ANALYSIS OF A DOUBLY PLATED GRILLAGE

UNDER IN-PLANE AND NORMAL LOADING

A Thesis presented for the degree of

Ph.D. (Engineering)

in the University of London

by

Donald Gatherer Williams, B.E., M.S.

Imperial College of Science and Technology,

London.

July 1969

ABSTRACT

Losses in the overall flexural and shear stiffness of plated grillages are studied with particular reference to the double-bottom structure. It is shown that in longitudinally framed ships, losses in flexural stiffness can be of the order of 15% in the longitudinal direction due primarily to shear lag, and can be in excess of 20% in the transverse direction due primarily to local panel bending. The latter effect is analysed by considering the large deflexion behaviour of initially deformed shell panels with restrained edges. Losses in shear stiffness due to perforations are shown to be of the order of 50% for hole sizes typical of the double-bottom structure.

Finite difference solutions to the orthotropic plate equations including shear deformation are given to show the effect of shear deformation on the behaviour of rectangular plated grillages under transverse and in-plane load. Flexural boundary conditions varying from simple support to fully clamped are treated. Within the practical range of plate dimensions the effect of shear deformation on stresses and deflexions can be of the order of ±40% and +100% respectively.

The above treatments are combined in order to analyse the results of tests conducted on a one-eighth scale steel model of a section of the double-bottom of a typical dry cargo ship. The agreement between measured and theoretical results for overall and local behaviour is satisfactory up to about 0.6 of the assumed working load. At this load non-linearity became evident in overall behaviour. Surface yielding of webs began at about 0.5 of the assumed working load and heart of plate yielding of the webs and surface yielding of shell panels began at about 0.75 of the assumed working load. The ultimate load for the model was 1.35 times the assumed working load.

ACKNOWLEDGEMENTS

The author wishes to express his thanks to the following:

Dr. J.C. Chapman, who supervised this work, for his guidance and encouragement.

Professor S.R. Sparkes for permission to pursue the work at Imperial College.

The British Ship Research Association, who sponsored this work, for their generous financial support.

The technical staff of the Structures Laboratory in general and Messrs. P. Guile, J. Neale, N. Scott and the late T. Wells in particular with special thanks to Mr. J. Galvin who was responsible for preparing the model for testing.

The staff and post-graduate students of the Structures Department for their valuable discussions, in particular Dr. B. Aalami and Dr. A.K. Basu.

Miss C. Collins for typing the thesis and Miss S. Rumble for tracing the figures.

CONTENTS

NOTATION

x, y, z	Cartesian co-ordinates - z normal to the plane of the plate, x and y parallel to principal axes of flexural symmetry
w	Deflexions of middle surface of plate in z direction
w_o	Initial deformation of local panels in the z direction
w_o/h	Initial deformation to plate thickness ratio at centre of panels
q	Intensity of lateral loading
q^*	Combined transverse pressure and in-plane load parameter
M_x, M_y	Bending moments per unit width of plate in x and y directions on y-z and x-z planes respectively
M_{xy}	Twisting moment per unit width of plate
Q_x, Q_y	Shear force per unit width of plate in z direction on y-z and x-z planes respectively
N_x, N_y	Tensile force per unit width of plate in x and y directions on y-z and x-z planes respectively (compression negative)
N_{xy}	Shear force per unit width of plate
P_x	Longitudinal in-plane thrust applied to double-bottom model expressed in tons/ram (13 rams each end)
D_x, D_y	Flexural stiffness of plate in x and y directions respectively; anticlastic bending unrestrained
$D = \frac{Eh^3}{12(1-\mu^2)}$	Flexural stiffness of homogeneous isotropic plate with anticlastic bending restrained
D_{xy}	Twisting stiffness of plate

S_x, S_y	Shear stiffness of plate in x and y directions respectively
E	Young's modulus for plate material
μ_x, μ_y	Poisson's ratios associated with bending moments in x and y directions respectively
μ	Poisson's ratio for plate material
h	Thickness of homogeneous isotropic plate
a, b	Length and width of plate in x and y directions respectively
k_{1x}, k_{1y}	Deflexion spring stiffnesses along $x = \pm a/2$ and $y = \pm b/2$ plate boundaries respectively
k_{2x}, k_{2y}	Normal rotation spring stiffnesses along $x = \pm a/2$ and $y = \pm b/2$ plate boundaries respectively
k_{3x}, k_{3y}	Tangential rotation spring stiffnesses along $x = \pm a/2$ and $y = \pm b/2$ boundaries respectively
k^*	External rotational restraint of local panels due to edge stiffeners
K	Effective rotational restraint of local panels taking account of k^* and continuity
λ_{1x}/b_1, λ_{1y}/b_1	Shell shear breadth factors in x and y directions respectively
λ_{2x}/a, λ_{2y}/b	Shell buckling breadth factors in x and y directions respectively
F_x, F_y	Effective web area factors in x and y directions respectively
σ_{xb}, σ_{yb}	Outer shell panel bending stresses in x and y directions respectively
σ_{xm}, σ_{ym}	Outer shell panel membrane stresses in x and y directions respectively
ϵ_{xi}, ϵ_{yi}	Inner shell surface strains at shell-web intersections in x and y directions respectively

ε_{xo}, ε_{yo}	Outer shell surface strains at shell-web intersections in x and y directions respectively
σ, τ	Theoretical applied web bending and shear stresses
γ_x', γ_y'	Shear strains in the x and y directions respectively

NOTE: For definition of non-dimensional orthotropic plate parameters see page 73.

CHAPTER I

INTRODUCTION

1. GENERAL

The basic structural elements in a doubly plated grillage are the plating or flanges and the grillage or web system. Depending on the particular design it may or may not be necessary to ensure the efficiency of these elements by local stiffening. The plating is usually continuous over the web system, except for isolated openings to allow access through or into the system. The webs may be solid or perforated and fabricated from sheet or rolled sections. In the latter case the section flanges will contribute to the plating flexural stiffness.

This form of construction is often dictated by the function of the structure. It has the advantage, as compared to single plating, of economy due to efficient material location but, where there is a choice, this must be weighed against difficulty of fabrication.

The flange and web plating is subjected to a combined stress system which arises from local (discrete panel) deformation, deformation of the grillage and deformation of the whole structure. While it is theoretically possible to incorporate all these modes of deformation into a single solution this is not at present a practical proposition, mainly because of the computer storage and time which would be required. Even if it were possible at the present time any such facility would only be of use as an analytical tool since, for design purposes, the costs involved would be

prohibitive. For practical purposes some form of idealization is required to take account of the loss of effectiveness due to local deformation in an overall solution which must then be followed by a separate local stress analysis.

This work is concerned with extending this practical approach to incorporate recent advances in the theoretical analysis of local behaviour in an extension to the orthotropic plate theory for overall behaviour, and to relate the results to the practical case of a ship's double-bottom structure.

2. THE DOUBLE-BOTTOM STRUCTURE

The double-bottom, which constitutes the bottom of the hull of many ships, including most dry cargo vessels, is made up of inner and outer shells the thicknesses of which can vary, depending on the overall size of the ship, from $\frac{1}{2}$ to $1\frac{1}{4}$ ins. The shells are separated by a web system which can be from 4 to 8 ft. deep and is usually of the order of $\frac{1}{2}$ in. thick. The webs may be solid, or perforated for lightening and inspection purposes. Webs in the transverse direction, spanning between the sides of the ship, are called floors and are spaced at from 5 to 10 ft. centres. Webs in the longitudinal direction are referred to as intercostals, except for the centre web which is called the centre girder, and are spaced at from 10 to 15 ft. centres.

Both shells and webs are usually stiffened. If the shell stiffening runs longitudinally the bottom is said to be longitudinally framed, if it runs transversely, transversely framed. Most modern ships of any size are longitudinally framed. The inner and outer

shell stiffeners are usually connected by a strut between floors to maintain shell spacing. There are also local web brackets, between floors, to provide additional stiffness immediately adjacent to the sides of the ship and the centre girder. Bulkheads, which are transverse diaphragms subdividing the ships hull into compartments, are spaced at between one and two times the width of the ship.

3. MODEL OF THE DOUBLE-BOTTOM

Because of the evolutionary nature of the development of ship design criteria, some practices have arisen which, although proven safe under service conditions, have only a semi-rational basis. In order to clarify such issues with respect to the double-bottom, a program of research was initiated at Imperial College involving both theoretical analysis and the fabrication and testing of a model of a section of a typical double-bottom. This model was based on the midship section of a single-deck dry-cargo ship, 400 ft. long, 56 ft. wide and 33 ft. deep, designed to Lloyd's 1956 Rules by the staff of the British Ship Research Association. It was fabricated in steel to one-eighth scale and represents that section of the bottom bounded by the sides of the ship and two adjacent bulkheads. In order to finalise fabrication techniques, construction of the main model was preceded by a single-floor model to the same scale. This represented a transverse section incorporating one floor only and was tested as a simply supported beam for various loading conditions. The latter work was reported by Chapman, Ho and Taylor [1].

The external load, under service conditions, on sections of the double-bottom bounded by the sides of the ship and two adjacent bulkheads is primarily:

(i) Transverse loading, due to water pressure from the outside, and cargo from the inside.

(ii) Longitudinal end thrust due to overall bending of the ship.

The model was tested under combinations of the above loading and also under local transverse load, such as would occur during dry docking.

The effective boundary conditions, at the sides and bulkheads of a section of the double-bottom of a real ship, vary from ship to ship and with the cargo loading. At the sides, since the double-bottom is usually much stiffer than the hull sides, the condition may approach simple support. At the bulkheads the condition depends primarily on the cargo load distribution between holds. For all holds equally loaded the effective restraint will approach the fully clamped condition whereas for alternate holds loaded the effective restraint will be considerably relaxed.

The model was supported on closely spaced pin ended rods on all edges. At the sides, which were free from any other restraint, this simulated simple support. At the bulkhead ends, which were stiffened beyond the line of the rods to ensure even distribution of the external in-plane load, the effective condition was partial rotational restraint.

4. ANALYSIS OF DOUBLY PLATED GRILLAGES

4.1 Overall Analysis

In the past, stresses due to transverse bending were evaluated using a beam or grillage approach. Only recently have attempts been made to allow for the substantial contribution to bending and torsional rigidities due to continuity of shell plating.

For the particular case of the double-bottom Schade [2], [3], [4] approximated the structure as a homogenous orthotropic plate, the stiffnesses of which are the same as those of the actual double-bottom, assumed to be uniformly spread. By means of an energy method Schade obtained solutions for the orthotropic plate's differential equations and presented design curves and tables for double-bottom structures, from which deflections, bending stresses and shear stresses can be estimated. The boundary conditions of the orthotropic plates considered were, all edges simply supported, all edges clamped or two opposite edges clamped and the others simply supported. Provision is made in the analysis to account for the variation in bending stiffness across the width of the plate for the cases when the centre girder section is stiffened by a keel plate.

Orthotropic plate theory was later applied by Chapman [5] to the overall behaviour of doubly-plated grillages in order to investigate the influence of the distribution of material between the flanges and the webs. The theoretical results obtained were confirmed by a model test.

More elaborate model tests were subsequently carried out and reported with reference to stiffened plates in ship structures in

conjunction with theoretical analyses [1], [6], [7], [8]. A survey of recent developments in the structural design of ships and a comprehensive list of references is given in Reference 9.

The orthotropic plate approach gives realistic design criteria provided allowance is made for the influence of the non-homogeneity of the real structure. Non-homogeneity has two basic effects. Firstly, local stress systems developed in transferring load between adjacent structural elements result in local distortions which must be accounted for in the overall flexural stiffness parameters. These effects are discussed in the following section. Secondly, the relatively wide spacing of webs results in effective shear stiffness parameters which are small enough to induce significant transverse shear deformation. The latter aspect of stiffened plate behaviour has received very little attention.

In this thesis, numerical solutions to the equations of Libove and Batdorf [10] for the linearised small deflexion behaviour of flat sandwich plates, including shear deformation, are presented for a range of plate and boundary parameters and several loading conditions. This particular theory may be regarded as a natural extension of the approximate theory for incorporating shear deflexion in beams [11]. A plated grillage can be idealised as a sandwich plate by considering the webs as corresponding to the sandwich core material.

The consideration of deflexion due to shear requires the specification of one more boundary condition than in ordinary plate theory [12]. Libove and Batdorf derived the resultant three boundary equations for each edge in terms of an idealised discrete spring system. By appropriate specification of spring stiffnesses it is possible to approximate continuous plate systems and plates supported

on edge beams.

The plate equations are derived to allow for orthotropic plate properties, making it possible to consider plate structures with differing flexural and differing shear properties in the two orthogonal directions. In evaluating equivalent stiffnesses the loss of overall effectiveness due to local behaviour must be taken into account. Provided this is done on a rational basis a wide range of structures can be analysed by the orthotropic plate approach.

Existing solutions which take account of shear deflexion are confined mainly to the simply supported boundary condition which incorporates zero tangential edge slope. These include solutions for isotropic plates by Ericksen [13], who considered rectangular plates under uniform transverse load, and by Yen, Gunturkun and Pohle [14], who considered square plates under uniform and concentrated transverse load. Reissner [15] demonstrated that for the case of isotropic plates with simply supported edges, subjected to uniform transverse load, deflexions but not stresses are modified by the inclusion of shear deformation. For orthotropic plates, Raville [16] considered the effect of shear orthotropy in rectangular plates under uniform transverse load and Robinson [17] gives solutions for combined transverse and in-plane load for a limited number of cases of flexural and shear orthotropy in rectangular plates. In the presence of orthotropy it is shown that both deflexions and stresses are affected by shear deformation.

The simply supported edge condition incorporating zero tangential edge slope implies that edge twisting moments are fully developed. The zero edge twisting moment condition has been considered by Kromm [18]

for a uniformly loaded square plate and by Schafer [19] for a sinusoidal heap on a rectangular plate. Carley and Langhaar [20] extended Schafer's solution to cover any symmetric load distribution. Numerical results given with these solutions are for relatively high values of shear stiffness and intermediate values of edge restraint against twist have not been considered.

There are also isolated solutions for square isotropic clamped plates under uniform transverse load [21], [22]. These show that the independence of edge slope due to shear deformation from normal rotational edge restraint results in significant modification to stresses as well as deflexions. Orthotropic plates with edge fixity have not been treated and intermediate values of normal rotational edge restraint have not been considered.

Since analysis of plate behaviour is considerably more involved if shear deformation is considered, it is desirable to have a guide as to whether the additional work is justified. With this objective, solutions are now presented which show the influence of shear deformation on stresses and deflexions for a broader range of plate parameters and boundary conditions than have previously been treated.

4.2 Local Analysis

4.2.1 Shell Panels: The basic double-bottom shell element is bounded on two (transverse) sides by adjacent floors and on two (longitudinal) sides by adjacent shell stiffeners or a shell stiffener and an intercostal. Typical dimensions are 40 in x 100 in with thickness varying from $\frac{1}{2}$ to $1\frac{1}{4}$ ins. and the panel may have an initial lack of flatness of the order of $\pm$ 50% of the plate thickness, at mid-panel relative to the sides. These panels are

subjected to transverse load due to water pressure on the outer shell and cargo load on the inner shell and also biaxial and longitudinal in-plane loads due to transverse bending of the double-bottom and overall bending of the ship respectively.

The local stresses in the panels can be derived from an analysis of the behaviour of a discrete initially deformed plate under combined load, provided the influence of continuity is accounted for in the boundary conditions. The type of plate theory to be used depends, for a given degree of accuracy, on the magnitude of the total deflexion relative to the plate thickness. Three categories of solution can be defined:

(i) Small deflexion solutions, which assume that the deflexions are so small that the transverse and in-plane load behaviour can be computed independently and superimposed.

(ii) Linearised solutions, which assume that the deflexions are large enough for the interaction between in-plane load and transverse deflexion to be significant, but still small enough for second order terms to be ignored. This implies that membrane stresses remain constant during deformation and the behaviour is linear with increments of transverse load.

(iii) Large deflexion solutions, which assume that the deflexions are large enough for second order terms to be significant in which case the membrane stresses do not remain constant throughout the plate and the behaviour is non-linear with increasing transverse load.

The historical development of plate analysis in general is well documented in the literature. In the field of ships plating in particular, one of the earlier workers was Conway [23] who derived linearised solutions for initially flat, simply supported rectangular panels subjected to uniform transverse pressure and uniaxial tension and compression. Lockwood [24] extended the method to include clamped square plates. Bleich [25] applied the more accurate large deflexion theory to solve cases of initially flat, square, simply supported panels subjected to similar loading. He concluded that in practice the deflexions were unlikely to be of sufficient magnitude to warrant the involved large deflexion analysis, and that linearised solutions could be used to give results of acceptable accuracy.

This conclusion was queried by Aalami [26] who derived solutions for various combinations of side ratio, loading, boundary conditions and initial deformation. He concluded that while the linearised solution proposed by Bleich for simply supported plates yields reasonably accurate results when the plate is acted upon by a uniform edge compression with unloaded edges free from stress, this approach may be grossly in error for other boundary conditions. Also, as pointed out above, practical panels may have initial deformations of the order of half the plate thickness which automatically makes the solution sensitive to non-linear effects.

While Aalami's work showed the necessity of considering large deflexion effects, practical application to double-bottom panels was dependent on an accurate assessment of the effective boundary conditions. Two flexural and two membrane conditions require definition. Of these four, the flexural condition for rotational

restraint is the most difficult to assess. This restraint depends on two factors, namely, the restraint afforded by continuity of plating having regard for total deflexion in adjacent panels, and that given by the shell stiffening. Murray [27], [28] considered this problem and produced a semi-emperical approach based on observed deformations for cases where the initial deformation was of the same sign in adjacent panels.

In this thesis a more analytical approach to the assessment of effective rotational restraint is presented and the results are utilised in the computer program developed by Aalami, to analyse the non-linear transverse deformation behaviour of local panels in the double-bottom model. This analysis provided an estimate of the loss of shell effectiveness in resisting in-plane load to be used in the analysis of overall behaviour of the model.

4.2.2 Web Panels: As part of the overall investigation into the behaviour of the double-bottom structure being carried out at Imperial College, of which Aalami's work was a part, the stress distribution, buckling and post buckling behaviour of perforated plates in shear was studied by Ho [29]. Historical development of analysis in this field is outlined in the latter reference. Finite difference solutions for stress distribution in square panels with central circular perforations of variable size were obtained for two limiting boundary conditions, namely, edges restrained to remain straight and uniform applied shear stress. Numerical values were also obtained for the classical solution for uniform shear applied to an infinite plate with a hole and for Wang's [30] solution for uniform shear applied to a discrete square plate with a hole.

In practice, the double-bottom webs are not discrete square panels with a single central hole but, as in the case of shell panels, a discrete panel analysis can give satisfactory results provided effective boundary conditions are realistically evaluated. It appeared possible, that the rigidity of the top and bottom shells and the web stiffening, could result in a condition approaching edges restrained to remain straight for discrete panel elements encompassing a single hole.

An attempt was made to apply the theory to tests on the single floor model described previously. It was found that stresses measured at the circumference of the holes agreed quite well with a solution for a discrete plate with rigid edges but better still with the classical solution for a hole in an infinite plate subjected to uniform shear. It appeared that deflexion due to shear, which was a measure of the additional flexibility due to perforation, agreed best with a solution for a discrete plate with edges subjected to uniform shear stress.

Although it was pointed out that the overall deflexions were influenced by loss of flange effectiveness no attempt was made to eliminate this effect before extracting deflexion due to shear. For this reason the value of the agreement noted as regards deflexions is suspect. Subject to further verification, it would seem that the infinite plate solution, which falls between the limiting cases mentioned, is the most realistic. It was noted that the comparison of theory and experiment must have been influenced by the fact that the depth of the floor panels was not equal to the hole spacing and that there were additional perforations to admit longitudinal stiffeners.

In order to clarify the above issues, a test on a beam incorporating the same web perforations and stiffening as the transverse floors, but with flanges such that loss of flange effectiveness was negligible, was carried out as part of the present work.

4.2.3 Shell-Web Interaction: The web spacing to overall span ratios along lontidudinal and transverse axes of most double-bottom structures are such that shear lag causes significant loss of overall bending stiffness. This is not strictly a local effect since it depends partly on the overall transverse load distribution. Shade[31] considered the particular case of ship structures and derived design curves for several typical cases. Unfortunatley, these solutions are not sufficiently general for direct application to the double-bottom and therefore, as part of this work, Shade's theoretical approach has been used as the basis of a computer program from which the required results were obtained.

5. SUMMARY OF OBJECTIVES OF THIS INVESTIGATION

5.1 To integrate, and extend where necessary, existing work on the analysis of loss of overall stiffness in plated grillages due to local deformation, with particular reference to the double-bottom structure.

5.2 To investigate the effect of shear deformation on the overall behaviour of plated grillages by obtaining numerical solutions to the orthotropic plate equations including this mode of deformation.

5.3 To utilise the preceding work in the analysis of tests on a model

of a section of the double-bottom structure in order to gain a better insight into both the overall and the local behaviour.

CHAPTER 2

MODEL AND TEST SET UP

1. GENERAL

Basic details of the double-bottom model are given in the Introduction. Work on the assembly of the model, which was done at Imperial College, started in 1959 under the supervision of P.F. Taylor. When construction was only partially completed B. Aalami took over the supervision and was responsible for strain gauging the model. Aalami also designed and supervised the construction of the transverse load rig. In 1965 when the model was in position and almost ready for testing it was handed over to the author who supervised all testing and was responsible for some modifications. The latter included the installation of tension links in the corners of the model to resist "lift-off" and the installation of the in-plane load and the local transverse load test arrangements.

Although much of the theoretical work discussed in later Chapters is of general application it was developed with the primary purpose of analysing the double-bottom model. This applies particularly to the analysis of local behaviour and for this reason it is desirable that the reader be familiar with the contents of this Chapter before proceeding to Chapter 3.

2. DESCRIPTION OF THE MODEL

Figure 1 shows the principal dimensions and some details of the model. Additional details (web perforations and local stiffening)

are given in Figure 2. The 0.064 in. and 0.080 in. plate thicknesses, which were determined by the availability of mild steel sheet, correspond closely to the correct scale thicknesses for the principal structural members.

Figure 3 shows the model prior to attachment of the inner shell and gives an appreciation of the complexity of the double-bottom structure. Figures 4 and 5 show details of the shell and web stiffening. Figures 6 and 7 are inner and outer shell views of the completed model. The inner shell view shows the margin and bulkhead brackets which stiffened the upstanding edge Tee section at intersections with the main and bracket floors at the sides, and the longitudinal webs and shell stiffeners at the ends.

3. FABRICATION OF THE MODEL

The main problem in constructing the model was to attach the second skin after the remainder of the structure had been welded, since it was not possible to weld internally. Various spot-welding methods were considered, but all suffered from the disadvantage that the web members would require to be flanged on their faying edges, and also, that the connexions would be intermittent. Furthermore the jigging of components for welding would have been difficult.

To achieve connexions as nearly continuous as possible, with access from outside the model only, a method was devised in which the faying edges of all members attached to the bottom shell and inner bottom (i.e. centre and intercostal girders, floors, bracket floors, and longitudinal stiffeners) had projecting teeth machined in their edges. These teeth fitted into corresponding slots machined in the

inner bottom and bottom shell plating. The depth of a tooth was equal to the thickness of the plate into which it fitted, so that when assembled the top of the tooth was flush with the outside of the plating. The plate was then welded in position by a run of weld along the top of the tooth on the outside of the plate, making a continuous connexion over the length of the tooth. In general the tooth length was about 3 in. and the space between teeth varied between 1 and 2 ins., the closer spacing being used where high shear stresses were expected.

Consideration was given to attaching one skin by fillet welding, but it would have been difficult to manipulate an electrode in the cramped spaces inside the model, and some parts would have been completely inaccessible. Furthermore, the distortion of the plating would have been greater. Both skins were therefore slotted and welded externally.

To facilitate correct alignment of the web members it was convenient to provide half-depth slots at their intersections, eggbox fashion. In this way the web structure was self-jigging and could be accurately assembled and welded before the plating was added. The longitudinal stiffeners and the channel struts were prefabricated with the web structure.

Cooling was effected by applying a jet of compressed air to the welds after the slag had been chipped away. Each weld was individually cooled before proceeding with the next weld. A welding sequence was evolved, during construction, to compensate for the observed distortions.

4. LOADING ARRANGEMENTS

4.1 Transverse Loading Frame

Details of the transverse loading frame are shown in Figure 8. Transverse load was transmitted from the edge Tee brackets, via a system of vertical rods, to a stiff rectangular box section frame. This frame was tied to three transverse wide flanged beams which were friction bolted to six solid circular steel columns. These columns reacted against the "strong floor". The seating between the box section and the beams was packed to ensure a uniform distribution of load. Despite the rigidity of this arrangement, small but finite deflexions of the rig due to transverse load were recorded. Figure 9 shows the loading frame bolted in position for a transverse pressure test.

4.2 Attachment of Model to Box Section Frame

The vertical rods, which can be seen along the sides and ends of the model in Figure 9, were located on the edge Tee sections in line with each margin and bulkhead bracket. The rods were seated as shown in Figure 10. Rods at the centres of each edge were restrained against movement parallel to their respective edges. The model was therefore restrained in space along both horizontal axes but the edges were free to translate normal to themselves. The restrained rods were housed in the circular appendages visible on the underside of the box section frame in Figure 11.

The corners of the model were restrained vertically by links which could develop tension and therefore resist corner "lift-off" under transverse load. These links were articulated to minimise lateral

restraint at the corners, as shown in Figure 10.

In the unloaded conditions the weight of the model was taken by 20 adjustable coil springs spaced at intervals around the edge of the model and attached to the box section frame. These springs were tightened prior to testing so that the model was held firmly against the rods, which were themselves adjusted so that all rods were firmly seated. This minimised the effect of local slackness on the overall reaction distribution.

4.3 Transverse Pressure Loading

Transverse pressure was applied to the flat portion of the outer bottom by means of a pressure bag, fabricated from 1/16th. in. sheets of rubber and clamped between steel bars at the edges. The bag was operated by water. Figure 12 shows this bag in position on the floor prior to installation of the model. With the pressure bag in position the model was placed on top of the bag as shown in Figure 11. The loading frame beams were then lowered and clamped in position such that, when the model was attached to the box section frame there was a gap of about 0.75 ins. to be taken up before water pressure became effective. In the foreground of Figure 9, which shows the rig in readiness for a transverse load test, can be seen the arrangement used to regulate transverse pressure. This incorporated a gravity operated safety valve by means of which, with the inlet valve open, the pressure automatically cut out at within about 0.1 p.s.i. of the required load. The final adjustment, made with reference to a water manometer and not the dial gauge shown in Figure 9, was achieved by hand operation of the inlet valve. Once any surge had damped out the pressure bag was sealed off and always remained stable within about 0.02 p.s.i. of the required load.

4.4 Longitudinal Thrust Loading

Longitudinal thrust was applied, in combination with transverse pressure, by means of 26 - 20 ton capacity lapped rams, 13 at each end. They were located so as to distribute the load uniformly across the width and through the depth of the model. Final adjustment was achieved by means of the adjustable ram seatings shown in Figure 13. Figure 14 shows details of a ram in position. The rams reacted against concrete piers bolted to the strong floor. Figure 15 is a general view of the longitudinal thrust rig at one end of the model. The rams were operated by an Amsler loading cabinet with a piping system arranged to load both ends of the model simultaneously and thus minimise differential thrust. Ram pressure was adjusted and maintained to within 0.01 tons/ram.

4.5 Local Transverse Load

Local transverse load was applied along the centre girder, at points of intersection with the transverse floors, by means of 10 ton capacity lapped rams held vertically under the model. The transverse beams, box section frame and model had previously been raised and reclamped so that the underside of the model was 35 ins. clear of the strong floor. Figure 14 gives details of the ram set up. The pad, seated on top of the ram, was designed to distribute load sufficiently to avoid a premature local web failure. Figure 16 is a view of several rams in position under the model. Figure 17 is a general view of the first local transverse load case of 8 rams, one at each floor. Tests were conducted for four different cases, obtained by successively removing rams in pairs from the ends of the line. As in the case of

the longitudinal thrust load, the system was operated with an Amsler load cabinet reading to within 0.01 tons/ram and connected by a piping set up arranged to ensure, as nearly as possible, symmetrical load application.

5. INSTRUMENTATION

5.1 Strain Measurement

Strains were measured using electrical wire resistance gauges bonded to the model and the supporting rods with epoxy based adhesive. Figure 18 shows the location of web gauges. Figure 19 shows the location of gauges at intersections of the inner and outer shells with longitudinal and transverse webs. Figure 20 shows the locations of gauges on stringers and on centre lines of three outer shell panels. Figure 21 shows the rod numbering system and the location of the rods which were strain gauged to measure reactions.

Strains were recorded automatically at the rate of 10 gauges per second by a "Solartron" data-logger which had a specified sensitivity of $\pm$ 2 microstrain. Temperature compensation was provided by dummy gauges bonded to steel plate. Output from the data-logger was of two forms. A printed output, which was used as a guide to critical behaviour during tests, and a punched tape output, which was sent directly to the computer for reduction.

5.2 Deflexion Measurement

Local deflexion was measured for three outer shell panels using inductive displacement transducers located as shown in Figure 22.

They were held in a frame resting on the inner shell of the model. Contact with the outer shell was provided by $\frac{1}{8}$ in. diameter extension spindles attached to the transducers and passing through holes drilled in the inner shell. These spindles seated in moulded recepticles bonded to the inside of the outer shell. The transducers had a travel of 0.5 ins. and deflexions were measured on a meter which was read to a specified accuracy of $\pm$ 0.001 ins.

Overall deflexions, transverse to and in the plane of the model, were recorded at the locations shown on Figure 22. Gauges prefixed R recorded the in-plane displacements. Gauges 20 and 21 recorded vertical displacement of the box frame. Deflexions were measured with 0.5 in. travel mechanical dial gauges, sensitive to 0.0001 ins., held in a rig resting directly on the strong floor. Because of the complexity of the loading and deflexion rigs considerable care was necessary to ensure that no fouling occurred.

6. TEST PROCEDURE

6.1 Combined Transverse Pressure and In-plane Load

A total of 10 combined load tests were conducted. These were for ten values of longitudinal thrust varying from 0 to 9 tons/ram. In each case the transverse pressure was first brought up to 0.5 p.s.i. and the longitudinal thrust then applied. The transverse pressure was then readjusted to 0.5 p.s.i., if required, and this became the datum load for successive increments, of 0.5 p.s.i., in the transverse pressure. The reason for using a small value of transverse pressure as a datum rather than zero pressure was, firstly, to minimise the

effects of any slackness in the rig, and secondly, to stabilize the model against any longitudinal force arising out of unequal end loads. The maximum value of transverse pressure in each test was determined by the approach of yielding, indicated by the printed strain record. For low values of longitudinal thrust the web strains governed but as thrust was increased the shell panel strains became the governing factor.

6.2 Local Transverse Load

As for the combined load tests a datum load, of 0.25 tons/ram, was applied to eliminate any slackness in the rig. In each case the load was increased in increments of 0.25 tons/ram, up to a load at which local yielding was almost reached.

CHAPTER 3

ANALYSIS OF PLATING EFFECTIVENESS

1. GENERAL

The orthotropic plate approach to the analysis of plated grillages follows the sequence below.

(i) An analysis of local element behaviour in order to determine the losses in overall effectiveness to be allowed in computation of orthotropic plate properties for use in;

(ii) An analysis of overall behaviour to determine force distributions for use in;

(iii) A local stress analysis

At first sight it would seem that this approach must involve an iterative procedure because of the interdependence of the above steps. It will be shown however that, with certain limitations, it is possible to make a good estimate of losses in effectiveness from the geometry of the particular structure.

This Chapter deals with an investigation into these losses with particular reference to the double-bottom model. Where possible existing theoretical work, mainly in relation to large deflexion plate behaviour, has been used but it has been necessary to develop some work, relating to the evaluation of realistic boundary conditions for plate panels.

The local stress systems considered in this respect are as follows:

(i) In connection with flange effectiveness, two effects must be distinguished

The first effect, commonly called shear lag, arises because load transfer across the flanges is dependent on a plane stress system. The associated shear distortion is reflected in the longitudinal stress distribution across the flange and results in an overall moment of resistance which is less than that given by the idealised assumption that stress is proportional to curvature. This effect is taken into account by using a reduced flange breadth in computing overall flexural stiffness where the ratio of reduced to fully effective flange breadth due to shear lag is termed the shear breadth factor in this thesis.

Secondly, the longitudinal stress distribution is influenced by out of plane, flange deformation. Out of plane deformation is initiated by either local transverse pressure and/or initial lack of flatness and the resultant increase in in-plane flexibility must be reflected in the overall flexural stiffness. As with shear lag this effect is taken into account by using a reduced flange breadth in computing overall stiffness where the ratio of reduced to fully effective flange breadth due to transverse deformation is termed the buckling breadth factor in this thesis.

(ii) In connection with web effectiveness

Perforations and local restraints must be accounted for in evaluating the effective web area to be used in computing the overall shear stiffness. The complexity of the floor (transverse web) perforations and stiffening make a theoretical analysis difficult but an attempt is made to rationalise an existing solution [29] with the aid of experimental results from floor beam tests.

2. SHEAR BREADTH FACTOR

This factor is defined as follows:

x axis: λ_{1x}/b_1

y axis: λ_{1y}/b_1

Where λ_{1x} and λ_{1y} are the effective flange dimensions and b_1 is the corresponding actual flange dimension, between webs, in the respective directions.

Numerical values of this factor, for the double-bottom model, were obtained from a computer program, based on a solution by Schade [31], which was written as part of the present work. A brief account of Schade's solution is given in Appendix A.

As noted by Schade the shear breadth factor depends upon:

(i) The boundary conditions along the sides of the flange. The program is written for full lateral restraint, a condition

approached in the case of multiple webs.

(ii) The form of the bending moment distribution. This depends on the applied loading and the support conditions. In the case of the double-bottom various loading conditions are examined and the boundaries are assumed simply supported.

(iii) The geometrical properties of the section. The program is written for doubly flanged sections specified as follows (reference Figure 25); flange breadth (b_1, equal top and bottom), flange thickness top and bottom (t_1 and t_2, not necessarily equal), web depth (s) and web thickness (t_3). No account is taken at this stage of the effect of flange stiffeners, which is discussed later in this section.

Figures 23 and 24 show results from solutions for the overall behaviour of the double-bottom model. These were obtained to examine the moment (M_x, M_y) and shear (Q_x, Q_y) distribution in order to determine if they had a form analogous to the corresponding beam distribution for similar applied loading conditions. It can be seen that inclusion of the effect of shear deformation causes some modification to the distributions in the loaded regions but for practical purposes the analogy is valid and beam solutions were assumed to be applicable. The reason for using stepped rather than constant load, as shown in the cross sections, was that the theoretical solution for plate behaviour including shear deformation is extremely sensitive to load discontinuities and the numerical limitations of the solution are minimised if the load is distributed in this manner. It might also be argued that the stepped load section is more

realistic. As can be seen from the deflection profiles the proportion of overall deflection due to shear is very significant.

Solutions for the variation of shear breadth factor over the span for longitudinal and transverse beam sections of the double-bottom model, under various loading conditions, are shown in Figure 25. The loads correspond to cases actually applied to the model. Since the overall analysis of the model assumes constant stiffness along respective axes an equivalent shear breadth factor was calculated for each case on the basis of overall beam flexibility such that it gave the same central deflection as the corresponding beam with stiffness varying in proportion to the calculated shear breadth factor. It will be noted that it is possible for the shear breadth factor to exceed 1.0. This occurs for laterally restrained flanges only, where this restraint allows the biaxial strength of the plate to develop so that the maximum theoretical effectiveness is $1/(1-\mu^2)$ or 1.099 for $\mu = 0.3$. To avoid confusion with later work the equivalent shear breadth factor are quoted as a percentage of the maximum 1.099 in the following table. The same values apply to top and bottom flanges.

Equivalent Percentage Shear Breadth Factor					
H/L	1.0	0.667	0.444	0.222	0.092
x axis	94.0	93.8	93.6	93.2	-
y axis	94.0	-	-	-	93.0

The preceding analysis ignores the influence of stiffeners on flange effectiveness. Longitudinal stiffeners increase the overall flexural stiffness without contributing to the flange shear rigidity so that the flange shear distortion is greater compared to an unstiffened flange section of comparable flexural stiffness under the same applied load. A further reduction factor is required to take account of this behaviour. Ferahian [32] examined the influence of flange stiffeners in the case of single web beams (no lateral flange restraint) and produced the curve shown in Figure 26 (ii), which gives reduction factors (K_1) to be applied to the corresponding unstiffened flange solution for shear breadth in simply supported beams under uniformly distributed load.

Ideally, corresponding curves should be produced for the particular case of the double-bottom, incorporating the effect of multiple webs, but reduction factors of sufficient accuracy can be obtained directly from Figure 26 (ii). This is justified on the basis of the comparison between single and multiple web solutions for unstiffened flanges shown in Figure 26 (i). It can be seen that for beams with L/b_1 greater than about 4 the ratio of λ_1/b_1 for single webs to λ_1/b_1 for multiple webs, for any given L/b_1, is reasonably constant. Therefore for the double-bottom model ($L/b_1 \simeq 6$, both axes) the correction to shear breadth to allow for stiffeners was taken directly from Figure 26 (ii). For the model the two values of K_1 shown in Figure 26 (ii) correspond to the inner and outer shell and take into account the linear stress distribution through the depth of the beam. Thus the percentages by which the corresponding shear breadth solutions must be multiplied to account for stiffeners are,

x axis only :

Inner Shell : 91.0%

Outer Shell : 92.5%

3. BUCKLING BREADTH FACTOR

3.1 Definition of the Typical Model Shell Panel

The evaluation of loss of flange effectiveness due to transverse deflection of a typical double-bottom shell panel was carried out with the aid of a computer program giving solutions for the large deflection behaviour of rectangular orthotropic plates, developed by Aalami [26]. The following factors had to be considered before this program could be utilised.

3.1.1 Basic Panel Element: This was resolved in part by the limitations of the program since, there being no facility for the specification of interior restraint, the basic element could not surround an interior support such as a channel strut. The choice was thus reduced to several rectangular isotropic plate elements of different dimensions. From Figure 1 it can be seen that the $14\frac{1}{2}$ in. x $4\frac{3}{8}$ in. panel bounded by adjacent floors and adjacent shell stiffeners (or a shell stiffener and an intercostal) was the predominant element and hence this was chosen for more detailed analysis.

3.1.2 Effective Panel Boundary Conditions: The plate equations required the definition of two flexural and two membrane boundary

conditions as follows:

(i) Flexural:

(a) Vertical deflexion restraint: The most flexible edges were those bounded by shell stiffeners which had an unsupported span equal to the distance between a floor and a channel strut. However, these stiffeners were sufficiently inflexible to make edge deflexions very small relative to deflexions in the interior of the panel and vertical deflexion restraint was taken as infinity.

(b) Normal slope restraint: Evaluation of this restraint has been considered by Murray [27], [28]. The results are of limited application however and it was apparent that a more detailed analysis of the problem was required. This was done as part of the present investigation and is presented in detail in the next section of this Chapter. The conclusion reached is that, for the particular case of the double-bottom model, the edges of individual panels were restrained such as to develop about 75% of the fully clamped edge moment.

(ii) Membrane:

Normal in-plane restraint: Since the double-bottom model was effectively free in space there was no external restraint to be transmitted to individual interior panels. Compatible displacements at the edges of adjacent panels required however that the edges remain straight, resulting in a non-uniform distribution of membrane forces normal to the edges. Aalami's program has the facility for specifying that edges remain straight and the applied force is prescribed as the mean force on each edge. The final distribution of the applied force is

determined by the solution, subject to satisfaction of the straight edge condition.

(b) Tangential in-plane restraint: As with normal in-plane restraint the external restraint is zero and compatible panel edge shear displacements are assumed to correspond to zero tangential in-plane restraint of individual panels.

3.1.3 Initial Lack of Flatness: This is of primary importance with respect to the behaviour of a panel as an isolated plate and as regards interaction with adjacent panels. Figure 27 is a contour plot of the initial lack of flatness over the central area of the bottom shell of the double-bottom model. It is of note that whereas in practice welding techniques lead to inward deformation for most panels, the model exhibited inward and outward initial deformations in approximately equal proportion. This antisymmetry was the primary factor which prevented the fully clamped edge condition for individual panels from developing. Some approximation as to the magnitude of the deformations was necessary and this was done by taking a mean of central deflexions between adjacent edges, giving values of +0.019 in. and -0.025 in. for inward and outward central deformation respectively. The plating was 0.080 in. thick and based on the above mean measurements a value of central initial deformation to plate thickness ratio (w_o/h) of ± 0.25 was used in the calculation of effective rotational restraint to be applied to model panels. In Aalami's program initial deformation may be defined as either a sinusoidal distribution along both axes for a given central value of w_o/h, or actual (axially symmetric) deformations can be prescribed at nodal points. The former method was utilised in the present analysis.

3.1.4 Loading: Figure 28 shows the various types of panel loading considered. The combinations of these loads to which a particular panel was subjected depended on its location in the shell. In the model, only the outer shell panels experienced transverse pressure (q), distributed evenly on panels over the flat section of the bottom. The in-plane load on each panel due to overall flexure of the model (N_{qx}, N_{qy}) was proportional to the corresponding bending moment and of opposite sign in the inner and outer shells. The in-plane load due to externally applied forces (N_x') was assumed to be constant across the breadth of the model. This corresponds to overall bending of the ship's hull and variation between inner and outer shells due to differences in section moduli was assumed to be negligible. Hence in the model test the in-plane load was applied at the neutral axis of the double-bottom.

3.2 Evaluation of Effective Local Panel Rotational Restraint

In isolating a panel from an array of panels, boundary conditions must be derived which reflect the restraint due to local stiffeners and the forces imposed by the surrounding system. Of the four boundary conditions required only the effective restraint against normal rotation is not immediately apparent. This problem would not arise for transversely loaded panels if there were no initial deformation or if the initial deformation was identical in all panels, in which case it would be reasonable to assume the interior panels were fully clamped. It is the variation of initial deformation in adjacent panels, interacting with the in-plane load which relaxes the fully clamped condition.

The relatively large aspect ratio of the panels under consideration ($\varepsilon = \frac{14.5}{4.375} = 3.31$) simplified the problem because for such cases the dominant behaviour is basically that of a beam spanning the short (y) direction. This led to a consideration of the idealised continuous beam-column shown in Figure 29 (i). The assumptions, apart from the initial assumption that the problem could be treated as a beam-column, are that the initial deformation was of the antisymmetric sinusoidal form shown, that the in-plane load was constant and that external rotational restraint (k^*) was equal and vertical displacement zero, at all supports.

The first problem, having made the above idealisation, was to assess the value of k^*, the external rotational restraint due to the longitudinal shell stiffeners. Having done this the beam-column solution could be used to determine a value of effective rotational restraint such that, when applied to a single span, it gave the same solution for forces as the original continuous span solution.

3.2.1 External Rotational Restraint:

The required restraint is defined as follows:

$$k^* = M/\theta$$

Where: M = torque applied to stiffener/unit length

θ = total rotation at corresponding cross section

Two alternative methods of evaluating this quantity were considered, both of which could be expected to give roughly the same value for k^*.

(i) Torque Solution:

The total rotation (θ) is assumed to be made up of θ_1 due to twisting as a thin walled section about an enforced centre of rotation to which must be added θ_2 due to local bending.

Defining: $k_1^* = M/\theta_1$

$k_2 = M/\theta_2$

Then: $k^* = M/(\theta_1 + \theta_2) = k_1^* k_2/(k_1^* + k_2)$

(a) Solution for k_1^*:

Governing Equation: For the parameters defined in Figure 30 (i) the governing equation for torque of an angle section about an enforced centre of rotation is: (Reference 33)

$$\frac{d^4\theta_1}{dx^4} - \frac{GK}{Dd^2}\frac{d^2\theta_1}{dx^2} = -\frac{M}{Dd^2}$$

In the case of the double-bottom the enforced centre of rotation is at the stiffener-shell interface. Because of the channel strut restraint at the middle of the side of a panel the torque distribution cannot be predicted so for the purposes of this analysis a uniform distribution was assumed. This is shown to be conservative (give lower values of k_1^*), compared to a parabolic distribution, for the limiting case of d = 0.

Boundary Conditions: In the double-bottom model end restraints were provided by the channel strut at one end and the stiffened floor at the other. Two limiting cases were considered:

Firstly, ends restrained against rotation but free to warp:

$$\theta_1 = 0$$

$$\frac{d^2\theta_1}{dx^2} = 0$$

Secondly, ends restrained against rotation and warping:

$$\theta_1 = 0$$

$$\frac{d\theta_1}{dx} = 0$$

Of these two cases the latter is more realistic for the model but both cases were analysed to show the influence of restraint against warping.

Solution of Equations: The above equations were solved using first order finite difference approximations to the derivatives. The numerical values of the coefficients for the particular case of double-bottom model stiffeners are given in Figure 30 (i). Values of $k_1 = M/\theta_1$ were computed at each mesh point. The minimum value, which occurs at $x = L/2$ is denoted k_1^*. Figure 31 (i) shows the convergence behaviour of k_1^* as the number of finite difference mesh divisions per span is increased. Figure 31 (ii) shows the effect of span dimension on k_1^*. The restraint due to the channel strut, which reduces the span by a factor of 2, results in an increase in k_1^* by a multiple of the order of 2^4.

Figure 32 shows the variation of k_1 across the span in the case of a stiffener restrained by a channel strut (L = 6")

for the two alternative end conditions. It can be seen that taking $k_1^* = M/\theta_1$ at x = L/2 gives a conservative estimate of the external rotational restraint for the assumed torque distribution.

Figure 30 (ii) shows the effect on k_1^* of varying the distance of the enforced centre of rotation from the shear centre (d). As d increases the flexural stiffness of the angle flange becomes more effective. This is more marked for ends restrained against warping such that, for d = 0.9" (restrained at the shell-stiffener interface) k_1^* is about $3\frac{1}{2}$ times greater when the ends are restrained against warping.

For d = 0 the solutions are independent of restraint against warping since when torque is applied at the shear centre there is no tendency to warp. The pure torque solution for uniformly distributed applied torque gives $k_1^* = 296$ which is less than the corresponding solution for sinusoidally distributed applied torque, $k_1^* = 364$ (constant for all x). Although the true distribution is not known this indicates that the solution for k_1^* based on uniformly distributed torque is conservative.

The value taken as the external rotational restraint associated with torque was (reference Figure 30 (ii)):

$$k_1^* = 3.58 \times 10^3 \text{ in.lb./in.}$$

It is of note that taking account of:(i) the reduced span due to support at channel struts,(ii) the enforced centre of rotation and (iii) the restraint against warping, increases k_1^* relative to the pure torque value for full span between floors,

by a multiple of about 50.

(b) Solution for k_2 (local bending):

The preceding calculation takes no account of local deformation of the angle arm connected to the shell. The assumed conditions are illustrated in Figure 33 (i). This gives $k_2 = M/\theta_2 = 3EI/\ell = 2.22 \times 10^3$ in.lb./in.

Total Restraint:

$$k^* = k_1^* \; k_2/(k_1^* + k_2) = 1.37 \times 10^3 \text{ in.lb./in.}$$

(ii) Plate Solution:

The alternative solution is to consider the angle as acting as plate simply supported along the connection with the shell, where the moment is applied, and elastically supported by the outstanding leg on the opposite edge. Because of the large aspect ratio (ε>6) it was sufficient to treat this plate as a beam as shown in Figure 33 (ii).

Assuming that the outstanding leg is clamped at the ends and that the transverse load (plate reaction) distribution is uniform, the vertical restraint is, approximately:

$$k' = \frac{384D}{L^4} = 4.35 \times 10^3 \text{ lb./in.}^2$$

Because of its geometry, the rotational restraint of the outstanding leg is not greatly affected by having an enforced centre of rotation at the edge. Hence, for a uniform applied torque

distribution, the rotational restraint is, approximately:

$$k'' = \frac{8GK_f}{L^2} = 0.1 \times 10^3 \text{ in. lb./in.}$$

Where: GK_f = torsional stiffness of outstanding leg

Substituting these values into the following solution for the moment-slope relationship:

$$\frac{M}{\theta_2} = \frac{4EI}{\ell}\left[\frac{3EI\,k''/\ell^3 + 3EI\,k'/\ell + k'k''}{12\,(EI)^2/\ell^4 + 12\,EI\,k''/\ell^3 + 4EI\,k'/\ell + k'k''}\right]$$

Gives: $$k^* = \frac{M}{\theta_2} = 1.35 \times 10^3 \text{ in.lb/in.}$$

This agrees closely with the torque solution.

3.2.2 Effective Rotational Restraint (beam-column solution)

The required restraint is defined as follows:

$$K = M/\theta$$

Where: M = beam-column moment at supports

θ = corresponding slope

(i) Equations: The governing equation for the continuous beam-column shown in Figure 29 (i) can be derived from a consideration of the equilibrium of forces acting on an element shown in Figure 29 (ii) and the small deflexion moment-curvature relationship.

This gives: $$\frac{d^4w}{dy^4} + \frac{p}{EI}\frac{d^2w}{dy^2} = \frac{q}{EI} - \frac{p}{EI}\frac{d^2w_o}{dy^2}$$

Where: w = deflexion due to applied load

w_o = initial deflexion (sinusoidal distribution)

The boundary conditions, which introduce the effect of external rotational restraint at the supports are as follows:

End supports: $w = 0$

$$M = k^* \frac{dw}{dy}$$

Interior supports: $w = 0$

$$\Sigma M = 0, \left(EI \frac{d\theta_A}{dy} - EI \frac{d\theta_B}{dy} + k^* \theta_C = 0\right)$$

$$\theta_A = \theta_B, (= \theta_C)$$

(ii) Solution of Equations: These equations were solved numerically using first order finite difference expressions for the derivatives. This required the solution for one fictitious point at each end and two fictitious points at each interior support as shown in Figure 29 (iii). A computer program (BEAMCOL) was written to solve the resulting simultaneous equations for N spans of equal length, M equal divisions per span. The total number of unknowns, including fictitious points, is therefore $M(N + 2) + 1$. The corresponding number of equations were solved directly, without partitioning, using a Gaussian reduction routine.The possibility of round off error using this routine limited the number of unknowns to about 120.

(iii) Accuracy of Solution: The accuracy of the program was checked against several known solutions, some of which are shown in Figure 34. The convergence behaviour as the number of divisions per span was increased, for the case of a two span beam under uniform transverse load, is shown in Figure 35 (ii).

It may be noted that the above equations are of the same form as those for the torque solution to determine external rotational restraint. By appropriate interchange of coefficients the BEAMCOL program duplicated solutions given by the torque program.

(iv) Parameters for model:

(a) Dimensions: Results are for model dimensions, given in Figure 36.

(b) Number of Spans: The choice of the number of spans to be used in solutions to determine effective rotational restraint was based on the criteria that; the central span should behave the same as a single clamped span for uniform transverse load and zero initial deformation. Figure 35 (i) (a) shows that an eleven span solution meets the latter criteria. Eight divisions per span were used for all cases giving 111 unknowns for eleven spans.

(c) Loading: The relationship between q, the transverse load, and P, the in-plane load, was based on a preliminary solution for the overall behaviour of the double-bottom model for uniform transverse pressure, simply supported edges and the shells assumed to be fully effective. At the centre of the model this gave, for a one inch strip (transverse, y axis)

$$q = 1 \text{ lb./in.}$$

$$P = 110 \text{ lb.}$$

These loads increase proportionally, and the combination is denoted by q^* such that $q^* = 1$ corresponds to the above combined load.

(d) Initial Deformation: As shown in Figure 29 (i) an anti-symmetric profile, relative to each support, was assumed. This is not necessarily the case in practice but did occur in the model and was chosen as the worst condition. Several w_o/h ratios are examined, a value of 0.25 being used in the final analysis.

(v) Results: Figure 36 shows the influence of external rotational restraint (k^*) on the bending moment distribution for two loading cases. It can be seen that in the absence of k^* (Figure 36 (i)) the effective restraint on a single span, as evidenced by the support moments, varies considerably, approaching zero for q = 5 lb/in., P = 550 lb. ($q^* = 5$). Such a variation in local restraint would cause, or at least magnify, any non-linearity in the overall behaviour. In fact the tests showed the overall behaviour to be almost linear up to the pressure corresponding to $q^* = 5$, indicating that effective restraint was relatively constant. Figure 36 (ii) shows that $k^* = 1000$ is sufficient to maintain a large degree of local restraint.

Figure 37 shows the effect of increasing load on K for three values of k^* and three values of central initial deformation ratio (w_o/h). The three solutions for $k^* = 0$ (external restraint zero) converged on K = 0 (effective restraint of individual spans zero-simple support), at about $q^* = 6$ (P = 660 lb.). At just slightly above this load all three solutions degenerated. The simply supported column buckling load for a single span ($\pi^2 EI/L^2$) is 665 lb. This

shows that degeneration of the beam-column solution is an accurate indication of column buckling load. Since the buckling load of the typical simply supported plate panel corresponds to $q^* = 7.7$ and the design pressure for the ship on which the model was based corresponds to $q^* = 10$, the importance of avoiding the simply supported edge condition is apparent. The specification of a minimum value of k^*, incorporating an adequate safety factor against approaching the simply supported condition within the working load range, seems a logical basis for design.

Figure 38 gives solutions for support moment in single span beam-columns for varying end restraint. Solutions are given for two load cases and three values of initial deformation ratio. The purpose of these curves was to give a measure of the degree of clamping in continuous beam-columns as a percentage of the fully clamped moment.

Figure 39 directly relates external rotational restraint (k^*) and effective rotational restraint (K) for three cases of initial deformation and two values of load. As w_o/h increases the rate of increase in K as k^* is increased drops off and becomes less sensitive to transverse load. For the particular case of the double-bottom model:

$$k^* = 1350 \text{ in.lb/in.}$$

$$w_o/h = 0.25$$

Giving:

$$K = 2000 \text{ in.lb/in. at } q^* = 1$$

$$K = 1530 \text{ in.lb/in. at } q^* = 5$$

The preceding solutions have been for the maximum value of P, relative to q, which occurs at the centre of the double-bottom. In fact, although q remains constant over the flat portion of the bottom, P reduces in proportion the overall bending moment. This means that the relaxing effect on K of the interaction between P and w_o will reduce toward the sides of the model. Figure 40 gives a measure of this effect for k^* = 1350 in.lb/in. and w_o/h = 0.25. Half way between the sides and the centre of the model K will exceed the centre value by about 10%.

As shown in Figure 37 all the preceding values of K refer to a span with initial deformation in the same direction as the transverse load. It might be expected that adjacent spans, where the initial deformation opposes the transverse load, would experience considerably different effective rotational restraint. This is in fact the case but since the main criteria for the influence of membrane stresses on panel behaviour, which is the determining factor as regards buckling breadth, is the magnitude of deflexion relative to plate thickness the comparison shown in Figure 41 was made. This shows that deflexions in the direction of transverse load are significantly greater than those opposite transverse load in the adjacent span. Hence, the buckling breadth calculations were based on discrete panels with initial deformation in the direction of transverse load subjected to an effective rotational edge restraint of K = 1530 in.lb/in.

3.3 Buckling Breadth Factor

This factor is defined as follows: x axis: λ_{2x}/a

y axis: λ_{2y}/b

Where λ_{2x} and λ_{2y} are the effective and a and b are the corresponding actual panel dimensions in the x and y directions.

Figure 28 gives details of the shell panel for which Aalami's program was used to obtain solutions for buckling breadth factors.

Two approaches were considered in determining buckling breadth factors:

(a) Buckling breadth based on deformation, given by the ratio of in-plane displacement with no transverse deflexion to in-plane displacement with actual transverse deflexion.

(b) Buckling breadth based on stress, given by the ratio of the mean stress to the actual maximum stress. This definition is analogous to that used for shear breadth.

Available analytical work on buckling breadth is for uniaxially loaded panels, whereas double-bottom shell panel in-plane loading is usually biaxial. The effect of biaxial as compared to uniaxial loading on buckling breadth for the panel shown in Figure 28 was therefore examined. Uniaxial solutions were derived by assuming that the biaxial in-plane loading due to transverse pressure could be separated so as to act independently along each axis.

Tables 1, 2 and 3 give solutions for buckling breadth factor of a clamped panel ($K_r \to \infty$), for three values of initial deformation ratio. These results were obtained to compare the alternative definitions of the factor for various load combinations.

The limitations of the buckling breadth definition based on deformation (a) became apparent in λ_{2y}/b for the case of biaxial load because, for certain load combinations, the in-plane displacement without

transverse deflexion was of opposite sign to that when transverse deflexion was included. Therefore, although some of the biaxial solutions did not exhibit this behaviour, all values of λ_{2x}/a and λ_{2y}/b given by definition (a) for biaxial load are omitted. The three remaining solutions for λ_{2y}/b (all w_o/h) agree very closely for $N_x' = 0$. The limitations of the uniaxial load solutions become apparent however, when the effect of increasing N_x' on the biaxial load solutions for λ_{2y}/b is observed. Also, biaxial load can be seen to have a significant effect on λ_{2x}/a for $N_x' = 0$.

On the basis of these observations it was decided to use the solutions given by the stress definition (b) for biaxial load for both λ_{2x}/a and λ_{2y}/b. Figure 42 shows solutions for the clamped edge case for $w_o/h = 0$, 0.25, 0.5 and 1.0. It can be seen that for this boundary condition λ_{2x}/a is significantly affected by both loading and initial deformation ratio, whereas λ_{2y}/b, which shows much more marked reductions in effectiveness, is primarily dependent on initial deformation ratio.

Figure 43 shows the corresponding solutions for simply supported edges. Some of the curves are incomplete because the program failed to converge for certain combinations of load and initial deformation. It can be seen that relaxation of rotational edge restraint causes the effectiveness to reduce drastically and to become much more dependent on loading. This condition, which would lead to much greater overall flexibility and non-linear behaviour, has been remarked upon previously in connection with beam-column solutions where the desirability of ensuring effective external rotational restraint was stressed.

The preceding cases represent limiting boundary conditions whereas in practice the effective rotational restraint will have some intermediate value. Solutions for K_r varied between these limits for the particular case of $w_o/h = 0.25$ and $q^* = 5$ are given in Figure 44. This initial deformation ratio corresponds to that assumed to have predominated in the double-bottom model and $q^* = 5$ corresponds to the maximum transverse load condition reached in elastic tests.

The analysis of effective rotational restraint for the typical model panel gave a value of:

$$K = 1530 \text{ in.lb./in.}$$

substituting in the following non-dimensional expression for rotational restraint:

$$K_r = K\, a/D$$

For: $a = 14.5$ in.

$$D = \frac{E\, h^3}{12\,(1-\mu^2)} = 14.18 \times 10^2 \text{ lb. in.}^2/\text{in.}$$

Gives: $$K_r = \frac{1530 \times 14.5}{14.18 \times 10^2} = 15.65 \quad \text{say } 16$$

From Figure 44, this gives values of effective breadth factor of the order of:

$$\lambda_{2y}/b = 0.77$$

$$\lambda_{2x}/a = 0.99$$

As compared to the fully clamped values:

$$\lambda_{2y}/b = 0.92$$

$$\lambda_{2x}/a = 0.99$$

Taking a mean (to allow for conservative approximations noted in preceding discussion): $\lambda_{2y}/b = 0.85$

$\lambda_{2x}/a = 0.99$

NOTE: Due to an oversight, a stiffness of EI, instead of the more correct $EI/(1 - \mu^2)$, has been used in preceding calculations involving beam idealization of long plate behaviour. The error involved is negligible, particularly in view of other approximations, and the conclusions regarding panel buckling load are still valid. For example, using $EI/(1 - \mu^2)$, instead of EI, increases the value taken for non-dimensional effective rotational restraint (K_r) from 16 to 16.7. As can be seen from Figure 44 this increases λ_{2y}/b by about 0.5%.

4. EFFECTIVE WEB AREA

4.1 Single Floor Test

As part of Ho's work an attempt was made to relate theoretical solutions for the behaviour of web panels with perforations and tests on a single floor model. This model was a transverse section of the double-bottom, 14½ inches wide, incorporating a single floor. The flange, stiffener, floor and bracket floor details were similar to the main model as shown in Figure 2.

From a comparison of measured beam deflexions and a theoretical solution including shear deformation for solid webs (no perforations), Ho arrived at a loss of shear stiffness due to perforations of about 50%. This result was then compared with three theoretical solutions for perforated plates in shear. Two of these were for discrete

square panels, with a central circular hole for alternative boundary conditions of uniform edge shear and rigidly restrained edges. The third was based on the classical solution for a circular hole in an infinite plate subjected to pure shear. Agreement was best with the discrete panel solution for uniform edge shear.

Ho also compared measured and theoretical stresses around the circumference of the holes. In this case agreement was best with the infinite plate solution. This solution corresponds to the case of a discrete panel with a high degree (although not fully rigid) of edge restraint. Ho attributed the agreement of measured deflexions and stresses with different theoretical solutions to the effect of the perforations in way of shell stiffeners which were considered to contribute significantly to shear deformation without greatly affecting stress concentration.

4.2 Thick Flange Beam Test

A closer examination of Ho's results showed that two compensating errors had been made in computing shear deformation. These were the omission of loss of flange stiffness due to shear lag, which was partially compensated by an assumed value of Young's modulus which was about 4% low. In order to clarify the issue a test was done, as part of the present work, on a beam with flanges sufficiently narrow relative to beam span to eliminate loss of flange stiffness due to shear lag. The web corresponded to a floor between intercostals. Figure 45 gives details of the beam and results of the test. Measured deflexions are compared to a theoretical solution incorporating web effectiveness factors (F) based on an empirical relationship proposed by Kuhn [35].

This relationship is as follows:

Effective web area = Solid web area x F/100

Where: $F = (1-D/b)(1-(D/h)^3) \times 100\ \%$

For: D = diameter of perforation

b = spacing between perforations

h = depth of web

The variation in F across the span is due to the change in the diameter of holes immediately adjacent to the centre girder. Agreement was sufficiently close to justify using Kuhn's solution as a basis for the final calculation reductions in shear stiffness due to perforations. The results also confirm the experimental value derived by Ho. Back substitution into Ho's results for F = 50%, taking account of the bracket floors and using the correct value for E, gives a loss of flange stiffness due to shear lag in the single floor test of about 9%. This is quite close to the corresponding computed loss of stiffness due to shear lag, derived in previous sections, namely 7.5%.

4.3 Web Effectiveness Factors (F) for Double-Bottom Model

4.3.1 Floors (y axis):

b = 4.375"

h = 5.5"

There were two different hole sizes to be considered,

(a) D = 2.125", gives: F_{ya} = 49%

(b) D = 1.875", gives: F_{yb} = 55%

Now, since the orthotropic plate solution for overall behaviour assumes uniform shear stiffness along each axis, some approximation was necessary to account for the above variation in F_y. Equating central deflexion for variable F_y, and central deflexion assuming uniform F_y, for a triangular distribution of shear varying from zero at the centre to a maximum at the supports, gave a uniform F_y = 70%. The latter shear distribution corresponds approximately to uniformly distributed load on the model. Bracket floors were assumed to have the same stiffness over their length as the main floors. For point load F_y would be of the order of 65%.

4.3.2 Longitudinal webs (x axis): Two cases had to be considered,

(a)	Centre girder:	F_{xa}	=	1 (no perforations)
(b)	Intercostals:	D	=	1.875"
		b	=	4.8125"
		h	=	5.5"
	Gives:	F_{xb}	=	60%

To accommodate the uniform shear stiffness requirement an equivalent value was computed on the basis of the longitudinal webs taking load in proportion to a triangular transverse distribution of longitudinal shear varying from zero at the sides to a maximum at the centre. This gave a uniform F_x = 80%.

5. MODEL PROPERTIES

5.1 Summary of Effectiveness Calculations:

5.1.1 Flange effectiveness expressed as a percentage of the full flange width:

Source of loss	Axis	
	x	y
Shear lag	86%*	93.5%
Local flexure	99%	85%
Product	85%	79.5%

(* This includes the effect of longitudinal stiffeners)

5.1.2 Web effectiveness expressed as a percentage of the solid web area:

x axis: 80%

y axis: 70%

5.2 Moments of Inertia and Web Areas for Double-Bottom Model

Figures 46 and 47 give details of typical longitudinal and transverse sections and corresponding section properties taking the above losses of effectiveness into account. The values shown were rounded off to a more realistic number of significant figures prior to the final orthotropic plate analysis of the model. One additional

loss of effectiveness appears in these calculations, namely, loss web flexural effectiveness due to perforations. In the case of the intercostals this was based on mean reduced moment of inertia, whereas, in the more complex case of the floors a reduction based simply on solid web area was used. In both cases the effect is very small relative to the total moment of inertia of the corresponding section.

One additional property, not shown on the above Figures, was required. This was the "product of inertia" which, for practical purposes is given by:

$$I_{fxy} = \frac{I_{fx} + I_{fy}}{2} = 0.9112 \text{ in.}^4/\text{in.}$$

A more accurate alternative calculation, using the computed flange distances from the neutral axes and applying a mean correction for loss of flange effectiveness, gave $I_{fxy} = 0.9111$ in.^{4}/in.

Summary of calculated values

x axis:
$I_{fx} = 0.9390$ in.^{4}/in
$I_{wx} = 0.0415$ "
$I_{sx} = 0.1428$ "
$A_{wx} = 0.0129$ in.^{2}/in

y axis:
$I_{fy} = 0.8834$ in.^{4}/in
$I_{wy} = 0.0511$ "
$A_{wy} = 0.0170$ in.^{2}/in

"product of inertia":
$I_{xy} = 0.9112$ in.^{4}/in

5.3 Elastic Properties of the Double-Bottom Model Material

The model was fabricated from mild-steel sheet and tests to determine Young's modulus and Poisson's ratio gave the following results:

5.3.1 Young's Modulus ($E \times 10^{-6}$ p.s.i.)

Material	Specimens			
	1	2	3	4
Outer shell (0.080")	29.61*	29.74*	31.00	30.52
Inner shell (0.064")	30.58	30.10	29.88	30.42

(* These specimens correspond to the longitudinal (x) axis. All the others were transverse (y) axis oriented).

A mean value of $E = 30.23 \times 10^6$ p.s.i. was assumed to govern for the purposes of analysis.

5.3.2 Poisson's ratio (μ)

Material	Specimens	
	1	2
Outer shell (0.080")	0.31	0.30
Inner shell (0.064")	0.29	0.29

Mean: $\mu = 0.30$

5.4 Section Properties for use in the Orthotropic Plate Analysis of the Double-Bottom Model

5.4.1 Flexural:

Define:

$i_{fx} = I_{fx}/(1-\mu^2) = 1.0319$ in^4/in

$i_{wx} = I_{wx} = 0.0415$ "

$i_{sx} = I_{sx} = 0.1428$ "

$i_x = i_{fx} + i_{wx} + i_{sx} = 1.2162$ "

$i_{fy} = I_{fy}/(1-\mu^2) = 0.9708$ "

$i_{wy} = I_{wy} = 0.0511$ "

$i_y = i_{fy} + i_{wy} = 1.0219$ "

$i_{fxy} = I_{fxy}/(1-\mu^2) = 1.0013$ "

Hence, equating corresponding coefficients in Shade's solution[2] for a stiffened cellular plate and Libove and Batdorf's solution[10] for an orthotropic plate, gives the following orthotropic plate idealizations for the double-bottom model flexural properties:

$\mu_x = (i_{fxy}/i_y)\,\mu = 0.294$

$\mu_y = (i_{fxy}/i_x)\,\mu = 0.247$

$D_x = E(1-\mu_x \mu_y) i_x = 34.082 \times 10^6$ in.lb

$D_y = E(1-\mu_x \mu_y) i_y = 28.637 \times 10^6$ "

$D_{xy} = \frac{E(1-\mu)}{4} (i_{fx} + i_{fy} + 2i_{fxy}) = 21.189 \times 10^6$ "

5.4.2 Shear:

The orthotropic plate idealizations of the double-bottom model shear properties were taken to be:

$$S_x = A_{wx}E/(2(1 + \mu)) = 1.50 \times 10^5 \text{ lb/in.}$$

$$S_y = A_{wy}E/(2(1 + \mu)) = 1.98 \times 10^5 \text{ lb/in.}$$

CHAPTER 4

BEHAVIOUR OF RECTANGULAR ORTHOTROPIC PLATES INCLUDING TRANSVERSE SHEAR DEFORMATION

1. THEORY

The governing equations and boundary conditions describing the small deflexion behaviour, including shear deformation, of flat rectangular orthotropic sandwich plates subjected to combined transverse and in-plane load as derived by Libove and Batdorf [10] are as follows. For an outline of the derivation of these equations see Appendix C.

1.1 Governing Equations

The following system of linear partial differential equations govern the plate behaviour for a given set of boundary conditions. The individual variables and coefficients are defined in the notation and the sign convention employed is shown in Figure 48.

$$\left.\begin{aligned}
&N_x \frac{\partial^2 w}{\partial x^2} + N_y \frac{\partial^2 w}{\partial y^2} + 2 N_{xy} \frac{\partial^2 w}{\partial x \partial y} + \frac{\partial Q_x}{\partial x} + \frac{\partial Q_y}{\partial y} = -q && \text{(a)}\\
&-\{D_{xy} + \frac{\mu_y D_x}{(1-\mu_x \mu_y)}\} \frac{\partial^3 w}{\partial x \partial y^2} - \frac{\mu_y D_x}{(1-\mu_x \mu_y)} \frac{\partial^3 w}{\partial x^3} + \frac{D_{xy}}{2S_x} \frac{\partial^2 Q_x}{\partial y^2}\\
&\quad + \frac{D_x}{(1-\mu_x \mu_y) S_x} \frac{\partial^2 Q_x}{\partial x^2} - Q_x + \{\frac{D_{xy}}{2S_y} + \frac{\mu_y D_x}{(1-\mu_x \mu_y) S_y}\} \frac{\partial^2 Q_y}{\partial x \partial y} = 0 && \text{(b)}\\
&-\{D_{xy} + \frac{\mu_x D_y}{(1-\mu_x \mu_y)}\} \frac{\partial^3 w}{\partial x^2 \partial y} - \frac{\mu_x D_y}{(1-\mu_x \mu_y)} \frac{\partial^3 w}{\partial y^3} + \{\frac{D_{xy}}{2S_x} + \frac{\mu_x D_y}{(1-\mu_x \mu_y) S_x}\} \frac{\partial^2 Q_x}{\partial x \partial y}\\
&\quad + \frac{D_{xy}}{2S_y} \frac{\partial^2 Q_y}{\partial x^2} + \frac{D_y}{(1-\mu_x \mu_y) S_y} \frac{\partial^2 Q_y}{\partial y^2} - Q_y = 0 && \text{(c)}
\end{aligned}\right\} \quad (1)$$

The terms involving shear stiffness (S_x, S_y) distinguish these equations from ordinary plate theory in which deflexions due to shear are neglected. The usual fourth-order equation for homogeneous isotropic plates [36] can be obtained from the above equations by writing:

$$S_x = S_y = \infty,\ \mu_x = \mu_y = \mu,\ D_x = D_y = D\ (1-\mu^2),\ D_{xy} = D(1-\mu).$$

Substitution into equations (1) and solving for w gives:

$$\frac{\partial^4 w}{\partial x^4} + 2\frac{\partial^4 w}{\partial x^2 \partial y^2} + \frac{\partial^4 w}{\partial y^4} = \frac{1}{D}\{q + N_x \frac{\partial^2 w}{\partial x^2} + N_y \frac{\partial^2 w}{\partial y^2} + 2N_{xy}\frac{\partial^2 w}{\partial x \partial y}\} \qquad (2)$$

This equation does not involve derivatives of q.

1.2 Boundary Conditions

The boundary equations, incorporating the discrete spring system defined in the notation, are shown below. The reactive moments and shear forces are distinguished from the internal moments and shear forces by the bar placed above the corresponding symbol. The co-ordinate system used is shown in Figure 49. Symmetry about the two axes is assumed and it is sufficient, therefore, to consider only the edges $x = a/2$, $y = b/2$.

At $x = a/2$:

$$\left.\begin{aligned}
&\bar{Q}_x = -k_{1x} w = Q_x + N_x \frac{\partial w}{\partial x} + N_{xy}\frac{\partial w}{\partial y} && \text{(a)}\\
&\bar{M}_x = k_{2x}\left(\frac{\partial w}{\partial x} - \frac{Q_x}{S_x}\right) = -\frac{D_x}{(1-\mu_x\mu_y)}\left\{\frac{\partial^2 w}{\partial x^2} - \frac{1}{S_x}\frac{\partial Q_x}{\partial x} + \mu_y\left(\frac{\partial^2 w}{\partial y^2} - \frac{1}{S_y}\frac{\partial Q_y}{\partial y}\right)\right\} && \text{(b)}\\
&\bar{M}_{xy} = -k_{3x}\left(\frac{\partial w}{\partial y} - \frac{Q_y}{S_y}\right) = \frac{D_{xy}}{2}\left\{2\frac{\partial^2 w}{\partial x \partial y} - \frac{1}{S_x}\frac{\partial Q_x}{\partial y} - \frac{1}{S_y}\frac{\partial Q_y}{\partial x}\right\} && \text{(c)}
\end{aligned}\right\} \qquad (3)$$

At $y = b/2$:

$$\left.\begin{aligned}
&\bar{Q}_y = -k_{1y} w = Q_y + N_y \frac{\partial w}{\partial y} + N_{xy}\frac{\partial w}{\partial x} && \text{(a)}\\
&\bar{M}_y = k_{2y}\left(\frac{\partial w}{\partial y} - \frac{Q_y}{S_y}\right) = -\frac{D_y}{(1-\mu_x\mu_y)}\left\{\frac{\partial^2 w}{\partial y^2} - \frac{1}{S_y}\frac{\partial Q_y}{\partial y} + \mu_x\left(\frac{\partial^2 w}{\partial x^2} - \frac{1}{S_x}\frac{\partial Q_x}{\partial x}\right)\right\} && \text{(b)}\\
&\bar{M}_{xy} = -k_{3y}\left(\frac{\partial w}{\partial x} - \frac{Q_x}{S_x}\right) = \frac{D_{xy}}{2}\left\{2\frac{\partial^2 w}{\partial x \partial y} - \frac{1}{S_x}\frac{\partial Q_x}{\partial y} - \frac{1}{S_y}\frac{\partial Q_y}{\partial x}\right\} && \text{(c)}
\end{aligned}\right\} \qquad (4)$$

The ordinary plate theory boundary conditions are obtained by setting S_x and S_y equal to infinity and eliminating one condition on each edge. For simply supported and clamped edges the condition on M_{xy} is omitted while for free edges the reduction to two conditions is achieved by the Kirchoff approximation of combining the shear force and derivatives of M_{xy} along each edge.

1.3 Limitations of the Discrete Spring Idealization

The discrete spring idealization for edge restraints implies that reactive forces are mutually independent. This type of support condition is usually only found in laboratory tests. An example is a plate supported on discrete vertical rods on all edges, for which $k_{2x} = k_{2y} = k_{3x} = k_{3y} = 0$ and k_{1x} and k_{1y} are related to the compressibility (and extensibility, in the corner regions) of the rods. For most practical cases, continuity of support contravenes the assumption of independence of reactive forces. An example is a plate with integral edge beams in which the edge shears and twisting moments are coupled - the beam suffers a change of deflexion due to twisting moment as well as to shear, and a change of slope due to shear as well as to twisting moment. This coupling is not recognised in the relationships for edge beams proposed by Frederick [37].

For integral edge beams the following mixed variable equations can be derived to replace the equations involving the discrete spring idealizations for vertical and tangential rotational restraints.

At $x = a/2$:

$$\left.\begin{aligned} B_y \frac{\partial^4 w}{\partial y^4} - Q_x + \frac{B_y}{A_y} \frac{\partial^2 Q_x}{\partial y^2} + \frac{\partial M_{xy}}{\partial y} &= 0 \qquad \text{(a)} \\ Q_x + \frac{A_y}{S_y} \frac{\partial Q_y}{\partial y} &= 0 \qquad \text{(b)} \end{aligned}\right\} \quad (5)$$

At $y = b/2$:

$$\left.\begin{aligned} B_x \frac{\partial^4 w}{\partial x^4} - Q_y + \frac{B_x}{A_x} \frac{\partial^2 Q_y}{\partial x^2} + \frac{\partial M_{xy}}{\partial x} &= 0 \qquad \text{(a)} \\ Q_y + \frac{A_x}{S_x} \frac{\partial Q_x}{\partial x} &= 0 \qquad \text{(b)} \end{aligned}\right\} \quad (6)$$

B_x, B_y and A_x, A_y are the beam flexural and shear stiffnesses. The other symbols are as previously defined. Solutions for these boundary conditions are not given in this thesis.

It is possible however, to derive equivalent discrete spring stiffnesses for edge beams if assumptions are made regarding the relationship between edge shear and twisting moment. If, for example, on the basis of the standard solution for simply supported plates, it is assumed that the shear forces (Q_x along $x = a/2$, Q_y along $y = b/2$) are related everywhere to M_{xy} by:

$$Q_x = 4 \frac{\partial M_{xy}}{\partial y} \quad , \quad Q_y = 4 \frac{\partial M_{xy}}{\partial x}$$

And, assuming these forces are distributed sinusoidally between corners, then:

$$k_{1x} = 4\pi^4 B_y/(5b^4) \quad , \quad k_{1y} = 4\pi^4 B_x/(5a^4)$$

$$k_{3x} = \pi^2 B_y/(5b^2) \quad , \quad k_{3y} = \pi^2 B_x/(5a^2)$$

The normal rotational restraints (k_{2x}, k_{2y}) can be found from the torsional stiffness of the beams and are independent of k_{1x}, k_{3x} and k_{1y}, k_{3y}. The accuracy of solutions incorporating the above approximations has not yet been examined.

1.4 Non-Dimensionalization of Plate Parameters

The generality of a single solution for the preceding equations was extended to include a set of dimensionally similar problems by making the following substitutions:

$$x = aX,\ y = aY$$

$$w = Wa^4/D_x,\ Q_x = aV_x,\ Q_y = aV_y$$

The coefficients can then be conveniently grouped such that a problem is defined by the following set of non-dimensional parameters:

Flexural stiffness parameter:	$\alpha = D_x/D_y$
Twisting stiffness parameter:	$\beta = D_{xy}/D_x$
Shear stiffness parameters:	$\gamma_x = a^2 S_x/D_x,\ \gamma_y = b^2 S_y/D_y$
In-plane load parameters:	$N'_x = a^2 N_x/D_x,\ N'_y = b^2 N_y/D_y$
Side ratio:	$\epsilon = a/b$
Poisson's ratios:	$\mu_x,\ \mu_y$
Edge restraint parameters:	
(a) vertical deflexion:	$K_{1x} = a^3 k_{1x}/D_x,\ K_{1y} = b^3 k_{1y}/D_y$
(b) normal rotation:	$K_{2x} = a\, k_{2x}/D_x,\ K_{2y} = b\, k_{2y}/D_y$
(c) tangential rotation:	$K_{3x} = a\, k_{3x}/D_x,\ K_{3y} = b\, k_{3y}/D_y$

1.5 Idealized Properties of Doubly Plated Grillages

Based on the work of Schade [38], and in conformity with definitions given in the Notation, the following relationships were derived for the idealized flexural properties of plated grillages:

$$D_x = E(1 - \mu_x \mu_y)\{I_{fx}/ (1-\mu^2) + I_{sx} + I_{wx}\}$$

$$D_y = E(1- \mu_x \mu_y)\{I_{fy}/ (1-\mu^2) + I_{sy} + I_{wy}\}$$

$$D_{xy}= E(I_{fx} + I_{fy} + 2I_{fxy}) /(4(1 + \mu))$$

$$\mu_x = \mu I_{fxy}/(I_{fy} + (1-\mu^2) (I_{sy} + I_{wy}))$$

$$\mu_y = \mu I_{fxy}/(I_{fx} + (1-\mu^2) (I_{sx} + I_{wx}))$$

I_{fx}, I_{sx} and I_{wx} are the unit moments of inertia in the x direction, taken about the neutral plane of the plate, of the flanges, flange stiffeners and webs respectively. I_{fy}, I_{sy} and I_{wy} are the corresponding inertias in the y direction. I_{fxy} is a biaxial (flange) moment of area and is approximately equal to $(I_{fx} + I_{fy})/2$ in many practical cases. The flange inertias must take account of the loss of effectiveness due to shear lag and local out of plane bending.

Shear properties:

$$S_x = A_{wx} E/(2(1 +\mu))$$

$$S_y = A_{wy} E/(2(1 +\mu))$$

A_{wx} and A_{wy} are the unit effective web areas in the x and y directions.

2. SOLUTION OF EQUATIONS

2.1 Check Solutions

The equations given in the preceding section were solved by the finite difference method. This gave a system of simultaneous equations in three unknowns (W, V_x, V_y), the formulation and solution of which was programmed for the University of London Atlas Computer. This is described in more detail in the following sub-section and also in Appendix C. In addition, two series and one alternative finite difference solution were programmed to give check results. These were for the particular case of simply supported edges. Details of the series solutions, one of which was based on Libove and Batdorf's equations and the other on Reissner's equations, are given in Appendix B. The alternative finite difference solution is described in Appendix D. This was based on Libove and Batdorf's equations but differed from the solution described below in that it was for a governing equation in w only, derived from Equation (1) by elimination of Q_x and Q_y. It has the limitation that only the simply supported boundary condition incorporating zero tangential edge slope is amenable to reduction to a single variable and hence, elsewhere in this thesis, this solution is referred to as the "solution for simply supported edges only". The mixed variable solution does not have this limitation and hence is referred to as the "solution for generalized boundary conditions".

2.2 Finite Difference Solution for Generalized Boundary Conditions

2.2.1 Finite Difference Nets: In order to allow for sufficient mesh divisions to ensure that errors due to the finite difference approximation were insignificant and at the same time satisfy computer

storage and round-off error limitations, solutions are restricted to cases of symmetry about the two axes. It is therefore sufficient to consider only a quarter of the plate as shown in Figure 49. Uniform plate properties are implicit in equations (1) and restraint is constant along each edge.

All derivatives are approximated as five point finite difference equations since it was found that three point equations, for first and second order derivatives, gave unsatisfactory results for certain boundary conditions. A single row of fictitious points are defined on each boundary requiring the governing and boundary equations to be formulated in off-centre form at each boundary node. Corresponding to the numbering shown in Figure 49, the total number of unknowns is $3(I + 2)(J + 2)$.

In the corner of the plate (nodes A, B, C and D) there are 12 unknowns but only 9 equations. Two methods of overcoming this deficiency were tried. Firstly node D was eliminated entirely by appropriate use of backward difference equations and secondly three additional equations were formulated by extrapolating the three variables independently along the diagonal. In all cases solutions for the variables at nodes away from the corner region were not significantly affected by the method used. Some differences occurred in the corner region for plates with low tangential rotational edge restraint but these diminished as mesh size was reduced. The diagonal extrapolation method converged more rapidly in such cases and all solutions involving low tangential rotational restraint used this method. In other cases the backward difference method was used since it involves three fewer variables and periodic checks against the alternative method agreed within less than 1%.

2.2.2 Matrix Operations: The finite difference operators give a set of simultaneous equations in three unknowns at each node which can be represented in matrix form as:

$$AX = K$$

Where: A is a square (pxp) coefficient matrix

X is a column (px1) unknown matrix

K is a column (px1) load matrix

These matrices were formulated so that the three unknowns at any given node appeared in successive rows, resulting in a broad single band coefficient matrix. Because of the large number of unknowns in even a relatively coarse mesh the solution incorporated partitioning of tri-diagonal form. It was found in some cases that when the size of sub-matrices approached 100 x 100, the method of solution involved significant round-off error. This was due partly to the larger differences in magnitude of coefficients in such cases and to minimise the effect an iterative procedure was used giving a solution of the form:

$$\Sigma X = X_1 + X_2 + X_3 + \ldots.$$

Where:

$$X_1 \simeq A^{-1} K$$

$$X_2 \simeq A^{-1} \{K - AX_1\} = A^{-1} K_2$$

$$X_3 \simeq A^{-1} \{K_2 - AX_2\} = A^{-1} K_3 \quad \text{etc.}$$

A limit on the number of cycles was set such that the residual solution was less than a specified percentage of the iterative solution.

2.2.3 Accuracy of Solutions: Table 4 shows a sample of checks made against numerical solutions from Reference 36. These correspond to the limiting case of infinite shear rigidity and agreement is quite satisfactory.

Table 5 shows the convergence behaviour of solutions for the simply supported case in Table 4 for four different mesh sizes. On the basis of these results and bearing in mind computer time involved, an 8 x 8 mesh was chosen for all future calculations except for rectangular plates, where it was found to be desirable to keep the side ratio of mesh divisions less than 3:1.

Table 6 shows comparisons with three alternative solutions for simply supported sandwich plates including shear deformation. Solutions based on References 17 and 39,which are series solutions for Libove and Batdorfs' and Reissners' equations respectively, were obtained from computer programs written specifically for the purpose of checking the finite difference solution. Values quoted from Reference 16 were taken directly from that source. The latter solution considers the facings and core as discrete elements whereas the other solutions are for an idealised homogeneous system. Bearing in mind this difference agreement can be considered quite satisfactory.

A series solution for a clamped square isotropic plate under uniform transverse load, including shear deformation, is given in Reference 21. This incorporates the unrealistic third boundary condition $M_{xy} = 0$. Table 7 shows a comparison between the series solution and solutions obtained from the finite difference program for two extreme values of tangential rotational edge restraint. The $M_{xy} = 0$ condition was approximated by low restraint - $K_{3x} = K_{3y} = 1$, and the

more realistic condition of high restraint was given by specifying $K_{3x} = K_{3y} = 10^4$. Surprisingly, the moments agree better for the former condition but the differences are small in both cases.

Although the $K_{3x} = K_{3y} = 0$ condition cannot be prescribed in the program in its present form (this reduces the number of independent equations by one and results in a singularity) a solution for $K_{3x} = K_{3y} = 1$ is shown in comparison with Kromm's solution in Figure 50. This is for a square homogeneous plate having a span/thickness ratio of 20. The effective shear stiffness parameter used in the finite difference solution is multiplied by a factor of 2/3 to allow for warping. The lack of exact agreement in the corner is attributed mainly to the fact that the $M_{xy} = 0$ boundary condition is not fully satisfied. It is possible however that numerical limitations due to finite difference errors and corner definition could have contributed to this.

All the preceding comparisons have been for uniform transverse load. Solutions for non-uniform transverse load was restricted to cases where the load varies continuously because this is implicit in equations(1). Discontinuities cause the results to oscillate about the true solution. The degree of oscillation depends on the severity of the discontinuity and the magnitude of the shear stiffness. Figure 51 shows the type of behaviour and the improvement obtained when the discontinuity is made less severe. As the shear stiffness is reduced the improved solution begins to degenerate and for this reason the solution for non-uniform transverse load given in the Results is for a triangular load distribution. This limitation could be overcome by solving a lower order form of the equations. Alternatively, the equations can be transformed into a single sixth order equation in one variable (w say) with derivatives of the load on the right hand side.

As already mentioned, a program was written to give solutions to the latter equation but it suffers from the limitation that only simply supported edges can be treated. This program was most useful, however, in the analyses of patch load test results, described in the next Chapter.

3. RESULTS

3.1 Presentation

3.1.1 Plate Parameters: The effect on plate behaviour of shear stiffness (γ_x,γ_y), flexural orthotropy (α), shear orthotropy (γ_y/γ_x), twisting stiffness (β) and side ratio (ε) are examined for the case of a clamped plate under uniform transverse load. The effects of α, γ_y/γ_x,β and ε are compared for γ_x = 50, 250 and 500. For shear-isotropic plates $\gamma_y = \alpha\gamma_x/\varepsilon^2$. These values were chosen to cover a broad range of practical structures - for example, in a ship's double-bottom γ_x and γ_y may be of the order of 75 while for a dock gate γ_x and γ_y may be of the order of 350. Values of γ_x or γ_y of less than 50 may occur when webs are omitted along one axis - for example, in the case of bridge decks without diaphragms.

3.1.2 Boundary Parameters: The effect on plate behaviour of normal and tangential rotational restraint are examined for a square isotropic plate under uniform transverse load. Again, comparisons are made for $\gamma_x = \gamma_y$ = 50, 250 and 500. The following table gives the numerical values of non-dimensional restraint applied along edges unless other values are specified. The values corresponding to infinite restraint were established by tests for convergence of results for successively greater values of the respective parameters.

Condition	K_{1x} , K_{1y}	K_{2x} , K_{2y}	K_{3x} , K_{3y}
Simple support	10^7	0	10^5
Clamped	10^7	10^5	10^5
Free	0	0	0

3.2 Effect of Shear Stiffness ($\gamma_x = \gamma_y$) in Clamped Isotropic Plates - Figures 52, 53

Figure 52 shows the variation of central deflexion and maximum edge moment and shear force for a clamped square isotropic plate under uniform load as both shear stiffness parameters are varied simultaneously from 10 to 10^4. It can be seen that stresses as well as deflexions are significantly affected - ignoring shear deflexions for $\gamma_x = \gamma_y = 50$ would result in values of $M_{x2} = M_{y3}$ which are about 15% too large. This relaxation of edge moment occurs because the edge clamping does not apply to the slope due to shear. Figure 53, which gives deflexion, moment and shear force distributions for $\gamma_x = \gamma_y = 50$, 250 and 500, shows the edge slope developing as shear stiffness is reduced. This results in a more even distribution of load as evidenced by the edge shear distribution (Q_y) and the bending moment distribution (M_x) across a centre line. The edge twisting moment falls off as shear stiffness increases. When $\gamma_x = \gamma_y$ is very large M_{xy} approaches the zero value which is implicit in ordinary plate solutions for clamped edges.

3.3 Effect of Flexural Orthotropy (α) - Figures 54, 55, 56

For the purposes of examining the effects of flexural orthotropy a doubly plated grillage with flanges of equal thickness, stiffened along the x axis only, is chosen. The webs are assumed to be plates of equal thickness and spacing in both directions. Based on the stiffened plate relationships given previously, the biaxial parameters for this type of structure are:

$$\mu_x = \mu$$

$$\mu_y = \mu/\alpha$$

$$\beta = (1-\mu)/(\alpha-\mu^2)$$

Figures 54 and 55 show the behaviour of a square, shear-isotropic plate under uniform transverse load as α varies from 1 (isotropic) to 2 for simply supported and clamped edges respectively. Solutions are compared for three cases of shear stiffness - γ_x = 50, 250 and 500. The relationship $\gamma_y = \gamma_x \alpha$ is simply a feature of the non-dimensionalization and does not conflict with the shear-isotropic assumption. For the simply supported case, moments are unaffected by shear stiffness in the isotropic case (α= 1). As α is increased some modification of the load distribution due to shear stiffness is reflected in the divergence of central moments. At α = 2 the maximum moment given by ordinary plate theory (M_{x1}) would be about 5% high for γ_x = 50. There is a similar increase in the error for clamped edges as α is increased but in this case, as noted previously, the error in the isotropic case is about 15%, making a total error of about 20% at α = 2. In the clamped case the error in M_{y3} reduces up to about α = 1.7 at which point the error changes sign.

Figure 56 shows distributions of bending moment and shear force for α= 1, 1.5 and 2 and γ_x = 50 for the clamped edge condition. Both moments and shears illustrate the load transfer to the stiffer axis. M_{y3}, at the edge, is least affected by the transfer. This is because, although the plate tends to flatten across the y axis as α increases, near the edges a local curvature is maintained by the rotational restraint.

3.4 Effect of Shear Orthotropy (γ_y/γ_x) - Figures 57, 58

Figure 57 shows the effect on central deflexion and maximum edge moment of the variation of transverse shear stiffness (γ_y) in a flexurally-isotropic clamped plate under uniform transverse load for three values of longitudinal shear stiffness - γ_x = 50, 250 and 500. These results apply to cases of doubly plated grillages in which the web area and/or spacing is varied in the transverse direction. They do not cover the case of bridge decks without transverse diaphragms in which the plate properties must account for local deformation.

As γ_y/γ_x is increased, more of the load is transferred along the stronger (y) axis and M_{y3} and M_{x2} diverge. In the shear-isotropic case (γ_y/γ_x = 1) for γ_x = 50, ordinary plate theory overestimates the maximum stress by about 15% but at γ_y/γ_x = 4.5 ordinary theory underestimates this stress by about 15%. The reversal takes place at γ_y/γ_x of the order of 1.5. Load transfer to the stronger direction is evidenced in the centre line bending moment and edge shear force distributions, for the case of γ_x = 50, shown in Figure 58.

3.5 Effect of Twisting Stiffness (β) - Figures 59, 60

To show the effect of twisting stiffness, an isotropic multi-cellular plate with similar flange stiffeners along both axes is considered. The twisting stiffness parameter (β) is varied by changing the stiffener size and/or spacing. For this case, the relationship between the expressions for the biaxial plate parameters given previously is:

$$\mu_x = \mu_y = -\frac{k}{2} + \sqrt{\left(\frac{k}{2}\right)^2 - 1}$$

Where: $k = (1-\mu) / \beta\mu$

Figure 59 shows the variation of central deflexion and maximum edge moment, for the case of a clamped plate under uniform transverse load, as β is varied from 0.1 to the value corresponding to no stiffeners - $1/(1+\mu) = 0.769$ for $\mu = 0.3$. Solutions for three values of shear stiffness are compared - $\gamma_x = \gamma_y = 50$, 250 and 500. The decrease in moment and deflexion as β increases is accentuated by a reduction in shear stiffness. For $\gamma_x = \gamma_y = 50$ the error in stresses given by ordinary plate theory increases from about 10% at $\beta = 0.1$ to about 15% at $\beta = 0.769$.

Figure 60 compares moment and shear force distributions in the $\gamma_x = \gamma_y = 50$ case for $\beta = 0.1$, 0.4 and 0.769. These show that the shear distribution to the boundaries is practically unaffected by β while edge bending moment exhibits a reduction associated with the increase in twisting moment as β is increased. The central bending moment remains constant for increasing β because the effect of the corresponding decrease in central curvature is offset by the increase

in $\mu_x = \mu_y$.

3.6 Effect of Side Ratio (ε) - Figures 61, 62

Figure 61 shows the influence of side ratio on central deflexion and central edge moments in an isotropic clamped plate under uniform transverse load for $\gamma_x = \gamma_y = 50$, 250 and 500. The solutions become insensitive to side ratio at about b/a = 3. Above this value the plate behaviour away from the short sides is essentially that of a beam of stiffness D spanning the x direction and the edge reaction is almost uniform. In the region of the short sides behaviour reverts to that of a plate with corresponding variation of reaction distribution. These distributions are shown in Figure 62 for the case of b/a = 3, for $\gamma_x = 50$ and 500. This distinction between reaction distributions is reflected in the effect on central edge moments of shear stiffness. The long edge moment (M_{x2}) becomes insensitive to shear stiffness because the relaxing effect on load distribution is lost as beam action begins to predominate. This is not the case along the short edges where biaxial behaviour remains significant. For b/a > = 2 a mesh division of 6 (x axis) by 12 (y axis) was used.

3.7 Effect of Tangential Rotational Edge Restraint (K_{3x}, K_{3y}) Figures 63, 64

Although variation of tangential rotational edge restraint cannot be treated directly in plate solutions which exclude shear deformation, the Kirchoff equation for edge shears along simply supported boundaries attempts to determine the effect on edge reaction of zero tangential rotational edge restraint ($M_{xy} = 0$) using the reactions

obtained from a solution which gives non-zero values of M_{xy} at the boundaries. Thus the standard solution for simply supported plates gives two alternative distributions of edge reaction, depending on whether or not the Kirchoff condition is employed. The reaction corresponding to the deflected shape of the plate, without discrete corner forces, is correct if $K_{3x} = K_{3y} = \infty$; the modified reaction obtained from the Kirchoff equation, which gives point corner forces, is correct (within the limitations of a solution which neglects shear deformation) if $K_{3x} = K_{3y} = 0$.

As shown by Kromm [18], who included shear deformation in the case of a square isotropic plate having a relatively high shear stiffness (a/h = 20) for the zero edge twisting moment condition, the Kirchoff equation gives accurate values of edge reaction except near the corners. In the latter regions the discrete point forces predicted by Kirchoff are distributed over a short distance either side of the corner. For plates having shear stiffnesses of the order investigated by Kromm ($\gamma_x = \gamma_y \simeq 1230$) only the forces in the immediate vicinity of the edges are sensitive to the degree of tangential rotational edge restraint. This is not so for plates having shear stiffnesses of less than about $\gamma_x = \gamma_y = 500$.

In the following discussion of the influence of tangential rotational edge restraint on plate behaviour, this restraint is assumed to be independent of vertical deflexion restraint (K_{1x} and K_{1y} kept constant at 10^7). As discussed previously this is not representative of many practical cases, such as plates supported on integral edge beams, where these restraints are coupled.

The effect of varying tangential rotational edge restraint on moment and shear force distributions in a simply supported square isotropic plate under uniform transverse load is shown in Figure 63 for $\gamma_x = \gamma_y = 50$. As $K_{3x} = K_{3y}$ is increased greater edge twisting moments can develop and hence the equilibrating shear forces, Q_y at $x = \pm a/2$ and Q_x at $y = \pm b/2$, decrease. When $K_{3x} = K_{3y} = 10^3$, M_{xy} approaches a limiting value and the above shear forces approach zero. At the same time the reversal in reactive shear distributions near the corners becomes less severe. Also, as $K_{3x} = K_{3y}$ and hence M_{xy} increases the internal bending moments reduce as a greater proportion of the load is transmitted to the edges by twisting moment. When $K_{3x} = K_{3y} = 10^3$ the moments and shear forces, but not deflexions, throughout the plate approach those given by ordinary plate theory.

Figure 64 shows the effect of varying shear stiffness in the presence of low tangential rotational edge restraint. For $K_{3x} = K_{3y} = 1$ bending moments and shear forces are compared for $\gamma_x = \gamma_y = 50$, 250 and 500. As shear stiffness increases the edge shears (Q_x and Q_y) becomes more pronounced. The increase in corner forces is reflected in the decrease in bending moments in the interior of the plate. For large shear stiffness the interior forces become the same as given by ordinary plate theory showing that the influence of K_{3x} and K_{3y} is restricted to the edge region in cases where shear deformation is insignificant.

3.8 Effect of Normal Rotational Edge Restraint (K_{2x}, K_{2y})

Figures 65, 66, 67, 68, 69, 70

An example of a case where the normal rotational restraint on an individual plate panel, due to the surrounding system, can be idealised as a spring is a panel within an array of panels continuous over vertical supports. In a 3 x 3 array of identical square isotropic panels in which only the centre panel is loaded (transversely), the outer panels may be replaced by normal rotational springs with non-dimensional restraint stiffnesses (K_{2x}, K_{2y}) of the order of 3 or 4 depending on whether the outer edges of the array are simply supported or clamped.

Another typical case is that of a plate supported on edge beams. If the edge moment is assumed to act at the shear centre of the edge beam and to have a sinusoidal distribution along the edge between corners, then the normal rotational edge restraints for a square isotropic plate due to identical edge beams of torsional rigidity C are given by:

$$K_{2x} = K_{2y} = a(\pi^2 C/a^2)/D_x$$

Three combinations of rotational edge restraint along adjacent boundaries, symmetrical about the two centre lines, are examined for the case of a square isotropic plate under uniform transverse load. The behaviour is compared for three values of shear stiffness; $\gamma_x = \gamma_y = 50, 250, 500$.

Figure 65 gives solutions for central deflexion and central edge moments for a plate with all edges equally restrained by springs

the stiffnesses of which are varied from zero, which corresponds to simple support, to 10^5, which approximates to the fully clamped condition. The influence of shear stiffness on central edge moment becomes evident at about $K_{2x} = K_{2y} = 5$ which is of the order of the effective restraint due to unloaded panels in an array. Figure 66 shows distributions of deflexion, shear force and bending and twisting moment for three values of $K_{2x} = K_{2y}$.

Figure 67 gives solutions for the case of two edges ($x = \pm a/2$) simply supported ($K_{2x} = 0$) while along the other edges ($y = \pm b/2$) K_{2y} is varied from 0 to 10^5. For $\gamma_x = \gamma_y = 50$ the relaxing effect of shear deformation in the clamped edge case ($K_{2y} = 10^5$) results in a maximum edge moment which is about 20% less than would be given if shear deformation were ignored. The more pronounced significance of shear deformation in this case, as compared to the case of both edges equally restrained, is due to the restrained edge reacting a greater proportion of the applied load. Figure 68 illustrates the load transfer to the restrained boundaries as restraint is increased.

Figure 69 gives solutions for two edges ($y = \pm b/2$) clamped ($K_{2y} = 10^5$) while along the other edges ($x = \pm a/2$) K_{2x} is increased from 0 to 10^5. This causes the influence of shear stiffness on central edge moment at the fully clamped edge (M_{y3}) to decrease as the load distribution between adjacent sides becomes more even. For lower values of shear stiffness this redistribution is accentuated and M_{x2} is greater up to about $K_{2x} = 20$ at which point the relaxing effect of the improved load distribution along the $x = \pm a/2$ boundaries becomes apparent. Figure 70 illustrates the effect of equalization of load distribution as K_{2x} approaches the fully clamped condition.

3.9 Effect of In-Plane Load (N'_x) - Figure 71

Figure 71 shows the effect of uniaxial in-plane compressive load on central deflexion and central edge moment in a square clamped isotropic plate subjected to a constant uniform transverse load. Solutions are compared for three values of shear stiffness - $\gamma_x = \gamma_y = 50$, 250 and 500. The results for N'_x greater than about 60% of the respective buckling loads, are shown as broken lines because there were signs that the numerical solution degenerated above this point.

Since N'_x operates on the total (flexural and shear) curvature, stresses increase more rapidly with N'_x for lower values of shear stiffness. The latter effect and the reduction in edge stress due to shear deformation along the clamped edge nullify one another at about $N'_x = -10$. Above this value solutions which ignore shear deformation underestimate the maximum stress. The critical in-plane loads for $\gamma_x = \gamma_y = 50$, 250 and 500 are about $N'_x = 40$, 80 and 90 respectively [40]. N'_x critical = 109 in the case of negligible shear deformation.

3.10 Effect of Non-Uniform Transverse Load - Figure 72

Figure 72 gives centre line bending moment and edge shear distributions in a square clamped isotropic plate under a non-uniform transverse load distribution for two values of shear stiffness - $\gamma_x = \gamma_y = 50$, 500. The load distribution is of triangular form in the y direction and constant in the x direction. The apex of the y distribution has been smoothed because of the sensitivity of the numerical solution to loading discontinuities. Ignoring shear

deformation would result in an overestimate of maximum edge moment by about 20% for $\gamma_x = \gamma_y = 50$. The corresponding error for uniform load was 15%.

4. CONCLUSIONS

4.1 The results show that the effects of transverse shear deformation may be of such a magnitude that an analysis which disregards this deformation gives values of deflexions and stresses which are appreciably in error. This error depends on plate properties, boundary conditions and type of loading. Particular combinations of these factors have been studied and the results can be seen in the graphs. Some features of the analysis are indicated below.

4.2 Isotropic homogeneous plates: In uniformly loaded rectangular plates with simply supported edges incorporating zero tangential edge slope ($M_{xy} \neq 0$) deflexions but not stresses are affected by shear stiffness. Stresses are influenced however for any other boundary condition or loading. In a square uniformly loaded plate with clamped edges for example, a shear stiffness parameter of $\gamma_x = \gamma_y = 50$ reduces the maximum stress by about 15%.

4.3 Flexurally orthotropic plates: In a square uniformly loaded plate with a shear stiffness parameter of $\gamma_x = \gamma_y = 50$ and flexural stiffness ratio of 2, the maximum stress is reduced by about 5% in the case of simply supported edges ($M_{xy} \neq 0$), and about 20% for clamped edges.

4.4 Shear orthotropic plates: In square uniformly loaded clamped plates increasing shear orthotropy increases the maximum stress. Thus, for $\gamma_x = 50$ the effect of shear deformation on maximum stress varies from a reduction of about 15% at $\gamma_y = 50$ to an increase of about 15% at $\gamma_y = 225$.

4.5 Plates with reduced twisting stiffness: The effect of shear deformation on stresses reduces as the twisting stiffness parameter (β) decreases. For a square uniformly loaded clamped plate the 15% reduction in maximum stress associated with $\gamma_x = \gamma_y = 50$ is for a homogeneous plate for which $\beta = 0.769$ and this decreases to about 10% at $\beta = 0.1$.

4.6 Rectangular plates: The effect of shear stiffness on the maximum stress in uniformly loaded clamped plates decreases as side ratio (b/a) increases, becoming negligible at about b/a = 3.

4.7 Elastically restrained plates

(a) Tangential rotational edge restraint: The development of corner forces in simply supported plates is associated with a reduction in tangential rotational edge restraint (K_{3x}, K_{3y}). For $K_{3x} = K_{3y}$ approaching zero in a square uniformly loaded plate, the intensity of the force at the corner is reduced by about 85% due to shear deformation for $\gamma_x = \gamma_y = 50$. This decrease is reflected in an increase in central stresses of about 10%.

(b) Normal rotational restraint: It has been noted that in a square uniformly loaded clamped plate the edge stresses are reduced by 15% for $\gamma_x = \gamma_y = 50$. This effect is magnified

when adjacent boundaries are unequally restrained. For two opposite edges simply supported and the other two clamped, the effect of $\gamma_x = \gamma_y = 50$ on the maximum stress, at the clamped edge, is a reduction of about 20%.

4.8 In-plane load: The increase in stresses due to in-plane load is accentuated by shear deformation. For a square clamped plate with combined transverse and uniaxial in-plane load the reduction in maximum stress due to shear deformation is reversed at about 10% of the critical load. At 20% of the critical load the maximum stress is increased by more than 30% for $\gamma_x = \gamma_y = 50$.

4.9 Non-uniform transverse load: For a clamped square plate subjected to a triangular load distribution across one axis, central deflexion increases by 135% for $\gamma_x = 50$ as compared to 110% for a uniform distribution. The corresponding reduction in maximum stress is about 20% as compared to 15% in the uniformly loaded case.

4.10 Certain combinations of plate properties, boundary conditions and loading may lead to larger discrepancies between the simple and more exact theories than those noted above. For a particular ship's bottom structure for example, shear deformation increases the central deflexion by 70% and reduces the maximum stress by 30%.

CHAPTER 5

ANALYSIS OF DOUBLE-BOTTOM MODEL TESTS

1. INTRODUCTION

The model test results are used to verify the applicability of the various theoretical solutions for overall and local behaviour of the double-bottom structure. Overall behaviour (reactions, deflexions and shell strains at shell-web intersections) is examined with reference to the orthotropic plate solution including shear deformation described in Chapter 4. Local behaviour of shell and web panels is analysed using Aalami's [26] solution for large deflexion of panels under combined transverse and in-plane load, and Ho's [29] work on the behaviour of perforated webs.

Details of the model and the various load cases are given in Chapter 2. The overall stiffness properties of the model, taking account of local behaviour, are computed in Chapter 3. Before analysis could proceed it was necessary to establish the effective boundary conditions appropriate to the method of support of the model described in Chapter 2. The coordinate axis orientation used in the analysis is as follows - x axis longitudinal, bisecting the bulkheads, y axis transverse, bisecting the sides of the ship.

2. OVERALL BOUNDARY CONDITIONS

The overall analysis, because it includes shear deformation, requires the specification of three boundary conditions on each edge and not two

as in ordinary plate theory. These were computed theoretically as follows, but as the discussion shows, all the required conditions were not immediately apparent.

2.1 Vertical Deflexion Restraint

Assuming that vertical edge flexibility was confined to the lengthening or shortening of the rod supports the corresponding restraint is given by:

$$k_1 = EA/dh$$

Where:

A = rod area

d = rod length, including vertical adjustment correction

h = rod spacing

This gives:

$$k_{1x} = 0.21 \times 10^6 \text{ lb/in}^2$$

$$k_{1y} = 0.26 \times 10^6 \text{ lb/in}^2$$

It was anticipated, and the experimental results confirmed, that the above values overestimated the vertical edge restraint. This was most evident at the bulkhead ends due to deflexion of the box section frame against which the rods reacted. The final values used, and the effect on overall behaviour of vertical edge flexibility, are discussed with reference to the analysis of the combined load tests.

2.2 Normal Rotational Restraint

At longitudinal (side of ship) edges it is apparent that there was no restraint against normal rotation ($k_{2y} = 0$). At transverse (bulkhead) edges the condition is not so clearly defined. It appeared possible that the torsional rigidity of the end extensions could have constituted some degree of normal rotational edge restraint. As discussed in Chapter 4, the magnitude of this restraint, if it was developed in conjunction with reactive end torques, is given by:

$$k_{2x} = \pi^2 C/b^2 = 1.64 \times 10^6 \text{ lb}$$

Where:

C = torsional rigidity of end extensions (1250×10^6 lb. in^2)

b = width of model

The experimental results do not confirm the effectiveness of this restraint and the value finally used was $k_{2x} = 0$. The basis of this conclusion is discussed with reference to the analysis of the combined load tests.

2.3 Tangential Rotational Restraint

The situation regarding theoretical evaluation of this restraint is similar to that for normal rotational edge restraint. At longitudinal edges it was negligible ($K_{3y} = 1$) while at transverse edges the flexural stiffness of the end extension may have constituted some degree of tangential rotational restraint. Since, as discussed in Chapter 4, any approximation is complicated in the case of edge beams by the limitations of the discrete spring idealization, it was decided to vary

k_{3x} and by comparison with experimental results for combined load behaviour establish the most appropriate value.

3. ANALYSIS FOR COMBINED TRANSVERSE AND IN-PLANE LOAD

Detailed comparisons between theory and experiment are made for a transverse pressure, only, of 1 p.s.i. Particular results are then studied for increments of transverse pressure up to 5 p.s.i. in the presence of constant in-plane thrust. This is done for four values of thrust, namely P_x = 0, 3, 6 and 9 tons/ram which correspond to average in-plane stresses of 0, -2.31, -4.62 and -6.93 tons/in^2. The average stress was computed as the total in-plane load divided by the total transverse cross-sectional area of the model. In all tests, transverse pressure was incremented from a datum of 0.5 p.s.i. This was done to eliminate slackness from the rig and thereby ensure constant datum strains. The results are given, however, for load incremented from a datum of zero p.s.i., by extrapolating backwards. In all cases the initial behaviour was practically linear and hence no significant error was incurred.

3.1 Overall Behaviour

Figure 73 gives details of the 1 p.s.i. transverse load distribution and the boundary conditions used in orthotropic plate solutions for overall behaviour. An 8 x 8 mesh was used for all solutions. The double step approximation to the discontinuity in the pressure in the transverse (y) direction was necessary because of a limitation in the theoretical solution. This is discussed in Chapter 4. The total load was computed on the assumption that full pressure operated over the area

covered by the water bag. In practice it is likely that the pressure tapered off at the edges and hence the total load was probably slightly less than the assumed value. This is confirmed in discussion on the equilibrium between applied load and measured reaction which follows. Overall reaction and deflexions are compared to solutions for boundary conditions 1, 1a, 2, 3, 3a and 4. By this means it was possible to clarify the uncertainties raised in the preceding section and establish one set of conditions on which all later analysis of behaviour under combined transverse and in-plane load could be based.

3.1.1 Reactions:

Figure 74 (i) shows theoretical distributions of edge shear for boundary conditions 1, 2, 3 and 4. Condition 3a is not included because it developed from an analysis of overall deflexions which is discussed in the next section. There was no significant difference in the distributions for conditions 1 and 1a, which correspond to conventional simple support. The same distributions would be given by a solution which does not include shear deformation and hence cannot develop tension in the corner regions. Condition 2 differs from 1 in that the tangential rotational restraint at the sides of the model is very low. This causes tension forces to develop in the corner regions. In condition 3 the tangential rotational restraint is low on all edges and the corner tension becomes more pronounced. The preceding conditions have zero normal rotational restraint on all edges. In condition 4 a degree of normal rotational restraint is introduced at the bulkhead ends on the assumption that the torsional rigidity of the end box extension is fully effective.

As a first attempt to determine the most appropriate combination of boundary conditions, theoretical and experimental edge reactions were compared on the basis of proportion of load taken by adjacent edges. This is shown in Table 8. The following comments take no account of errors in the theory due to assumptions and approximations made in computing flexural and shear stiffnesses of the orthotropic plate.

Boundary Condition	Edge Reaction				Total Reaction ΣQ lb.	$\frac{\Sigma Q}{\Sigma P}$
	ΣQ_x lb.	$\Sigma Q_x/\Sigma Q$	ΣQ_y lb.	$\Sigma Q_y/\Sigma Q$		
1 (1a)	951	0.416	1336	0.584	2287	1.001
2	805	0.352	1483	0.648	2288	1.002
3 (3a)	930	0.406	1358	0.594	2288	1.002
4	1187	0.519	1099	0.481	2286	1.001
Test	684	0.316	1481	0.684	2165	0.948

Table 8

The total test reaction (ΣQ) is about 5% less than the applied load (ΣP) assuming that full pressure was achieved over the whole bag area. This lack of equilibrium is attributed mainly to the fact that it is likely that the applied pressure tapered off at the edges of the bag. It can be seen in Figure 74 (ii) however, that negligible reaction was recorded by the rod located at the centre of the side of the model. This, and the corresponding rod on the opposite side, jammed in their guide blocks due to in-plane rigid body displacement of the model and

it is possible that some load was transferred to the rig by friction and not recorded, because the gauges were positioned above the guide blocks. Half of the discrepancy could have been due to this, but the adjacent peak in the distribution of rod loading indicates that in fact the jammed rod took no vertical load. Finally, it is possible that the load was not evenly distributed to all quadrants but checks on symmetry of deflexions, strains and reactions agreed remarkably well and tend to discount this. All the following theoretical solutions assume full ΣP so that stresses may be slightly overestimated although any effects will be small since the tapering off in load is adjacent to the edges.

From Table 8 it can be seen that the best agreement, between the alternative theoretical solutions and the test results on the proportion of load taken by adjacent edges, is for condition 2. The next best agreement is for condition 3 while condition 4 shows a disproportionate amount of load taken by the bulkhead ends. This indicates that the normal rotational restraint due to torsional rigidity of the end extensions was not developed.

Figure 74 (ii) shows a comparison between the measured reactions and the corresponding rod forces given by the edge shear distributions for conditions 2 and 3. It can be seen that the measured corner tension is bounded by these two solutions. From these observations it appears that some degree of tangential rotational restraint was achieved at the bulkhead end although not perhaps as high as specified in condition 3.

3.1.2 Deflexions

In Figure 75 (i) the measured overall deflexions are compared with theoretical solutions for boundary conditions 1, 1a, 2, 3 and 4.

The experimental values show much larger edge deflexions than predicted by theory. This is due partly to edge flexibility not accounted for in the rod calculations and partly to rigid body uplift of the model and rig. The latter effect is confirmed by the fact that whereas tension in the corners implies a downward displacement relative to the rig, an upward displacement relative to the floor was recorded by a dial gauge adjacent to the corner. The additional flexibility is attributed mainly to the bending of the box section frame against which the rods reacted. This is confirmed by the fact that the displacement was greatest at the bulkhead ends where the box frame spans over the full width of the model.

Theoretical edge deflexions of the right order of magnitude can be obtained by rational adjustment of vertical deflexion edge restraints. The question of the most appropriate condition as regards k_{3x} remains however. It is of note that whereas the difference in deflexions for conditions 1 and 2 is about 8%, the difference for conditions 2 and 3 is only 1½%. This is reflected in the stresses. Hence, since the difference between solutions 2 and 3 is small and since condition 3 behaves better numerically because the corner conditions are more compatible (all rotational restraints low) it was decided to incorporate an empirical adjustment in vertical deflexion edge restraint in condition 3.

This was done by subtracting a vertical rigid body displacement at the corner and the centres of the two edges, so that the resultant deflexions were of an order compatible with the corresponding rod stresses. The originally computed vertical edge restraints were then adjusted to correspond to these deflexions giving a condition, denoted 3a, solutions for which are shown in Figure 75 (ii).

The proportion of reaction taken by adjacent sides remains the same as for condition 3 although there is a slight redistribution resulting in very good agreement with the measured corner tension. Incorporation of the reduced vertical restraints in condition 2 would have increased the divergence from measured corner tension. The difference in central moments between conditions 3 and 3a is less than 1%. The measured central deflexion is within less than 5% of that given by condition 3a. This is remarkably good agreement considering the limitations of the orthotropic plate idealization. The lack of more exact agreement as regards proportion of reaction does however indicate that there may be some error in the relative effective overall stiffnesses. This is discussed further with regard to shell strains. Shear deformation accounts for 32% of the calculated total deflexion.

3.1.3 Shell Strains at Shell-Web Intersections

Figures 76 and 77 show a comparison between measured and theoretical shell strains at shell-web intersections for inner and outer shells respectively. The following discussion is with reference to the solution denoted 3a, solution 1a was included to show the effect on strains of allowing for shear deformation. The assumption made in the local panel analysis that vertical edge deflexion was zero, implied that tangential edge strains due to bending were zero and hence theoretically, the discrepancy between measured and theoretical values is due to variation in membrane stress across the panels.

(a) Inner Shell: Near the centre of the model the overall solution underestimates ε_{xi} by about 28% and overestimates ε_{yi} by about 37%. Corrections based on the losses of shell effectiveness used in computing overall stiffnesses reduces the error in ε_{xi} to about 5% and increases

the error in ε_{yi} slightly, to about 38%. The measured distributions of strain follow the form of theoretical solutions reasonably well except for ε_{xi} in the x direction. This may be due to a variation in effective plate properties or an error in the overall boundary conditions.

(b) Outer Shell: After correction, the errors in outer shell strains near the centre of the model are an underestimate of about 38% for ε_{xo} and an overestimate of about 13% for ε_{yo}.

The degree of agreement noted above is considered good in view of the complexity of the system. The differences are due mainly to local deformation and errors in the computation of loss of effectiveness. The errors due to local deformation are most apparent in ε_{xo}. The corresponding results for patch load cases, where the local panels were not subjected to transverse load, do not show the same large and distributed error. The errors in computation of loss of effectiveness appear to be most severe in the y direction as evidenced by the discrepancies in ε_{yi}. This indicates that the computed location of the neutral axis was too close to the outer shell and is attributed to failure to distinguish between losses in the inner and outer shells. Calculations were based on an analysis for outer shell panels and it is apparent that the loss of effectiveness was less for the inner shell. Allowance for this would have given an increased flexural stiffness in the y direction which is consistent with the discrepancies observed in overall deflexion and proportion of reaction taken by adjacent edges.

3.1.4 Combined In-Plane Thrust and Increasing Transverse Pressure

(a) Shell Stress and Strain at Shell-Web Intersections: Figures 78 and 79 show longitudinal shell stresses at points across the model, midway between floors D and C and between floors A and A' respectively, for increasing in-plane load. The experimental stresses were computed on the assumption of uniaxial stress (no overall bending). The in-plane loads were applied after a settling load of 0.5 p.s.i. transverse pressure had been applied. The measured values are compared with a theoretical average stress given by dividing the total in-plane load by the total transverse cross sectional area of the model. The model had a built-in overall outward deformation which was partially but no entirely compensated by the 0.5 p.s.i. transverse pressure. This is evident in the divergence of measured inner and outer shell stresses which is most apparent toward the centre of the model. The mean stress given by gauges 170, 171, 172 and 173, which was least affected by the assumption of uniaxial stress, agrees very closely with the calculated average stress. This verifies that in-plane load was applied at, or very near, the longitudinal neutral axis of the model.

Some inconsistencies are evident for in-plane loads of P_x = 7, 8 and 9 tons/ram. The patch load tests were conducted in between the P_x = 6 and 7 tons/ram tests. This was necessary because many of the outer shell surface gauges had begun to malfunction due to condensed water which had accumulated between the pressure bag and the model. It was decided that since replacement of these gauges involved raising the model, the patch load tests should be conducted while the model was in the raised position. When these were completed the model was restored to the combined load position. The inconsistencies are evidence that the original conditions were not exactly reproduced.

Figure 80 shows the behaviour of typical longitudinal (i) and transverse (ii) strains for increasing transverse pressure. Four cases of constant in-plane load are shown - P_x = 0, 3, 6 and 9 tons/ram. There is a small degree of non-linearity with increasing transverse load, most noticeable for outer shell strains in the y direction due to a greater sensitivity to local non-linear behaviour. The initial overall outward deformation of the model is evidenced by the non-coincidence of datum strains for $P_x > 0$.

(b) Deflexions: Figure 81 (i) shows measured central deflexion for the four load cases considered above. The slight degree of non-linearity with increasing transverse pressure, most noticeable for P_x = 3 and 6 tons/ram, is attributed to in-plane rigid body displacement of the model. This caused the dial gauge spindle to move transversely until further movement of the model was prevented by stops. The effect was most noticeable for dial gauges with long spindles which included gauge number 1. Interaction between in-plane and transverse load effects is evident in the slope of the curves. The non-coincidence of datum load deflexions is due to initial overall outward deformation of the model. The good agreement of corresponding deflexions in opposite quadrants, shown in Figure 81 (ii), is typical of the high degree of symmetry attained in all tests.

(c) Reactions: Figure 82 shows typical compression rod (i) and tension link (ii) strain measurements for increasing transverse load (P_x = 0). The difference in strains in each case is a measure of the bending of the rods. Mean strains, from which reactive forces were computed, can be seen to be reasonably linear. In the presence

of in-plane load reactive forces increased. For a transverse pressure of 1 p.s.i. and an in-plane load of P_x = 9 tons/ram the measured increase/quadrant was 55 lbs compared to a theoretical value, for boundary condition 3a, of 59 lbs.

3.2 Local Behaviour

3.2.1 Webs

In the analysis of the single floor model Ho[29] obtained good agreement between theoretical and experimental tangential stresses around lightening holes by superimposing the effects of shear and bending. The same approach is used here for distributions of shear force and bending moment given by the orthotropic plate solution including shear deformation for boundary condition 3a.

Ho showed that a reasonable approximation to the shear behaviour is obtained from a solution for a hole in an infinite plate subjected to uniform shear. Figure 83 (i) shows the distribution of tangential stress computed in this way for an applied shear stress of 1 ton/in^2. The theoretical applied shear stress was taken as the shear force per web at the particular section divided by the solid web area. The contribution due to bending is based on Howland and Stevenson's theory[41] for an infinitely long strip with a single hole on its centre line. Figure 83 (ii) shows the distribution of tangential stress computed in this way for an applied bending stress of 1 ton/in^2. The applied bending stress was taken as the mean shell-web interface stress at the particular section.

Experimental heart of plate tangential stresses around holes were derived by subtracting the bending component from strains recorded on opposite surfaces. Any bending was due to initial out of plane

deformation which the results showed to be considerable in some cases. Where stresses were deived at symmetric locations the mean value is plotted.

Figure 84 shows the results for the holes in floors A (A'), B, C and D at bay 7-8 (7'-8'). In all cases the experimental values conform remarkably well to the theoretical distributions around the circumference. The peak values are low, due mainly to the fact that strains were recorded 0.10 inches from the edge of the hole at which distance Ho's solution predicts a fall off in stress concentration of about 20%. At 0^{o} and 180^{o} the theoretical tangential stress is due to bending only and agreement with measured stresses is not good. This is not surprising considering that no account was taken of cut outs in way of stiffeners or of lack of symmetry.

Figure 85 (i) compares measured stresses around holes in floor A and side bracket A_1 at bay 8-9 with two theoretical solutions which differ in intensity of theoretical applied shear stress. In one, floor A is assumed to take all the shear force between the centre lines separating floor A and the adjacent floors and in the other this force is distributed equally between floor A and three side brackets. The experimental values for floor A indicate that the shear force was shared with the side brackets, although not in the assumed ratio. This is not confirmed in the results for side bracket A_1 but this may have been due to local effects.

Figure 85 (ii) compares measured and theoretical stresses around the hole in centre bracket A_1, bay 0-1. This case differs significantly from all others in that the primary source of theoretical applied stress is bending. The experimental results do not confirm the

existence of tangential stresses due to bending and this is probably a realistic result, rather than the influence of local effects as was suggested for side bracket A_1. These conclusions are confirmed by the results for patch load tests.

Figure 85 (iii) compares measured stresses around the intercostal holes immediately adjacent to bulkheads with a theoretical solution assuming that the intercostals resisted the shear force distributed from midway between the intercostals and centre girder to midway between the intercostals and the sides of the model. The effect of measuring strains a small distance from the edge of the hole is apparent in the peak stress. The discrepancy noted at 180^{o} in the floor hole stresses at bay 7-8 is not so apparent because the bending stress is much lower.

Centre girder shear stress was measured near the bulkhead ends. The recorded value was 0.75 tons/in^2 for q = 1 p.s.i. which is within 9% of the theoretical value of 0.83 tons/in^2. In the theoretical calculation it was assumed that the shear stress, due to shear force distributed between the centre lines separating the centre girder and the intercostals, varied uniformly through the depth of the web.

The behaviour under combined loading of typical web strains is shown in Figure 86. The effect of initial out of plane deformation is very apparent in (i) but despite the slight non-linearity in recorded strains the heart of plate strain is reasonably linear and, as would be expected, relatively insensitive to in-plane load.

3.2.2 Shell Panels

(a) Overall Transverse Load Only - q = 1 p.s.i.

Three outer shell panels were examined in detail. Figure 87

shows these panels and the initial deformation and in-plane loads which were used in theoretical solutions based on Aalami's[26] computer program for the large deflexion behaviour of rectangular orthotropic plates.

The initial deformation was based on contours measured prior to any testing. These are plotted in Figure 27 where it can be seen that there was some lack of symmetry within each panel. No account can be taken of this in the program and hence sinusoidal approximations were used with central deflexions equal to the maximum measured deflexions relative to the respective panel boundaries.

The program requires that applied in-plane load be specified as the average value in the x and y directions. These are the values shown and they were derived from the overall solution by applying reduction factors based on the analysis for loss of shell effectiveness used in the computation of overall flexural stiffnesses. Some averaging was also necessary to account for variation of moment in the y direction. It will be noted that the applied average in-plane edge stress in the y direction was computed to be less for panel 1 than panel 2 despite the fact that panel 1 was closer to the centre of the model. This arose because it was assumed that the centre bracket floors had negligible influence on the membrane stress distribution between floors. Hence, since the membrane stress varies between maximum values at the floors, the mean stress between intermediate centre brackets was considerably less than the mean stress between floors.

Boundary conditions were assumed to be the same as used in the transverse bending loss of effectiveness analysis except for the case

of rotational edge restraint in panel 1. This restraint was reduced to allow for the greater flexibility of the web panels, which bound panel 1 on three sides, as compared to the angle stiffener which bounds the fourth side. Assuming that the webs were solid and fixed at the inner shell side, the rotational restraint is of the order of 480 in.lb/in. as compared to about 1530 in.lb/in. for angle stiffeners. The lower value was used on all sides for panel 1 and the higher value on all sides for panels 2 and 3. It should be noted that the computation of the restraint due to angle stiffeners involved the assumption of antisymmetric initial deformation in adjacent panels in the y direction, a condition not ideally satisfied across panels 1, 2 and 3.

Measured values of deflexion, bending stress and membrane stress are compared with corresponding theoretical distributions in Figures 88, 89 and 90 respectively. The results cannot be viewed independently however because it is quite feasible, with the number of variables involved, to contrive a theoretical solution which accurately predicts deflexions say, but bears little relation to the true stress system. Despite apparent discrepancies, the theoretical solution, considering its limitations, predicted the experimental results remarkably well and the results for all three variables are reasonably consistent. A detailed discussion of the discrepancies would be difficult to justify but it is possible to comment on several possible sources of error in the theoretical solutions.

The most significant factor is the lack of antisymmetry in the initial deformation of adjacent panels. This is most apparent in the behaviour of panel 2 where the effects of the much larger deformations in panel 3 have swamped the flexural behaviour of panel 2 to such an

extent that the theoretical solutions for deflexions and bending stresses are of the wrong sign. This factor also probably contributed to the lower measured values of σ_{ym} in panels 2 and 1. In the latter case the panel on the opposite side of the centre girder had suffered significantly greater initial deformation.

A second major source of error was the restriction in the theoretical solution as regards symmetry of initial deformation within a panel. This applies mainly to panel 3 in which the effect of concentration of initial deformation toward the floor A' end, which can be seen in the contours, was reflected in the lower measured membrane stresses in this region.

(b) Combined Load Behaviour

The analysis of shell panel test results is now extended to include overall transverse pressures (q*) up to 5 p.s.i. for four cases of in-plane load - P_x = 0, 3, 6 and 9 tons/ram. As deflexions increase the non-linearity associated with large deflexion behaviour becomes more apparent and the limitations of the theoretical solution are accentuated. Nevertheless, there is sufficient agreement between theory and experiment to justify extending the analysis.

Figure 91 gives deflexions for panels 1, 2 and 3. Figures 92 and 93 give bending and membrane stresses at the centres of panels 1 and 2 respectively. Figures 94, 95 and 96 give these stresses for panel 3 at points a, b and c (see Figure 89) respectively. Results are plotted from datum loads of P_x = 0, 3, 6 and 9 tons/ram and q = 0 p.s.i. The lack of agreement between theory and experiment at these datum loads is due partly to effects of the initial overall sag of the model, noted

previously in connection with analysis of overall behaviour. Also, as noted previously, the experimental results for P_x = 9 tons/ram exhibit differences from the other three cases which are attributed to deformation caused during the patch load tests.

Panel 1: The inconsistency between results for P_x = 9 tons/ram and the other cases is particularly evident in the datum load results for Panel 1, which show a marked increase in deflexions and stresses. This is attributed to a modification, mainly local but also possibly overall, sustained during the patch load tests. For increasing transverse load (q*) the most marked divergence between theory and experiment is for σ_{yb} although deflexion, σ_{xb} and σ_{ym} show similar effects. This is attributed partly to underestimation of the influence of a higher degree of rotational restraint on the edge bounded by angle stiffener number 1, and partly to the influence of the significantly higher negative initial deformation of adjacent panels in the y direction. The relatively good agreement for σ_{ym} substantiates the observation regarding the overall flexural ineffectiveness of bracket floors, made in reference to tangential hole stresses.

Panel 2: As for comparisons made for q* = 1, agreement is poor and gets worse under increasing load for all measured quantities except σ_{xm}. This confirms the dominant role played, particularly on y axis behaviour, by the much larger deformation in adjacent panel 3. From the design point of view however, this is not very significant because the stresses affected are small relative to σ_{xm} in the presence of P_x, and agreement is excellent for σ_{xm}.

Panel 3: These results (and also those for panel 2) do not show, to the same degree, the inconsistency discussed previously in regard to the load case involving P_x = 9 tons/ram. This indicates that the effect was primarily due to local deformation in the vicinity of the point of application of the patch loads. The erratic behaviour of stresses at point a for P_x = 9 tons/ram is not attributed to the effects of patch load tests apart from the possibility that the gauge may have been damaged. The limitations of the theory when initial deformation is not symmetric within the panel are emphasised by these results. At points b and c, which are closer to the peak in the actual initial deformation profile, the effects on stresses of membrane effects is more apparent. The pronounced variation of membrane stress in the x direction, resulting in very high stresses at the shell-web interfaces, emphasises the necessity of allowing for a realistic amount of initial deformation in computing loss of shell effectiveness for design purposes.

3.2.3 Shell Stiffeners and Channel Struts

The shell stiffeners are subjected to axial forces due to overall bending and in-plane load and to transverse load and torque due to local deformation of adjacent shell panels. The load distribution is non-uniform. The stiffeners are restrained at floors and channel struts and the stiffener-shell interface constitutes an enforced centre of rotation. The complexity of this system does not lend itself to theoretical analysis at the present time.

Figures 97 and 98 give the experimental results for inner and outer shell stiffeners 3 and 8 between floors A and A' for the four combined load cases considered previously. Figure 99 gives experimental

stresses for channel struts X, Y and Z for the same four in-plane load cases for q = 1 p.s.i. only. The strut stresses are not plotted for increasing transverse load because they behaved linearly in nearly all cases.

Some non-linearity is apparent in the stiffener stresses for increasing transverse load, mainly for outer shell stiffener number 3 at cross sections b (e) and c (d). There is a significant variation in stiffener stresses between end restraints in all cases and for outer shell stiffener number 3 the stresses at section a, b and c show good agreement with stresses at symmetric sections f, e and d. For this stiffener the axial stresses due to overall bending for q = 1 p.s.i. are about -0.39 tons/in^2 at the outer surface and -0.24 tons/in^2 at the free leg. It can be seen that local deformations give rise to stresses of the same order. The combined stresses can be seen to reach high levels which emphasises the necessity of adequate safety margins since the behaviour of the panels and hence overall effectiveness is very sensitive to the degree of restraint afforded by the shell stiffeners.

Little can be said about the channel struts. They perform an important function not only in maintaining the separation of inner and outer shells but also in restraining the stiffeners, and thereby, greatly increasing the rotational edge restraint of the shell panels. This restraining influence is evident in the strut bending stresses which, despite some degree of non-symmetry, are consistent with deformation predictable from the antisymmetry of shell panels.

4. ANALYSIS FOR TRANSVERSE PATCH LOADING

Details of the patch load tests are given in Chapter 2. Four tests were conducted with load applied by 8, 6, 4 and 2 rams respectively, located symmetrically about the transverse centre line, along the centre girder at intersections with the transverse floors. Results are compared with theoretical solutions for a load of 1 ton/ram. Discussion of behaviour common to these tests and the combined distributed transverse and in-plane load tests, already covered in preceding sections will not be repeated in this section.

4.1 Overall Behaviour

Figure 100 shows the ram locations for the four patch load tests and the corresponding distributions used in theoretical solutions for overall behaviour. The theoretical distributions had the stepped form shown in order to minimise errors arising from discrete discontinuities. This limitation is due to the fact that when shear deformation is taken into account, the equations involve differentiation of the transverse load distribution.

The theoretical solution for simply supported edges only, described in Appendix D, was used because the solution for generalised boundary conditions, used to analyse the combined load tests, is even more sensitive to non-uniform transverse load. Zero vertical edge deflexion and zero tangential rotational edge slope are implicit in the solution for simply supported edges. These correspond to infinite vertical deflexion restraint and infinite tangential rotational restraint in the generalised boundary condition solution. In the analysis to determine the most appropriate boundary conditions it was found that

inclusion of appropriate vertical and tangential rotational edge flexibility resulted in an increase in central deflexion and central moments of the order of 10%. In addition, the shear force distribution was modified, as shown by the reversals of edge reaction in the corner regions. In the following analysis of the patch load tests these limitations to the theoretical solution should be borne in mind.

4.1.1 Reactions

Theoretical and experimental reaction distributions are compared in Figures 101 and 102. The inclusion of shear deformation has very little effect on the theoretical edge reaction distribution for simply supported edges with zero vertical displacement. The hump in the theoretical distribution, adjacent to the corner at the bulkhead end, is due to the unequal rod spacing in this region. Two limitations in the theoretical solution are apparent. The first follows from the above discussions on boundary conditions wherein the development of large corner tension forces cannot be directly accounted for. The second relates to the idealization of discrete webs as a homogeneous medium. This is very pronounced for load cases P8 and P6 where the experimental reaction distribution shows a distinct increase in the vicinity of the centre girder. As for the combined load case, there are also peaks in the side of ship distributions at the floors. The equilibrium between measured reaction and applied load is excellent for load cases P2 and P4. For load cases P6 and P8 the discrepancies are 5% and 4% respectively although in the former case the failure of two rods to record load, possibly due to equipment malfunction, may have caused this.

4.1.2 Deflexions

Theoretical and experimental overall deflexions are compared in Figures 103 and 104. The theoretical solution including shear deformation underestimates the measured central deflexion by 9%, 7%, 6% and 8% for cases P8, P6, P4 and P2. Assuming a +10% correction to account for edge flexibilities makes agreement remarkably good. Of the total theoretical central deflexions, shear deformation accounts for 26%, 28%, 32% and 37% for cases P8, P6, P4 and P2 respectively. The theoretical and experimental distributions of deflexion agree remarkably well even for cases P2 and P4, where a distinct hump develops under the load. The variation in curvature at the edge of the patch in the x direction becomes very apparent in theoretical strains.

4.1.3 Shell Strains at Shell-Web Intersections

The total theoretical corrections to the strains given by the overall solution, to account for local deformation and incorrect boundary conditions, are of the order of +30% and +10% in the x and y directions respectively. Applying these corrections to the solutions shown in Figures 105 and 106 for inner and outer shell strains - load case P8, gives errors relative to measured central region strains of the order of +45%, +45%, -25% and +15% in ε_{xi}, ε_{yi}, ε_{xo} and ε_{yo} respectively. These errors confirm the conclusion made in reference to combined loading, that the computed neutral axes were too close to the outer shell. This was because the loss of effectiveness, which was assumed to be equal in both shells, was in fact more severe in the outer, compression shell. The measured strains conform remarkably well to the theoretical distributions considering the limitations due to the effects of local behaviour. It was noted with reference to combined load results that

these limitations were less severe in patch load cases because of the absence of local transverse panel loading. Results for inner and outer shell strain for load cases P6, P4 and P2 are given in Figures 107 and 108, 109 and 110, and 111 and 112 respectively. The theory shows how the effect of shear deformation on bending strains under the load becomes more severe as the patch size diminishes.

4.2 Local Behaviour

4.2.1 Webs

As for the combined load analysis, theoretical solutions for tangential web hole stresses were computed by the summation of the effects of shear and bending. Particular cases were obtained by taking multiples of the two distributions given in Figure 83.

Figures 113, 114, 115 and 116 compare measured and theoretical tangential stresses for the holes located at bay 7-8 (7'-8') in floors A (A'), B, C and D respectively. All four load cases are shown on each Figure. As for the combined load results the experimental values fit the theoretical distributions remarkably well although the maximum values are again predictably low.

Figure 117 gives results for holes located at bay 8-9, in floor A and side bracket A_1, for the four load cases. Two theoretical distributions are shown, one in which all the shear force is taken by floor A and one in which this force is shared with the side brackets. Again, as for the combined load results, the floor A stresses indicate that the shear was shared with the side brackets to some degree but this is not confirmed by the results for side bracket A_1.

Figure 118 gives results for centre bracket A_1 for the four load cases. In this case there is a significant difference from the combined load results. Whereas in the latter case there was insignificant shear force so close to the centre of the model, in the patch load cases the shear distribution rises rapidly and contributes significantly to the applied web loading at bay 0-1. It was noted that the lack of stress recorded in the combined load test indicated that the centre brackets contribution to overall flexural stiffness was insignificant. This was confirmed by the shell panel analysis of σ_{ym} for panel 1. The patch load results show that the centre brackets do contribute significantly to shear stiffness since the measured stress at 135^{o} is, theoretically, entirely due to applied shear stress. This justifies the inclusion of centre and side brackets in the analysis to determine overall shear stiffness.

Figure 119 gives results for the intercostal holes immediately adjacent to bulkhead ends. Agreement is comparable with the combined load results.

The measured centre girder shear stresses adjacent to the bulkheads were 2.56, 1.36, 0.73 and 0.32 tons/in^2 for load cases P8, P6, P4 and P2 respectively. The corresponding theoretical values are 2.08, 1.10, 0.60 and 0.28 tons/in^2 giving errors of 19%, 19%, 18% and 13%. The decrease in percentage error corresponds to an improvement in load distribution as the distance from the applied load increases.

4.2.2 Shell Panels

Figures 120, 121, 122 and 123 compare two theoretical solutions for deflexions of outer shell panels 1, 2 and 3 with experimental results

for load cases P8, P6, P4 and P2 respectively. The corresponding results for bending stresses are given in Figures 124, 125, 126 and 127 and for membrane stresses in Figures 128, 129, 130 and 131. The theoretical solutions are for two cases of elastic rotational edge restraint:— one for the same values used in the combined load analysis, and the other for zero rotational edge restraint which corresponds to simply supported edges. An analysis using the beam-column solution described in Chapter 3 showed that, in the absence of distributed transverse pressure, the effective rotational restraint for an antisymmetric distribution of initial deformation ($w_o/h=0.25$) reduced the effective rotational restraint by about a half. However, it was decided to use the zero restraint condition and discuss differences between theory and experiment with reference to the preceding calculation. Loading was entirely in-plane. The theoretical values for average in-plane stress were taken from corresponding solutions for overall behaviour, including shear deformation, with adjustments for loss of effectiveness and non-uniform distribution.

Measured deflexions in panels 2 and 3 fall about midway between the two theoretical distributions which indicates the theoretical estimate of loss of elastic restraint in the absence of transverse load was quite accurate. This observation must however be examined with reference to stresses. It is of note that, in the absence of transverse load, the high relative initial deformation of panel 3 does not appear to have exerted the marked influence on flexural behaviour of panel 2 observed in the combined load tests. The measured deflexion in panel 1 is considerably greater than both theoretical solutions. There is little difference between the latter solutions because the effective rotational restraint assumed for panel 1 was relatively low. The greater

measured deflexion is attributed to an increase in the initial deformation of panel 1. This has already been discussed with reference to the inconsistencies between combined load results for P_x = 0, 3, 6 tons/ram and P_x = 9 tons/ram where the patch load tests were conducted in the interim between the 6 and 9 tons/ram tests.

Measured bending stresses in all panels agree more closely with solutions for simply supported edges but considering the approximation involved agreement is remarkably good.

Measured membrane stresses show the same effects noted in the combined load tests. In some cases the difference between theoretical membrane stresses for the two boundary conditions was insignificant and only the restrained edge results are given. Agreement in the x direction is good allowing for the effect of non-symmetry in panel 3. In the y direction the theoretical values are high, probably due to an overestimate of applied edge stress.

4.2.3 Shell Stiffeners and Channel Struts

Figures 132, 133, 134 and 135 give inner and outer shell stiffener stresses in stiffeners numbered 3 and 8, between floors A and A', for load cases P8, P6, P4 and P2 respectively. The overall stresses at the shell-stiffener intersection for outer shell stiffener number 3 are of the order of -1.1, -1.1, -1.0 and -0.7 tons/in^2 for the four load cases. Comparing these values to the measured stresses emphasises the very significant influence of local deformation. This is even more apparent in stiffener number 8 in which stresses are higher than in

number 3 in some cases, despite the much greater distance from the centre line. Figure 136 gives channel strut stresses.

4.3 Non-Linearity with Increasing Load

The various measured values exhibited about the same degree of non-linearity under increasing load as observed in the combined load tests.

5. FAILURE TEST

5.1 Preliminary Local Failure

It was decided to precede the final failure test with one additional elastic test. This was for the model subjected to a constant transverse pressure of 5 p.s.i. and increments of in-plane thrust in excess of the previous maximum (P_x = 9 tons/ram). The purpose was to give more extensive experimental data on the large deflexion behaviour of local shell panels under combined thurst.

As the in-plane load was being incremented from P_x = 15 tons/ram to P_x = 16 tons/ram, (which was to be the maximum) there was an unexpected outer shell buckling failure at one end. Figure 137 is a view of the underside of the model after this failure. Although it cannot be seen very clearly, there was also evidence that a similar failure was imminent at the other end and elsewhere the permanent outer shell deformation was in excess of the original initial deformation.

The maximum thrust was about $P_x = 15\frac{1}{2}$ tons/ram corresponding to an average compressive stress of -12 tons/in^2. The lowest theoretical panel buckling load under longitudinal compression is -17.1 tons/in^2,

for simply supported edges. This would correspond to a three half wave buckle but as can be seen in Figure 138 the actual buckle was of a local nature and this premature failure is attributed to two main factors. Firstly, the shell stiffeners were not continuously welded around their section at the ends and hence they only become effective in sharing the thrust at some distance from the ends. Secondly, the intermittent welding of the stiffeners and webs to the shell constituted a local weakness at gaps in the weld in so far as the restraint against antisymmetric buckling of adjacent panels was reduced. As can be seen in Figure 138 it was across a line of gaps in the welding that the buckle occurred. These factors were obviated in the inner shell by the margin brackets.

Because of the local nature of the failure and since it was not in the region of the expected critical area so far as the final failure test was concerned, it was decided to repair the model by cutting out the buckles and welding additional shell plating at both ends. This additional plating was $\frac{1}{8}$ in. thick and extended one floor spacing from the ends, except at the centre, where it extended as far as the second bracket floor. It was welded in panels across the whole width of the buckled end and on every second panel at the other end. Some realignment of the end extension was necessary at the buckled end. After repair the model was realigned in the rig and elastic tests under combined load showed virtually no difference from the pre-failure tests.

5.2 Final Failure Test

The repaired model was failed under combined transverse pressure and in-plane thrust, incremented simultaneously at the rate of $q = 1$ p.s.i. and $P_x = 1$ ton/ram. These corresponded to theoretical

overall central longitudinal outer bottom stresses of about -0.45 and -0.77 tons/in^2 respectively. Working load was assumed, for the purposes of defining an overall safety factor against collapse, to be q = 10 p.s.i. (full draft, empty hold condition) and P_x = 10 tons/ram (approximately maximum hogging condition), corresponding to maximum theoretical overall longidudinal outer bottom stresses of -4.5 tons/in^2 and -7.7 tons/in^2 respectively. Thus the elastic analysis, for the assumed losses in plating effectiveness, gave a combined overall maximum longitudinal compressive stress at the assumed working load, of -12.2 tons/in^2. The corresponding theoretical transverse stress was -8.3 tons/in^2. The yield stress for the material was about 15 tons/in^2.

At about q = 13.5 p.s.i. and P_x = 13.5 tons/ram the loading could no longer be sustained. This corresponds to a nominal double-bottom safety factor of 1.35. In practice it may be slightly higher due to rotational restraint at the sides. Subject to a more detailed analysis it appeared that failure was due to degeneration in outer shell transverse panel effectiveness, combined with extensive local yielding. At the failure load the theoretical maximum combined overall central longitudinal outer shell stress was of the order of -16½ tons/in^2. The corresponding transverse stress was in excess of -11 tons/in^2. The theoretical local bending stresses in some panels were of the same order of magnitude. Even allowing for the fact that overall and local maximum stresses do not occur at the same locations, the combined elastic stresses were in excess of yield at the assumed working load indicating that at failure the yielded areas must have been extensive.

Figure 139 is an overall view of the bottom of the model after failure. Figure 140 shows details of local deformation in the centre region. Figure 141 shows details of a buckle which extends roughly

diagonally toward the corners at one end. This buckling is thought to have precipitated the final collapse.

To test the central shell panel ultimate load hypothesis, additional solutions were obtained from the BEAMCOL program (described in Chapter 3) for a transverse outer shell section subjected to combined load. Rotational restraint at supports due to stiffeners (k^*) was taken as 1350 in. lb/in. and the central initial deformation was taken as a quarter of the plate thickness ($w_o/h = 0.25$). The solution degenerated, which has been shown in Chapter 3 to be a good measure of the column buckling load, at slightly above 10.25 p.s.i. transverse pressure and 1127.5 lb. in-plane load. For zero rotational restraint the column buckling load was found to be 665 lb. compared to 850 lb. for the corresponding panel. Increasing the restrained beam-column buckling load in the same proportion gives a restrained panel buckling load of about 1435 lb. which corresponds to about 13 p.s.i. transverse pressure or 1.3 times the assumed working load. It would seem possible therefore, that panel buckling combined with extensive yielding due to overall and local bending, could relate directly to the observed collapse load.

Figure 142 is a plot of overall central deflexion, and local deflexions in panels 1 and 3, for the failure test. The beam-column solution for effective rotational restraint and corresponding central deflexion is also shown. Non-linearity becomes apparent in the overall deflexion at about 0.6 of the assumed working load. The overall stiffness decreased rapidly beyond the assumed working load which is very close to the beam-column buckling load.

CHAPTER 6

CONCLUSIONS

1. LOSSES IN PLATING EFFECTIVENESS

1.1 Shell Plating

An elastic analysis of overall behaviour of plated grillages using the orthotropic plate approach should take account of loss of shell plating effectiveness caused by shear lag and local panel bending. For the model, which was typical of many dry cargo ships, shear lag dominated the longitudinal losses and local panel bending dominated the transverse losses. The span to flange width ratio was about 6 in both directions for which the unstiffened flange shear lag loss would be about 7½% but due to longitudinal framing this was doubled in the longitudinal direction. The 3:1 side ratio of shell panels (3 longitudinal) resulted in negligible longitudinal and about 15% transverse loss of flange effectiveness due to local panel bending.

Losses due to shear lag depend on section geometry, boundary conditions and the distribution (but not the magnitude) of applied transverse load. Losses due to panel bending are sensitive to magnitude of loading (in-plane and transverse) in addition to the other factors. However, provided the rotational edge restraint is sufficiently high, which was the case in the model for transverse loads up to 5 p.s.i., the magnitude of the load is of secondary importance compared to the effect of initial deformation. Hence, it appears that local panel as well as shear lag effectiveness calculations may be made, in certain cases, without reference to actual stress levels.

In the case of the model, calculation of panel bending effectiveness was based on a measured mean central initial deformation to plate thickness ratio (w_o/h) of 0.25. For clamped or nearly clamped edges loss of effectiveness due to panel bending increases in almost direct proportion to w_o/h where it is possible that w_o/h may exceed 0.5 in practice.

The combined losses used in the overall analyses of the model were 15% in the x direction and 20% in the y direction. These were assumed to be the same in top and bottom shells and to be constant throughout the model. Losses of this order must significantly affect overall behaviour and the degree of agreement between theory and experiment indicates that they represent a reasonable assessment. Agreement would have been better if a distinction had been made between inner and outer shell panel bending losses.

The preceding conclusions must be qualified for external load in excess of that applied during the elastic tests, in which load was restricted such that no local yielding was recorded by any of the strain gauges. In the case of distributed transverse pressure only, this meant that loading had to be stopped at 5 p.s.i., half the full draft pressure, because yielding was imminent in several perforated floors. In the case of combined distributed transverse load and longitudinal thrust, loading had to be stopped at 4 p.s.i. and -6.93 tons/in^2 (9 tons/ram) because yielding was imminent in central bottom shell panels. In the final failure test, combined load was applied in increments of 1 p.s.i. and -0.77 tons/in^2 (1 ton/ram) and non-linearity became evident in the overall central deflexion at about 6 p.s.i. and -4.62 tons/in^2 (6 tons/ram). By 10 p.s.i. (full draft pressure) and -7.7 tons/in^2 (10 tons/ram) the measured central deflexion had diverged from the linear solution by

about 15%, of which only 2½% could be accounted for by elastic interaction between in-plane load and overall transverse deformation. This indicates a significant fall off in flange effectiveness which is attributed to inelastic deformation and a reduction in effective panel restraint below a value at which panel effectiveness could be computed without reference to stress levels.

1.2 Web Plating

Accounting for shear deformation in the orthotropic plate approach to plated grillage analysis requires the idealization of discrete webs as a continuous media. In the double-bottom structure, where shear deformation can account for more than 50% of the total deflexion, this idealization requires an accurate assessment of loss of web shear stiffness due to perforations. In the model, perforations reduced the shear stiffness by about 50%. It has been shown by Ho that the theoretical solution for a hole in an infinite plate subjected to pure shear gives good agreement with test results for loss of web shear stiffness although for design purposes an empirical equation proposed by Kuhn has been shown to give satisfactory results.

The form of the orthotropic plate equations solved as part of this investigation precluded consideration of non-uniform section properties and hence local variations were accounted for by taking equivalent uniform properties. In the double-bottom model, equivalent shear properties had to take account of the fact that the longitudinal centre girder, with no perforations, was almost twice as stiff as the intercostals and that the bracket floors gave local increases in transverse stiffness near the centre girder and the sides of the model. The equivalent losses of shear stiffness were 20% longitudinally and 30%

transversely. Agreement between overall theoretical and experimental deflexions indicates that this was a reasonable assessment.

No account was taken of loss of shear effectiveness due to out of plane web deformation. That considerable out of plane deformation did take place, due to initial deformation of the webs, was evidenced by the measured strains on opposite surfaces. At some locations this effect was severe enough to result in local surface yielding at half full draft pressure. The agreement noted between measured and theoretical overall deflexions up to 5 p.s.i., indicates that the error incurred by omitting this factor was not very significant but it is possible that it became significant at higher loads and contributed to the observed decrease in overall stiffness.

2. EFFECT OF WEB SHEAR DEFORMATION ON MODEL BEHAVIOUR

2.1 General

The following observations are made with respect to the double-bottom model. Practical cases will arise where the significance of shear deformation is of greater importance than observed in the model and these are remarked upon in passing. More general conclusions relating to the influence of shear deformation on orthotropic plate behaviour, for a broad range of plate and boundary parameters, are given in Chapter 4.

2.2 Deflexions

Measured and theoretical overall deflexions agreed within 5%. For distributed transverse loading the theoretical solution showed that shear deformation accounted for 32% of the total deflexion. For patch loads

the contribution due to shear was about 26%, 28%, 32% and 37% for the P8, P6, P4 and P2 cases respectively. The patch load results were obtained, of necessity, from a solution restricted to cases of simply supported, undeflecting edges. The distributed transverse load case was, however, amenable to analysis by a solution for elastically restrained deflecting edges and the actual boundary conditions could therefore be more accurately simulated. The reason for this distinction was the relative sensitivity of the two solutions to variation in transverse load distribution. The more general solution was unsatisfactory for the patch load cases because the effect of variation appeared in the variable coefficient matrix (left hand side), whereas in the simply supported edge condition solution this effect appeared in the loading matrix (right hand side) and provided the load was stepped, rather than cut off abruptly at discontinuities, the results were satisfactory.

For other boundary conditions, such as clamped ends and elastically restrained sides, shear deformation could account for more than 50% of the total deflexion. An effect of this magnitude might be important when, for example, propeller shaft distortion is a consideration.

2.3 Reactions

As discussed in Chapter 4, the inclusion of shear deformation in the plate equations obviates the necessity of resorting to the Kirchoff equation to compute corner forces. These forces arise when tangential rotational restraint is low, which was the case in the double-bottom model.

Total measured and theoretical reactions agreed within less than 5% in all cases. The distribution of measured reaction was used as a basis for determining the effective boundary conditions because there was some doubt as to the influence of the in-plane loading beams welded at the ends of the model. It was concluded that restraint due to the loading beams had negligible effect on the overall behaviour of the model.

The limitations of the orthotropic plate approach to analysis of the double-bottom was most evident in the end reaction distributions for patch loads where a peak, in line with the centre girder, was quite pronounced in the measured values. The theoretical solution predicts a smooth distribution. Much less significant peaks were apparent in line with other continuous webs in all tests. Despite this limitation, the orthotropic plate approach gave satisfactory results for other variables, for patch load as well as distributed transverse load cases.

2.4 Stresses

For distributed transverse load the theoretical effect of shear deformation on overall stresses in the model was of the order of 10%. This was due primarily to the influence of reduced tangential rotational edge restraint at the sides, an effect which can only be accounted for in the orthotropic plate solution when shear deformation is included. As already mentioned, this reduced restraint could not be accounted for in the solutions for patch loads, but the solution used did give localised increases of the same order under the loaded areas.

Theoretical shell panel in-plane edge forces due to transverse load were derived from overall solutions including shear deformation. The

agreement between measured and theoretical centre panel stresses showed that these edge forces were of reasonable accuracy for both the distributed and the local transverse load cases.

Solutions for the double-bottom model subjected to combined in-plane and transverse load showed that, for loading of practical interest, interaction between in-plane load and overall transverse deflexion due to load (including shear deflexion) is negligible. The results confirmed this, although measurable deflexions did occur due to interaction between the in-plane load and the initial overall outward deformation of the model. Thus, for practical purposes, direct superposition can be used to evaluate the combined overall stresses and the combined panel in-plane edge forces.

Practical cases do arise where accounting for shear deformation can have a more significant effect on stresses. For example, for clamped ends and elastically restrained sides the maximum end stresses may be reduced by more than 30%. Shear-orthotropy may result in increases in maximum stress of the same order of magnitude.

3. LOCAL ELASTIC BEHAVIOUR

3.1 Shell Panels

Good agreement between theory and experiment has justified the analysis of shell panels as discrete, initially deformed, isotropic plates subjected to transverse pressure and edge loads. The following conclusions relate to behaviour for loads of the order applied in the elastic tests and are qualified in the later discussion on behaviour observed during the failure test.

The analysis is dependent on an accurate assessment of local boundary conditions which must take account of continuity. This was done by analysing the moment-slope characteristics of a transverse outer shell section idealised as an initially deformed beam-column. The effect of stiffeners was accounted for by applying rotational restraint at each support. This restraint was derived from a torque analysis for angle sections restrained against warping at end supports and constrained to rotate about an enforced centre of rotation at the shell-stiffener interface. It was shown that this restraint can be considerable and it is in fact essential, if premature buckling of outer shell panels is to be prevented. The latter analysis was for angle section stiffeners. For bulb section stiffeners the restraint would be considerably reduced. The channel struts, which connected top and bottom shell stiffeners midway between floors, had a considerable effect on shell panel behaviour, since, by halving the stiffener span between restraints they increased the effective panel rotational restraint by a factor of about 16.

Initial deformation of shell panels in the model was of sufficient magnitude, relative to plate thickness, to induce large deflexion behaviour. Although there is very little quantitative data available it appears likely that in ships in service the centre panel deformation to plate thickness ratio will be in excess of that observed in the model. Hence, design data based on linearised solutions for local panel behaviour cannot be assumed to be sufficiently accurate for practical purposes.

3.2 Web Panels

The distribution of measured heart of plate tangential stresses around web lightening holes conformed very well to a theoretical solution

based on superposition of bending and shear effects. The maximum theoretical tangential stress, due to the shear component of applied web load, was derived from a solution based on the equations for a hole in an infinite plate subjected to pure shear. Previous work has shown that this solution corresponds to the case of a discrete perforated panel with edges partially restrained. Actual measured maximum stresses were about 20% lower than the theoretical values because they were recorded at 0.1 inches in from the edges of the holes. A fall off in stress concentration of this order was predicted by the theory.

Applied shear forces used in the theoretical solutions were derived from the overall orthotropic plate solutions by lumping the distributed shear at the webs. At cross sections including discontinuous webs (bracket floors), measured stresses were compared to two solutions, one in which all the shear was taken by the continuous web and another where the shear was shared equally between all webs. The experimental results showed that the discontinuous webs were sharing the load although not apparently on an equal basis. This indicates that a lower shear effectiveness factor should be applied to discontinuous webs. Due to intial deformation there was considerable out of plane bending of perforated web panels. In some locations this was sufficient to give local surface stresses approaching yield at half full draft pressure (5 p.s.i.). The corresponding maximum heart of plate tangential stress at this load was of the order of 10 tons/in^2. Although the surface yielding may not in itself be a critical factor the corresponding deformation may contribute to loss of web effectiveness at higher loads. If necessary, additional stiffness could be achieved, without necessitating additional material, by bending the circumference at 45^o to give a flanged effect as is presently done in aircraft construction.

Measured and theoretical centre girder web shear stresses agreed within 9% for the distributed transverse load case. For local transverse load the error varied from 19% to 13%. The increase in error is indicative of limitations in the orthotropic plate approach to analysis of plated grillages when webs are widely spaced. Even so, for practical purposes the method appears satisfactory for spacings characteristic of the double-bottom structure.

3.3 Shell Stiffeners and Channel Struts

The shell panel rotational edge restraint function of the shell stiffeners and channel struts has already been commented upon. Although no quantitative analysis was attempted, the observed stresses in these members were consistent with this function. The shell stiffener stresses due to local deformation exceeded the stresses due to overall bending at some points, indicating that design for local buckling may be desirable since this could initiate overall failure of the double-bottom.

4. FAILURE

In the final failure test transverse pressure and in-plane thrust were increased simultaneously at the rate of 1 p.s.i. and 1 ton/ram (-0.77 tons/in^2) respectively. Working load was assumed to occur at 10 p.s.i. and 10 tons/ram (-7.7 tons/in^2) where 10 p.s.i. corresponded to the full draft empty hold condition. The theoretical maximum overall longitudinal compressive stresses at this load were -4.5 tons/in^2 and -7.7 tons/in^2 due to transverse pressure and in-plane thrust

respectively. Failure occurred at about 1.35 times this assumed working load and appeared to have been initiated by collapse of the central outer shell panels.

According to the orthotropic plate theory (including shear deformation and loss of shell effectiveness) the load required to cause compressive yielding of the outer shell at the centre of the model was 1.25 times the assumed working load. If loss of effectiveness is ignored this factor becomes 1.56, increasing to 1.74 if, in addition, shear deformation is ignored. Local surface yielding of central shell panels, and heart of plate web hole circumference yielding, began at about 0.75 of the assumed working load. An approximate calculation of the buckling load of a typical shell panel gave a central panel buckling load which corresponded to about 1.3 times the assumed working load.

In the single floor test [1] the failure appeared to have resulted from a combination of shell and floor buckling at a solid floor shear stress, in way of the buckle, of about 7.3 tons/in^2. The corresponding theoretical maximum solid floor shear stress at failure of the double-bottom model was about 6.75 tons/in^2. The corresponding average solid floor shear stress was about 5.4 tons/in^2. The theoretical solid intercostal shear stress in way of the holes immediately adjacent to the ends was about 8.1 tons/in^2 at failure. There was no external evidence of a shear failure in the double-bottom model but this remains to be confirmed when the model is cut open.

An approximate yield line analysis, taking the in-plane thrust as fixed at 13.5 tons/ram (-10.4 tons/in^2), gives an ultimate transverse pressure of about 19 p.s.i. This solution is outlined in Appendix E.

These observations indicate that a reasonable estimate of ultimate load may be obtained from the orthotropic plate solution, based on compressive yielding of the outer shell at the centre of the double-bottom, provided loss of shell effectiveness and shear deformation are taken into account. This would have to be viewed in conjunction with a panel buckling and web shear stress analysis.

REFERENCES

1. CHAPMAN J.C., HO D. and TAYLOR P.F. Transverse bending of an element of a ship's double bottom. Trans. N.E.C.I.E.S., 1965.

2. SCHADE H.A. Bending theory of ship bottom structure. Soc. Nav. Arch. Mar. Eng. Trans., Vol. 46, 1938.

3. SCHADE H.A. The orthogonally stiffened plate under uniform lateral load. A.S.M.E. Trans., Vol. 62, 1940.

4. SCHADE H.A. Design curves for cross stiffened plating under uniform bending load. Soc. Nav. Arch. Mar. Eng. Trans., Vol. 49, 1941.

5. CHAPMAN J.C. Doubly plated grillages under uniform lateral pressure. B.S.R.A. Report R.B. 1566, 1958.

6. CHAPMAN J.C. The structural behaviour of ship's double bottom (failure test). B.S.R.A. Report N.S.11, Nav. Arch. Report No. 1, 1963.

7. SCHULZ H.G. Buckling and post-buckling behaviour of transversely stiffened ship hull model. Journal of Ship Research, Sept. 1964.

8. HARRISON R.P. and RICHARDSON W.S. Experiments on compression of double bottom plating: Part II. B.S.R.A. Report R.B. 1582, S.S. 190, 1958.

9. CHAPMAN J.C. Developments in ship structures. The Structural Engineer, Feb. 1966.

10. LIBOVE C. and BATDORF S.B. A general small-deflection theory for flat sandwich plates. N.A.C.A. Report No. 899, 1948.

11. TIMOSHENKO S.P. Strength of Materials, Part I. D. Van Nostrand Co. Inc., 3rd Edition, 1955.

12. REISSNER E. The effect of transverse shear deformation on the bending of elastic plates. Jour. Appl. Mech., Vol. 12, 1945.

13. ERICKSEN W.S. Effects of shear deformation in the case of a flat rectangular sandwich panel. Deflection under uniform load of sandwich panels having facings of unequal thickness. F.P.L. Report 1583-C, 1950.

14. YEN K.T., GUNTURKUN S. and POHLE F.V. Deflections of a simply supported rectangular sandwich plate subjected to transverse loads. N.A.C.A., T.N. No. 2581, 1951.

15. REISSNER E. Small bending and stretching of sandwich-type shells. N.A.C.A., T.N. No. 1832, 1949.

16. RAVILLE M.E. Deflection and stresses in a uniformly loaded, simply supported, rectangular sandwich plate. F.P.L. Report 1847, 1962.

17. ROBINSON J.R. The buckling and bending of orthotropic sandwich panels with all edges simply supported. Aero. Quart., Vol. 6, 1955.

18. KROMM A. Uber die Randquerkrafte bei gestutzten platten. Z. Angew. Math. Mech., Vol. 35, 1955.

19. SCHAFER M. Uber eine verfeinerung der klassischen theorie dunner schwach gebogener platten. Z. Angew. Math. Mech., Vol. 32, 1952.

20. CARLEY T.G. and LANGHAAR H.L. Transverse shearing stress in rectangular plates. Proc. A.S.C.E., Vol. 94, 1968.

21. LOCKWOOD TAYLOR J. Strength of sandwich panels. Proc. VII Int. Congr. Appl. Mech., Vol. 1, 1948.

22. MARCH H.W. Effects of shear deformation in the case of a flat rectangular sandwich panel. F.P.L. Report 1583, 1948.

23. CONWAY H.D. Bending of rectangular plates subjected to a uniformly distributed lateral load and tensile or compressive forces in the plane of the plate. Jour. of Appl. Mech., Vol. 16, Sept. 1949.

24. LOCKWOOD J. Rectangular flat plates under combined bending and compression. The Shipbuilder and Marine Engine-Builder, Vol. 57, Jan. 1950.

25. BLEICH J.F. Buckling strength of metal structures. London: McGraw-Hill Book Co., 1952.

26. AALAMI B. Non-linear behaviour of rectangular orthotropic plates under transverse and in-plane loads, Ph.D. Thesis, University of London (Imperial College), 1967.

27. MURRAY J.M. Notes on deflected plating in compression and tension. Trans. I.N.A., Vol. 87, 1945.

28. MURRAY J.M. Corrugation of bottom shell plating. Trans. I.N.A., Vol. 97, 1954.

29. HO D. The buckling of perforated web plates. Ph.D. Thesis London University (Imperial College), 1964.

30. WANG C.T. Theoretical analysis of perforated shear webs. Jour. Appl. Mech., Vol. 13, 1946.

31. SCHADE H.A. The effective breadth of stiffened plating under bending loads. Trans. Am. Soc. Nav. Arch. and Mar. Eng., 1952.

32. FERAHIAN R.H. Shear lag and buckling in plated grids. M.Sc. Thesis, University of London (Imperial College), 1963.

33. ZBIROHOWSKI-KOSLIA K. Thin walled beams, 1st edition, Crosby Lockwood and Sons Ltd., 1967.

34. GODDEN W.G. Numerical analysis of beam and column structures. Prentice Hall Inc., 1965.

35. KUHN P. The strength and stiffness of shear webs with lightening holes having 45° flanges. N.A.C.A./ARR/323, 1942.

36. TIMOSHENKO S.P. and WOINOWSKY-KRIEGER S. Theory of plates and shells. McGraw-Hill Co., 1959.

37. FREDERICK D. Thick rectangular plates on an elastic foundation. Trans. A.S.C.E., Vol. 122, 1957.

38. SCHADE H.A. Bending theory of ship bottom structure. Soc. Nav. Arch. Mar. Eng. Trans., Vol. 46, 1938.

39. SALERNO V.L. and GOLDBERG M.A. Effect of shear deformation on the bending of rectangular plates. Jour. Appl. Mech., Vol. 27, 1960.

40. THURSTON G.A. Bending and buckling of clamped sandwich plates. Jour. Aero. Sci., Vol. 24, 1957.

41. HOWLAND R.C. and STEVENSON A.C. Biharmonic analysis of a perforated strip. Phil. Trans., Series A, Vol. 232, 1934.

42. JONES L.L. and WOOD R.H. Yield line analysis of slabs. Thames and Hudson, Chatto and Windus, 1st edition, 1967.

APPENDIX A

OUTLINE OF SHADE'S SOLUTION FOR COMPUTATION OF SHEAR BREADTH FACTOR[31]

Any function describing the plane stress behaviour of the flanges of a beam must satisfy the LaGrange equation:

$$-\nabla^4 F = 0$$

Where: F = Airey stress function defining stresses :

$$\sigma_x = \frac{\partial^2 F}{\partial y^2}$$

$$\sigma_y = \frac{\partial^2 F}{\partial x^2}$$

$$\tau = -\frac{\partial^2 F}{\partial x \partial y}$$

The solution for a particular beam depends on the boundary conditions, the loading distribution and the section geometry. The case of interest to this investigation (multiple webs) is shown in Figure 143.

Two series solutions solutions, representing alternative end conditions ($x = 0, L$), were considered:

(i) $F_n = f_n \sin \omega x$

Where:

$\omega = n\pi/L$,

n = any integer

Gives:

$$\left.\begin{aligned} \sigma_x &= \frac{\partial^2 f}{\partial y^2} \sin \omega x = 0 \\ \sigma_y &= -\omega^2 f \sin \omega x = 0 \\ \tau &= \omega \frac{\partial f}{\partial y} \cos \omega x \neq 0 \end{aligned}\right| \text{at } x = 0, L$$

This corresponds to free ends except for $\tau \neq 0$.

(ii) $$F_n = f_n \cos \omega x$$

Gives:

$$\left.\begin{aligned} \sigma_x &= \frac{\partial^2 f}{\partial y^2} \cos \omega x \neq 0 \\ \sigma_y &= -\omega^2 f \cos \omega x \neq 0 \\ \tau &= -\omega \frac{\partial f}{\partial y} \sin \omega x = 0 \end{aligned}\right| \text{at } x = 0, L$$

This corresponds to clamped ends.

Satisfaction of the LaGrange equation gives (for both series)

$$f_n = (A_n + C_n \omega y)\cosh \omega y + (B_n + D_n \omega y)\sinh \omega y$$

Three of the four coefficients can be directly defined from satisfaction of the independent boundary conditions:

$$\left.\begin{aligned} v &= \text{normal displacement} = 0 \\ \tau &= \text{shear stress} = 0 \end{aligned}\right| \text{at } y = 0,\ x = 0 \rightarrow L$$

$$v = 0; \quad \text{at } y = b, \quad x = 0 \rightarrow L .$$

Substituting the stress function into the relevant stress-strain and strain-displacement equations for the above boundary conditions gives:

$$B_n = C_n = O$$

$$D_n = \frac{-A_n \tanh \omega b}{(\omega b - j \tanh \omega b)} = A_n K_n$$

$$j = (1-\mu)/(1+\mu)$$

Gives:

$$f_n = A_n(\cosh \omega y + K_n \omega y \sinh \omega y)$$

The remaining boundary condition is:

$$\overline{\sigma}_x = \frac{M_x}{Z_x}$$

Where:

M_x = beam bending moment at a particular section

Z_x = beam section modulus at that section.

This is the simple beam stress for the reduced flange breadth and is dependent on the flange effectiveness, yet to be evaluated. One way of solving for this would be to use an iterative procedure starting from an assumed Z_x distribution along the span (L). Shade avoids the necessity of iteration by defining a "boundary function" - the effective breadth for any given n, which he shows to be independent of x, i.e. independent of longitudinal stress distribution. This eliminates A and Shade then derives the actual effective breadth by a summation involving the $\overline{\sigma}_x$ boundary

condition, for M_x defined in harmonic form (gives n series) and taking account of the "boundary functions" in Z_x.

Thus, for a given n, the loss of effectiveness based on web stress is (see Figure 143(ii)):

$$\bar{\lambda}_n = \frac{\int_o^b \sigma_{xn} dy}{\bar{\sigma}_{xn}} = \frac{\left.\frac{\partial f}{\partial y}\right|_o^b}{\left.\frac{\partial^2 f}{\partial y^2} + \mu \omega^2 f\right|_{y=b}}$$

Substituting for f_n gives:

$$\frac{\bar{\lambda}_n}{b} = \frac{4}{\alpha} \frac{(\cos \alpha - 1)}{(3+\mu)\sinh \alpha - (1+\mu)\alpha}$$

Where:

$$\alpha = 2 \omega b$$

This is the required "boundary function" for the particular section, A has cancelled out and the expression is independent of x.

Now, if the moment distribution is defined as a harmonic function (Fourier series):

$$M_x = \Sigma M_n \sin \omega x$$

Then for a particular n:

$$M_{nx} = M_n \sin \omega x$$

$$\bar{\sigma}_{nx} = \frac{M_{nx}}{Z_{nx}}$$

$$X_{nx} = \int_o^b \sigma_{nx} = \bar{\lambda}_n \bar{\sigma}_{nx}$$

Finally, the actual effective breadth is:

$$\lambda_1 = \frac{\sum X_{nx} \sin \omega x}{\sum \bar{\sigma}_{nx} \sin \omega x}$$

Or; Shear Breadth Factor:

$$\frac{\lambda_{1x}}{b} = \frac{\sum (\frac{\bar{\lambda}_n}{b})(\frac{M_{nx}}{Z_{nx}})}{\sum (\frac{M_{nx}}{Z_{nx}})}$$

Shade gives values of shear breadth factor for a limited number of beam sections and load distributions. In order to obtain the factors required as part of this investigation, the preceding expressions were programmed for solution on the University of London Atlas Computer. The generality of the solution is defined in Chapter 3. The results confirmed Shade's suggestion that although section geometry does significantly influence local loss of effectiveness in the case of patch loads, the overall (beam) loss of effectiveness can be based on uniform load and is independent of section geometry for practical purposes.

The double-bottom model analysis required solutions for the distribution of stress across the flange so that stresses could be estimated at points removed from the flange-web interface. These were obtained by extending Shade's solution for the simply supported end case as follows:

We require:

$$\sigma_x = \frac{\partial^2 F}{\partial y^2} = \sum \omega^2 A_n \left[(1+2K)\cosh \omega y + K_n \omega y \sinh \omega y \right] \sinh \omega x$$

To evaluate A_n, consider:

$$\overline{\sigma}_{nx} = \left(\frac{\partial^2 f}{\partial y^2} + \mu \omega^2 f\right) \sin \omega x = \frac{M_{nx} \sin \omega x}{Z_{nx}}$$

Gives:

$$A_n = \frac{\left(\frac{M_{nx}}{Z_{nx}}\right)}{\omega^2 L_n}$$

$$L_n = (1 + 2K_n + \mu)\cosh \omega b + (1+\mu)K_n \omega b \sinh \omega b$$

Hence σ_x distributions were derived by summation of the above expressions.

APPENDIX B

SERIES SOLUTIONS FOR PLATE EQUATIONS INCLUDING SHEAR DEFORMATION

Two alternative series solutions, based on the work of Robinson[17] and Salerno and Goldberg[39], were programmed for the purposes of establishing the practical significance of shear deformation in relation to deflexions in the double-bottom model, and also to give check values for the finite difference solutions. This Appendix outlines the derivation of the series, the programs for the solution of which were written for the University of London Atlas Computer as part of the present work.

The basic difference between the two solutions is that Salerno and Goldberg attempt a more rigorous satisfaction of the simply supported boundary condition. The results in Table 6 show that the effect is insignificant.

Except where noted otherwise, the notation used conforms to that in the main text. In both solutions the origin of the co-ordinate axes is taken at the corner of the plate and not at the centre as shown in Figure 49.

1. ROBINSON'S SOLUTION

This is a solution for Libove and Batdorf's[10] equations for rectangular orthotropic sandwich plates under combined transverse and in-plane load. The plate properties are implicitly constant throughout the plate.

The particular loading considered is uniform in-plane load in the x direction, N_x, and uniform transverse load, defined by the following double Fourier series :

$$q = \sum_{m=1,3,5\ldots}^{\infty} \sum_{n=1,3,5\ldots}^{\infty} q_{mn} \sin \frac{m\pi x}{a} \sin \frac{n\pi y}{b}$$

Where: $q_{mn} = 16q/(\pi^2 mn)$

The following series were assumed to describe the three variables, w, Q_x and Q_y, in the governing equations (1), given in Chapter 4.

$$w = \sum_{m=1,3,5\ldots}^{\infty} \sum_{n=1,3,5\ldots}^{\infty} A_{mn} \sin \frac{m\pi x}{a} \sin \frac{n\pi y}{b}$$

$$Q_x = \sum_{m=1,3,5\ldots}^{\infty} \sum_{n=1,3,5\ldots}^{\infty} B_{mn} \cos \frac{m\pi x}{a} \sin \frac{n\pi y}{b}$$

$$Q_y = \sum_{m=1,3,5\ldots}^{\infty} \sum_{n=1,3,5\ldots}^{\infty} C_{mn} \sin \frac{m\pi x}{a} \cos \frac{n\pi y}{b}$$

These implicitly satisfy the following simply supported boundary conditions.

At $x = 0, a$: $w = 0$

$$M_x = 0$$

$$\frac{\partial w}{\partial y} - \frac{Q_y}{S_y} = 0 \rightarrow Q_y = 0$$

At $y = 0, b$: $w = 0$

$$M_y = 0$$

$$\frac{\partial w}{\partial x} - \frac{Q_x}{S_x} = 0 \rightarrow Q_x = 0$$

Infinite tangential rotational restraint is implicit in the above equations

($K_{3x} = K_{3y} = \infty$). The constants A_{mn}, B_{mn} and C_{mn} can be obtained by substituting the above series into equations (1) and solving term by term, to give:

$$A_{mn} = -q_{mn}\frac{W_{mn}}{Z_{mn}}, \quad B_{mn} = q_{mn}\frac{X_{mn}}{Z_{mn}}, \quad C_{mn} = -q_{mn}\frac{Y_{mn}}{Z_{mn}}$$

Where:

$$W_{mn} = a_1m^4 + a_2m^2 + a_3m^2n^2 + a_4n^2 + a_5n^4 - 1$$

$$X_{mn} = b_1m^5 + b_2m^3 + b_3m^3n^2 + b_4mn^2 + b_5mn^4$$

$$Y_{mn} = c_1m^4n + c_2m^2n + c_3m^2n^3 + c_4n^3 + c_5n^5$$

Defining:

$$P_y = 4\pi^2D_y/(b^2(1-\mu_x\mu_y))$$

$$r = P_y/(4S_y)$$

$$k = D_x/D_y$$

$$\varepsilon = S_x/S_y$$

$$\eta = D_{xy}/D_y$$

$$\beta = a/b$$

$$\mu_x = \mu$$

$$\mu_y = \mu D_y/D_x \quad \text{(from Maxwell's reciprocal law)}$$

Then:

$$\alpha_1 = -\alpha_1 k\eta/(2\beta^4)$$

$$\alpha_2 = -\, r(k/\varepsilon + \eta(k-\mu^2)/(2k))/\beta^2$$

$$\alpha_3 = -\alpha_1(k-\eta\mu)/\beta^2$$

$$\alpha_4 = -\, r(1+\eta(k-\mu^2)/(2k\varepsilon))$$

$$\alpha_5 = -\alpha_1\eta/2$$

$$\alpha_1 = r^2(1-\mu^2/k)/\varepsilon$$

$$b_1 = \alpha_3 k\eta/(2\beta^4)$$

$$b_2 = \alpha_2 k/\beta^2$$

$$b_3 = \alpha_3(k-\eta\mu)/\beta^2$$

$$b_4 = \alpha_2(\eta(k-\mu^2)/k + \mu)$$

$$b_5 = \alpha_3\eta/2$$

$$\alpha_2 = P_y\pi/(4b\beta)$$

$$\alpha_3 = \alpha_2 r(k-\mu^2)/k$$

$$c_1 = -\alpha_5\, k\eta/(2\beta^4)$$

$$c_2 = -\alpha_4(\eta(k-\mu^2)/(k\beta^2) + \mu/\beta^2)$$

$$c_3 = -\alpha_5(k-\eta\mu)/\beta^2$$

$$c_4 = -\alpha_4$$

$$c_5 = -\alpha_5\eta/2$$

$$\alpha_4 = P_y\pi/(4b)$$

$$\alpha_5 = \alpha_4\, r(k-\mu^2)/(\varepsilon\, k)$$

Hence deflexions and shears were computed by the evaluation of the preceding coefficients and summation of respective series. In addition, moments were computed from the following relationships, derived by

substituting the series expressions into equations (41) given in Appendix C.

$$M_x = \sum_{m=1,3,5\ldots}^{\infty} \sum_{n=1,3,5\ldots}^{\infty} (f_1 m^6 + f_2 m^4 + f_3 m^4 n^2 + f_4 m^2 n^2 + f_5 m^2 n^4 + f_6 n^4 + f_7 n^6 + f_8 m^2 + f_9 n^2) \frac{q_{mn}}{Z_{mn}} \sin \frac{m\pi x}{a} \sin \frac{n\pi y}{b}$$

$$M_y = \sum_{m=1,3,5\ldots}^{\infty} \sum_{n=1,3,5\ldots}^{\infty} (f_{10} m^6 + f_{11} m^4 + f_{12} m^4 n^2 + f_{13} m^2 n^2 + f_{14} m^2 n^4 + f_{15} n^4 + f_{16} n^6 + f_{17} m^2 + f_{18} n^2) \frac{q_{mn}}{Z_{mn}} \sin \frac{m\pi x}{a} \sin \frac{n\pi y}{b}$$

$$M_{xy} = \sum_{m=1,3,5\ldots}^{\infty} \sum_{n=1,3,5\ldots}^{\infty} (f_{19} m^5 n + f_{20} m^3 n + f_{21} m^3 n^3 + f_{22} m n^3 + f_{23} m n^5 + f_{24} m n) \frac{q_{mn}}{Z_{mn}} \cos \frac{m\pi x}{a} \cos \frac{n\pi y}{b}$$

Where:

$$f_1 = e_1 a_1 + e_3 b_1$$

$$f_2 = e_1 a_2 + e_3 b_2$$

$$f_3 = e_1 a_3 + e_2 a_1 + e_3 b_3 + e_4 c_1$$

$$f_4 = e_1 a_4 + e_2 a_2 + e_3 b_4 + e_4 c_2$$

$$f_5 = e_1 a_5 + e_2 a_3 + e_3 b_5 + e_4 c_3$$

$$f_6 = e_2 a_4 + e_4 c_4$$

$$f_7 = e_2 a_5 + e_4 c_5$$

$$f_8 = -e_1$$

$$f_9 = -e_2$$

$$e_1 = -\alpha_6\alpha_7^2$$
$$e_2 = -\alpha_6\alpha_8^2\mu$$
$$e_3 = -\alpha_6\alpha_7/S_x$$
$$e_4 = \alpha_6\alpha_8\mu/S_y$$

$$\alpha_6 = D_x/(1-\mu^2)$$
$$\alpha_7 = \pi/a$$
$$\alpha_8 = \pi/b$$

$$f_{10} = e_6a_1 + e_8b_1$$
$$f_{11} = e_6a_2 + e_8b_2$$
$$f_{12} = e_5a_1 + e_6a_3 + e_7c_1 + e_8b_3$$
$$f_{13} = e_5a_2 + e_6a_4 + e_7c_2 + e_8b_4$$
$$f_{14} = e_5a_3 + e_6a_5 + e_7c_3 + e_8b_5$$
$$f_{15} = e_5a_4 + e_7c_4$$
$$f_{16} = e_5a_5 + e_7c_5$$
$$f_{17} = -e_6$$
$$f_{18} = -e_5$$

$$e_5 = -\alpha_{10}\alpha_8^2$$
$$e_6 = \alpha_{10}\alpha_7^2\mu$$
$$e_7 = \alpha_{10}\alpha_8/S_y$$
$$e_8 = -\alpha_{10}\alpha_7\mu/S_x$$

$$\alpha_{10} = D_y/(1-\mu^2)$$

$$f_{19} = e_9a_1 + e_{10}c_1 + e_{11}b_1$$
$$f_{20} = e_9a_2 + e_{10}c_2 + e_{11}b_2$$

$$f_{21} = e_9 a_3 + e_{10} c_3 + e_{11} b_3$$
$$f_{22} = e_9 a_4 + e_{10} c_4 + e_{11} b_4$$
$$f_{23} = e_9 a_5 + e_{10} c_5 + e_{11} b_5$$
$$f_{24} = -e_9$$

$$e_9 = -\alpha_7 \alpha_8 D_{xy}$$
$$e_{10} = \alpha_7 D_{xy}/(2S_y)$$
$$e_{11} = -\alpha_8 D_{xy}/(2S_x)$$

Solutions for deflexion, shears and moments were checked against isotropic plate solutions for negligible shear deformation from Reference 36, and also against solutions for shear-orthotropic plates including shear deformation from Reference 16. Agreement was quite satisfactory.

For plate properties of the order of those for the double-bottom model it was found that shear deformation accounted for about 30% of the total deflexion. This showed the practical significance of shear deformation and indicated the desirability of further investigation into the effect of shear deformation on plate behaviour, for alternative boundary conditions.

2. SALERNO AND GOLDBERG'S SOLUTION

This is a Levy type solution of Reissner's equations[12] for the case of simply supported rectangular homogeneous isotropic plates under transverse load. These equations are the same as Libove and Batdorf's if the terms relating to stress and strain normal to the plane of the plate are removed. In the following presentation Salerno and Goldberg's solution is modified for the case of non-homogeneous plates and the notation is modified to

conform to the preceding theory.

Assuming infinite flexual stiffness normal to the plane of the plate, Reissner's equations are as follows:

Governing equations:

$$\frac{\partial Q_x}{\partial x} + \frac{\partial Q_y}{\partial y} = - q \tag{7}$$

$$Q_x - \frac{(1-\mu)D}{2C_s} \nabla^2 Q_x = -D \frac{\partial \nabla^2 w}{\partial x} - \frac{(1+\mu)D}{2C_s} \frac{\partial q}{\partial x} \tag{8}$$

$$Q_y - \frac{(1-\mu)D}{2C_s} \nabla^2 Q_y = -D \frac{\partial \nabla^2 w}{\partial y} - \frac{(1+\mu)D}{2C_s} \frac{\partial q}{\partial y} \tag{9}$$

Where: $C_s = S_x = S_y$

$$\nabla^2 = \frac{\partial^2}{\partial x^2} + \frac{\partial^2}{\partial y^2}$$

Moments:

$$M_x = -D\left(\frac{\partial^2 w}{\partial x^2} + \mu \frac{\partial^2 w}{\partial y^2}\right) + \frac{(1-\mu)D}{C_s} \frac{\partial Q_x}{\partial x} - \frac{\mu D}{C_s} q \tag{10}$$

$$M_y = -D\left(\frac{\partial^2 w}{\partial y^2} + \mu \frac{\partial^2 w}{\partial x^2}\right) + \frac{(1-\mu)D}{C_s} \frac{\partial Q_y}{\partial y} - \frac{\mu D}{C_s} q \tag{11}$$

$$M_{xy} = -(1-\mu)D \frac{\partial^2 w}{\partial x \partial y} + \frac{(1-\mu)D}{2C_s}\left(\frac{\partial Q_x}{\partial y} + \frac{\partial Q_y}{\partial x}\right) \tag{12}$$

Eliminating Q_x and Q_y from equations (7,8,9) gives:

$$D \nabla^4 w = q - \frac{D}{C_s} \nabla^2 q \tag{13}$$

Where: $\nabla^4 = \nabla^2 \nabla^2$

Salerno and Goldberg separate the solution into two main parts.

Firstly they use a stress function approach to derive solutions for Q_x and Q_y satisfying equations (7,8,9) in terms of w, q and four constants. Secondly they define a deflexion function, $w = f(x,y)$, undetermined in y and satisfying the boundary conditions on $x = O,a$. They use equation (13) to derive an expression for the y function which involves two coefficients which, together with the coefficients in the shear solutions, are then eliminated using conditions of symmetry and boundary conditions.

Shear Solution:

Particular integrals (satisfying equations (7,8,9)) are given by:

$$Q_{x1} = -D\frac{\partial \nabla^2 w}{\partial x} - \frac{D}{C_s}\frac{\partial q}{\partial x} \qquad (14)$$

$$Q_{y1} = -D\frac{\partial \nabla^2 w}{\partial y} - \frac{D}{C_s}\frac{\partial q}{\partial y} \qquad (15)$$

Where: $$Q_x = Q_{x1} + Q_{x2} \qquad (16)$$

$$Q_y = Q_{y1} + Q_{y2} \qquad (17)$$

In which Q_{x2} and Q_{y2} are the complementary functions which, in order to satisfy the homogeneous parts of equations (7,8,9), are given by a stress function, ϕ, such that:

$$Q_{x2} = \frac{\partial \phi}{\partial y} \qquad (18)$$

$$Q_{y2} = -\frac{\partial \phi}{\partial x} \qquad (19)$$

Where: $$\phi - k^2 \nabla^2 \phi = O \qquad (20)$$

In which: $k^2 = (1-\mu)D/(2C_s)$

The solution of (20) is:

$$\phi = (C_1 \sin px + C_2 \cos px) \cosh \eta y + (C_3 \sin px + C_4 \cos px) \sinh \eta y \quad (21)$$

Where: $\eta^2 = 1/k^2 + p^2$

Hence:

$$Q_x = -D \frac{\partial \nabla^2 w}{\partial x} - \frac{D}{C_s} \frac{\partial q}{\partial x} + \eta \left[(C_1 \sin px + C_2 \cos px) \sinh \eta y + (C_3 \sin px + C_4 \cos px) \cosh \eta y \right] \quad (22)$$

$$Q_y = -D \frac{\partial \nabla^2 w}{\partial y} - \frac{D}{C_s} \frac{\partial q}{\partial y} + p \left[(C_1 \cos px - C_2 \sin px) \cosh \eta y + (C_3 \cos px - C_4 \sin px) \sinh \eta y \right] \quad (23)$$

Deflexion Solution:

In addition to the simply supported boundary conditions satisfied by Robinson's solution, Salerno and Goldberg attempt to satisfy a curvature condition which reflects the effect of shear deformation, namely, normal curvature $\neq 0$.

For this purpose they choose a deflexion function of the form:

$$w = \frac{q}{24D} \sum_{1,3,5\ldots}^{\infty} \left[\frac{96}{av^2} Y(y) \sin vx + \frac{12D}{C_s} (ax - x^2) \right] \quad (24)$$

Where: $v = m\pi/a$, $m = 1,3,5\ldots..$

Satisfaction of the non-homogeneous governing equation (13) defines the y function. Substituting (24) into (13) gives:

$$\frac{d^4Y}{dy^4} - 2v^2 \frac{d^2Y}{dy^2} + v^4 Y = v^4 \tag{25}$$

The solution for which is:

$$Y = C_5 \cosh vy + C_6 vy \sinh vy + 1 \tag{26}$$

Hence the deflected shape is given by (26) and (24) and the shear forces by (26), (24), (22) and (23) thus:

$$Q_x = -\frac{4q}{a} \sum_{1,3,5\ldots}^{\infty} \frac{1}{v^4}\left[\frac{d^2Y}{dy^2} - v^2Y\right] \cos vx$$

$$+ \sum \eta C_4 \cos px \cosh \eta y \tag{27}$$

$$Q_y = -\frac{4q}{a} \sum_{1,3,5\ldots}^{\infty} \frac{1}{v^5}\left[\frac{d^3Y}{dy^3} - v^2 \frac{dY}{dy}\right] \sin vx$$

$$+ \sum p C_4 \sin px \sinh \eta y \tag{28}$$

Where $C_1 = C_2 = C_3 = O$ from symmetry. The remaining constants can now be eliminated from satisfaction of the boundary conditions.

On $x = O, a$: $w = O$ (29)

$M_x = O$ (30)

$$\frac{\partial w}{\partial y} - \frac{Q_y}{C_s} = O \tag{31}$$

(29) and (30 are automatically satisfied.

(31) gives:

$$p = \frac{m\pi}{a} - v$$

On $y = O, b$: $w = O$ (32)

$M_y = O$ (33)

$$\frac{\partial w}{\partial x} - \frac{Q_x}{C_s} = O \quad (34)$$

(32) gives:

$$C_5 \cosh \alpha_m + C_6 \alpha_m \sinh \alpha_m + 1 + \frac{D}{C_s} v^2 = O \quad (35)$$

Where:

$$\alpha_m = vb/2$$

(33) gives:

$$C_6 = 1/(2 \cosh \alpha_m) \quad (36)$$

(34) gives:

$$2C_6 \cosh \alpha_m - \frac{av^2}{4p} C_4 \eta \cosh \left(\frac{\eta b}{2}\right) - 1 = O \quad (37)$$

Substituting (36) into (35) gives:

$$C_5 = -(1 + \frac{Dv^2}{C_s} + \alpha_m \tanh \alpha_m/2)/\cosh \alpha_m \quad (38)$$

Substituting (36) into (37) gives:

$$C_4 = O \quad (39)$$

Hence:

$$w = \frac{4q}{aD} \sum_{1,3,5\ldots}^{\infty} \left[\frac{1}{v^5} (1 + C_5 \cosh vy + C_6 vy \sinh vy) + \frac{D}{C_s v^3} \right] \sin vx$$

Where: $$(x^2 - ax) = -\frac{8}{a} \sum_{1,3,5\ldots}^{\infty} \frac{1}{v^3} \sin vx$$

$$Q_x = -\frac{4q}{a} \sum_{1,3,5\ldots}^{\infty} \frac{1}{v^2} \left[2C_6 \cosh vy - 1\right] \cos vx$$

$$Q_y = -\frac{4q}{a} \sum_{1,3,5\ldots}^{\infty} \frac{1}{v^2} \left[2C_6 \sinh vy\right] \sin vx$$

$$M_x = \frac{4q}{a} \sum_{1,3,5\ldots}^{\infty} \left[\frac{1}{v^3} (1 + C_5 \cosh vy + C_6 vy \sinh vy)\right.$$

$$- \frac{\mu}{v^3} (C_5 \cosh vy + 2C_6 \cosh vy + C_6 vy \sinh vy)$$

$$\left. + \frac{(1-\mu)D}{v\, C_s} (2C_6 \cosh vy)\right] \sin vx$$

$$M_y = \frac{4q}{a} \sum_{1,3,5\ldots}^{\infty} \left[\frac{\mu}{v^3} (1 + C_5 \cosh vy + C_6 vy \sinh vy)\right.$$

$$- \frac{1}{v^3} (C_5 \cosh vy + 2C_6 \cosh vy + C_6 vy \sinh vy)$$

$$\left. - \frac{(1-\mu)D}{v\, C_s} (2C_6 \cosh vy)\right] \sin vx$$

$$M_{xy} = -\frac{(1-\mu)4q}{a} \sum_{1,3,5\ldots}^{\infty} \left[\frac{1}{v^3} ((C_5 + C_6) \sinh vy + C_6 vy \cosh vy)\right.$$

$$\left. + \frac{2D}{v C_s} C_6 \sinh vy\right] \cos vx$$

Hence deflexions, shears and moments could be computed at various points throughout a plate by calculating C_5 and C_6 and summing the respective series to any desired degree of accuracy. It was found that Salerno and Goldberg's and Robinson's solutions differed only slightly, near the boundaries, and agreed almost exactly at the centre of the plate, as shown in Table 6.

Salerno and Goldberg's solution exhibited a slight lack of symmetry in problems where the behaviour was implicitly symmetrical.

APPENDIX C

DETAILS OF FINITE DIFFERENCE SOLUTION OF MIXED VARIABLE ORTHOTROPIC PLATE EQUATIONS INCLUDING TRANSVERSE SHEAR DEFORMATION

(GENERALISED BOUNDARY CONDITIONS)

1. OUTLINE OF DERIVATION OF EQUATIONS[10]

1.1 Displacement Equations

Shear deformation is accounted for by defining the shear contribution to slope of the middle surface of the plate along the x and y axes as follows:

$$\frac{\partial w}{\partial x} = \gamma_x' = \frac{Q_x}{S_x}$$

$$\frac{\partial w}{\partial y} = \gamma_y' = \frac{Q_y}{S_y}$$

These expressions give additional terms to be added to the ordinary plate theory expressions for curvature and twist in terms of forces for an internal plate element (Figure 48) thus:

$$\left.\begin{aligned}
\frac{\partial^2 w}{\partial x^2} &= -\frac{M_x}{D_x} + \mu_y \frac{M_y}{D_y} + \frac{1}{S_x}\frac{\partial Q_x}{\partial x} \qquad (a)\\
\frac{\partial^2 w}{\partial y^2} &= -\frac{M_y}{D_y} + \mu_x \frac{M_x}{D_x} + \frac{1}{S_y}\frac{\partial Q_y}{\partial y} \qquad (b)\\
\frac{\partial^2 w}{\partial x \partial y} &= \frac{M_{xy}}{D_{xy}} + \frac{1}{2}\frac{1}{S_x}\frac{\partial Q_x}{\partial y} + \frac{1}{2}\frac{1}{S_y}\frac{\partial Q_y}{\partial x} \qquad (c)
\end{aligned}\right\} \quad (40)$$

Solving in terms of moments gives:

$$\left.\begin{aligned} M_x &= -\frac{D_x}{1-\mu_x\mu_y}\left[\frac{\partial}{\partial x}\left(\frac{\partial w}{\partial y}-\frac{Q_x}{S_x}\right)+\mu_y\frac{\partial}{\partial y}\left(\frac{\partial w}{\partial y}-\frac{Q_y}{S_y}\right)\right] && \text{(a)}\\ M_y &= -\frac{D_y}{1-\mu_x\mu_y}\left[\frac{\partial}{\partial y}\left(\frac{\partial w}{\partial y}-\frac{Q_y}{S_y}\right)+\mu_x\frac{\partial}{\partial x}\left(\frac{\partial w}{\partial x}-\frac{Q_x}{S_x}\right)\right] && \text{(b)}\\ M_{xy} &= \tfrac{1}{2}D_{xy}\left[\frac{\partial}{\partial x}\left(\frac{\partial w}{\partial y}-\frac{Q_y}{S_y}\right)+\frac{\partial}{\partial y}\left(\frac{\partial w}{\partial x}-\frac{Q_x}{S_x}\right)\right] && \text{(c)} \end{aligned}\right\} \quad (41)$$

1.2 Equilibrium Equations

As for ordinary plate theory (Reference 36)

Equilibrium of vertical forces requires:

$$\left.\begin{aligned} &\frac{\partial^2 M_x}{\partial x^2}-2\frac{\partial^2 M_{xy}}{\partial x\partial y}+\frac{\partial^2 M_y}{\partial y^2}=-\left(q+N_x\frac{\partial^2 w}{\partial x^2}+N_y\frac{\partial^2 w}{\partial y^2}+2N_{xy}\frac{\partial^2 w}{\partial x\partial y}\right) && \text{(a)}\\ &\text{Equilibrium of moments about y and x axes requires:}\\ &Q_x=-\frac{\partial M_{xy}}{\partial y}+\frac{\partial M_x}{\partial x} && \text{(b)}\\ &Q_y=-\frac{\partial M_{xy}}{\partial x}+\frac{\partial M_y}{\partial y} && \text{(c)} \end{aligned}\right\} \quad (42)$$

1.3 Governing Differential Equations

The governing equations, (1), are given in full in Section 1.1 of Chapter 4. Equation (1), (a) was derived by substituting for derivatives of moments in (42), (a) from (42), (b) and (c). Equations (1), (b) and (c)

were derived by substituting for derivatives of moments in (42), (b) and (c) from (41), (a), (b) and (c). This gave three independent mixed variable (w, Q_x, Q_y) equations. It is possible to reduce these equations to three independent single variable equations but this places restrictions on the boundary conditions which can be treated, because only the simply supported condition is amenable to reduction to a single variable. Solution of this single variable form of the equation is discussed further in Appendix D.

1.4 Boundary Conditions

For a system of edge forces denoted by $\overline{M}_x$, $\overline{M}_y$ and $\overline{Q}_x$ along those boundaries parallel to the y axis, and $\overline{M}_y$, $\overline{M}_{xy}$ and $\overline{Q}_y$ along those boundaries parallel to the x axis, Libove and Batdorf[10] derived the expression for the total potential energy of the system. Minimisation of this expression gave the following boundary conditions relating internal and external edge forces:

$$\left.\begin{aligned} \text{At } x = \pm a/2: \quad Q_x + N_x \frac{\partial w}{\partial x} + N_{xy} \frac{\partial w}{\partial y} &= \overline{Q}_x \qquad \text{(a)} \\ M_x &= \overline{M}_x \qquad \text{(b)} \\ M_{xy} &= \overline{M}_{xy} \qquad \text{(c)} \end{aligned}\right\} \tag{43}$$

$$\left.\begin{aligned} \text{At } y = \pm b/2: \quad Q_y + N_y \frac{\partial w}{\partial y} + N_{xy} \frac{\partial w}{\partial x} &= \overline{Q}_y \qquad \text{(a)} \\ M_y &= \overline{M}_y \qquad \text{(b)} \\ M_{xy} &= \overline{M}_{xy} \qquad \text{(c)} \end{aligned}\right\} \tag{44}$$

Substituting for moments from equations (41) and relating the

external forces to a discrete spring system gives equations (3) and (4) (Chapter 4).

1.5 Equations in Non-Dimensional Form

By making the substitutions given in section 1.4 of Chapter 4, the equations become:

Governing equations:

$$\left.\begin{aligned} &A1\frac{\partial^2 W}{\partial X^2} + A2\frac{\partial^2 W}{\partial Y^2} + A3\frac{\partial^2 W}{\partial X \partial Y} + A4\frac{\partial V_x}{\partial X} + A5\frac{\partial V_y}{\partial Y} = AO && (a)\\ &A6\frac{\partial^3 W}{\partial X^3} + A7\frac{\partial^3 W}{\partial X \partial Y^2} + A8\frac{\partial^2 V_x}{\partial Y^2} + A9\frac{\partial^2 V_x}{\partial X^2} + A10\ V_x + A11\frac{\partial^2 V_y}{\partial X \partial Y} = O && (b)\\ &A12\frac{\partial^3 W}{\partial Y^3} + A13\frac{\partial^3 W}{\partial X^2 \partial Y} + A14\frac{\partial^2 V_x}{\partial X \partial Y} + A15\frac{\partial^2 V_y}{\partial X^2} + A16\frac{\partial^2 V_y}{\partial Y^2} + A17\ V_y = O && (c)\end{aligned}\right\} \quad (45)$$

Boundary conditions:

At $x = a/2$:

$$\left.\begin{aligned} &A21\ W + A22\frac{\partial W}{\partial X} + A23\frac{\partial W}{\partial Y} + A24\ V_x = O && (a)\\ &A25\frac{\partial^2 W}{\partial X^2} + A26\frac{\partial^2 W}{\partial Y^2} + A27\frac{\partial W}{\partial X} + A28\ V_x + A29\frac{\partial V_x}{\partial X} + A30\frac{\partial V_y}{\partial Y} = O && (b)\\ &A31\frac{\partial^2 W}{\partial X \partial Y} + A32\frac{\partial W}{\partial Y} + A33\frac{\partial V_x}{\partial Y} + A34\ V_y + A35\frac{\partial V_y}{\partial X} = O && (c)\end{aligned}\right\} \quad (46)$$

At $y = b/2$:

$$\left.\begin{aligned} &A41\ W + A42\frac{\partial W}{\partial X} + A43\frac{\partial W}{\partial Y} + A44\ V_y = O && (a)\\ &A45\frac{\partial^2 W}{\partial X^2} + A46\frac{\partial^2 W}{\partial Y^2} + A47\frac{\partial W}{\partial Y} + A48\frac{\partial V_x}{\partial X} + A49\ V_y + A5O\frac{\partial V_y}{\partial Y} = O && (b)\\ &A51\frac{\partial^2 W}{\partial X \partial Y} + A52\frac{\partial W}{\partial X} + A53\ V_x + A54\frac{\partial V_x}{\partial Y} + A55\frac{\partial V_y}{\partial X} = O && (c)\end{aligned}\right\} \quad (47)$$

Where:

$AO = -q$

$A1 = N'_x$

$A2 = \varepsilon^2 N'_y/\alpha$

$A3 = 2N'_{xy}$

$A4 = 1$

$A5 = 1$

$A6 = -1/(1-\mu_x\mu_y)$

$A7 = -\beta - \mu_y/(1-\mu_x\mu_y)$

$A8 = \beta/(2\gamma_x)$

$A9 = 1/(\gamma_x(1-\mu_x\mu_y))$

$A1O = -1$

$A11 = \alpha\beta/(2\varepsilon^2\gamma_y) + \alpha\mu_y/(\varepsilon^2\gamma_y(1-\mu_x\mu_y))$

$$A12 = -1/(\alpha(1-\mu_x\mu_y))$$

$$A13 = -\beta - \mu_x/(\alpha(1-\mu_x\mu_y))$$

$$A14 = \beta/(2\gamma_x) + \mu_x/(\alpha\gamma_x(1-\mu_x\mu_y))$$

$$A15 = \alpha\beta/(2\varepsilon^2\gamma_y)$$

$$A16 = 1/(\varepsilon^2\gamma_y(1-\mu_x\mu_y))$$

$$A17 = 1$$

$$A21 = K_{1x}$$

$$A22 = N'_x$$

$$A23 = N'_{xy}$$

$$A24 = 1$$

$$A25 = 1$$

$$A26 = \mu_y$$

$$A27 = K_{2x}(1-\mu_x\mu_y)$$

$$A28 = -K_{2x}(1-\mu_x\mu_y)/\gamma_x$$

$$A29 = -1/\gamma_x$$

$$A30 = -\alpha\mu_y/(\varepsilon^2\gamma_y)$$

$$A31 = \beta$$

$$A32 = K_{3x}$$

$$A33 = -\beta/(2\gamma_x)$$

$$A34 = -K_{3x}\alpha/(\varepsilon^2\gamma_y)$$

$$A35 = -\alpha\beta/(2\varepsilon^2\gamma_y)$$

$$A41 = K_{1y}\,\varepsilon^3/\alpha$$

$$A42 = N'_{xy}$$

$$A43 = \varepsilon^2 N'_y/\alpha$$

$$A44 = 1$$

$$A45 = \mu_x/\alpha$$

$$A46 = 1/\alpha$$

$$A47 = K_{2y}\,\varepsilon\,(1-\mu_x\mu_y)/\alpha$$

$$A48 = -\mu_x/(\alpha\gamma_x)$$

$$A49 = -K_{2y}(1-\mu_x\mu_y)/(\varepsilon\gamma_y)$$

$$A50 = -1/(\varepsilon^2\gamma_y)$$

$$A51 = \beta$$

$$A52 = K_{3y}\,\varepsilon/\alpha$$

$$A53 = -K_{3y}\,\varepsilon/(\alpha\gamma_x)$$

$$A54 = -\beta/(2\gamma_x)$$

$$A55 = -\alpha\beta/(2\,\varepsilon^2\gamma_y)$$

2. FINITE DIFFERENCE APPROXIMATIONS TO THE DERIVATIVES

The computer program incorporated a subroutine for the derivation of finite difference coefficients based on the LaGrangian polynomial for five points. This gave the facility for using a graded mesh which it was proposed to use for cases of patch loading. It was found, however, that this did not overcome problems associated with discontinuities in load distribution and all solutions given in this thesis were for uniform mesh along each axis.

For the curve shown in Figure 144 the LaGrangian polynomial is as follows:

Denote:

$$a_o = x - x_o$$
$$a_1 = x - x_1$$
$$a_2 = x - x_2$$
$$a_3 = x - x_3$$
$$a_4 = x - x_4$$

And:

$$k_o = (x_o-x_1)(x_o-x_2)(x_o-x_3)(x_o-x_4)$$
$$k_1 = (x_1-x_o)(x_1-x_2)(x_1-x_3)(x_1-x_4)$$
$$k_2 = (x_2-x_o)(x_2-x_1)(x_2-x_3)(x_2-x_4)$$
$$k_3 = (x_3-x_o)(x_3-x_1)(x_3-x_2)(x_3-x_4)$$
$$k_4 = (x_4-x_o)(x_4-x_1)(x_4-x_2)(x_4-x_3)$$

Then:

$$w = (a_1a_2a_3a_4/k_o)w_o + (a_oa_2a_3a_4/k_1)w_1 + (a_oa_1a_3a_4/k_2)w_2 + (a_oa_1a_2a_4/k_3)w_3 + (a_oa_1a_2a_3/k_4)w_4$$

Hence, general expressions for the required derivatives:

Denote:

$$b_o = a_oa_1a_2, \quad b_5 = a_oa_3a_4$$
$$b_1 = a_oa_1a_3, \quad b_6 = a_1a_2a_3$$
$$b_2 = a_oa_1a_4, \quad b_7 = a_1a_2a_4$$
$$b_3 = a_oa_2a_3, \quad b_8 = a_1a_3a_4$$
$$b_4 = a_oa_2a_4, \quad b_9 = a_2a_3a_4$$

Then:

$$\frac{\partial w}{\partial x} = ((b_9+b_8+b_7+b_6)/k_1)w_o + ((b_3+b_4+b_5+b_9)/k_1)w_1$$

$$+ ((b_1+b_2+b_5+b_8)/k_2)w_2 + ((b_o+b_2+b_4+b_7)/k_3)w_3$$

$$+ ((b_o+b_1+b_3+b_6)/k_4)w_4$$

Denote:

c_o	=	$a_o a_1$,	c_5	=	$a_1 a_3$
c_1	=	$a_o a_2$,	c_6	=	$a_1 a_4$
c_2	=	$a_o a_3$,	c_7	=	$a_2 a_3$
c_3	=	$a_o a_4$,	c_8	=	$a_2 a_4$
c_4	=	$a_1 a_2$,	c_9	=	$a_3 a_4$

Then:

$$\frac{\partial^2 w}{\partial x^2} = (2(c_4+c_5+c_6+c_7+c_8+c_9)/k_o)w_o$$

$$+ (2(c_1+c_2+c_3+c_7+c_8+c_9)/k_1)w_1$$

$$+ (2(c_o+c_2+c_3+c_5+c_6+c_9)/k_2)w_2$$

$$+ (2(c_o+c_1+c_3+c_4+c_6+c_8)/k_3)w_3$$

$$+ (2(c_o+c_1+c_2+c_4+c_5+c_7)/k_4)w_4$$

And:

$$\frac{\partial^3 w}{\partial x^3} = (6(a_1+a_2+a_3+a_4)/k_o)w_o + (6(a_o+a_2+a_3+a_4)/k_1)w_1$$

$$+ (6(a_o+a_1+a_3+a_4)/k_2)w_2 + (6(a_o+a_1+a_2+a_4)/k_3)w_3$$

$$+ (6(a_o+a_1+a_2+a_3)/k_4)w_4$$

For the particular case of even mesh divisions the preceding expressions give the following solutions for difference coefficients (5 point).

For:

$$\left.\frac{\partial^m w}{\partial x^m}\right|_n = \frac{1}{D^*}(A_o w_o + A_1 w_1 + A_2 w_2 + A_3 w_3 + A_4 w_4)$$

Where:

m = order of the derivative

n = node at which derivative taken

h = length of mesh division

m	n	D*	A_o	A_1	A_2	A_3	A_4
1	O	12 h	-25	48	-36	16	-3
	1	12 h	-3	-10	18	-6	1
	2	12 h	1	-8	O	8	-1
	3	12 h	-1	6	-18	10	3
	4	12 h	3	-16	36	-48	25
2	O	$12\ h^2$	35	-104	114	-56	11
	1	$12\ h^2$	11	-20	6	4	-1
	2	$12\ h^2$	-1	16	-30	16	-1
	3	$12\ h^2$	-1	4	6	-20	11
	4	$12\ h^2$	11	-56	114	-104	35
3	O	$4\ h^3$	-10	36	-48	28	-6
	1	$4\ h^3$	-6	20	-24	12	-2
	2	$4\ h^3$	-2	4	O	-4	2
	3	$4\ h^3$	2	-12	24	-20	6
	4	$4\ h^3$	6	-28	48	-36	10

Table 9

The derivative coefficient notation used in the program is given in Figure 146. Thus, for example, the coefficients for the central difference approximation to $\frac{\partial}{\partial X}$ and $\frac{\partial}{\partial Y}$ for even mesh would be as follows:

$\frac{\partial}{\partial X}$			$\frac{\partial}{\partial Y}$		
EO	=	1/(12 hx),	E15	=	1/(12 hy)
E1	=	-8/(12 hx),	E16	=	-8/(12 hy)
E2	=	O,	E17	=	O
E3	=	8/(12 hx),	E18	=	8/(12 hy)
E4	=	-1/(12 hx),	E19	=	-1/(12 hy)

Where:

hx	=	1/(2 I)
hy	=	1/(2 E J)

3. LOCATION OF SPECIFIC FORMS OF DERIVATIVES

Figure 147 shows the forms of derivatives used at various nodes in a plate quadrant. The two alternative treatments of the corner deficiency (one more unknown than there are equations) are shown. The extrapolation method was based on the assumption that the fourth derivatives of the variables (W, V_x, V_y) along the diagonal were independently zero, i.e. a cubic extrapolation.

For the mesh notation shown in Figure 145 this gives:

$$\frac{\partial^4 w}{\partial r^4} = 24(w_o/k_o + w_1/k_1 + w_2/k_2 + w_3/k_3 + w_4/k_4) = O$$

Where:

$$k_o = (r_o-r_1)(r_o-r_2)(r_o-r_3)(r_o-r_4)$$

$$k_1 = (r_1-r_o)(r_1-r_2)(r_1-r_3)(r_1-r_4)$$

$$k_2 = (r_2-r_o)(r_2-r_1)(r_2-r_3)(r_2-r_4)$$

$$k_3 = (r_3-r_o)(r_3-r_1)(r_3-r_2)(r_3-r_4)$$

$$k_4 = (r_4-r_o)(r_4-r_1)(r_4-r_2)(r_4-r_3)$$

$$r_o = O$$

$$r_1 = \left[(x_1-x_o)^2 + (y_1-y_o)^2\right]^{\frac{1}{2}}$$

$$r_2 = r_1 + \left[(x_2-x_1)^2 + (y_2-y_1)^2\right]^{\frac{1}{2}}$$

$$r_3 = r_2 + \left[(x_3-x_2)^2 + (y_3-y_2)^2\right]^{\frac{1}{2}}$$

$$r_4 = r_3 + \left[(x_4-x_3)^2 + (y_4-y_3)^2\right]^{\frac{1}{2}}$$

For the case of even mesh along each axis the extrapolation equations reduce to the form:

$$w_o - 4w_1 + 6\,w_2 - 4w_3 + w_4 = O$$

4. PLATE EQUATIONS IN FINITE DIFFERENCE FORM

Figure 148 shows the general form of the governing equations and boundary conditions. The coefficients were given by the product of the

appropriate plate constants and derivative coefficients. As two typical examples of the governing equations and boundary conditions, expressions for the coefficients in regions A and B (Figure 147) respectively are given below.

4.1 Governing equations (A - all central differences)

Equation (45),(a)

d_o = E7A1 + E22A2 + FOA3, d_9 = E9A1 + F9A3

d_1 = E8A1 + F1A3, d_{10} = E24A2 + F1OA3

d_2 = E23A2 + F2A3, d_{11} = E5A1 + F11A3

d_3 = E6A1 + F3A3, d_{12} = E2OA2 + F12A3

rest: $d_n = F_nA3$

e_o = E2A4, e_9 = E4A4

e_1 = E3A4, e_{11} = EOA4

e_3 = E1A4,

rest: $e_n = O$

f_o = E17A5, f_{10} = E19A5

f_2 = E18A5, f_{12} = E15A5

f_4 = E16A5,

rest: $f_n = O$

K = AO

Equation (45),(b):

d_o = E12A6 + HOA7, d_9 = E14A6 + H9A7

d_1 = E13A6 + H1A7, d_{11} = E1OA6 + H11A7

d_3 = E11A6 + H3A7 ,

rest: $d_n = H_nA7$

e_o = E22A8 + E7A9 + A1O, e_9 = E9A9

e_1 = E8A9, e_{10} = E24A8

e_2 = E23A8, e_{11} = E5A9

e_3 = E6A9, e_{12} = E2OA8

e_4 = E21A8,

rest: $e_n = O$

$f_n = F_nA11$, $n = O \rightarrow 24$

K = O

Equation (45),(c)

d_o = E27A12 + GOA13, d_{10} = E29A12 + G1OA13

d_2 = E28A12 + G2A13, d_{12} = E25A12 + G12A13

d_4 = E26A12 + G4A13,

rest: $d_n = G_nA13$

$e_n = F_nA14$, $n = O \rightarrow 24$

f_o = E7A15 + E22A16 + A17, f_9 = E9A15

f_1 = E8A15, f_{10} = E24A16

f_2 = E23A16, f_{11} = E5A15

f_3 = E6A15, f_{12} = E2OA16

f_4 = E21A16,

rest: $f_n = O$

$K = O$

4.2 Boundary conditions (B - x derivatives backward, y central)

Equation (46),(a):

d_o = E2A22, d_9 = E4A22

d_1 = A21 + E3A22 + E17A23, d_{11} = EOA22

d_3 = E1A22, d_{14} = E19A23

d_5 = E18A23, d_{19} = E15A23

d_8 = E16A23,

rest: $d_n = O$

e_1 = A24 ; rest: $e_n = O$

$f_n = O$, $n = O \rightarrow 24$

$K = O$

Equation (46),(b):

d_o = E7A25 + E2A27, d_9 = E9A25 + E4A27

d_1 = E8A25 + E22A26 + E3A27, d_{11} = E5A25 + EOA27

d_3 = E6A25 + E1A27, d_{14} = E24A26

d_5 = E23A26, d_{19} = E2OA26

d_8 = E21A26,

rest: $d_n = O$

e_o = E2A29, e_9 = E4A29

e_1 = A28 + E3A29, e_{11} = EOA29

e_3 = E1A29,

rest: e_n = O

f_1 = E17A3O, f_{14} = E19A3O

f_5 = E18A3O, f_{19} = E15A3O

f_8 = E16A3O,

rest: f_n = O

K = O

Equation (46),(c):

d_1 = F1A31 + E17A32, d_{14} = F14A31 + E19A32

d_5 = F5A31 + E18A32, d_{19} = F19A31 + E15A32

d_8 = F8A31 + E16A32,

rest: d_n = F_nA31

e_1 = E17A33, e_{14} = E19A33

e_5 = E18A33, e_{19} = E15A33

e_8 = E16A33,

rest: e_n = O

f_o = E2A35, f_9 = E4A35

f_1 = A34 + E3A35, f_{11} = EOA35

f_3 = E1A35,

rest: f_n = O

K = O

APPENDIX D

DETAILS OF FINITE DIFFERENCE SOLUTION OF SINGLE VARIABLE ORTHOTROPIC PLATE EQUATIONS INCLUDING TRANSVERSE SHEAR DEFORMATION (SIMPLY SUPPORTED EDGES ONLY)

1. INTRODUCTION

It is possible to separate the variables in equations (1) (Chapter 4) to give three independent sixth order equations for the respective variables in terms of q. Any one of these equations can then be solved provided the boundary conditions are expressible in terms of the corresponding variable. Libove and Batdorf[10] derived the single variable form of the governing equations but not the boundary conditions. In order to attempt a single variable solution it was therefore necessary to reduce the mixed boundary conditions to equations in the corresponding variable and it was found that only the simply supported condition was amenable to such treatment.

Having established the required boundary equations, a finite difference solution of the sixth order equation for w was obtained. The shear forces were then obtained by the solution of fourth order equations for Q_x and Q_y respectively, in terms of w. These equations were derived from equations (1),(b) and (1),(c). An alternative approach to the shear solutions would have been to solve the second order equations given by equations (1),(a) and (1),(b), and (1),(a) and (1),(c) for Q_x and Q_y respectively, in terms

of q and w. Although the latter approach would have been simpler to formulate numerically, it was thought to be desirable to keep differential terms on q to a minimum. This was later justified when the sensitivity of solution to discontinuities in transverse loading became evident. Having solved for w, Q_x and Q_y the moments were obtained by direct substitution into equations (41) (Appendix C)

2. EQUATIONS IN TERMS OF w

2.1 Governing equation

The three equations (1) can be solved to obtain a differential equation for w alone in terms of q. This separation is accomplished most easily, for the case in which N_x, N_y and N_{xy} are constant throughout the plate, by treating the three differential equations as though they were algebraic equations and solving for w, Q_x and Q_y by means of determinants. The terms in the determinants are the differential-operator coefficients of w, Q_x and Q_y appearing in the three equations. In expanding these determinants, the rule for multiplication of linear operators must be used. For example:

$$\frac{\partial^2}{\partial y^2}\ \frac{\partial^2}{\partial x \partial y} = \frac{\partial^4}{\partial x \partial y^3}$$

As a result of such a solution, the following differential equation is obtained for w:

$$[D]w = - [M]q \qquad (48)$$

The differential operators are:

$$D = A1\frac{\partial^6}{\partial x^6} + A2\frac{\partial^6}{\partial x^5 \partial y} + A3\frac{\partial^6}{\partial x^4 \partial y^2} + A4\frac{\partial^6}{\partial x^3 \partial y^3} + A5\frac{\partial^6}{\partial x^2 \partial y^4}$$

$$+ A6\frac{\partial^6}{\partial x \partial y^5} + A7\frac{\partial^6}{\partial y^6} + A8\frac{\partial^4}{\partial x^4} + A9\frac{\partial^4}{\partial x^3 \partial y} + A10\frac{\partial^4}{\partial x^2 \partial y^2}$$

$$+ A11\frac{\partial^4}{\partial x \partial y^3} + A12\frac{\partial^4}{\partial y^4} + A13\frac{\partial^2}{\partial x^2} + A14\frac{\partial^2}{\partial x \partial y} + A15\frac{\partial^2}{\partial y^2}$$

$$M = B1\frac{\partial^4}{\partial x^4} + B2\frac{\partial^4}{\partial x^2 \partial y^2} + B3\frac{\partial^4}{\partial y^4} + B4\frac{\partial^2}{\partial x^2} + B5\frac{\partial^2}{\partial y^2} + B6$$

Where:

$A1 = D_{xy}D_x\ X16/(2S_y)$

$A2 = D_{xy}D_x\ N_{xy}/(S_xS_y)$

$A3 = D_{xy}D_x\ X17/(2S_x) + X18\ X16/S_y$

$A4 = 2\ X18\ N_{xy}/(S_xS_y)$

$A5 = D_{xy}D_y\ X16/(2S_y) + X18\ X17/S_x$

$A6 = D_{xy}D_y\ N_{xy}/(S_xS_y)$

$A7 = D_{xy}D_y\ X17/(2S_x)$

$A8 = -D_xX16 - D_{xy}(1-\mu_x\mu_y)N_x/(2S_y)$

$A9 = -2\ N_{xy}(D_{xy}(1-\mu_x\mu_y)/2S_y) + D_x/S_x)$

$A10 = -2D_{xy}(1-\mu_x\mu_y)(1+ N_y/(4\ S_y) + N_x/(4\ S_x))$

$-D_x(\mu_y + N_y/S_x) - D_y(\mu_x + N_x/S_y)$

$A11 = -2N_{xy}(D_{xy}(1-\mu_x\mu_y)/(2S_x) + D_y/S_y)$

$A12 = -D_yX17 - D_{xy}(1-\mu_x\mu_y)N_y/(2S_x)$

$A13 = (1-\mu_x\mu_y)N_x$

$A14 = 2(1-\mu_x\mu_y)N_{xy}$

$A15 = (1-\mu_x\mu_y)N_y$

Where:

$$X16 = 1 + N_x/S_x$$

$$X17 = 1 + N_y/S_y$$

$$X18 = D_x D_y - \mu_y D_x D_{xy}/2 - \mu_x D_y D_{xy}/2$$

And:

$$B1 = D_{xy} D_x/(2 S_x S_y)$$

$$B2 = X18/(S_x S_y)$$

$$B3 = D_{xy} D_y/(2 S_x S_y)$$

$$B4 = -((1-\mu_x \mu_y) D_{xy}/(2 S_y) + D_x/S_x)$$

$$B5 = -((1-\mu_x \mu_y) D_{xy}/(2 S_x) + D_y/S_y)$$

$$B6 = 1 - \mu_x \mu_y$$

2.2 Boundary Conditions

For the co-ordinate system shown in Figure 49 the simply supported boundary conditions are:

At $x = \pm a/2$:

$$w = 0 \qquad (49)$$

$$M_x = 0 \qquad (50)$$

$$\frac{\partial w}{\partial y} - \frac{Q_y}{S_y} = 0 \qquad (51)$$

At $y = \pm b/2$:

$$w = 0 \qquad (52)$$

$$M_y = 0 \qquad (53)$$

$$\frac{\partial w}{\partial x} - \frac{Q_x}{S_x} = 0 \qquad (54)$$

As part of the present work these equations were reduced to functions of the single dependent variable, w, as follows:

At $x = \pm a/2$:

Since the boundary equations are continuous between $y = \pm b/2$,

(49) gives: $$\frac{\partial^n w}{\partial y^n} = 0 \qquad (55)$$

(51) gives: $$Q_y = 0 \qquad (56)$$

$$\frac{\partial^n Q_y}{\partial y^n} = 0 \qquad (57)$$

Substituting into equation (41),(a) for (50), (55) and (57) gives:

$$\frac{\partial Q_x}{\partial x} = S_x \frac{\partial^2 w}{\partial x^2} \qquad (58)$$

Substituting into equation (1),(a) for (58) gives one of the required equations:

$$C1 \frac{\partial^2 w}{\partial x^2} + C2 \frac{\partial^2 w}{\partial x \partial y} = C3 \qquad (59)$$

Where: $C1 = X16$

$C2 = 2N_{xy}/S_x$

$C3 = -q/S_x$

Also:

(58) gives: $$\frac{\partial^2 Q_x}{\partial x \partial y} = S_x \frac{\partial^3 w}{\partial x^2 \partial y} \qquad (60)$$

Substituting for (55), (56), (57) and (6O) in Equation (1),(c) gives:

$$\frac{\partial^2 Q_y}{\partial x^2} = S_y \frac{\partial^3 w}{\partial x^2 \partial y} \qquad (61)$$

$$\frac{\partial^{2+n} Q_y}{\partial x^2 \partial y^n} = S_y \frac{\partial^{3+n} w}{\partial x^2 \partial y^{1+n}} \qquad (62)$$

Hence, the remaining equation on $x = \pm a/2$ is given by eliminating Q_x from (1),(a) and (1),(b) and substituting for (57) and (62), thus:

$$D1 \frac{\partial^4 w}{\partial x^4} + D2 \frac{\partial^4 w}{\partial x^3 \partial y} + D3 \frac{\partial^4 w}{\partial x^2 \partial y^2} + D4 \frac{\partial^4 w}{\partial x \partial y^3}$$

$$+ D5 \frac{\partial^2 w}{\partial x^2} + D6 \frac{\partial^2 w}{\partial x \partial y} = D7 \frac{\partial^2 q}{\partial x^2} + D8 \frac{\partial^2 q}{\partial y^2} + D9q \qquad (63)$$

Where:

$$D1 = -D_x X16/(1-\mu_x \mu_y)$$

$$D2 = -2D_x N_{xy}/((1-\mu_x \mu_y)S_x)$$

$$D3 = -D_{xy} X16/2 - D_x(S_y + N_y)/((1-\mu_x \mu_y)S_x)$$

$$D4 = -D_{xy} N_{xy}/S_x$$

$$D5 = N_x$$

$$D6 = 2N_{xy}$$

$$D7 = D_x/((1-\mu_x \mu_y)S_x)$$

$$D8 = D_{xy}/(2S_x)$$

$$D9 = -1$$

Thus (49), (59) and (63) constitute the required three boundary conditions at $x = \pm a/2$ in terms of the single variable w.

Similarly, the required boundary equations at $y = \pm b/2$ are as follows:

$$w = 0 \tag{52}$$

$$E1 \frac{\partial^2 w}{\partial y^2} + E2 \frac{\partial^2 w}{\partial x \partial y} = E3 \tag{64}$$

$$F1 \frac{\partial^4 w}{\partial y^4} + F2 \frac{\partial^4 w}{\partial y^3 \partial x} + F3 \frac{\partial^4 w}{\partial y^2 \partial x^2} + F4 \frac{\partial^4 w}{\partial y \partial x^3}$$

$$+ F5 \frac{\partial^2 w}{\partial y^2} + F6 \frac{\partial^2 w}{\partial x \partial y} = F7 \frac{\partial^2 q}{\partial y^2} + F8 \frac{\partial^2 q}{\partial x^2} + F9q \tag{65}$$

Where:

$E1 = X17$

$E2 = 2N_{xy}/S_y$

$E3 = -q/S_y$

$F1 = -D_y X17/(1-\mu_x \mu_y)$

$F2 = -2D_y N_{xy}/((1-\mu_x \mu_y)S_y)$

$F3 = -D_{xy}X17/2 - D_y(S_x + N_x)/((1-\mu_x \mu_y)S_y)$

$F4 = -D_{xy} N_{xy}/S_y$

$F5 = N_y$

$F6 = 2N_{xy}$

$F7 = D_y/((1-\mu_x \mu_y)S_y)$

$F8 = D_{xy}/(2 S_y)$

$F9 = -1$

3. FINITE DIFFERENCE APPROXIMATIONS TO THE DERIVATIVES

The simplest possible finite difference approximations were used for all derivatives, thus:

(i) Central differences

(ii) First order (no error terms)

(iii) Even mesh divisions

(iv) Minimum number of points consistent with the order of the derivative.

This gives the following coefficients, for uniaxial derivatives of the form

$$\left.\frac{\partial^m w}{\partial x^m}\right|_n = \frac{1}{D^*} \sum_{r=o}^{q-1} A_r w_r$$

Where:

m = order of derivatives

n = point at which derivative taken

q = number of points

h = length of mesh division

m	n	q	D*	A_o	A_1	A_2	A_3	A_4	A_5	A_6
1	1	3	$1/2h$	-1	O	1				
2	1	3	$1/h^2$	1	-2	1				
3	2	5	$1/2h^3$	-1	2	O	-2	1		
4	2	5	$1/h^4$	1	-4	6	-4	1		
5	3	7	$1/2h^5$	-1	4	-5	O	5	-4	1
6	3	7	$1/h^6$	1	-6	15	-20	15	-6	1

Table 10

The required mixed derivatives were obtained by taking the product of the appropriate uniaxial derivatives.

4. PLATE EQUATIONS IN FINITE DIFFERENCE FORM

Figures 149 and 150 show the general form of the finite difference nets formulated for the governing equations and boundary conditions. The coefficients, given by the product of derivative coefficients and their respective constants are given below. The constants incorporate the appropriate mesh factors:

$$D^* = 1/(h_x^m h_y^n)$$

4.1 Governing equation

$$a_o = -20\,A1 - 12\,A3 - 12\,A5 - 20\,A7 + 6\,A8 + 4\,A10 + 6\,A12 - 2\,A13 - 2\,A15$$

$$a_1 = a_3 = 15\,A1 + 8\,A3 + 6\,A5 - 4\,A8 - 2\,A10 + A13$$

$$a_2 = a_4 = 6\,A3 + 8\,A5 + 15\,A7 - 2\,A10 - 4\,A12$$

$$a_5 = a_7 = 5\,A2 - 4\,A3 + 4\,A4 - 4\,A5 + 5\,A6 - 2\,A9 + A10 - 2\,A11 + A14$$

$$a_6 = a_8 = -5\,A2 - 4\,A3 - 4\,A4 - 4\,A5 - 5\,A6 + 2\,A9 + A\,10 + 2\,A11 - A14$$

$$a_9 = a_{11} = -6\,A1 - 2\,A3 + A8$$

$$a_{10} = a_{12} = -2\,A5 - 6\,A7 + A12$$

$$a_{13} = a_{17} = -4\,A2 + A3 - 2\,A4 + A9$$

$$a_{14} = a_{18} = -2\,A4 + A5 - 4\,A6 + A11$$

$$a_{15} = a_{19} = 2\,A4 + A5 + 4\,A6 - A11$$

$a_{16} = a_{20} = 4\ A2 + A3 + 2\ A4 - A9$

$a_{21} = a_{23} = A1$

$a_{22} = a_{24} = A7$

$a_{25} = -a_{30} = a_{31} = -a_{36} = A2$

$a_{26} = -a_{29} = a_{32} = -a_{35} = A4$

$a_{27} = -a_{28} = a_{33} = -a_{34} = A6$

$b_o = 6\ B1 + 4\ B2 + 6\ B3 - 2\ B4 - 2\ B5 + B6$

$b_1 = b_3 = -4\ B1 - 2\ B2 + B4$

$b_2 = b_4 = -2\ B2 - 4\ B3 + B5$

$b_5 = b_6 = b_7 = b_8 = B2$

$b_9 = b_{11} = B1$

$b_{10} = b_{12} = B3$

4.2 Boundary conditions

At $x = \pm a/2$,	At $y = \pm b/2$
$c_o = 1$,	$c_o = 1$
$d_o = d_2 = d_4 = O$,	$d_o = d_1 = d_3 = O$
$d_1 = d_3 = C1$,	$d_2 = d_4 = E1$
$d_5 = -d_6 = d_7 = -d_8 = C2$,	$d_5 = -d_6 = d_7 = d_8 = E2$
$d_9 = C3$,	
$e_o = e_2 = e_4 = e_{10} = e_{12} = O$,	$e_o = e_1 = e_3 = e_9 = O$
$e_1 = e_3 = -4\ D1 - 2\ D3 + D5$,	$e_2 = e_4 = -4\ F1 - 2\ F3 + F5$

$e_5 = e_7 = -2\,D2 + D3 - 2\,D4 + D6,$ $\quad e_5 = e_7 = -2\,F2 + F3 - 2\,F4 + F6$

$e_6 = e_8 = 2\,D2 + D3 + 2\,D4 - D6,$ $\quad e_6 = e_8 = 2\,F2 + F3 + 2\,F4 - F6$

$e_9 = e_{11} = D1,$ $\quad e_{10} = e_{12} = F1$

$e_{13} = -e_{16} = e_{17} = -e_{20} = D2,$ $\quad e_{13} = -e_{16} = e_{17} = -e_{20} = F4$

$e_{14} = -e_{15} = e_{18} = -e_{19} = D4,$ $\quad e_{14} = -e_{15} = e_{18} = -e_{19} = F2$

$f_o = -2\,D7 - 2\,D8 + D9,$ $\quad f_o = -2\,F7 - 2\,F8 + F9$

$f_1 = f_3 = D7,$ $\quad f_1 = f_3 = F8$

$f_2 = f_4 = D8,$ $\quad f_2 = f_4 = F7$

5. SOLUTION FOR SHEAR FORCES - Q_x

5.1 Equations

Governing Equation

The governing equation for Q_x, given by eliminating Q_y from equations (1),(b) and (1),(c) is as follows:

$$G1\frac{\partial^4 Q_x}{\partial x^4} + G2\frac{\partial^2 Q_x}{\partial x^2} + G3\frac{\partial^4 Q_x}{\partial x^2 \partial y^2} + G4\frac{\partial^2 Q_x}{\partial y^2} + G5\frac{\partial^4 Q_x}{\partial y^4}$$

$$+ G6\,Q_x = G7\frac{\partial^5 w}{\partial x^5} + G8\frac{\partial^3 w}{\partial x^3}$$

$$+ G9\frac{\partial^5 w}{\partial x^3 \partial y^2} + G10\frac{\partial^3 w}{\partial x\,\partial y^2} + G11\frac{\partial^5 w}{\partial x \partial y^4} \qquad (66)$$

For $S_x = S_y = \infty$ and isotropic plate properties this reduces to:

$$Q_x = -D\left(\frac{\partial^3 w}{\partial x^3} + \frac{\partial^3 w}{\partial x \partial y^2}\right)$$

Where:

$$G1 = D_x D_{xy}/(2(1-\mu_x\mu_y)S_x S_y)$$

$$G2 = -D_{xy}/(2S_y) - D_x/((1-\mu_x\mu_y)S_x)$$

$$G3 = X18/((1-\mu_x\mu_y)S_x S_y)$$

$$G4 = -D_{xy}/(2S_x) - D_y/((1-\mu_x\mu_y)S_y)$$

$$G5 = D_y D_{xy}/(2(1-\mu_x\mu_y)S_x S_y)$$

$$G6 = 1$$

$$G7 = D_x D_{xy}/(2(1-\mu_x\mu_y)S_y)$$

$$G8 = -D_x/(1-\mu_x\mu_y)$$

$$G9 = X18/((1-\mu_x\mu_y)S_y)$$

$$G10 = -D_{xy} + \mu_y D_x/(1-\mu_x\mu_y)$$

$$G11 = D_y D_{xy}/(2(1-\mu_x\mu_y)S_y)$$

Boundary Equations

As noted previously, it is possible to derive a second order form of the governing equation for Q_x in terms of q and w. This implies that there is only one boundary condition on each edge as follows:

At $x = \pm a/2$: (as previously derived)

$$H1 \frac{\partial Q_x}{\partial x} = H2 \frac{\partial^2 w}{\partial x^2} \qquad (58)$$

Where:

$$H1 = 1$$

$$H2 = S_x$$

At $y = \pm b/2$:

(52) gives $\dfrac{\partial^n w}{\partial x^n} = O$

Substituting with (54) gives

$$Q_x = O \qquad (67)$$

Since the solution of (66) requires two independent equations on each edge a second equation, which is in fact a general equation and applicable to both edges, was obtained by eliminating Q_y from (1),(a) and (1),(b), thus:

$$J1 \frac{\partial^2 Q_x}{\partial x^2} + J2 \frac{\partial^2 Q_x}{\partial y^2} + J3\, Q_x = J4 \frac{\partial^3 w}{\partial x^3} + J5 \frac{\partial^3 w}{\partial x^2 \partial y} + J6 \frac{\partial^3 w}{\partial x \partial y^2} + J7 \frac{\partial q}{\partial x} \qquad (68)$$

Where:

$J1 = D_x/((1-\mu_x \mu_y)S_x) - X2O$

$J2 = D_{xy}/(2S_x)$

$J3 = -1$

$J4 = D_x/(1-\mu_x \mu_y) + X2O\, N_x$

$J5 = 2\, X2O\, N_{xy}$

$J6 = D_{xy} + \mu_y D_x/(1-\mu_x \mu_y) + X2O\, N_y$

$J7 = X2O$

Where:

$$X2O = D_{xy}/(2S_y) + \mu_y D_x/((1-\mu_x\mu_y)\ S_y)$$

5.2 Finite Difference Approximations to Equations

Figure 151 shows the general form of the finite difference approximations to the governing equation and boundary conditions for the solution of Q_x. Substituting for the central difference derivative coefficients based on Table 10 gives the expressions for the node points below. The equation constants incorporate the appropriate mesh factors (D*) in their denominators.

Governing equation (66)

$$g_o = 6\ G1 - 2\ G2 + 4\ G3 - 2\ G4 + 6\ G5 + G6$$

$$g_1 = g_3 = -4\ G1 + G2 - 2\ G3$$

$$g_2 = g_4 = -2\ G3 + G4 - 4\ G5$$

$$g_5 = g_6 = g_7 = g_8 = G3$$

$$g_9 = g_{11} = G1$$

$$g_{10} = g_{12} = G5$$

$$h_o = h_2 = h_4 = h_{10} = h_{12} = O$$

$$h_1 = -h_3 = 5\ G7 - 2\ G8 + 4\ G9 - 2\ G10 + 6\ G11$$

$$h_5 = -h_6 = -h_7 = h_8 = -2\ G9 + G10 - 4\ G11$$

$$h_9 = -h_{11} = -4\ G7 + G8 - 2\ G9$$

$$h_{13} = -h_{16} = -h_{17} = h_{20} = G9$$

$$h_{14} = -h_{15} = -h_{18} = h_{19} = G11$$

Boundary conditions

At $x = \pm a/2$ (58):

$i_o = O,$ $\quad k_o = -2\ H2$

$i_1 = -i_3 = H1,$ $\quad k_1 = k_3 = H2$

At $y = \pm b/2$ (67):

$l_o = 1$

General boundary equation (68):

$m_o = -2\ J1 - 2\ J2 + J3$

$m_1 = m_3 = J1$

$m_2 = m_4 = J2$

$n_o = O$

$n_1 = -n_3 = -2\ J4 - 2\ J6$

$n_2 = -n_4 = -2\ J5$

$n_5 = -n_7 = J5 + J6$

$n_6 = -n_8 = J5 - J6$

$n_9 = -n_{11} = J4$

$p_o = O$

$p_1 = -p_3 = J7$

Similarly, the corresponding equations for the solution of Q_y were expressed in finite difference form.

6. SPECIAL NOTE ON CORNER TREATMENT

6.1 w solution

In the corner region there are nine nodes, eight fictitious and the corner node, bounded by the two axes passing through the corner. The finite difference equations were formulated so that, of these, all except the corner node and the two fictitious nodes immediately adjacent to the corner were eliminated. Hence only three boundary equations were required in the corner, thus:

$$w = 0 \qquad (69)$$

$$\frac{\partial^2 w}{\partial x^2} = 0 \qquad (70)$$

$$\frac{\partial^2 w}{\partial y^2} = 0 \qquad (71)$$

(70) and (71) follow from the conditions applying along $y = \pm b/2$ and $x = \pm a/2$ respectively. This implies discontinuities since immediately adjacent to the corner along $x = a/2$, and $y = b/2$, (70) and (71) revert to (59) and (64) respectively. The effects of this approximation do not appear to significantly influence the results.

The twisting moment calculation for the corner point required the definition of the fictitious value for w on a diagonal line through the corner. Since this was not evaluated in the solution for w, a value was obtained using a cubic extrapolation along the diagonal.

6.2 Q_x solution (similarly for Q_y)

The Q_x solution was formulated so that all three corner fictitious nodes were eliminated. Thus only a single corner equation was required and this was taken as $Q_x = 0$.

APPENDIX E

APPROXIMATE YIELD LINE ANALYSIS OF MODEL FAILURE[42]

A very approximate yield line analysis was used to determine a value for the ultimate pressure which the double-bottom model could sustain in the presence of a constant in-plane thrust. This thrust was taken as the value at failure, namely -10.4 tons/in^2.

Assuming that yield lines developed as shown below and that the ultimate moment per unit length was equal for all lines, the geometry of the lines for minimum load is given by:

$$\tan \phi_{min} = -\frac{1}{\lambda} \pm \sqrt{\frac{1}{\lambda^2} + 3}$$

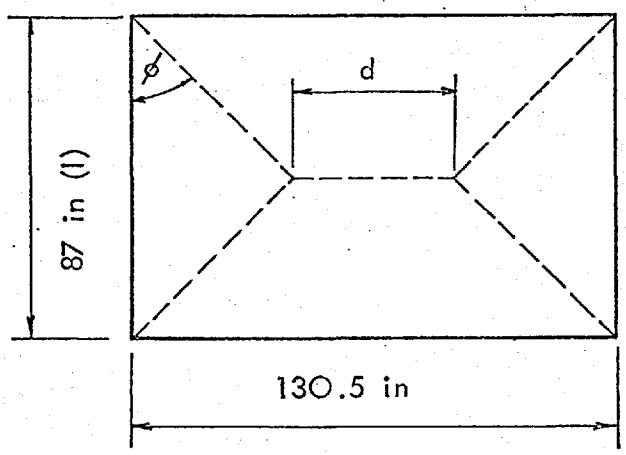

$$\lambda = \frac{130.5}{87} = 1.5$$

Hence: $\phi_{min} \simeq 50^\circ$

$d \simeq 27$ in

The ultimate moment was computed for the diagonal yield lines as follows:

$$M_u = t \sigma j$$

Where: t = outer shell thickness = 0.08 in

σ = (yield stress) - (component of applied thrust across yield line)

$$= (15 - 10.4 \cos \phi_{min}) \text{ tons/in}^2$$

$$= 6.7 \text{ tons/in}^2$$

$$l = \text{lever arm} = 5.573 \text{ in}$$

Giving: $M_u = 8{,}300$ in.lb/in

In the above calculation for M_u, the effect of the stiffeners appears in the value for the component of in-plane thrust but is ignored so far as transverse pressure is concerned.

The expression for ultimate pressure is as follows:

$$p_{min} = \frac{8 M_u}{l^2} \frac{(1/\tan \phi + \lambda)}{(\lambda - \tan \phi/3)} = \frac{M_u}{446}$$

Gives:

$$p_{min} = \frac{8300}{446} = 18.7 \text{ p.s.i.}$$

If it is assumed that the plating used to repair the end buckles which occurred in the preliminary failure, forced the diagonal yield lines to develop from the first floor in from the bulkheads, then a yield line solution similar to the above gives a value of p_{min} equal to about 23 p.s.i.

These values do not appear to bear any relation to the observed failure pressure despite the occurrence of buckles, in the outer shell, along lines which bore a resemblance to the assumed yield line pattern. It is possible, however, that a less approximate yield line solution may give better agreement.

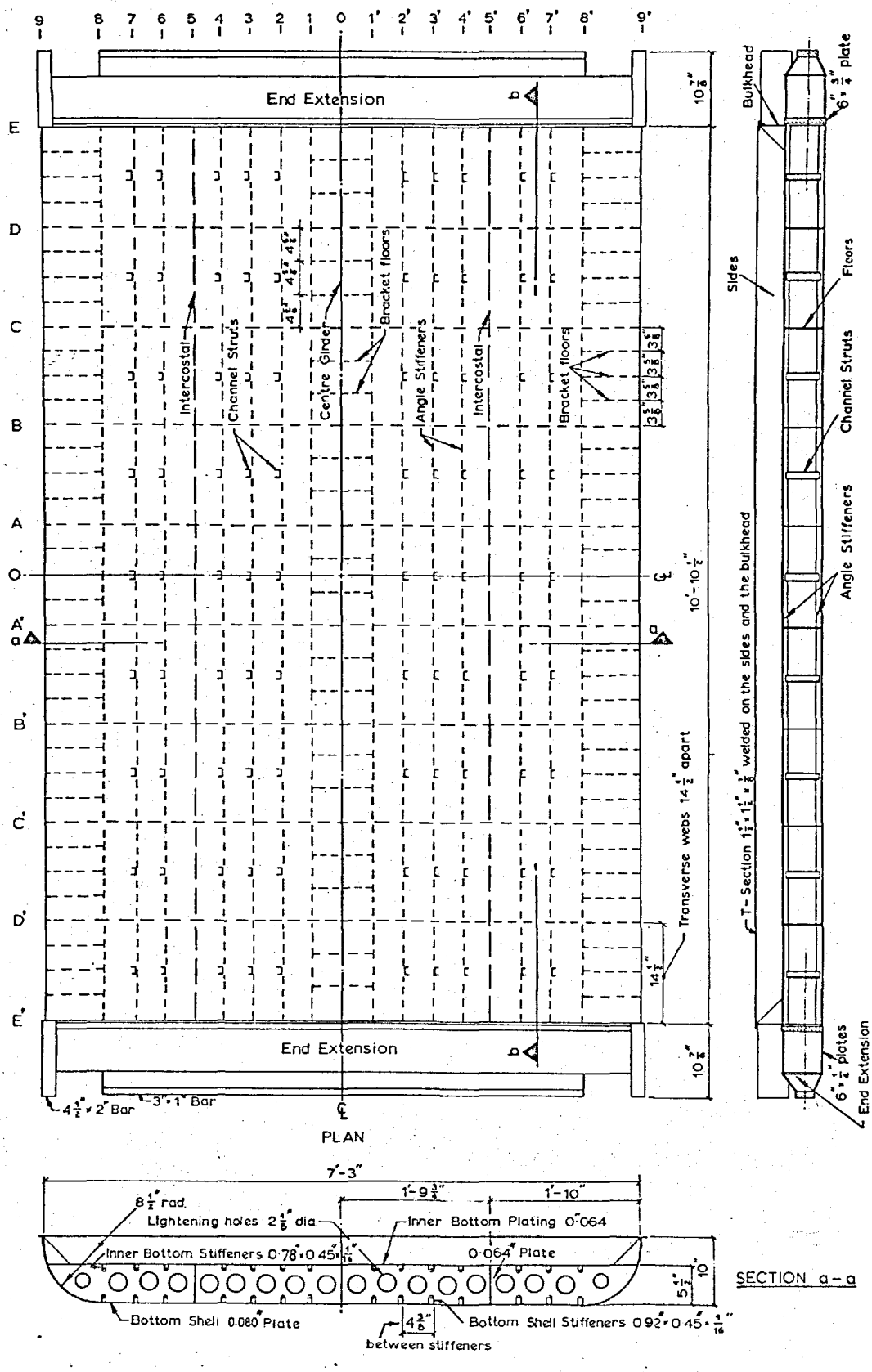

Fig. 1 : Principal Dimensions of Double-Bottom Model

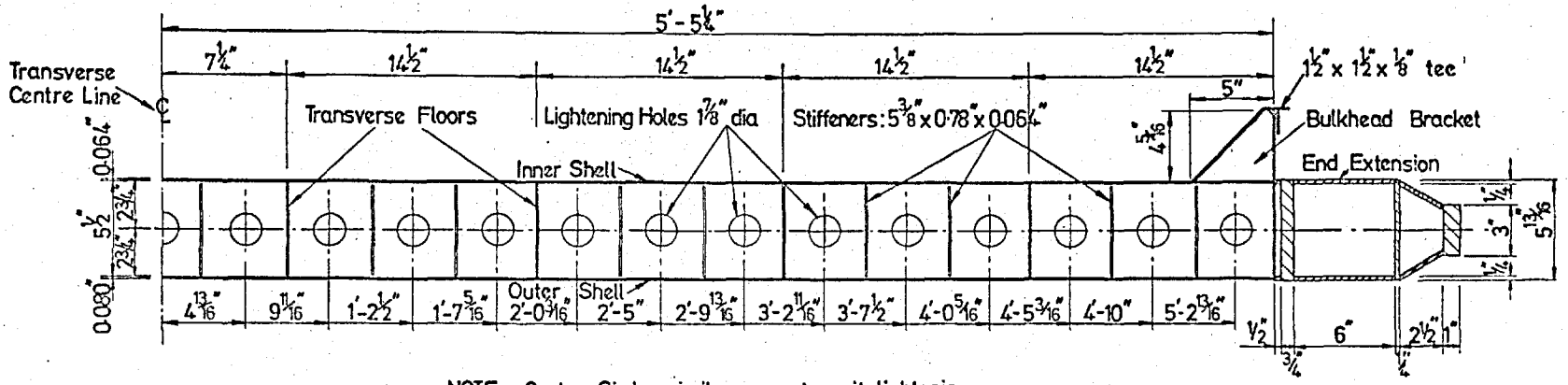

NOTE: Centre Girder similar except omit lightening holes and bracket floors replace stiffeners

DETAIL OF INTERCOSTALS AND END EXTENSION

NOTE: Centre girder and side bracket floors similar to main floors over corresponding frame spacing with ½" flange on free edges

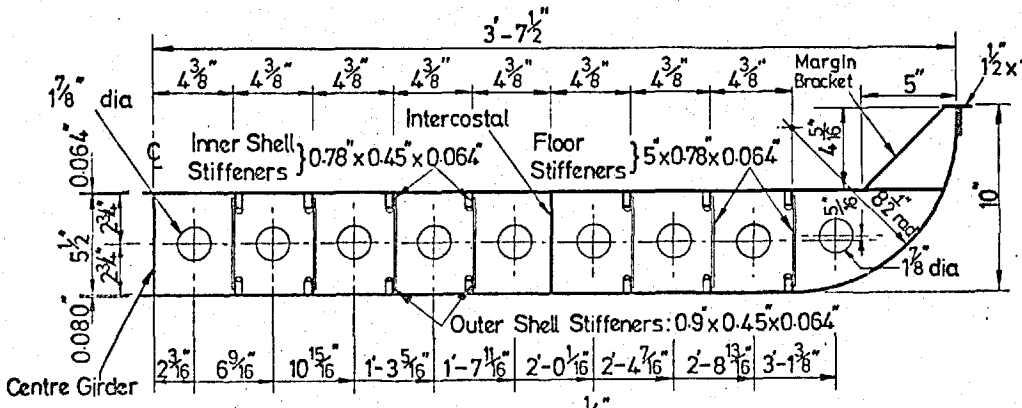

NOTE: All lightening holes 2⅛" dia except as shown

DETAIL OF TRANSVERSE FLOORS (See also Fig. 1)

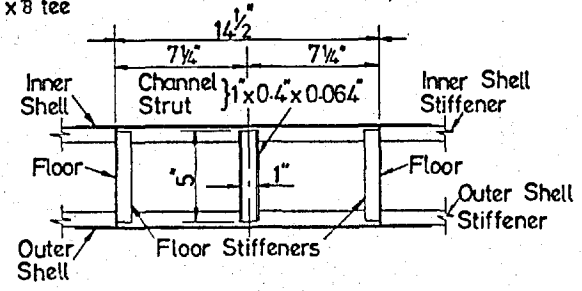

DETAIL OF CHANNEL STRUTS

Figure. 2 : Details of Model

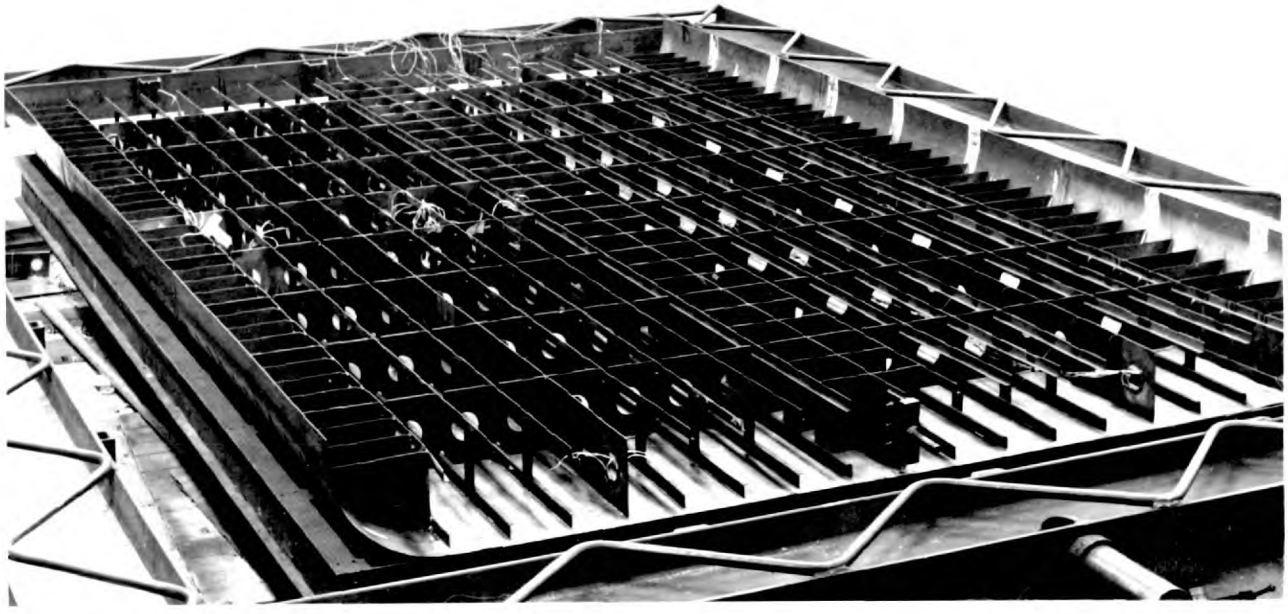

Fig. 3: Model Prior to Fixing Inner Bottom and End Extensions

Fig. 4: Detail of Shell and Floor Stiffening

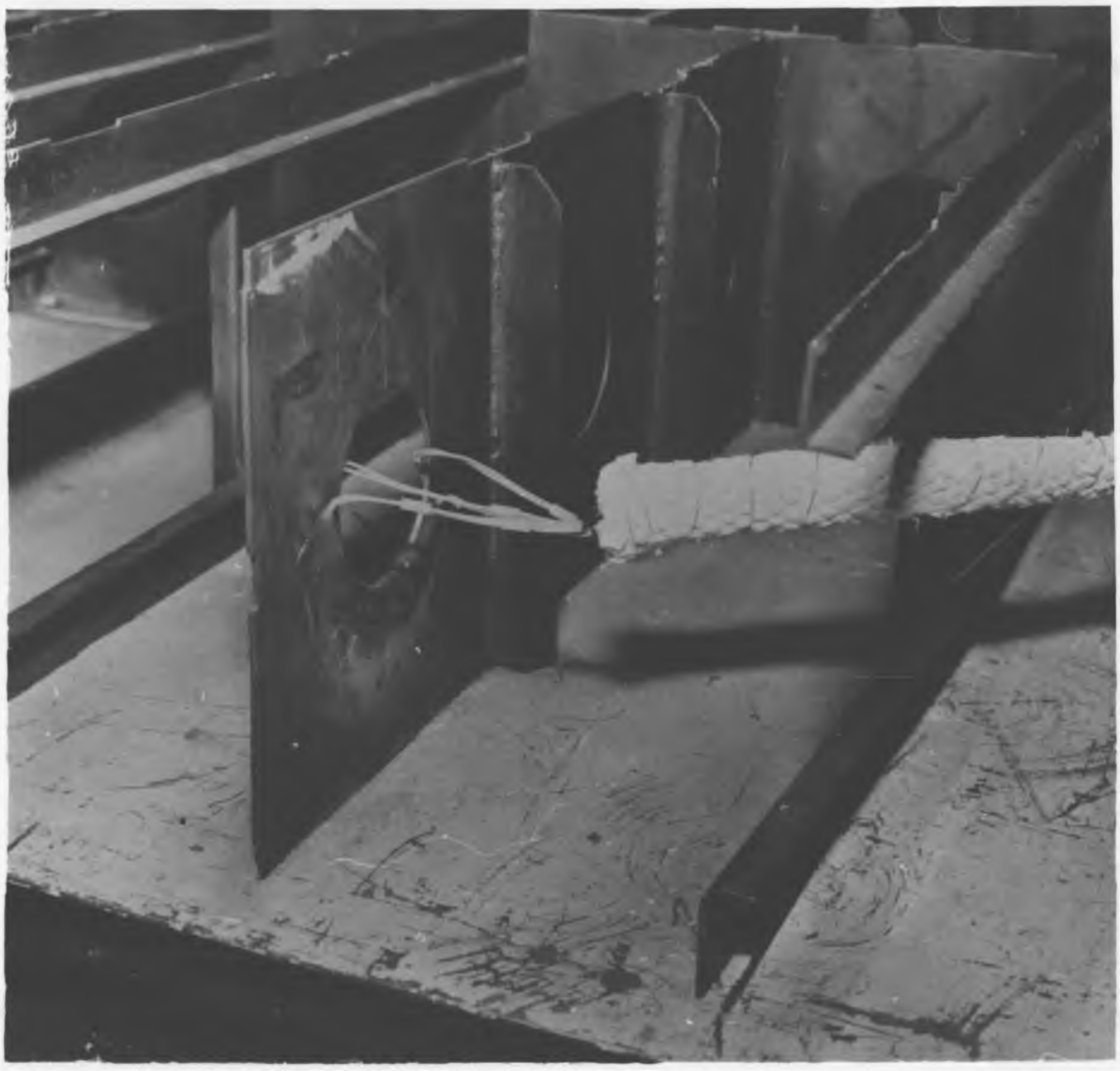

Fig. 5: Detail of Intercostal Stiffening

Fig. 6: Completed Model - Inner Shell View

Fig. 7: Completed Model - Outer Shell View

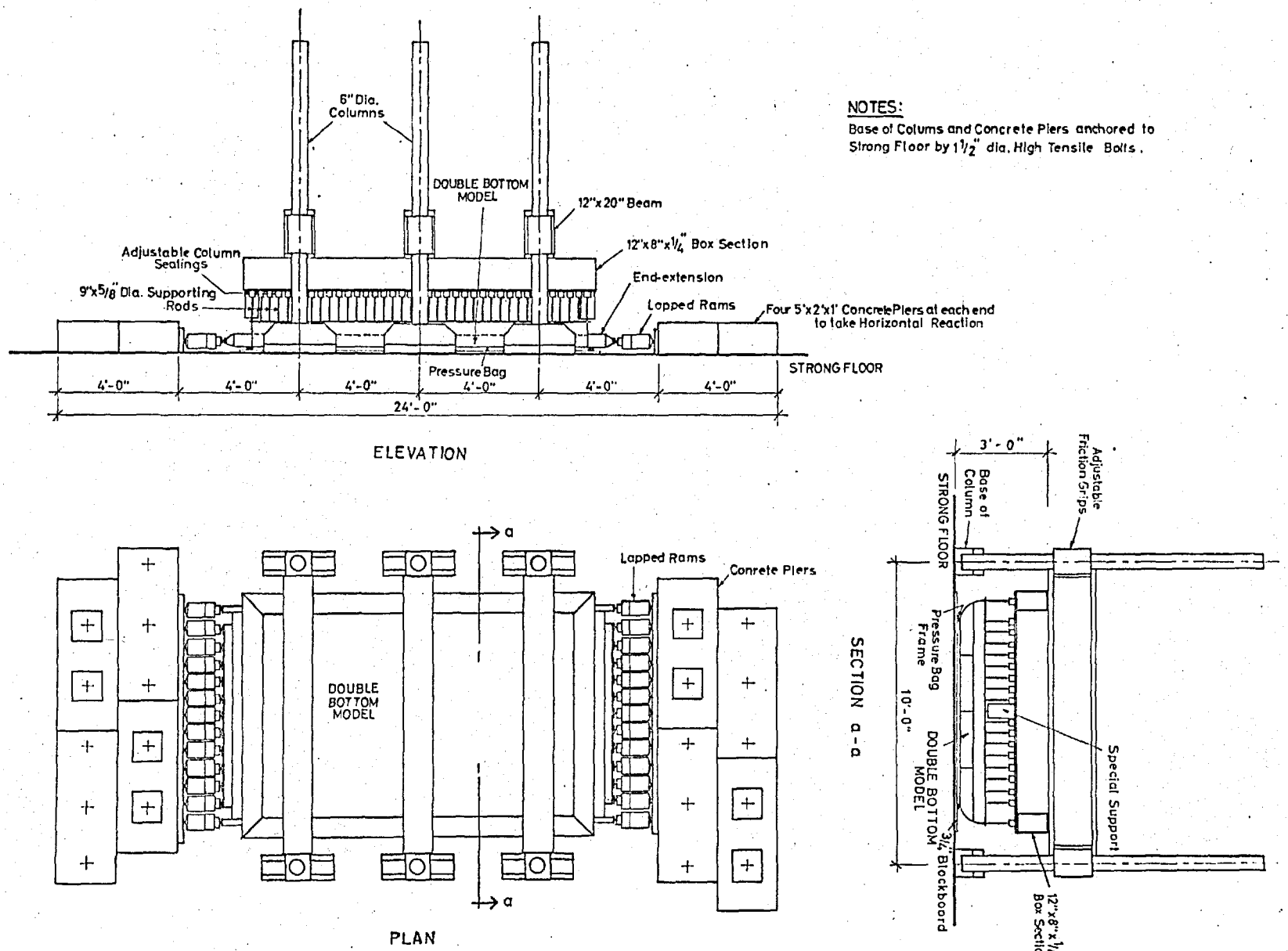

Fig. 8 : General Details of Combined Load Test Arrangement

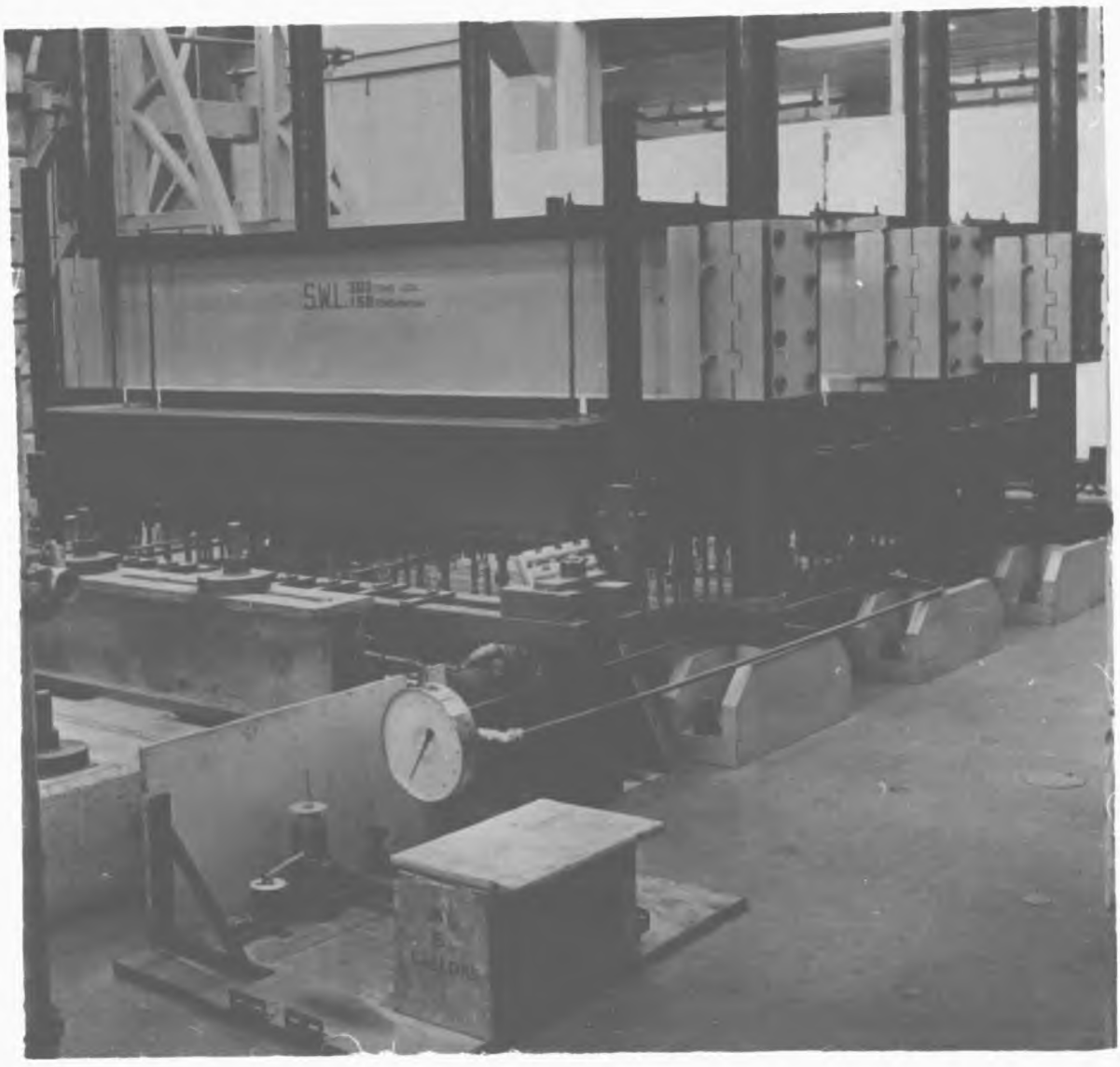

Fig. 9: General View Showing Loading Frame and Model in Position for Combined Load Test

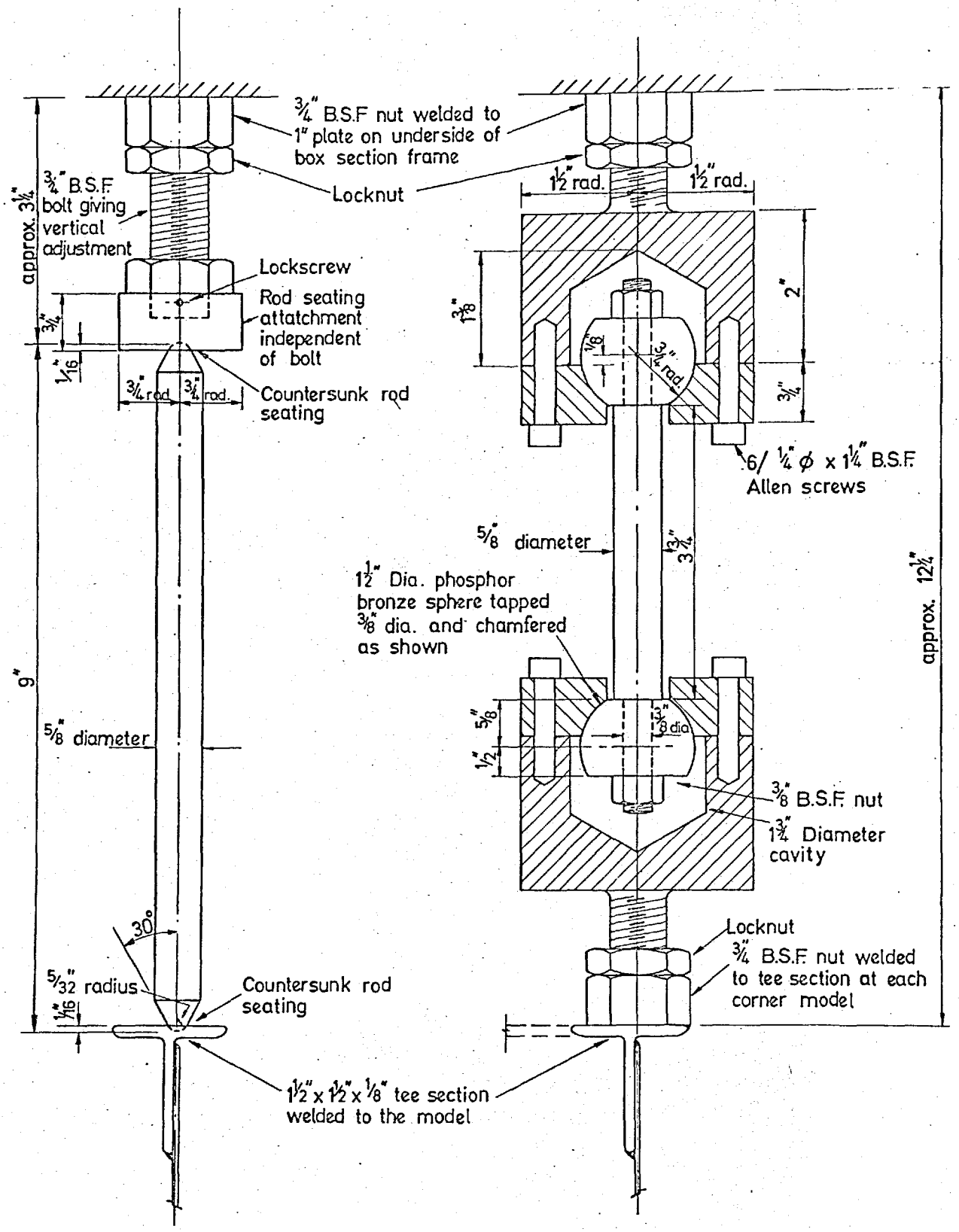

DETAIL OF ROD SUPPORT
Located at Bulkhead and Margin Brackets

DETAIL OF TENSION LINK SUPPORT
Located at Each Corner

Figure. 10 : Support of Model

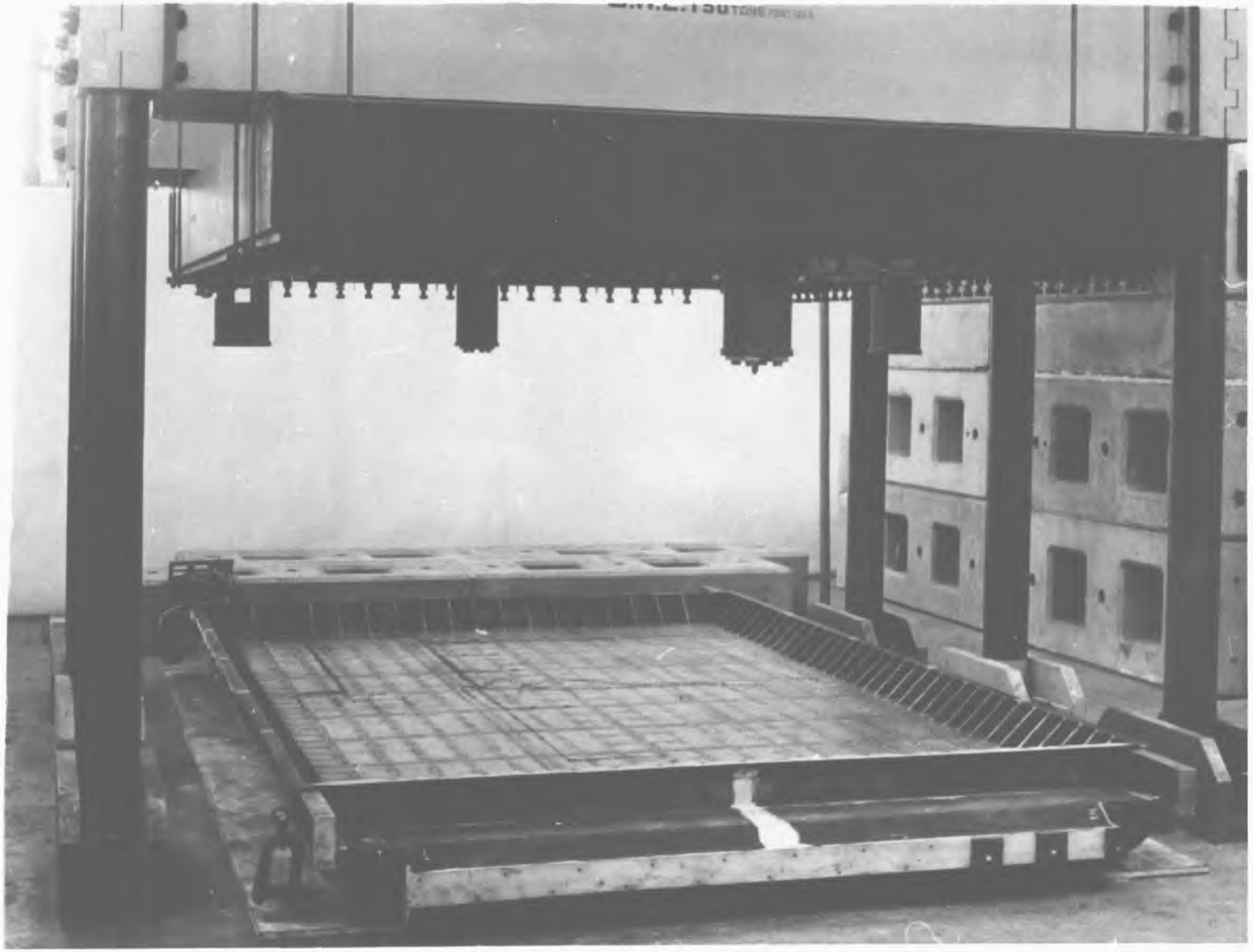

Fig. 11: Model in Position Prior to Lowering Loading Frame Beams

Fig. 12: Pressure Bag in Position in Loading Frame

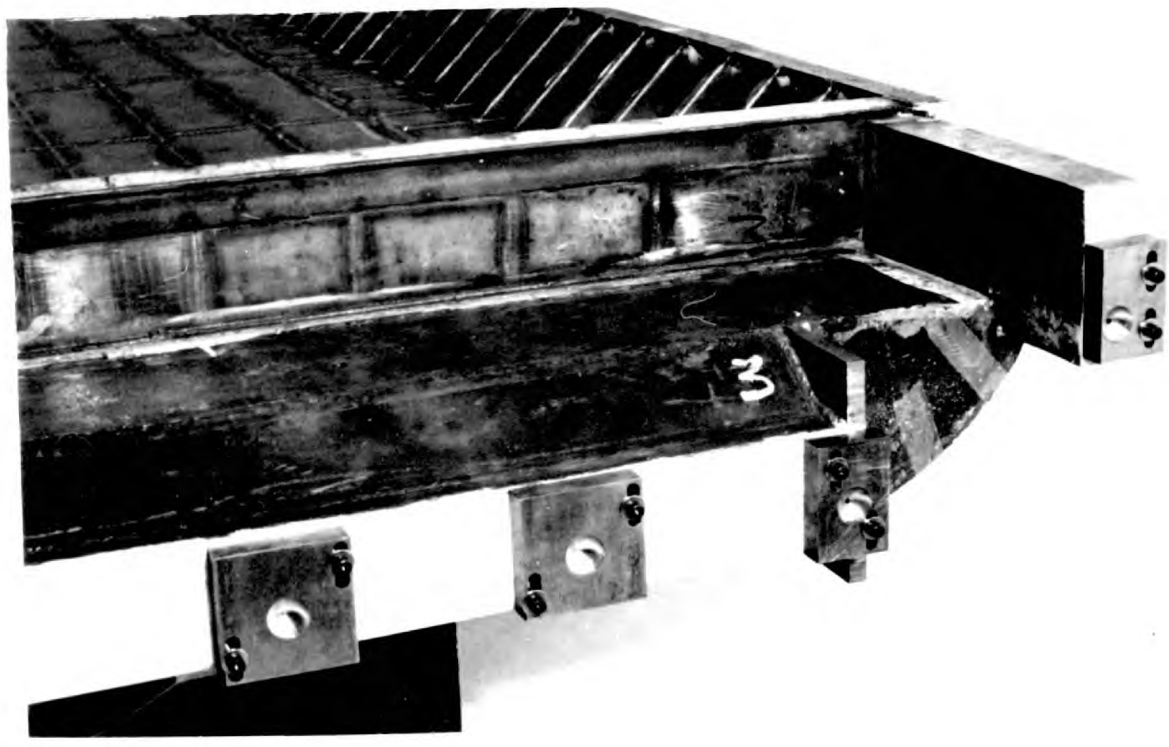

Fig. 13: Detail of End Extension and Adjustable Ram Seatings

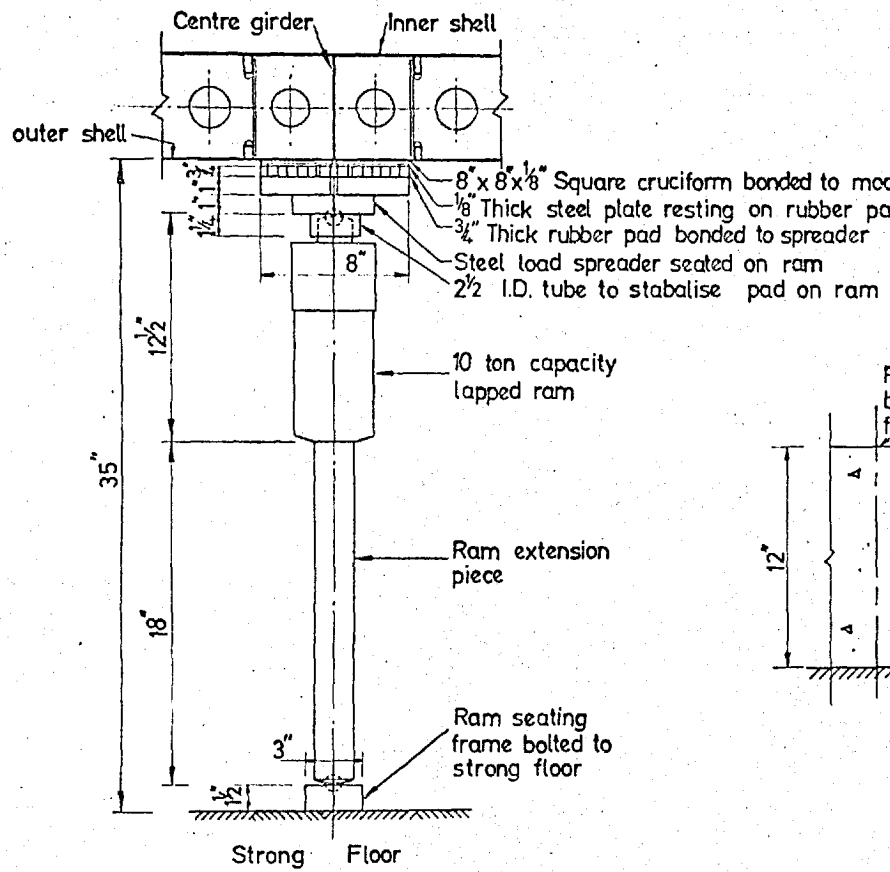

DETAIL OF VERTICAL RAM SET UP

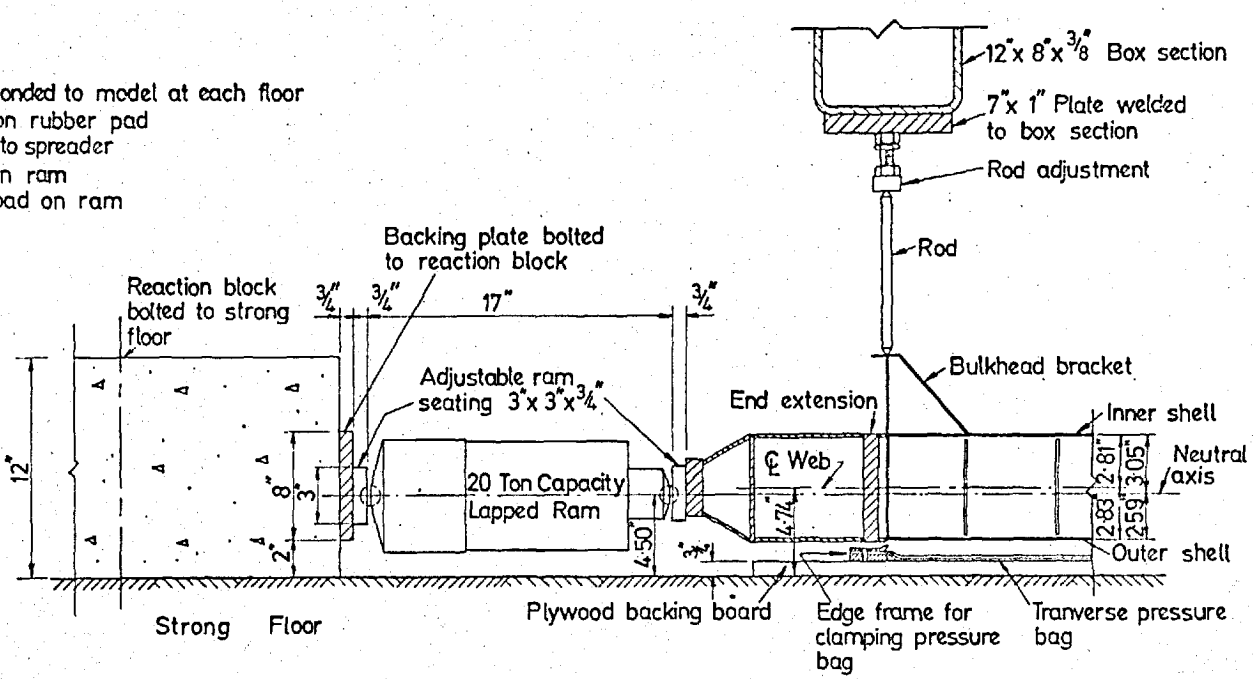

NOTE: Height of Ram above floor varies to accomadate change of model section toward sides

DETAIL OF MID - SECTION LONGITUDINAL RAM SET UP

Figure. 14 : Details of Ram Loading Arrangements

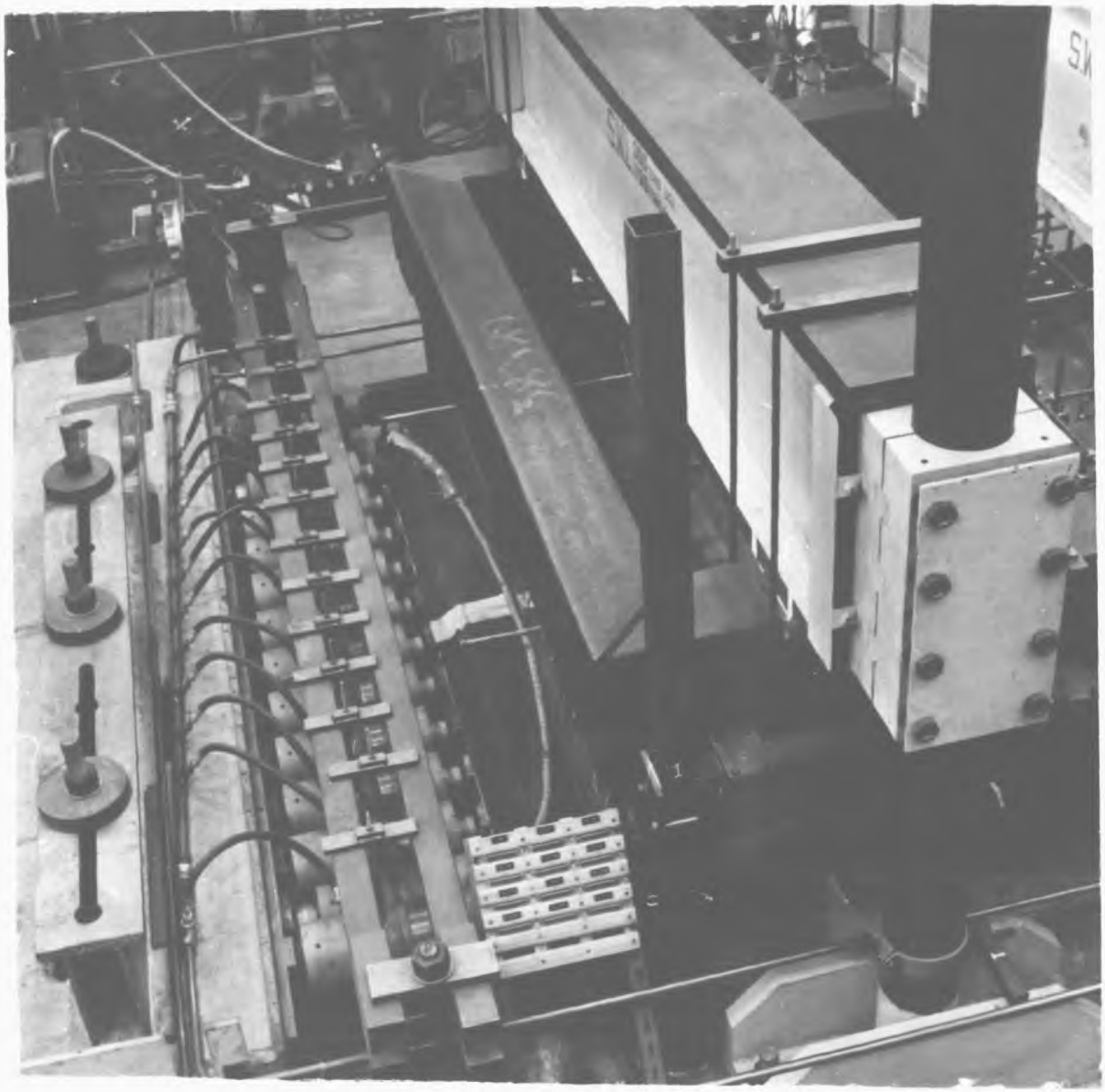

Fig. 15: Longitudinal Rams in Position at Bulkhead End

Fig. 16: Vertical Rams in Position Under the Model

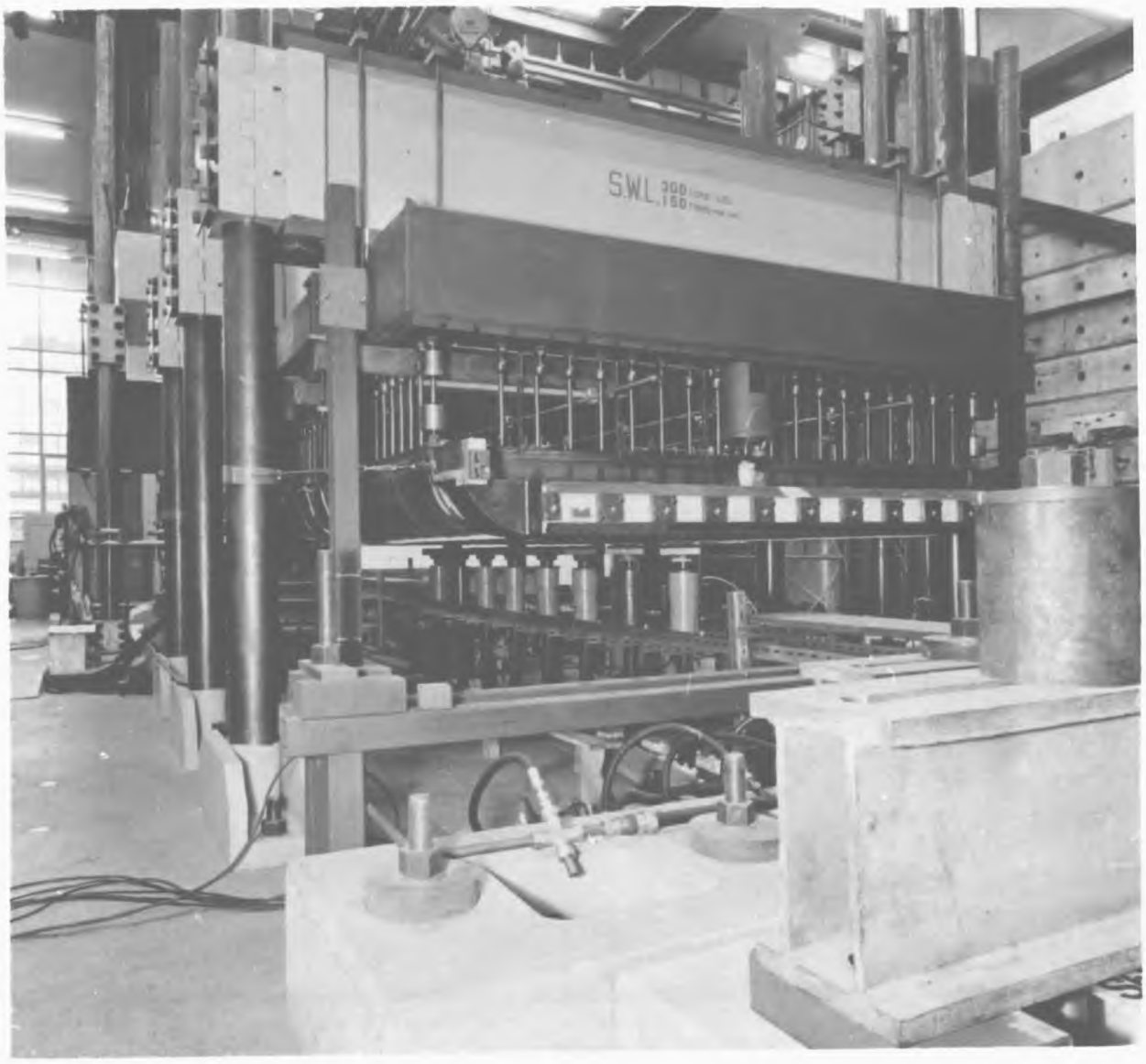

Fig. 17: General View of Local Transverse Load Test (8 rams)

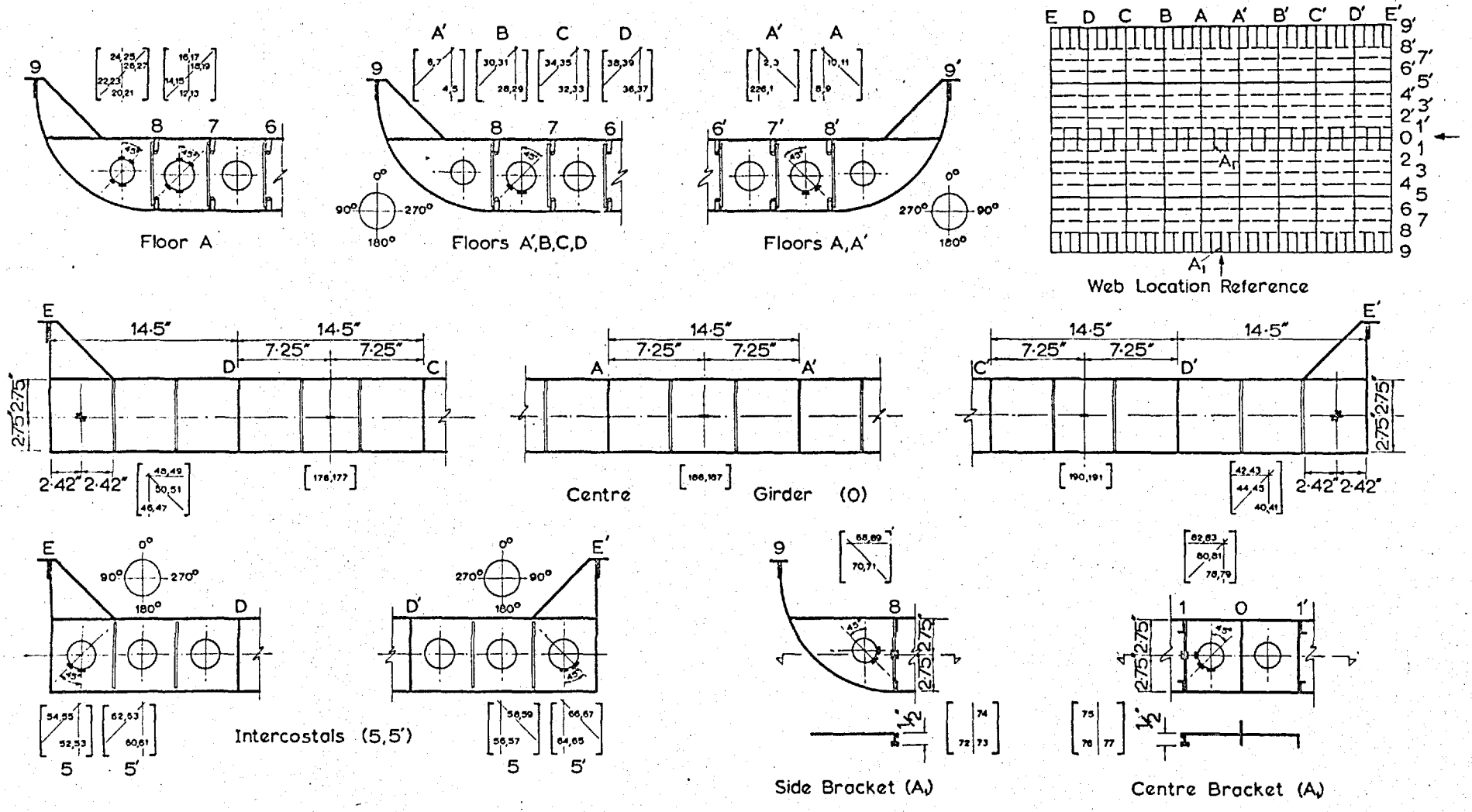

(Gauge numbering refers to Solartron output)

Fig. 18 : Instrumentation (1) Location of Web Strain Gauges

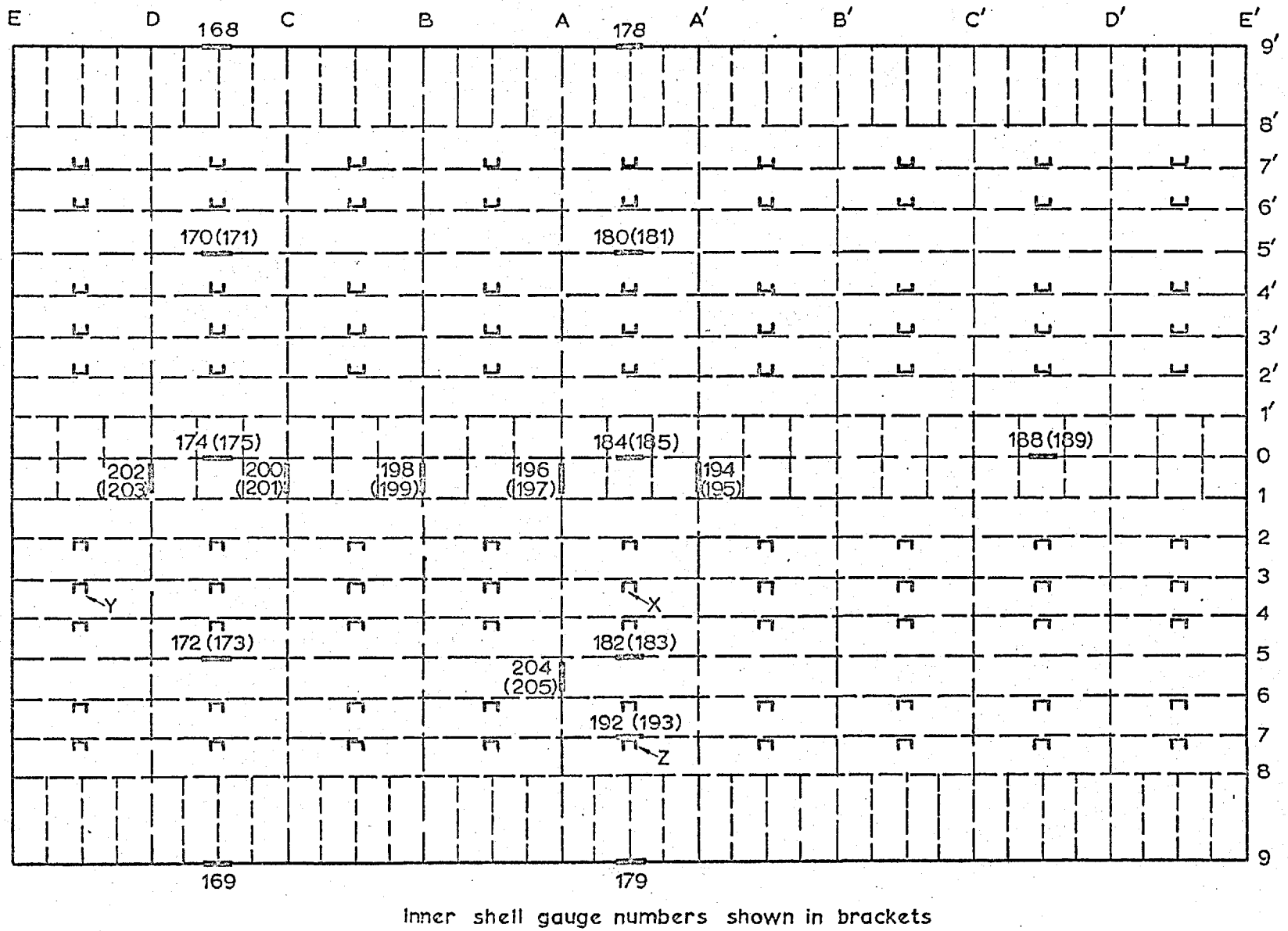

Fig. 19 : Instrumentation (2) - Location of Shell Strain Gauges at Intersections with Webs

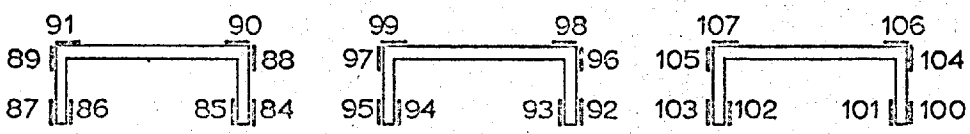

gauges located midway between shells

gauges located $1\frac{1}{2}$" from inside of outer shell

Strut X Strut Y Strut Z

Sections viewed from Inner Shell side

Strut Gauges

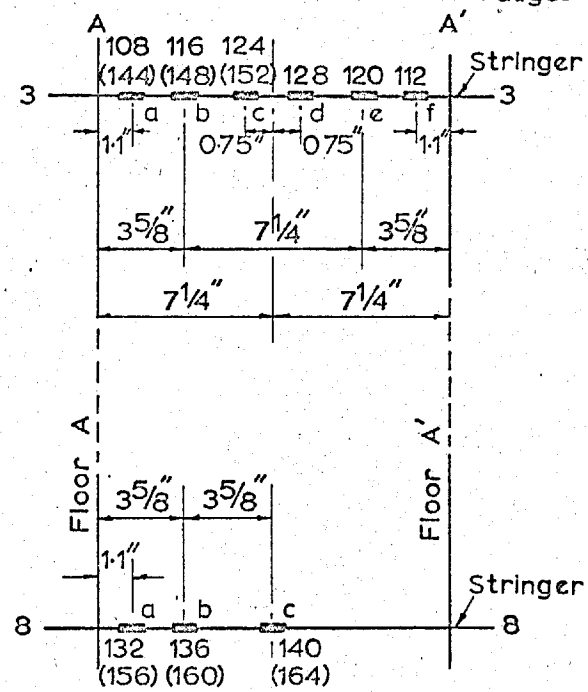

Shell - Stringer Gauges

Inner shell gauge numbers shown in brackets

Stringer Gauges

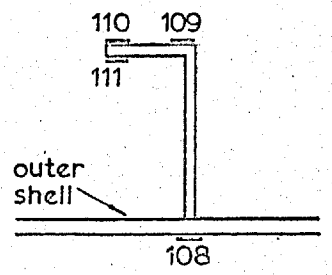

Stringer Flange Gauges

3 Stringer flange gauges numbered sequentially as above at each shell - stringer gauge location.

Refer Fig. 19 for Strut and Stringer locations

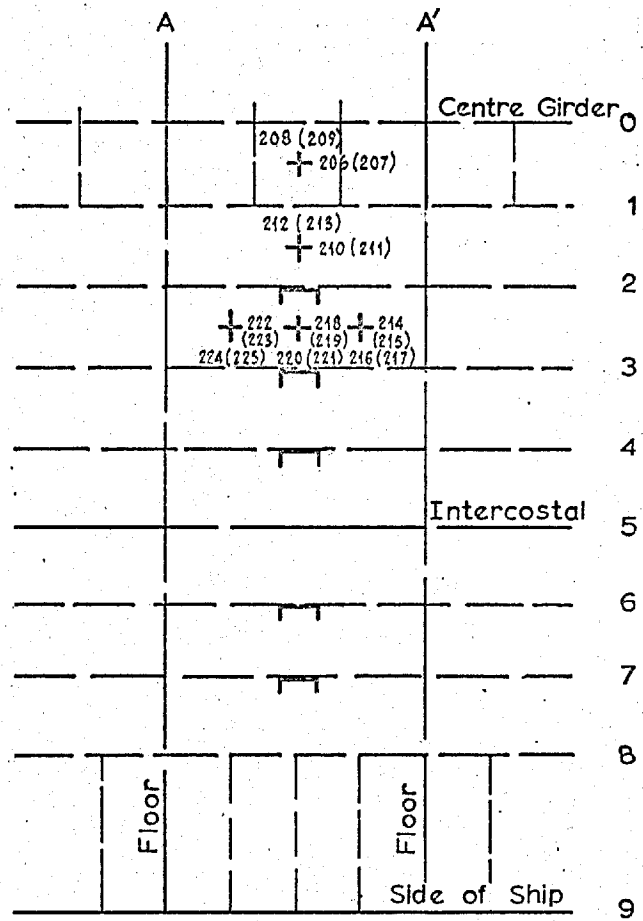

Numbers of Gauges on inside of outer shell shown in brackets

Refer Fig. 19 for general location.

Outer Shell Panel Strain Gauges

Fig. 20: Instrumentation (3) - Location of Strut, Stringer and Outer Shell Panel Strain Gauges

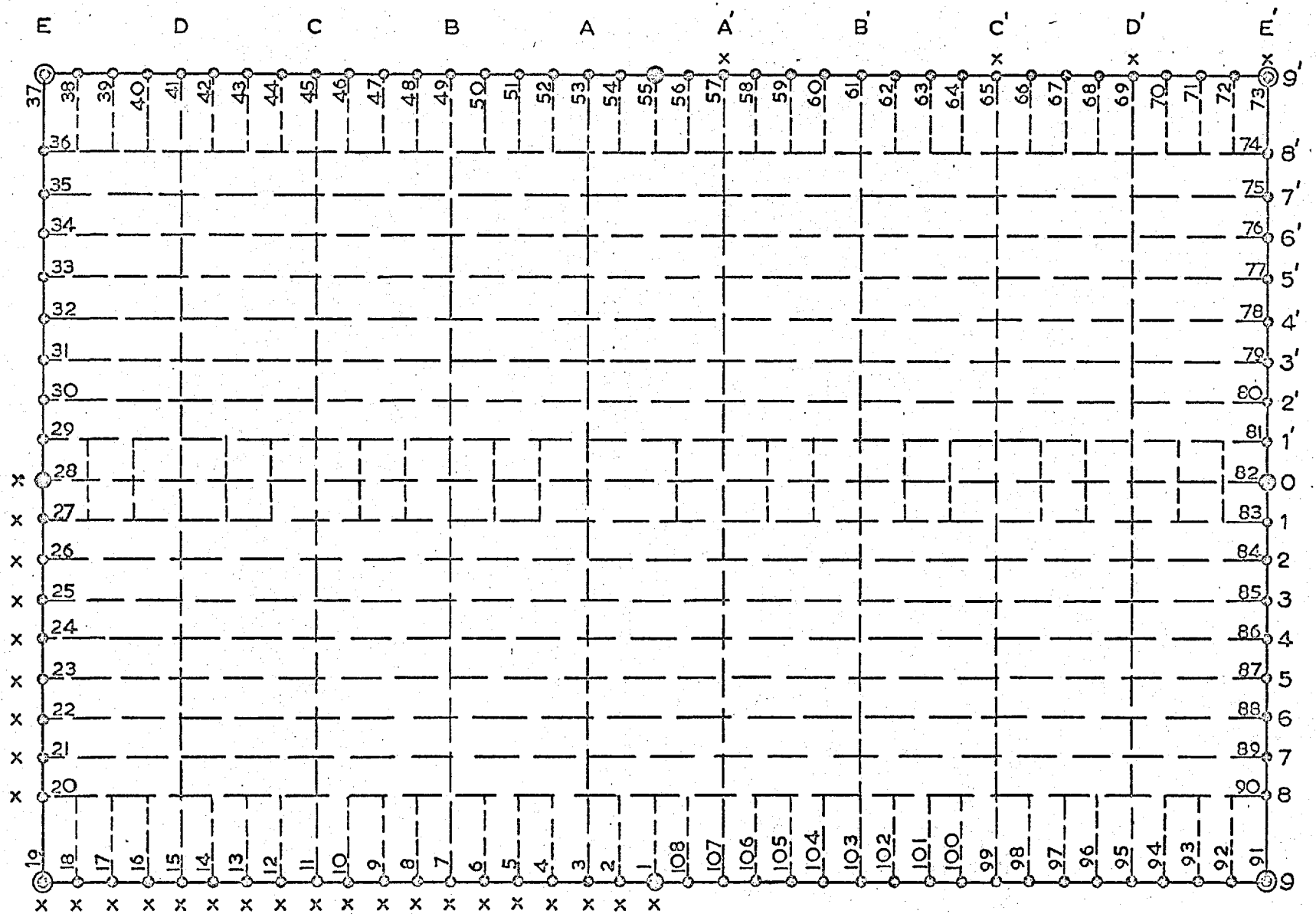

o Compression rod

⊙ Compression rod restrained by guide blocks

◎ Tension link

x Rods and links with strain gauges attached

Fig. 21 : Instrumentation (4) – Rod Numbering System and Location of Rod Strain Gauges

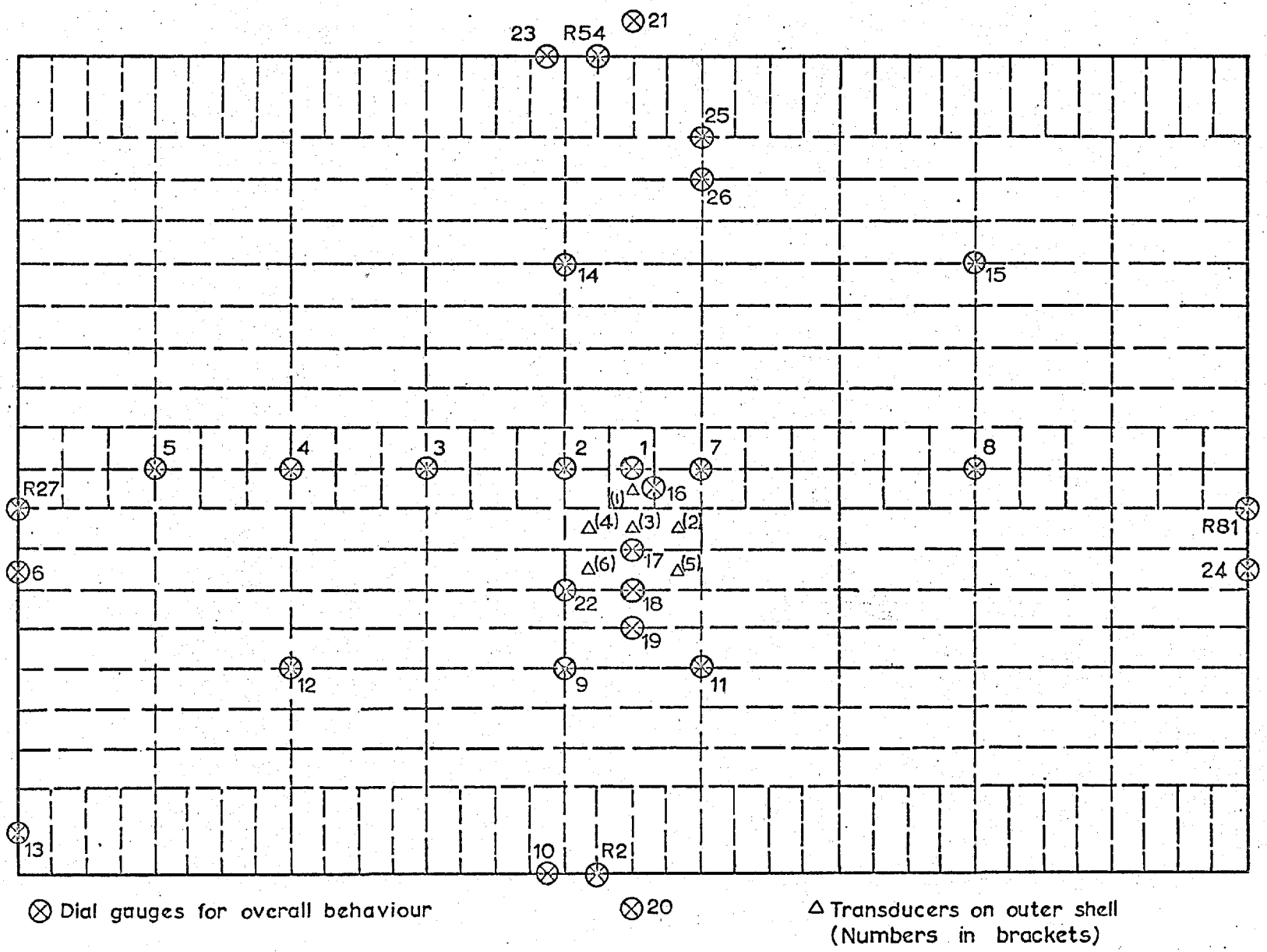

Fig. 22: Instrumentation (5) - Location of Dial Gauges and Transducers

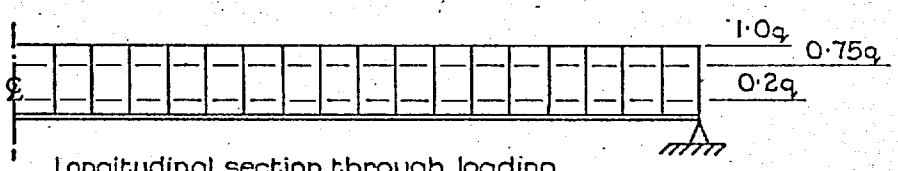

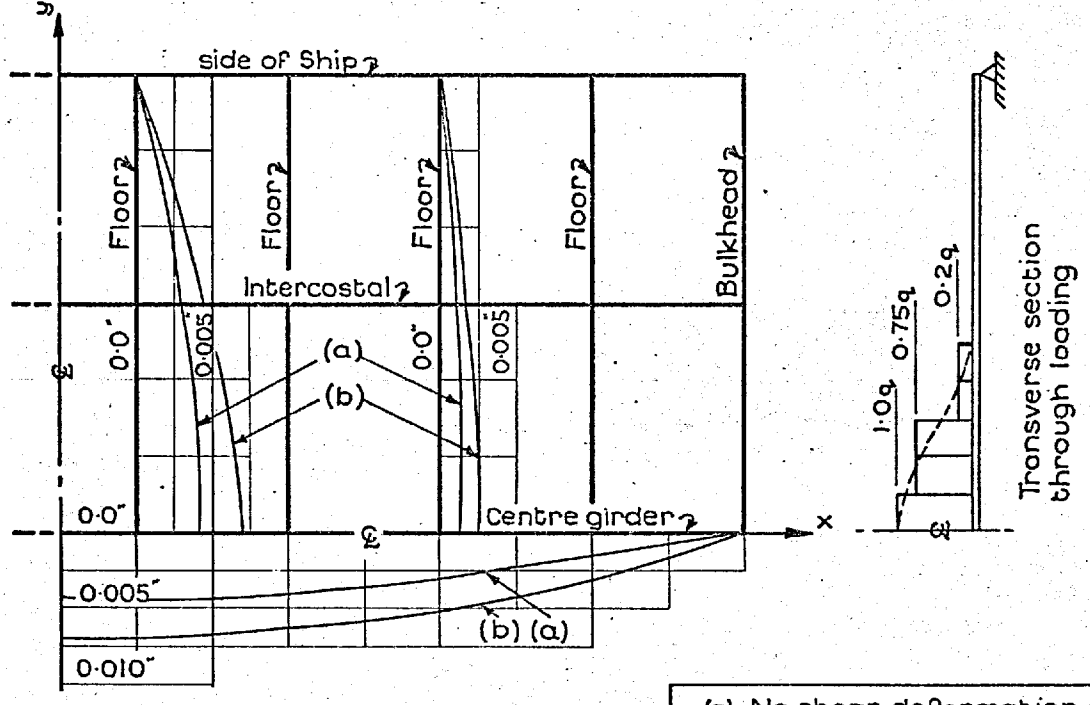

(i) Comparison of Deflexion Profiles

(a) No shear deformation
(b) Including shear deformation
Loading q* lp.s.i.

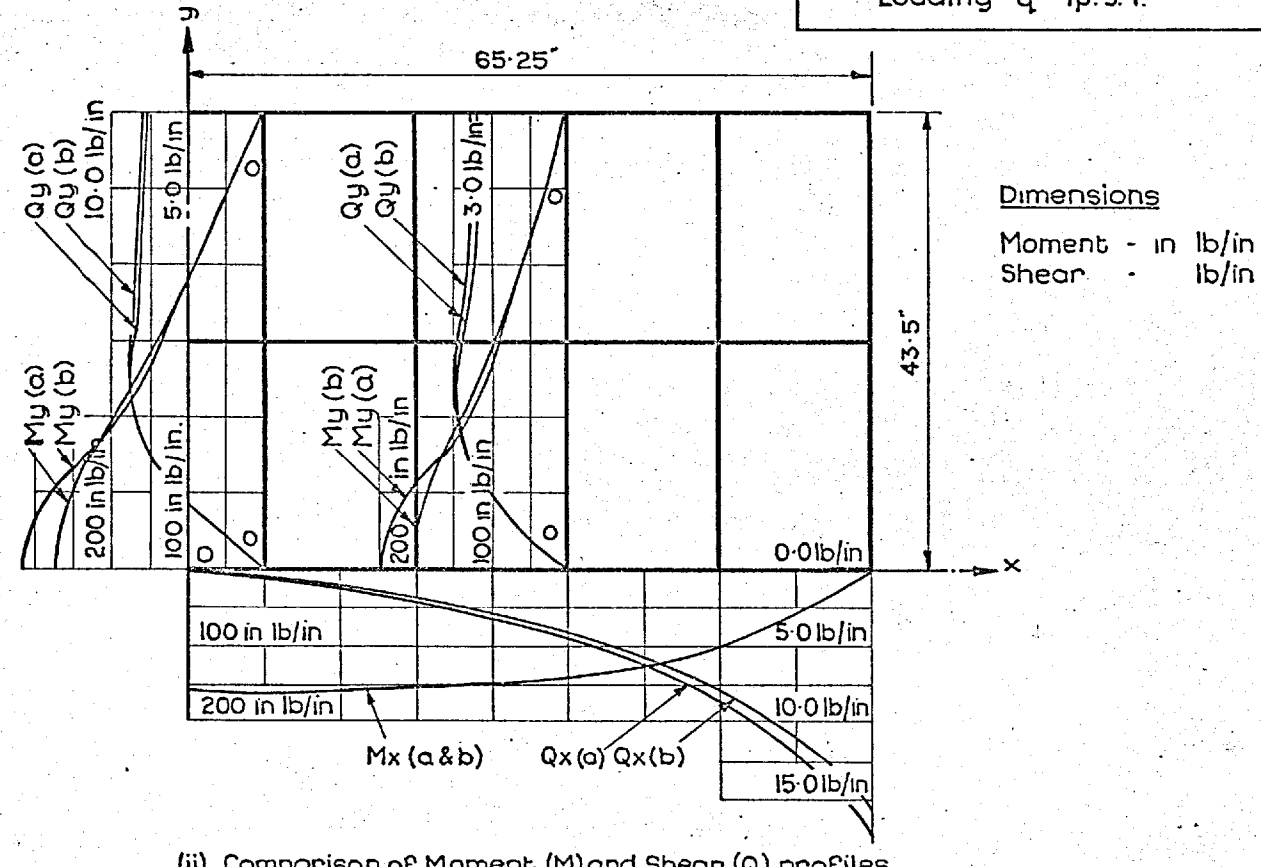

Dimensions

Moment - in lb/in
Shear - lb/in

(ii) Comparison of Moment (M) and Shear (Q) profiles

FIG.23:TYPICAL RESULTS FOR DOUBLE BOTTOM MODEL UNDER A TRANSVERSE LINE LOAD.

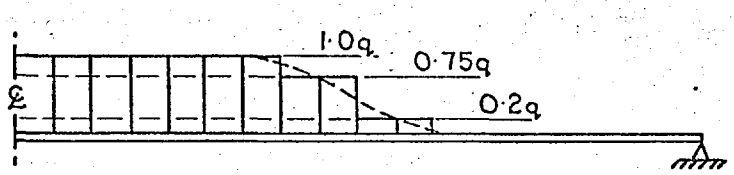

Longitudinal section through patch load

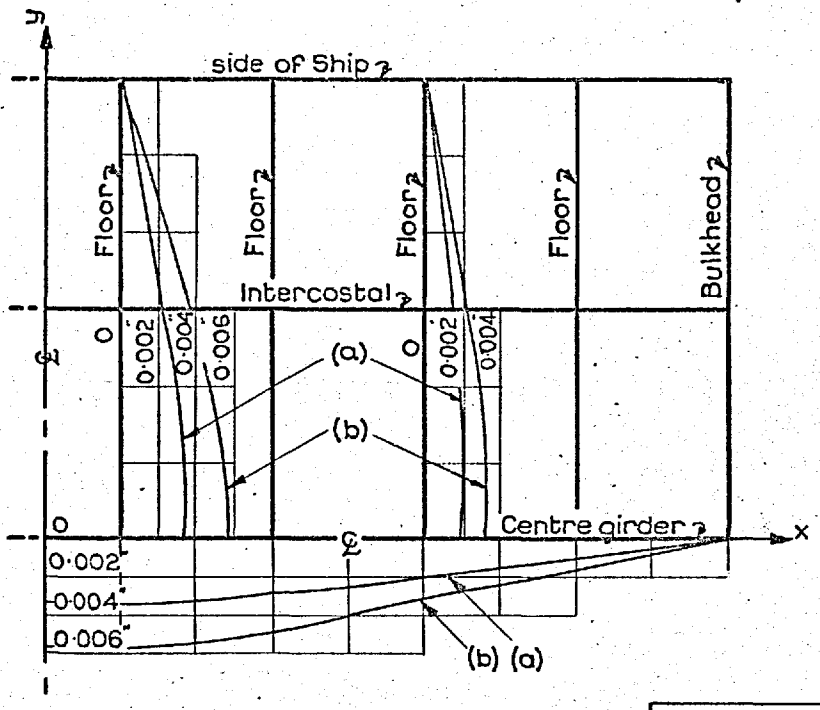

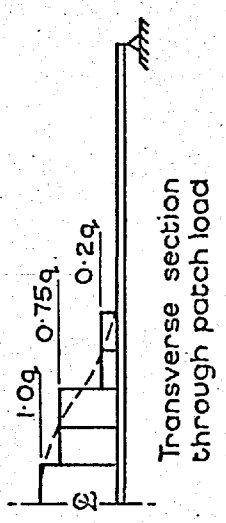

(i) Comparison of Deflexion Profiles

(a) No shear deformation
(b) Including shear deformation
Loading : q = 1 p.s.i.

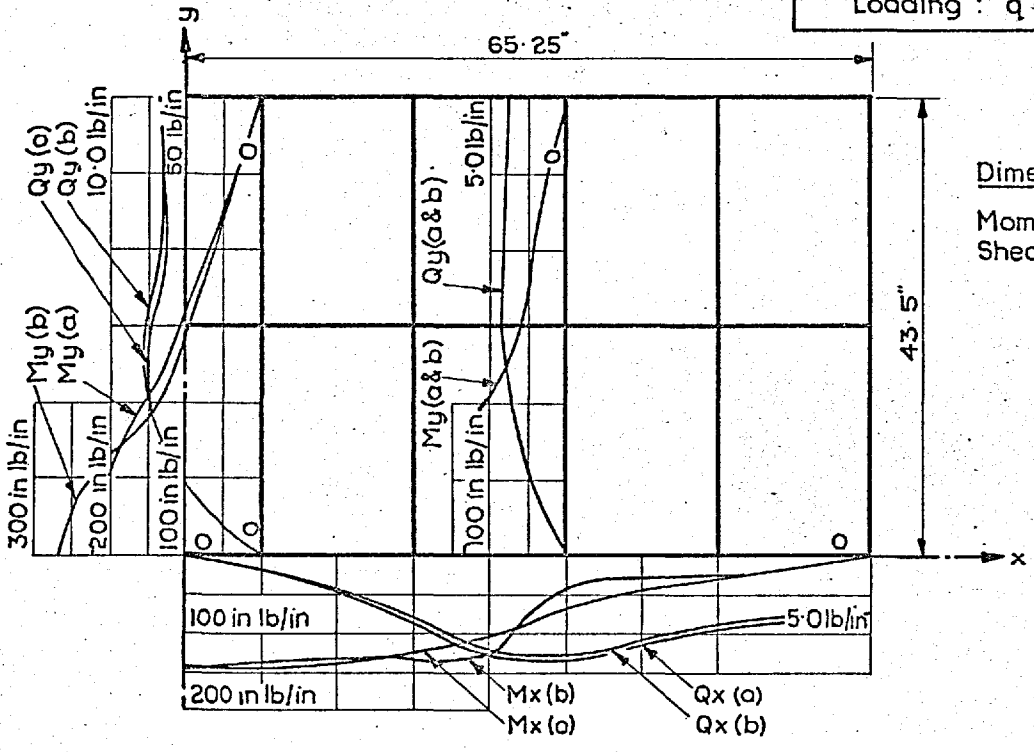

Dimensions

Moment - in lb/in
Shear - lb/in

(ii) Comparison of Moment (M) and Shear (Q) profiles

FIG. 24 : TYPICAL RESULTS FOR DOUBLE BOTTOM MODEL UNDER A PATCH LOAD

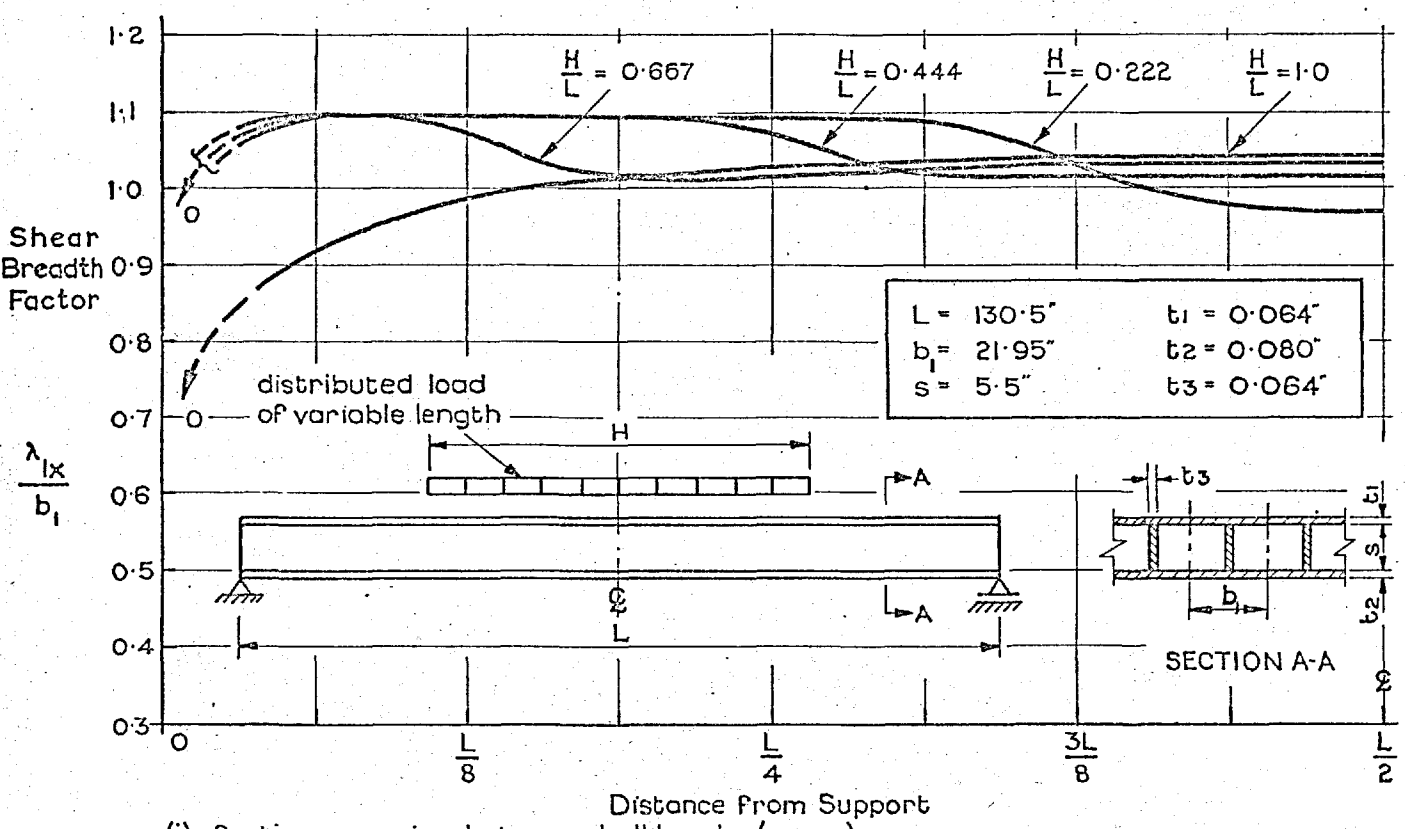

(i) Section spanning between bulkheads (x axis)

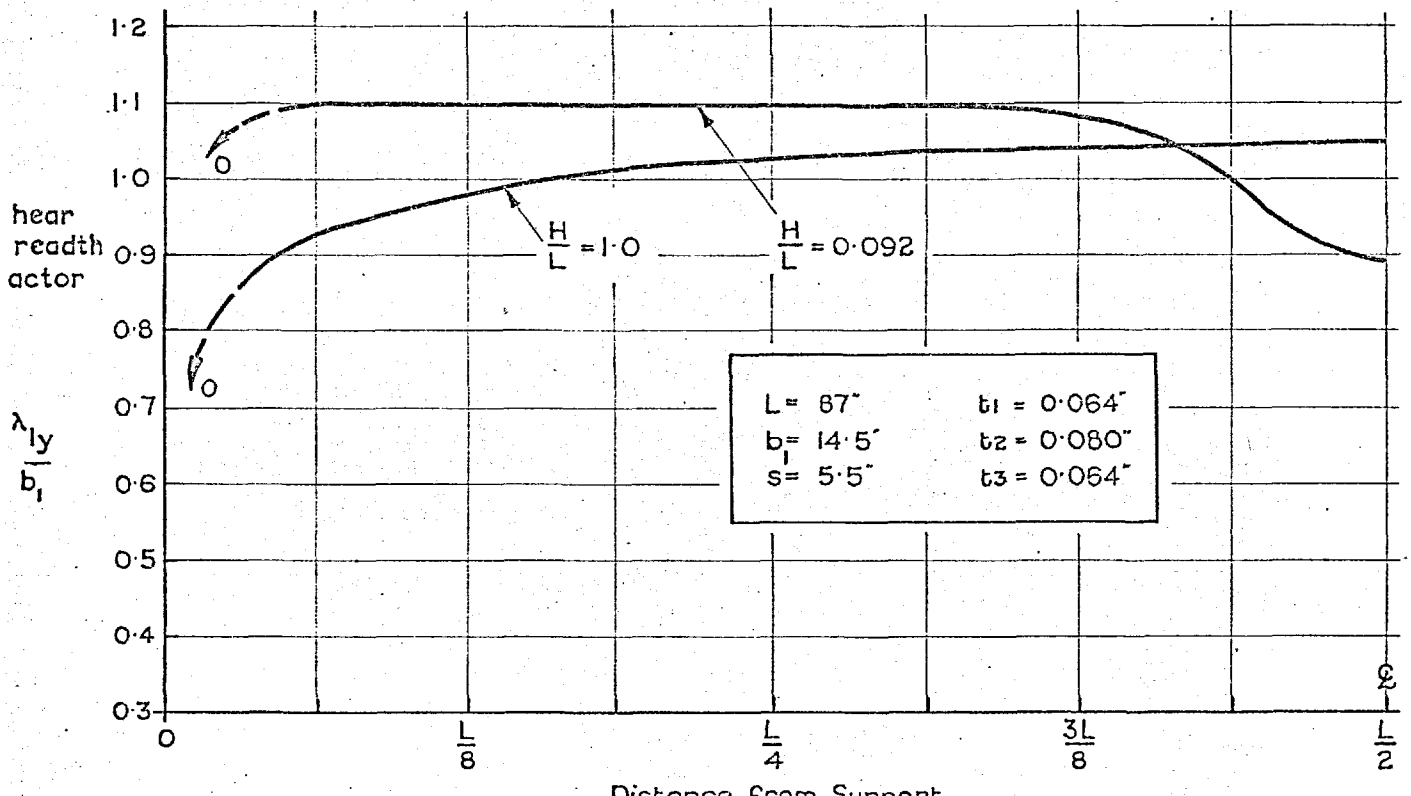

(ii) Section spanning between sides of ship (y axis)

FIG.25: VARIATION OF SHEAR BREADTH FACTOR WITH SPAN BETWEEN SUPPORTS FOR MULTIPLE WEB SECTIONS TYPICAL OF THE DOUBLE BOTTOM MODEL

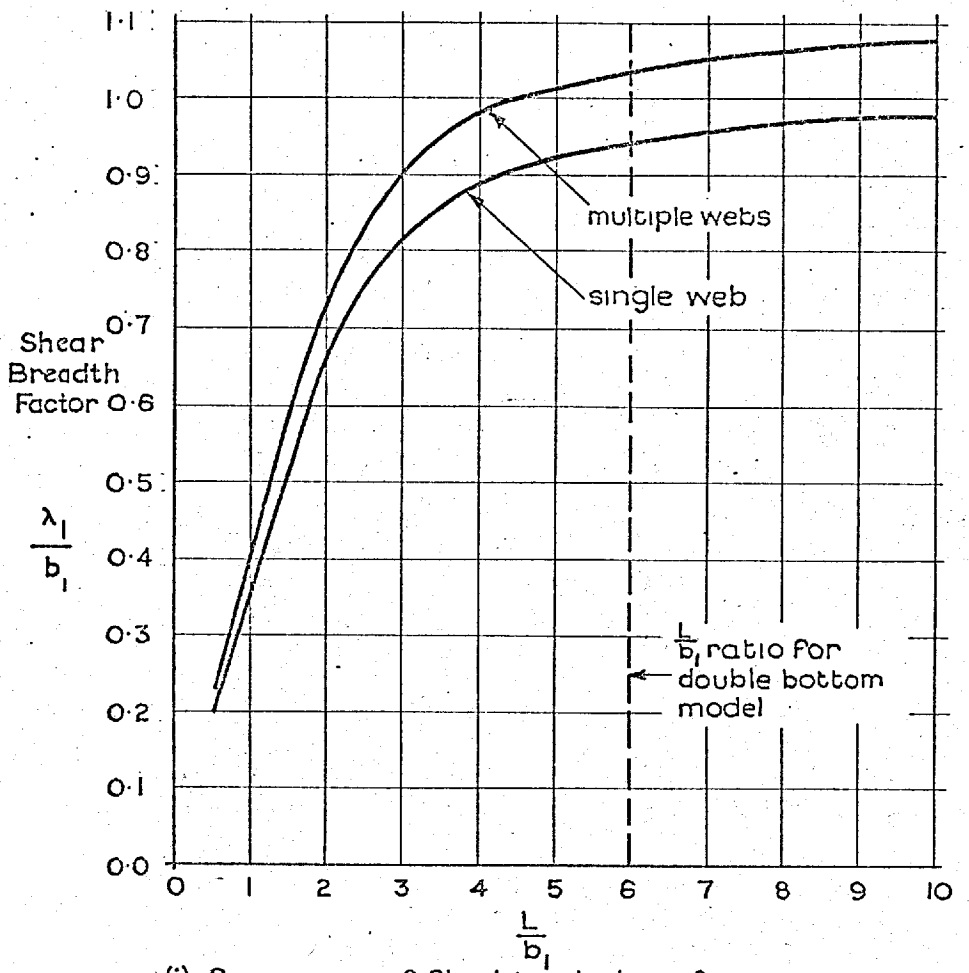

$\frac{L}{b_1}$ = Ratio of span between supports to the flange breadth

(i) Comparison of Shade's solutions of shear breadth for single and multiple web sections with unstiffened flanges subjected to uniformly distributed load.

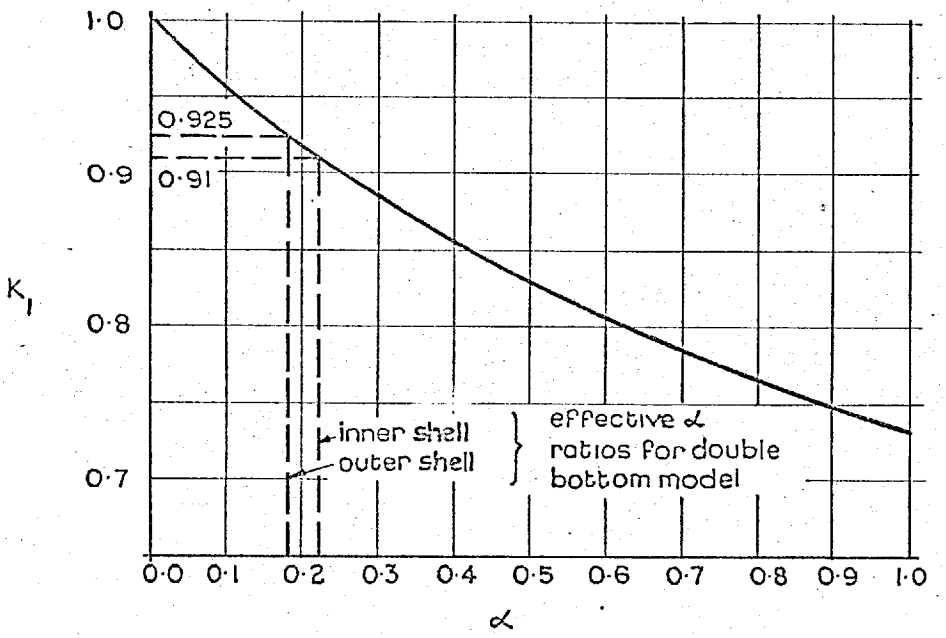

Note:
Both Shade's and Ferahian's solutions are for simply supported ends

K_1 = Reduction factor to be applied to the unstiffened flange solution.

α = Ratio of stiffener area to plate area between stiffeners, assuming stiffener develops full plate stress

(ii) Ferahian's solution for the effect of Longitudinal stiffeners on shear breadth of single web sections.

FIG.26: CURVES USED TO EVALUATE THE LOSS OF EFFECTIVENESS DUE TO LONGITUDINAL STIFFENERS

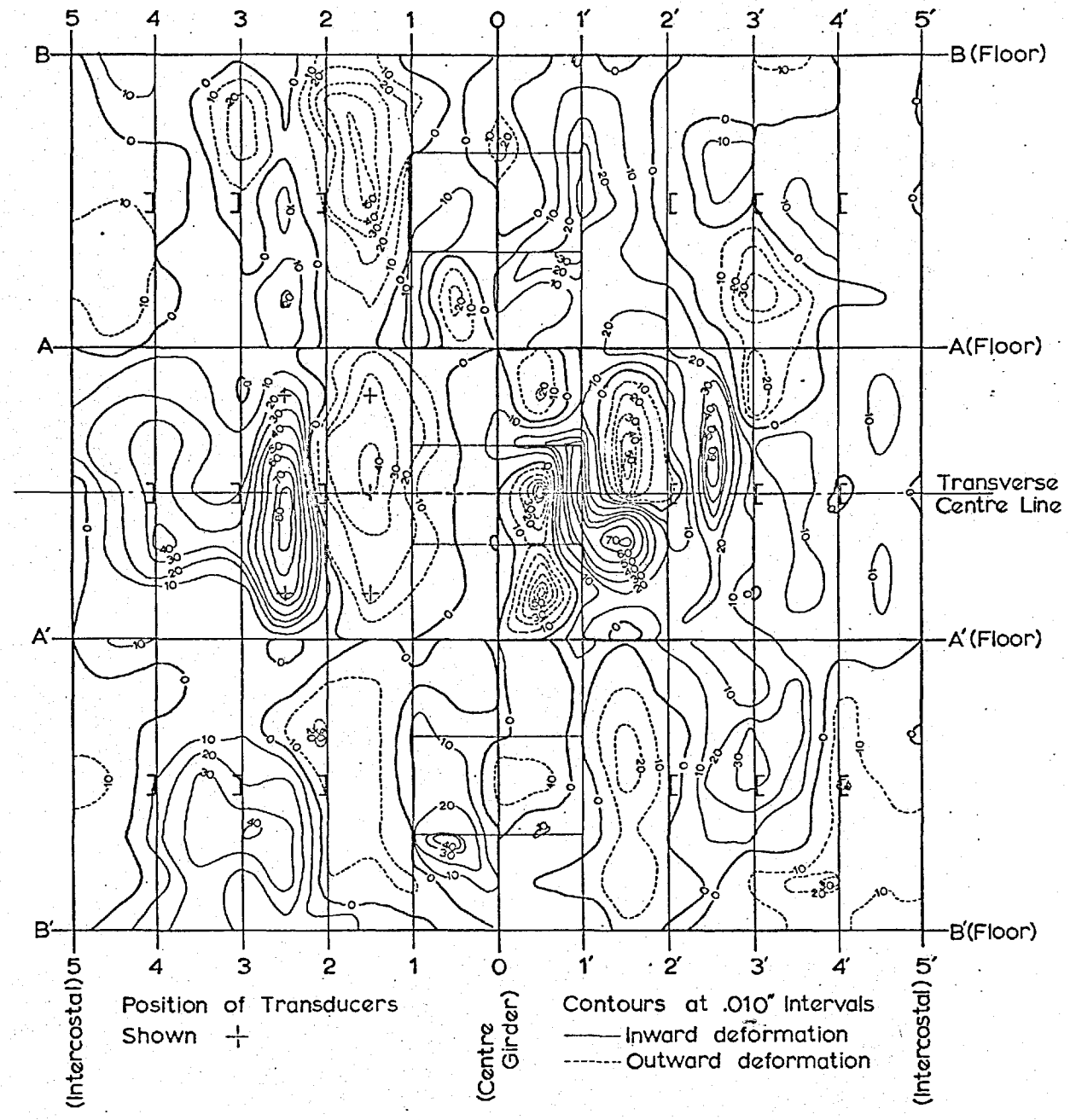

Fig. 27: Double Bottom Model - Contours of Initial Lack of Flatness over Central Panel of Outer Shell

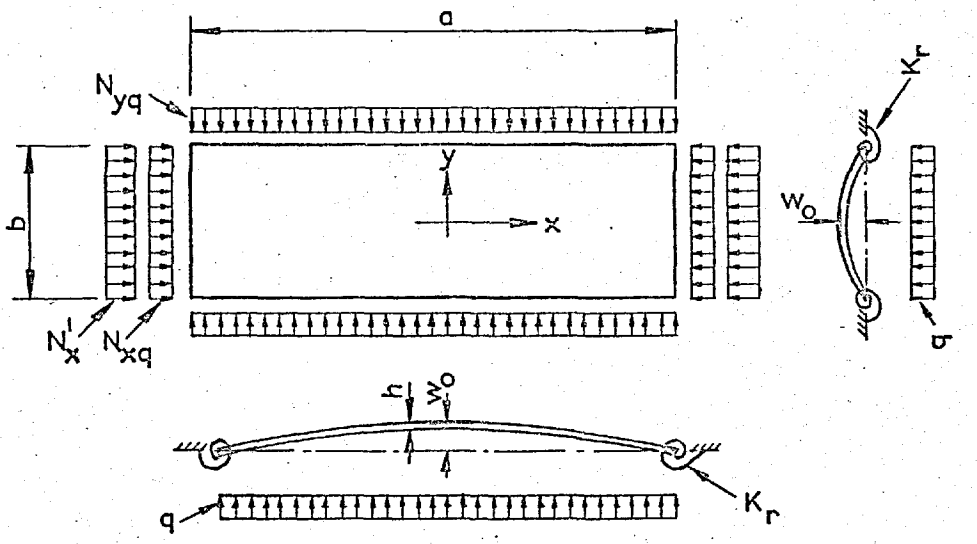

NOTATION : Buckling Breadth Factor { x axis : $\lambda 2x/a$; y axis : $\lambda 2y/b$

panel dimensions : a = 14·5 in.
b = 4·375 in.
h = 0·080 in.

initial deformation : sinusoidal distribution about both axis maximum , w_o at x = y = 0

boundary conditions :

(i) flexural (a) zero vertical displacement
(b) restrained against rotation (K_r)

(ii) membrane (a) edges remain straight
(b) zero shear stress

loading (i) transverse pressure - q p.s.i.

(ii) in-plane load

(a) due to flexure of double bottom where

q = 1 p.s.i. → { N_{xq} = -765 p.s.i. ; N_{yx} = -1385 p.s.i.

NOTE : the symbol q^* denotes transverse and corresponding in-plane load

(b) externally applied

$N'_x = 1^T$ = -1765 p.s.i.

Fig. 28 : Details of Outer Shell Panel

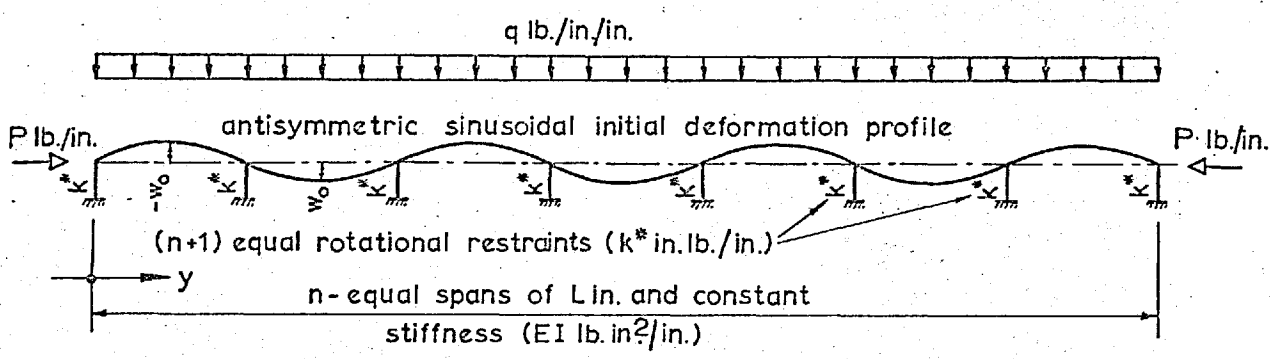

(i) General details of beam-column idealization.

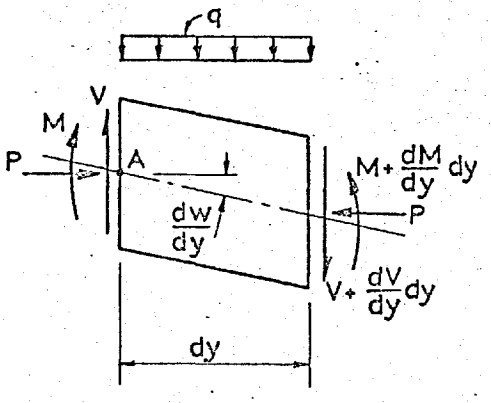

(ii) Forces acting on a beam-col. element.

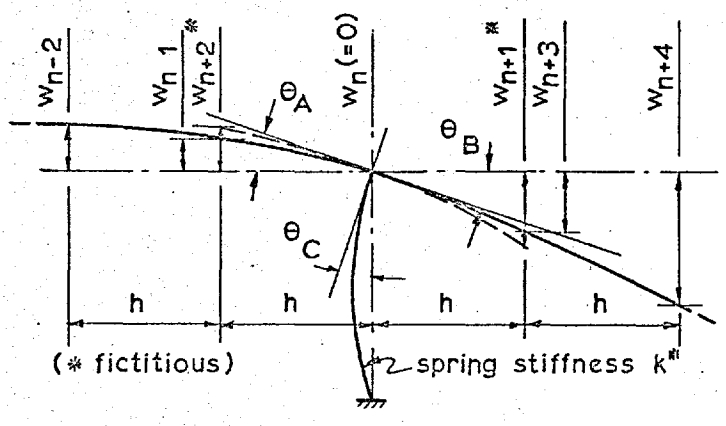

(iii) Finite difference points at an interior support. (deflexion due to applied load)

Fig. 29: Definition of Terms Relevant to Beam-Column Solution.

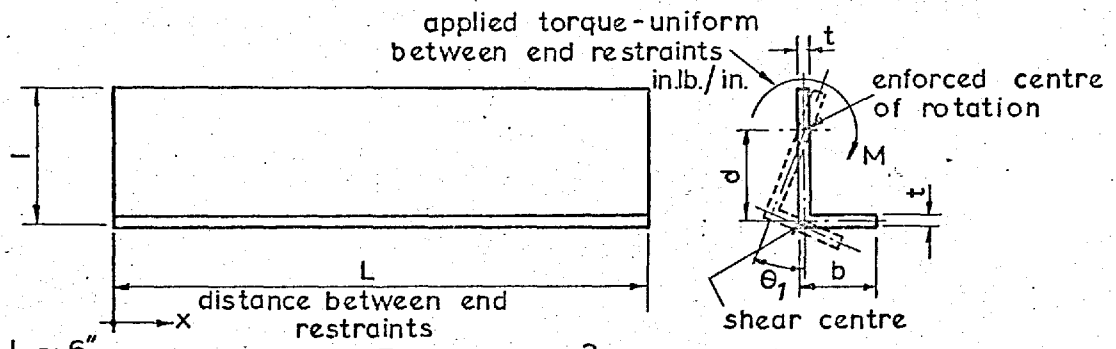

$L = 6''$
$l = 0.92''$
$b = 0.45''$
$t = 0.064''$

$$GK = \frac{E}{2(1+\mu)} \times (l+b-t)\frac{t^3}{3} = 1.327 \times 10^3 \text{ lb.in}^2$$

$$D = EI_f = \frac{Etb^3}{12} = 14.6 \times 10^3 \text{ lb.in}^2$$

(i) Angle properties and loading

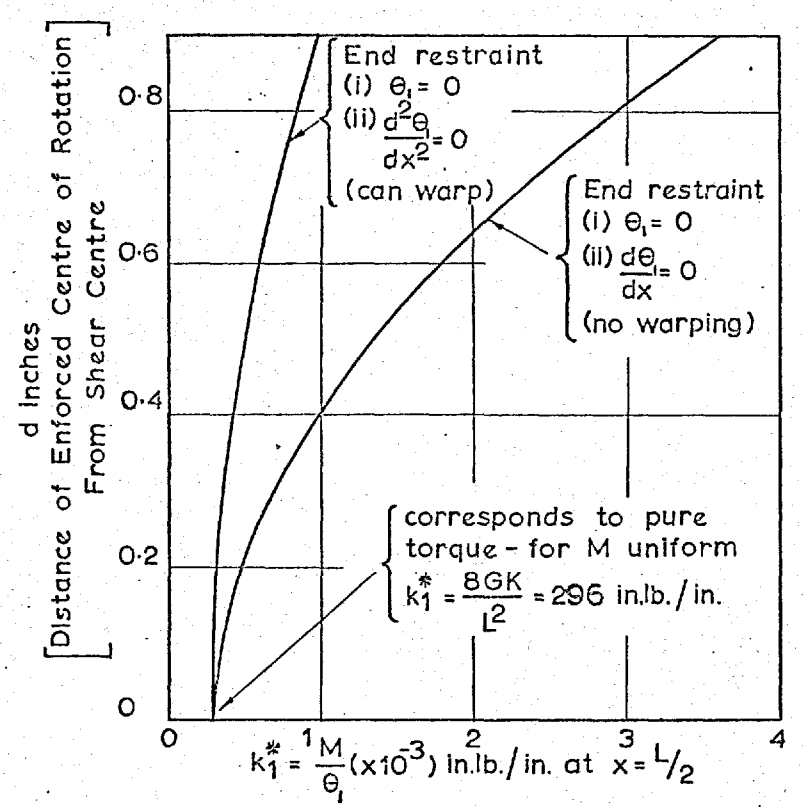

(ii) Effect of enforced centre of rotation

Fig. 30 : External Rotational Restraint of Shell Panels Due to Torsional Rigidity of Angle Stiffeners

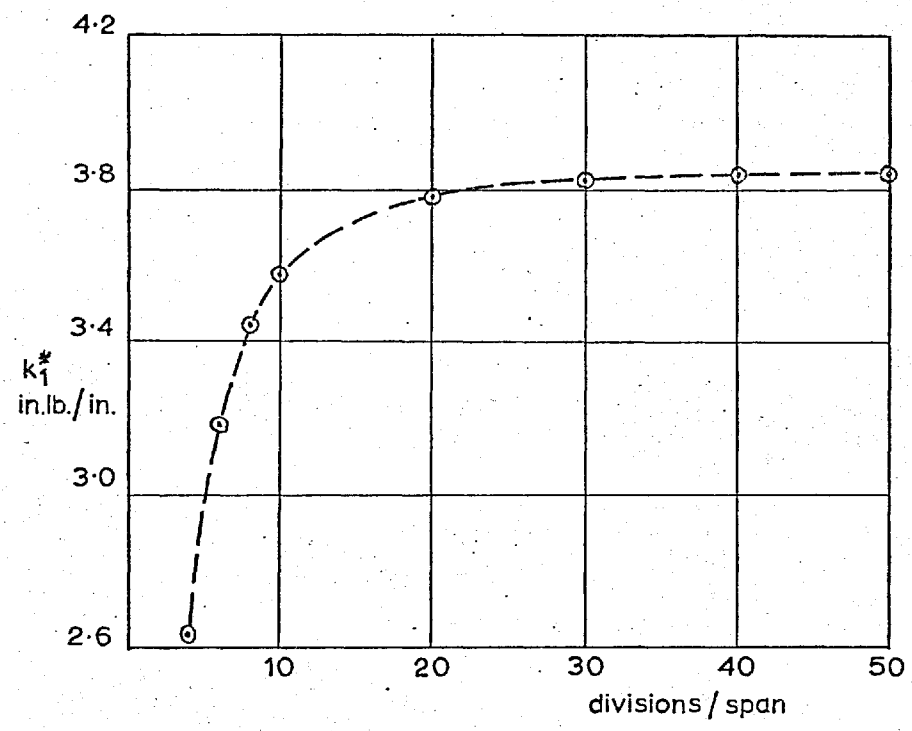

(i) Convergence Behaviour – No Warping

Note: Refer Fig.30 for definition of k_1^* and angle dimensions.

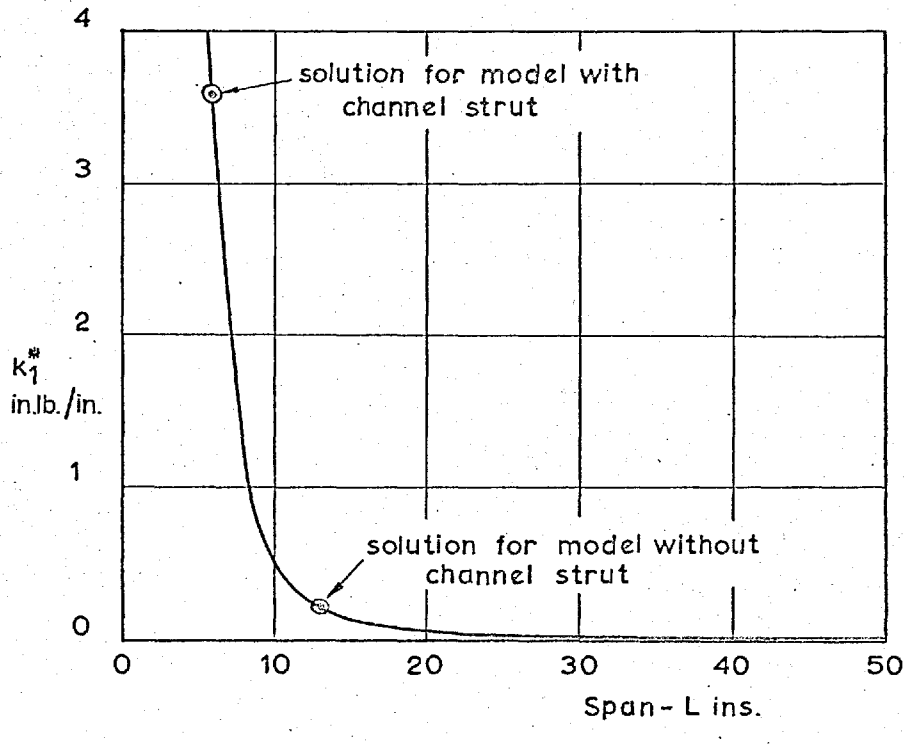

(ii) Effect of Span – No warping

Fig. 31 : Solutions for Torque of Double Bottom Angle Section Shell Stiffener

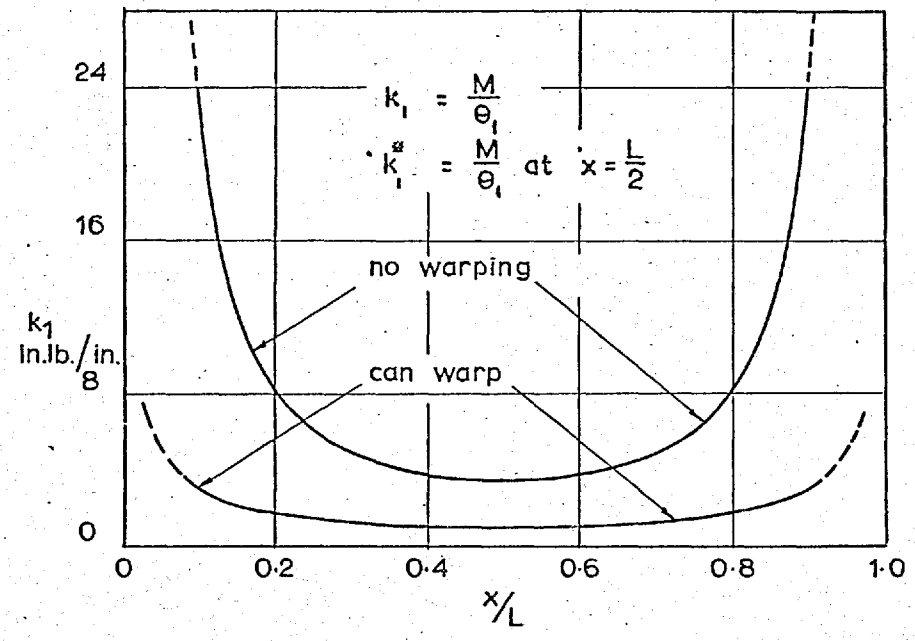

Fig. 32 Variation of k_1 Across Span

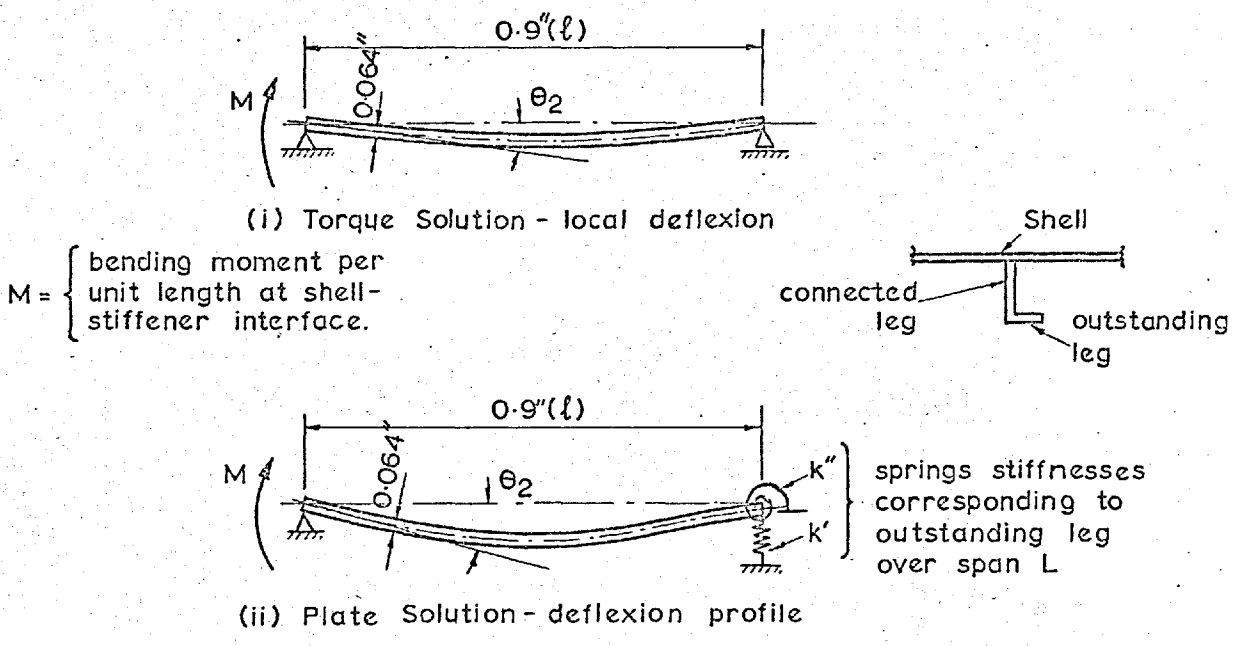

Fig. 33: Beam Idealization of Connected Leg Used to Establish External Rotational Restraint.

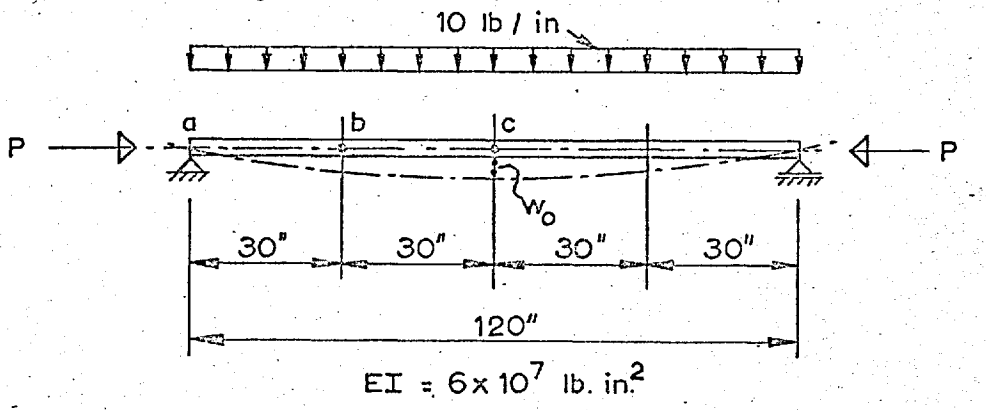

$EI = 6 \times 10^7$ lb. in.^{2}

Case	Solution	Divisions per span	Deflection due Load		Bending Moment	
			w_b in	w_c in	M_b in. lb.	M_c in. lb.
$P=20\times10^3$ lb, $w_o = 0$	Numark	4	0·624	0·878	$2{\cdot}600\times10^4$	$3{\cdot}552\times10^4$
	BEAMCOL	4	0·690	0·971	$2{\cdot}730\times10^4$	$3{\cdot}742\times10^4$
		16	0·627	0·883	$2{\cdot}604\times10^4$	$3{\cdot}566\times10^4$
$P=30\times10^3$ lb, $w_o = 0{\cdot}15$"	Numark	4	0·142	0·197	$6{\cdot}15\times10^3$	$7{\cdot}60\times10^3$
	BEAMCOL	4	0·143	0·198	$5{\cdot}86\times10^3$	$7{\cdot}33\times10^3$
		16	0·141	0·196	$6{\cdot}07\times10^3$	$7{\cdot}59\times10^3$

Note : For details of Numark solution see Ref. 34

(i) Simply Supported Span Under Combined Load With and Without Initial Deformation

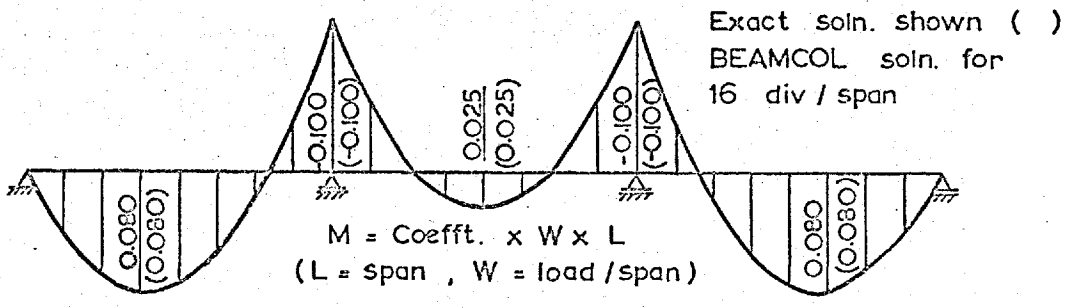

(ii) Bending Moment Distribution For 3 Span Beam Under Uniform Transverse Load Only

Fig. 34 : Accuracy Checks - BEAMCOL Program

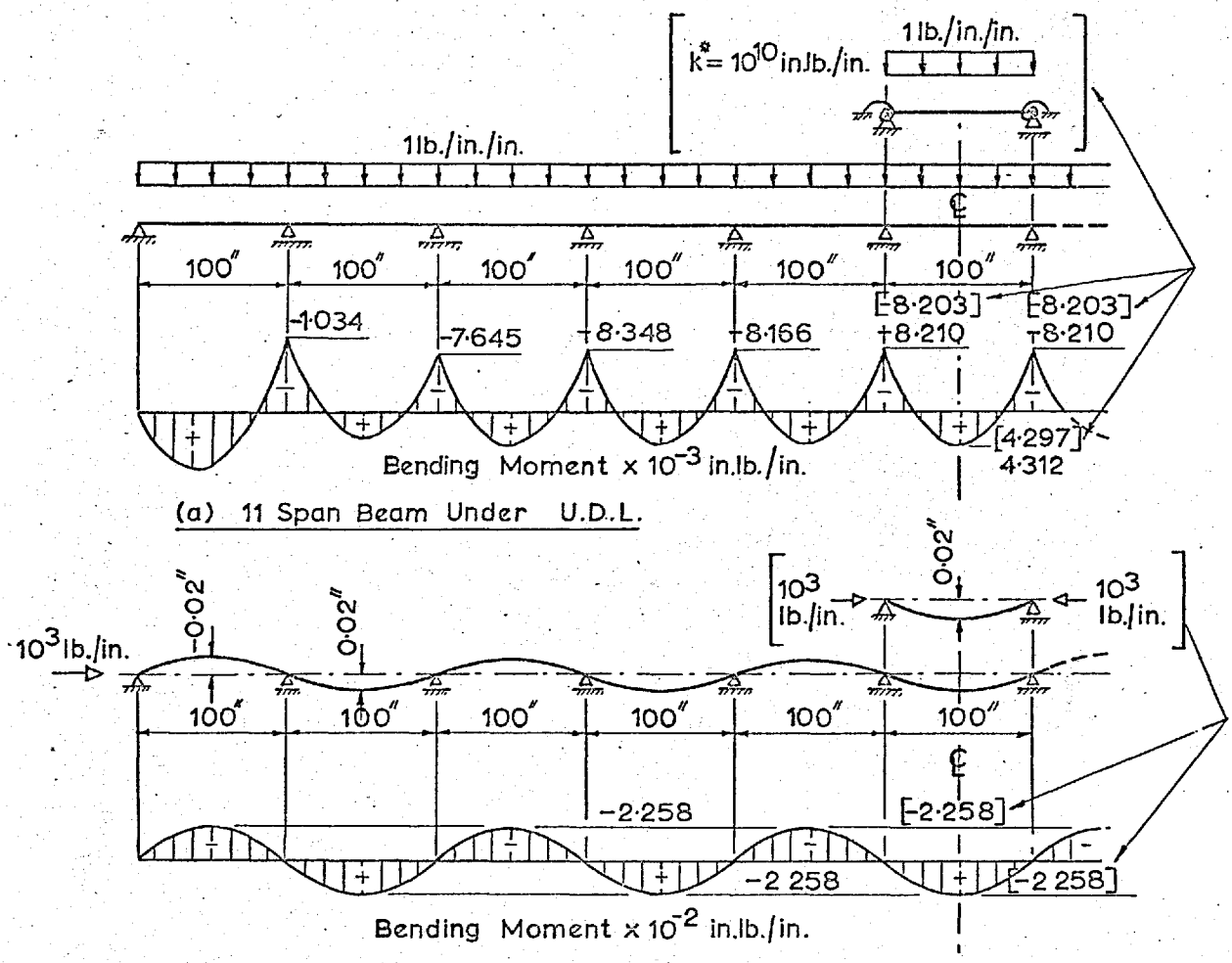

(i) Comparison of Equivalent Multiple and Single Span Solutions.

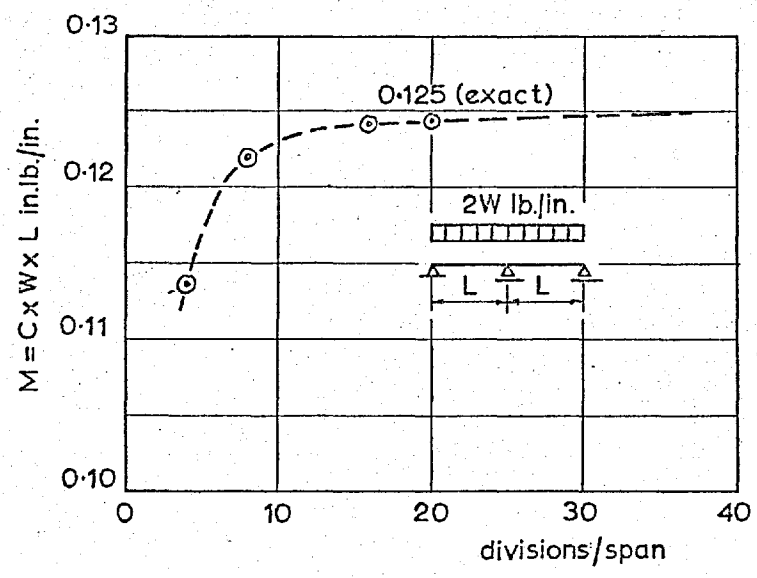

(ii) Convergence Behaviour of Central Support Moment for 2 Span Beam Under U.D.L.

Fig. 35 : Accuracy Checks — BEAMCOL Program.

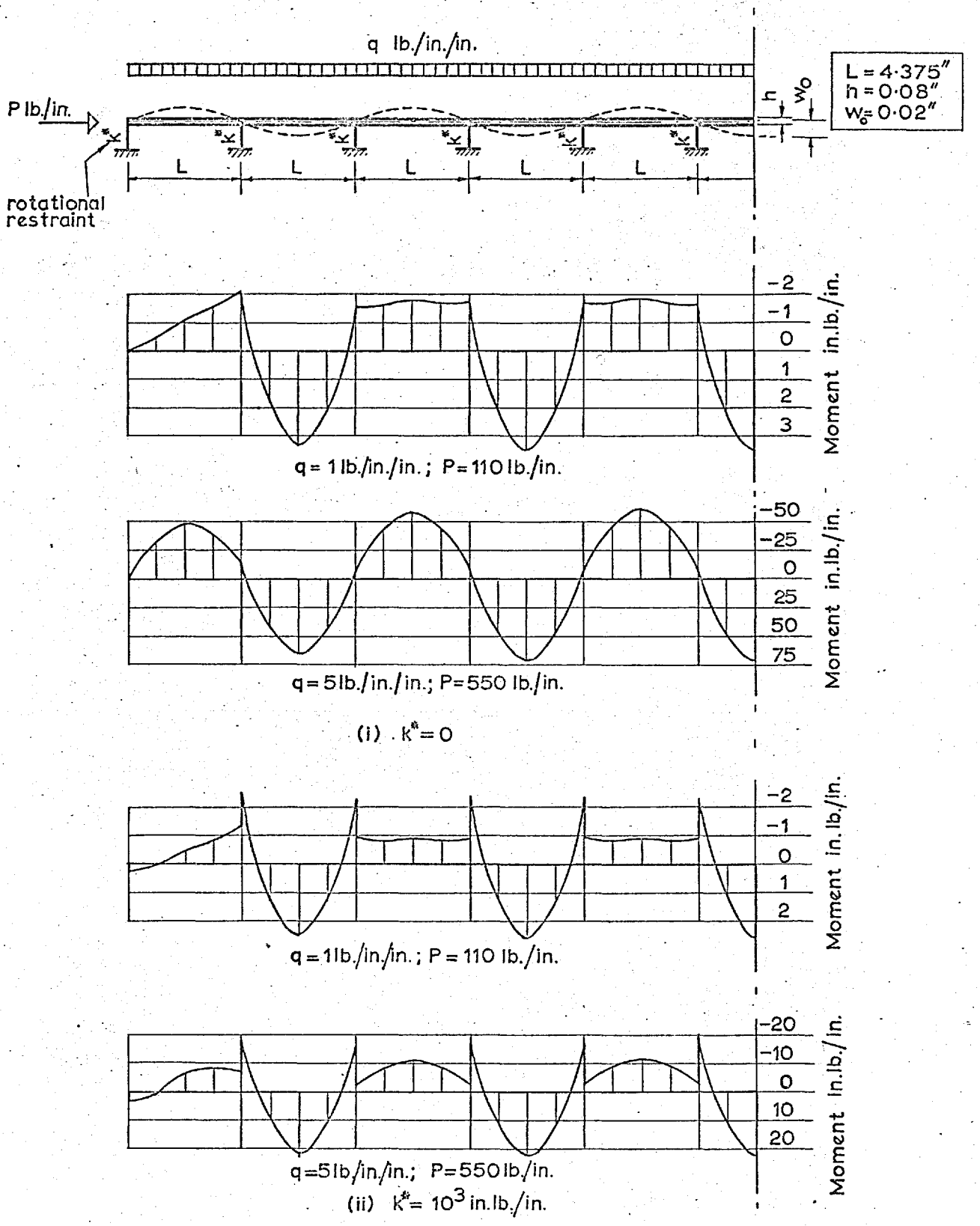

Fig.36 : Double Bottom Shell Idealised as Continuous Beam-Column: Effect of Loading on Moment Distribution.

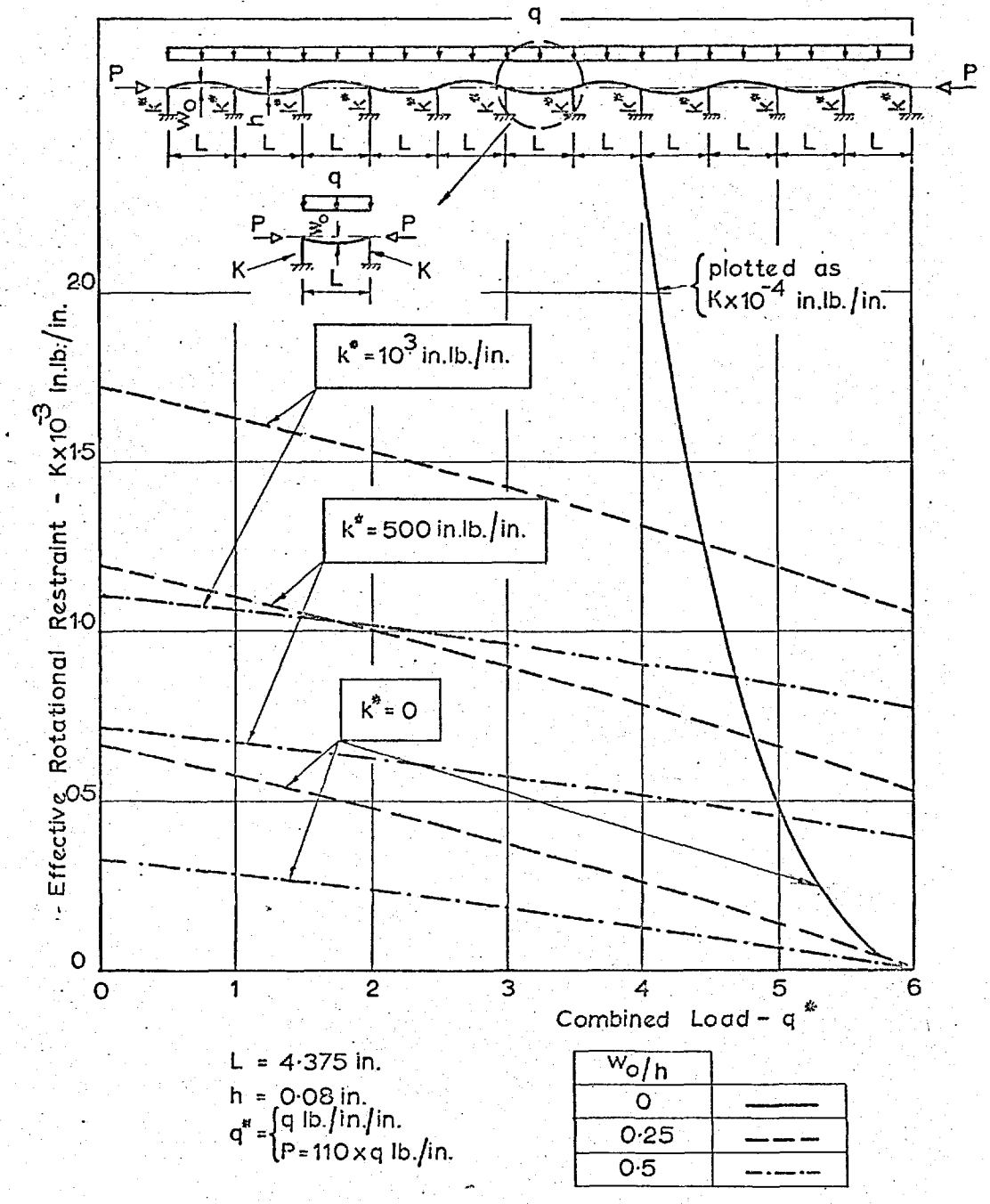

Fig. 37 : Double Bottom Shell Idealised As Continuous Beam-Column Effective Rotational Restraint for Single Span.

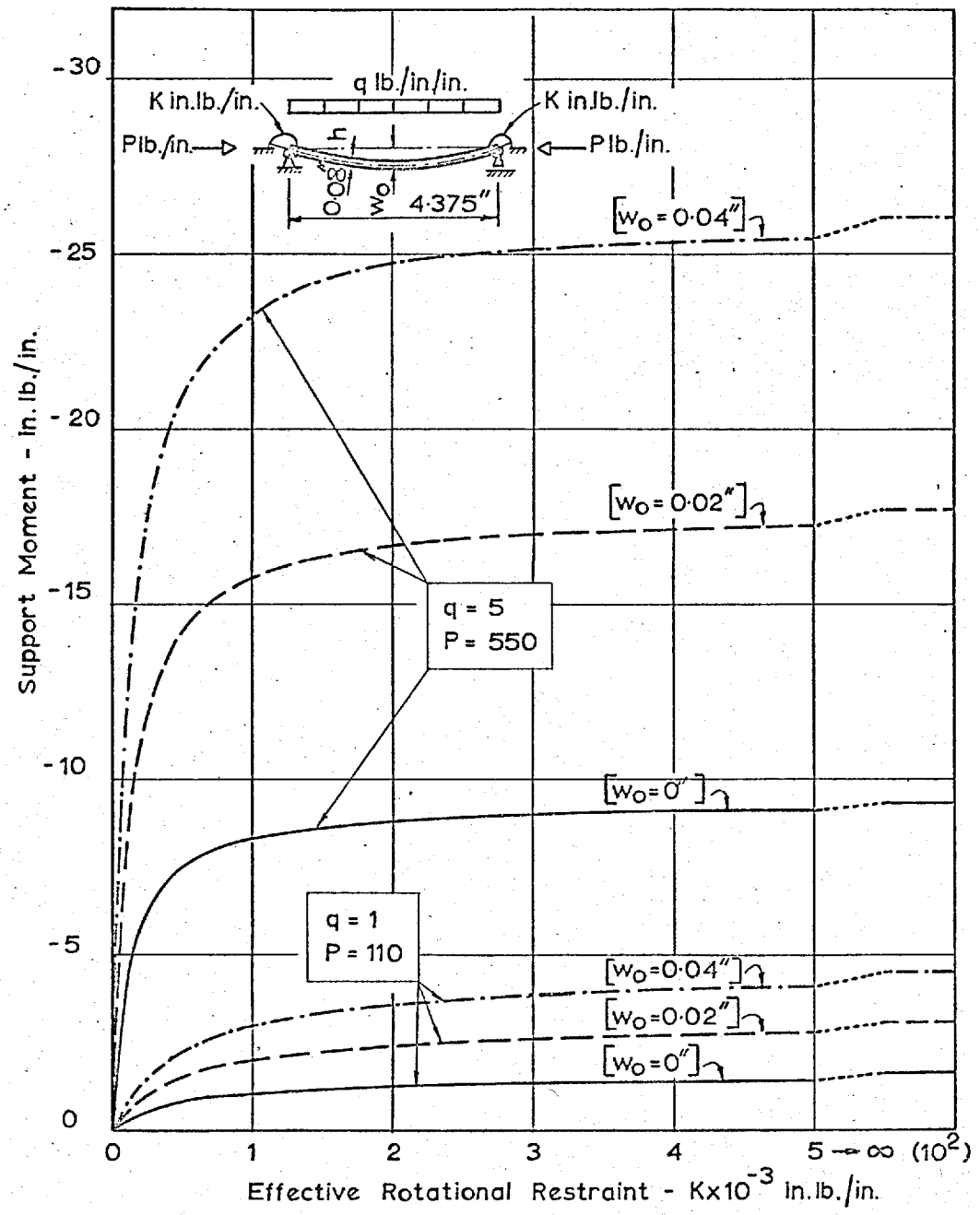

Fig.38: Double Bottom Shell Idealised as Single Span Beam - Column
Support Moment as a Function of Effective Rotational Restraint

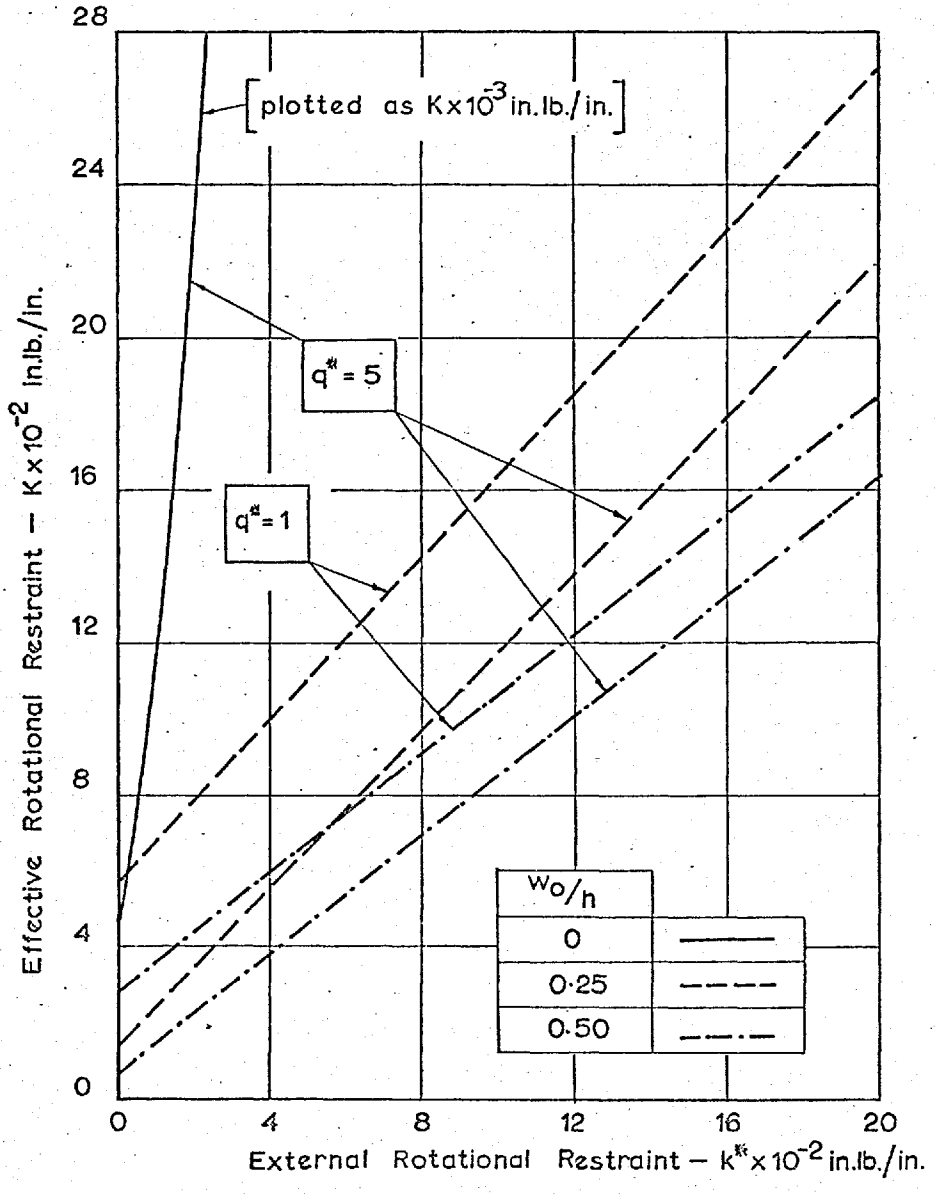

Fig. 39: Relationship between External and Effective Rotational Restraint for Model Shell Panels

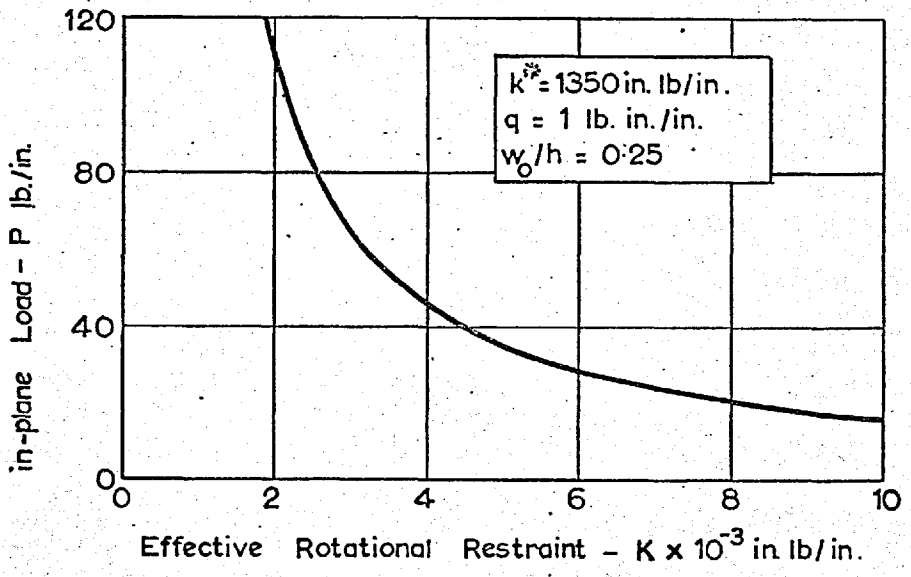

Fig. 40 : Increase in Effective Rotational Restraint Away From Centre of Model

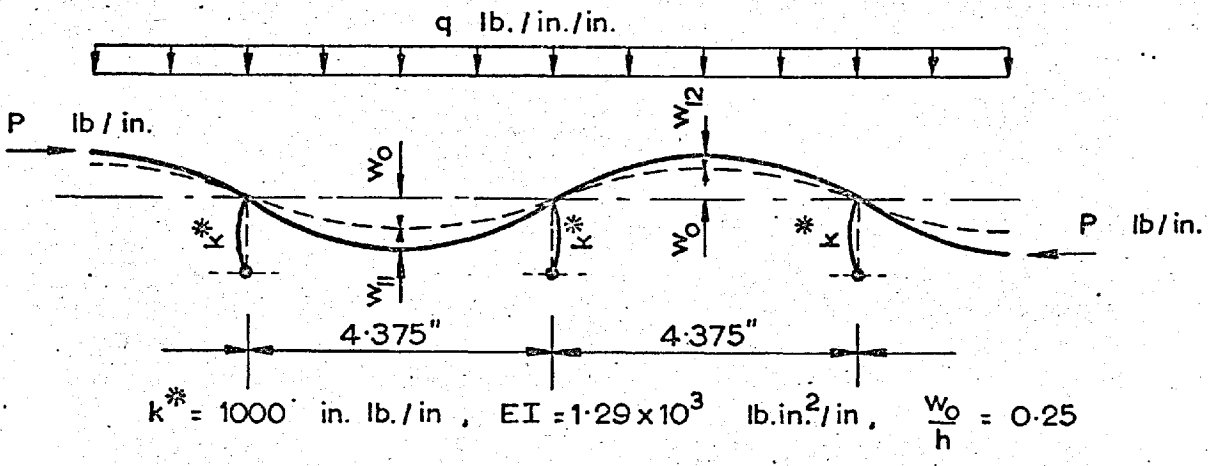

q*	w_{11} in.	w_{12} in.
1	0·00334	0·00160
2	0·00743	0·00379
3	0·01261	0·00689
4	0·01945	0·01144
5	0·02905	0·01851

Fig. 41 : Comparison of Deflexions in Adjacent Spans

TABLE 1

Buckling Breadth Factors for Typical Double-Bottom Panel

$W_o/h = 0$

(i) $N'_x = 0^T$

q^* p.s.i.	λ_{2x}/a				λ_{2y}/b			
	uniaxial load		biaxial load		uniaxial load		biaxial load	
	a	b	a	b	a	b	a	b
0	-	-	-	-	-	-	-	-
1	1	1	-	1	1	1	-	1
2	1	1	-	1	1	1	-	1
3	1	1	-	1	1	1	-	1
4	1	1	-	1	1	1	-	1
5	1	1	-	1	0.99	1	-	1

(ii) $N'_x = 5^T$

q^* p.s.i.	λ_{2x}/a				λ_{2y}/b			
	uniaxial load		biaxial load		uniaxial load		biaxial load	
	a	b	a	b	a	b	a	b
0	1	1	-	1	-	-	-	-
1	1	1	-	1	-	-	-	1
2	1	1	-	1	-	-	-	1
3	1	1	-	1	-	-	-	1
4	1	1	-	1	-	-	-	1
5	1	1	-	1	-	-	-	0.99

(iii) $N'_x = 10^T$

q^* p.s.i.	λ_{2x}/a				λ_{2y}/b			
	uniaxial load		biaxial load		uniaxial load		biaxial load	
	a	b	a	b	a	b	a	b
0	1	1	-	1	-	-	-	-
1	1	1	-	1	-	-	-	1
2	1	1	-	1	-	-	-	1
3	1	1	-	1	-	-	-	1
4	1	1	-	1	-	-	-	1
5	1	1	-	1	-	-	-	0.99

Note: Refer Figure 28 for details of panel and loading

T A B L E 2

Buckling Breadth Factors for Typical Double-Bottom Panel

$W_o/h = 0.5$

(i) $N'_x = 0^T$

q^* p.s.i.	λ_{2x}/a				λ_{2y}/b			
	uniaxial load		biaxial load		uniaxial load		biaxial load	
	a	b	a	b	a	b	a	b
0	-	-	-	-	-	-	-	-
1	0.99	0.99	-	0.98	0.90	0.89	-	0.89
2	0.99	0.99	-	0.97	0.84	0.85	-	0.84
3	0.99	0.99	-	0.97	0.83	0.84	-	0.83
4	0.99	0.99	-	0.97	0.82	0.83	-	0.82
5	0.99	0.99	-	0.96	0.81	0.82	-	0.81

(ii) $N'_x = 5^T$

q^* p.s.i.	λ_{2x}/a				λ_{2y}/b			
	uniaxial load		biaxial load		uniaxial load		biaxial load	
	a	b	a	b	a	b	a	b
0	1	1	-	1	-	-	-	-
1	1	1	-	1	-	-	-	0.84
2	1	1	-	1	-	-	-	0.84
3	1	1	-	0.99	-	-	-	0.81
4	1	1	-	0.99	-	-	-	0.81
5	1	1	-	0.99	-	-	-	0.80

(iii) $N'_x = 10^T$

q^* p.s.i.	λ_{2x}/a				λ_{2y}/b			
	uniaxial load		biaxial load		uniaxial load		biaxial load	
	a	b	a	b	a	b	a	b
0	1	1	-	1	-	-	-	-
1	1	1	-	1	-	-	-	0.80
2	1	1	-	1	-	-	-	0.81
3	1	1	-	1	-	-	-	0.80
4	1	1	-	0.99	-	-	-	0.79
5	1	1	-	0.99	-	-	-	0.79

Note: Refer Figure 28 for details of panel and loading

TABLE 3

Buckling Breadth Factors for Typical Double-Bottom Panel

$W_o/h = 1.0$

(i) $N'_x = 0^T$

q^* p.s.i.	λ_{2x}/a				λ_{2y}/b			
	uniaxial load		biaxial load		uniaxial load		biaxial load	
	a	b	a	b	a	b	a	b
0	-	-	-	-	-	-	-	-
1	0.98	0.97	-	0.93	0.69	0.70	-	0.69
2	0.98	0.97	-	0.91	0.65	0.67	-	0.66
3	0.98	0.97	-	0.91	0.64	0.66	-	0.65
4	0.98	0.97	-	0.91	0.63	0.65	-	0.64
5	0.98	0.97	-	0.90	0.62	0.64	-	0.63

(ii) $N'_x = 5^T$

q^* p.s.i.	λ_{2x}/a				λ_{2y}/b			
	uniaxial load		biaxial load		uniaxial load		biaxial load	
	a	b	a	b	a	b	a	b
0	1	1	-	0.99	-	-	-	-
1	1	1	-	0.99	-	-	-	0.60
2	1	0.99	-	0.99	-	-	-	0.62
3	0.99	0.99	-	0.98	-	-	-	0.62
4	0.99	0.99	-	0.97	-	-	-	0.61
5	0.99	0.99	-	0.96	-	-	-	0.61

(iii) $N'_x = 10^T$

q^* p.s.i.	λ_{2x}/a				λ_{2y}/b			
	uniaxial load		biaxial load		uniaxial load		biaxial load	
	a	b	a	b	a	b	a	b
0	1	1	-	0.99	-	-	-	-
1	1	1	-	0.99	-	-	-	0.53
2	1	1	-	0.99	-	-	-	0.58
3	1	0.99	-	0.98	-	-	-	0.59
4	0.99	0.99	-	0.98	-	-	-	0.59
5	0.99	0.99	-	0.98	-	-	-	0.59

Note: Refer Figure 28 for details of panel and loading

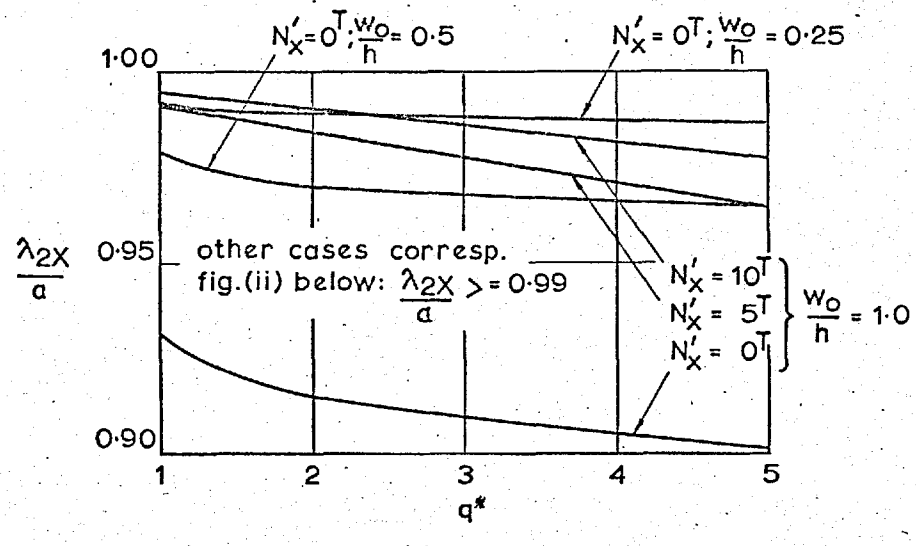

(i) X axis

Refer Fig. for definition of symbols

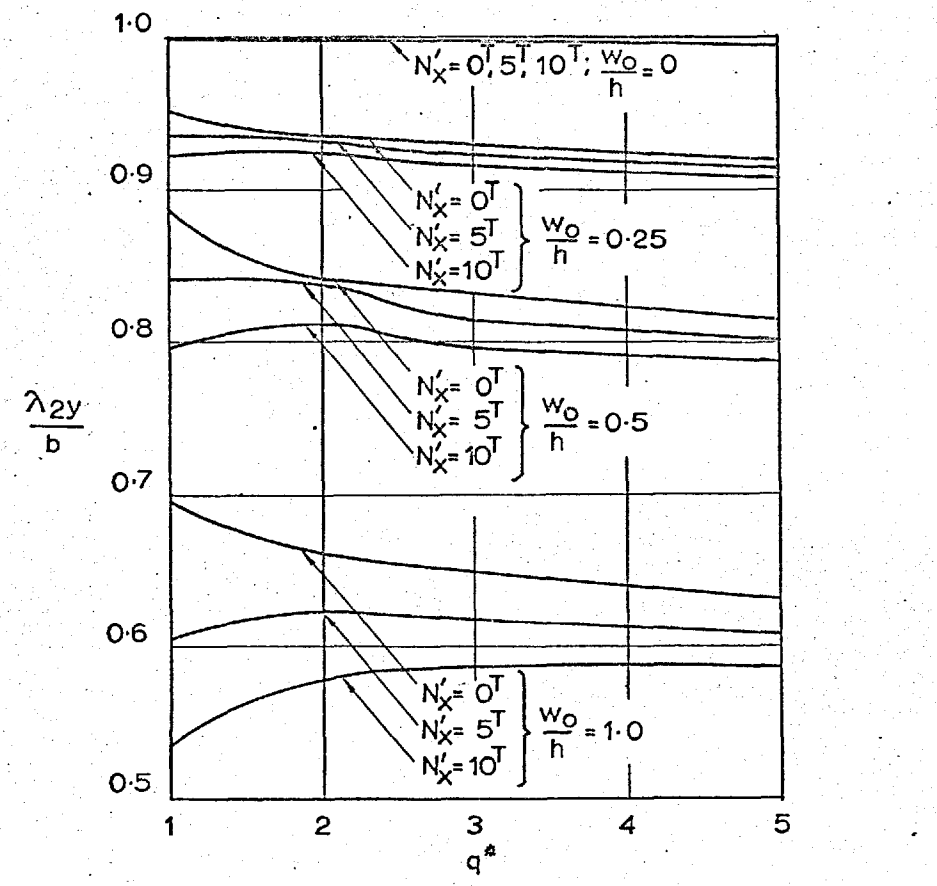

(ii) y axis

Fig. 42 : Loss of Shell Effectiveness Due to Local Bending
Panels Clamped

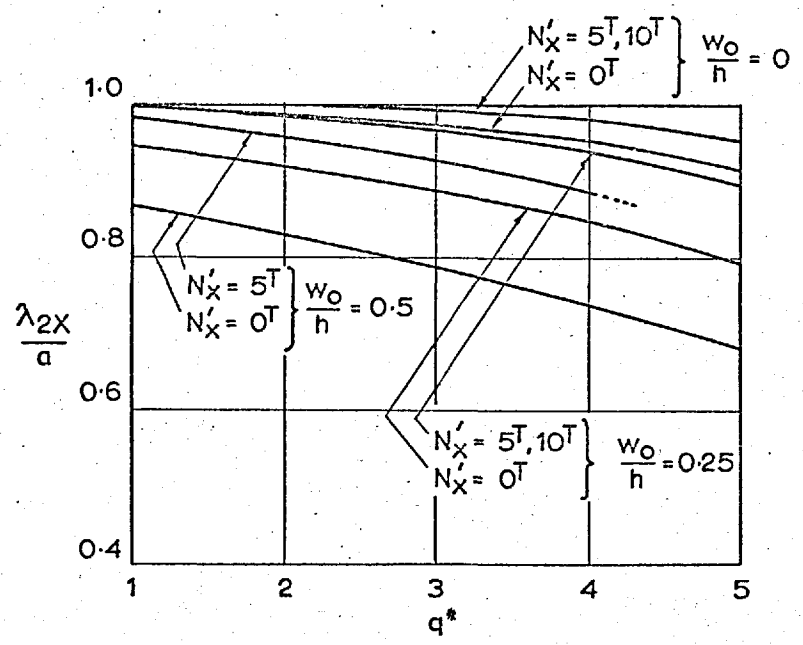

(i) X axis

Refer Fig. for definition of symbols

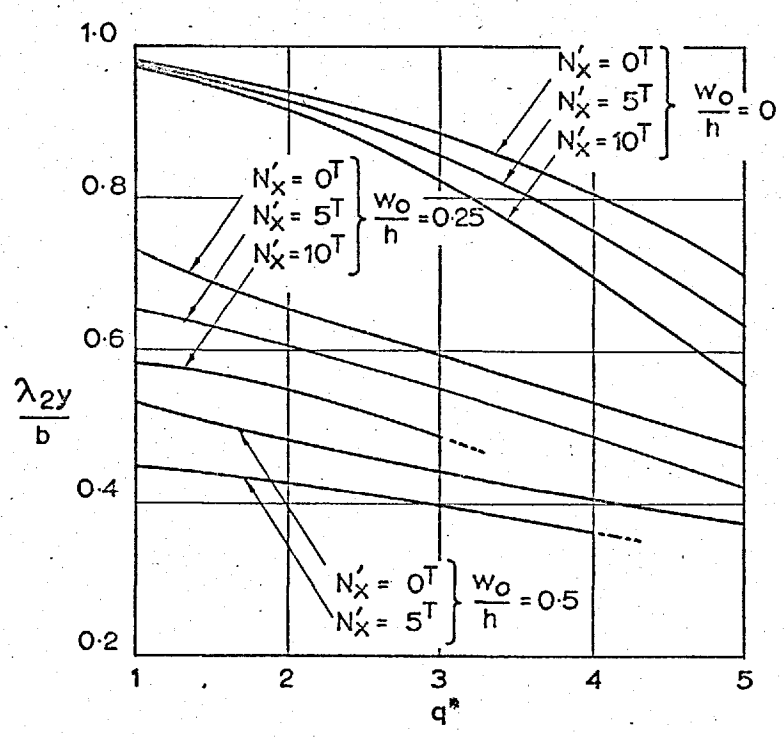

(ii) y axis

Fig.43: Loss of Shell Effectiveness Due to Local Bending Panels Simply Supported

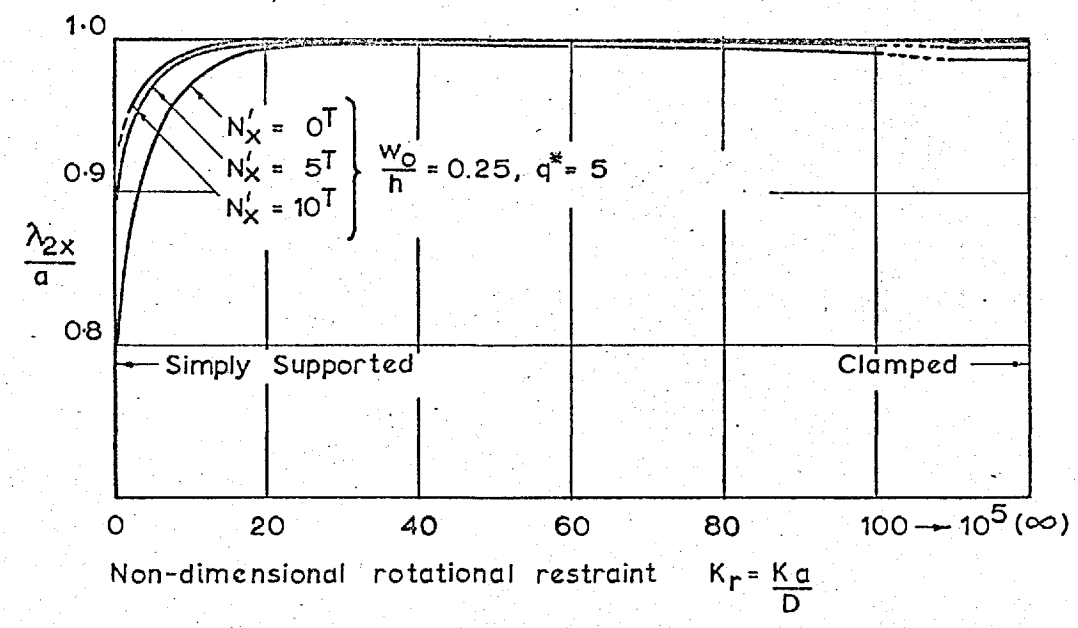

(i) X axis

Refer Fig. for definition of symbols

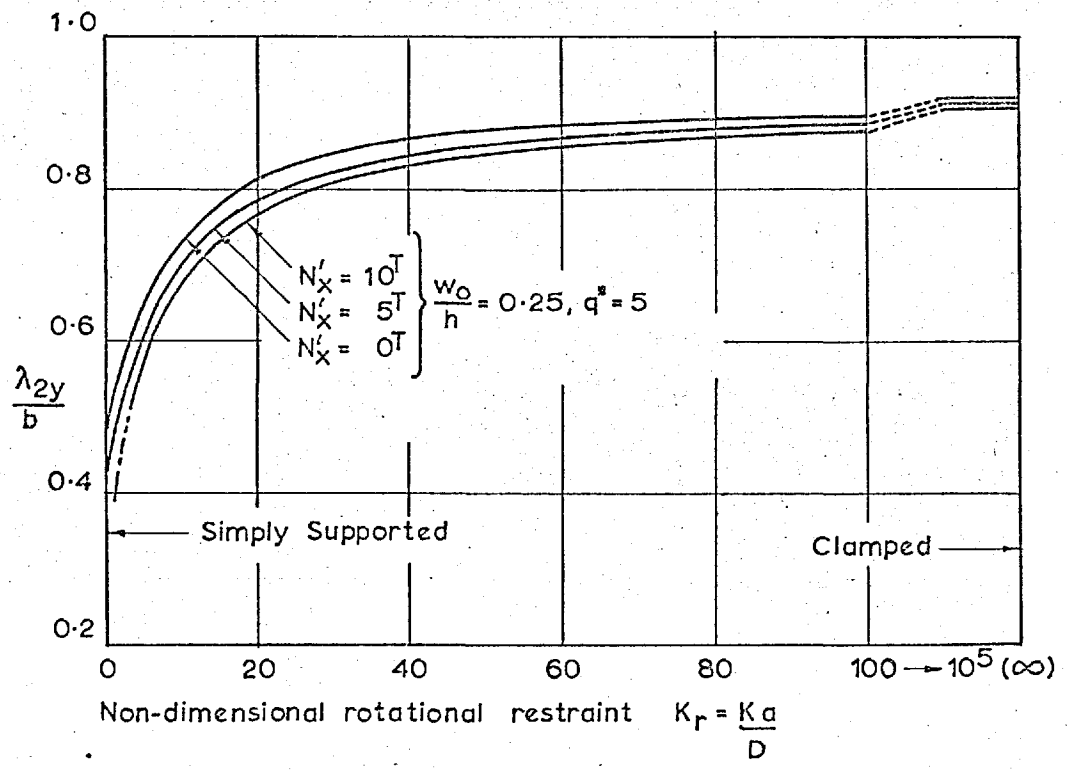

(ii) y axis

Fig. 44 : Loss of Shell Effectiveness Due to Local Bending Effect of Elastic Restraint

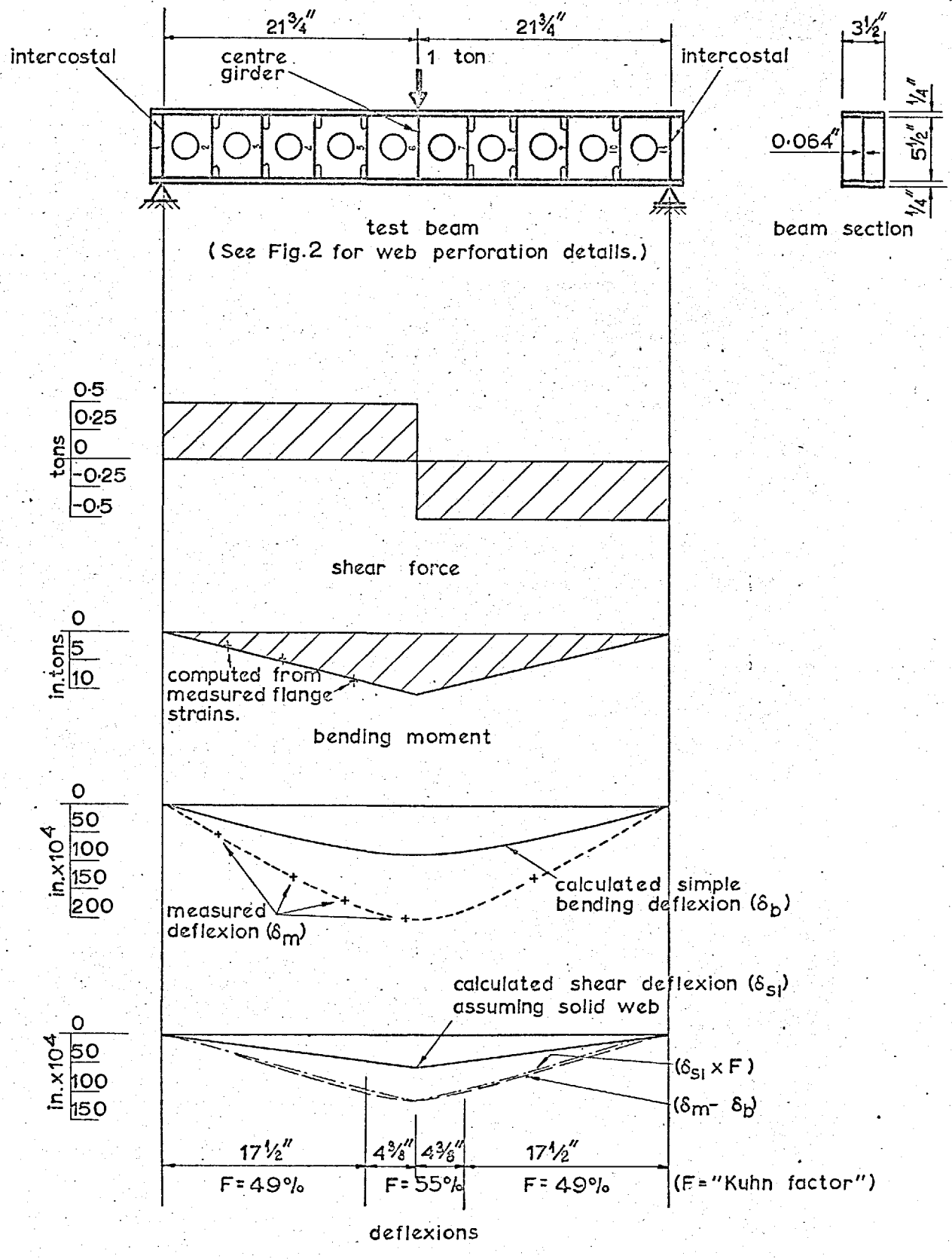

Fig. 45 : Test to Determine Effective Web Shear Stiffness.

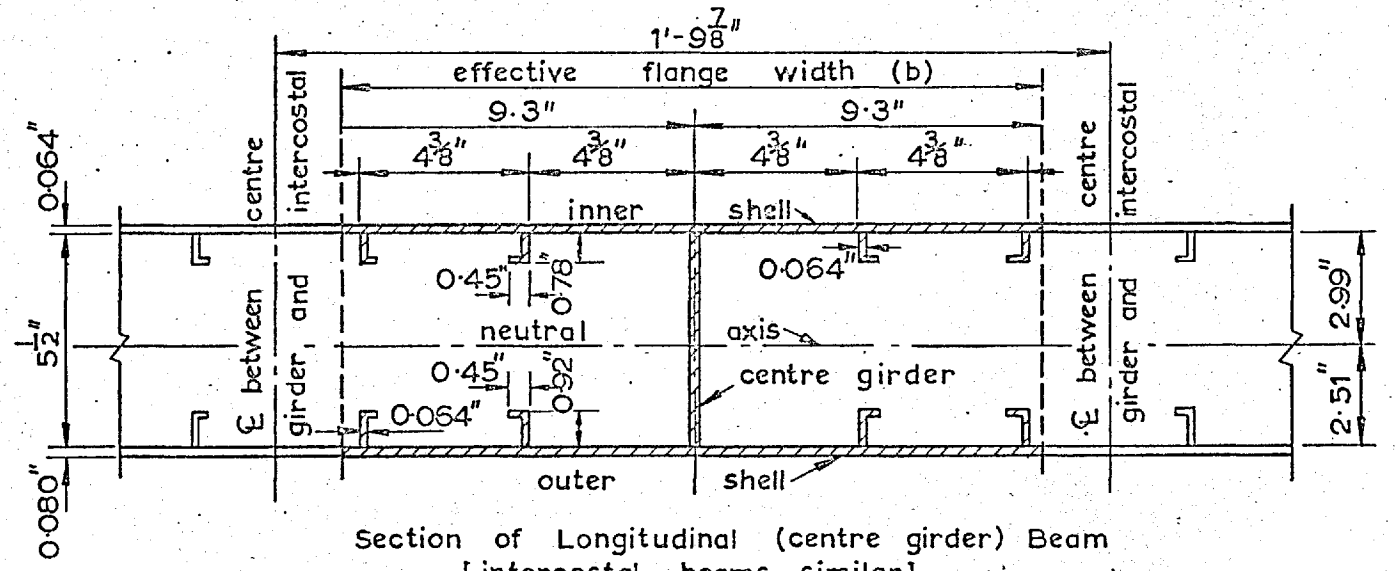

Section of Longitudinal (centre girder) Beam
[intercostal beams similar]

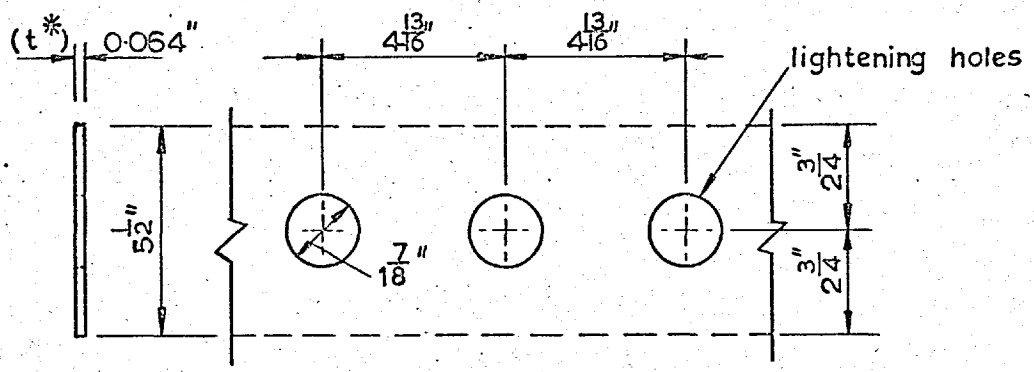

Detail of Intercostal Perforations
[centre girder solid]

Notes : (i) loss of flange effectiveness due to shear lag and out plane flange bending taken as 15% gives : $b = 21{\cdot}875 \times 0{\cdot}85 = 18{\cdot}594$ in

(ii) loss of web flexural effectiveness due to perforations
centre girder - nil
intercostal - 1%
} t^* taken as 0·064 in

(iii) the position of the neutral axis computed for these effective dimensions shown above

(iv) the corresponding 2nd moments of area are :
flanges : $I_{fx} = 20{\cdot}1880$ in^4 = 0·9390 in^4/in.
webs : $I_{wx} = 0{\cdot}9081$ in^4 = 0·0415 in^4/in.
stiffeners : $I_{sx} = 3{\cdot}1237$ in^4 = 0·1428 in^4/in.

(v) solid web cross sectional area
A'_{wx} 0·352 in^2 = 0·0161 in^2/in.

(vi) effective web area (20% loss due perforations)
$A_{wx} = 0{\cdot}0161 \times 0{\cdot}80 = 0{\cdot}0129$ in^2/in.

Fig. 46 : Details of Longitudinal Beam Element (x = axis)

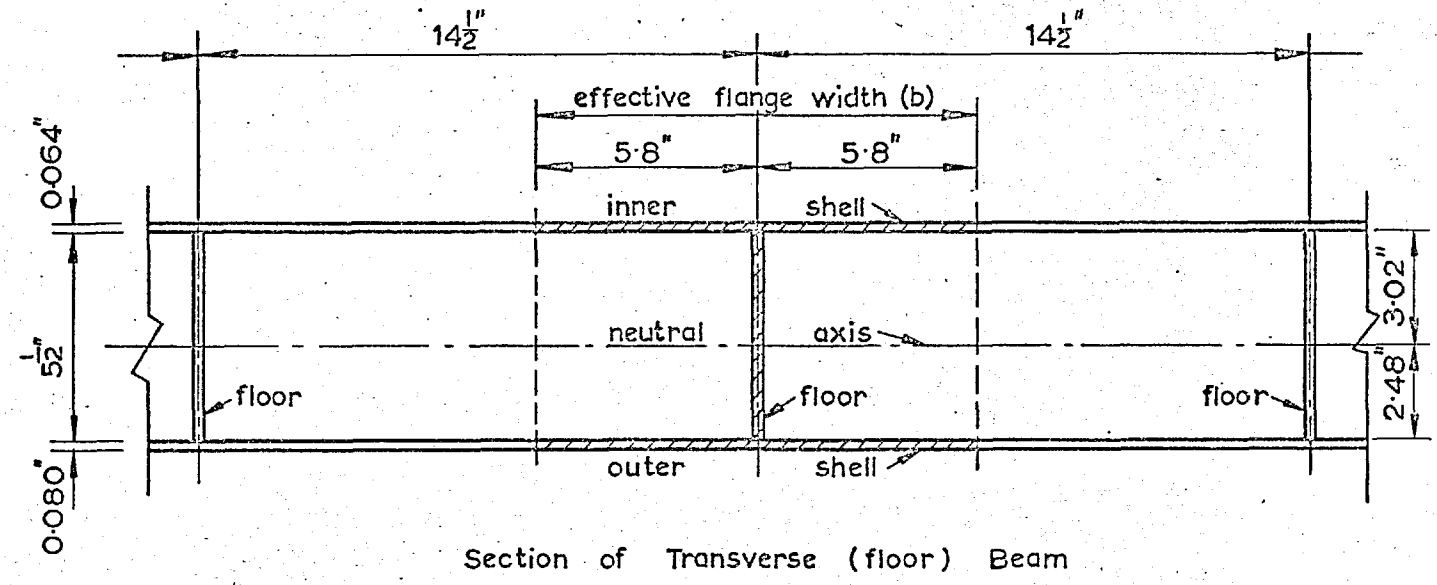

Section of Transverse (floor) Beam

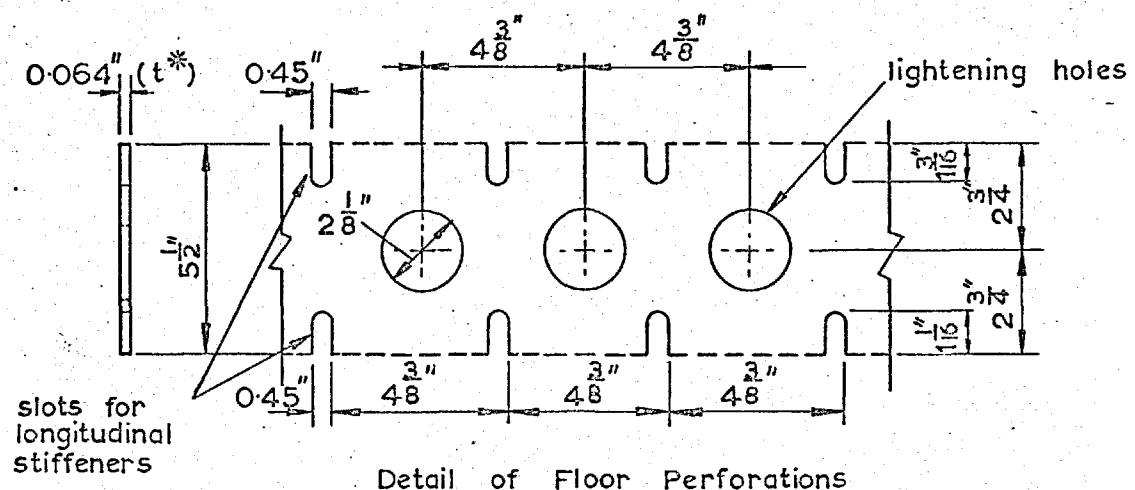

Detail of Floor Perforations

Notes : (i) loss of flange effectiveness due to shear lag and out of plane flange bending taken as 20%
gives : b = 14·5 x 0·8 = 11·6 in.

(ii) loss of floor flexural effectiveness due to perforations accounted for by taking reduced floor thickness
where : area perforation / solid area = 0·19
gives : effective t^* = 0·064 x 0·81 = 0·052 in.

(iii) the position of the neutral axis computed for these effective dimensions is shown above

(iv) the corresponding 2nd moments of area are :
flanges : I_{fy} = 12·8095 in^4 = 0·8834 in^4/in.
floors : I_{wy} = 0·7415 in^4 = 0·0511 in^4/in.

(v) solid floor cross sectional area
A'_{wy} = 0·352 in^2 = 0·0243 in^2/in.

(vi) effective web area (30% loss due perforations)
A_{wy} = 0·0243 x 0·70 = 0·0170 $in.^2$ / in.

Fig. 47 : Details of Transverse Beam Element (y axis)

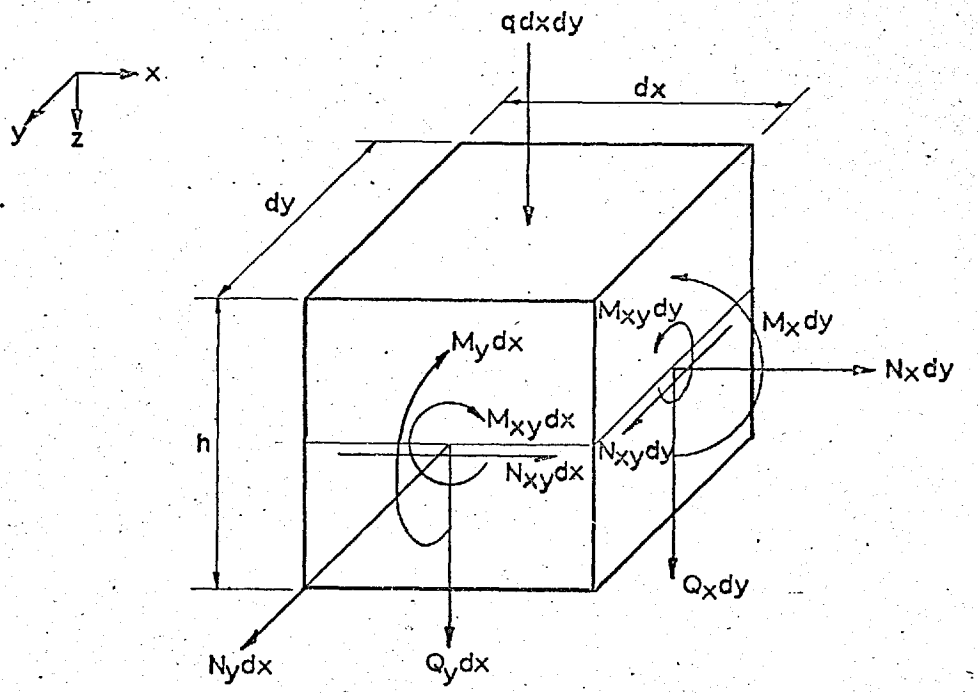

Fig.48 : Positive directions of forces and moments acting on differential element dxdy.

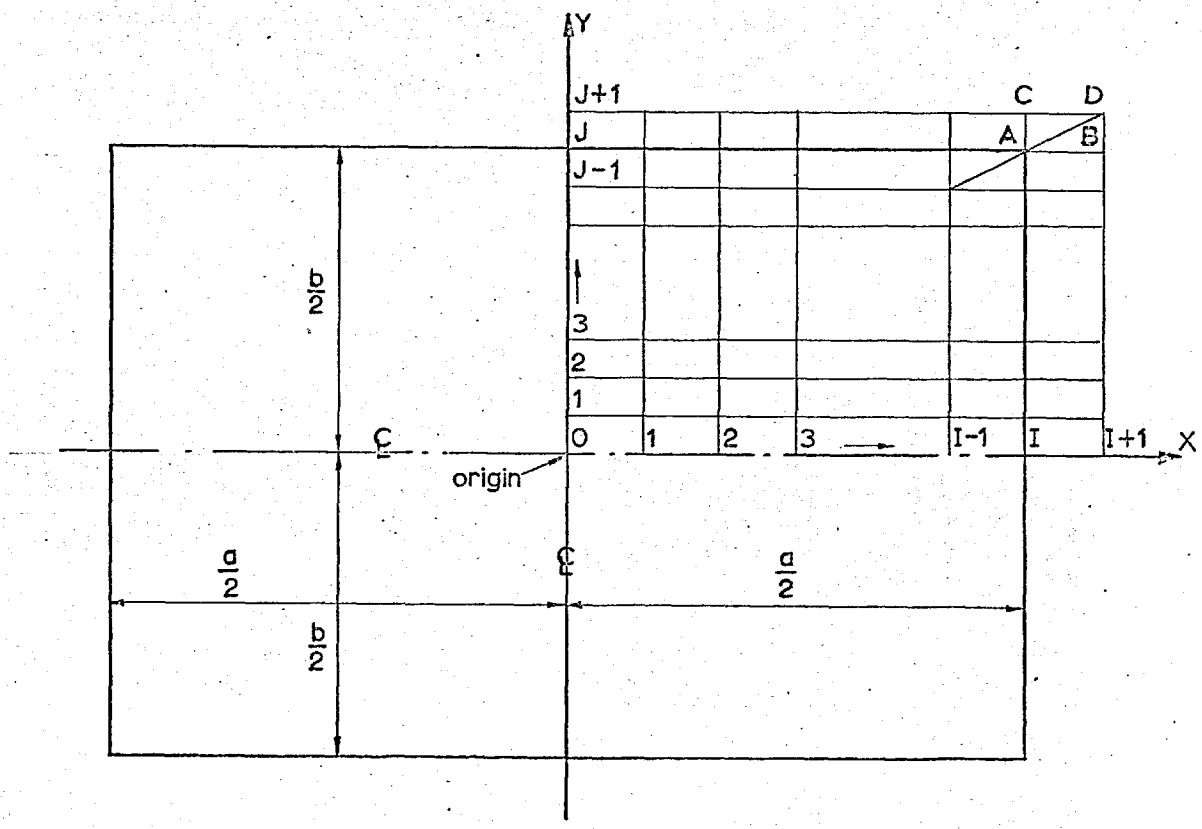

Fig.49 : Rectangular Plate Showing Co-ordinate Axes and Finite Difference Mesh..

Case	Boundary Condition		w_1 $(=k_1\frac{a^4}{D}q)$	w_3 $(=k_2\frac{a^4}{D}q)$	M_{x1} $(=k_3a^2q)$	M_{y1} $(=k_4a^2q)$	M_{x2} $(=k_5a^2q)$	M_{y3} $(=k_6a^2q)$	Scource
	$x=\pm a/2$	$y=\pm b/2$	k_1	k_2	k_3	k_4	k_5	k_6	
1	simple support	simple support	0.00402	0	0.0472	0.0472	0	0	*
			0.00406	0	0.0479	0.0479	0	0	Ref.35
2	"	clamped	0.00190	0	0.0241	0.0330	0	-0.0697	*
			0.00192	0	0.0244	0.0332	0	-0.0697	Ref.35
3	"	free	0.01308	0.01500	0.1230	0.0290	0	0	*
			0.01309	0.01509	0.1225	0.0271	0	0	Ref.36
4	clamped	clamped	0.00124	0	0.0227	0.0227	-0.0501	-0.0501	*
			0.00126	0	0.0231	0.0231	-0.0513	-0.0513	Ref.36

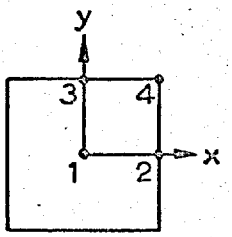

$\alpha = 1$ ($D = D_x/(1-\mu^2)$)
$\beta = 0.769$
$\gamma_x = \gamma_y = 10^4$
$\mu_x = \mu_y = \mu = 0.3$
$\varepsilon = 1$
} *

Table 4

Comparison With Ordinary Plate Theory Solutions
For Uniform Transverse Load

* I = J	w_1 $(=k_1\frac{a^4}{D}q)$ k_1	$M_{x1}=M_{y1}$ $(=k_2a^2q)$ k_2	M_{xy4} $(=k_3a^2q)$ k_3	$Q_{x2}=Q_{y3}$ $(=k_4aq)$ k_4	Equm. Check $\frac{\Sigma \text{Edge } Q}{\Sigma \text{Load}}$
4	0.00395	0.0453	0.0324	-0.3336	100.78%
6	0.00400	0.0467	0.0321	-0.3362	100.39%
8	0.00402	0.0472	0.0322	-0.3369	100.22%
10	0.00404	0.0475	0.0322	-0.3372	100.14%
Ref.36	0.00406	0.0479	0.0325	-0.338	-

* (I, J = number of mesh divisions in quarter of plate along x and y axis respectively)

Table 5

Convergence Behaviour of Case 1 - Table 4
For Decreasing Mesh Size

b in.	S_x lb/in.	S_y lb/in.	w_1 in.	M_{x1} in.lb/in.	M_{y1} in.lb/in.	C in. lb/in.	Scource
100	3·39 ($\times 10^4$)	3·39 ($\times 10^4$)	0.0293	473.8	473.8	331.7	*
			0.0292	478.6	478.6	335.0	based on Ref.17
			0.0292	478.9	478.9	335.2	based on Ref.39
			0.0282	–	–	326.8	Ref.16
200	3·39 ($\times 10^4$)	3·39 ($\times 10^4$)	0.0523	1009	463.0	870.1	*
			0.0523	1017	463.2	878.0	based on Ref.17
			0.0523	1017	463.5	878.0	based on Ref.39
			0.0507	–	–	856.4	Ref. 16
100	8·475 ($\times 10^4$)	3·39 ($\times 10^4$)	0.0215	620.8	339.5	519.0	*
			0.0215	621.2	336·0	520.4	based on Ref.17
			0.0209	–	–	503.4	Ref. 16
200	8·475 ($\times 10^4$)	3·39 ($\times 10^4$)	0.0346	1090	392·1	972·4	*
			0.0346	1094	385.9	978.2	based on Ref. 7
			0.0338	–	–	951.3	Ref. 16

$$C = (M_{x1} - \mu M_{y1})$$

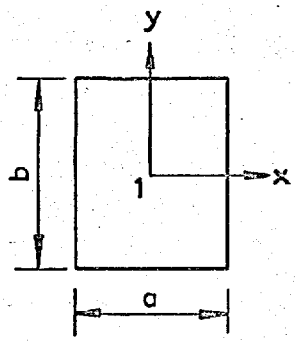

$D_x = D_y = 49{\cdot}2 \times 10^6$ in. lb.
$D_{xy} = 37{\cdot}9 \times 10^6$ in. lb.
$a = 100$ in.
$\mu_x = \mu_y = 0{\cdot}3$
$q = 1$ lb/in^2 } *

Table 6

Comparison With Solutions for Shear-Weak Simply Supported Plate Under Uniform Transverse Load

Torsional Edge Restraint	w_1 $(=k_1 \frac{a^4}{D} q)$ k_1	$M_{x1}=M_{y1}$ $(=k_2 a^2 q)$ k_2	$M_{x2}=M_{y3}$ $(=k_3 a^2 q)$ k_3	Scource
high	0.00319	0.0233	-0.0437	*
low	0.00321	0.0235	-0.0443	*
zero	0.00325	-	-0.0410	Ref. 21

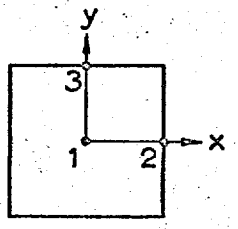

$\alpha = 1 \quad (D = D_x/(1-\mu^2))$
$\beta = 0.769$
$\gamma_x = \gamma_y = 43.4$
$\mu_x = \mu_y = \mu \quad 0.3$
$\varepsilon = 7$
} *

Table 7
Comparison With Solutions for Shear - Weak Clamped Plate Under Uniform Transverse Load

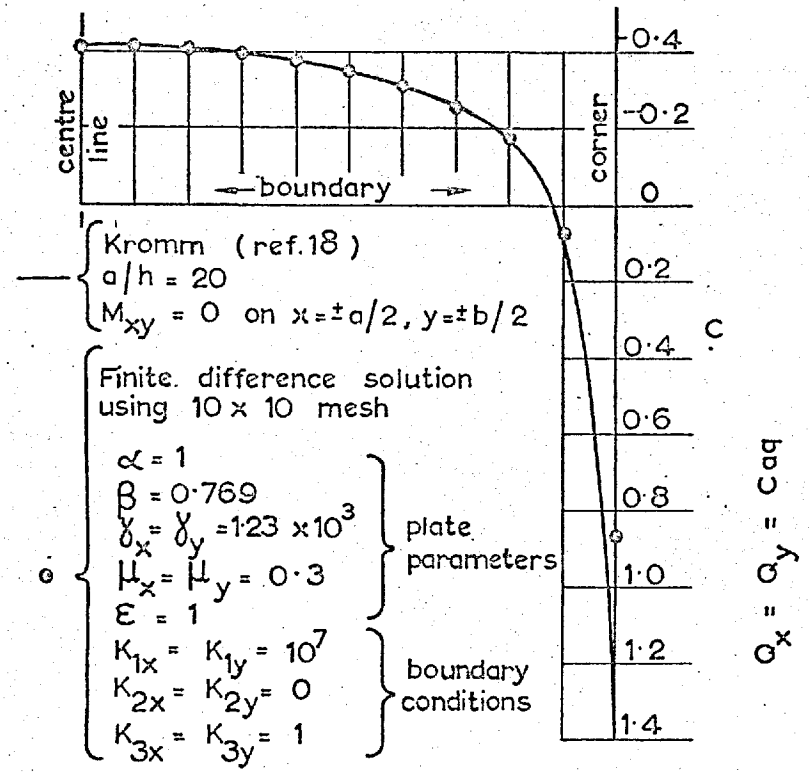

Fig. 50 : Comparison With Kromm's Solution of Edge Reaction For Homogeneous, Simply Supported Plate Under Uniform Transverse Load

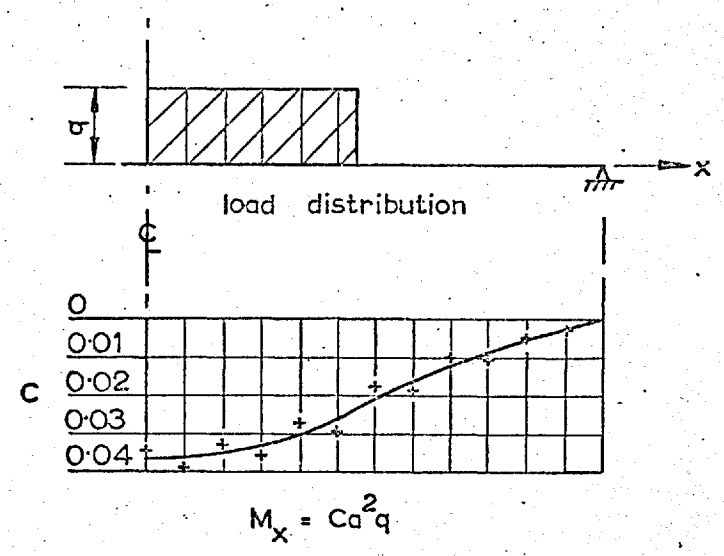

(i) Discrete discontinuity in transverse load distribution (constant along y axis)

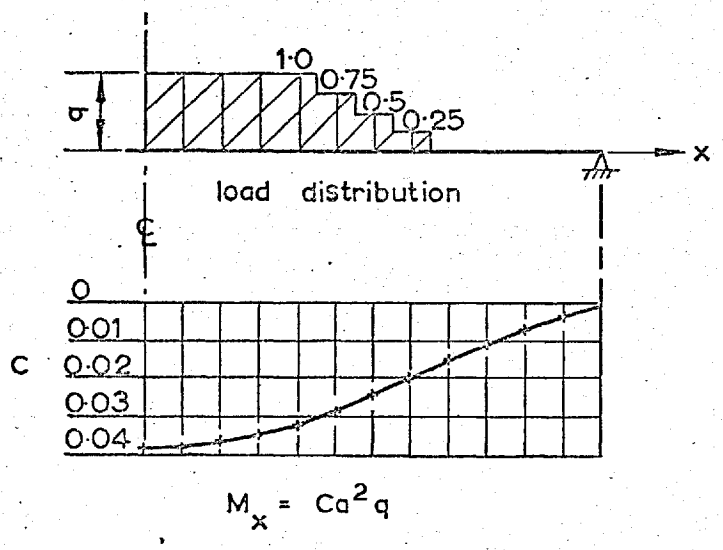

(ii) Stepped discontinuity in transverse load distribution (constant along y axis)

$\alpha = 1$ $\quad \mu_x = \mu_y = 0.3$ —— { solution excluding shear deformation

$\beta = 0.769$

$\varepsilon = 1$ $\quad \gamma_x = \gamma_y = 10^4$ + { solution including shear deformation

Fig. 51 : Simply Supported Plate
Effect of Discontinuous Transverse Load

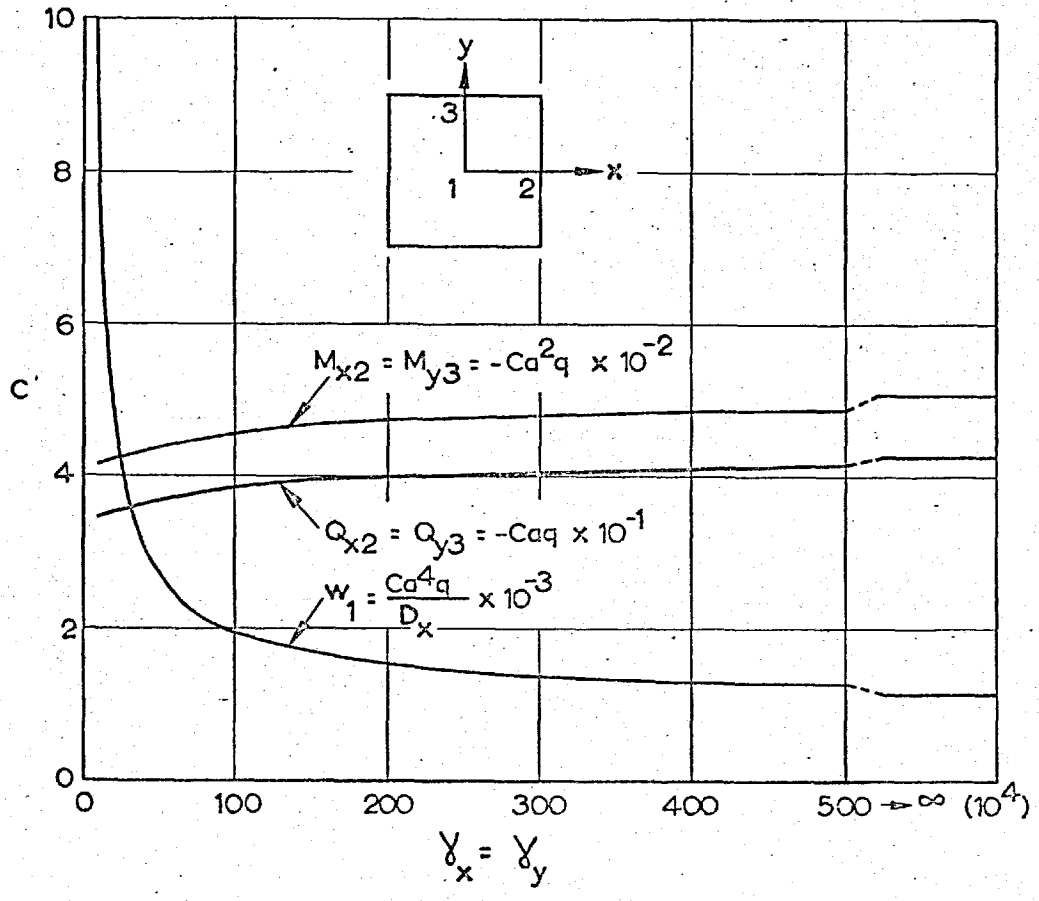

$\alpha = 1$ $\qquad$ $\varepsilon = 1$

$\beta = 0.769$ $\qquad$ $\mu_x = \mu_y = 0.3$

Fig. 52 : Clamped Plate Under Uniform Transverse Load
Effect of Shear Stiffness

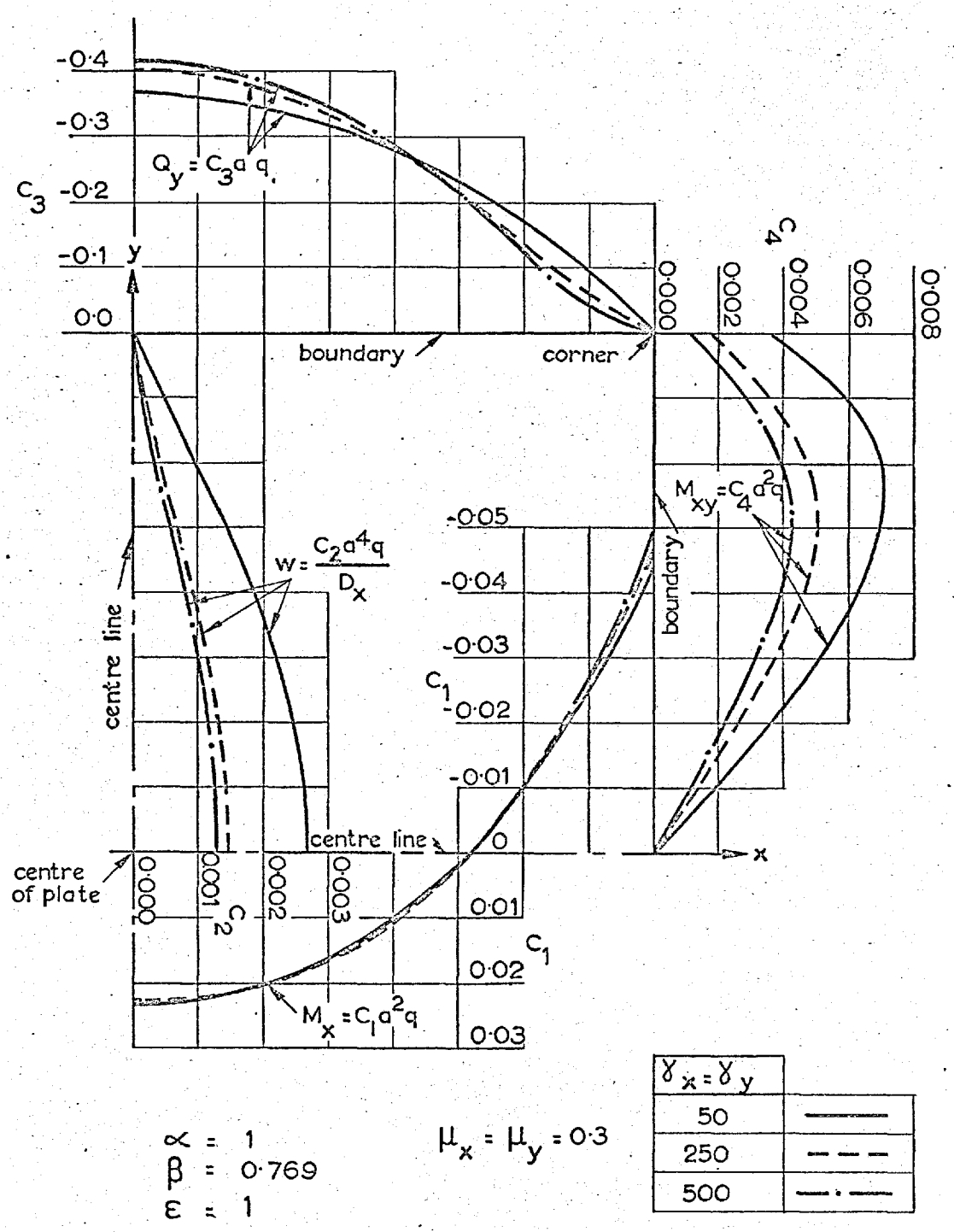

Fig. 53 : Clamped Plate Under Uniform Transverse Load
Effect of Shear Stiffness

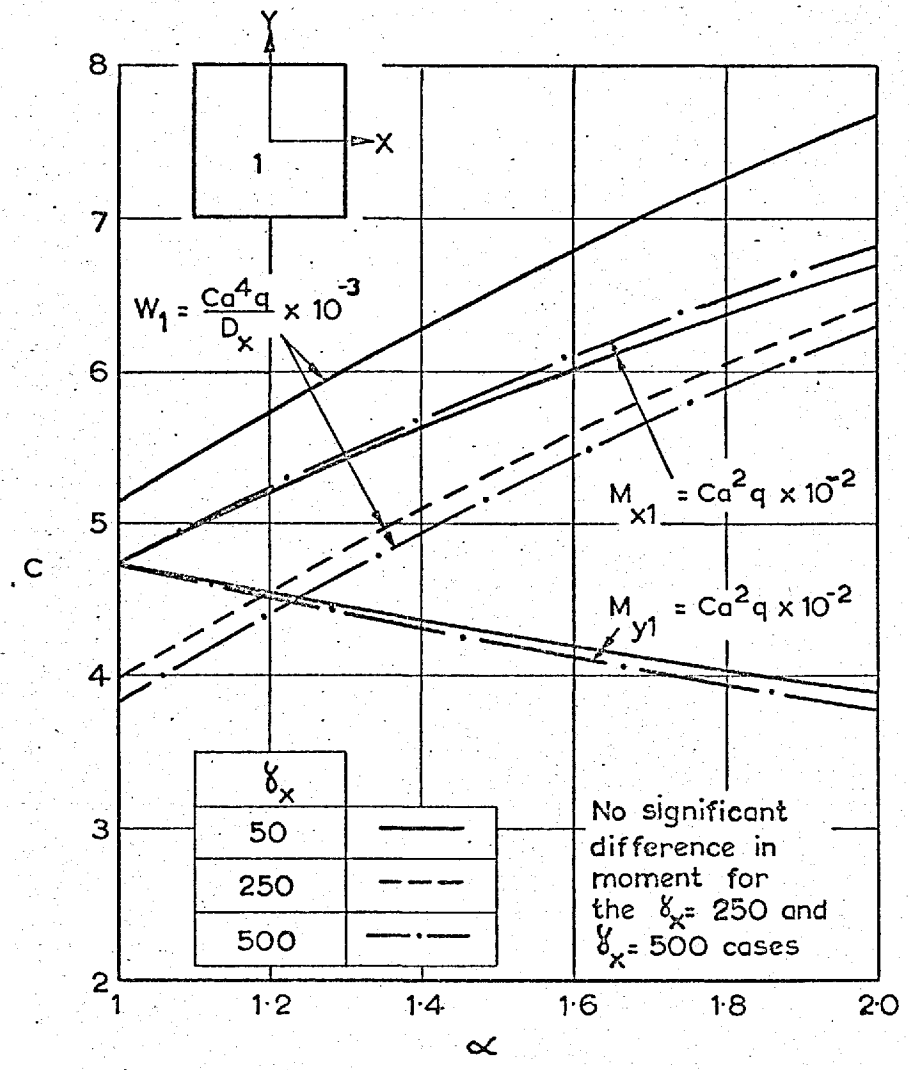

$\beta = (1-\mu)/(\alpha - \mu^2)$
γ_x as shown
$\gamma_y = \gamma_x \alpha$

$\varepsilon = 1$
$\mu_x = \mu = 0{\cdot}3$
$\mu_y = \mu/\alpha$

Fig. 54 : Simply Supported Plate Under Uniform Transverse Load Effect of Orthotropic Flexural Properties

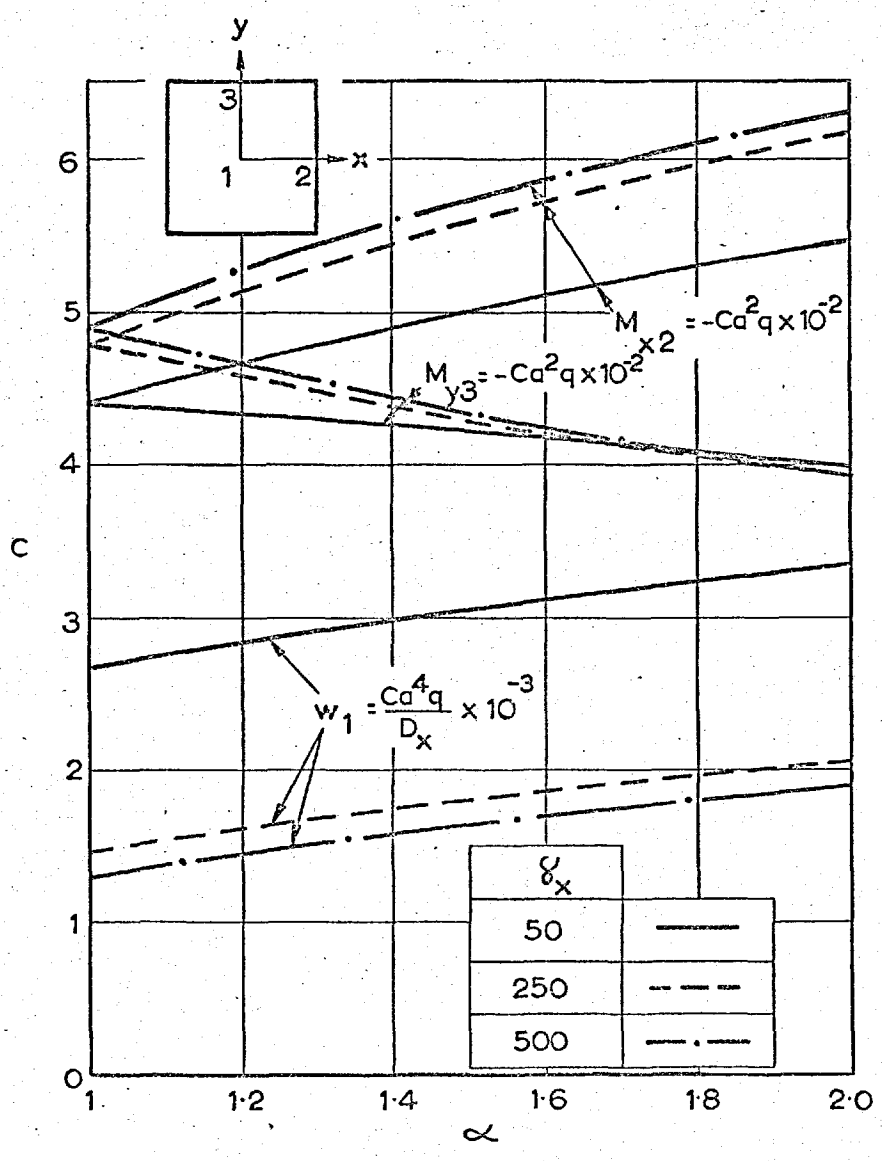

$\beta = (1-\mu)/(\alpha-\mu^2)$ $\qquad$ $\varepsilon = 1$

γ_x as shown $\qquad$ $\mu_x = \mu = 0.3$

$\gamma_y = \gamma_x \alpha$ $\qquad$ $\mu_y = \mu/\alpha$

Fig. 55 : Clamped Plate Under Uniform Transverse Load
Effect of Orthotropic Flexural Properties

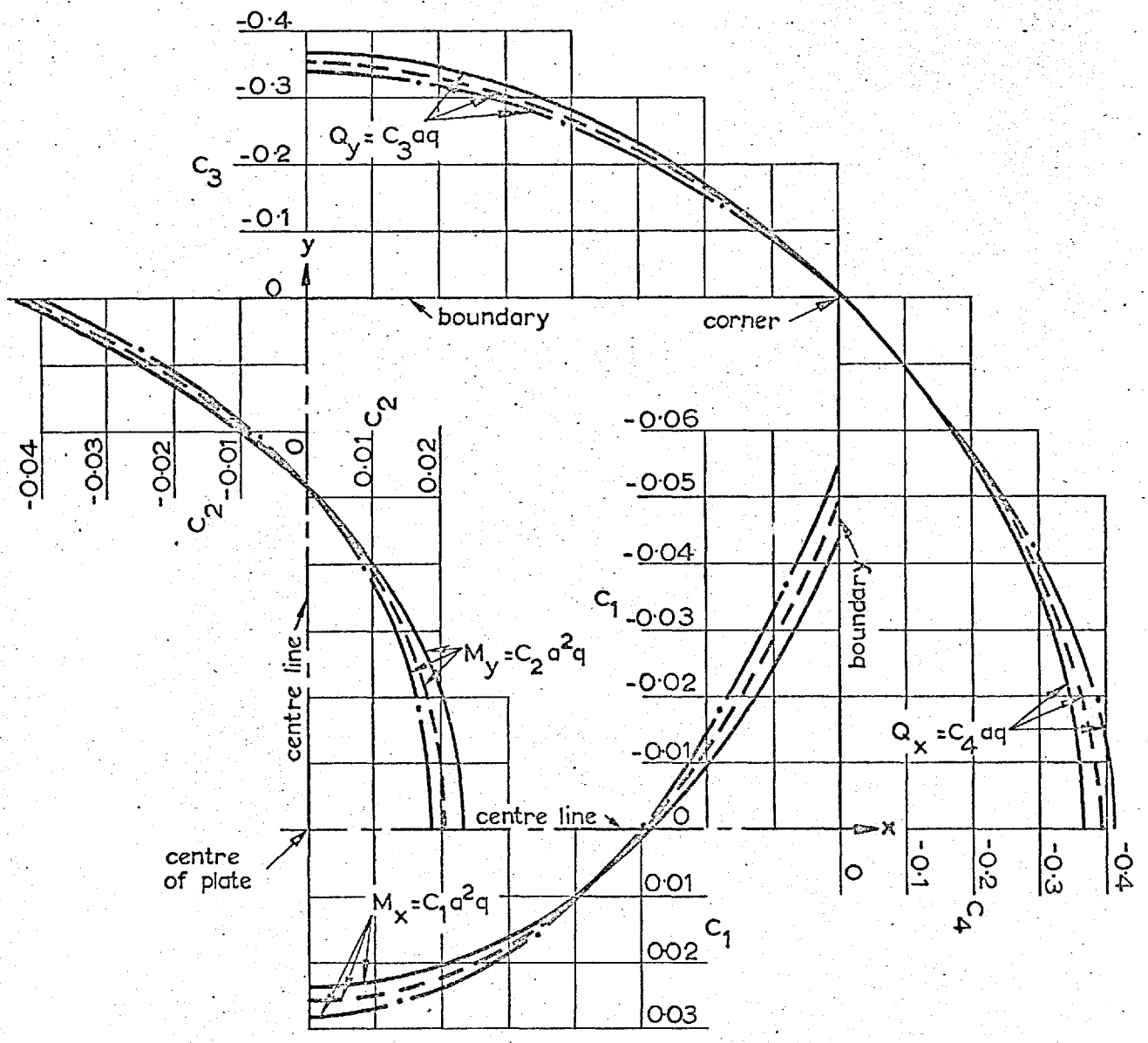

$\beta = (1-\mu)/(\alpha - \mu^2)$ $\quad \varepsilon = 1$

$\gamma_x = 50$ $\quad \mu_x = \mu = 0{\cdot}3$

$\gamma_y = \gamma_x \alpha$ $\quad \mu_y = \mu/\alpha$

α	
1	———
1·5	– – –
2	—·—

Fig. 56 : Clamped Plate Under Uniform Transverse Load
Effect of Orthotropic Flexural Properties

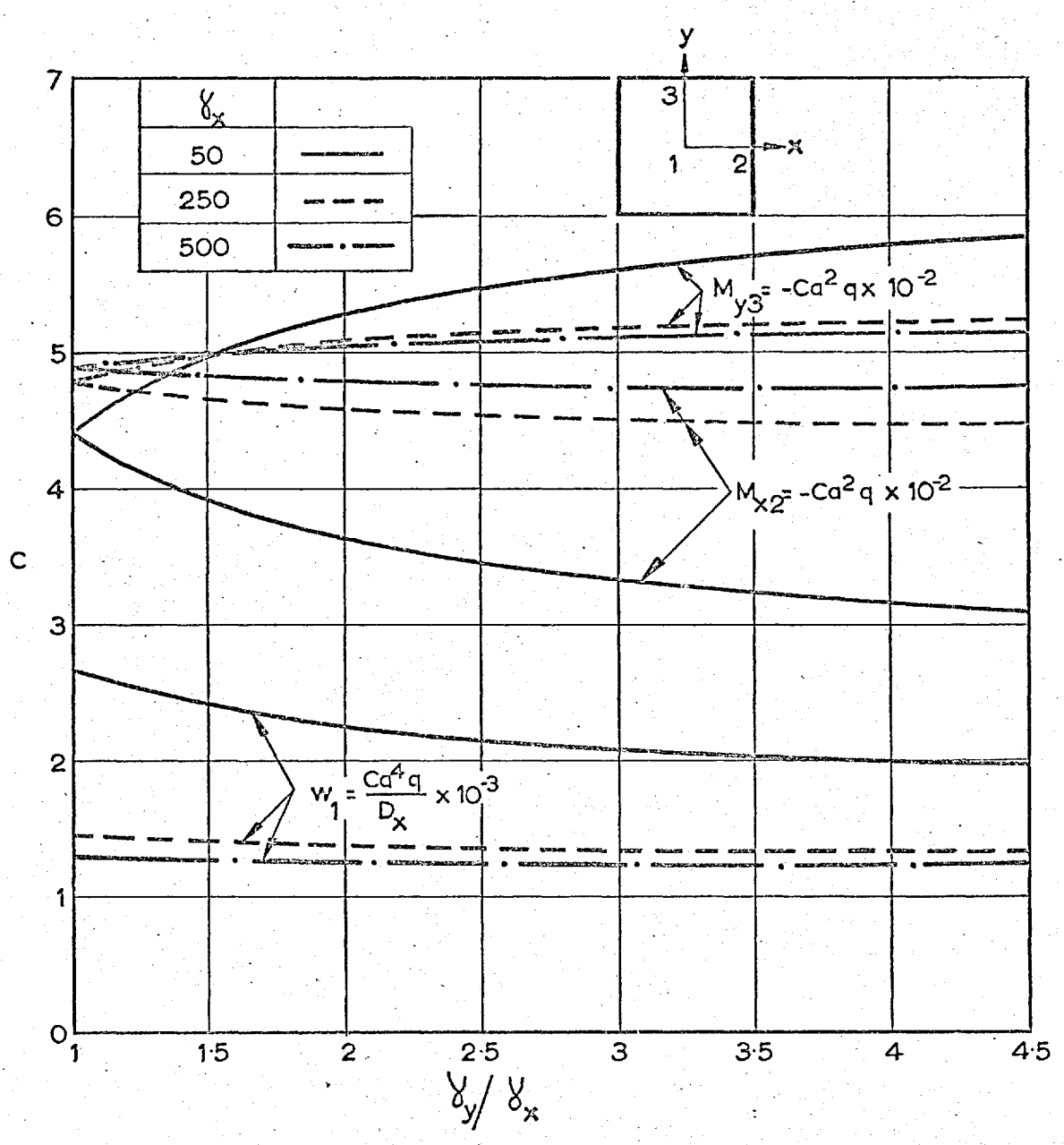

$\alpha = 1$ $\quad \varepsilon = 1$

$\beta = 0{\cdot}769$ $\quad \mu_x = \mu_y = 0{\cdot}3$

Fig. 57 : Clamped Plate Under Uniform Transverse Load
Effect of Orthotropic Shear Properties

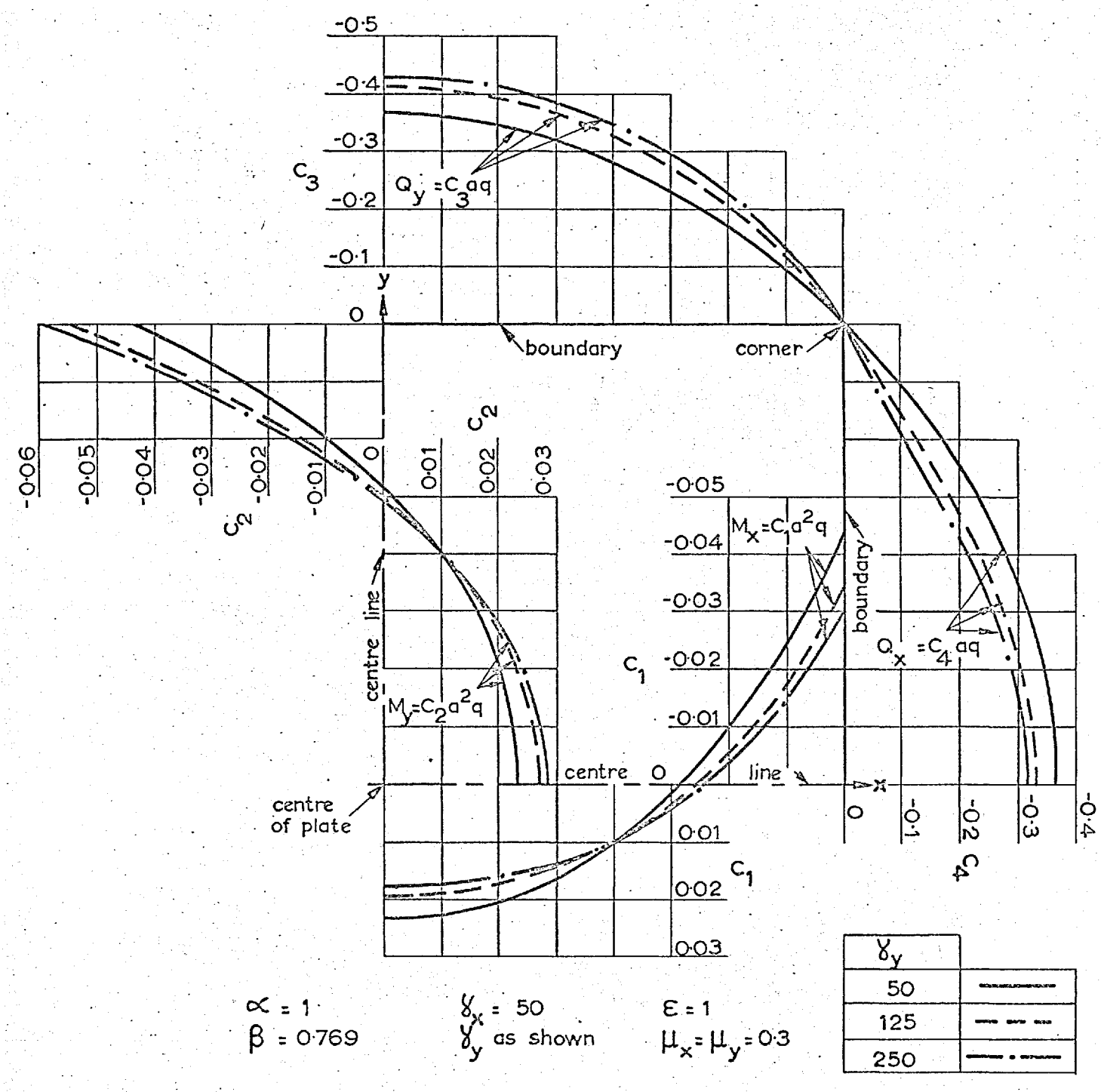

Fig. 58 : Clamped Plate Under Uniform Transverse Load
Effect of Orthotropic Shear Properties

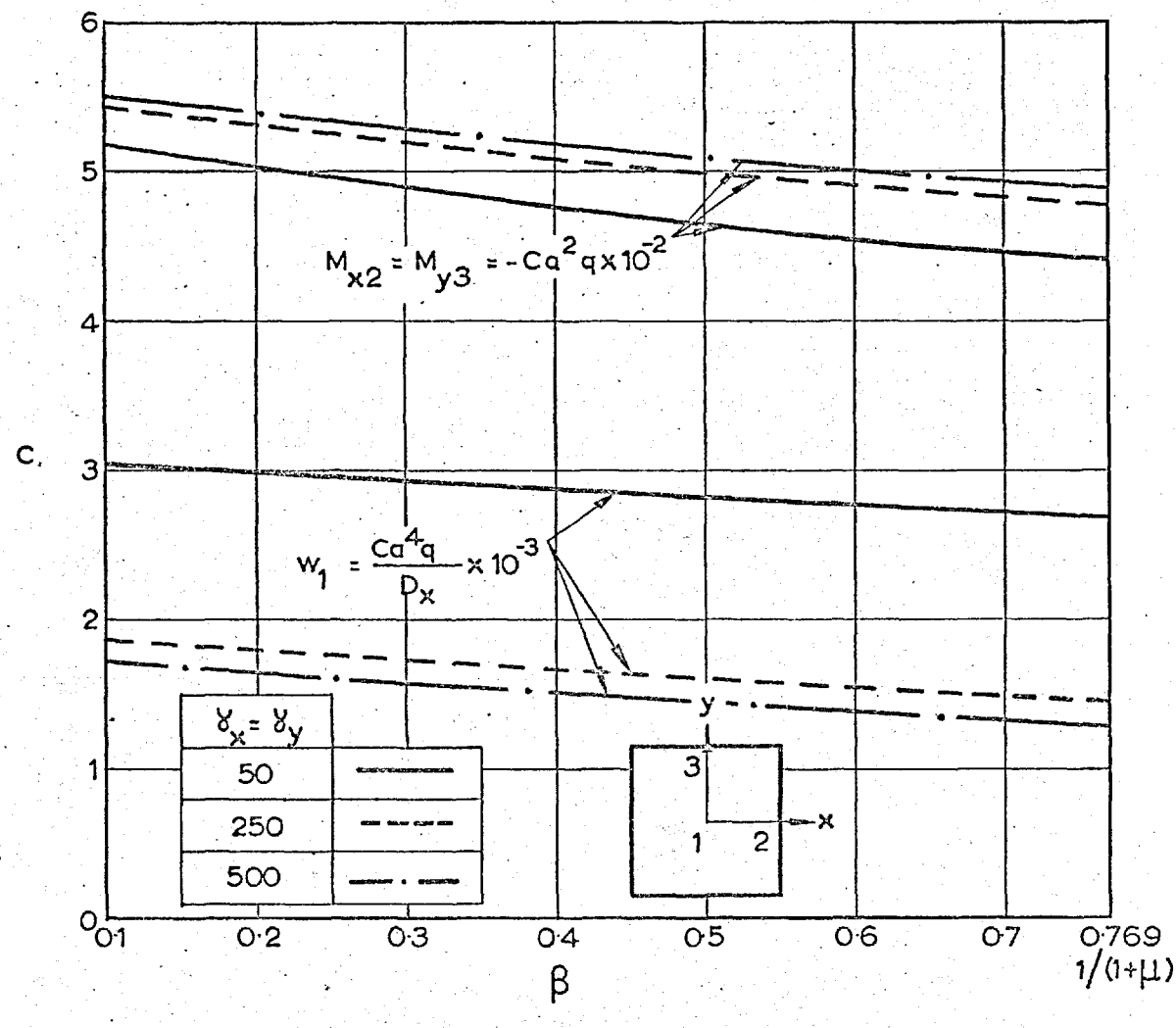

$\alpha = 1$
$\varepsilon = 1$
$\mu = 0{\cdot}3$

$$\mu_x = \mu_y = -\frac{k}{2} + \sqrt{\left(\frac{k}{2}\right)^2 + 1}$$

$$k = (1-\mu)/\beta\mu$$

Fig. 59 : Clamped Plate Under Uniform Transverse Load
Effect of Twisting Stiffness

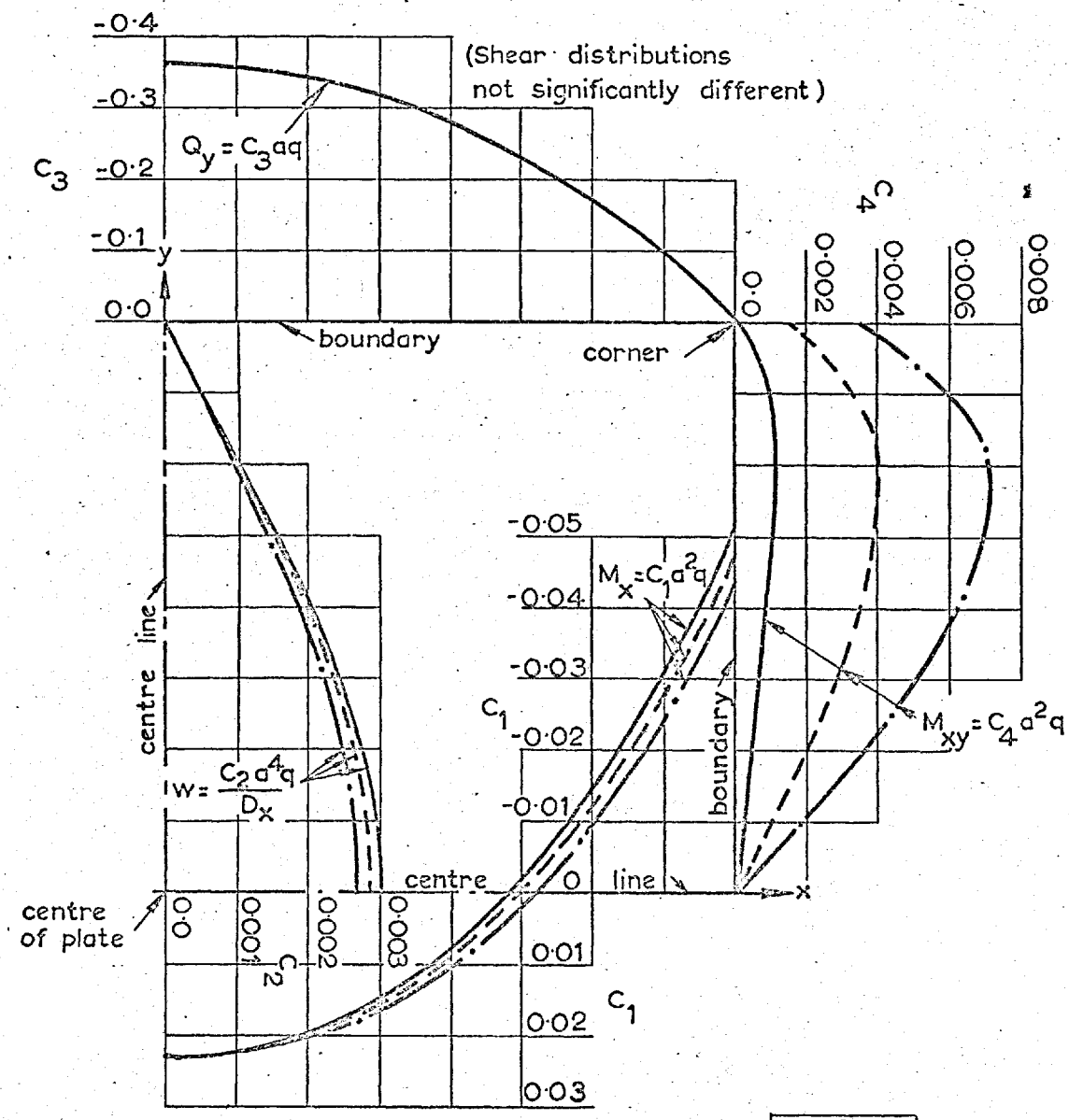

β	
0·1	———
0·4	- - - -
0·769	—·—

$\alpha = 1$ β as shown

$\gamma_x = \gamma_y = 50$ $\mu_x = \mu_y = -\frac{k}{2} + \sqrt{\left(\frac{k}{2}\right)^2 + 1}$

$\mu = 0{\cdot}3$ $k = (1-\mu)/\beta\mu$

Fig. 60 : Clamped Plate Under Uniform Transverse Load
Effect of Twisting Stiffness

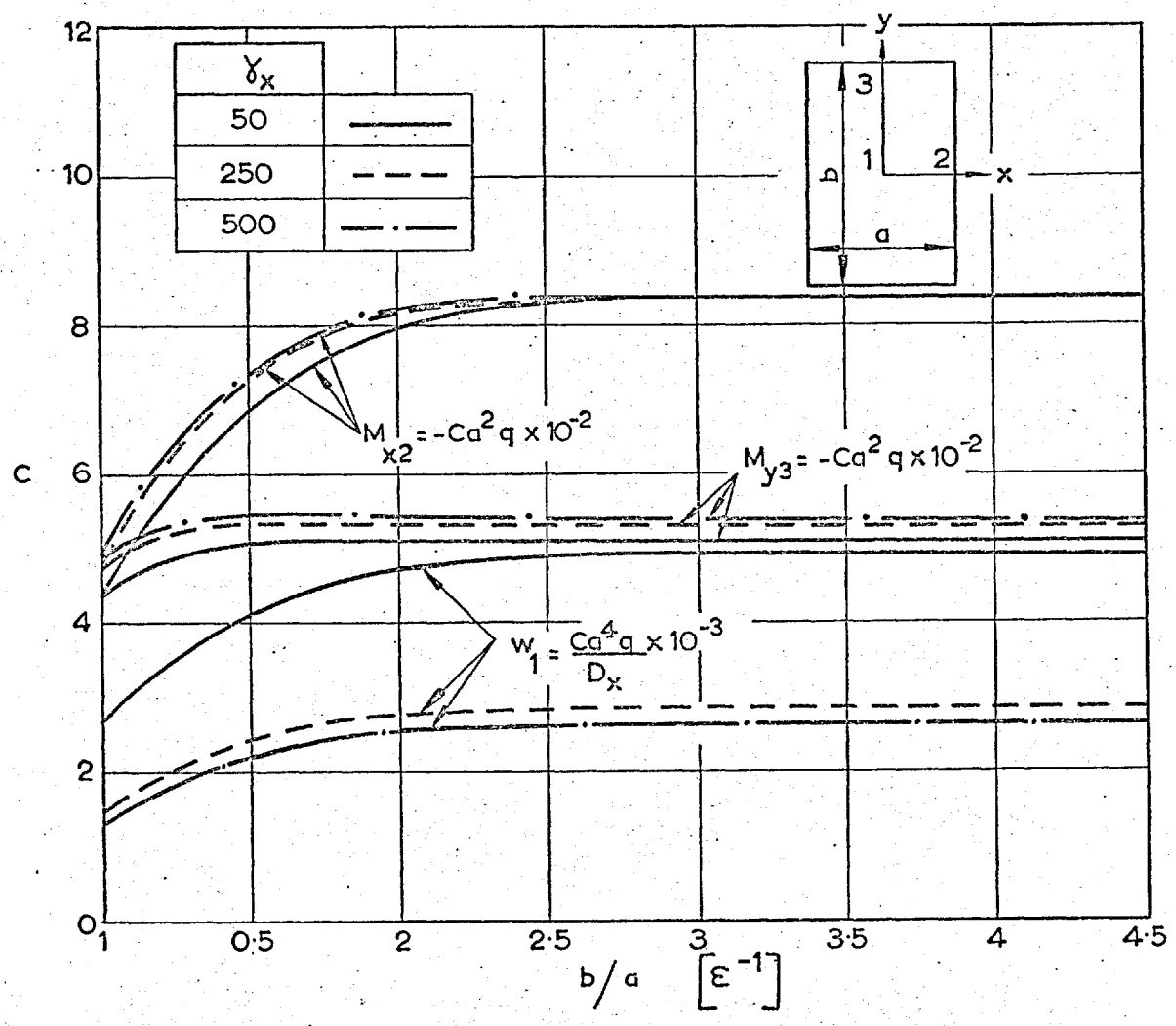

$\alpha = 1$ $\quad \beta = 0.769$ $\quad \gamma_x$ = as shown $\quad \gamma_y = \gamma_x/\varepsilon^2$ $\quad \mu_x = \mu_y = 0.3$

Fig. 61 : Clamped Plate Under Uniform Transverse Load
Effect of Side Ratio

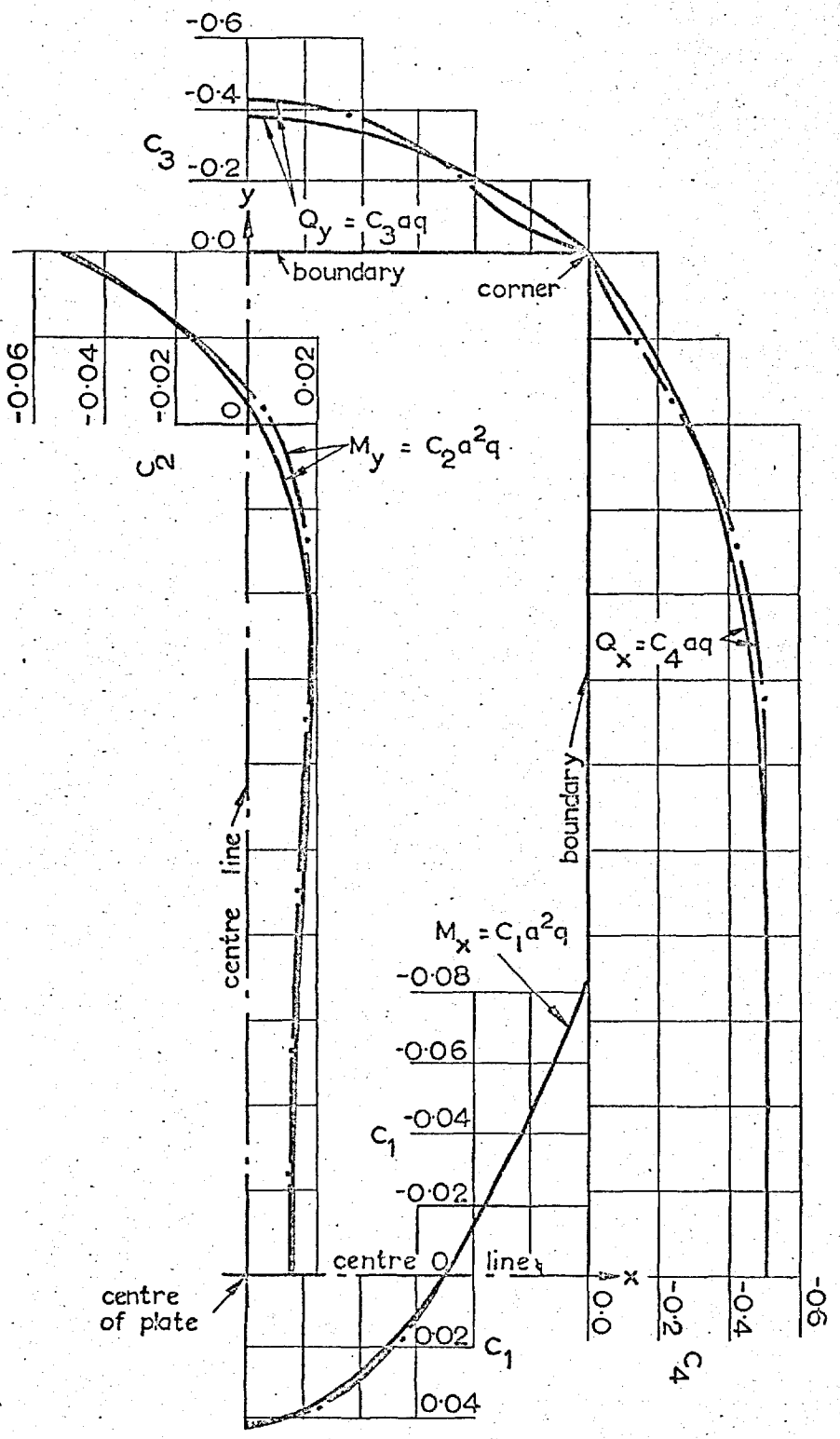

$\alpha = 1$ $\quad \varepsilon = 0.333$

$\beta = 0.769$ $\quad \mu_x = \mu_y = 0.3$

γ_x as shown

$\gamma_y = \gamma_x/\varepsilon^2 = 9\gamma$

γ_x	
50	———
500	— · —

Fig. 62 : Clamped Plate Under Uniform Transverse Load
Effect of Side Ratio

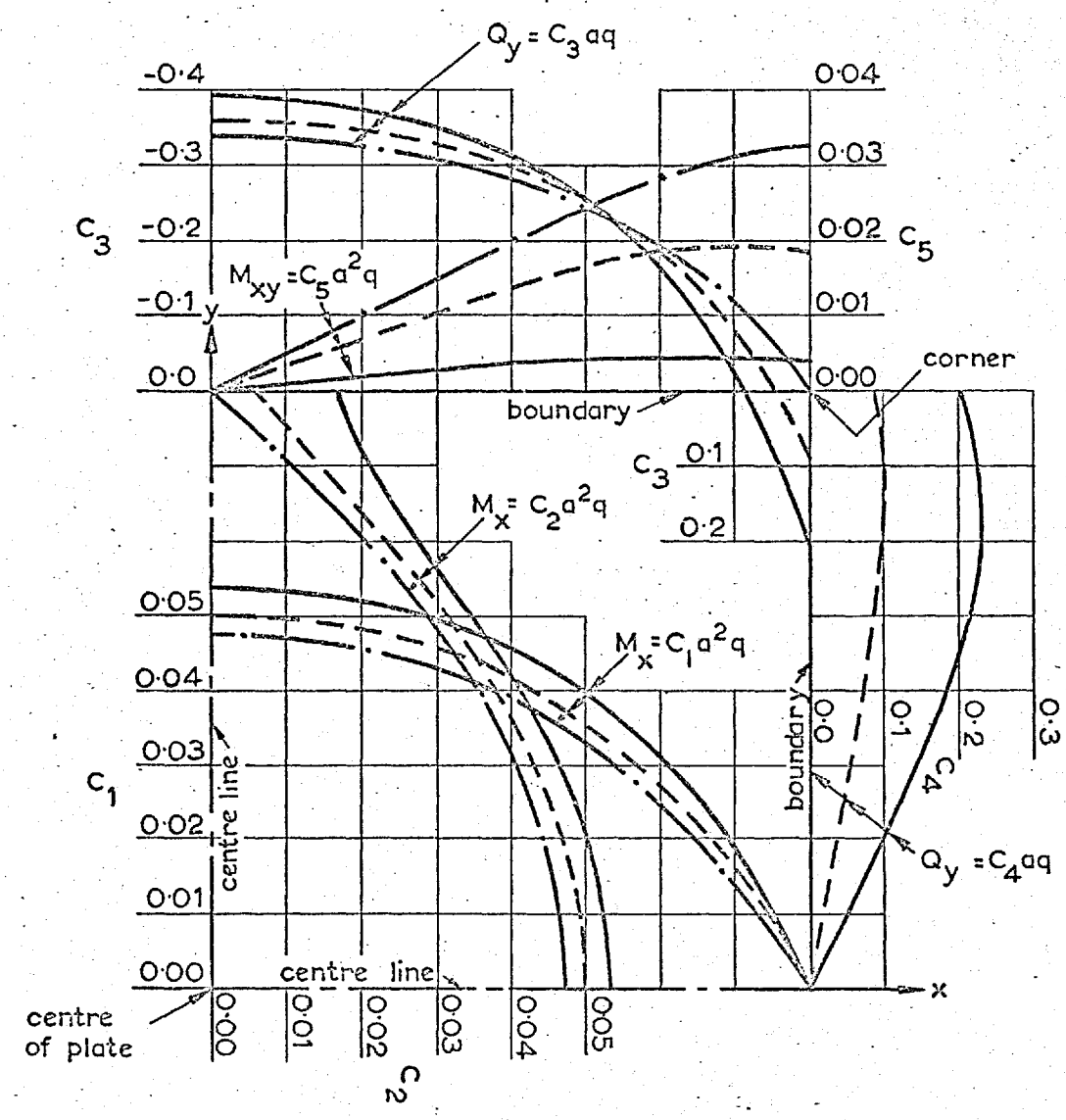

$\alpha = 1$ $\quad \varepsilon = 1$

$\beta = 0{\cdot}769$ $\quad \mu_x = \mu_y = 0{\cdot}3$

$\gamma_x = \gamma_y = 50$

$K_{3x} = K_{3y}$	
1	———
10	— — —
10^3	— · —

Fig. 63 : Simply Supported Plate Under Uniform Transverse Load Effect of Torsional Edge Restraint

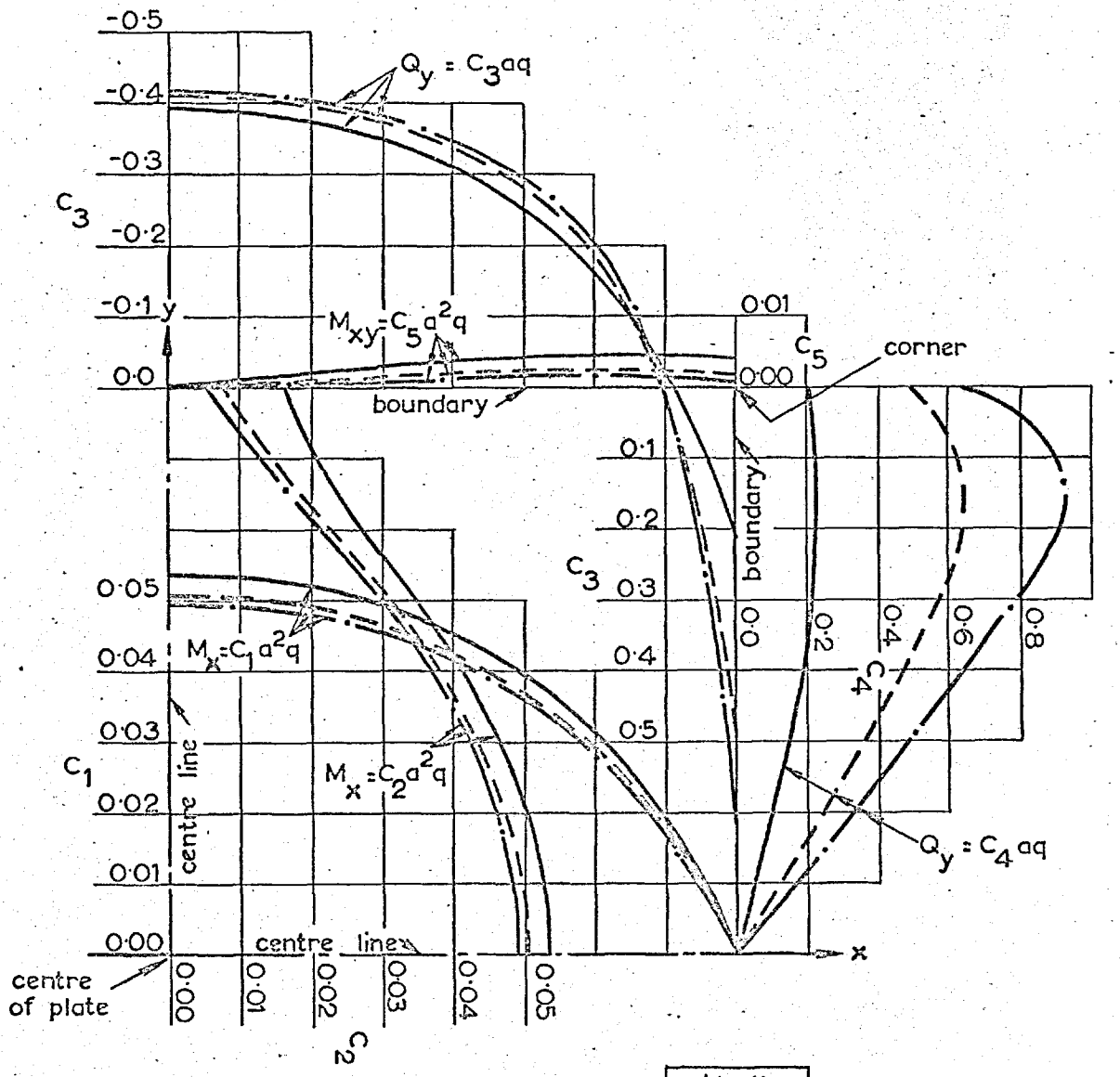

Fig. 64 : Simply Supported Plate Under Uniform Transverse Load
Effect of Shear Stiffness - Low Torsional Edge Restraint

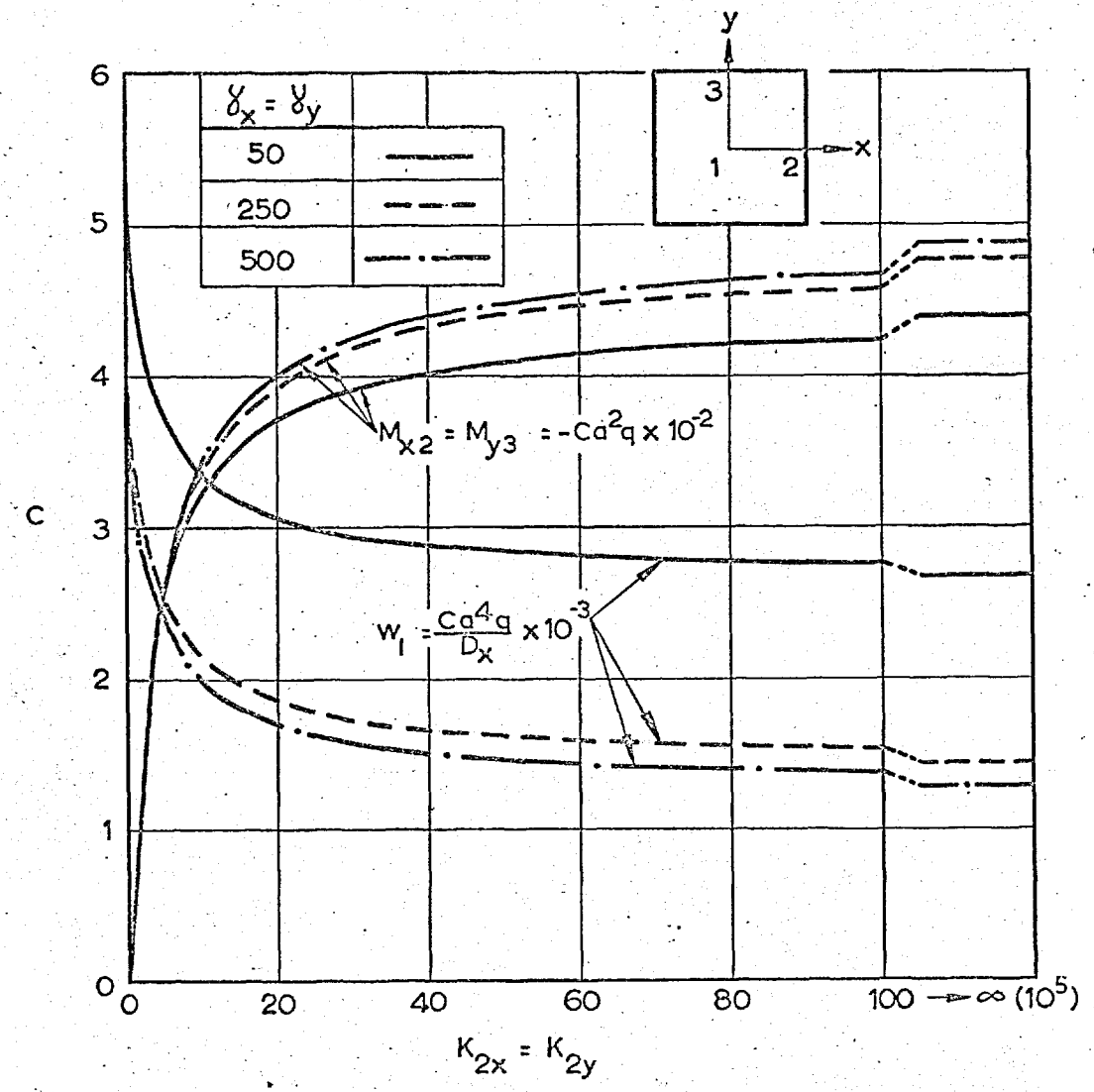

$\alpha = 1$ $\quad \varepsilon = 1$ $\quad K_{1x} = K_{1y} \to \infty$ (10^7)

$\beta = 0.769$ $\quad \mu_x = \mu_y = 0.3$ $\quad K_{3x} = K_{3y} \to \infty$ (10^5)

Fig. 65 : Plate Under Uniform Transverse Load
Effect of Equal Elastic Rotational Restraint
on Both Boundaries

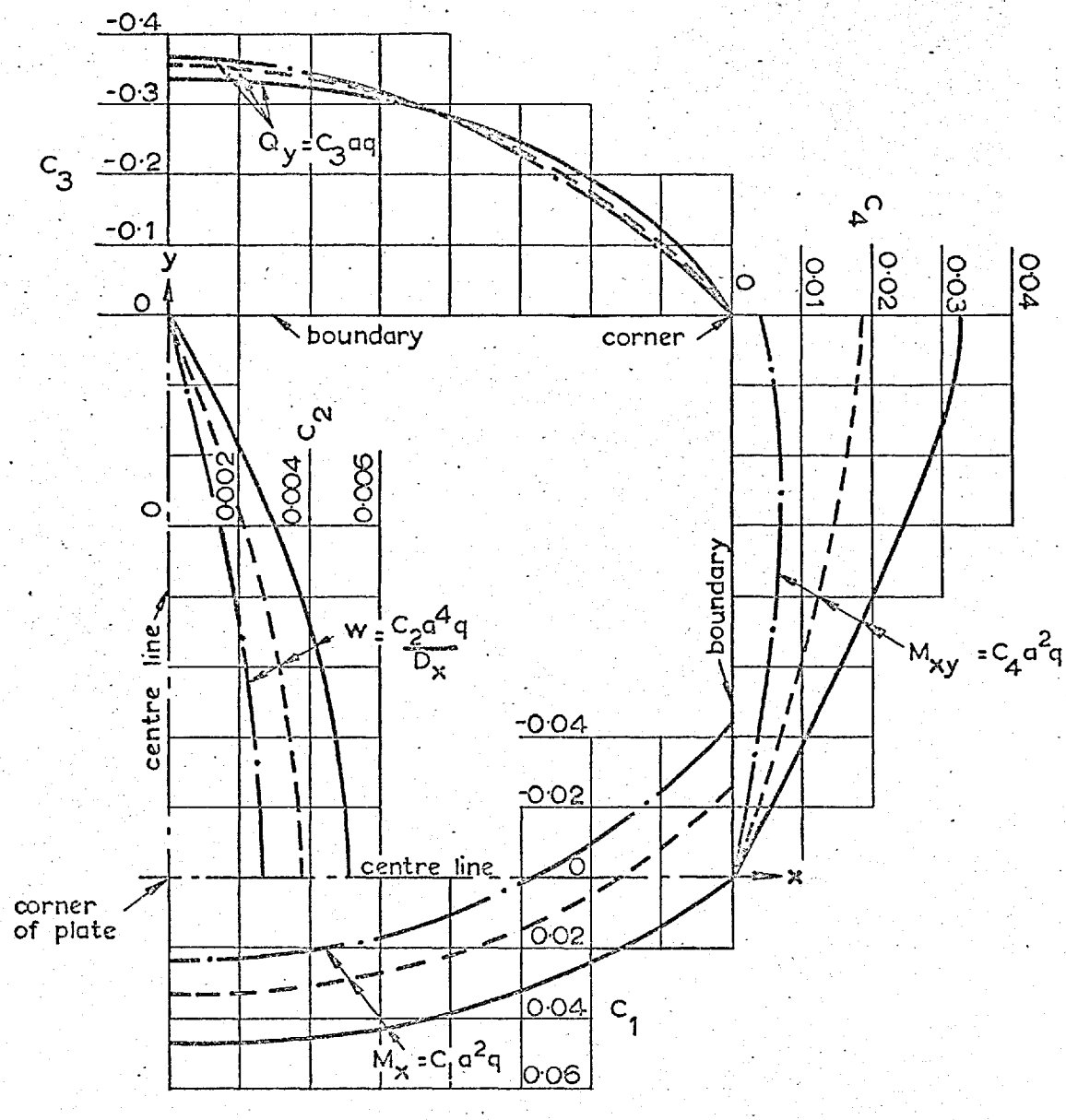

$\alpha = 1$ $\quad \mu_x = \mu_y = 1$

$\beta = 0.769$ $\quad K_{1x} = K_{1y} \to \infty (10^7)$

$\gamma_x = \gamma_y = 50$ $\quad K_{3x} = K_{3y} \to \infty (10^5)$

$\varepsilon = 1$

$K_{2x} = K_{2y}$	
0	———
5	— — —
10^5	—·—

Fig. 66 : Plate Under Uniform Transverse Load
Effect of Equal Elastic Rotational Restraint
On Both Boundaries

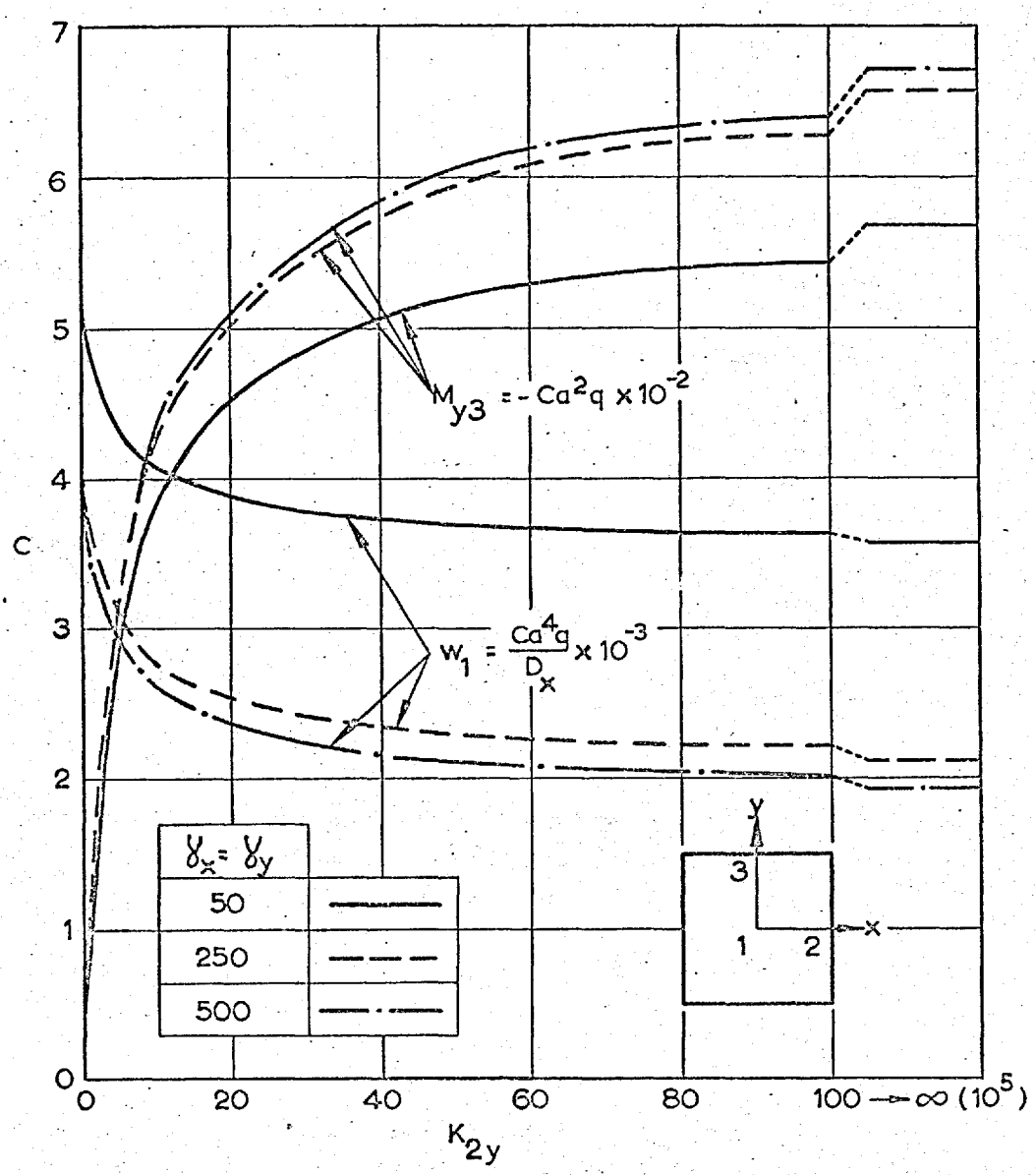

$\alpha = 1$ $\quad \varepsilon = 1$ $\quad K_{1x} = K_{1y} \to \infty$ (10^7)

$\beta = 0.769$ $\quad \mu_x = \mu_y = 0.3$ $\quad K_{2x} = 0$

$K_{3x} = K_{3y} \to \infty$ (10^5)

Fig. 67 : Plate Under Uniform Transverse Load
Effect of Elastic Rotational Restraint Along $y = \pm b/2$
Boundary , $x = \pm a/2$ Boundary Simply Supported

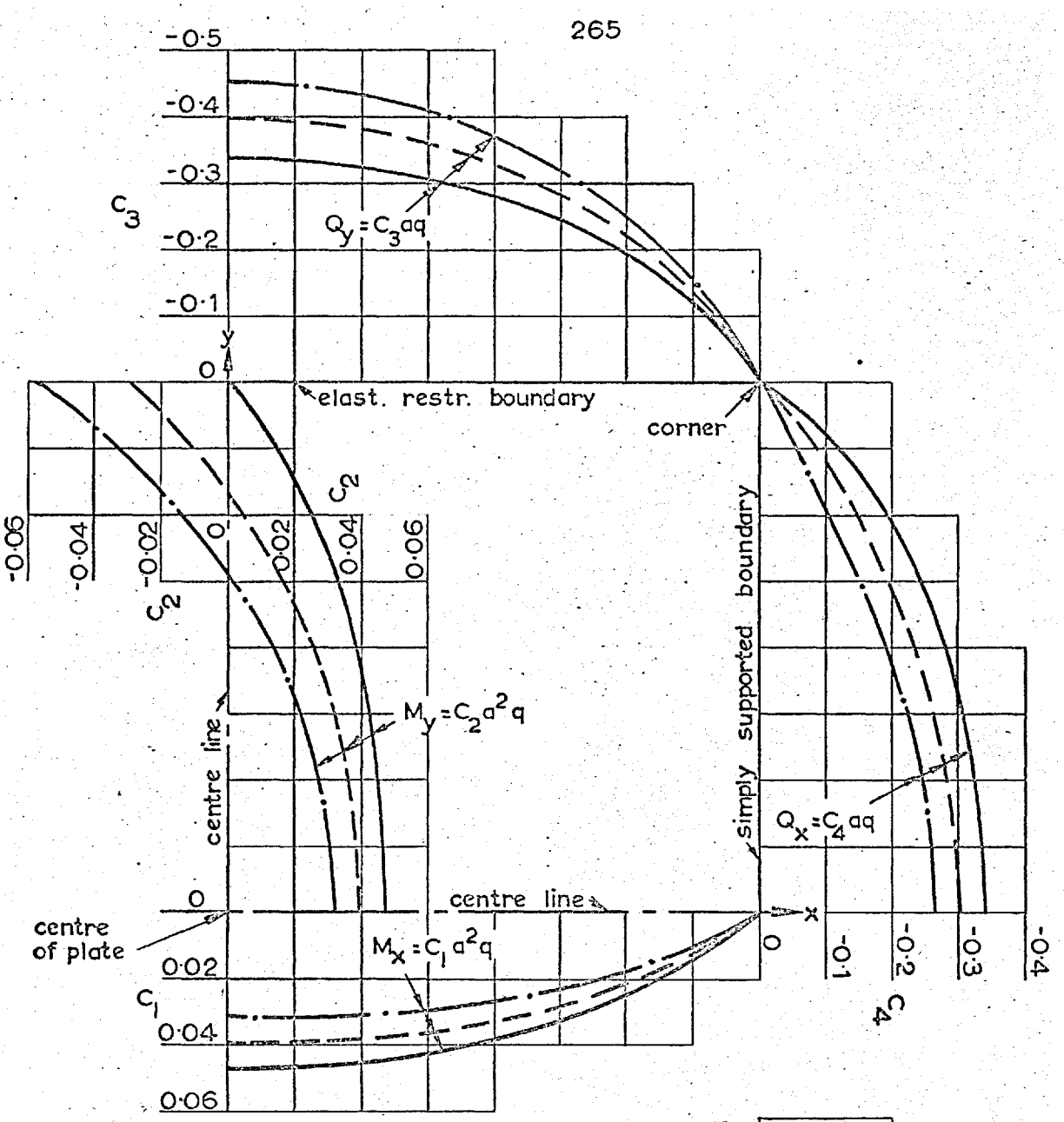

Fig. 68 : Plate Under Uniform Transverse Load
Effect of Elastic Rotational Restraint Along $y = \pm b/2$
Boundary, $x = \pm a/2$ Boundary Simply Supported

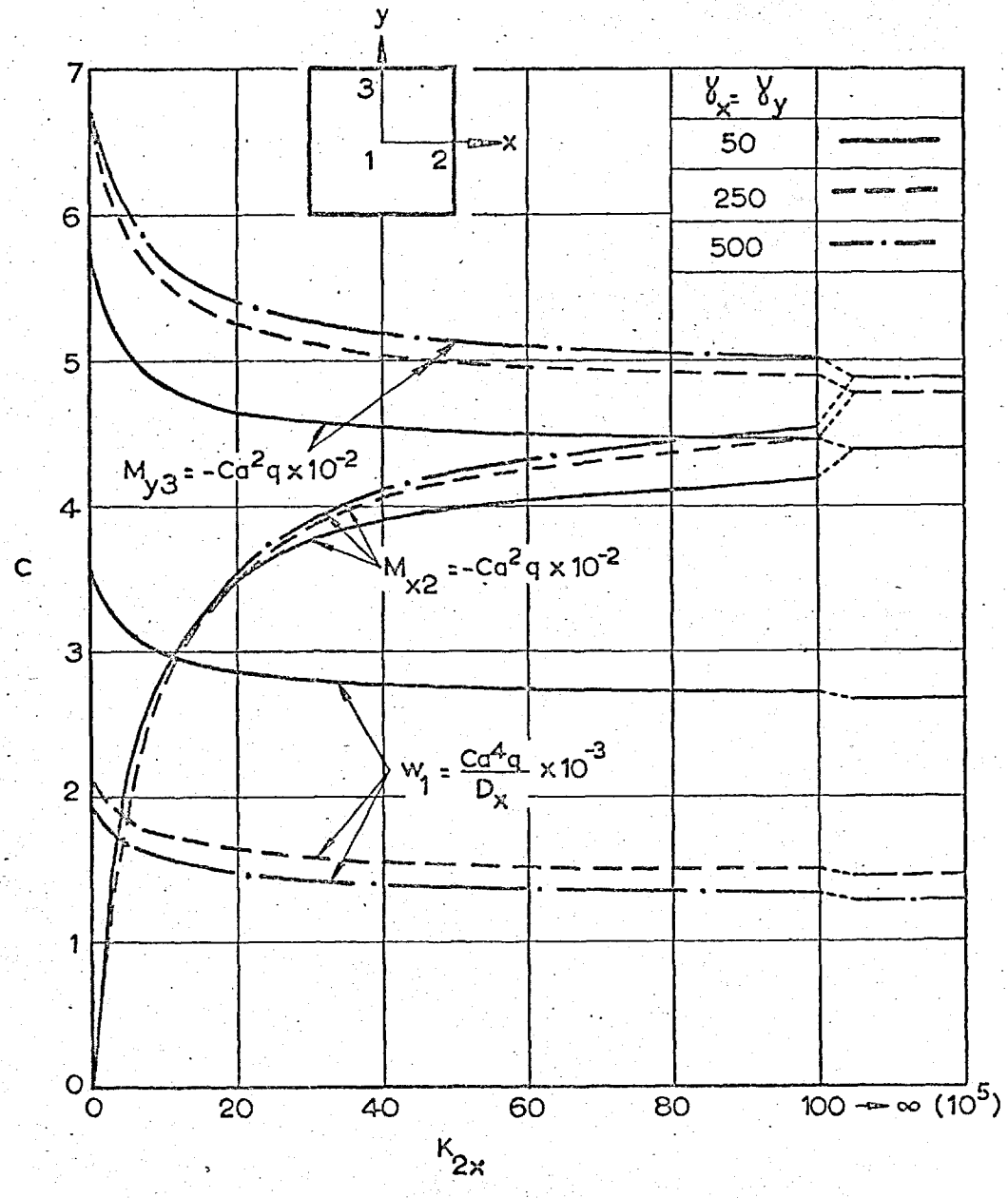

$\alpha = 1$ $\quad \varepsilon = 1$ $\quad K_{1x} = K_{1y} \to \infty$ (10^7)

$\beta = 0.769$ $\quad \mu_x = \mu_y = 0.3$ $\quad K_{2y} \to \infty$ (10^5)

$K_{3x} = K_{3y} \to \infty$ (10^5)

Fig. 69 : Plate Under Uniform Transverse Load
Effect of Elastic Rotational Restraint Along $x = \pm a/2$
Boundary , $y = \pm b/2$ Boundary Clamped

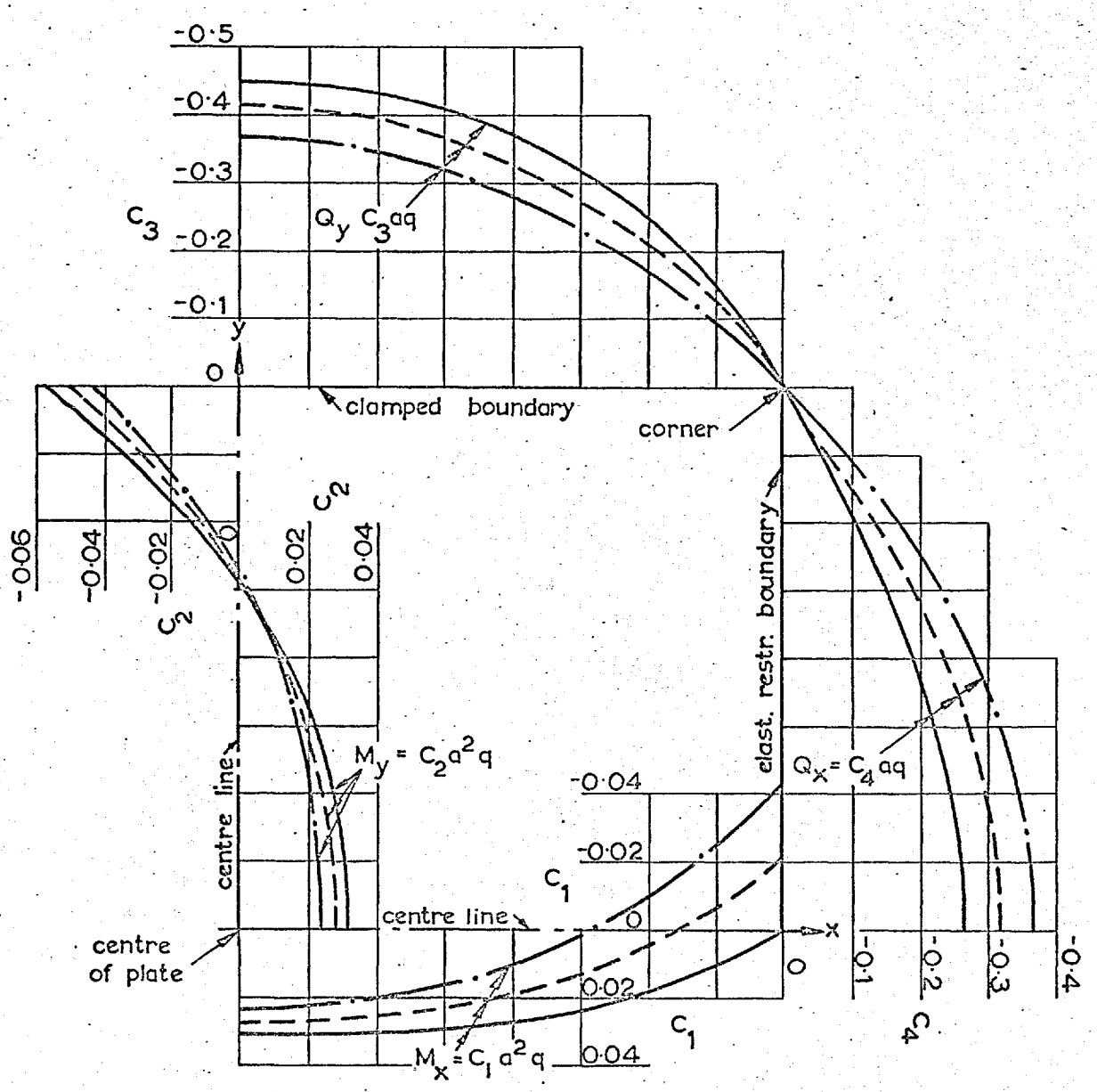

Fig. 70 : Plate Under Uniform Transverse Load
Effect of Elastic Rotational Restraint Along $x = \pm a/2$ Boundary , $y = \pm b/2$ Boundary Clamped

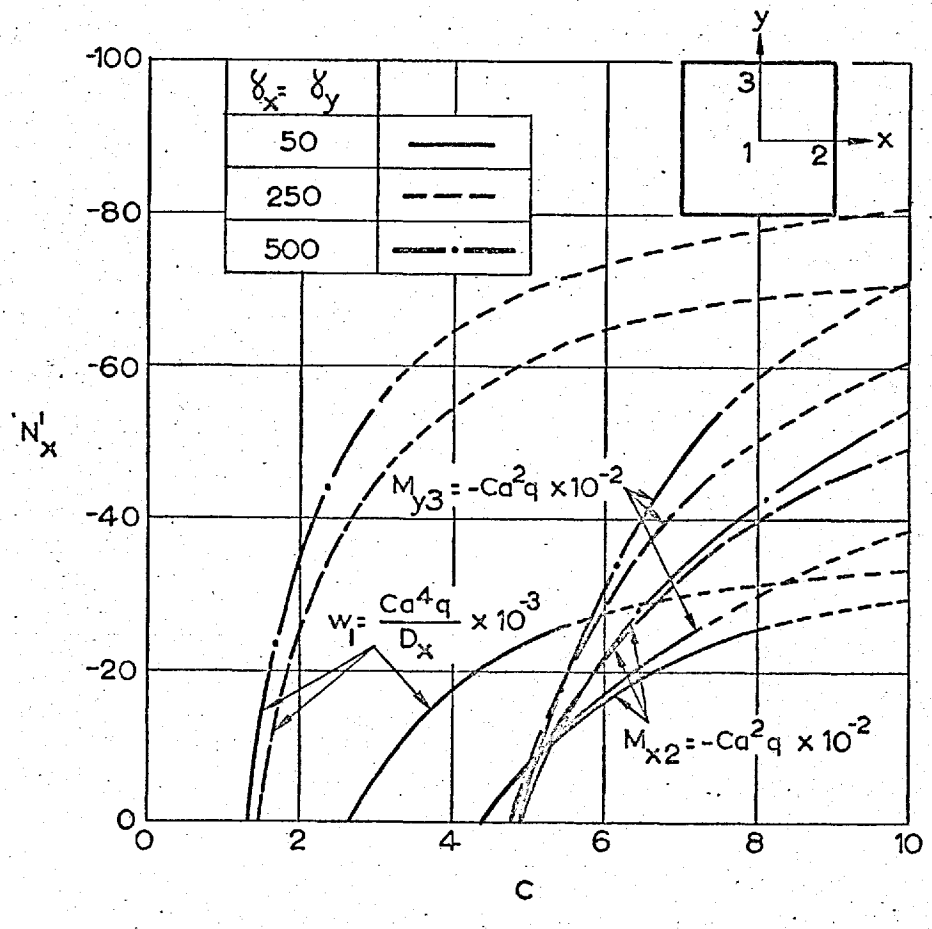

$\alpha = 1$ $\quad \varepsilon = 1$

$\beta = 0.769$ $\quad \mu_x = \mu_y = 0.3$

Fig. 71 : Clamped Plate Under Uniform Transverse Load and Uniaxial In-plane Load

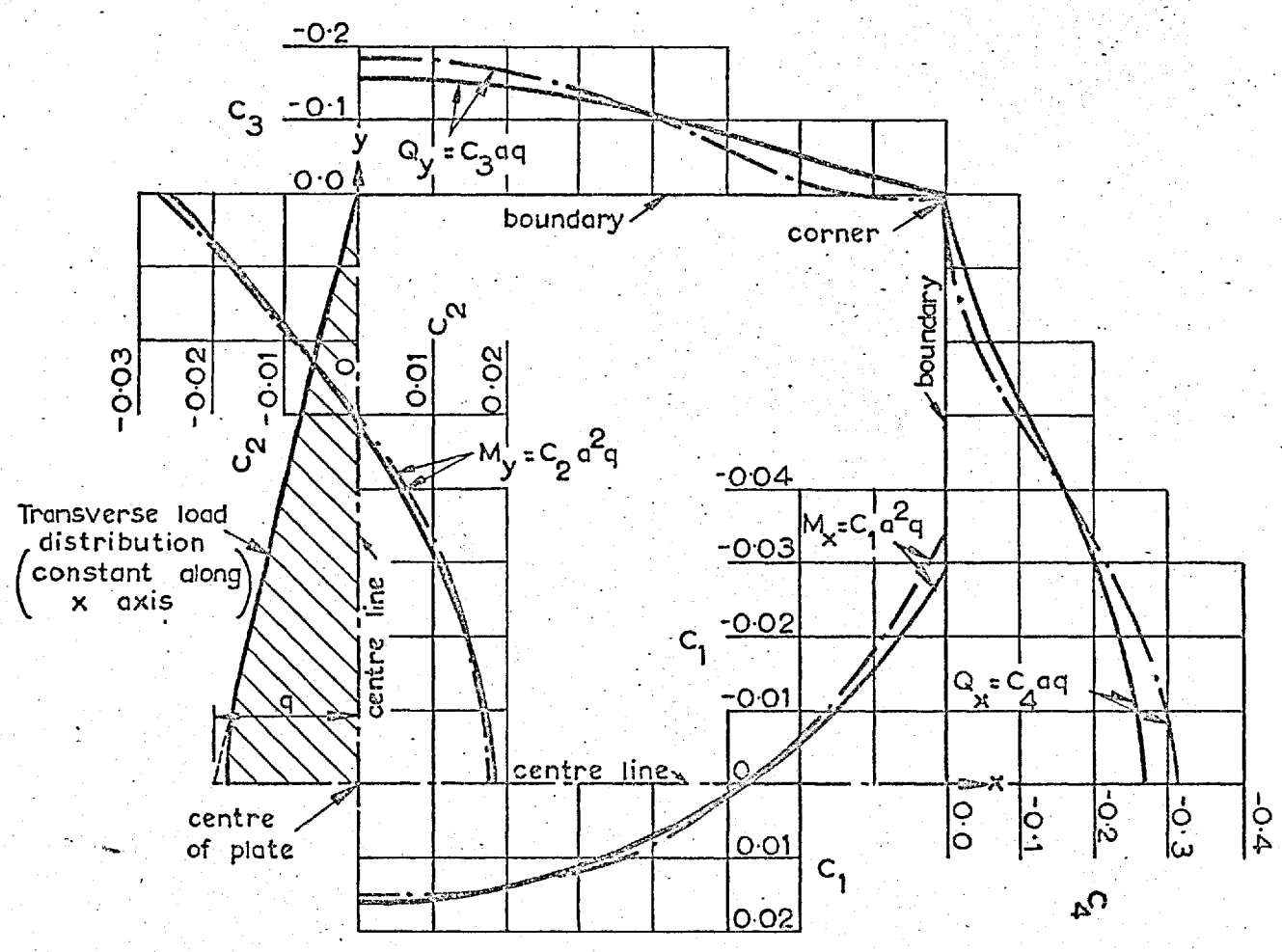

$\alpha = 1$

$\beta = 0.769$

$\varepsilon = .1$

$\mu_x = \mu_y = 0.3$

$\gamma_x = \gamma_y$	
50	———
500	— · —

Fig. 72 : Clamped Plate
Effect of Non-Uniform Transverse Load

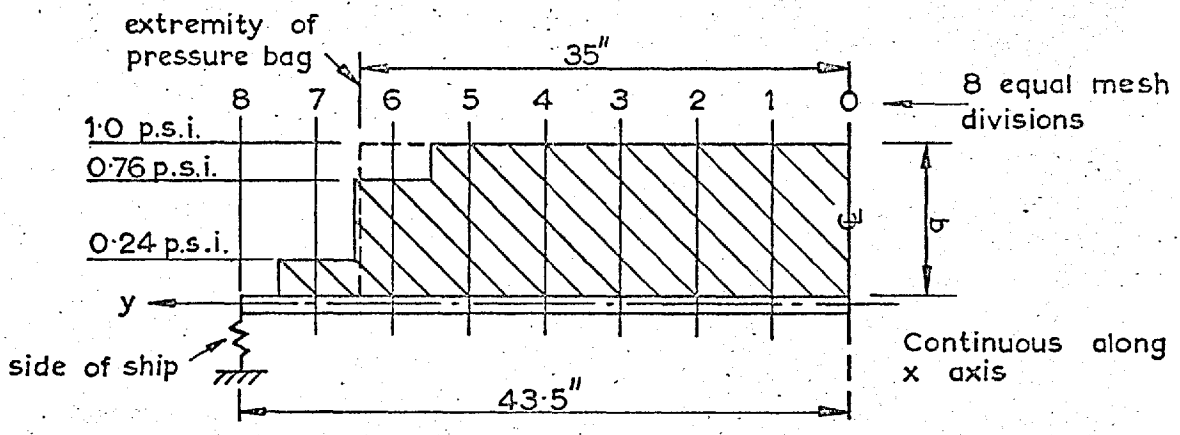

(i) Transverse load distribution

Boundary Condition		Non Dimensional Restraint						Remarks
		vertical		normal rotational		tangential rotational		
No.	plotted	K_{1x}	K_{1y}	K_{2x}	K_{2y}	K_{3x}	K_{3y}	
1a	------	10^7	10^7	0	0	10^5	10^5	ordinary simple support shear stiffness → ∞
1	———	$13{\cdot}76\times10^3$	$5{\cdot}86\times10^3$	0	0	10^5	10^5	as for 1a , with shear deformation
2	— — —	$13{\cdot}76\times10^3$	$5{\cdot}86\times10^3$	0	0	10^5	1	as for 1 , with low K_{3y}
3	—·—·	$13{\cdot}76\times10^3$	$5{\cdot}86\times10^3$	0	0	1	1	as for 2 , with low K_{3x}
3a	—·—·	$2{\cdot}06\times10^3$	$2{\cdot}52\times10^3$	0	0	1	1	as for 3 , with reduced K_{1x} and K_{1y}
4	—··—··	$13{\cdot}76\times10^3$	$5{\cdot}86\times10^3$	6·26	0	1	1	as for 3 , with normal restraint , K_{2x}

NOTE : There was very little difference between results for $K_{1x} = K_{1y} = 10^7$ and $K_{1x} = 13{\cdot}76\times10^3$, $K_{1y} = 5{\cdot}86\times10^3$ and therefore only the latter are given for cases including shear deformation.

(ii) Definition of boundary conditions

Fig. 73 : Double Bottom Analysis - Transverse Loading and Boundary Conditions Used in Theoretical Solutions For Overall Behaviour

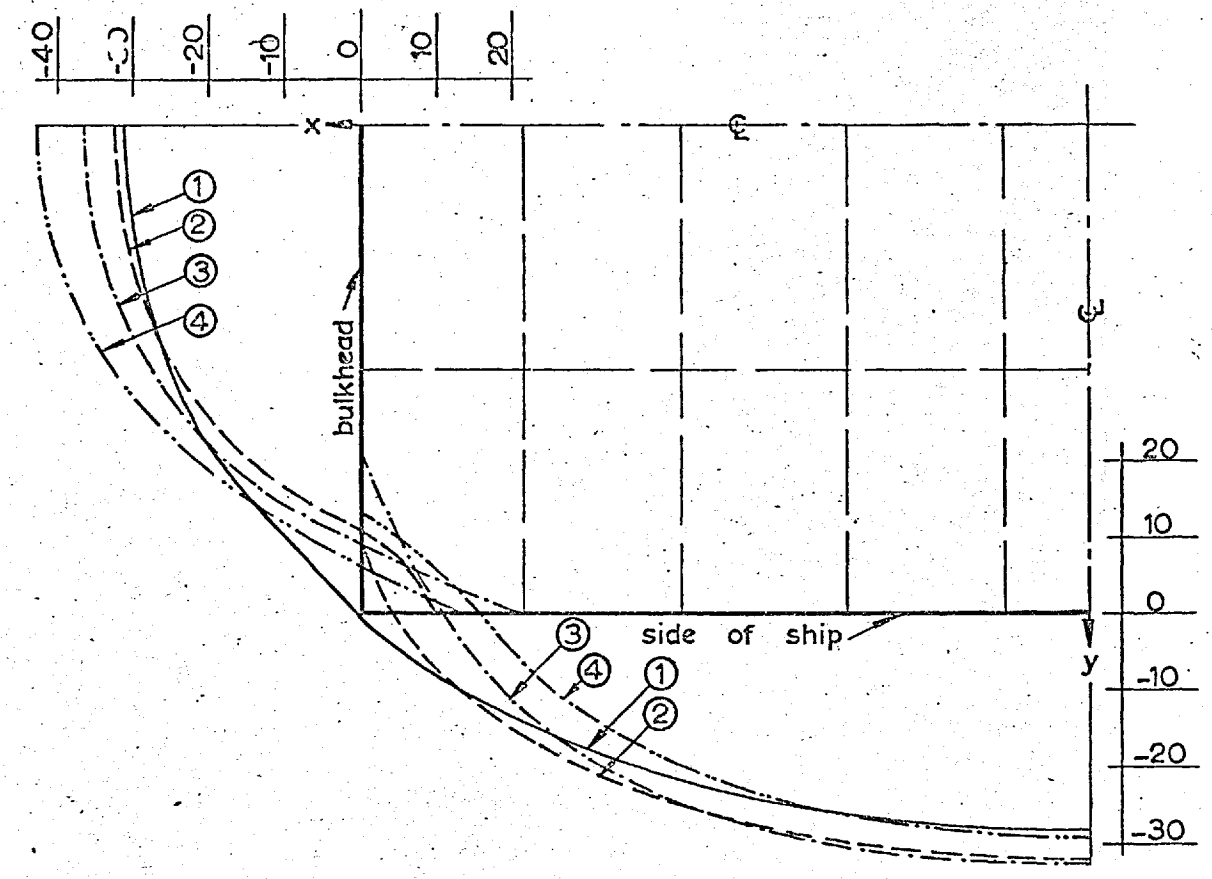

(i) Edge shear distributions in lbs./inch

NOTE : (i) Experimental values shown ⊙
(ii) For details of theoretical solutions, indicated ○, see Fig. 73

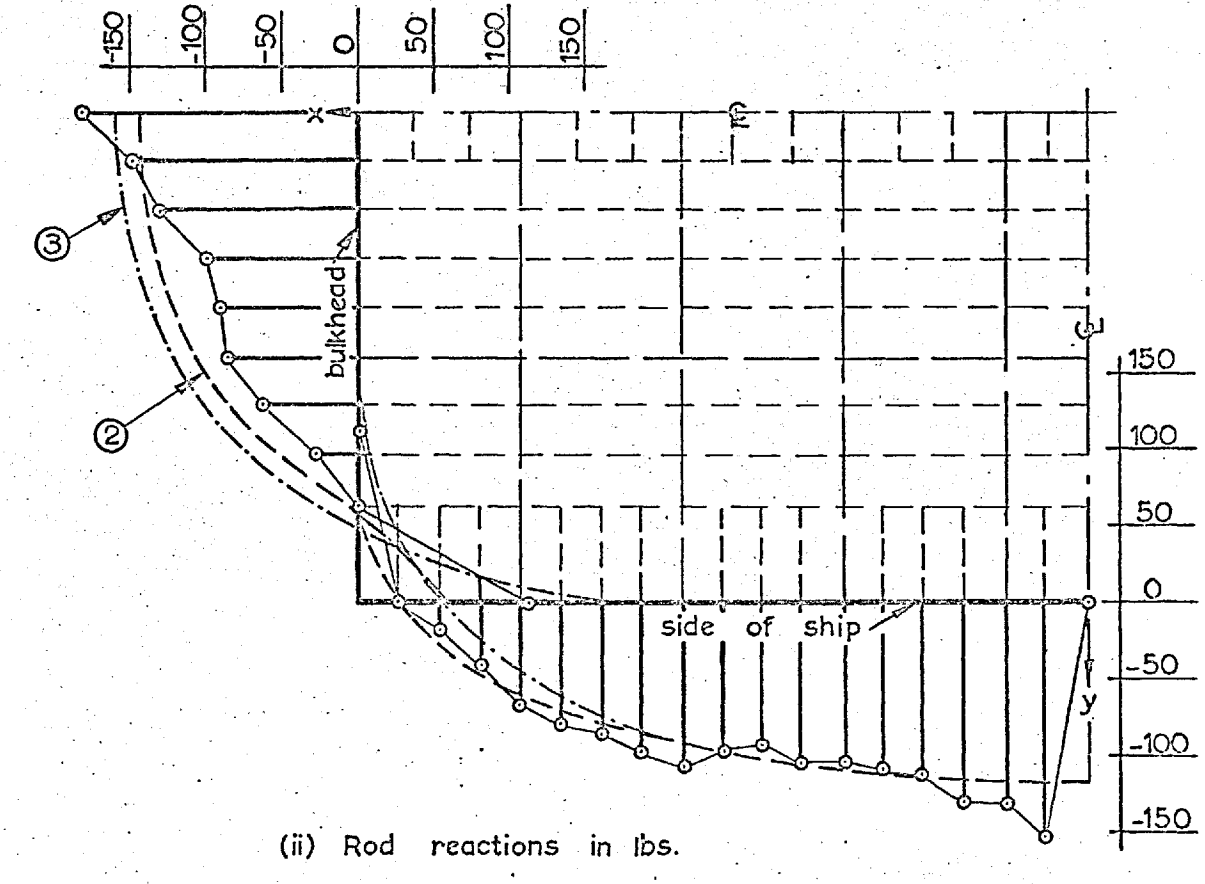

(ii) Rod reactions in lbs.

Fig. 74 : Double Bottom Analysis - Reactions for Distributed Transverse Load : q = 1p.s.i.

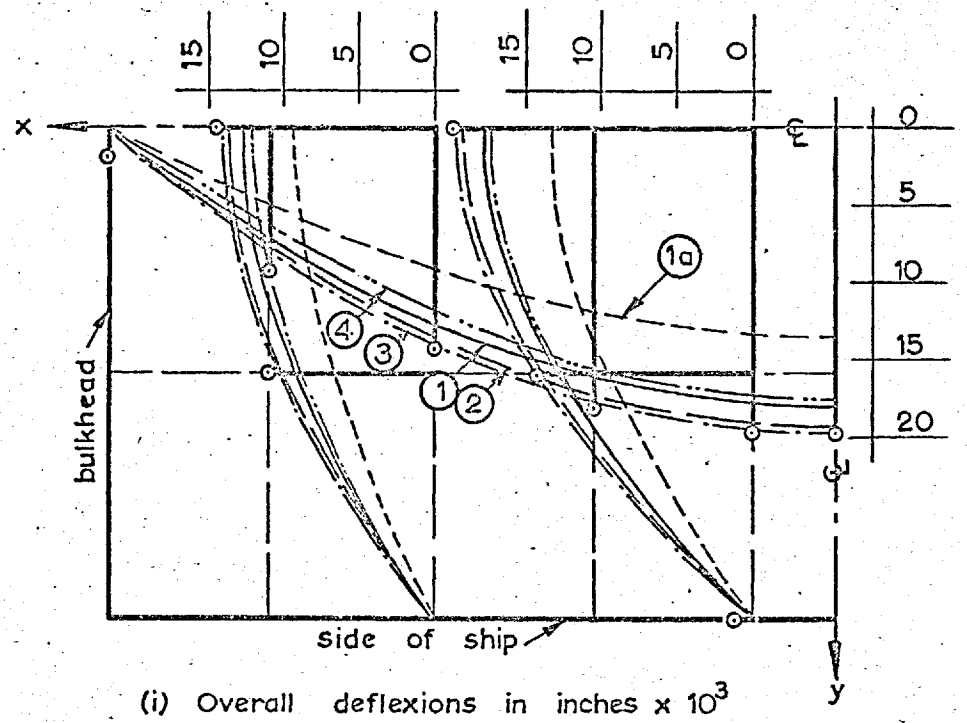

(i) Overall deflexions in inches x 10^3

NOTE : (i) Experimental values shown ⊙
(ii) For details of theoretical solutions, indicated ○, see Fig. 73

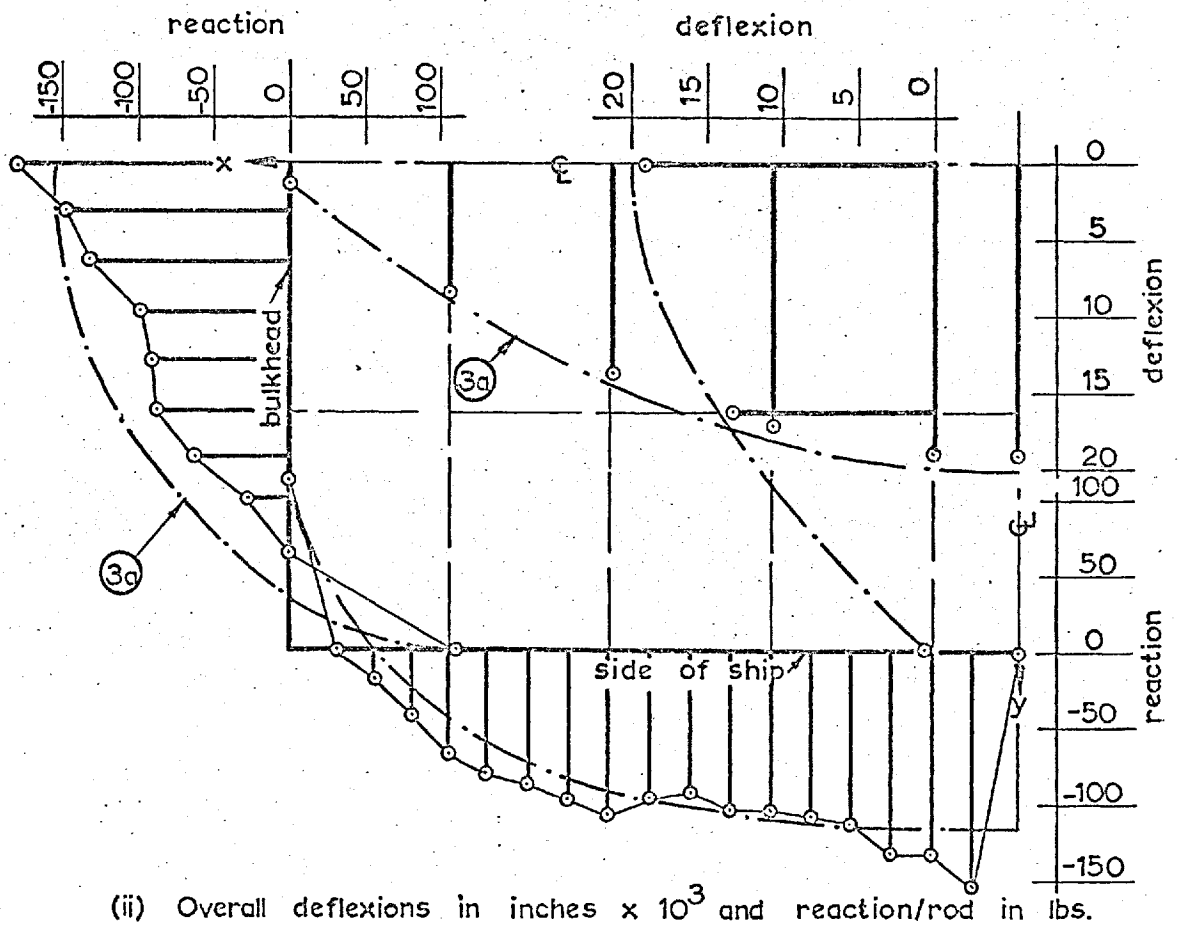

(ii) Overall deflexions in inches x 10^3 and reaction/rod in lbs.
Alternative theoretical boundary condition - 3a

Fig. 75 : Double Bottom Analysis - Deflexions and Reactions For Distributed Transverse Load : q = 1p.s.i

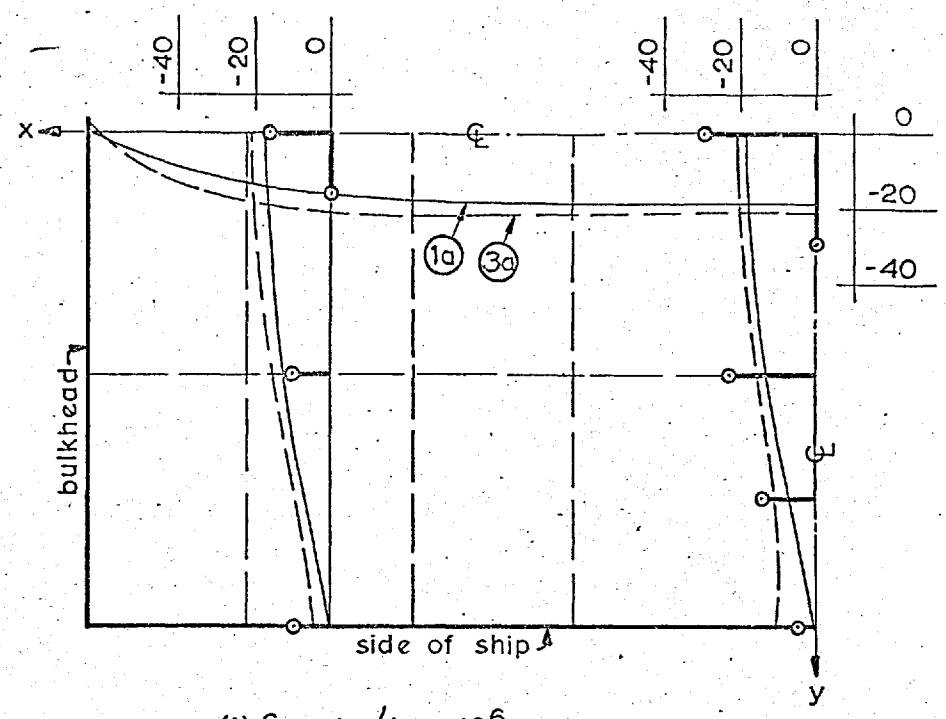

(i) ε_{xi} in./in. x 10^6

Note: (i) Experimental values shown thus: ⊙

(ii) For details of theoretical solutions, indicated ◯, see Fig. 73

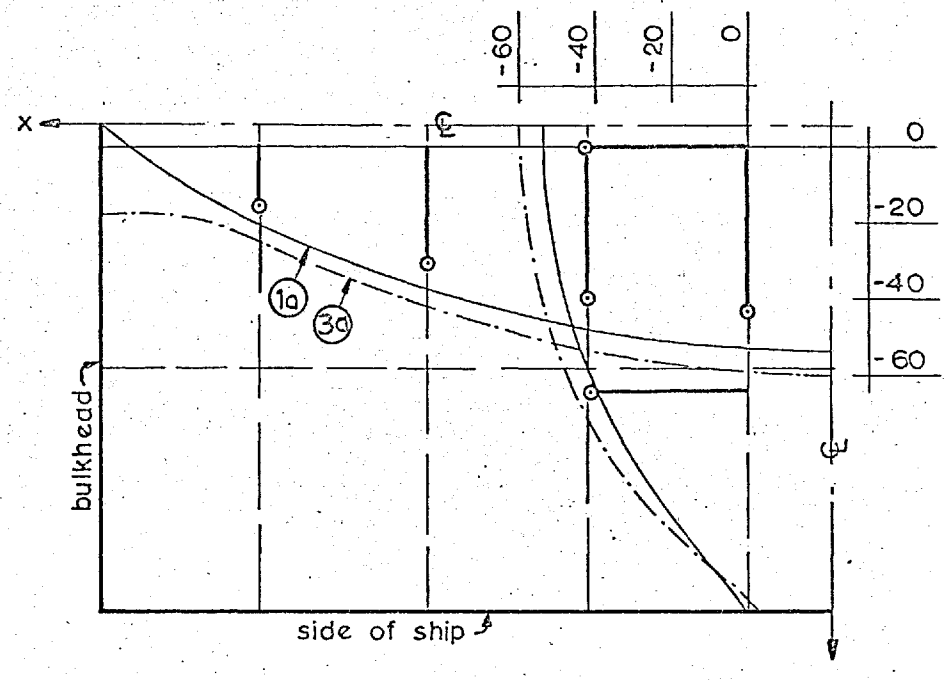

(ii) ε_{yi} in./in. x 10^6

Fig. 76 : Double Bottom Analysis – Inner Shell Strains For Distributed Transverse Load : q = 1 p.s.i.

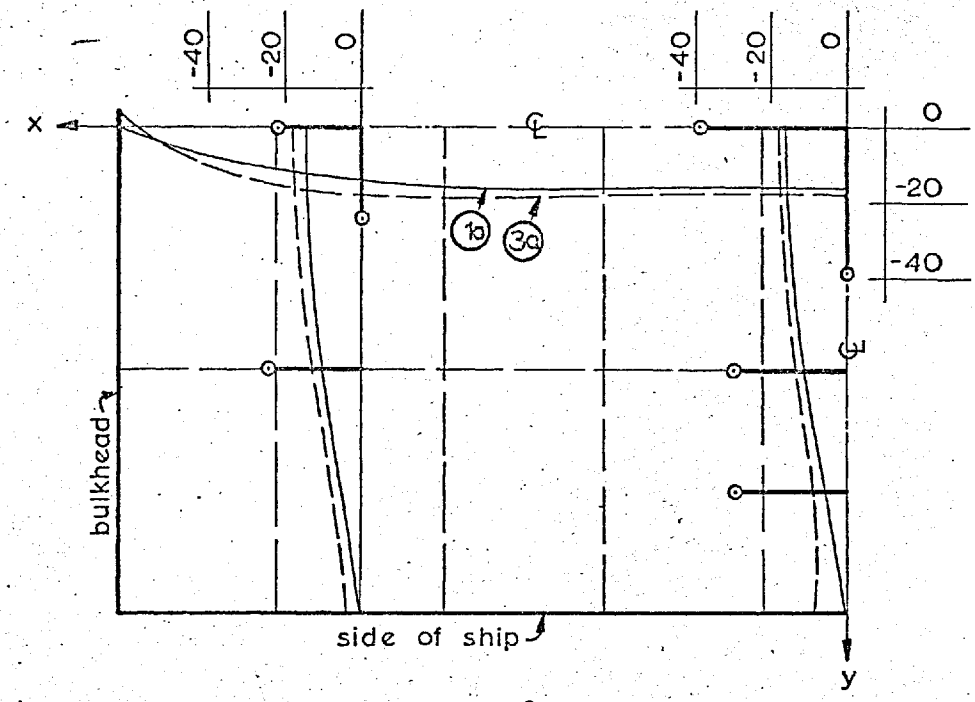

(i) ε_{xo} in./in. x 10^6

Note: (i) Experimental values shown thus: ⊙

(ii) For details of theoretical solutions, indicated ◯, see Fig. 73

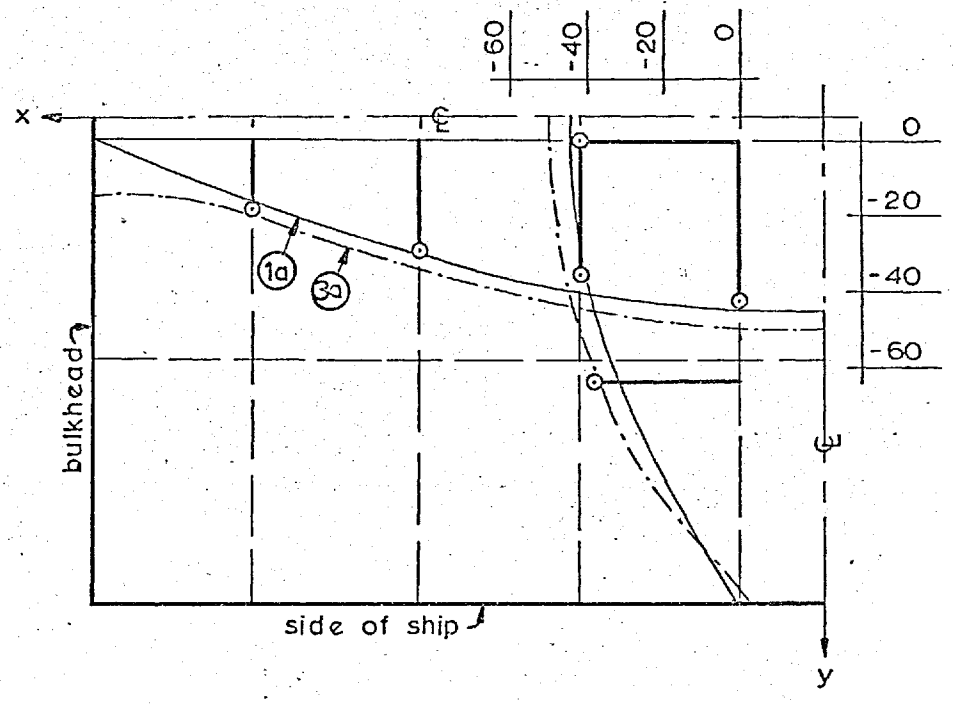

(ii) ε_{yo} in./in. x 10^6

Fig. 77 : Double Bottom Analysis – Outer Shell Strains For Distributed Transverse Load: q = 1 p.s.i.

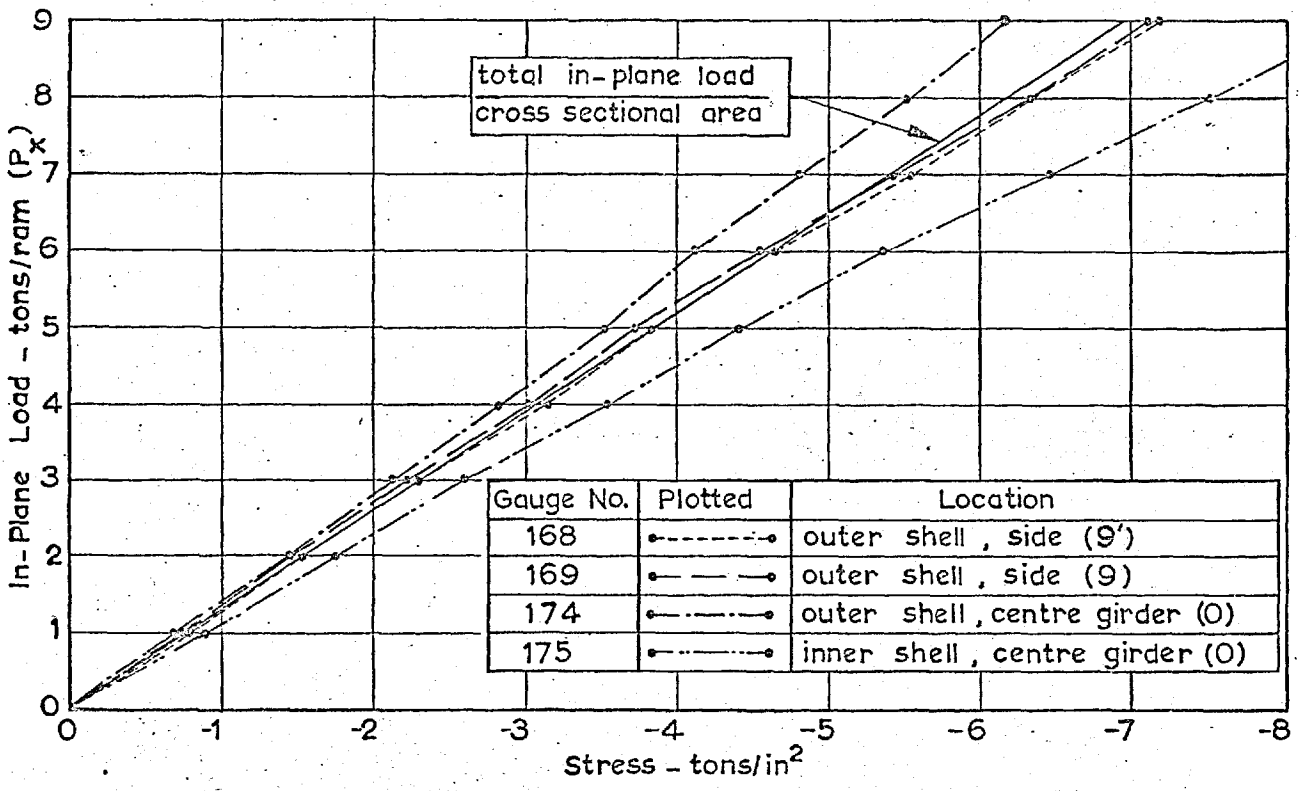

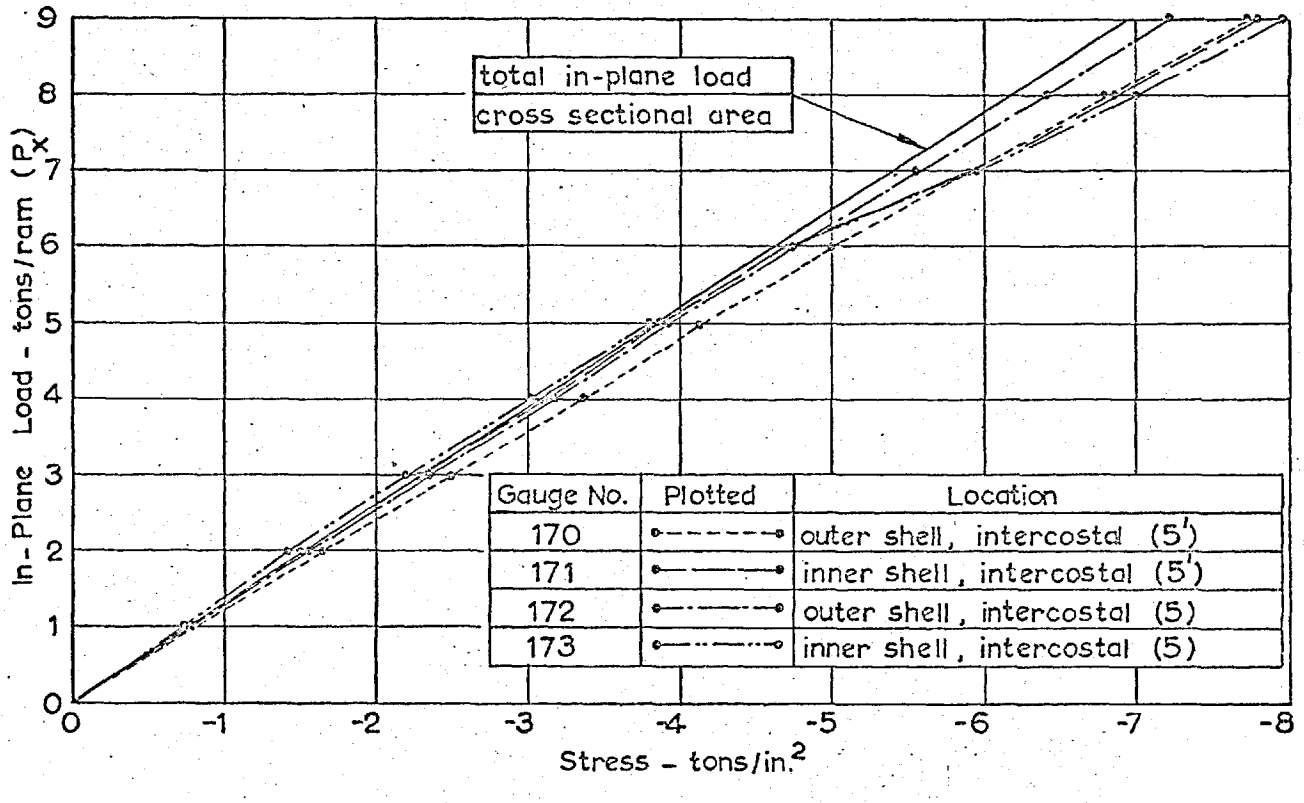

NOTE : For gauge locations see Fig. 19

Fig. 78 : Double Bottom Analysis - Longitudinal Shell Stresses (σ_{xm}) Between Floors D and C Due to In-Plane Load

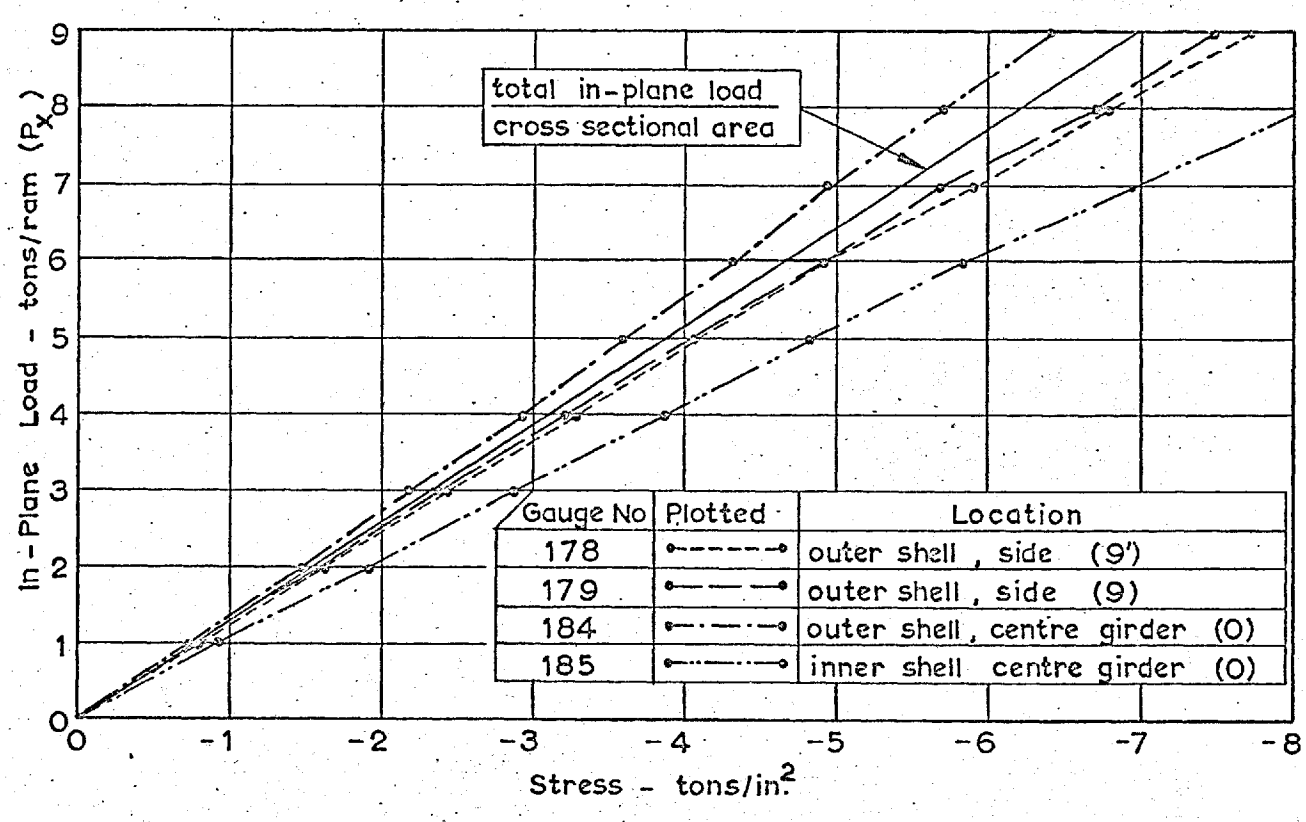

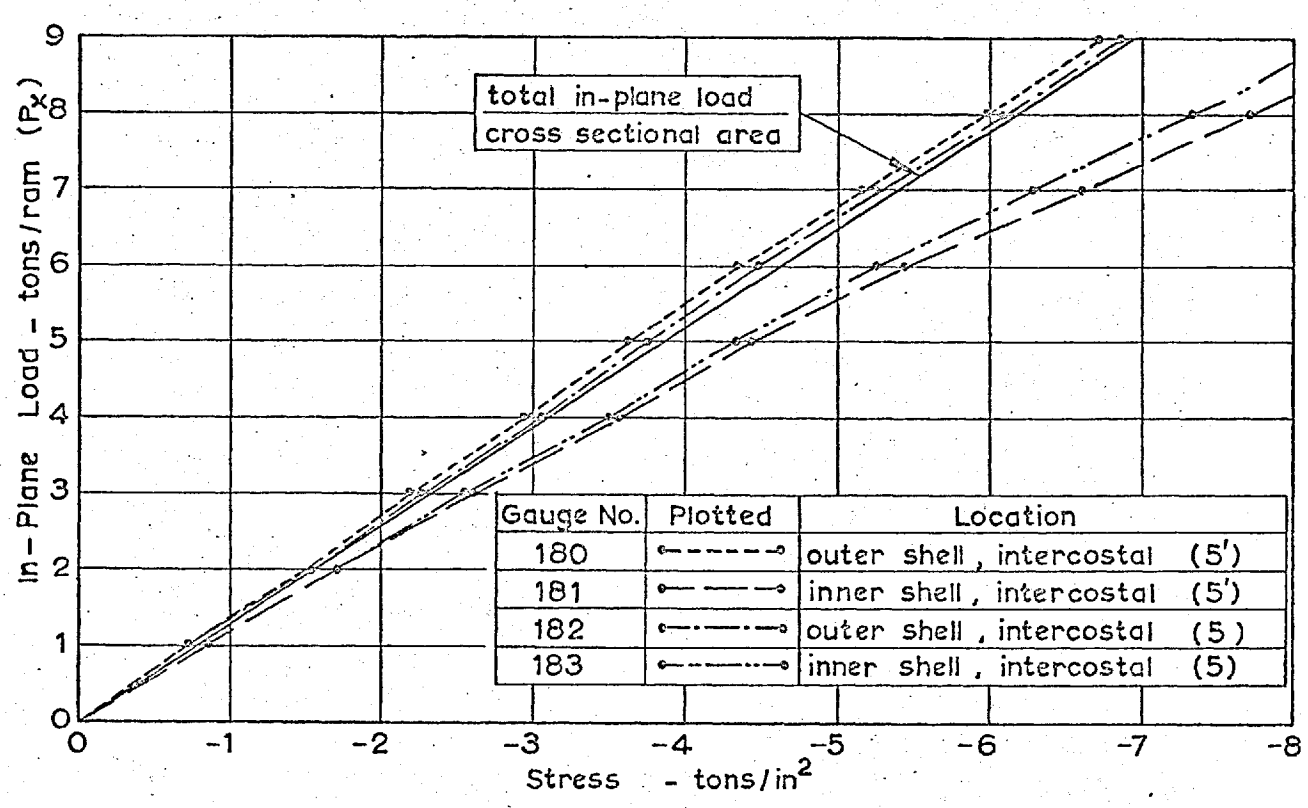

NOTE : For gauge locations see Fig. 19

Fig. 79 : Double Bottom Analysis - Longitudinal Shell Stresses (σ_{xm}) Between Floors A and A' Due to In-Plane Load

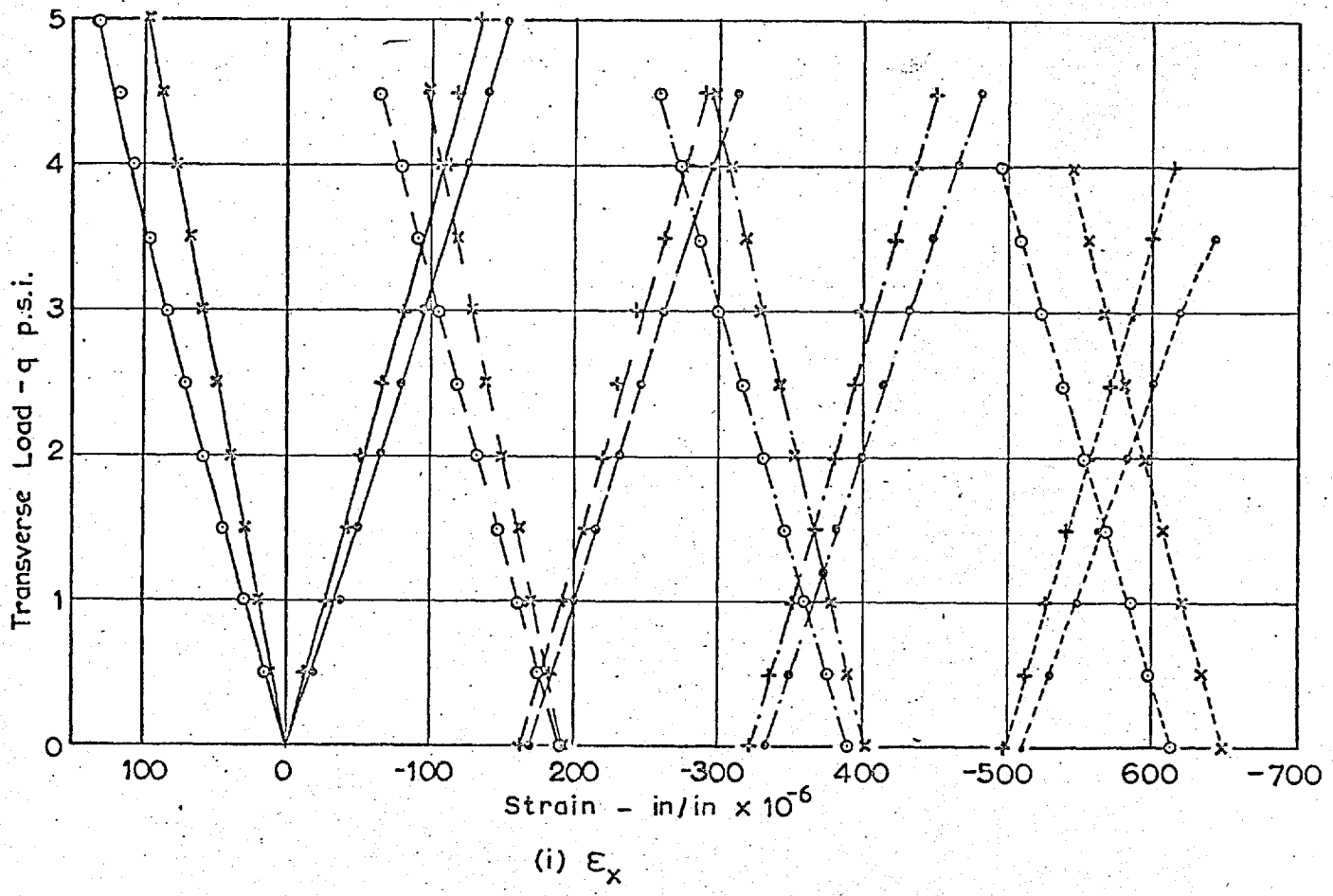

(i) ε_x

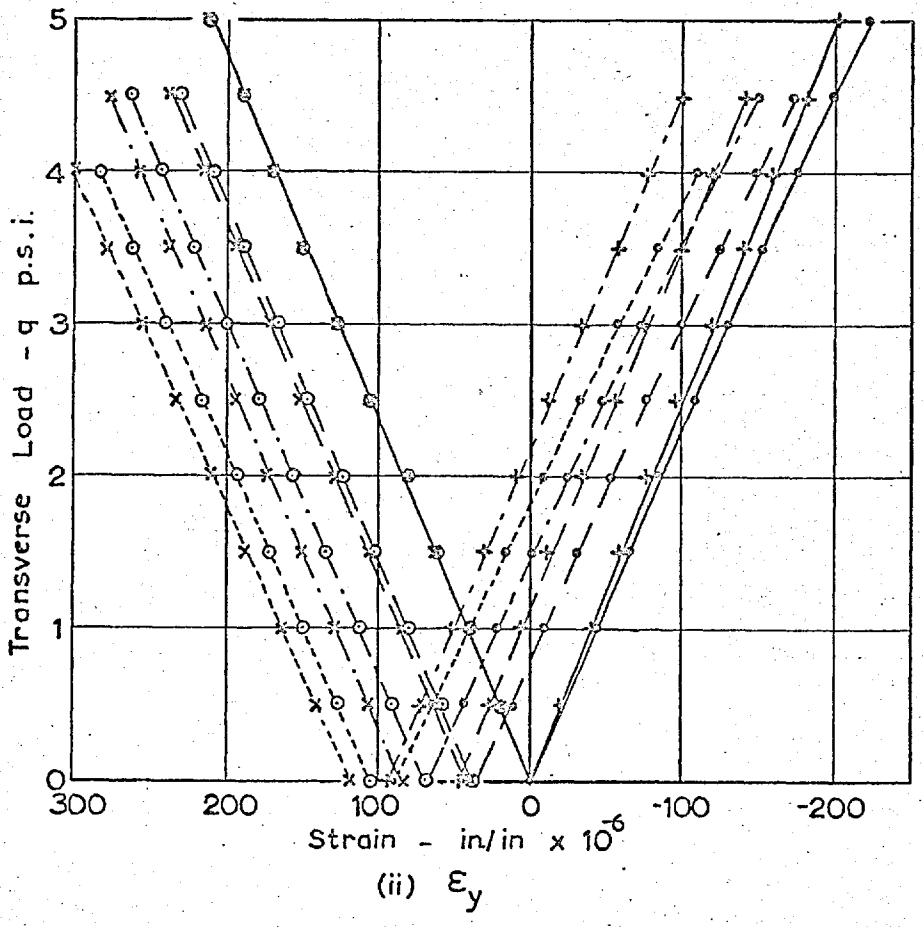

(ii) ε_y

LEGEND

Gauge Number		Symbol
(i) ε_x	(ii) ε_y	
180	194	+
181	195	×
182	196	•
183	197	⊙

See Fig. 19 for gauge locations

In - Plane Load		Plotted
P_x tons/ram	average stress tons/in^2	
0	0	———
3	-2·31	— —
6	-4·62	— · — ·
9	-6·93	- - - - -

Fig. 80 : Double Bottom Analysis - Typical Shell Strains For combined Transverse and In - Plane Load

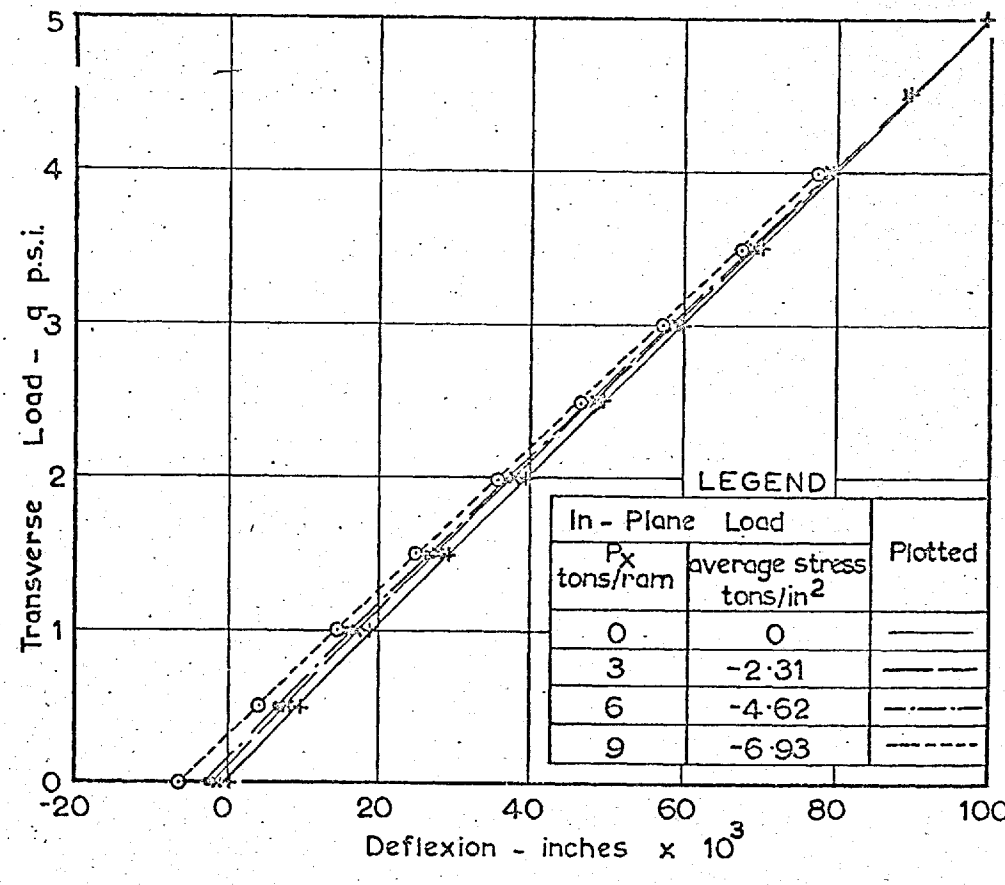

(i) Effect of comined load on central deflexion (gauge No. 1)

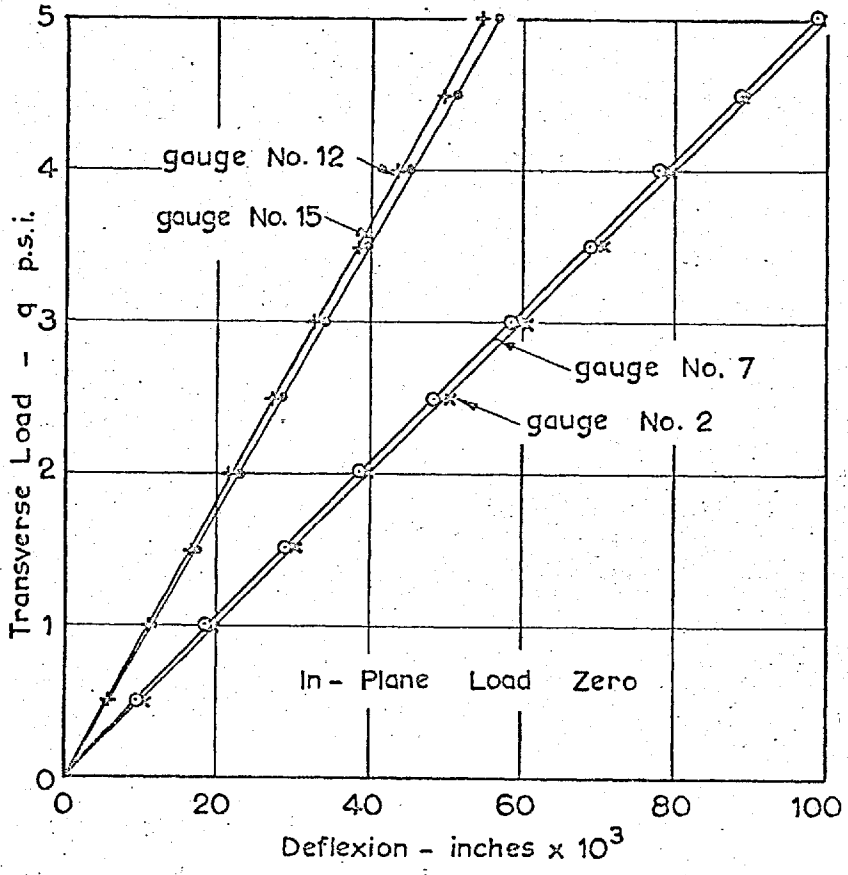

NOTE

See Fig. 22 for gauge locations

(ii) Symmetry of deformation for increasing transverse load

Fig. 81 : Double Bottom Analysis - Overall Deflexions For Increasing Transverse and In-Plane Load.

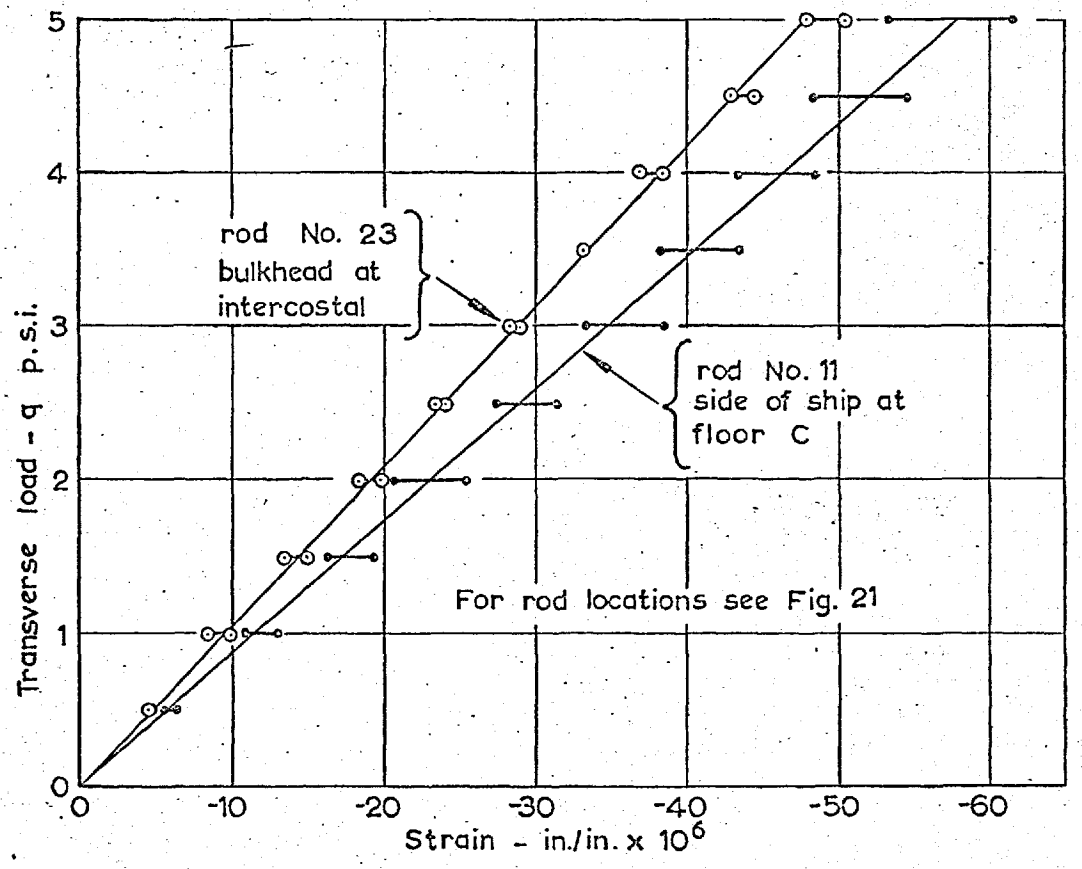

(i) Typical compression rods

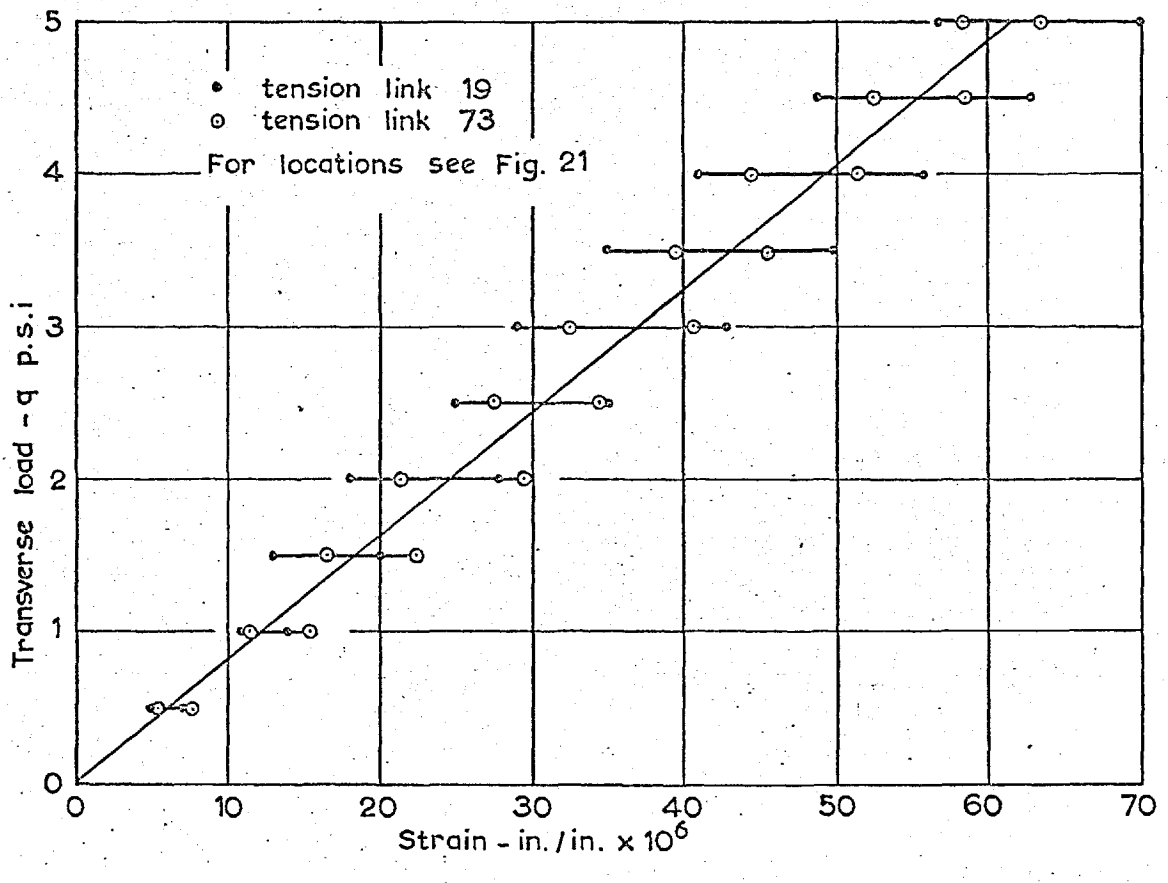

(ii) Tension links

Fig. 82 : Double Bottom Analysis - Linearity of Strains With Distributed Transverse Load

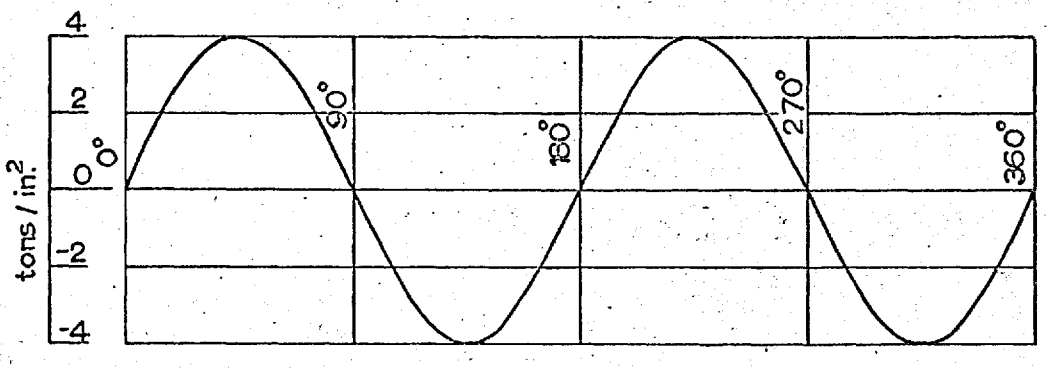

(i) Due to an applied shear stress : τ = 1 ton/in.^{2}

Note : See Fig. 18 for orientation of 0° datum

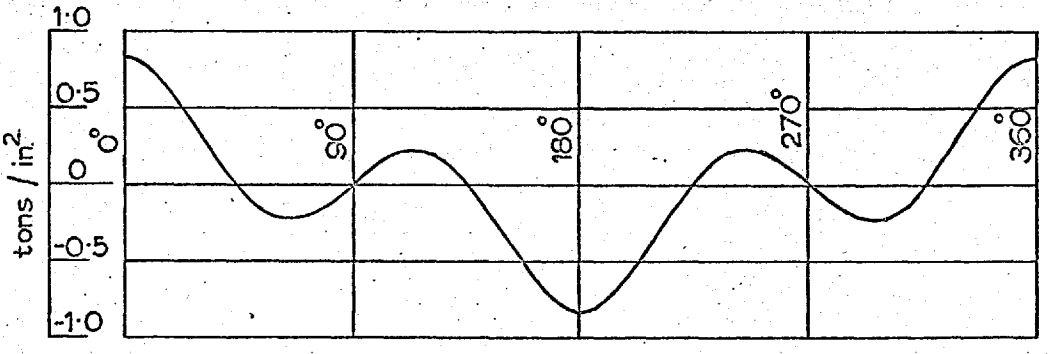

(ii) Due to an applied bending stress : σ = 1 ton./in.^{2}

Fig. 83 : Double Bottom Analysis - Theoretical Tangential Stresses Around Circumference of Lightening Holes

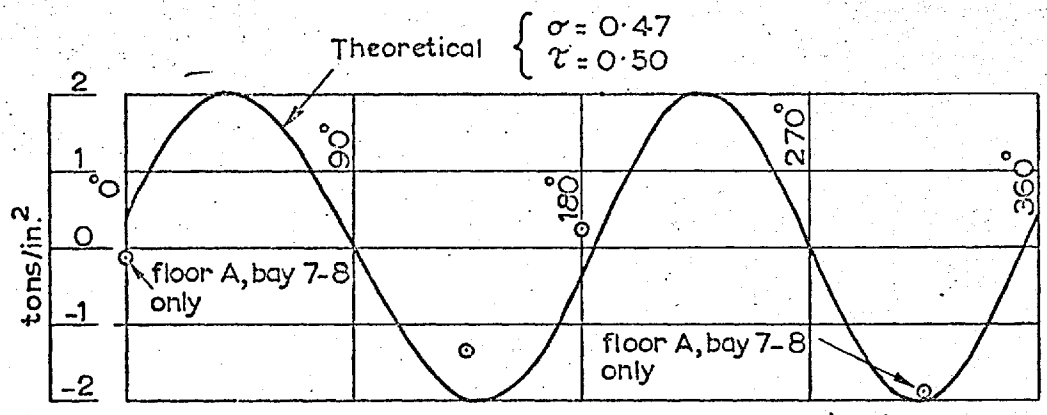

(i) Floors A and A′ , Bays 7 - 8 and 7′ - 8′

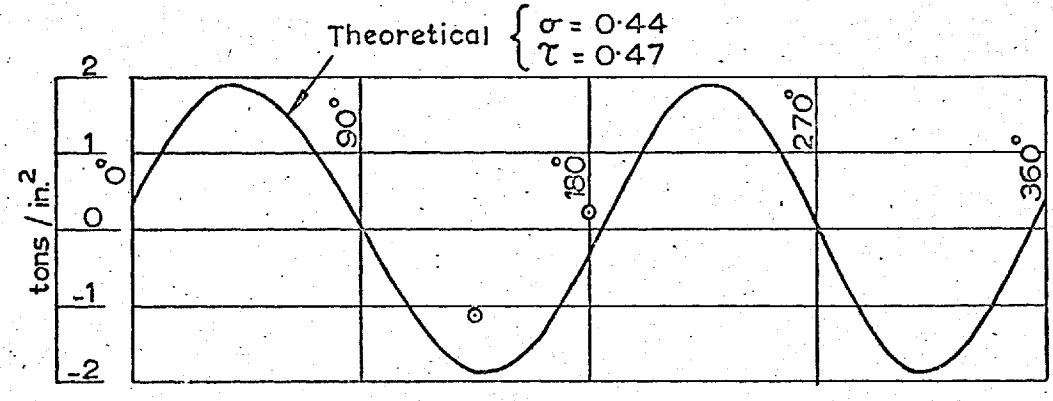

(ii) Floor B , Bay 7 - 8

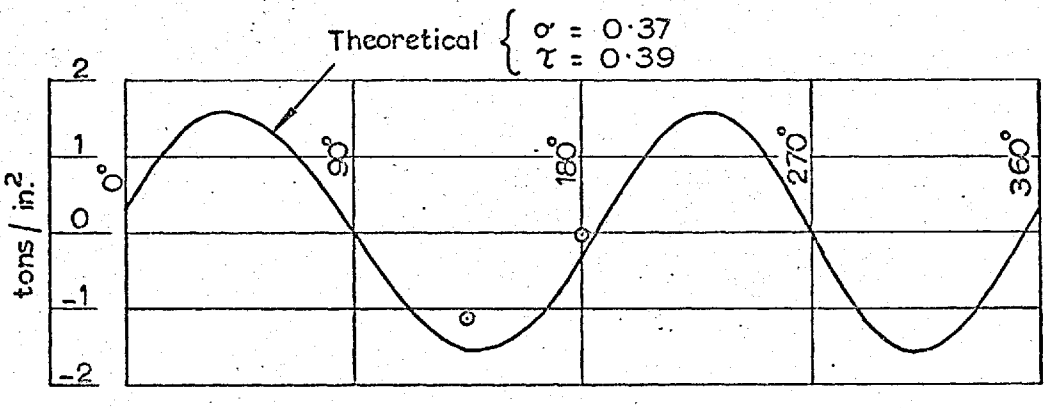

(iii) Floor C , Bay 7 - 8

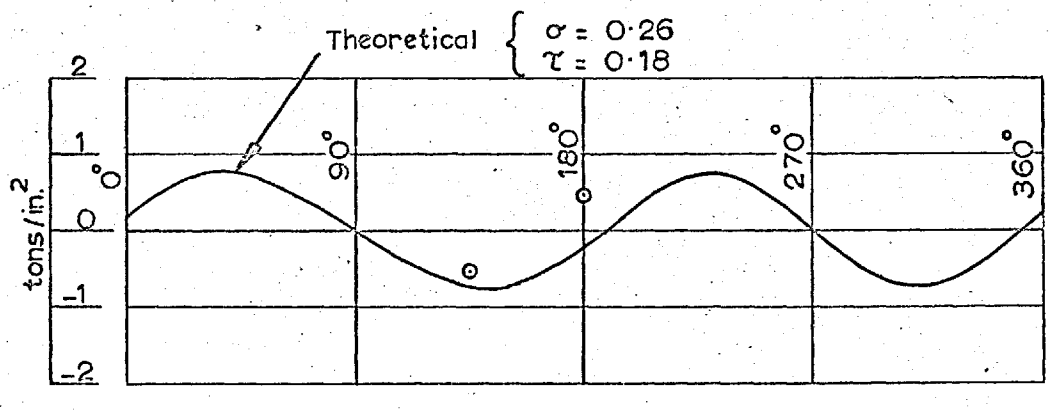

(iv) Floor D , Bay 7 - 8

NOTE: (i) Experimental values shown ⊙

(ii) Flexural (σ tons/in.^{2}) and shear (τ tons/in.^{2}) stresses shown for theoretical solutions were obtained from results for boundary condition 3a – see Fig. 73

(iii) For hole locations and orientation of 0° datum see Fig. 18

Fig. 84 : Double Bottom Analysis - Web Hole Stresses For Distributed Transverse Load : q = 1 p.s.i.

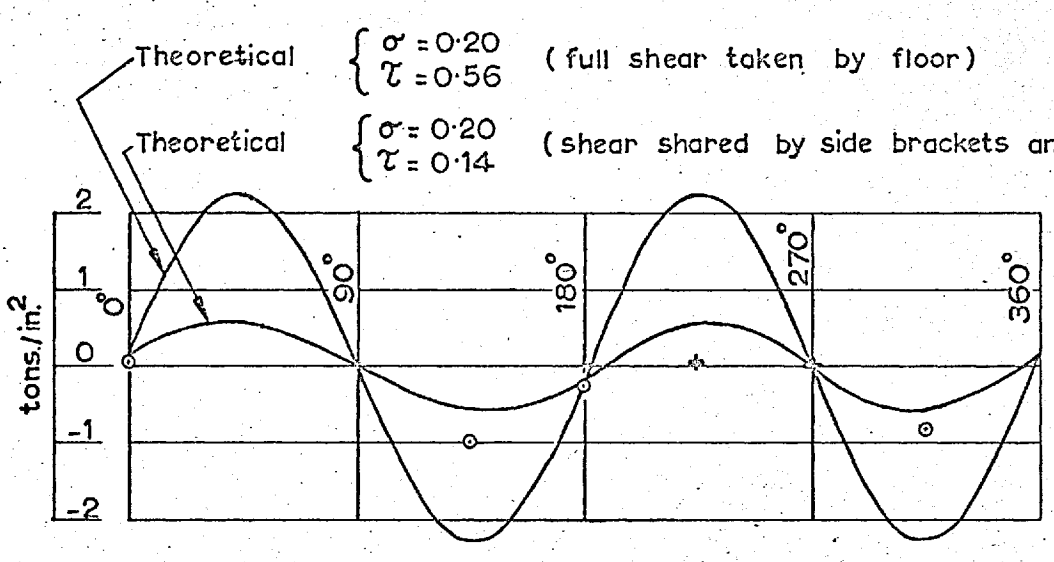

(i) Floor A (⊙) and Side Bracket A_1, (+), Bay 8-9

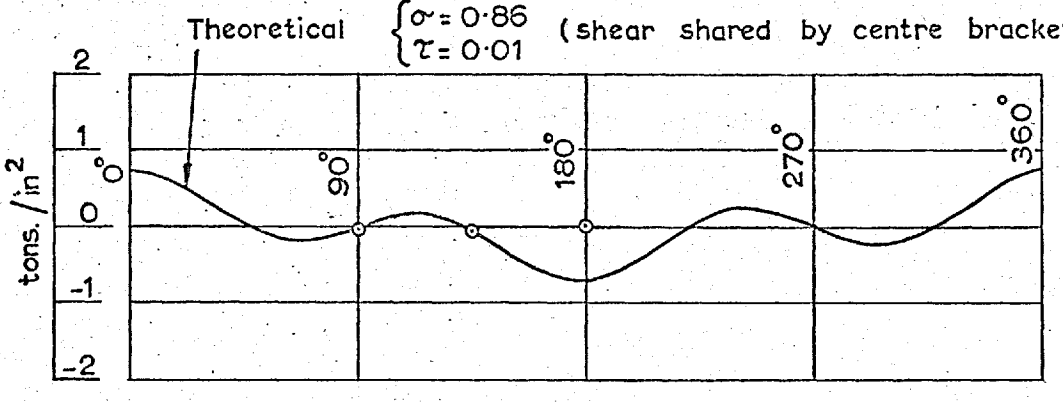

(ii) Centre Bracket A_1, Bay 0-1

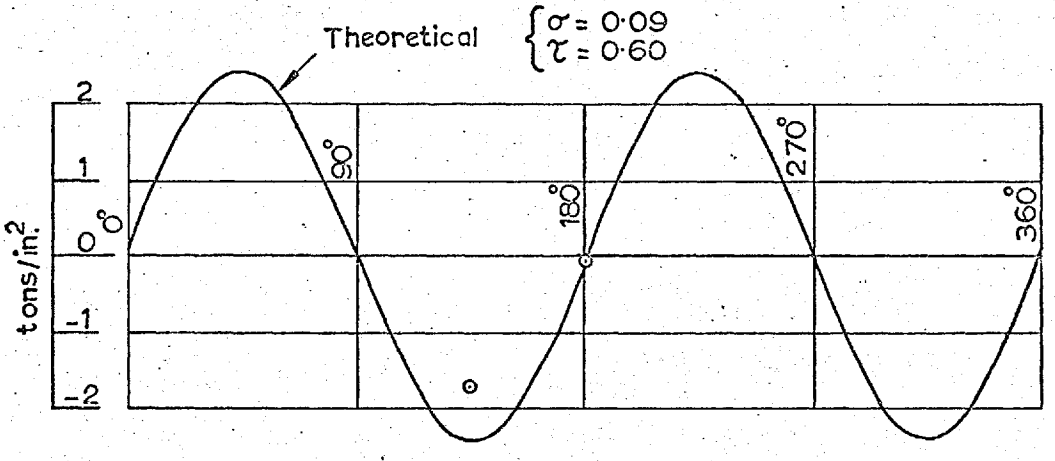

(iii) Intercostals (5 and 5'). Holes Adjacent to E and E'

NOTE: (i) Experimental values shown ⊙ and +
(ii) Flexural (σ tons/in^2) and shear (τ tons/in^2) stresses shown for theoretical solutions were obtained from results for boundary condition 3a - see Fig. 73
(iii) For hole locations and orientation of 0° datum see Fig. 18

Fig. 85 : Double Bottom Analysis - Web Hole Stresses For Distributed Transverse Load : q =1p.s.i.

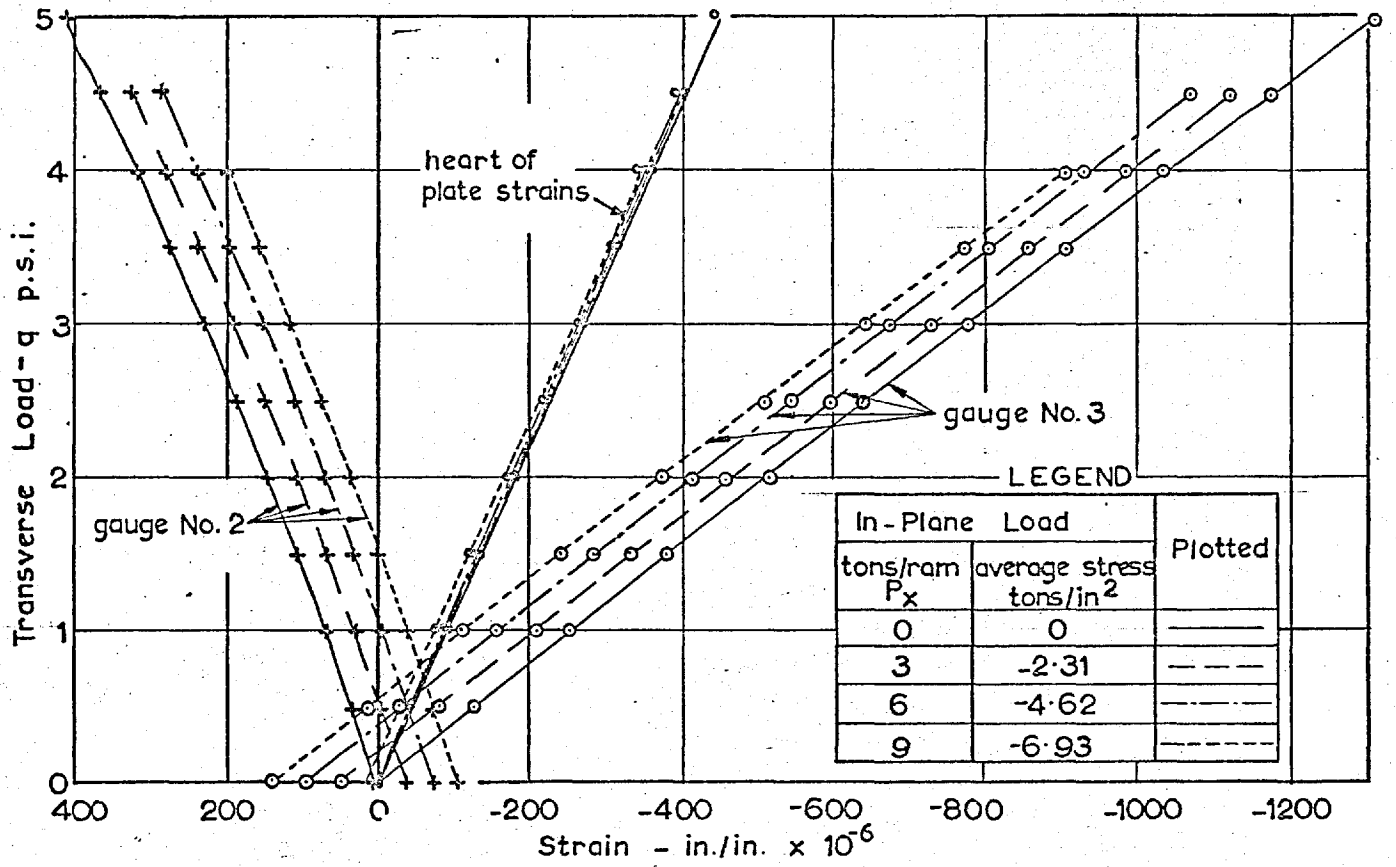

(i) Floor A' - Bay 7'-8'-135°

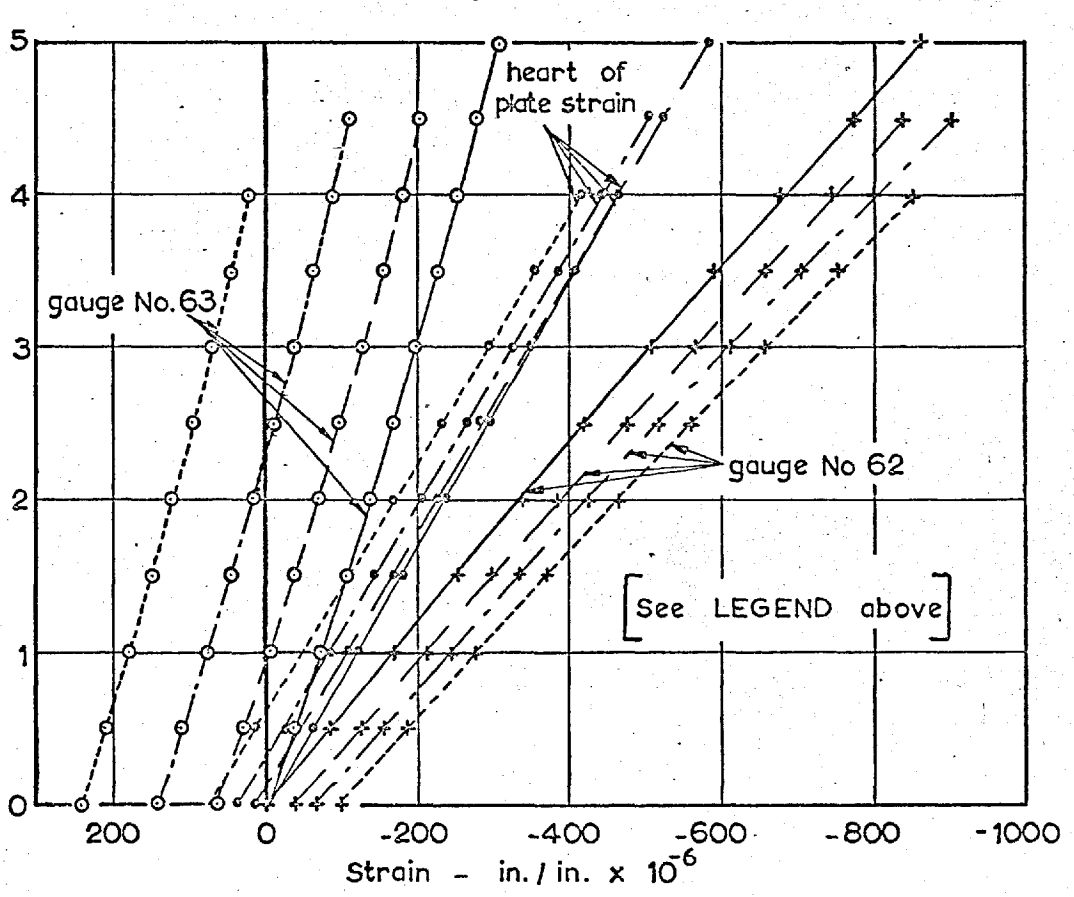

(ii) Intercostal 5' - Hole adjacent to E - 135°

NOTE
See Fig. 18 for gauge locations

Fig. 86 : Double Bottom Analysis - Typical Web Hole Strains For Combined Transverse and In - Plane Load

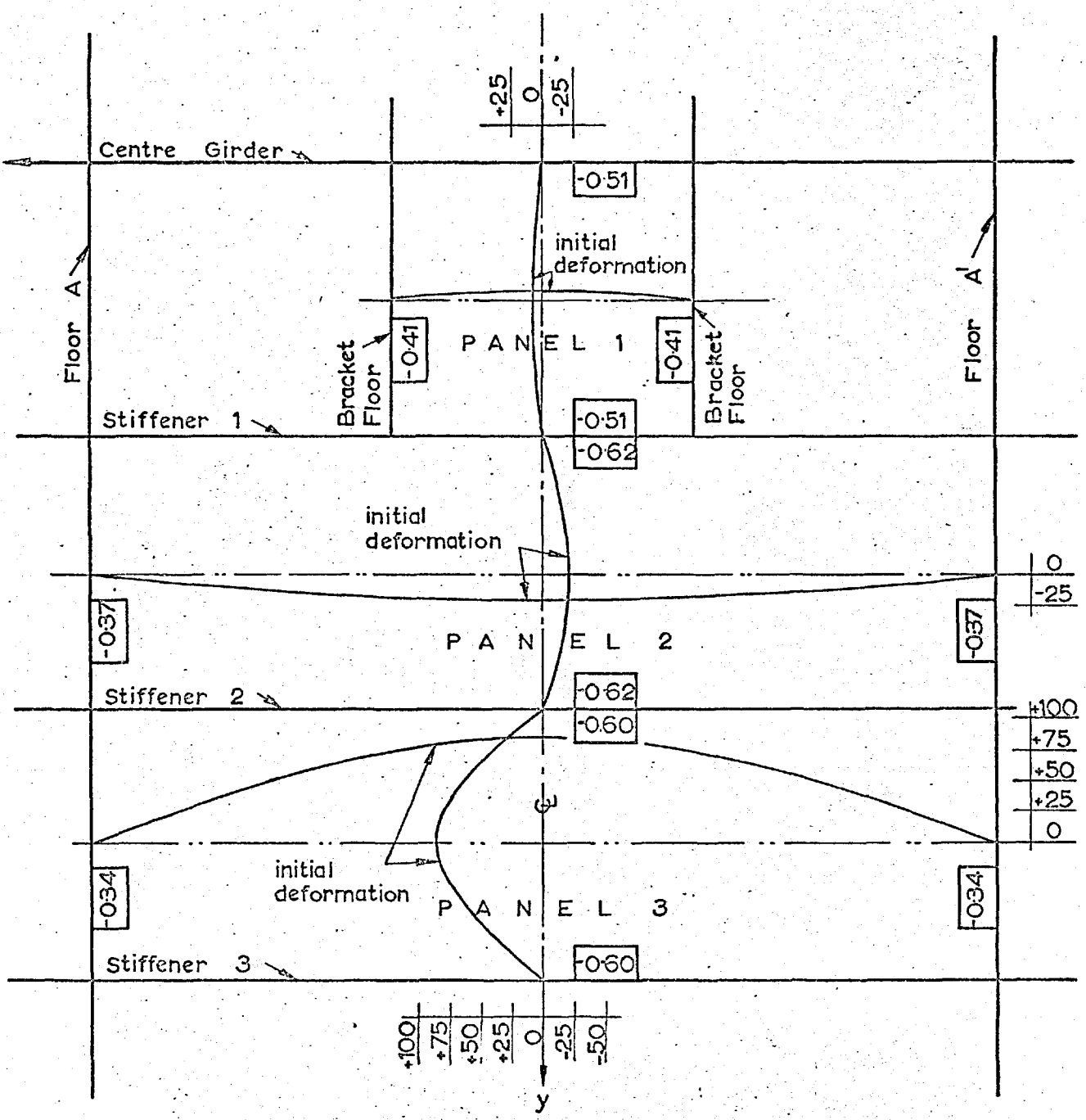

NOTE : (1) Initial deformation in inches $\times 10^3$ (positive inwards), based on measured contours shown in Fig. 27

(ii) Mean in-plane edge stresses, shown -0·60, in tons/in^2 computed from overall solution for boundary condition 3a and q = 1 p.s.i. - see Fig. 73.

(iii) For analysis of panel behaviour with increasing load in-plane stresses increased lineally with q.

Fig. 87 : Double Bottom Analysis - Initial Deformation and Loading Used In Outer Shell Panel Analysis For Distributed Transverse Load

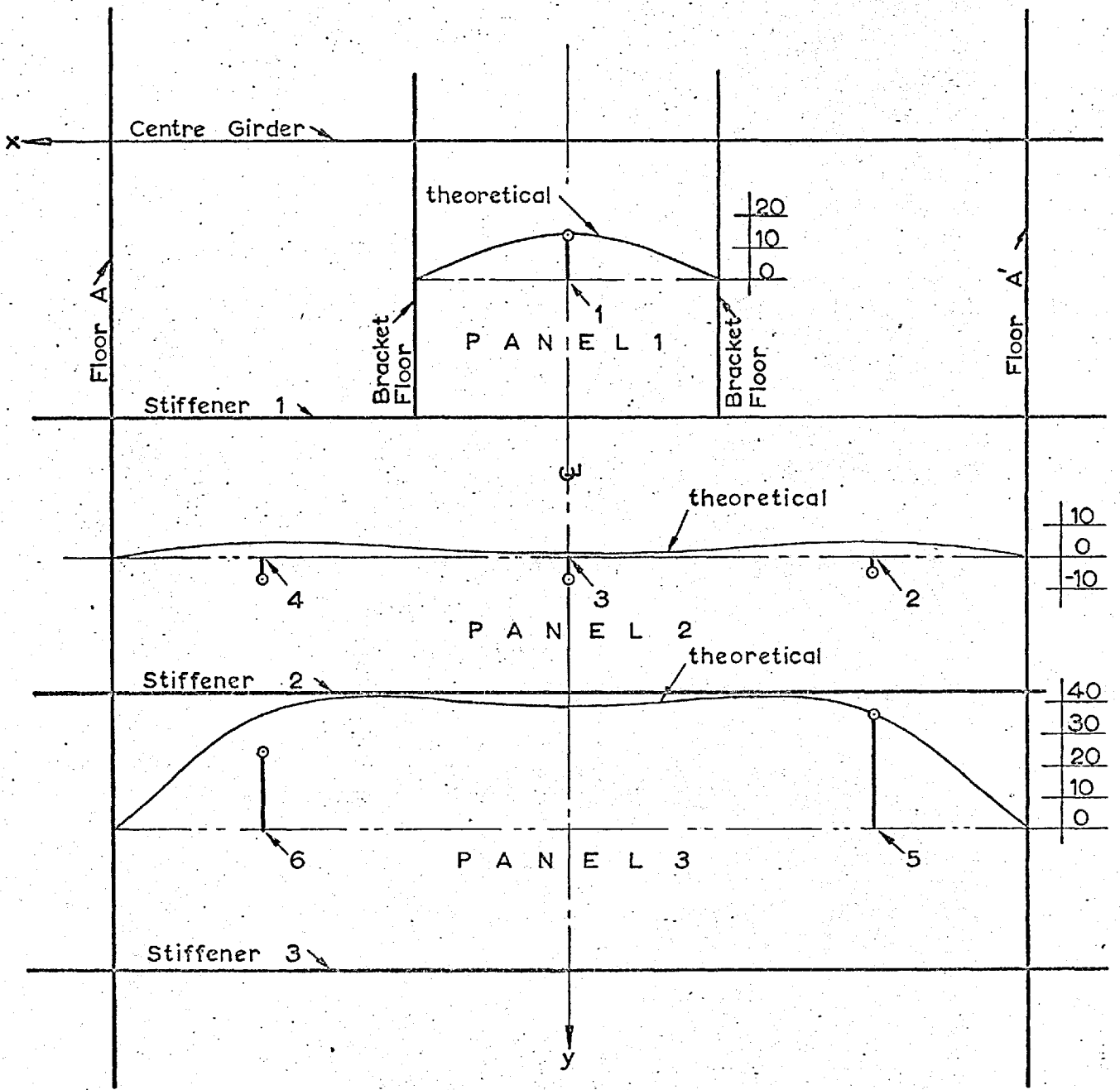

NOTE : (i) Deflexions in inches x 10^4 (positive inwards)
(ii) Experimental values shown o
(iii) For details of initial deformation and loading ($q^* = 1$) see Fig. 87

Fig. 88 : Double Bottom Analysis - Deflexions of Outer Shell Panels For Distributed Transverse Load : $q^* = 1$

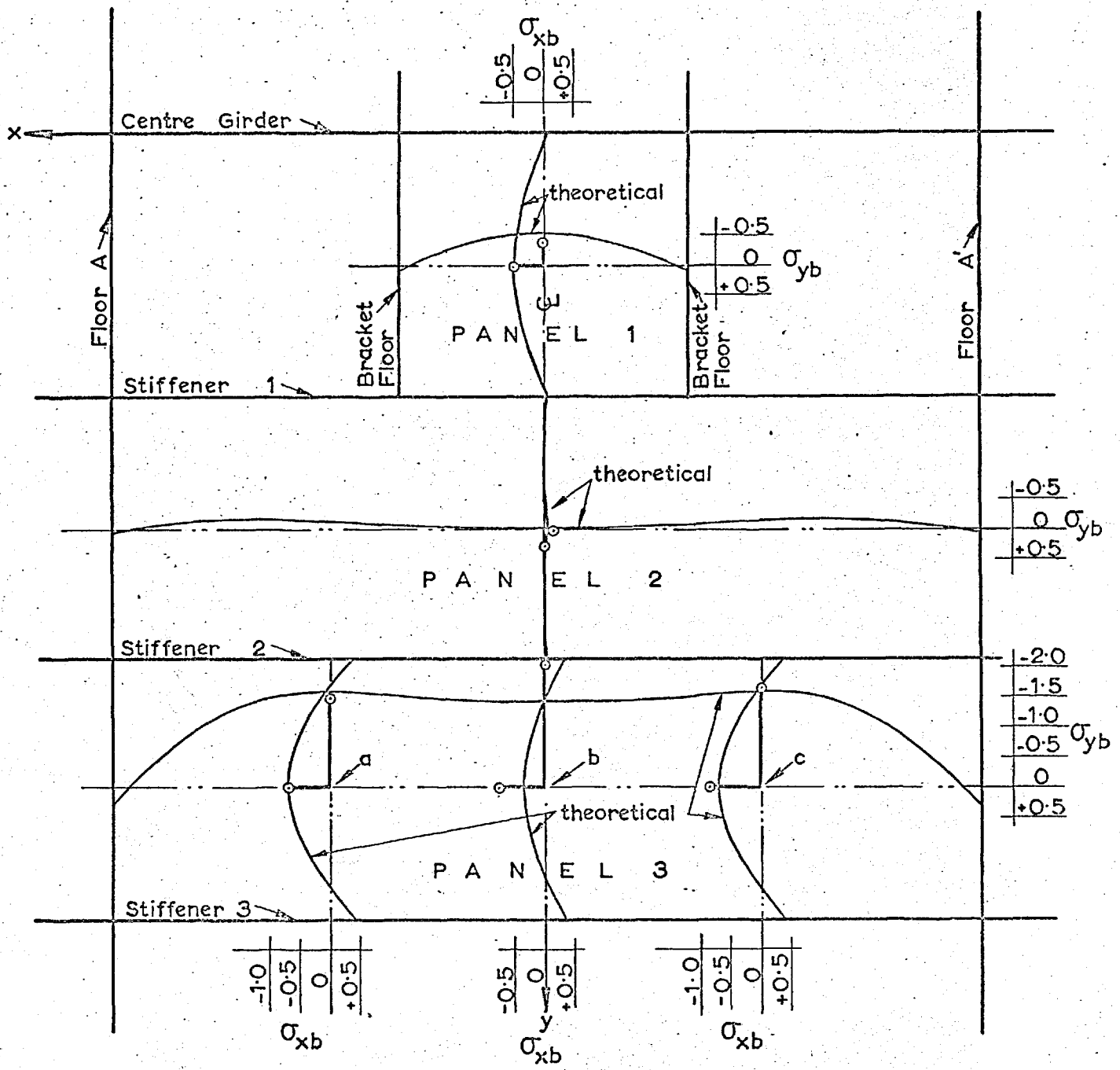

NOTE : (i) Stresses in. tons/in^2
(ii) Experimental values shown ⊙
(iii) For details of initial deformation and loading ($q^* = 1$) see Fig. 87

Fig. 89 :Double Bottom Analysis - Bending Stresses at Outer Surface of Outer Shell Panels For Distributed Transverse Load : $q^* = 1$

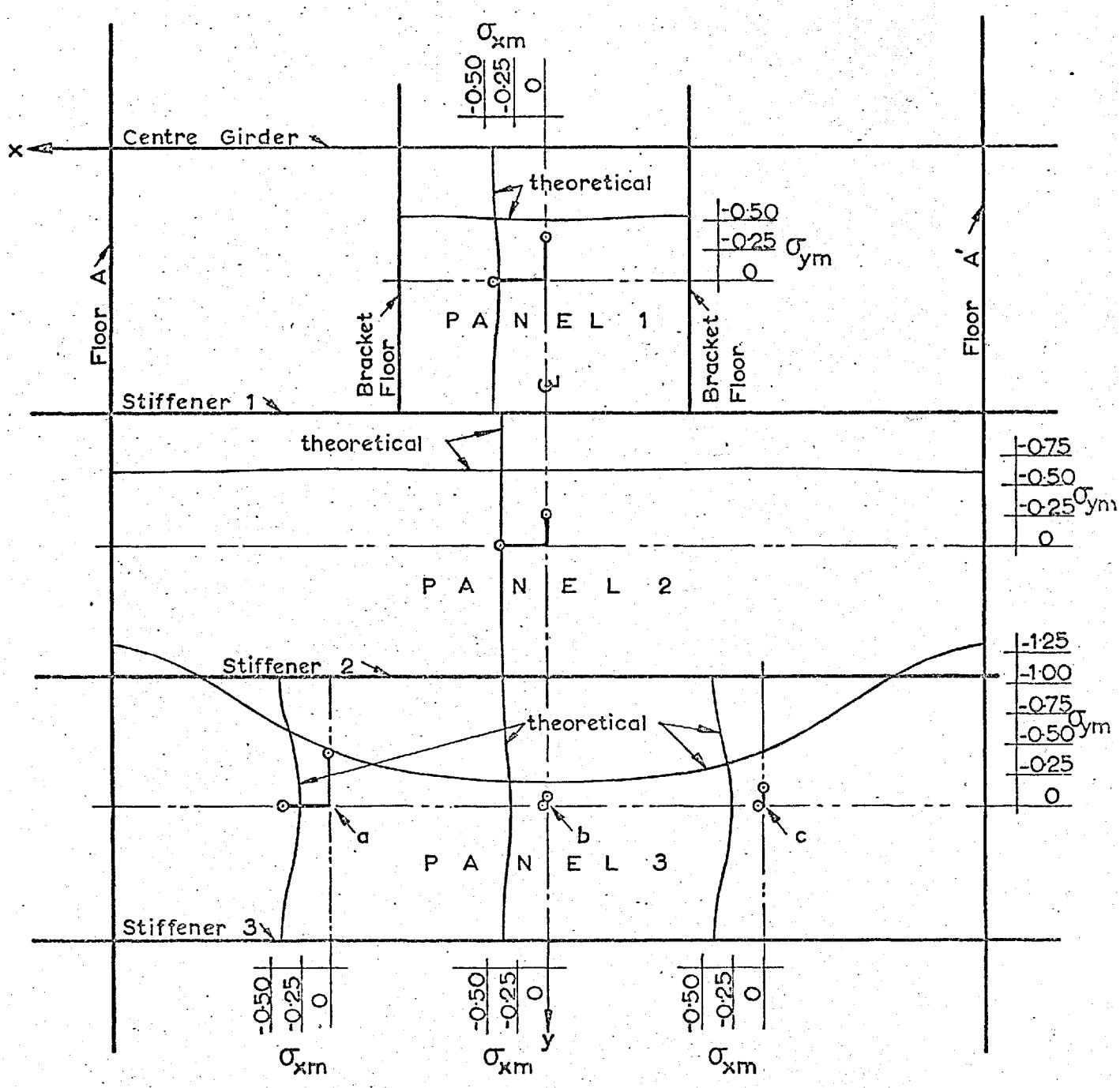

NOTE : (i) Stresses in tons/in^2
(ii) Experimental values shown ⊙
(iii) For details of initial deformation and loading ($q^* = 1$) see Fig. 87

Fig. 90 : Double Bottom Analysis - Membrane Stresses in Outer Shell Panels For Distributed Transverse Load : $q^* = 1$

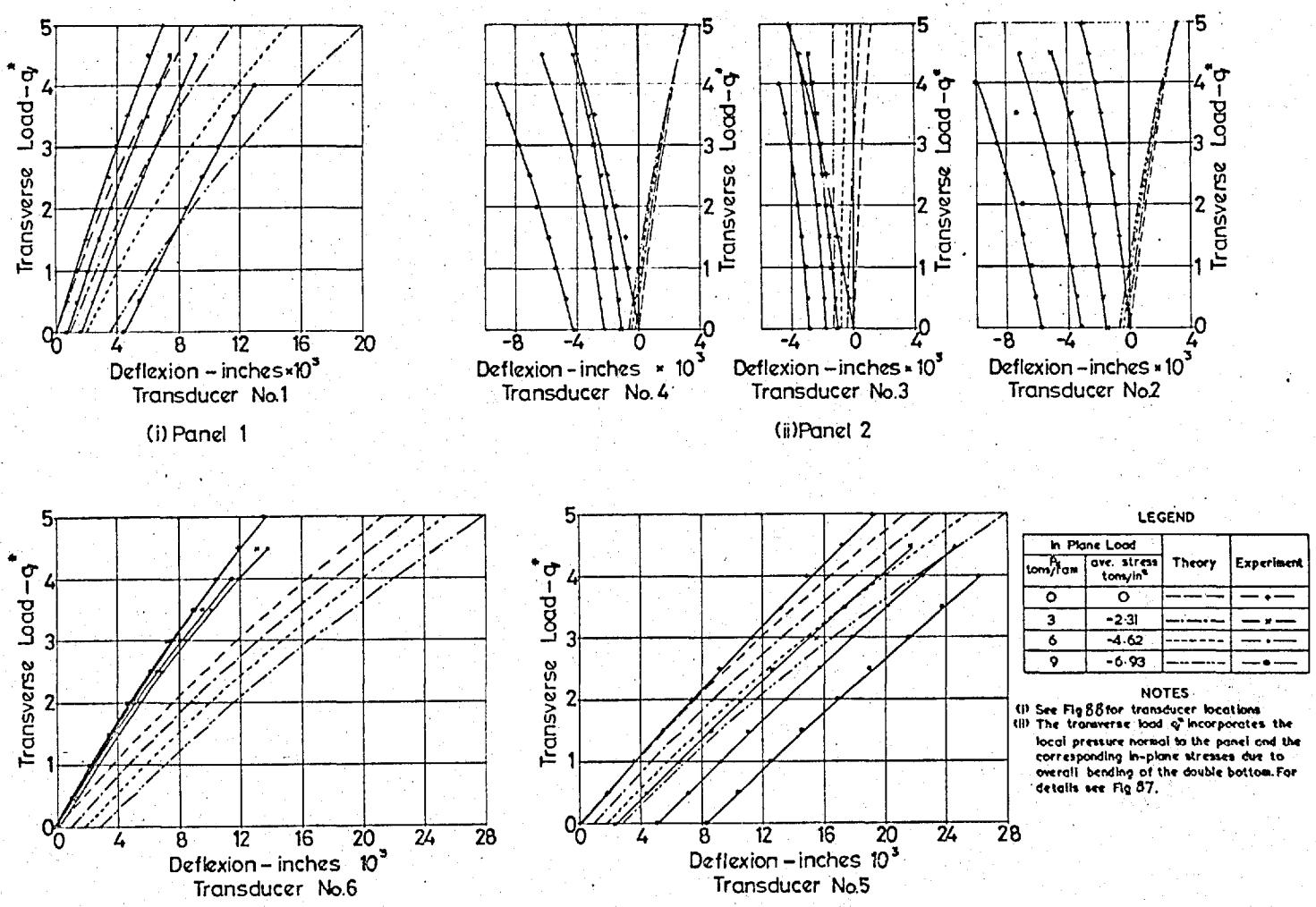

Fig. 91 : Double Bottom Analysis – Deflexion of Outer Shell Panels For Combined Transverse and In-Plane Loading.

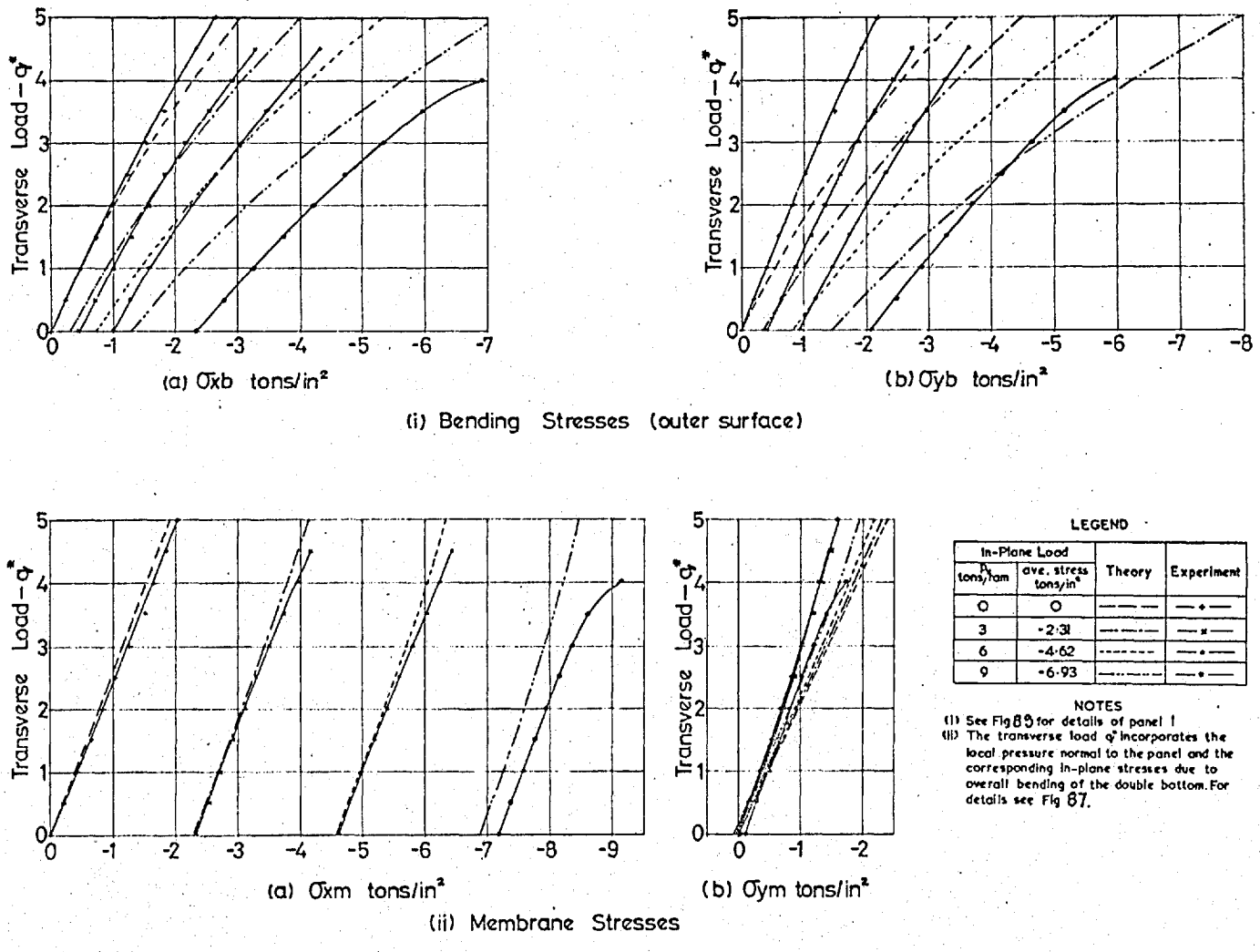

Fig. 92 : Double Bottom Analysis – Stresses at Centre of Panel 1 For Combined Transverse and In-Plane Loading.

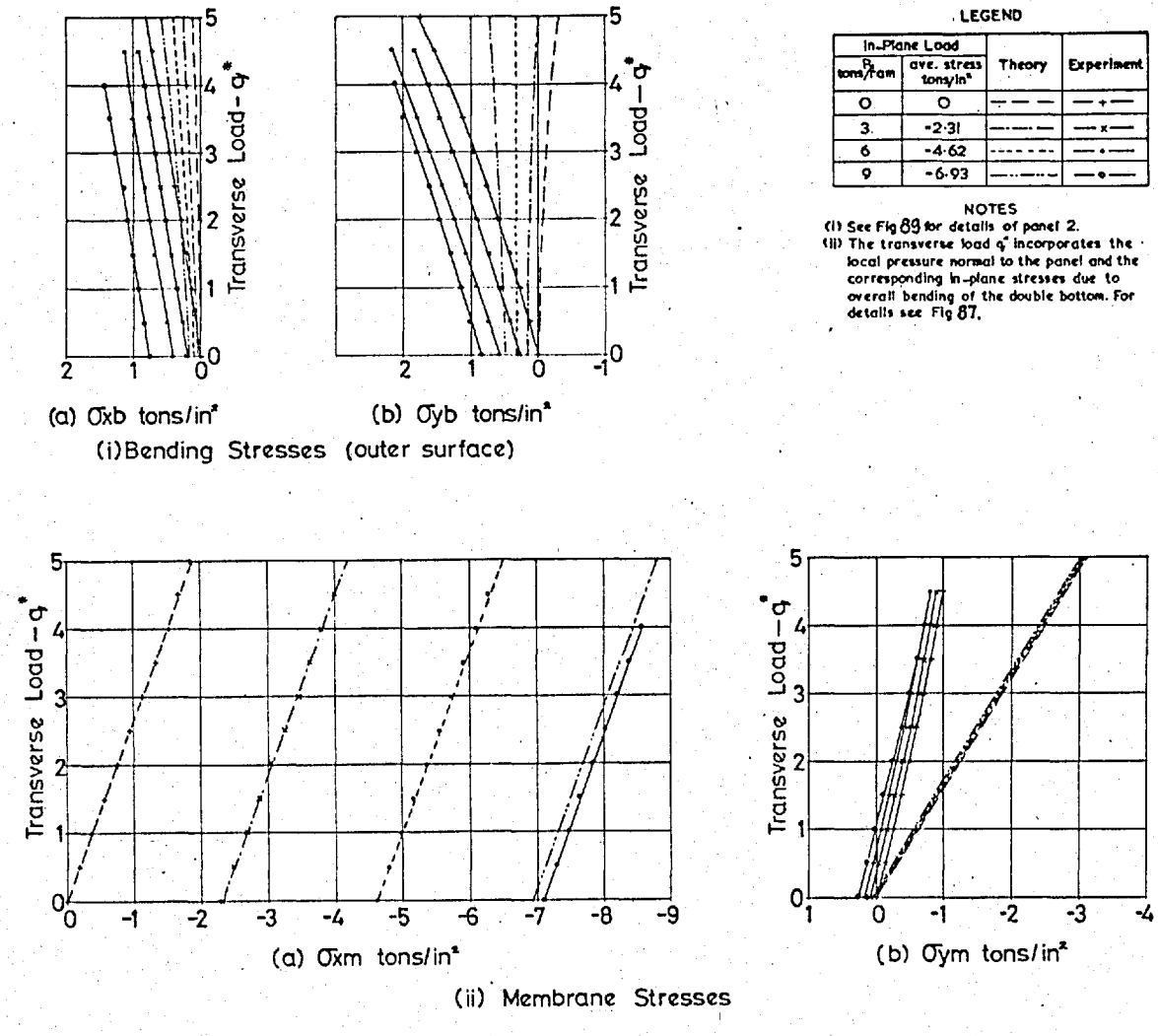

LEGEND

In-Plane Load		Theory	Experiment
p_x tons/ft/m	ave. stress tons/in²		
0	0	— — —	—+—
3	-2·31	—·—·—	—x—
6	-4·62	- - - - -	—•—
9	-6·93	—··—··—	—•—

NOTES

(i) See Fig 89 for details of panel 2.

(ii) The transverse load q^* incorporates the local pressure normal to the panel and the corresponding in-plane stresses due to overall bending of the double bottom. For details see Fig 87.

Fig. 93 : Double Bottom Analysis – Stresses at Centre of Panel 2 For Combined Transverse and In-Plane Loading.

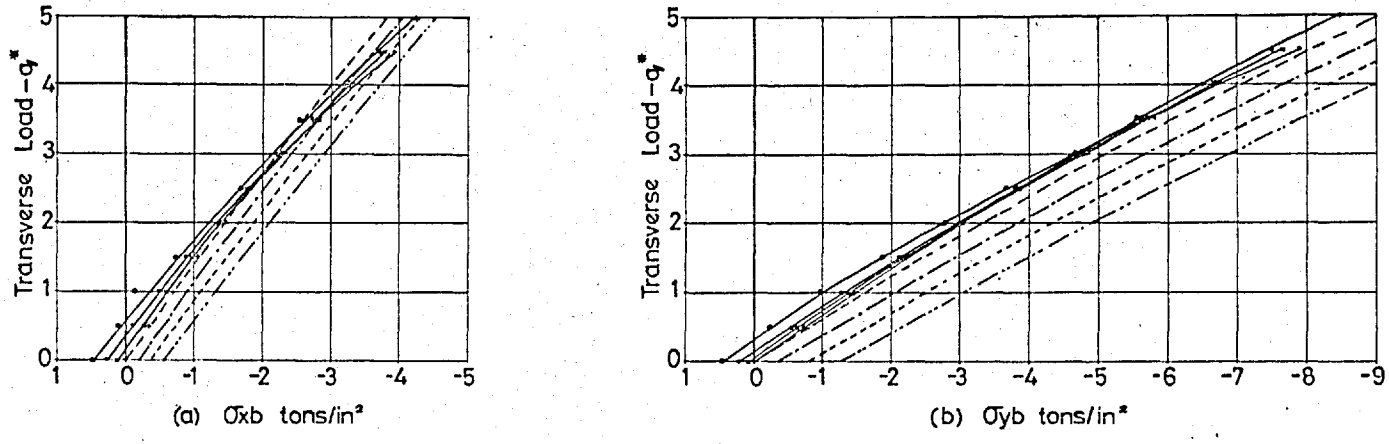

(i) Bending Stresses (outer surface)

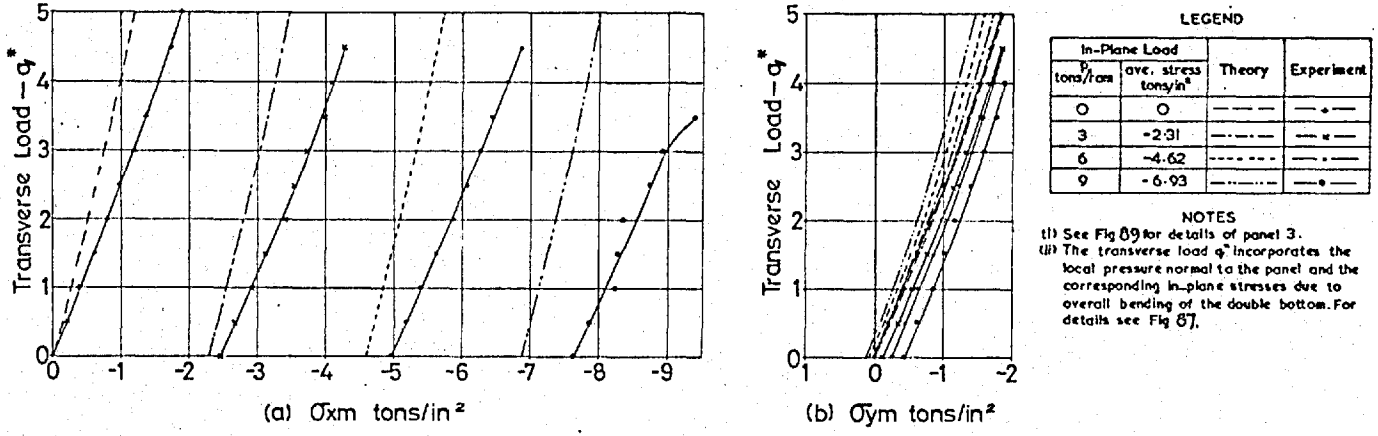

(ii) Membrane Stresses

Fig. 94 : Double Bottom Analysis – Stresses at Point a of Panel 3 For Combined Transverse and In – Plane Loading.

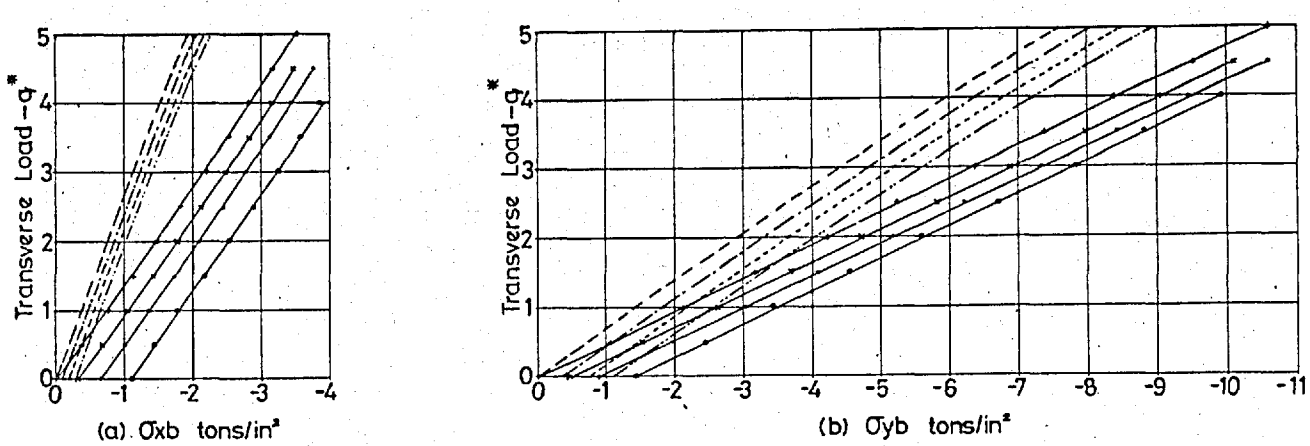

(i) Bending Stresses (outer surface)

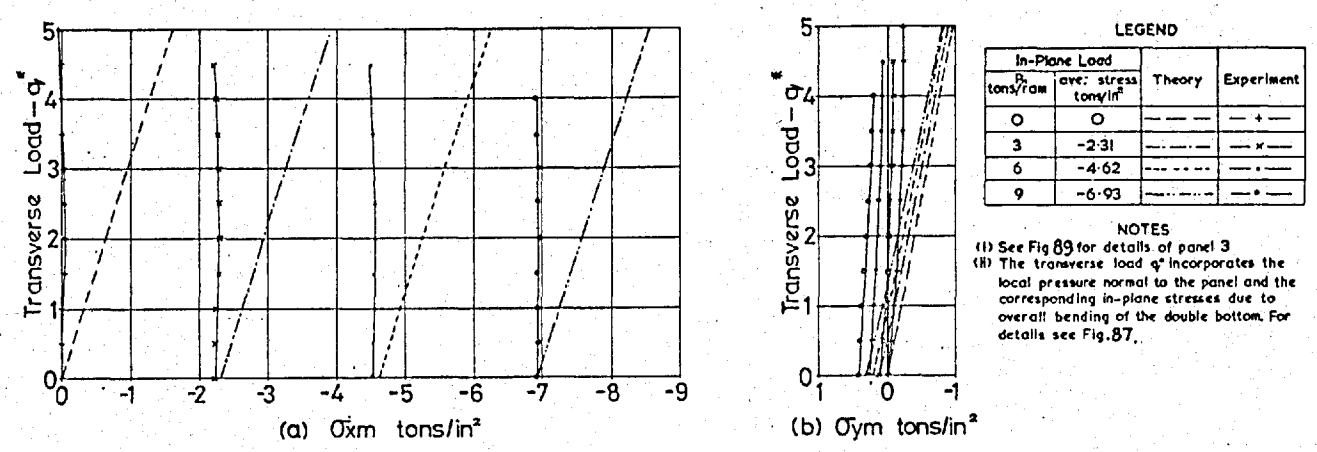

(ii) Membrane Stresses

Fig.95 : Double Bottom Analysis – Stresses at Point b (centre) of Panel 3 For Combined Transverse and In – Plane Loading.

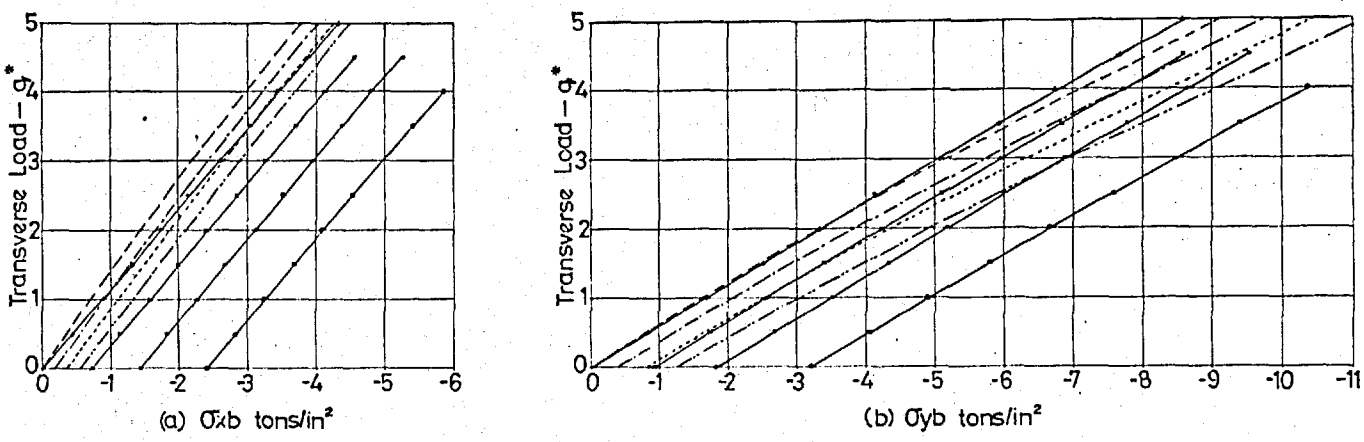

(i) Bending Stresses (outer surface)

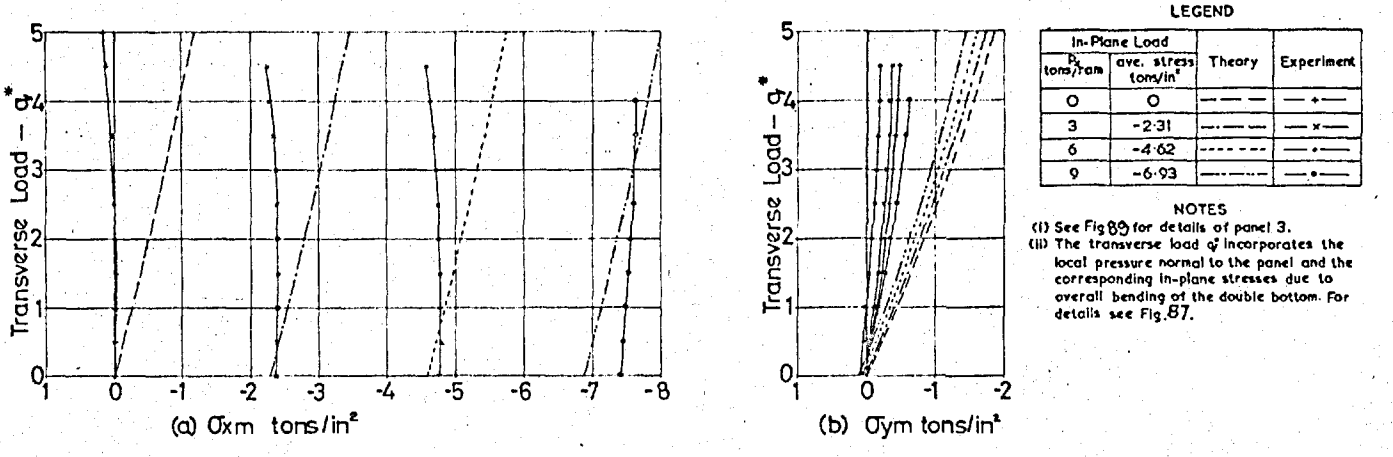

(ii) Membrane Stresses

Fig. 96 : Double Bottom Analysis – Stresses at Point c of Panel 3 For Combined Transverse and In - Plane Loading.

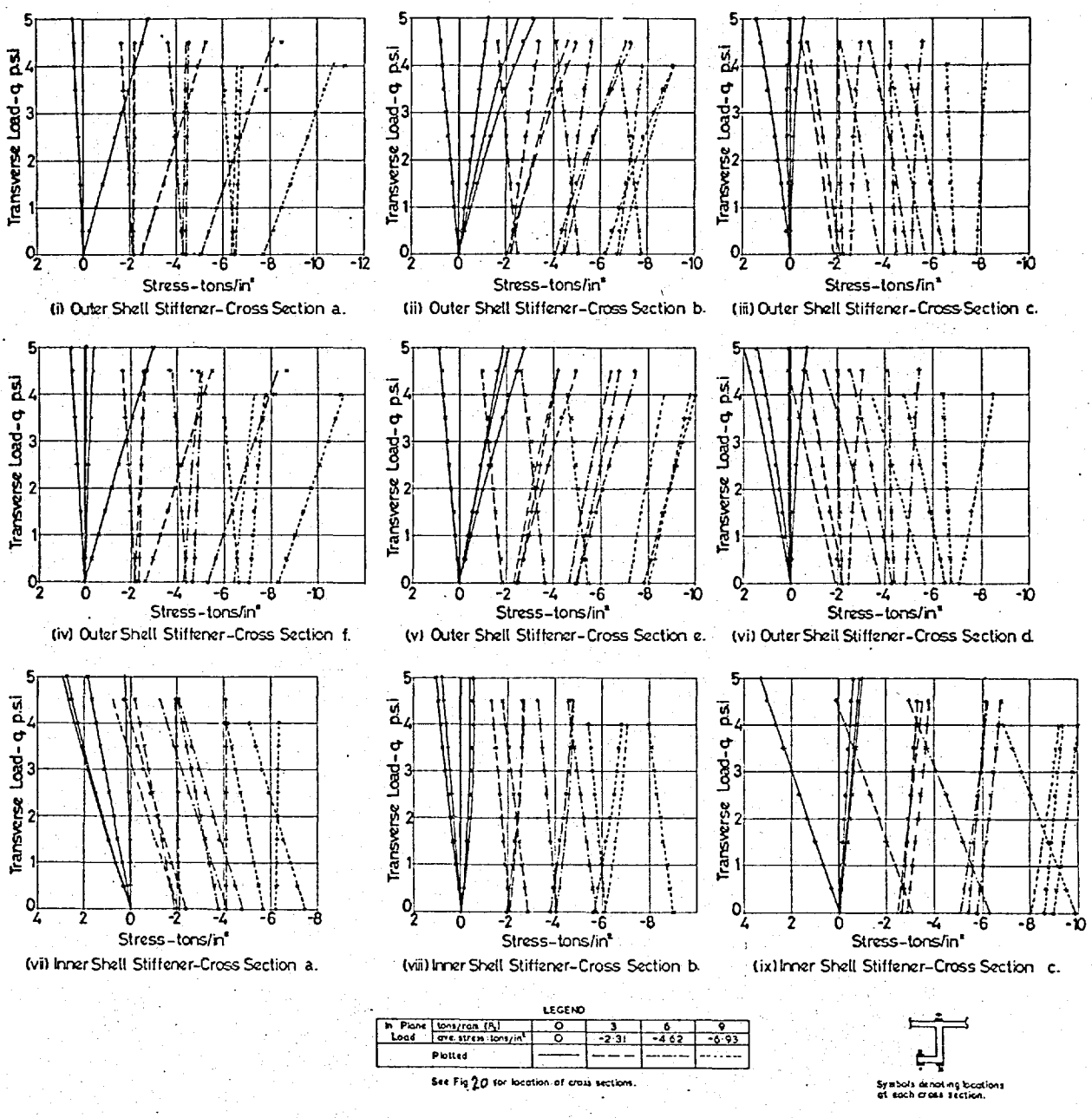

Fig.97: Double Bottom Analysis – Stresses in Shell Stiffeners No 3. For Combined Transverse and In-Plane Load.

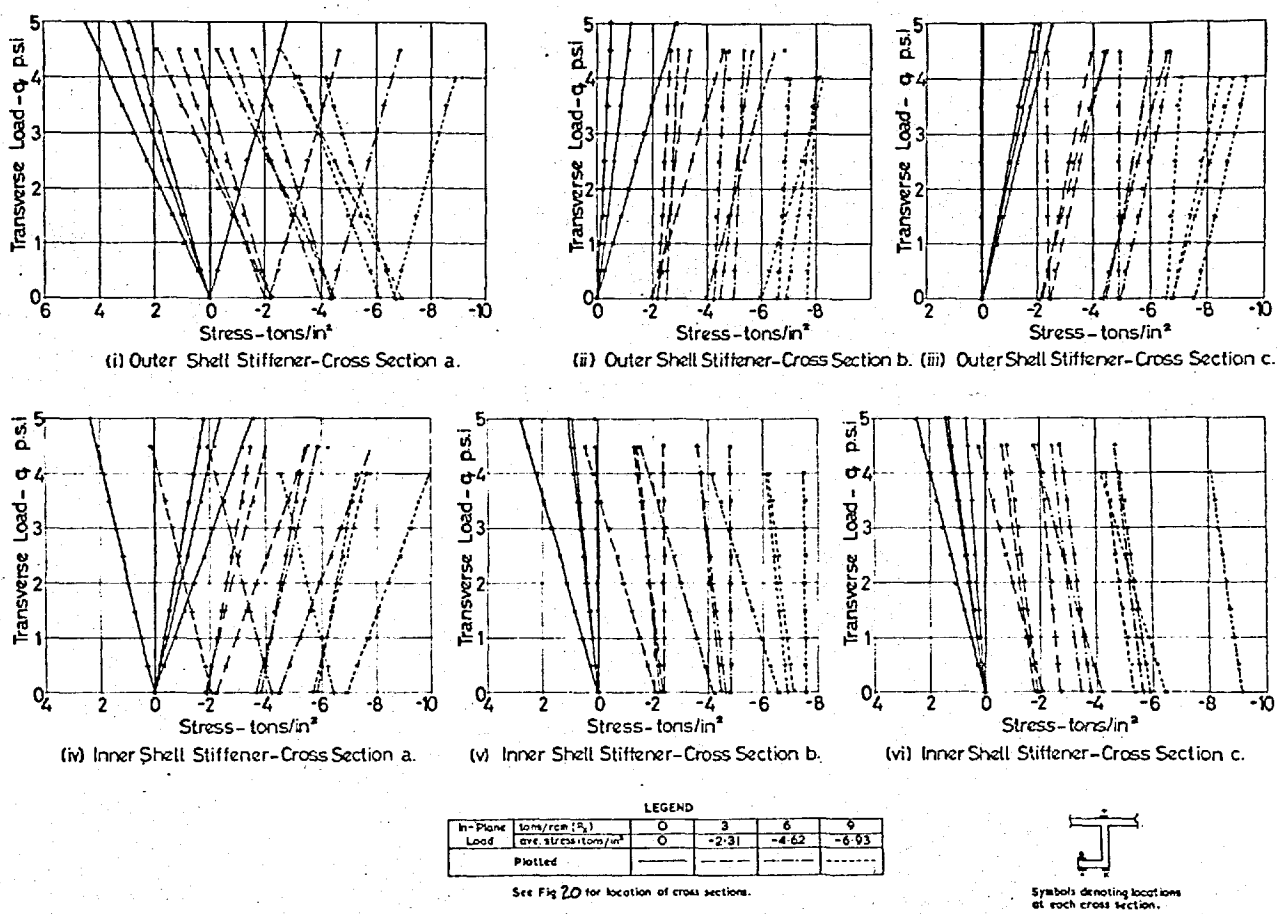

Fig.98 : Double Bottom Analysis - Stresses in Shell Stiffeners No 8.
For Combined Transverse and In-Plane Load.

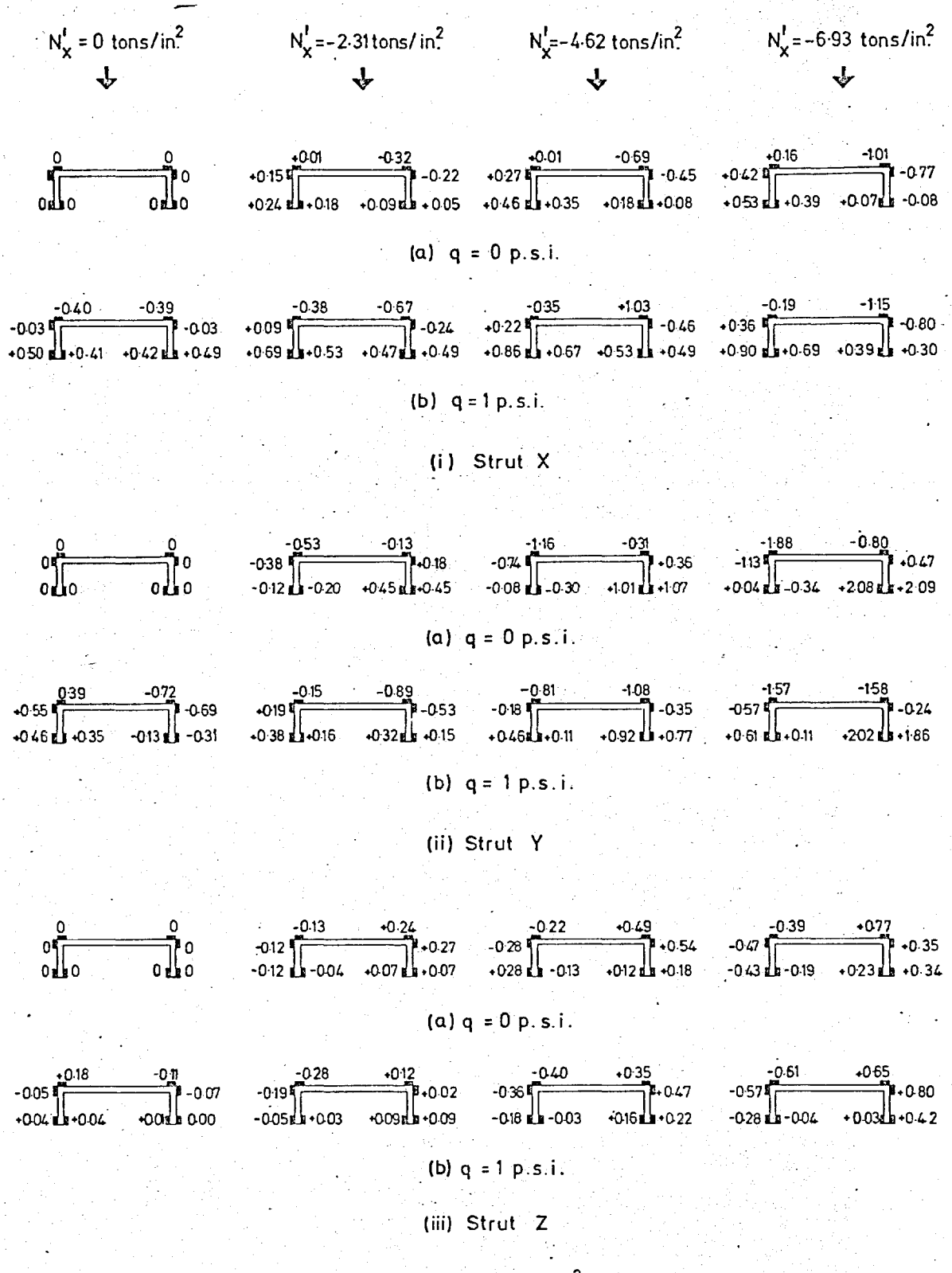

NOTE : (i) Stresses in tons/in^2
(ii) Loading - N'_x = in-plane load (average stress)
q = transverse pressure
(iii) See Fig. 20 for strut locations

Fig. 99 : Double Bottom Analysis - Strut Stresses For Combined Transverse and In-Plane Loading

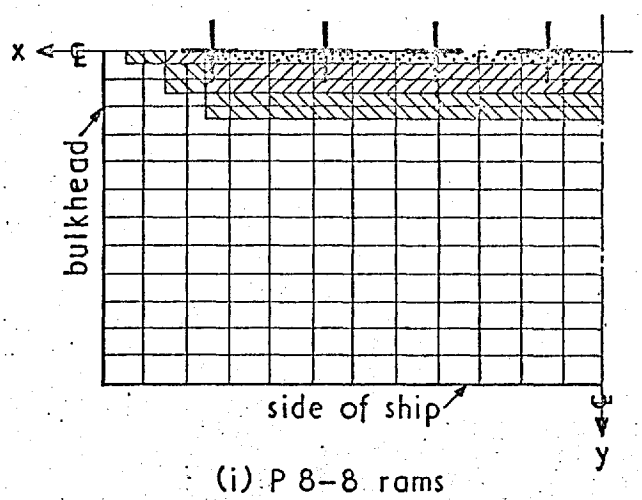

(i) P 8–8 rams

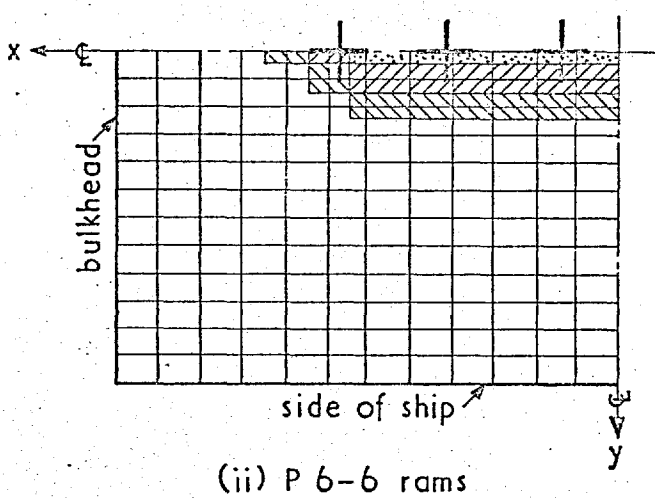

(ii) P 6–6 rams

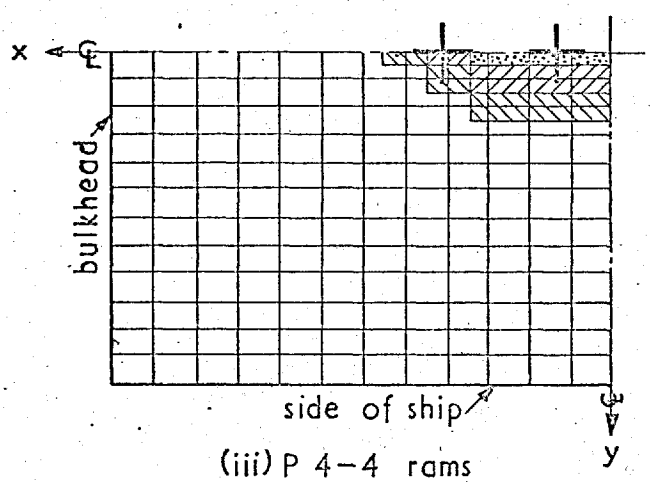

(iii) P 4–4 rams

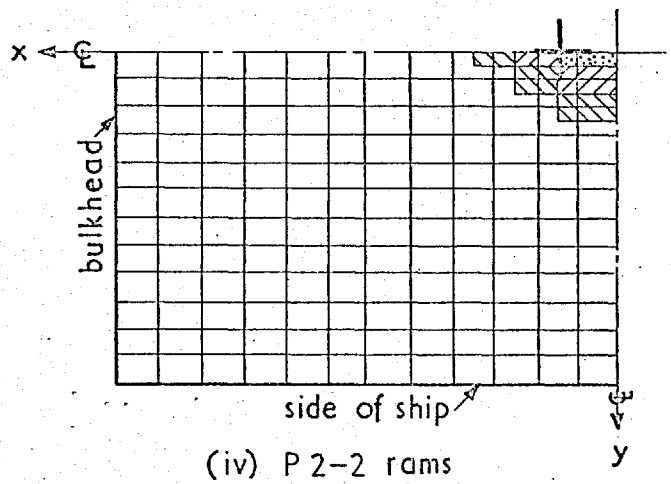

(iv) P 2–2 rams

NOTE : (i) Rams load through 8″ × 8″ × ⅛″ square cruciform – shown
(ii) Theoretical solutions for 12×12 mesh in quadrant
(iii) All data is plotted for a load of 1 ton/ram which in theoretical solutions was distributed as shown by shaded areas in the ratio

: : = 1.2 : 0.7 : 0.2

Fig. 100 : Double Bottom Analysis — Definition of Patch Loads

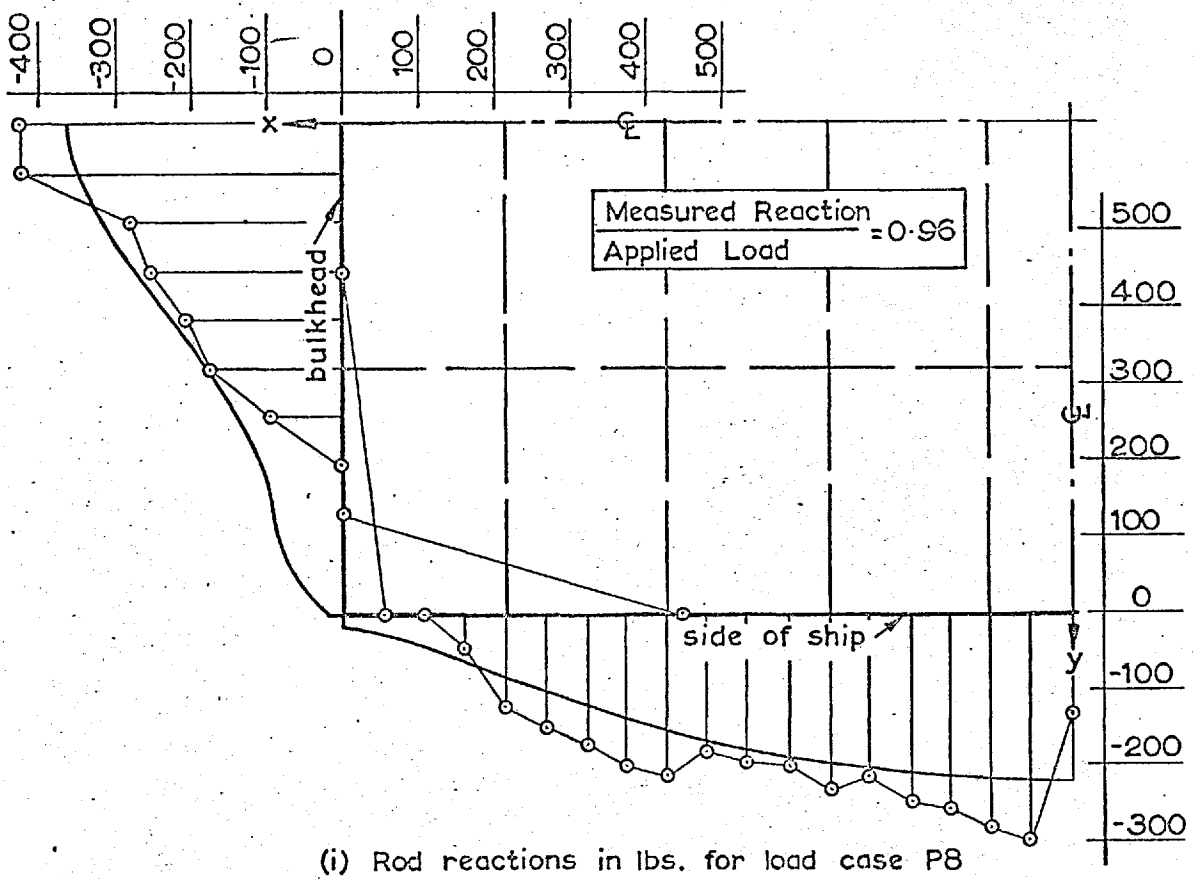

(i) Rod reactions in lbs. for load case P8

NOTE: (i) See Fig. 100 for definition of load cases
(ii) Experimental values shown ⊙
(iii) Theoretical solution shown —— for ordinary simple support and including shear deformation

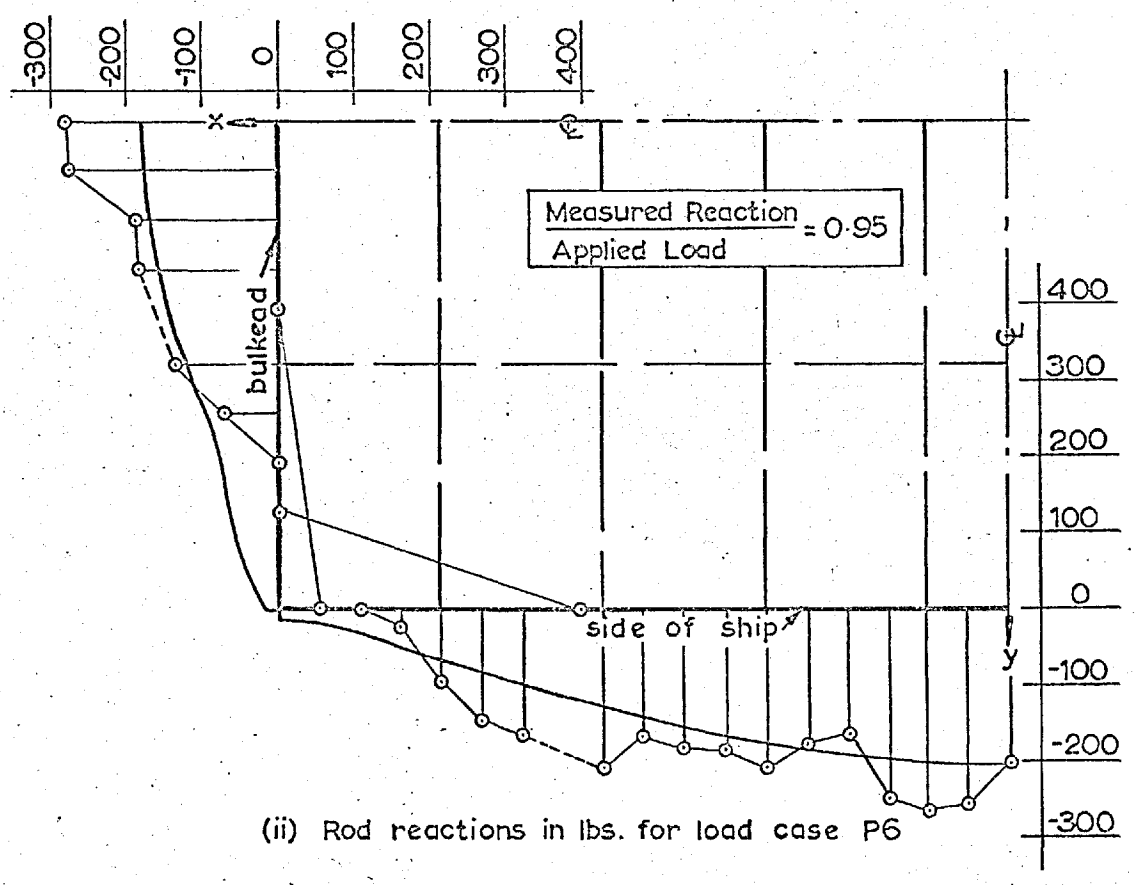

(ii) Rod reactions in lbs. for load case P6

Fig. 101 : Double Bottom Analysis - Reactions for Patch Loads

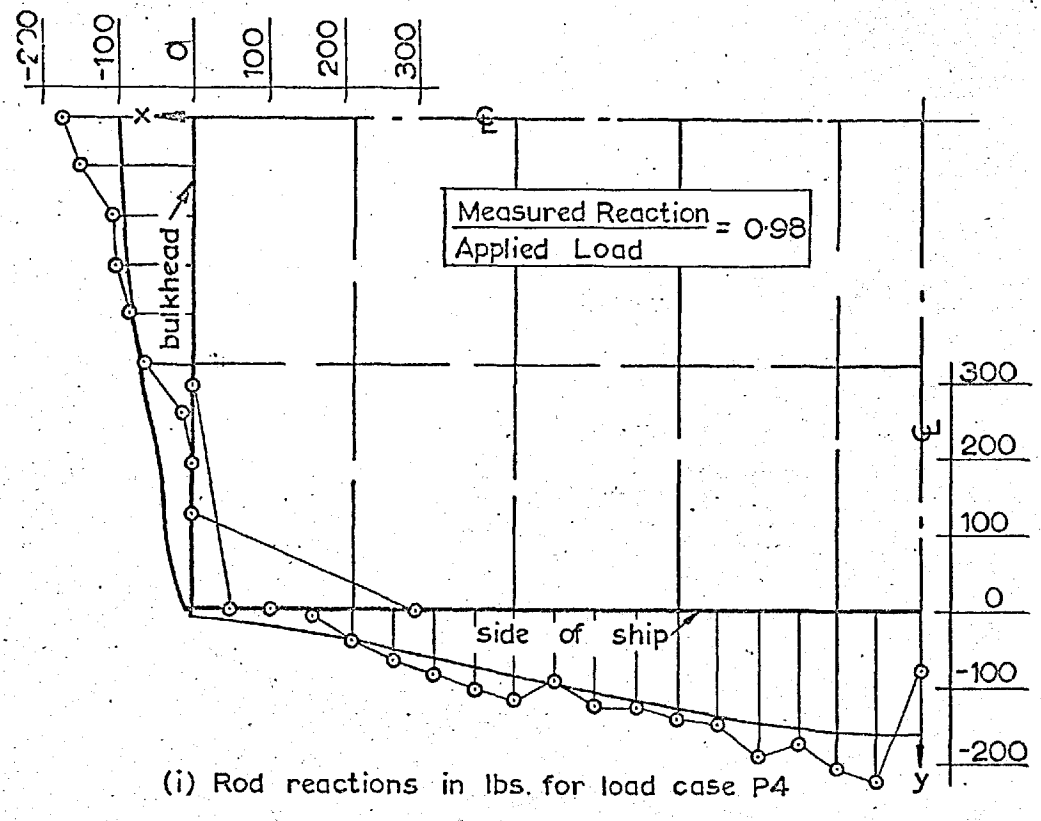

(i) Rod reactions in lbs. for load case P4

NOTE : (i) See Fig. 100 for definition of load cases
(ii) Experimental values shown ⊙
(iii) Theoretical solution shown —— for ordinary simple support and including shear deformation

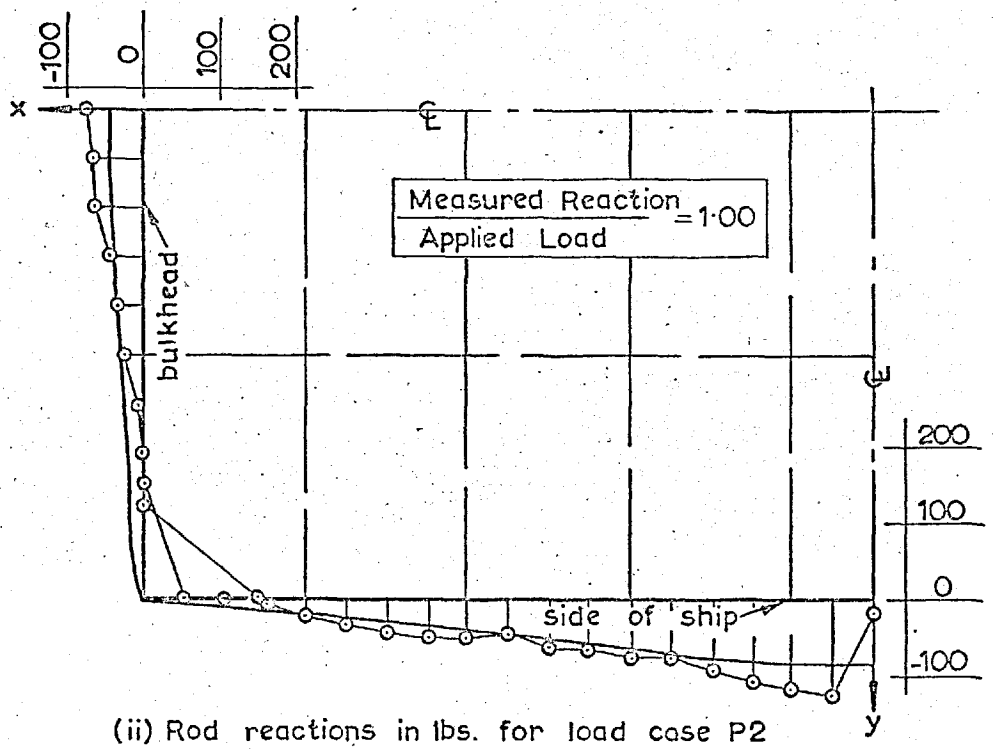

(ii) Rod reactions in lbs. for load case P2

Fig. 102 : Double Bottom Analysis - Reactions For Patch Loads

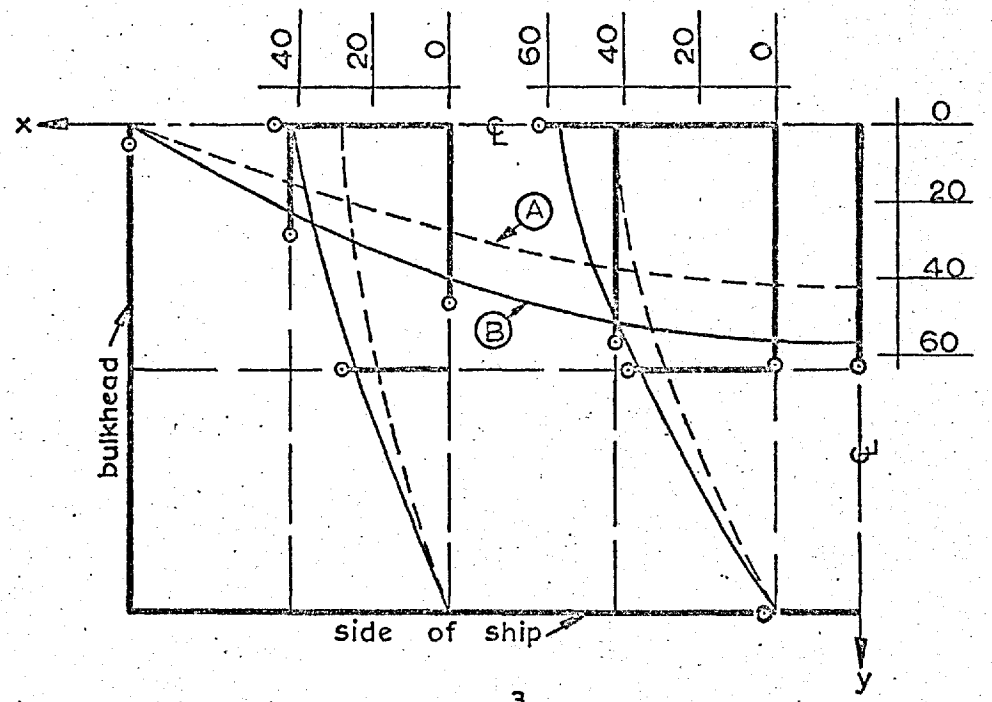

(i) Deflexions in inches x 10^3 for load case P8

NOTE : (i) See Fig. 100 for definition of load cases
(ii) Experimental values shown ⊙
(iii) Theoretical solutions (ordinary simple support) { (A) - no shear deformation; (B) - including shear deformation

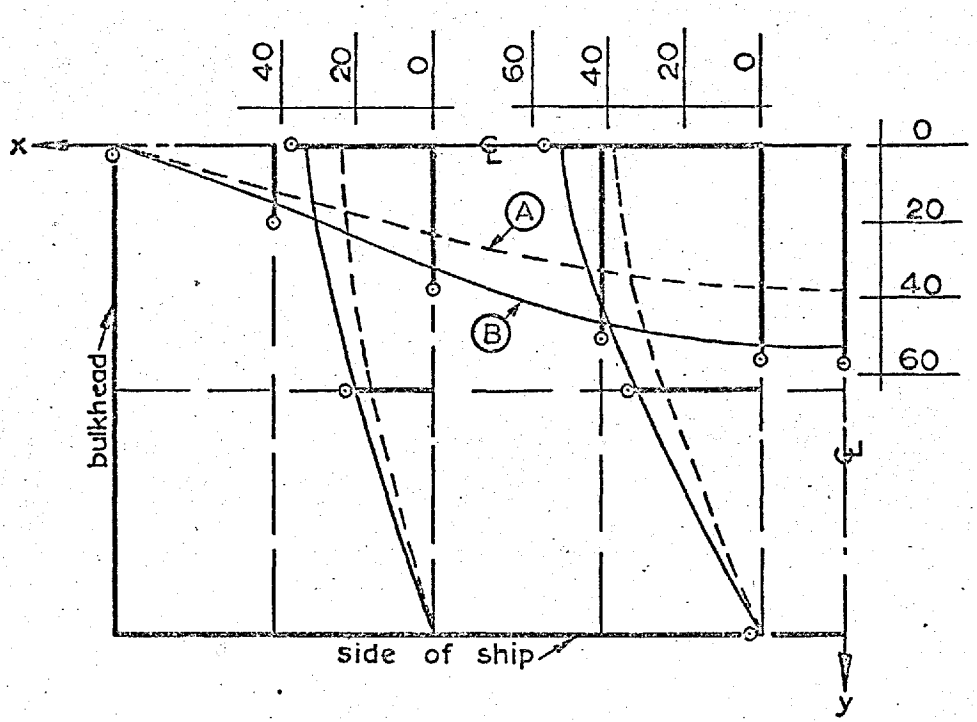

(ii) Deflexions in inches x 10^3 for load case P6

Fig. 103 : Double Bottom Analysis – Overall Deflexions For Patch Loads

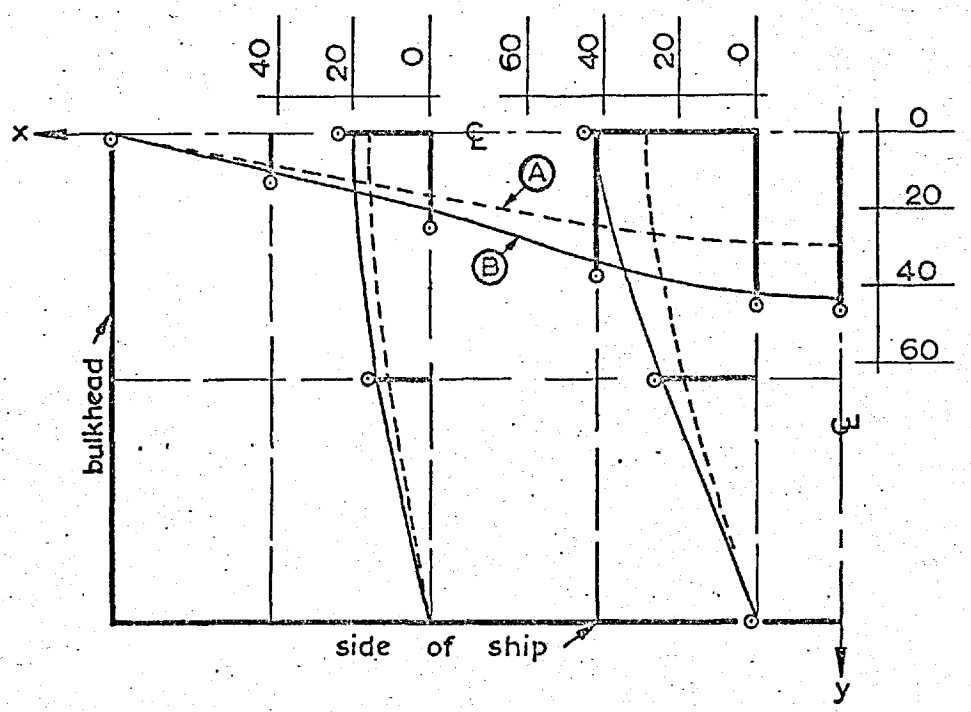

(i) Deflexions in inches x 10^3 for load case P4

NOTE : (i) See Fig. 100 for definition of load cases
(ii) Experimental values shown ⊙
(iii) Theoretical solutions (ordinary simple support) { (A) - no shear deformation; (B) - including shear deformation

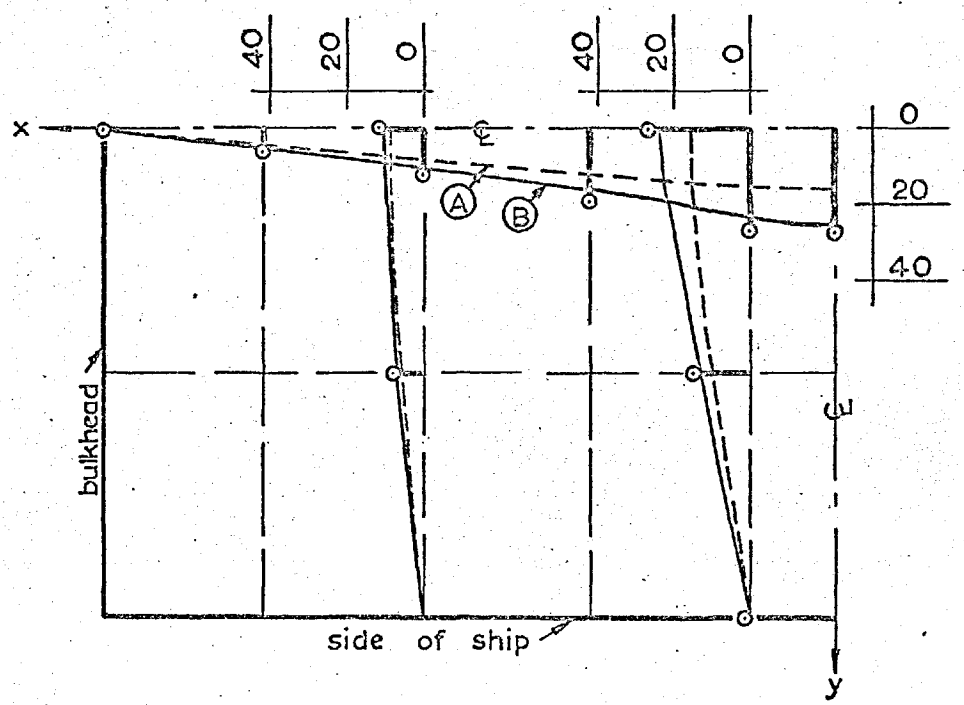

(ii) Deflexions in inches x 10^3 for load case P2

Fig. 104 : Double Bottom Analysis - Overall Deflexions For Patch Loads

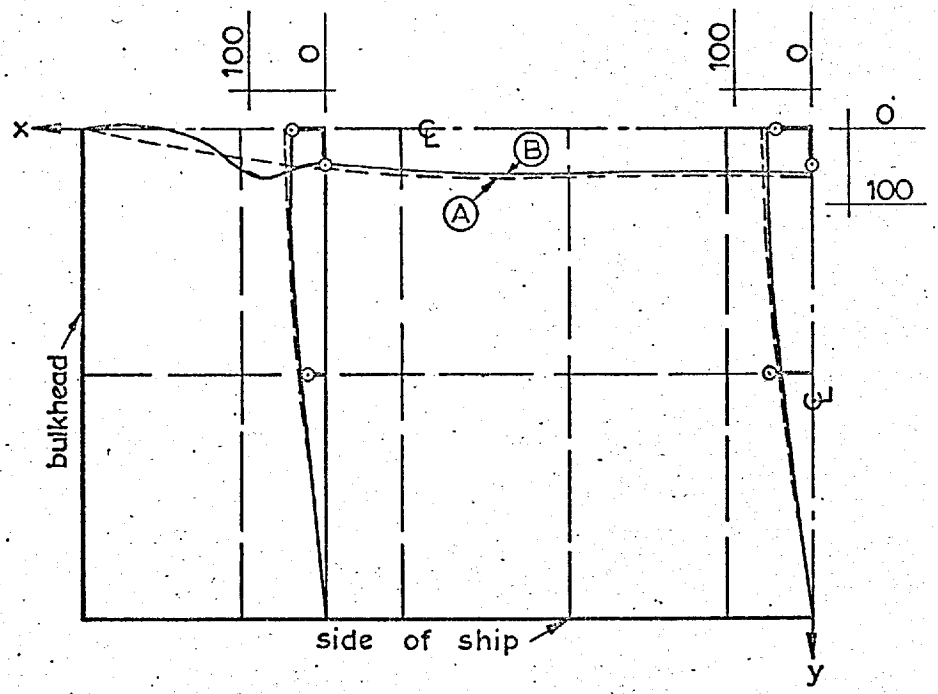

(i) ε_{xi} in./in. x 10^6

NOTE : (i) See Fig.100 for definition of loading
(ii) Experimental values shown ⊙
(iii) Theoretical solutions (ordinary simple support) { Ⓐ – no shear deformation; Ⓑ – including shear deformation

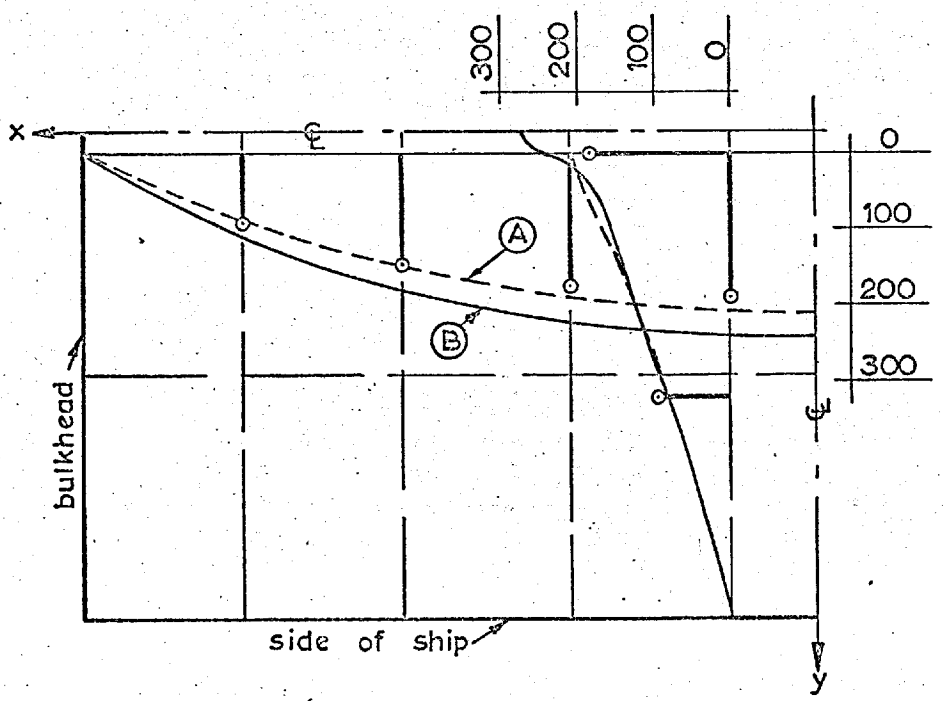

(ii) ε_{yi} in./in. x 10^6

Fig. 105 : Double Bottom Analysis – Inner Shell Strains For Patch Load P8

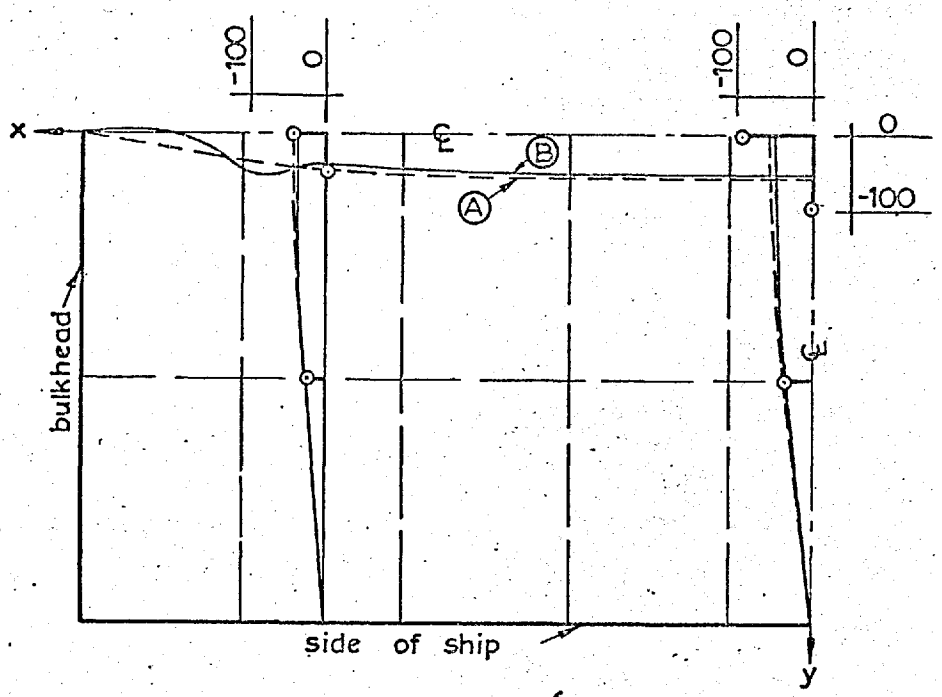

(i) ε_{xo} in./in. x 10^6

NOTE : (i) See Fig.100 for definition of loading
(ii) Experimental values shown o
(iii) Theoretical solutions (ordinary simple support) { (A) - no shear deformation; (B) - including shear deformation

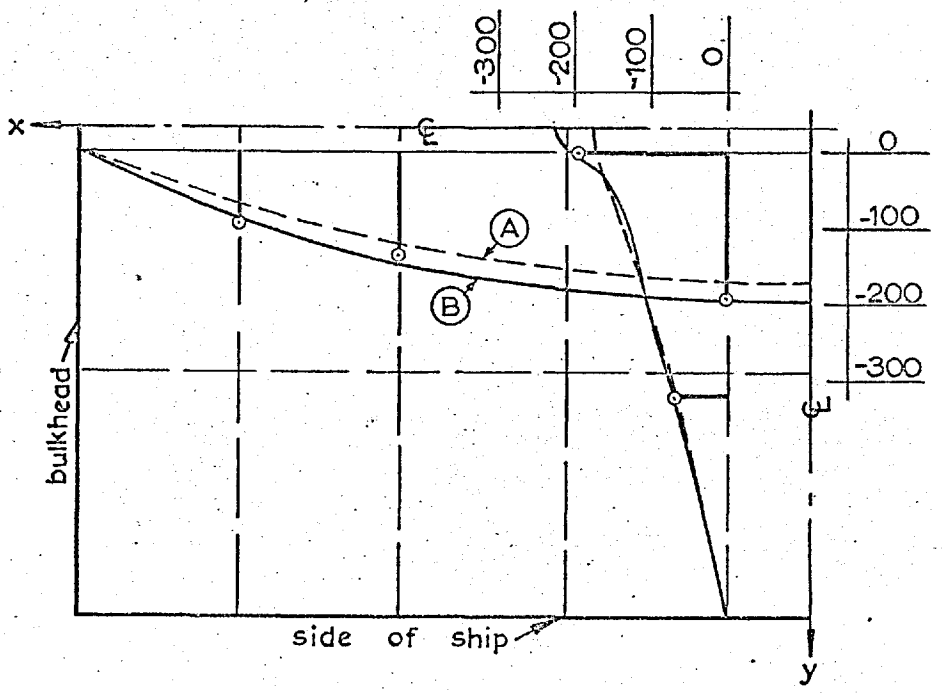

(ii) ε_{yo} in./in. x 10^6

Fig. 106 : Double Bottom Analysis - Outer Shell Strains For Patch Load P8

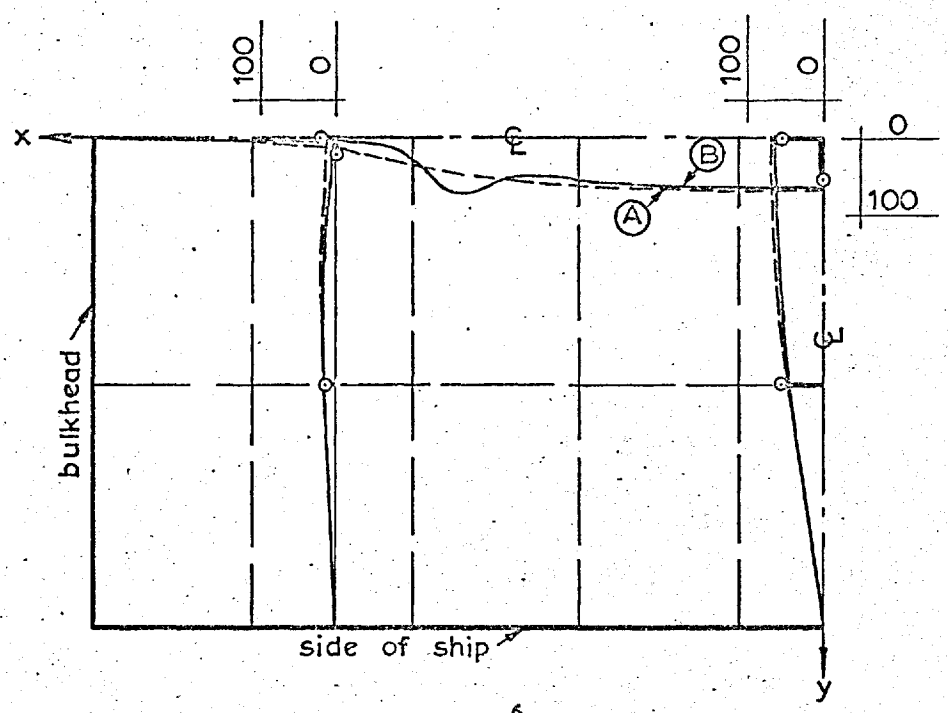

(i) ε_{xi} in./in. x 10^6

NOTE : (i) See Fig.100 for definition of loading
(ii) Experimental values shown ⊙
(iii) Theoretical solutions (ordinary simple support) {Ⓐ - no shear deformation; Ⓑ - including shear deformation

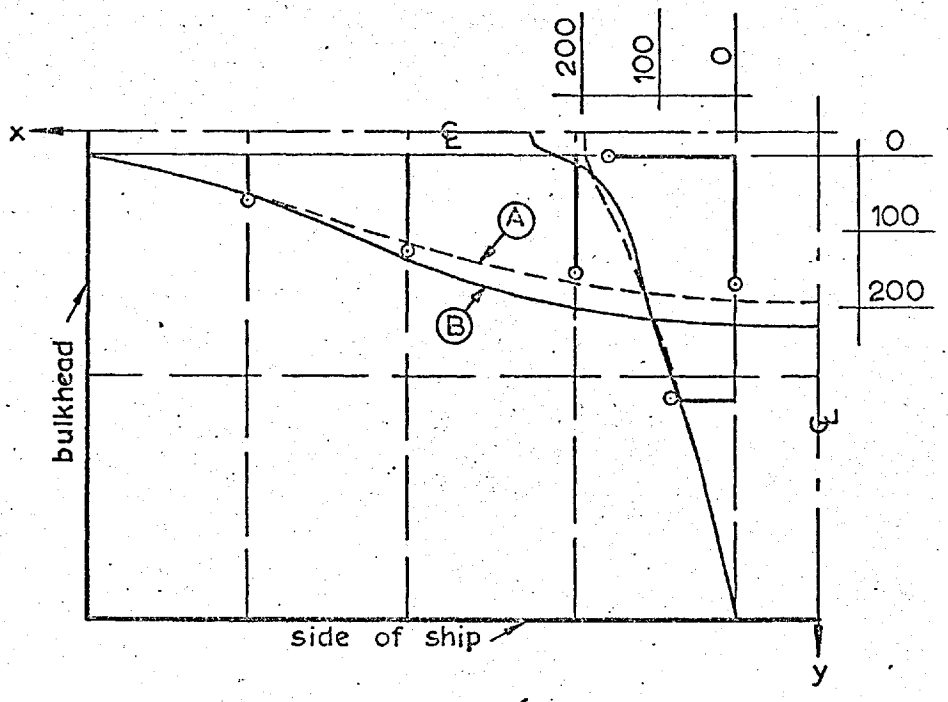

(ii) ε_{yi} in./in. x 10^6

Fig. 107 :Double Bottom Analysis - Inner Shell Strains For Patch Load P6

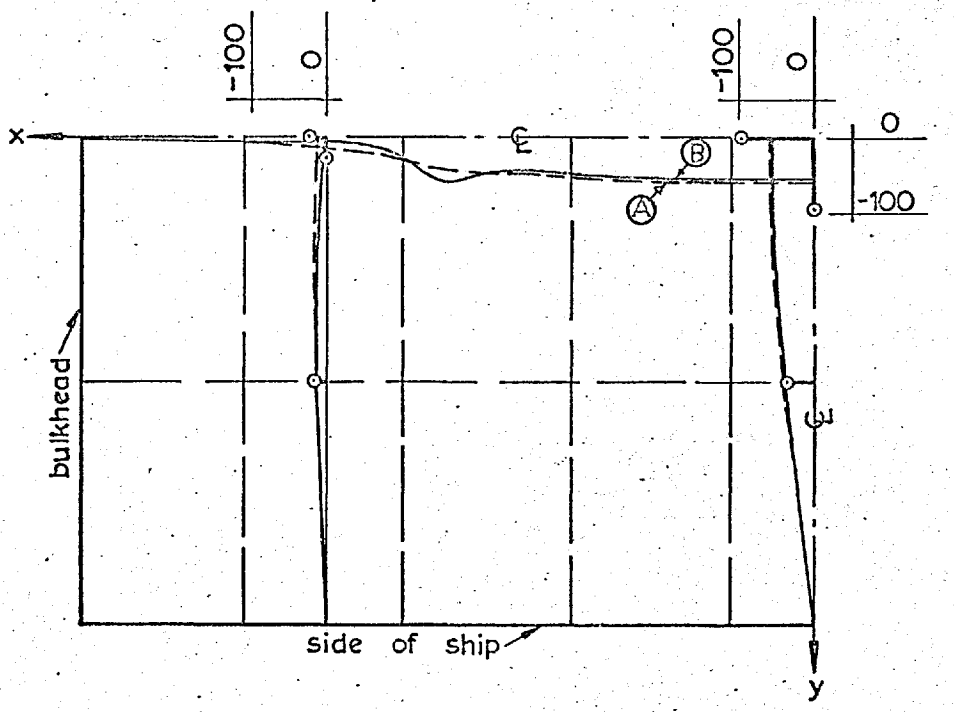

(i) ε_{xo} in./in. x 10^6

NOTE: (i) See Fig.100 for definition of loading
(ii) Experimental values shown ⊙
(iii) Theoretical solutions (ordinary simple support) { (A) - no shear deformation; (B) - including shear deformation

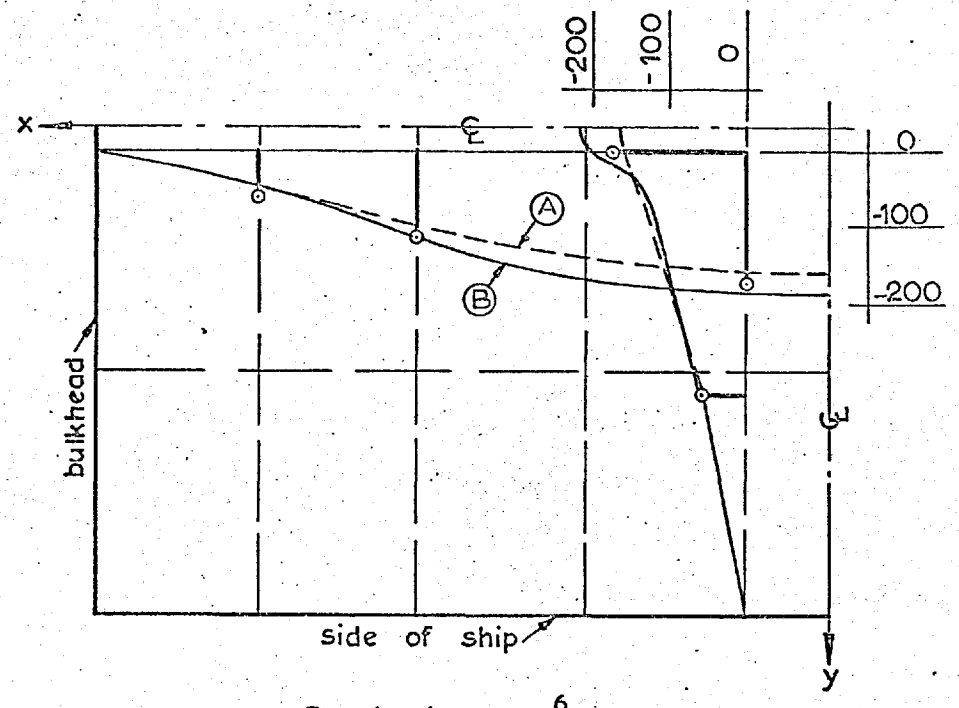

(ii) ε_{yo} in./in. x 10^6

Fig. 108 : Double Bottom Analysis - Outer Shell Strains For Patch Load P6

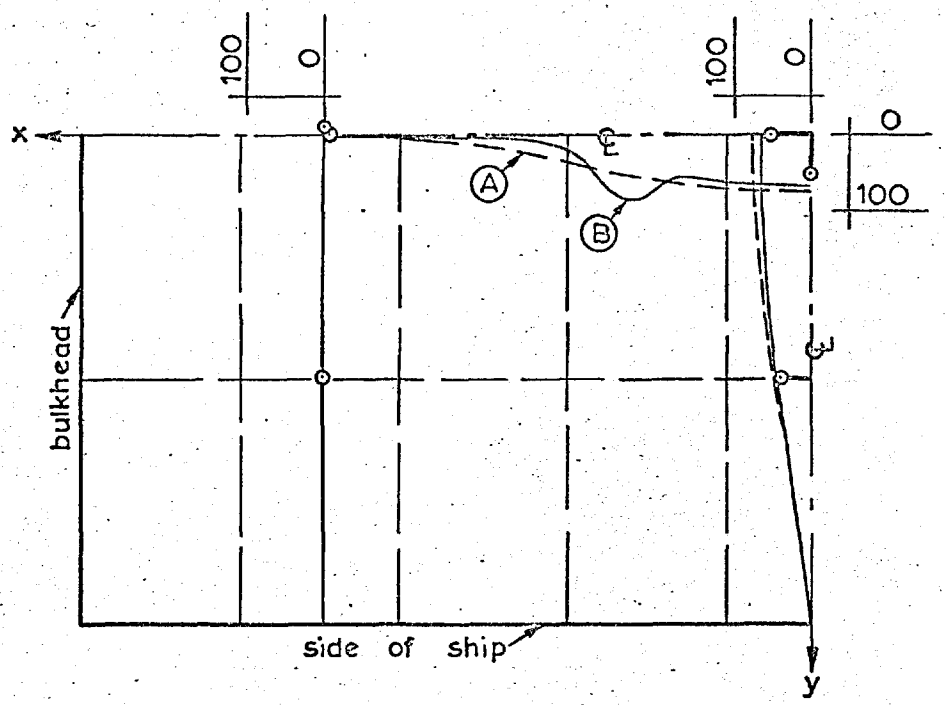

(i) ε_{xi} in./in x 10^6

NOTE : (i) See Fig.100 for definition of loading
(ii) Experimental values shown ⊙
(iii) Theoretical solutions (ordinary simple support) (A) - no shear deformation (B) - including shear deformation

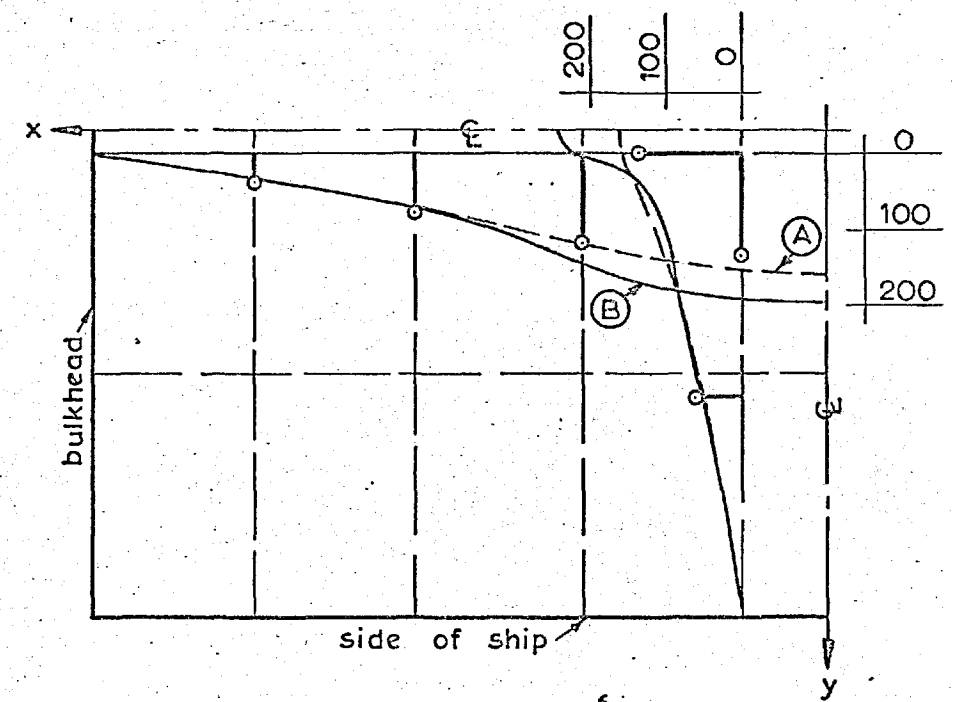

(ii) ε_{yi} in./in. x 10^6

Fig. 109 : Double Bottom Analysis - Inner Shell Strains For Patch Load P4

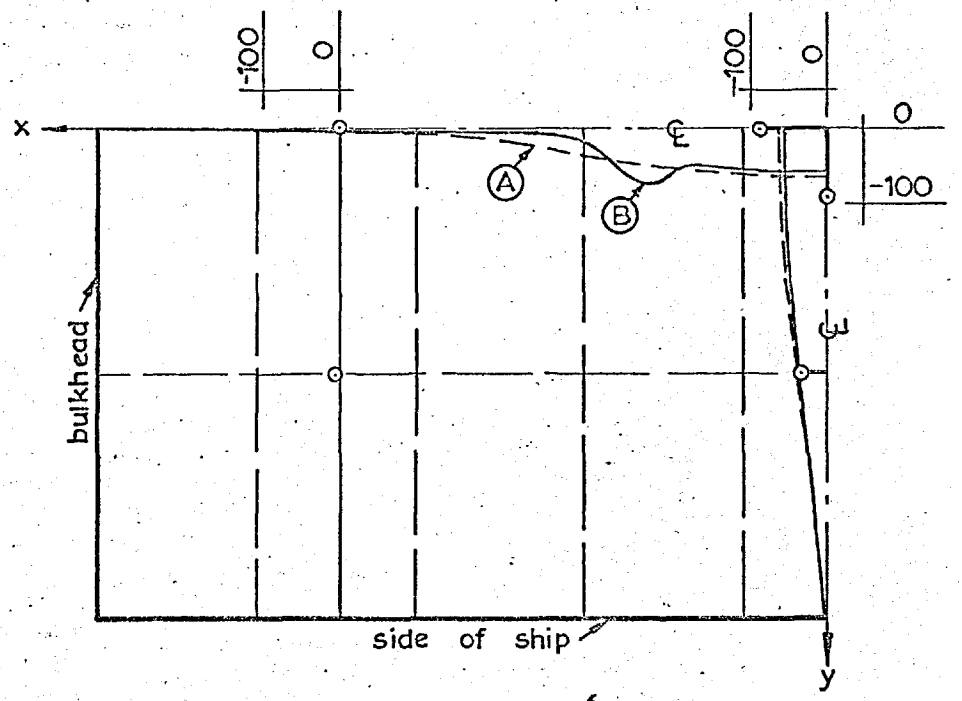

(i) ε_{xo} in./in. x 10^6

NOTE : (i) See Fig. 100 for definition of loading
(ii) Experimental values shown ⊙
(iii) Theoretical solutions (ordinary simple support) { (A) - no shear deformation; (B) - including shear deformation

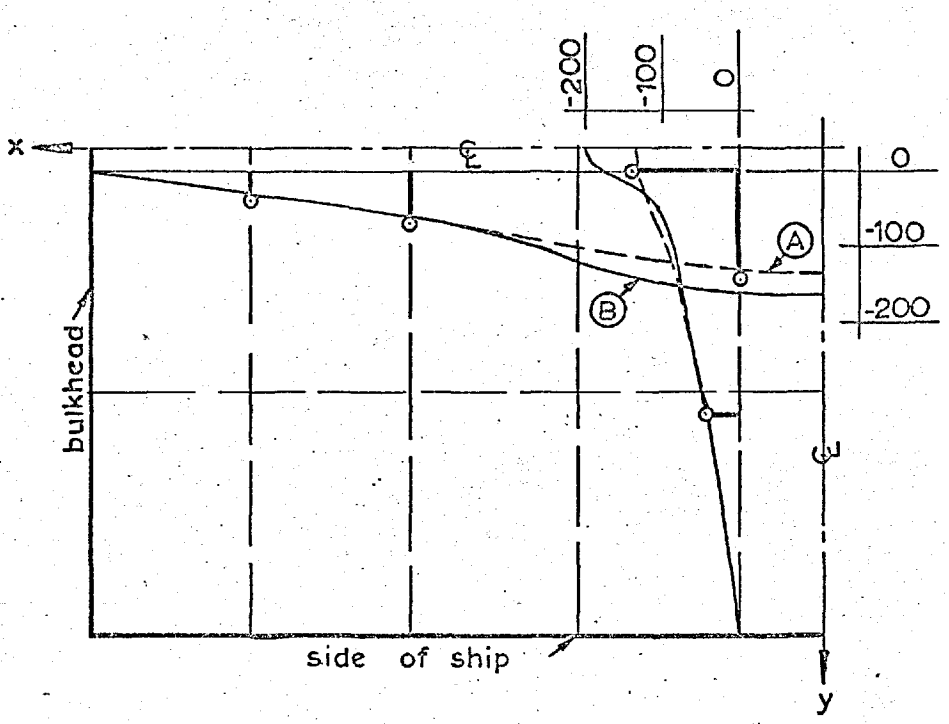

(ii) ε_{yo} in./in x 10^6

Fig. 110 : Double Bottom Analysis - Outer Shell Strains For Patch Load P4

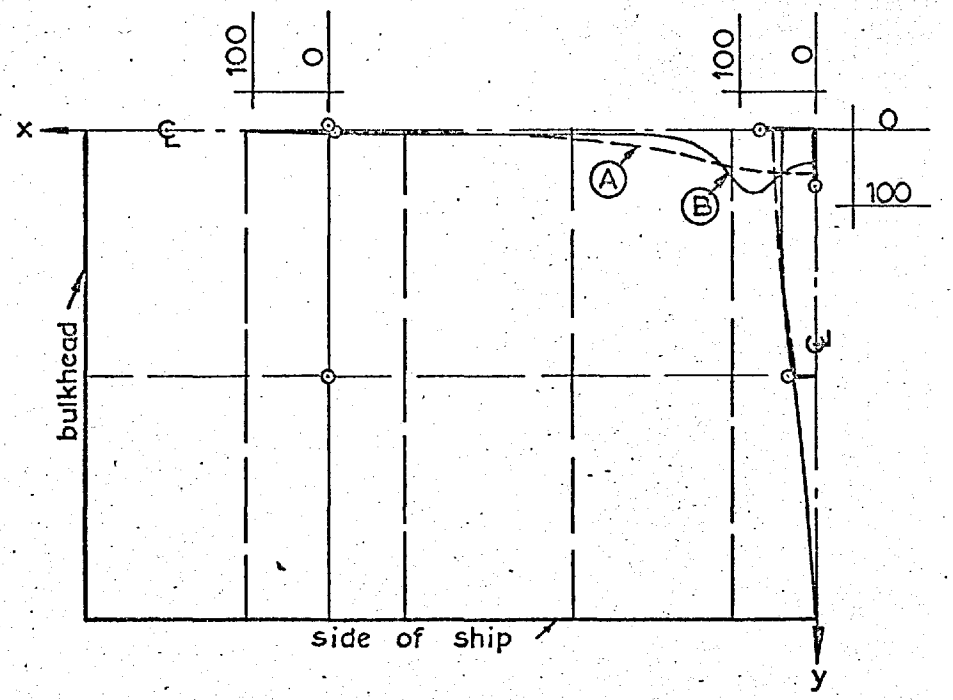

(i) ε_{xi} in./in. x 10^6

NOTE : (i) See Fig. 100 for definition of loading
(ii) Experimental values shown ⊙
(iii) Theoretical solutions (ordinary simple support) { (A) - no shear deformation; (B) - including shear deformation

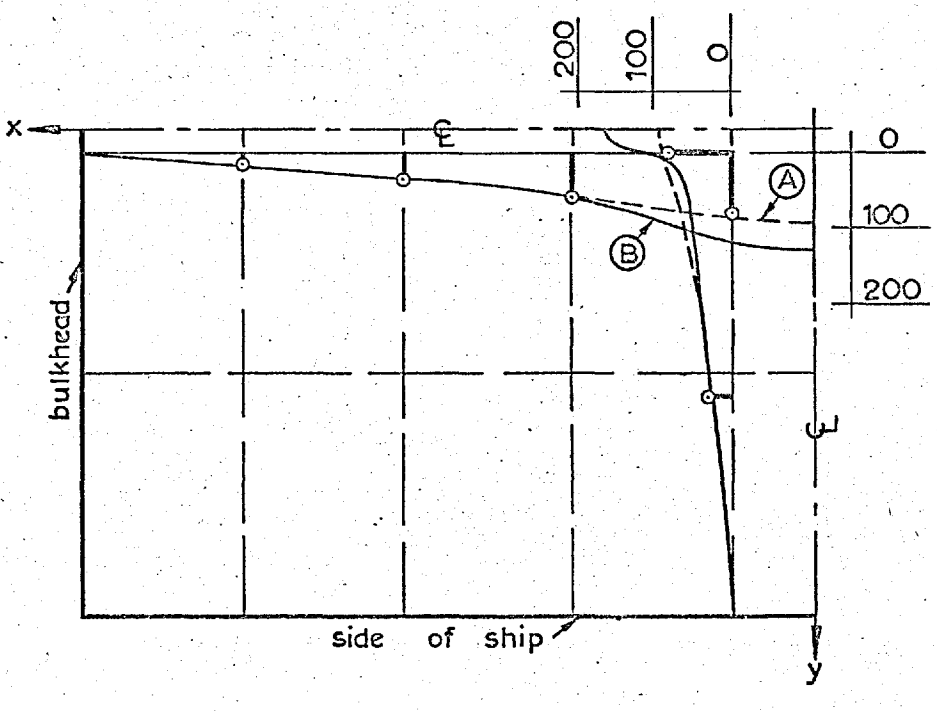

(ii) ε_{yi} in./in. x 10^6

Fig. 111 : Double Bottom Analysis – Inner Shell Strains For Patch Load P2

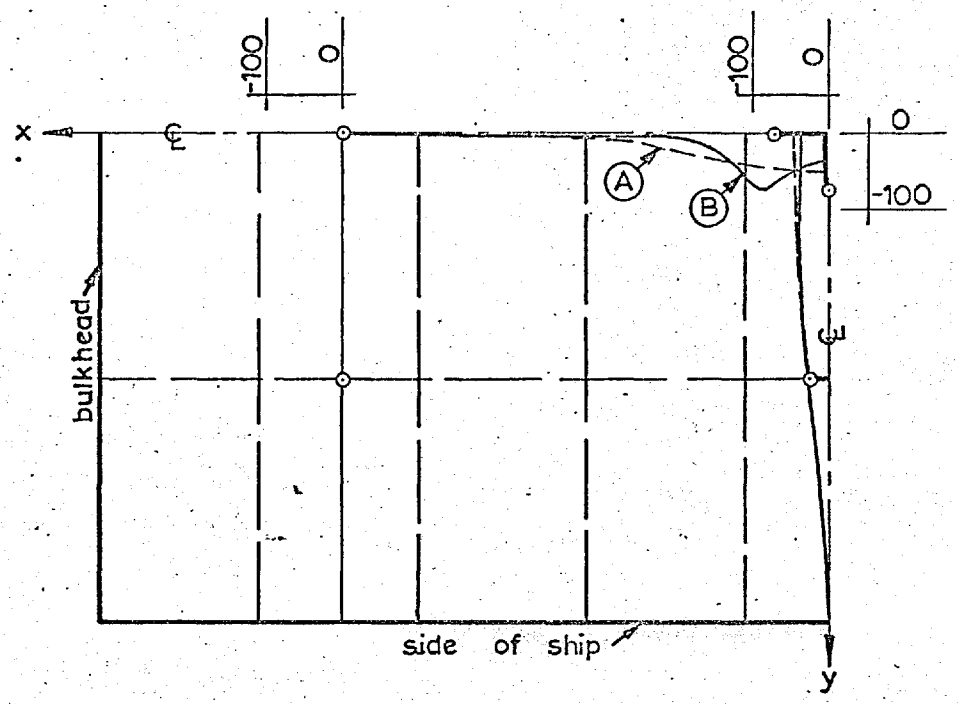

(i) ε_{xo} in./in. x 10^6

NOTE : (i) See Fig.100 for definition of loading
(ii) Experimental values shown o
(iii) Theoretical solutions ordinary simple support { (A) no shear deformation (B) including shear deformation

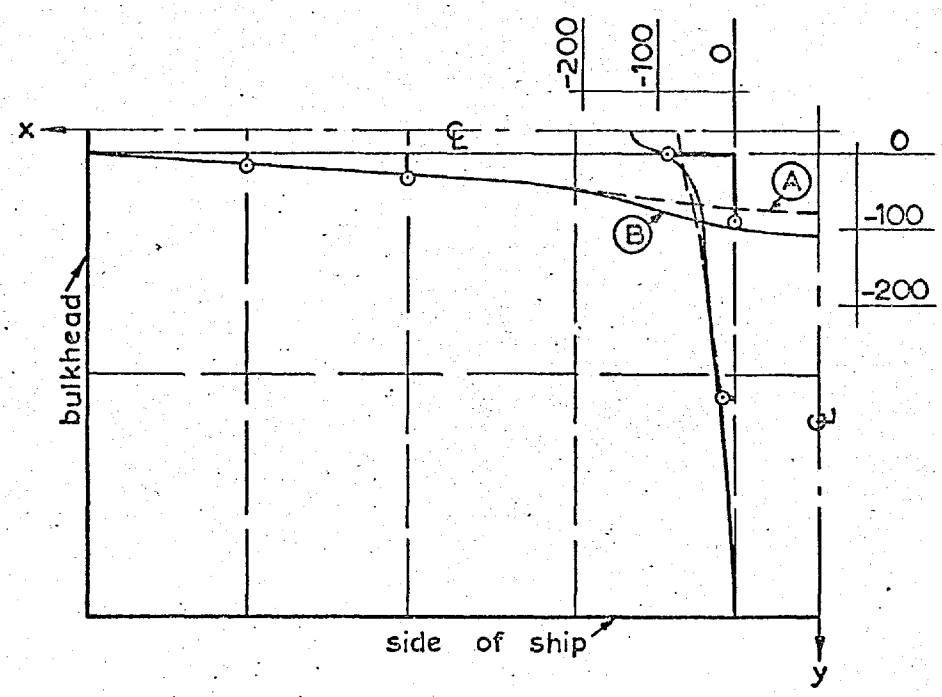

(ii) ε_{yo} in./in. x 10^6

Fig. 112 : Double Bottom Analysis - Outer Shell Strains For Patch Load P2

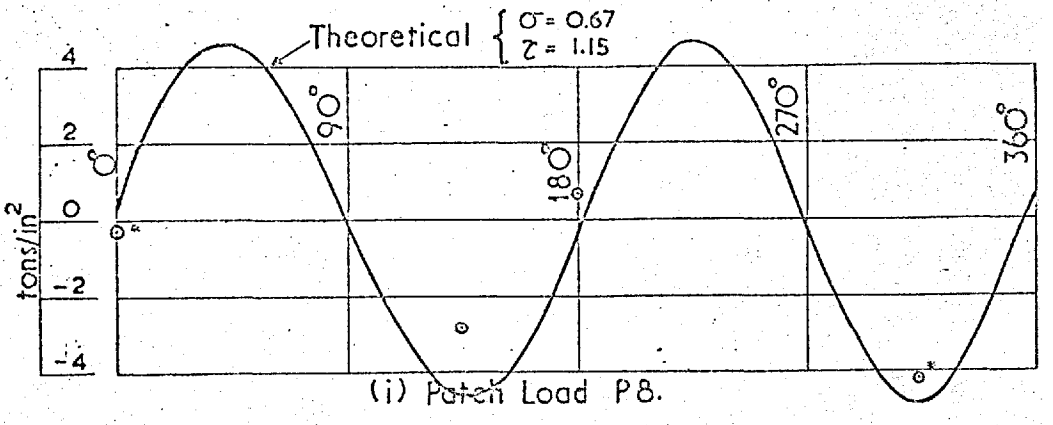

(i) Patch Load P8.

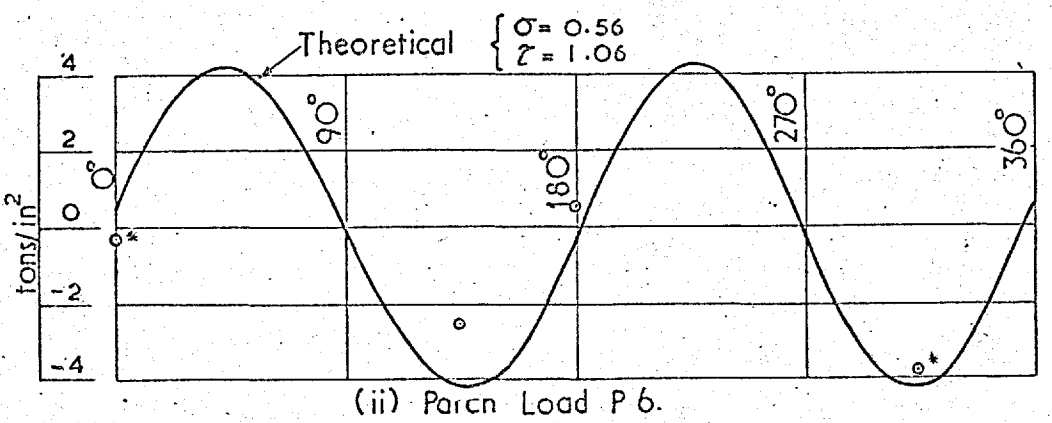

(ii) Patch Load P 6.

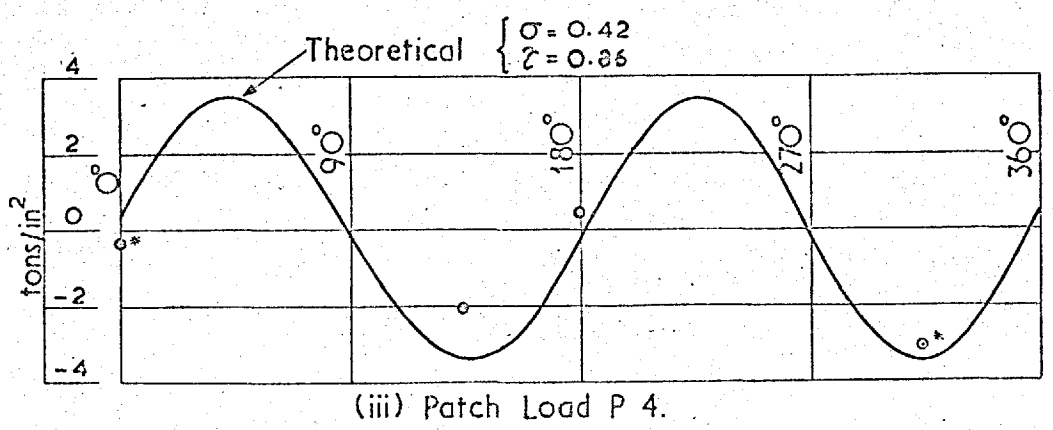

(iii) Patch Load P 4.

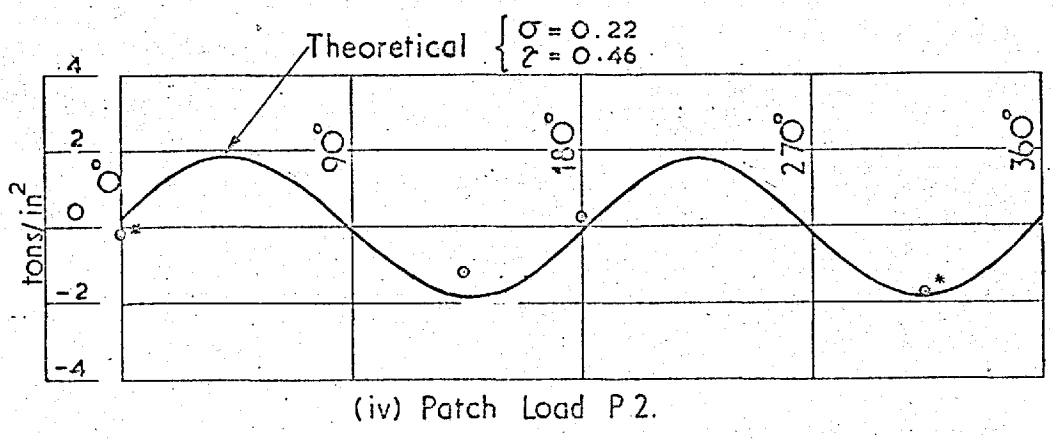

(iv) Patch Load P 2.

NOTE: (i) Experimental values shown ⊙. Those shown ⊙* were recorded at hole in floor A, bay 7-8 only.

(ii) Flexural (σ tons/in^2) and shear (τ tons/in^2) stresses shown for theoretical solutions were obtained from the solution including shear deformation for the load cases defined in Fig. 100

(iii) For hole locations and orientation of O° datum see Fig. 18

Fig. 113 : Double Bottom Analysis — Web Hole Stresses For Patch Loads Floor A (A') Ba· 7-8 (7'-8')

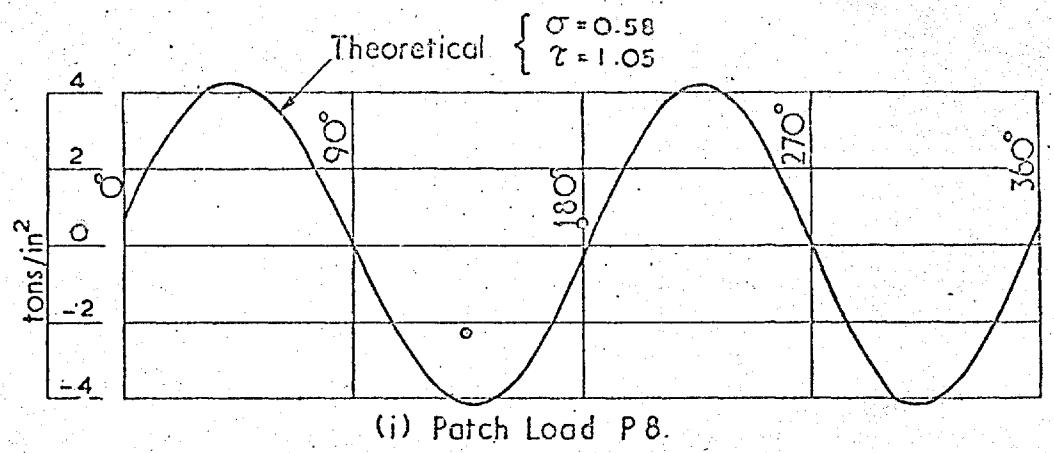

(i) Patch Load P 8.

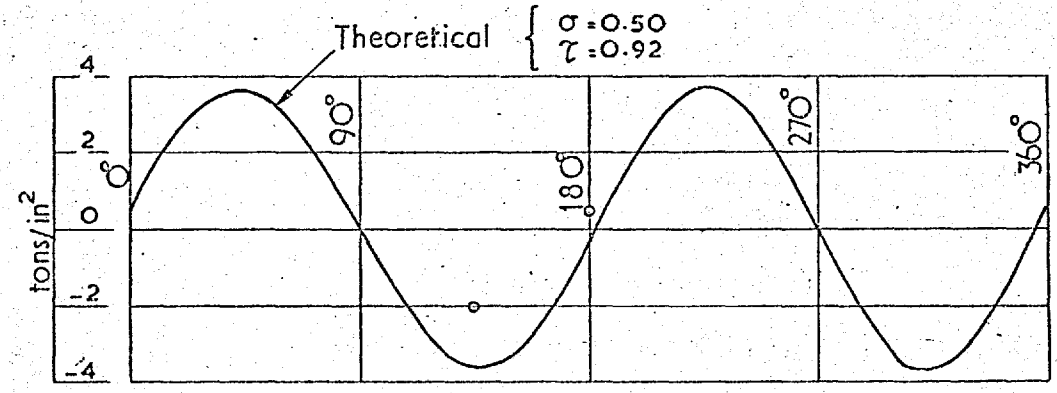

(ii) Patch Load P 6.

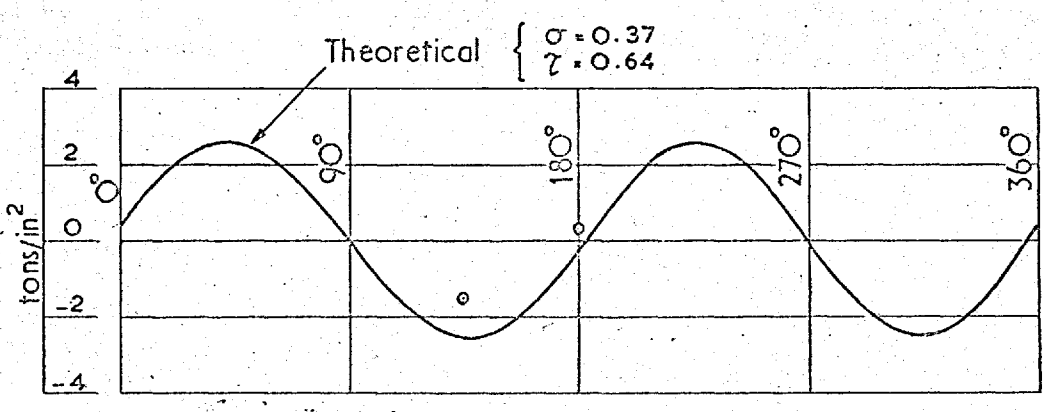

(iii) Patch Load P 4.

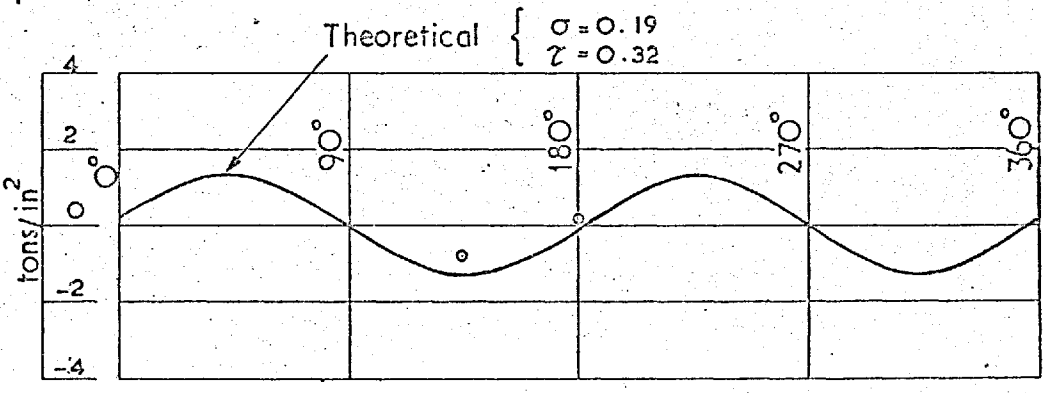

(iv) Patch Load P 2.

NOTE: (i) Experimental values shown ⊙
(ii) Flexural (σ tons/in^2) and shear (τ tons/in^2) stresses shown for theoretical solutions were obtained from the solutions including shear deformation for the load cases defined in Fig. 100
(iii) For hole locations and orientation of 0° datum see Fig. 18

Fig. 114 : Double Bottom Analysis – Web Hole Stresses For Patch Loads Floor B, Bay 7-8

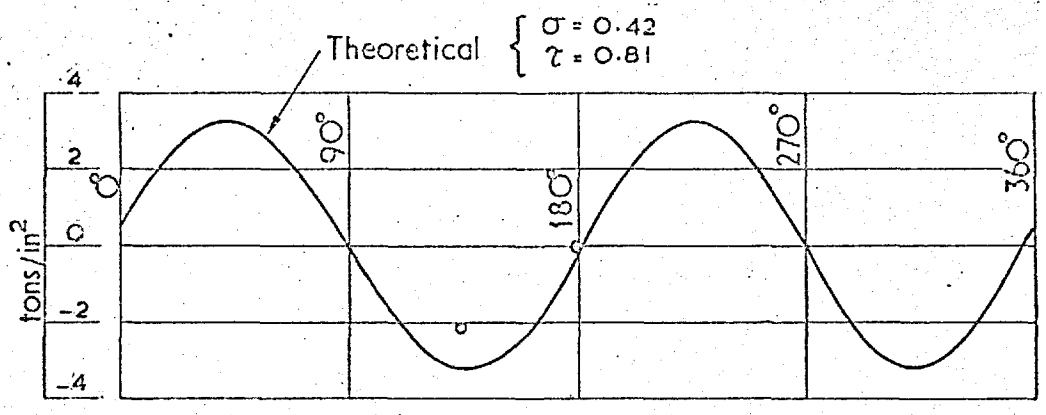

(i) Patch Load P 8.

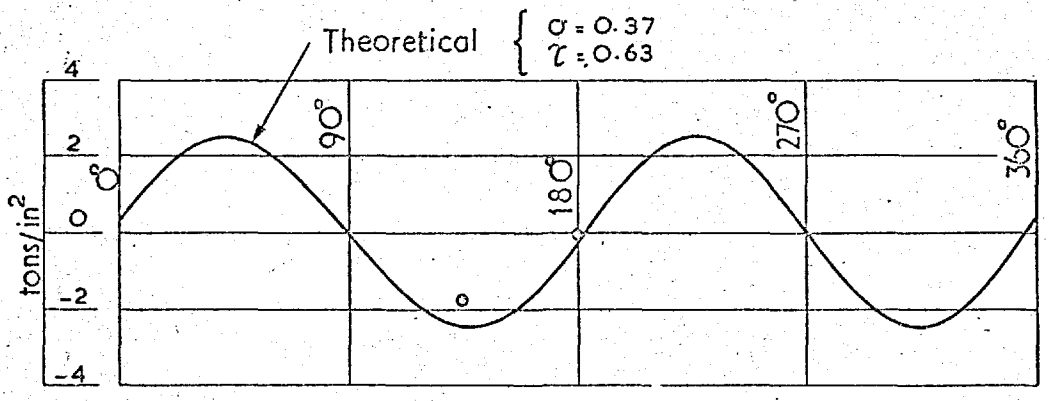

(ii) Patch Load P 6.

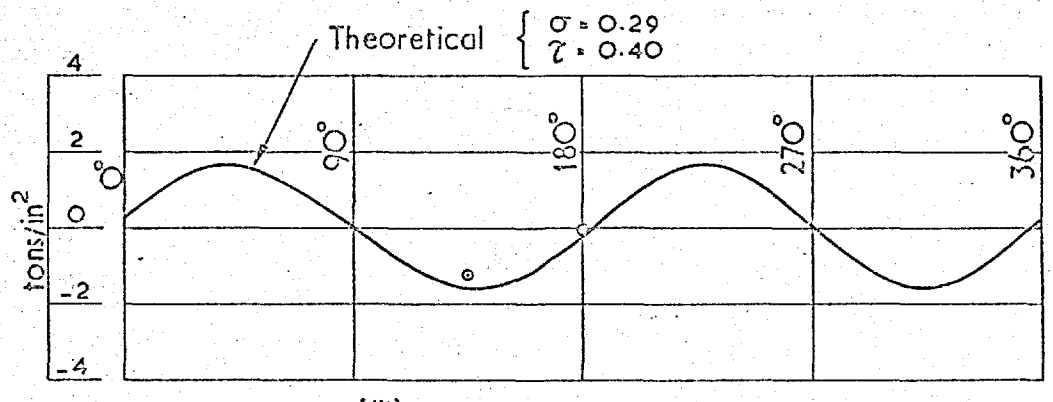

(iii) Patch Load P 4.

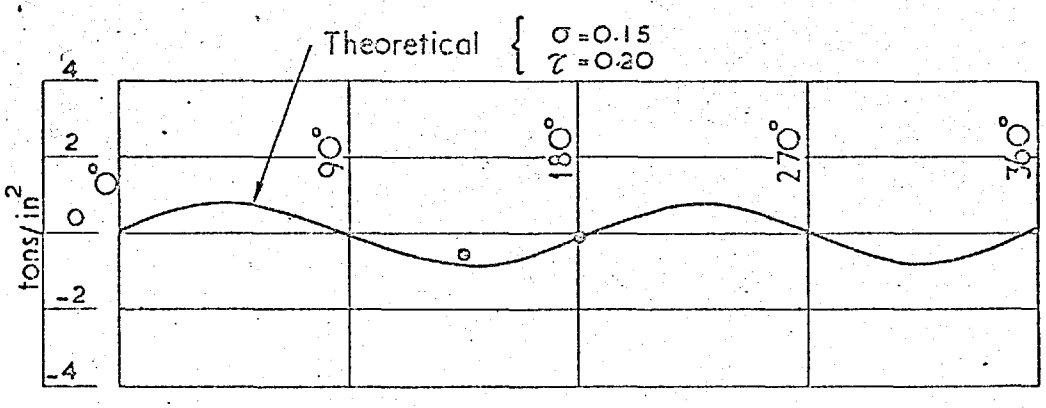

(iv) Patch Load P 2.

NOTE: (i) Experimental values shown o
(ii) Flexural (σ tons/in^2) and shear (τ tons/in^2) stresses shown for theoretical solutions were obtained from the solutions including shear deformation for the load cases defined in Fig. 100
(iii) For hole locations and orientation of 0° datum see Fig. 18

Fig. 115 : Double Bottom Analysis – Web Hole Stresses For Patch Loads

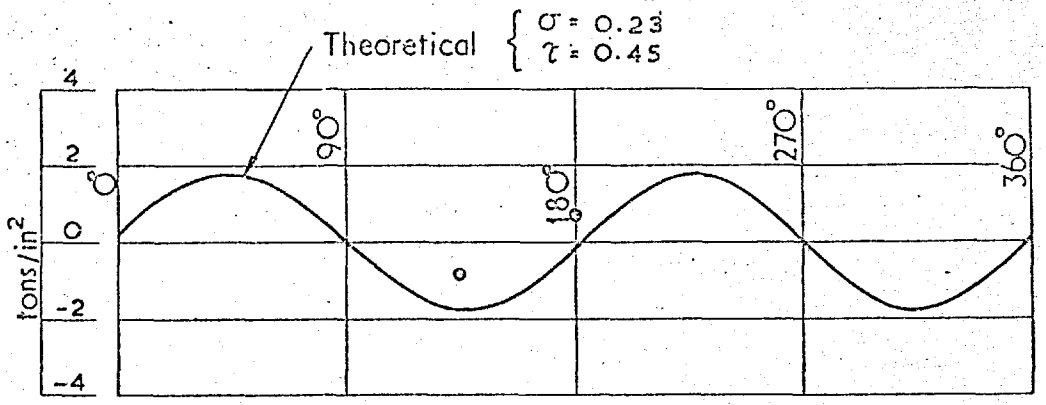

(i) Patch Load P 8.

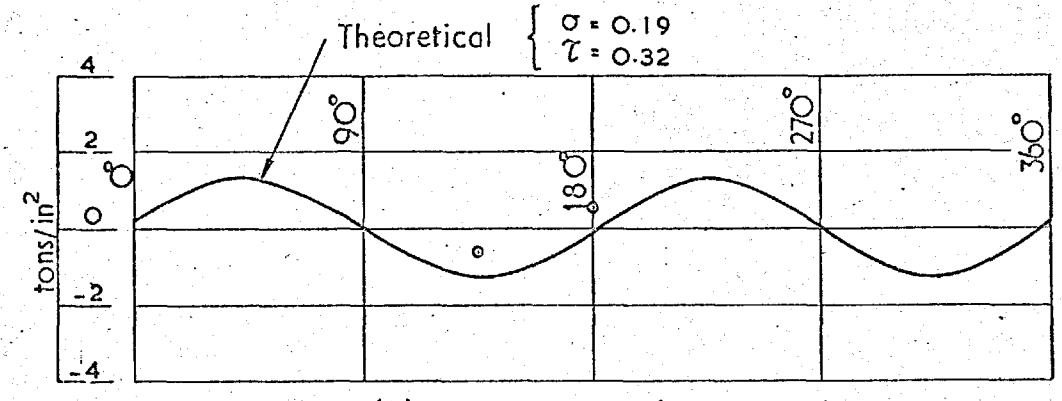

(ii) Patch Load P 6.

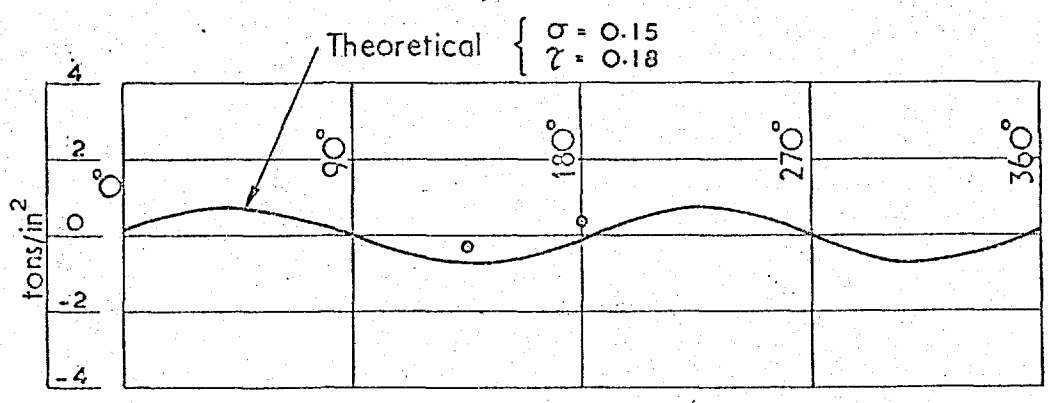

(iii) Patch Load P 4.

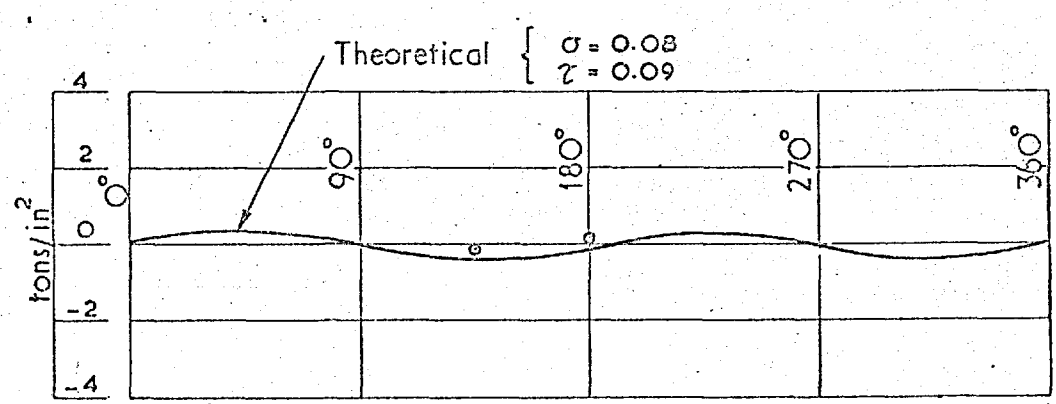

(iv) Patch Load P 2.

NOTE: (i) Experimental values shown o
(ii) Flexural (σ tons/in^2) and shear (τ tons/in^2) stresses shown for theoretical solutions were obtained from the solutions including shear deformation for the load cases defined in Fig. 100
(iii) For hole locations and orientation of O° datum see Fig. 18

Fig. 116 : Double Bottom Analysis – Web Hole Stresses For Patch Loads Floor D, Bay 7 – 8

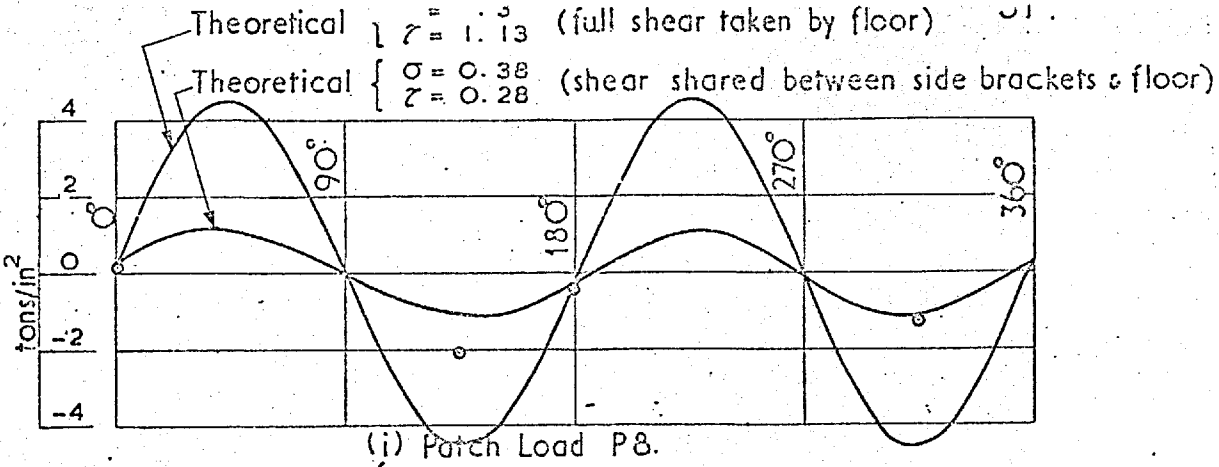

(i) Patch Load P8.

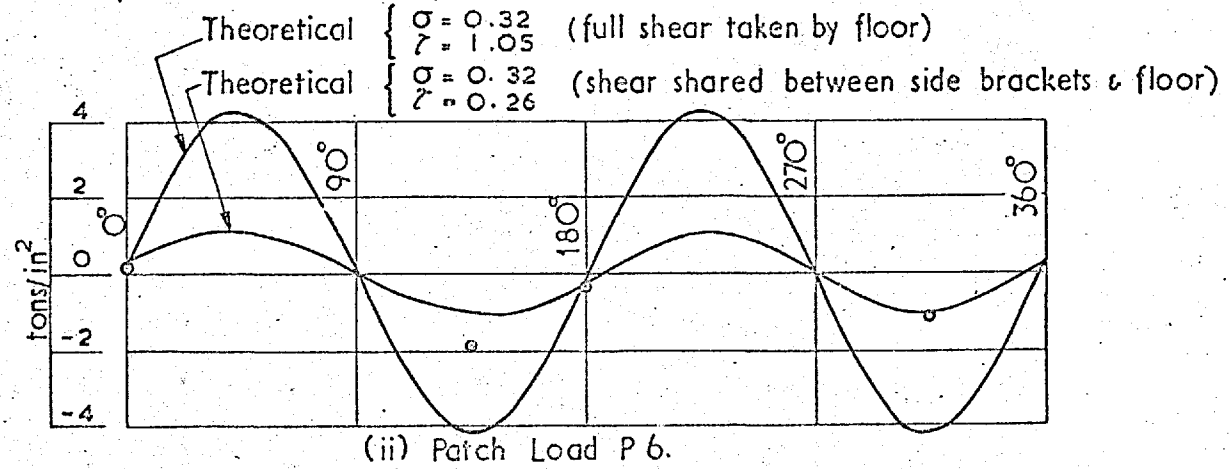

(ii) Patch Load P 6.

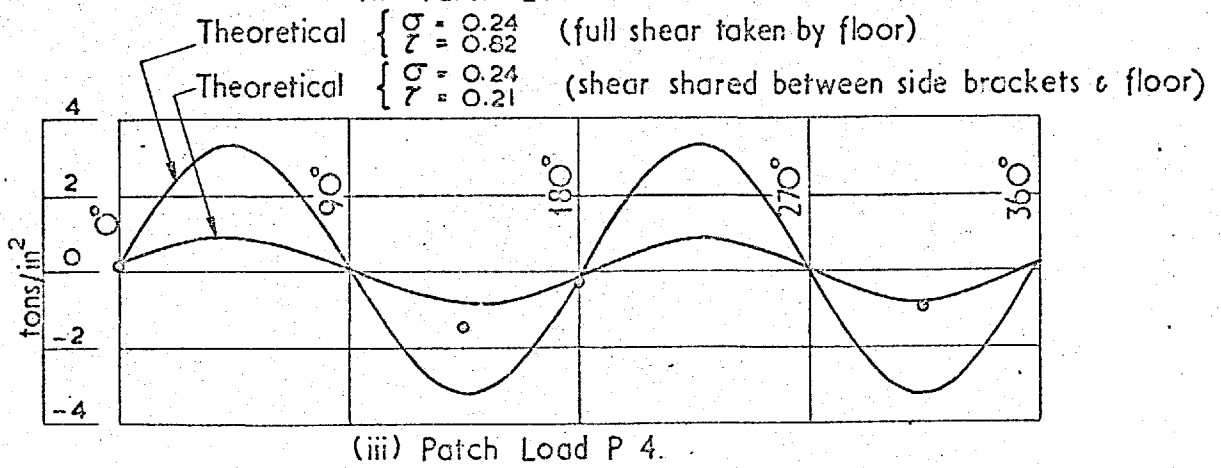

(iii) Patch Load P 4.

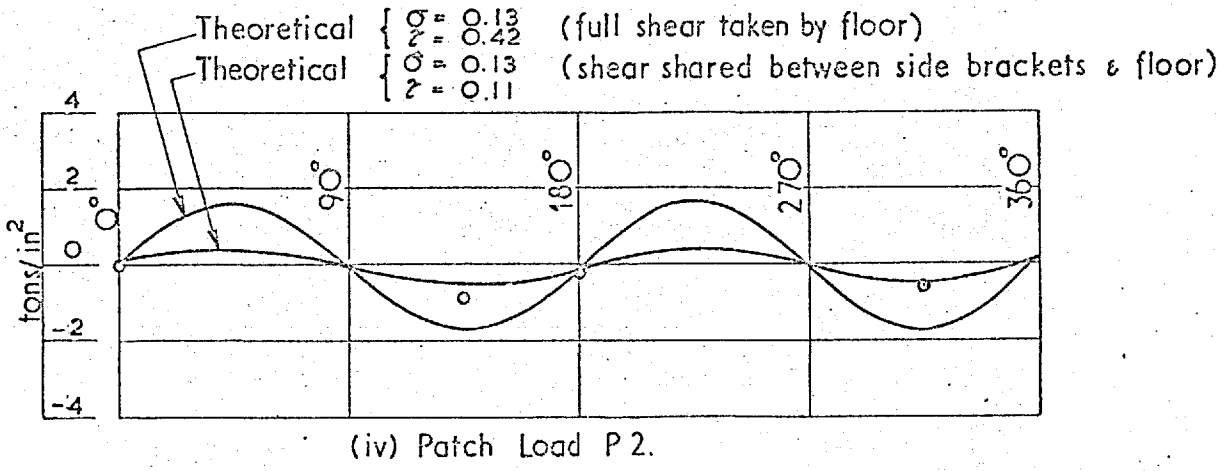

(iv) Patch Load P 2.

NOTE:

(i) Experimental values shown ∘ (floor A) and ÷(side bracket A_1)

(ii) Flexural (σ tons/in^2) and shear (τ tons/in^2) stresses shown for theoretical solutions were obtained from the solution including shear deformation for the load cases defined in Fig. 100

(iii) For hole locations and orientation of O° datum see Fig. 18

Fig. 117 : Double Bottom Analysis — Web Hole Stresses For Patch Loads Floor A and Side Bracket A_1 Ba 8-9

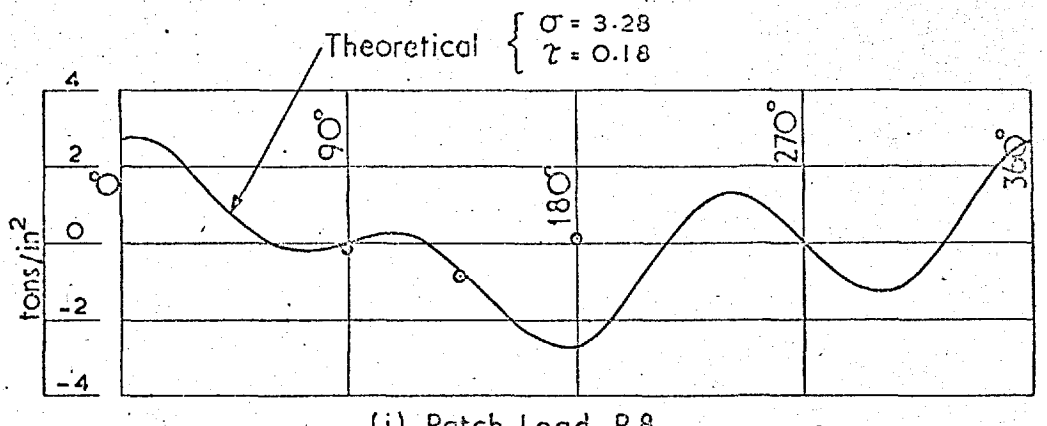

(i) Patch Load P 8.

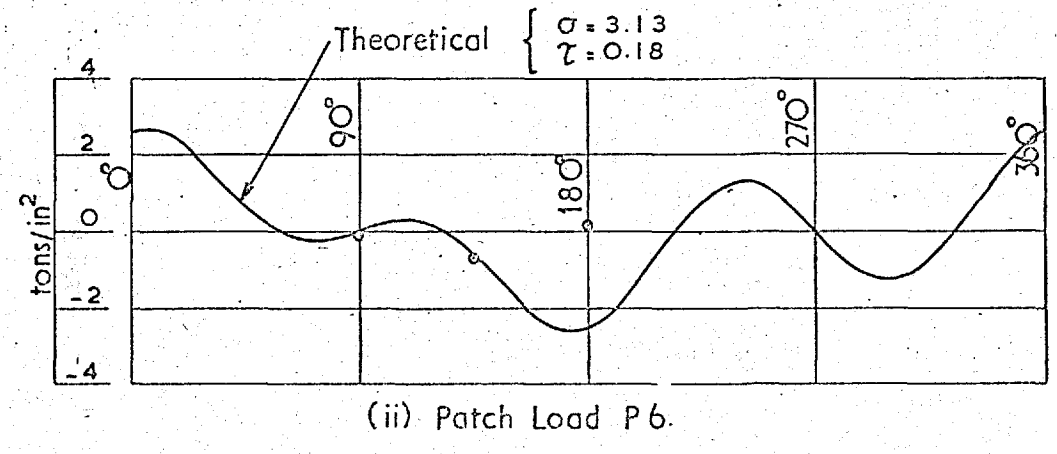

(ii) Patch Load P 6.

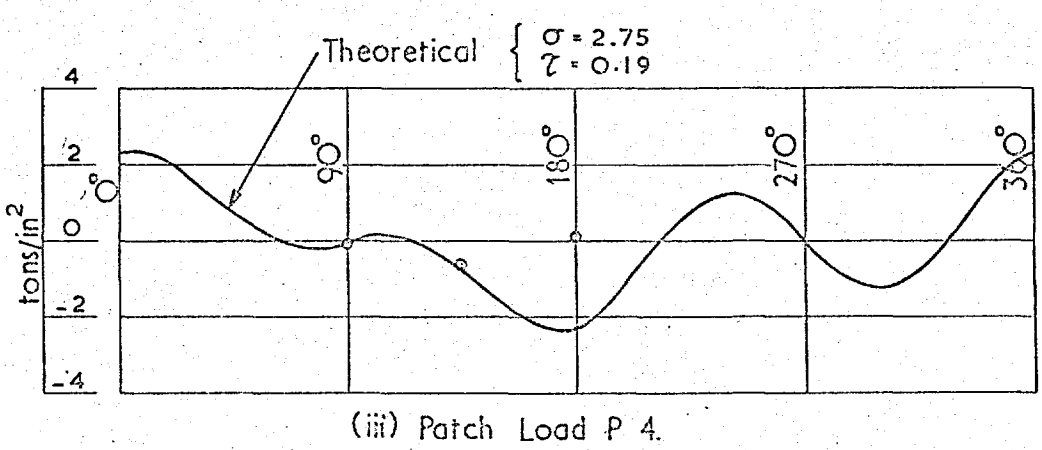

(iii) Patch Load P 4.

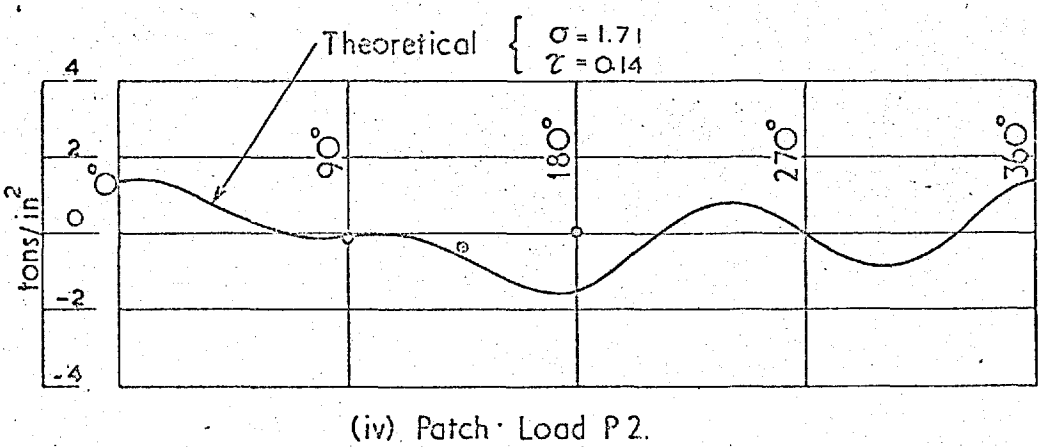

(iv) Patch Load P 2.

NOTE: (i) Experimental values shown o
(ii) Flexural (σ tons/in^2) and shear (τ tons/in^2) stresses shown for theoretical solutions were obtained from the solutions including shear deformation for the load cases defined in Fig. 100
(iii) For hole locations and orientation of O° datum see Fig. 18

Fig. 118 : Double Bottom Analysis – Web Hole Stresses For Patch Loads Centre Bracket A_1, Bay O-1

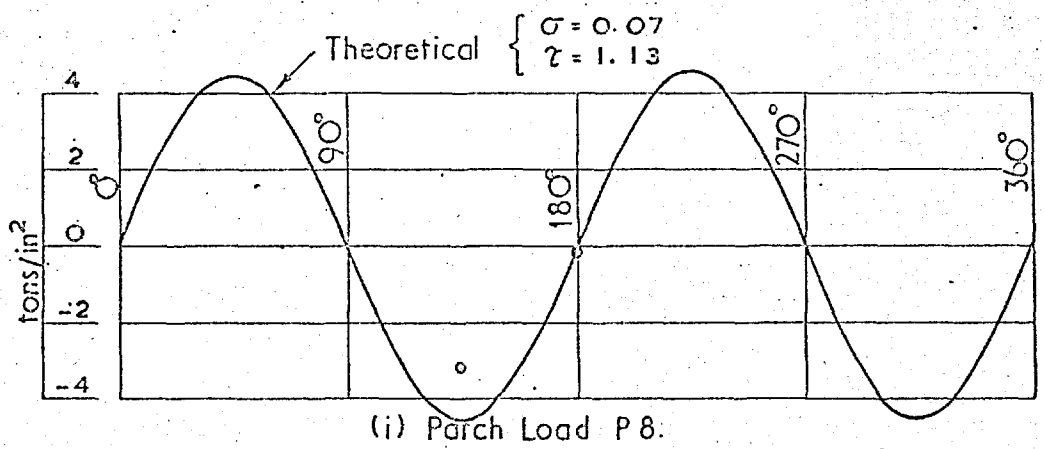

(i) Patch Load P 8.

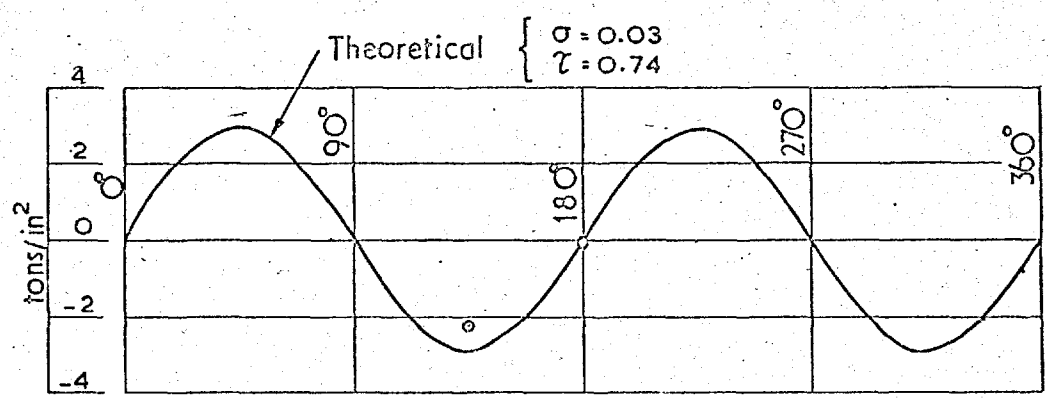

(ii) Patch Load P 6.

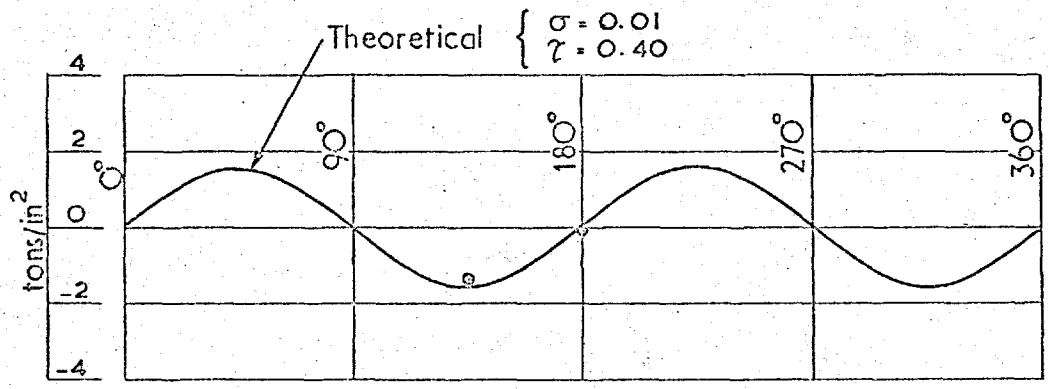

(iii) Patch Load P 4.

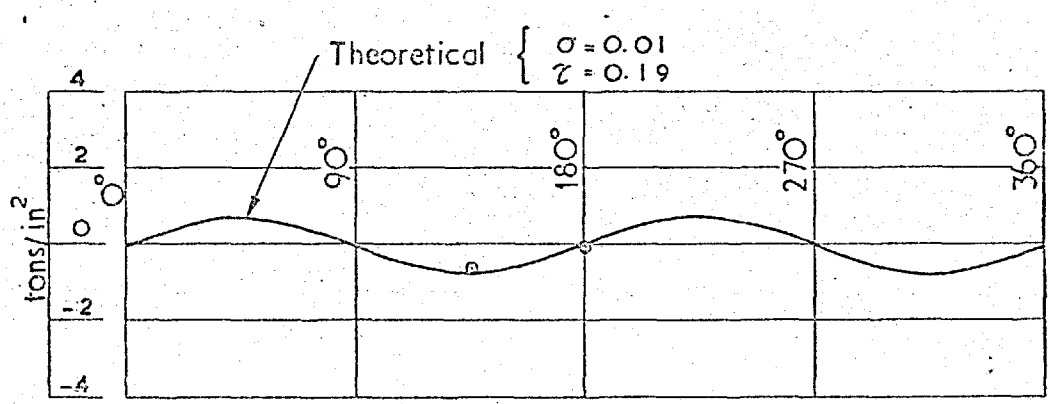

(iv) Patch Load P 2.

NOTE: (i) Experimental values shown o
(ii) Flexural (σ tons/in^2) and shear (τ tons/in^2) stresses shown for theoretical solutions were obtained from the solutions including shear deformation for the load cases defined in Fig. 100
(iii) For hole locations and orientation of O° datum see Fig. 18

Fig. 119 : Double Bottom Analysis – Web Hole Stresses For Patch Loads Intercostal 5 (5'), Holes Adjacent to E (E')

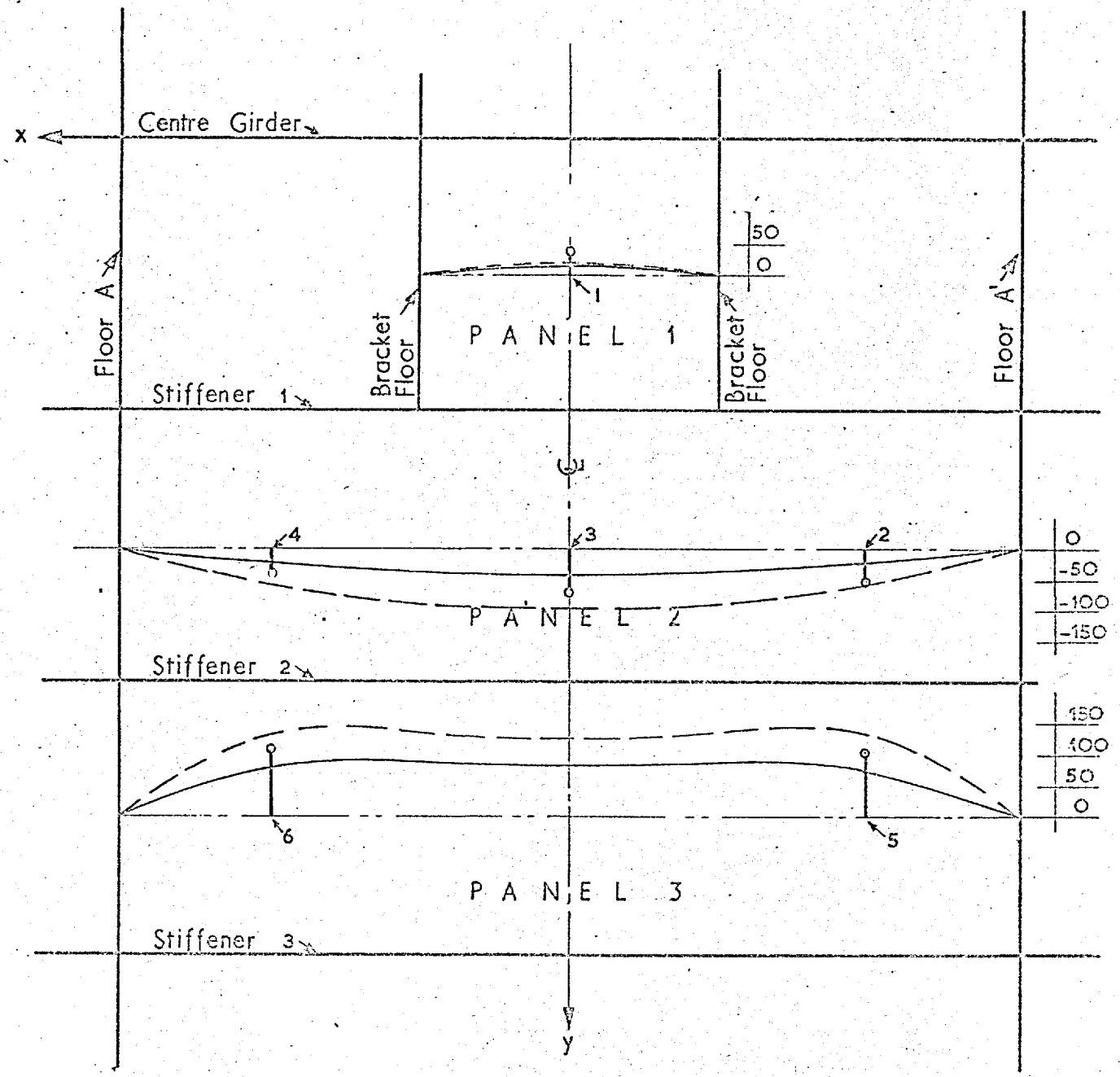

NOTE: (i) Deflexions in inches x 10^{-4} (positive inwards)
(ii) Experimental values shown o
(iii) Theoretical solutions
——— rotational elastic restraint
– – – – simple support
(iv) Patch load P8 defined in Fig. 100

Fig. 120 : Double Bottom Analysis – Deflexions of Outer Shell Panels For Patch Load P8.

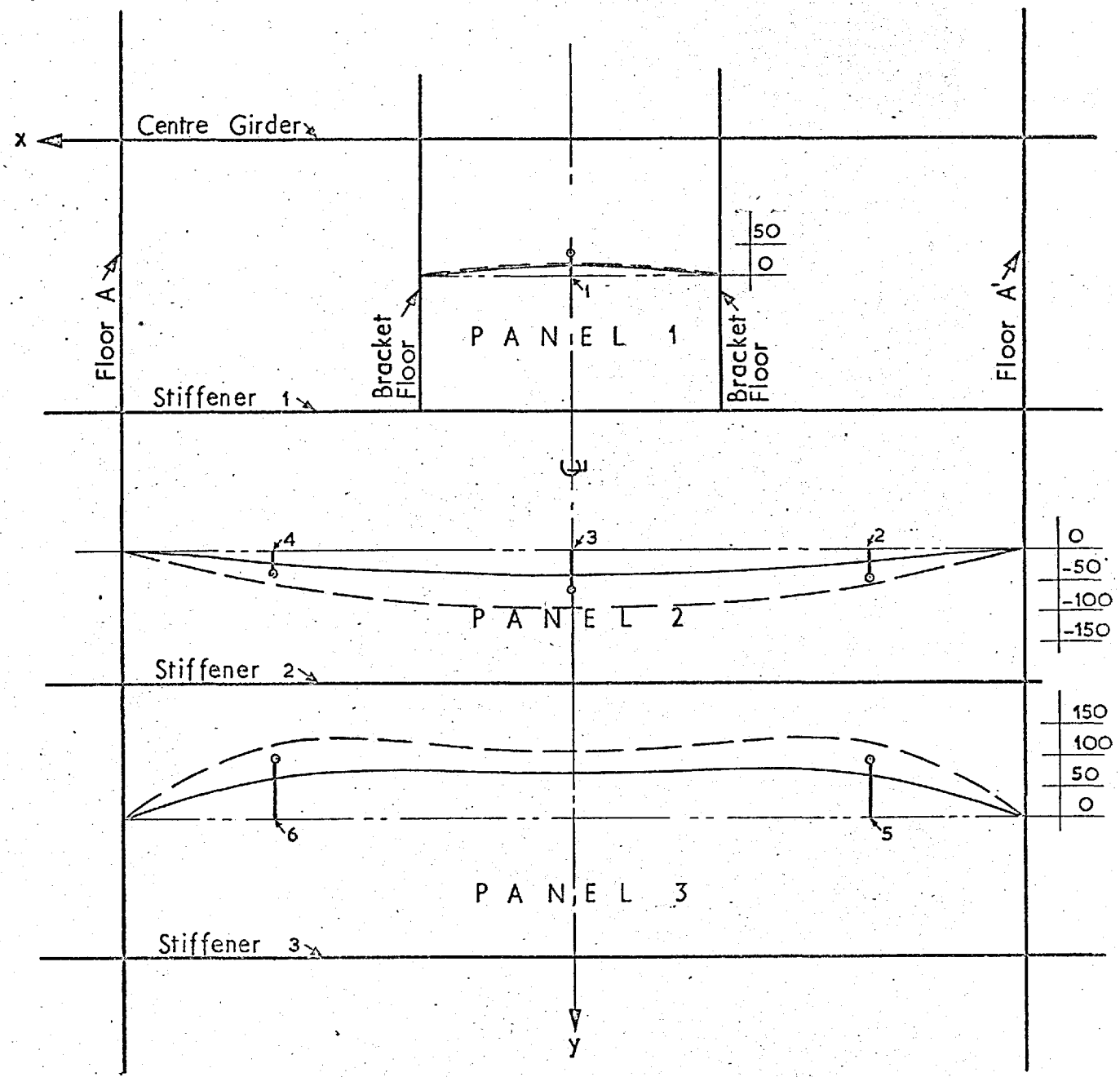

NOTE: (i) Deflexions in inches x 10^{-4} (positive inwards)
(ii) Experimental values shown ∘
(iii) Theoretical solutions
——— rotational elastic restraint
— — — simple support
(iv) Patch load P6 defined in Fig. 100

Fig. 121 : Double Bottom Analysis – Deflexions of Outer Shell Panels For Patch Load P6

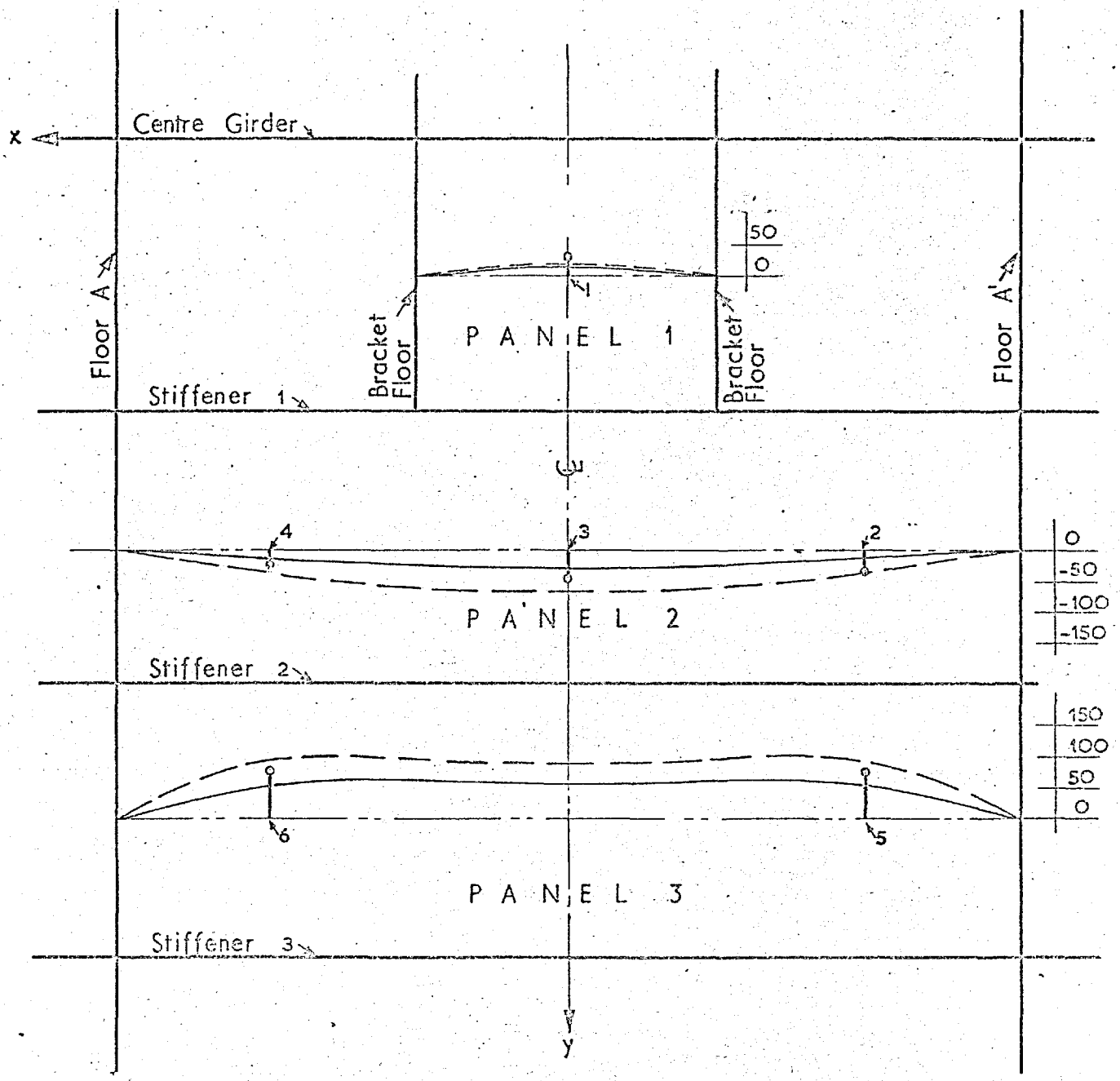

NOTE: (i) Deflexions in inches $\times 10^{-4}$ (positive inwards)
(ii) Experimental values shown o
(iii) Theoretical solutions
——— rotational elastic restraint
— — — simple support
(iv) Patch load P4 defined in Fig. 100

Fig. 122 : Double Bottom Analysis – Deflexions of Outer Shell Panels For Patch Load P4

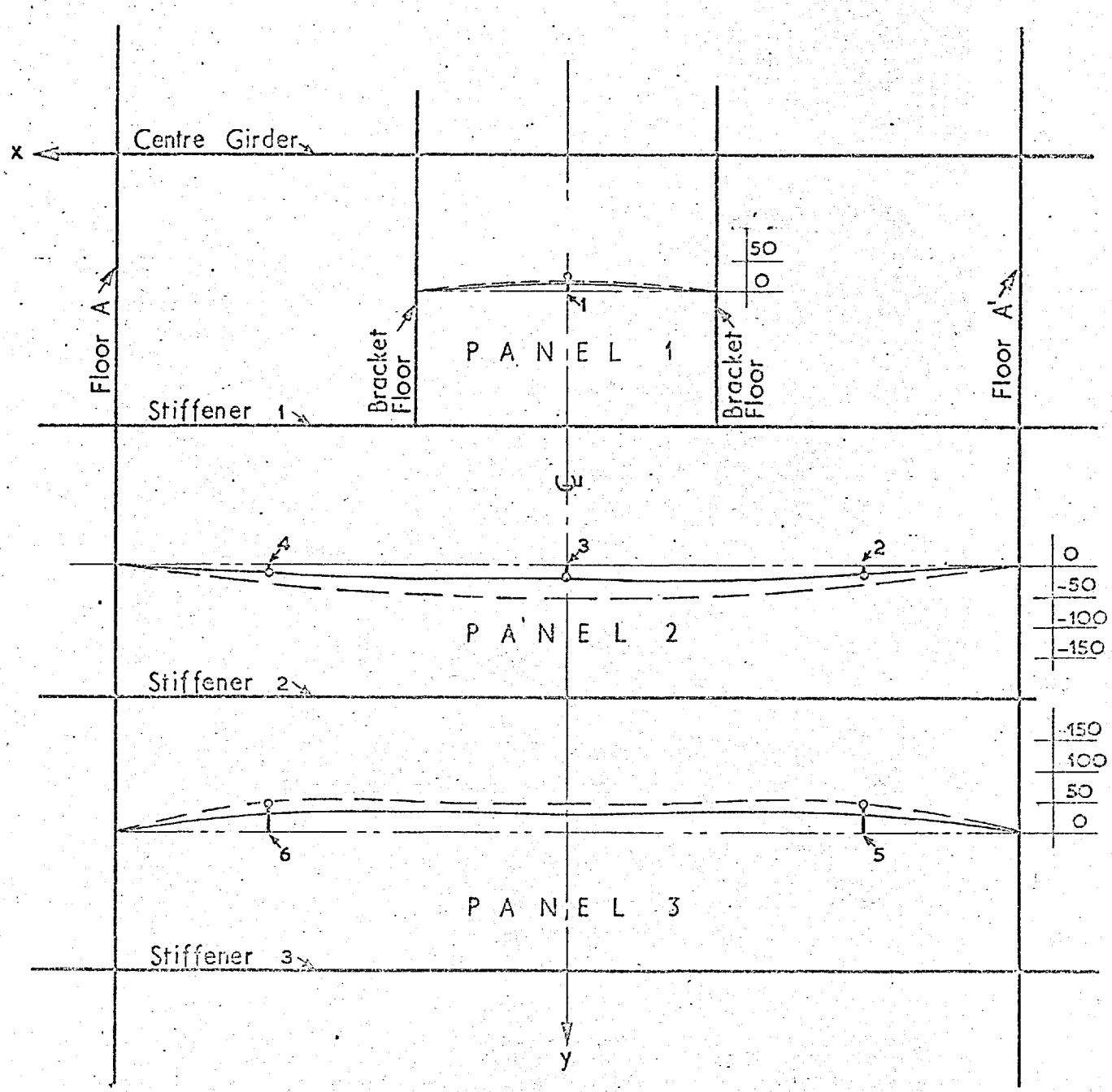

NOTE: (i) Deflexions in inches $\times 10^{-4}$ (positive inwards)
(ii) Experimental values shown ∘
(iii) Theoretical solutions
——— rotational elastic restraint
– – – – simple support
(iv) Patch load P2 defined in Fig. 100

Fig. 123 : Double Bottom Analysis – Deflexions of Outer Shell Panels For Patch Load P2

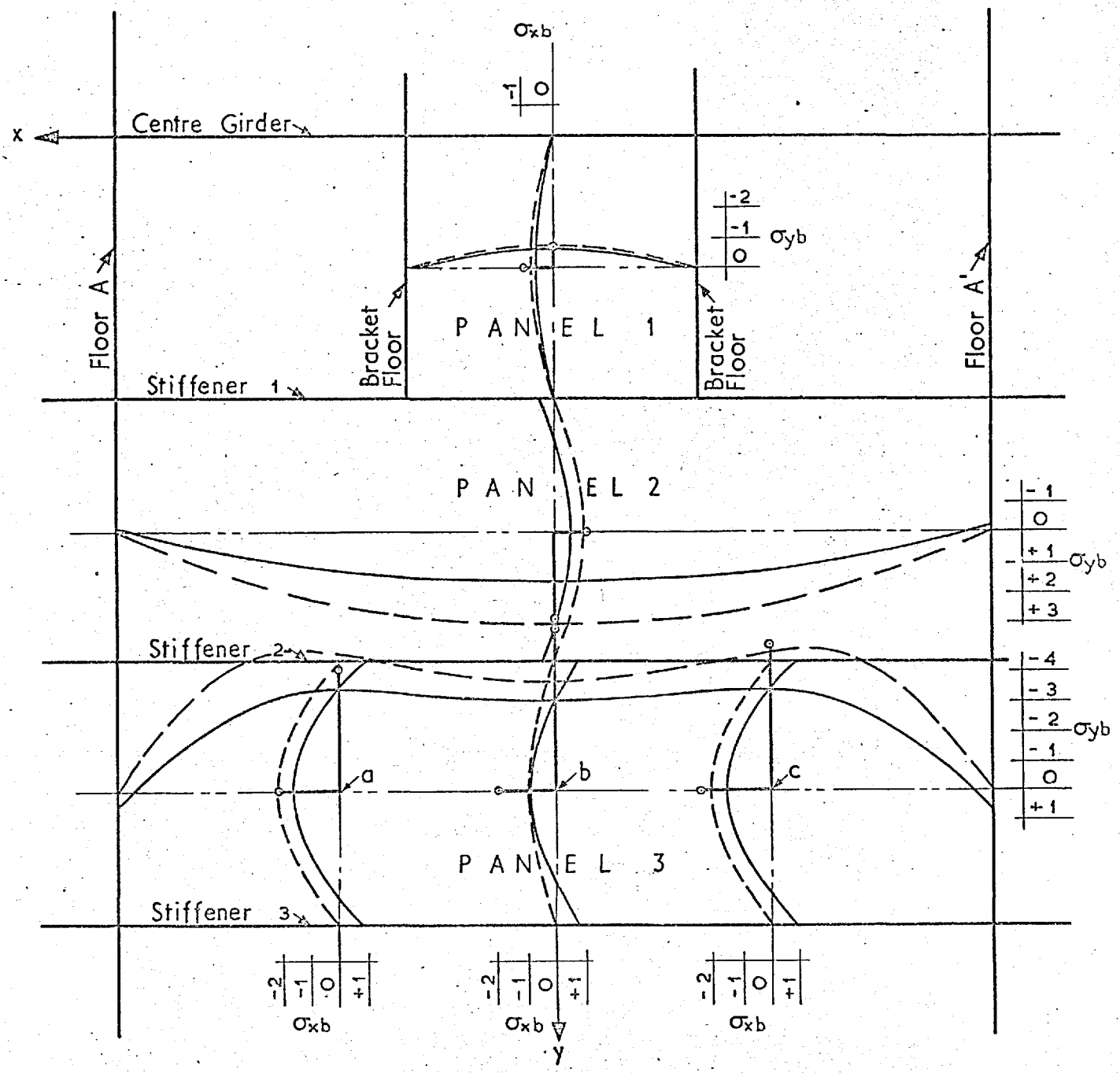

NOTE: (i) Stresses in tons/in^2
(ii) Experimental values shown ∘
(iii) Theoretical solutions
——— rotational elastic restraint
– – – – simple support
(iv) Patch load P8 defined in Fig. 100

Fig. 124 : Double Bottom Analysis – Bending Stresses at Outer Surface of Outer Shell Panels For Patch Load P8

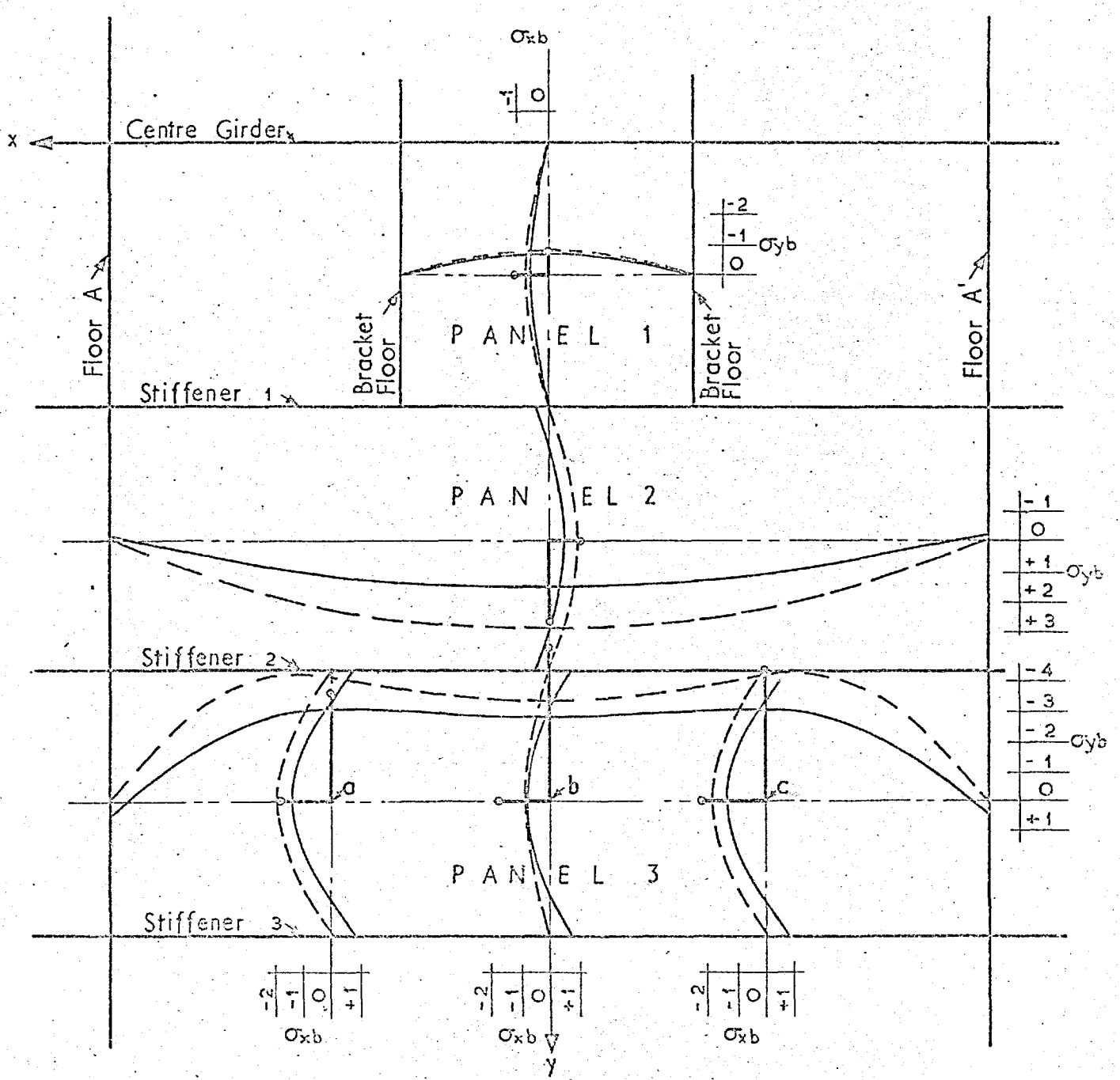

NOTE : (i) Stresses in tons/in^2
(ii) Experimental values shown ⊙
(iii) Theoretical solutions
——— rotational elastic restraint
— — — simple support
(iv) Patch load P6 defined in Fig. 100

Fig. 125 : Double Bottom Analysis – Bending Stresses at Outer Surface of Outer Shell Panels For Patch Load P6

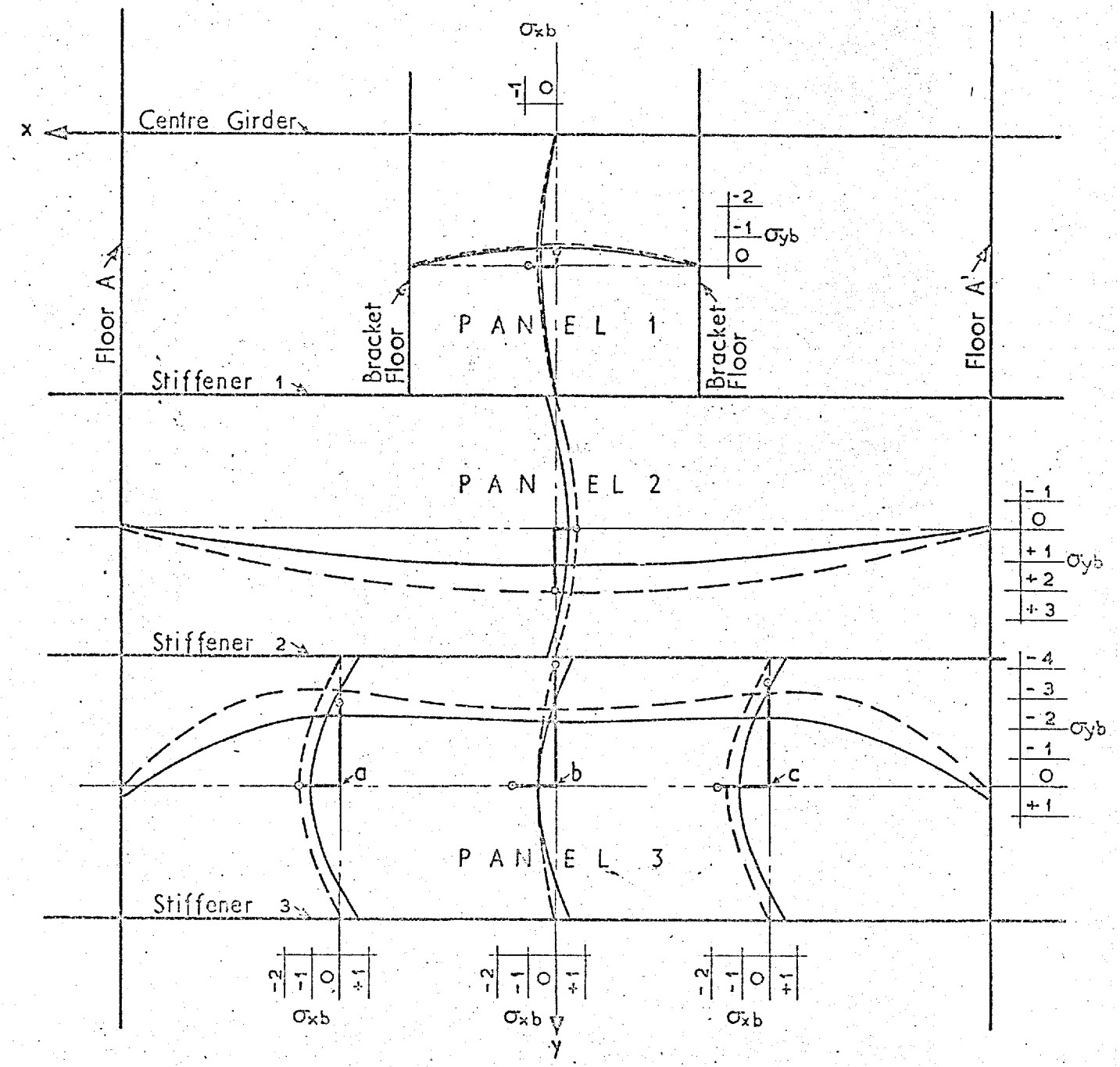

NOTE : (i) Stresses in tons/in^2
(ii) Experimental values shown ⊙
(iii) Theoretical solutions
——— rotational elastic restraint
— — — simple support
(iv) Patch load P4 defined in Fig. 100

Fig. 126 : Double Bottom Analysis – Bending Stresses at Outer Surface of Outer Shell Panels For Patch Load P4

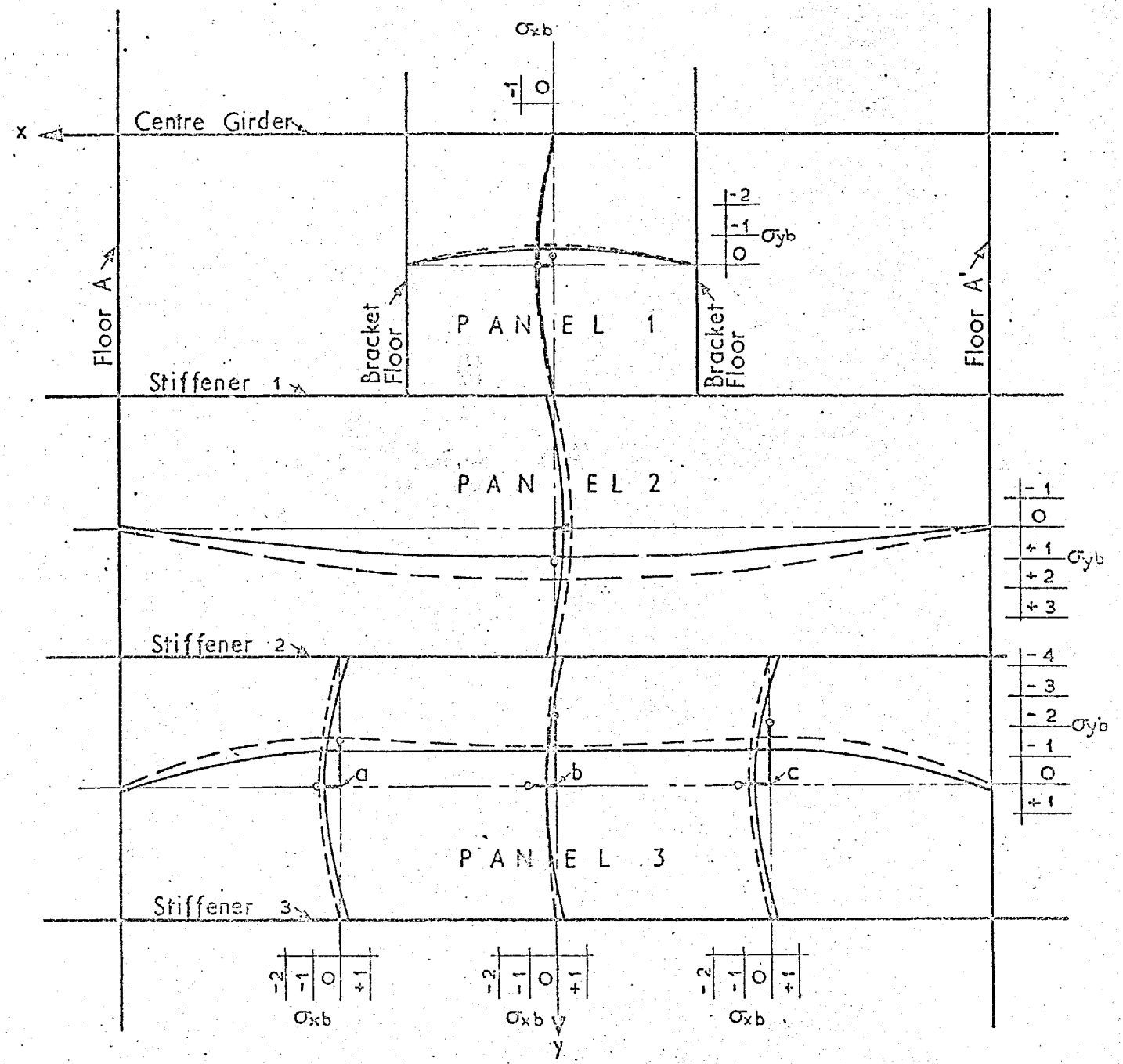

NOTE: (i) Stresses in tons/in^2
(ii) Experimental values shown ∘
(iii) Theoretical solutions
——— rotational elastic restraint
— — — simple support
(iv) Patch load P2 defined in Fig. 100

Fig. 127 : Double Bottom Analysis – Bending Stresses at Outer Surface of Outer Shell Panels For Patch Load P2

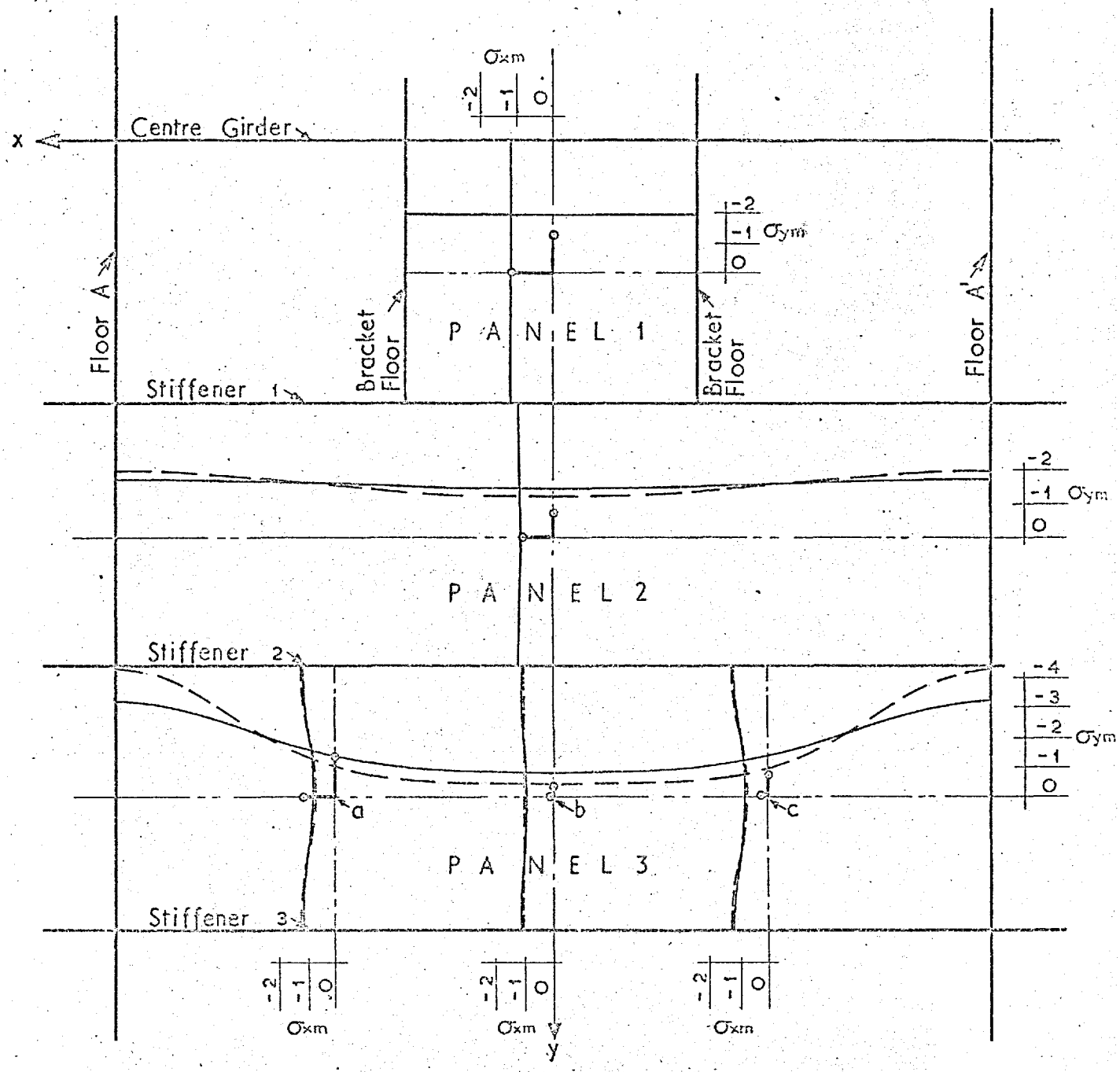

NOTE: (i) Stresses in tons/in^2
(ii) Experimental values shown ∘
(iii) Theoretical solutions
——— rotational elastic restraint
— — — simple support
(iv) Patch load P8 defined in Fig. 100

Fig. 128 : Double Bottom Analysis – Membrane Stresses in Outer Shell Panels For Patch Load P8

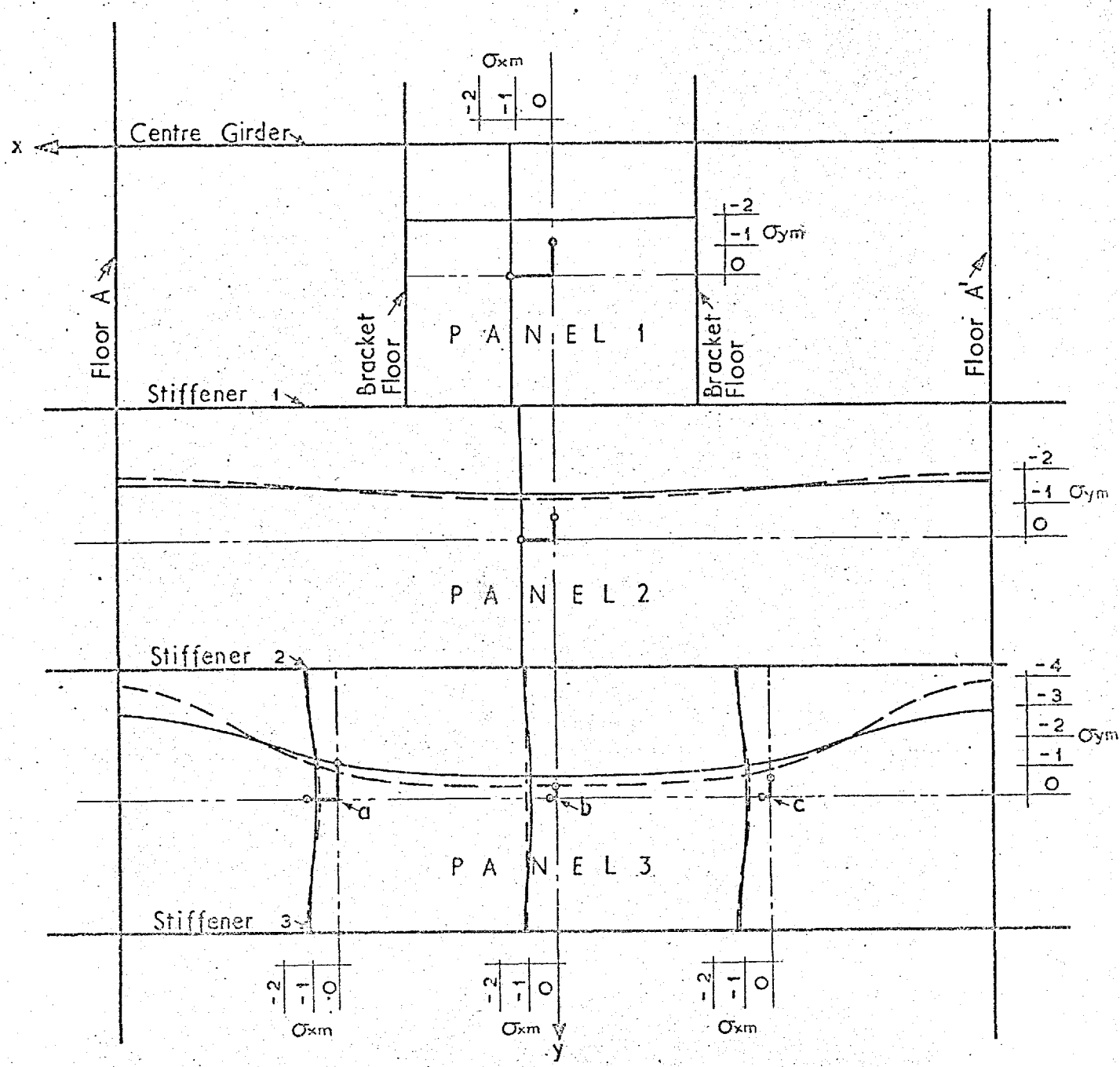

NOTE: (i) Stresses in tons/in^2
(ii) Experimental values shown.
(iii) Theoretical solutions
——— rotational elastic restraint
— — — simple support
(iv) Patch load P6 defined in Fig. 100

Fig. 129 : Double Bottom Analysis – Membrane Stresses in Outer Shell Panels For Patch Load P6

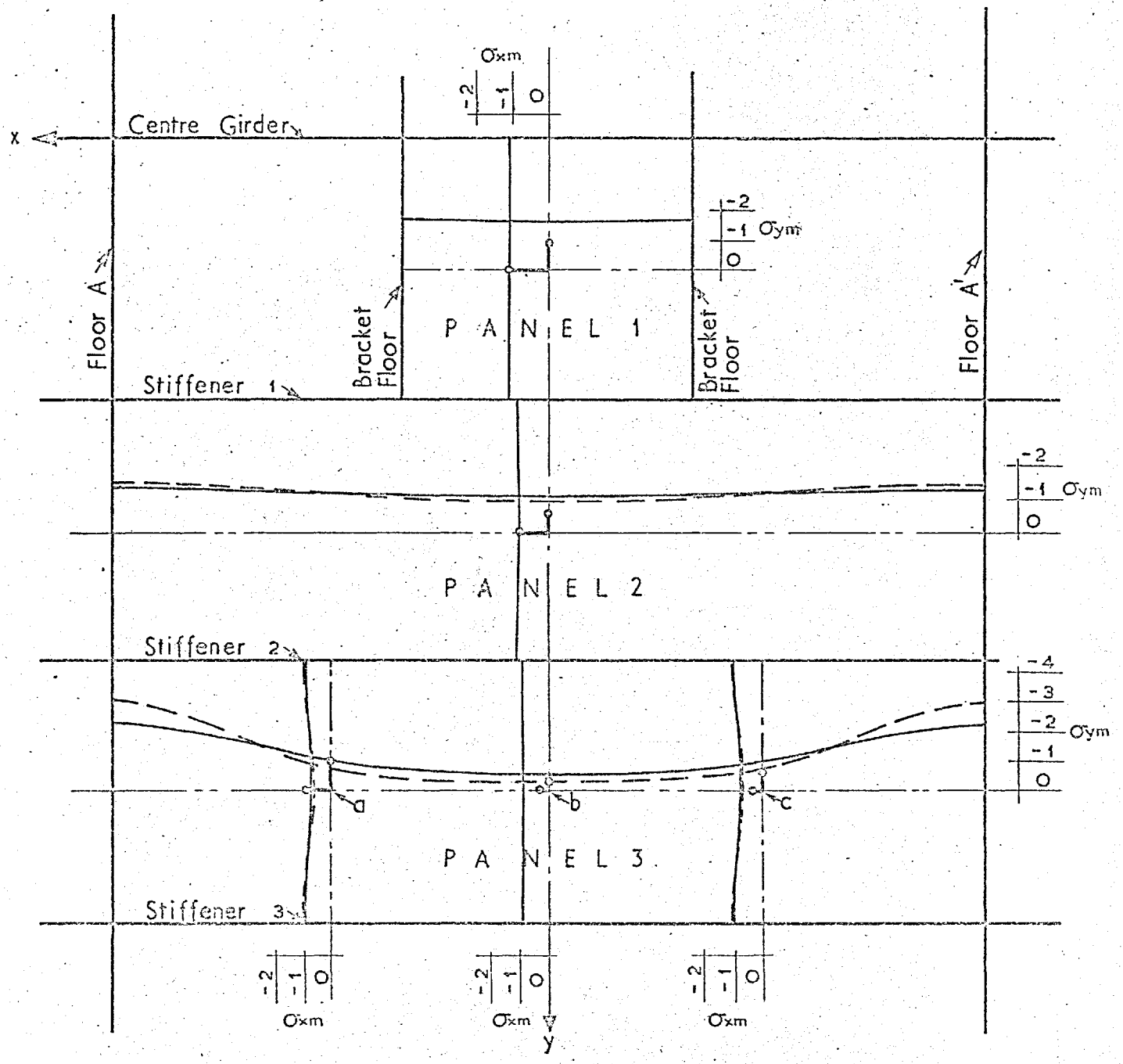

NOTE: (i) Stresses in tons/in^2
(ii) Experimental values shown ∘
(iii) Theoretical solutions
——— rotational elastic restraint
— — — simple support
(iv) Patch load P4 defined in Fig. 100

Fig. 130 : Double Bottom Analysis – Membrane Stresses in Outer Shell Panels For Patch Load P4

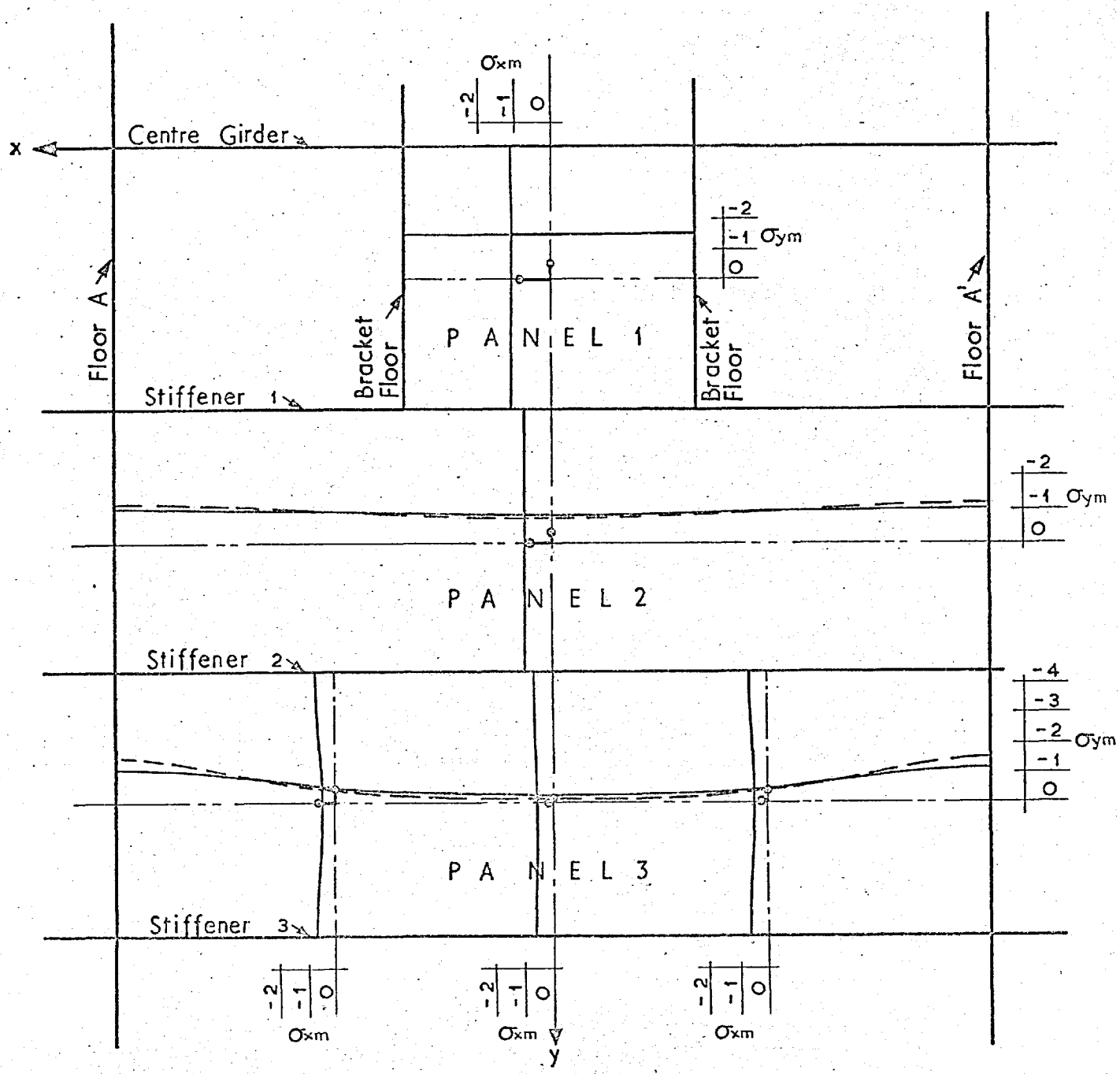

NOTE: (i) Stresses in tons/in^2
(ii) Experimental values shown ∘
(iii) Theoretical solutions
——— rotational elastic restraint
— — — simple support
(iv) Patch load P2 defined in Fig. 100

Fig. 131 : Double Bottom Analysis – Membrane Stresses in Outer Shell Panels For Patch Load P2

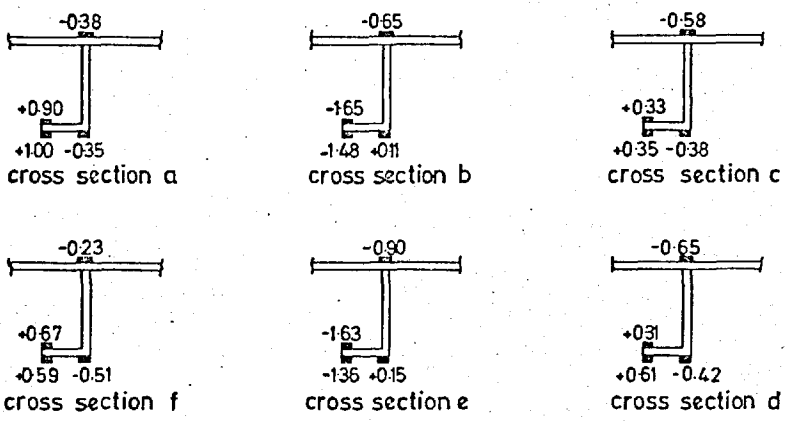

(i) Outer shell stiffener No. 3

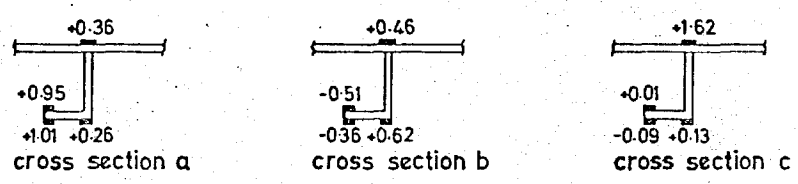

(ii) Inner shell stiffener No. 3

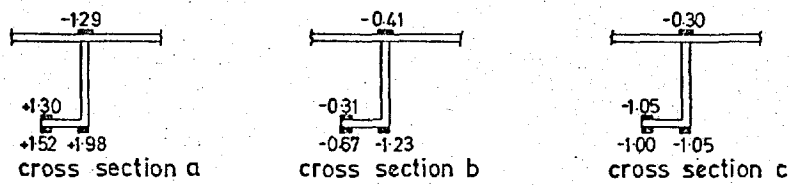

(iii) Outer shell stiffener No. 8

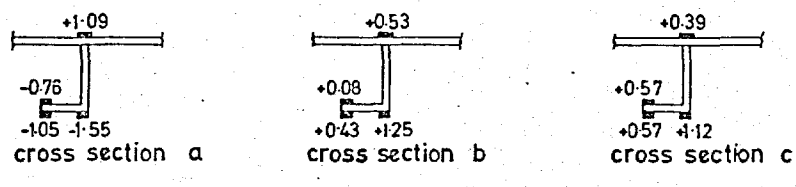

(iv) Inner shell stiffener No. 8

NOTE : (i) Stresses in tons/in.
(ii) See Fig. 100 for definition of load
(iii) See Fig. 20 for location of cross sections

Fig. 132 : Double Bottom Analysis - Shell Stiffener Stresses for Patch Load P8

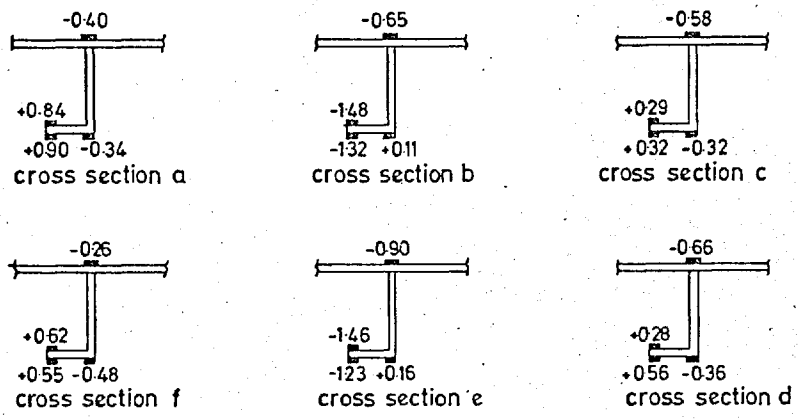

(i) Outer shell stiffener No. 3.

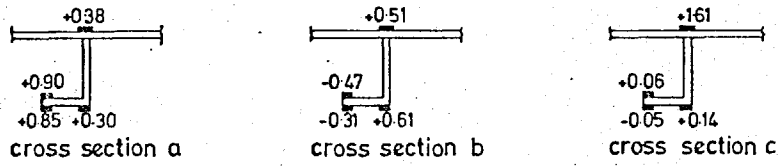

(ii) Inner shell stiffener No. 3.

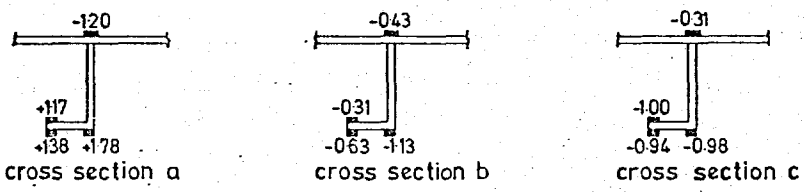

(iii) Outer shell stiffener No. 8.

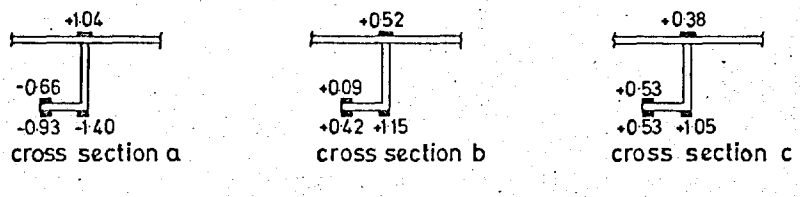

(iv) Inner shell stiffener No. 8.

NOTE: (i) Stresses in tons/in.^{2}
(ii) See Fig. 100 for definition of load
(iii) See Fig. 20 for location of cross sections

Fig. 133 : Double Bottom Analysis - Shell Stiffener Stresses for Patch Load P6

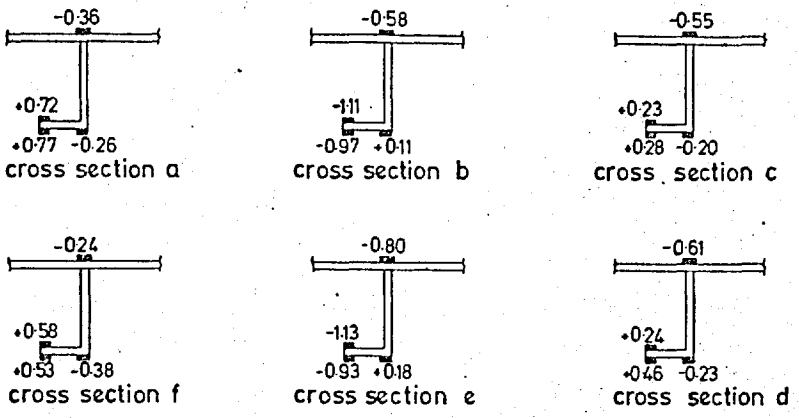

(i) Outer shell stiffener No. 3.

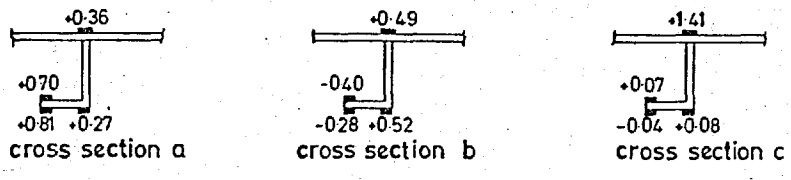

(ii) Inner shell stiffener No. 3.

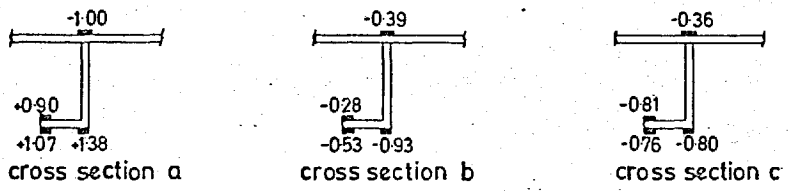

(iii) Outer shell stiffener No. 8.

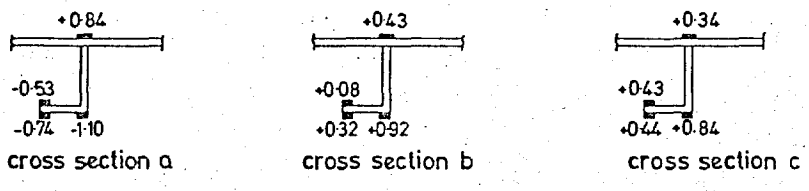

(iv) Inner shell stiffener No. 8.

NOTE : (i) Stresses in tons / in^2.
(ii) See Fig. 100 for definition of load
(iii) See Fig. 20 for location of cross sections

Fig. 134 : Double Bottom Analysis - Shell Stiffener Stresses for Patch Load P4

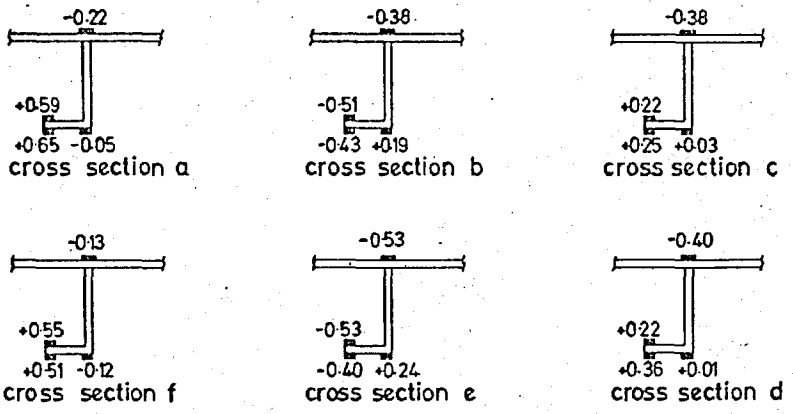

(i) Outer shell stiffener No. 3.

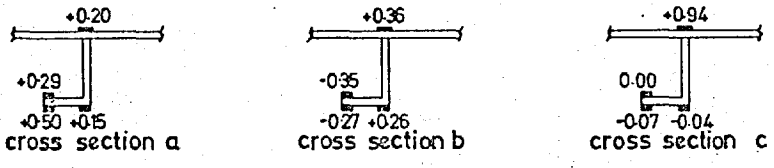

(ii) Inner shell stiffener No. 3.

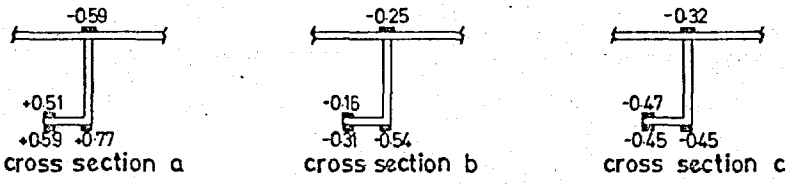

(iii) Outer shell stiffener No. 8.

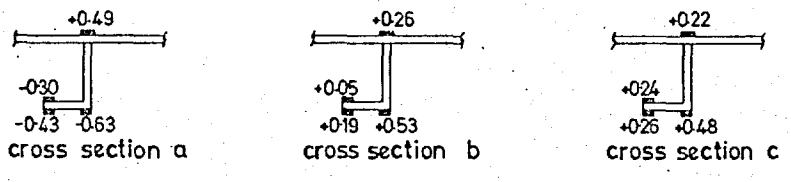

(iv) Inner shell stiffener No. 8.

NOTE : (i) Stresses in tons / in^2
(ii) See Fig. 100 for definition of load
(iii) See Fig. 20 for location of cross sections

Fig. 135 : Double Bottom Analysis - Shell Stiffener Stresses for Patch Load P2

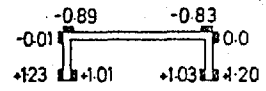

Strut X

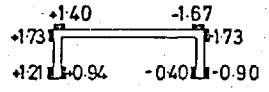

Strut Y

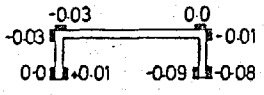

Strut Z

(i) Patch Load P8

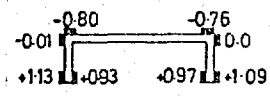

Strut X

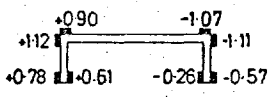

Strut Y

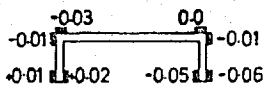

Strut Z

(ii) Patch Load P6

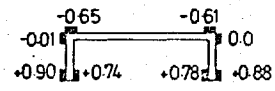

Strut X

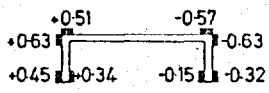

Strut Y

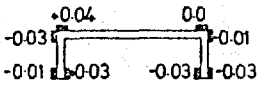

Strut Z

(iii) Patch Load P4

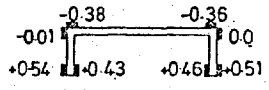

Strut X

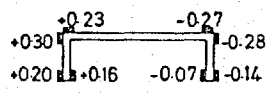

Strut Y

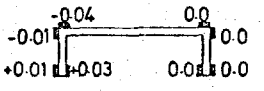

Strut Z

(iv) Patch Load P2

NOTE (i) Stress in tons/in^2
(ii) See Fig. 100 for definition of load cases
(iii) See Fig. 20 for strut locations

Fig. 136 : Double Bottom Analysis - Strut Stresses For Patch Loads

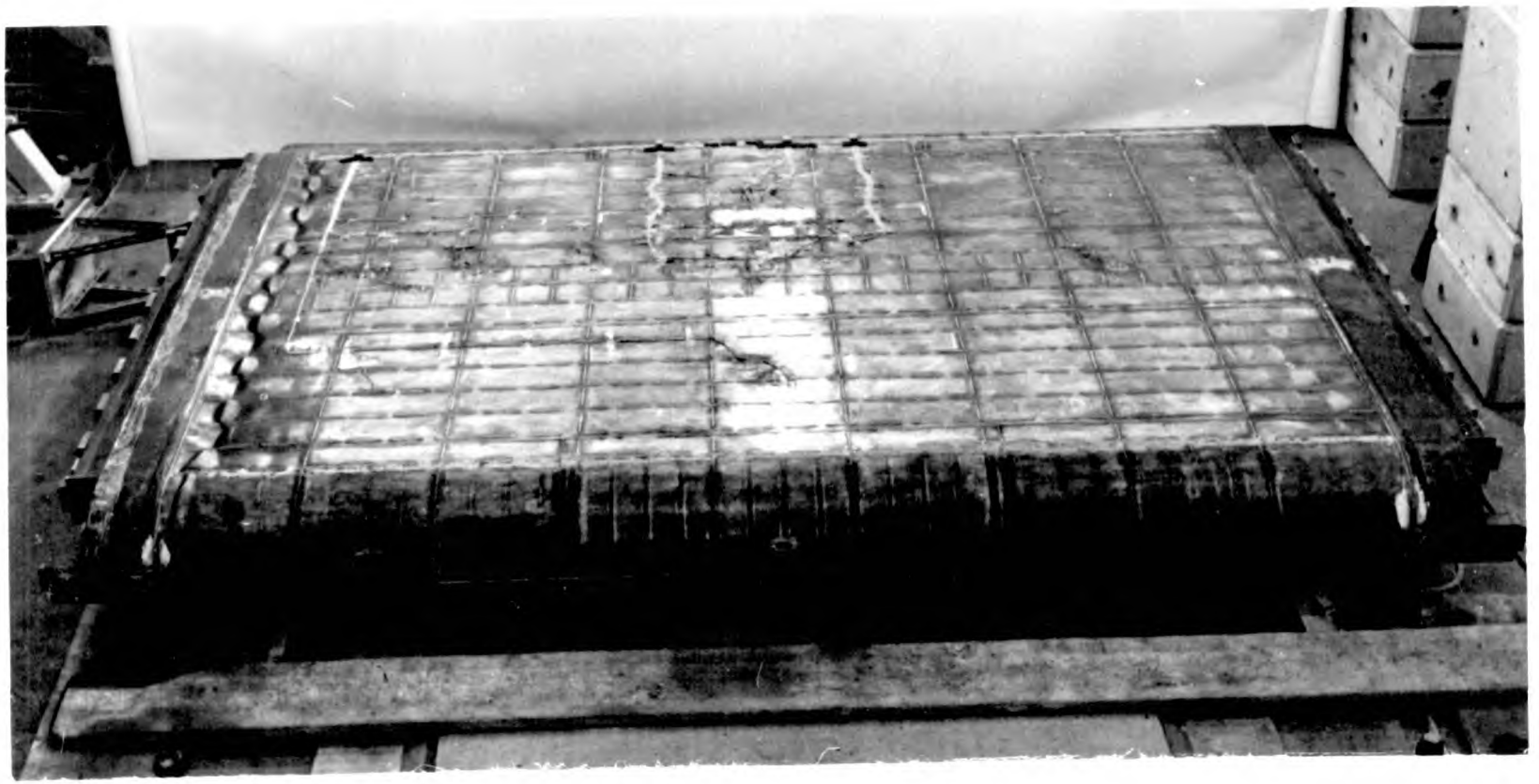

Fig. 137: Outer Shell After Local Failure

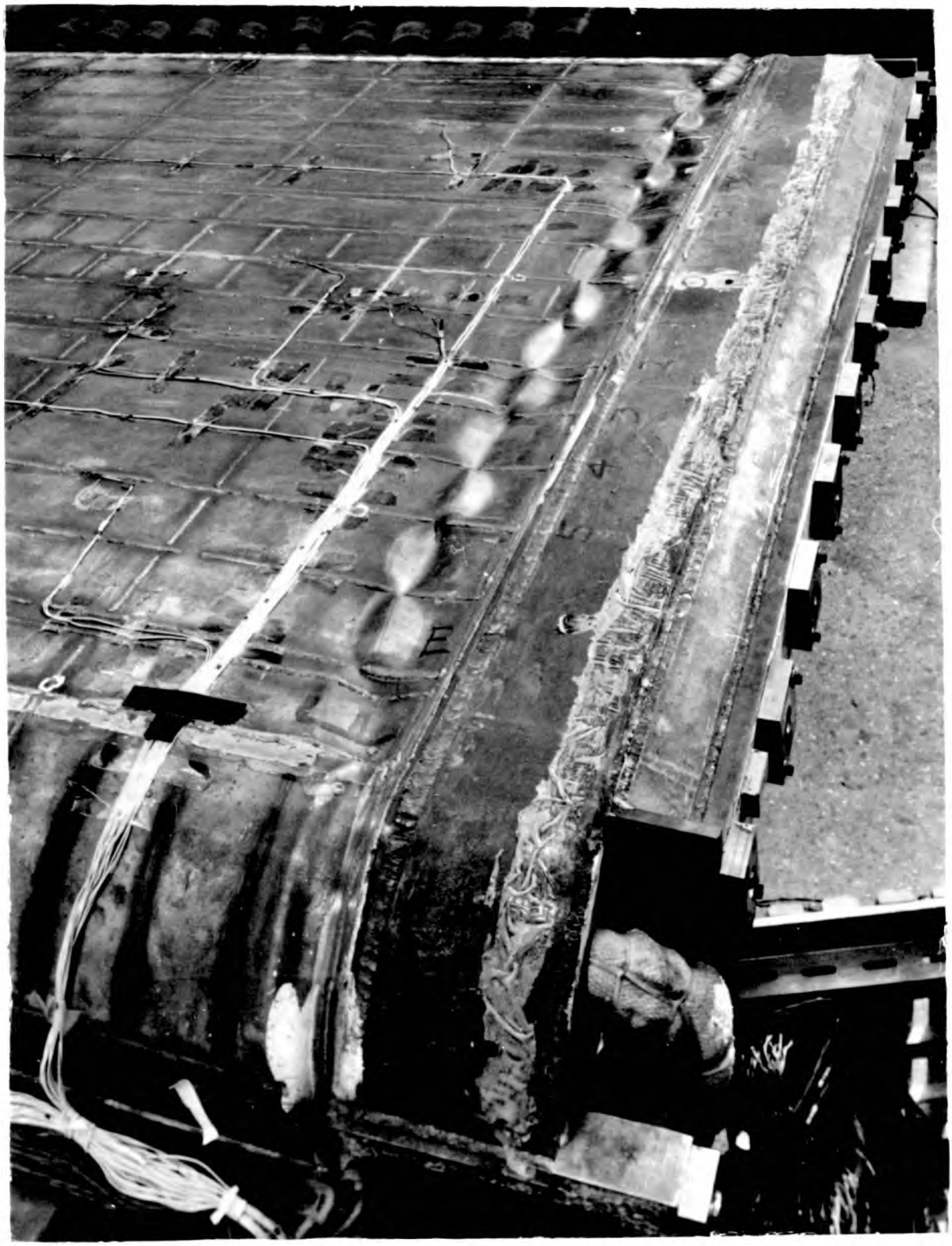

Fig. 138: Detail at Bulkhead End of Outer Shell After Local Failure

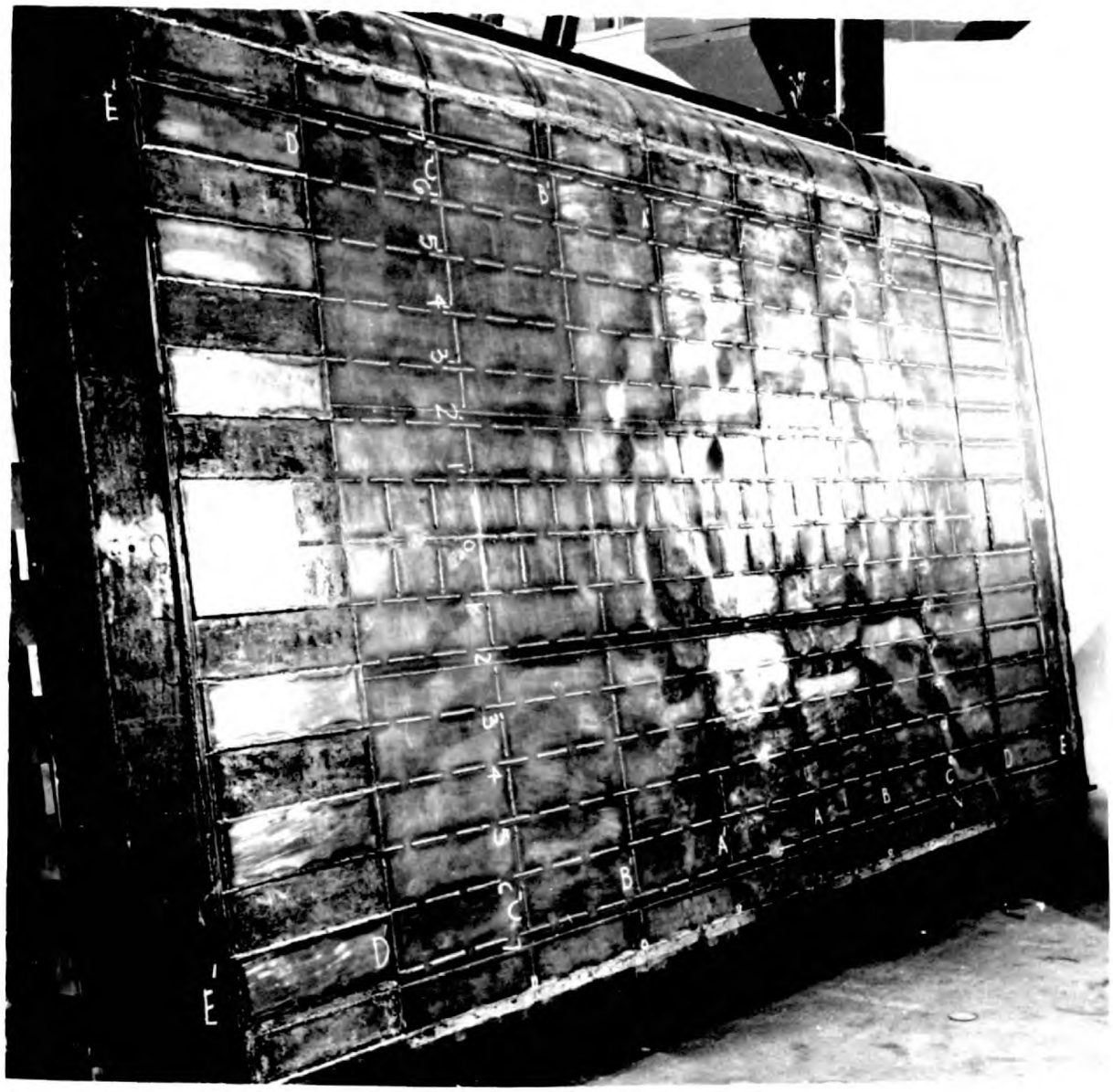

Fig. 139: Outer Shell After Overall Failure

Fig. 140: Detail of Central Region of Outer Shell After Overall Failure

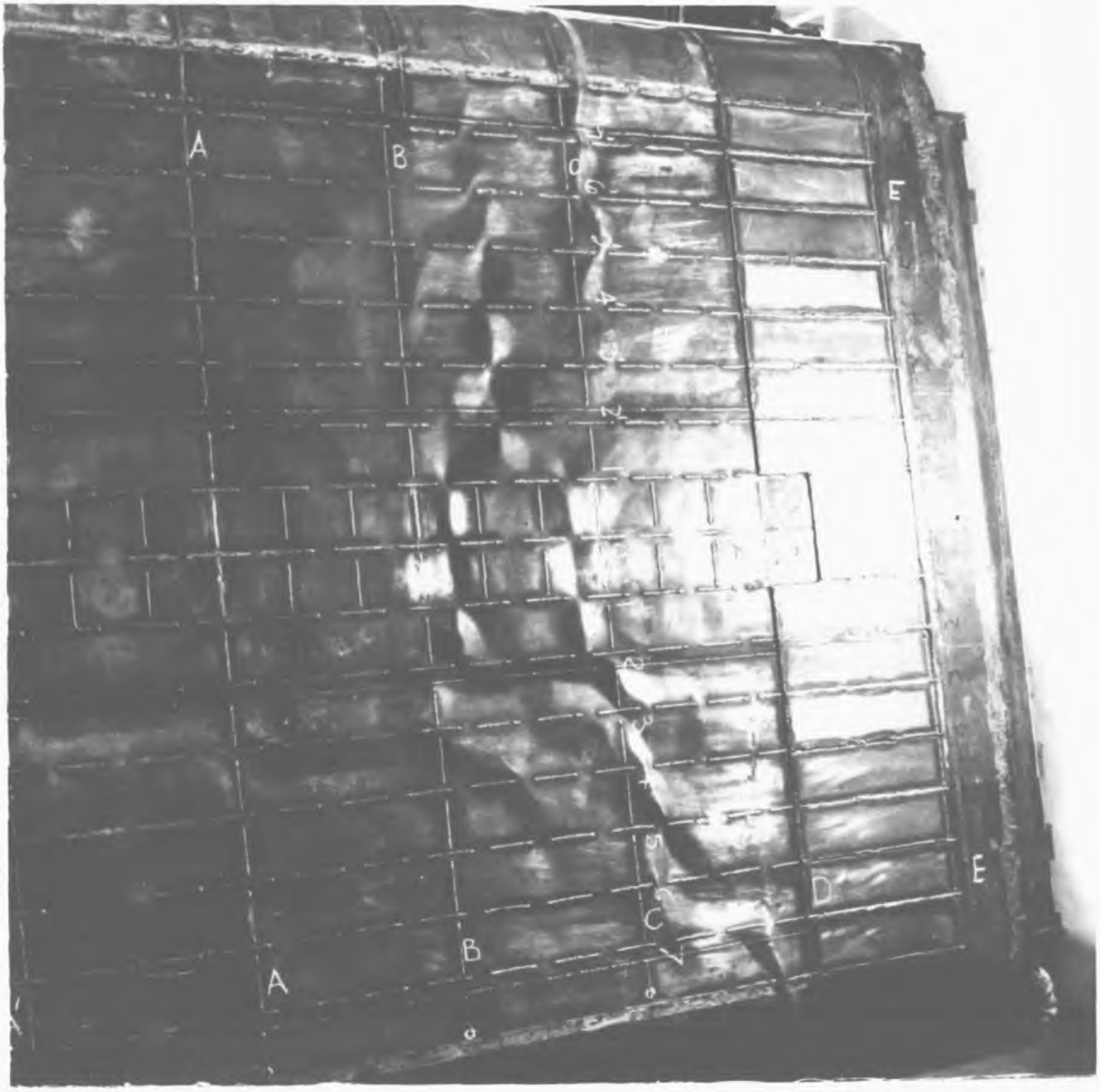

Fig. 141: Detail of End Region of Outer Shell After Overall Failure

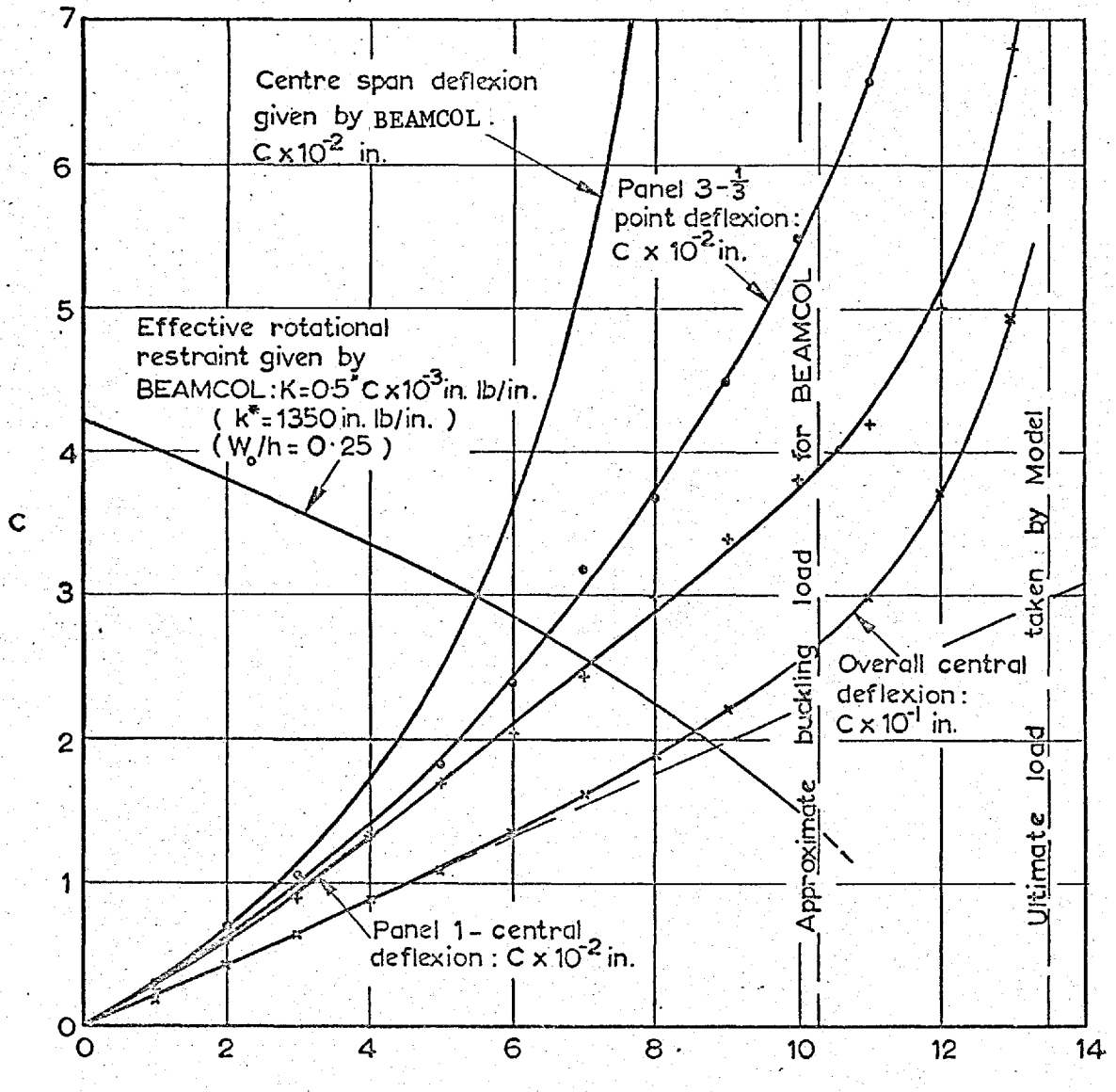

Fig. 142 : Double Bottom Analysis: Overall and Local Deflexions Compared to BEAMCOL Analysis for Failure Test

Note: End (x=0,L) boundary conditions implicit in stress function.

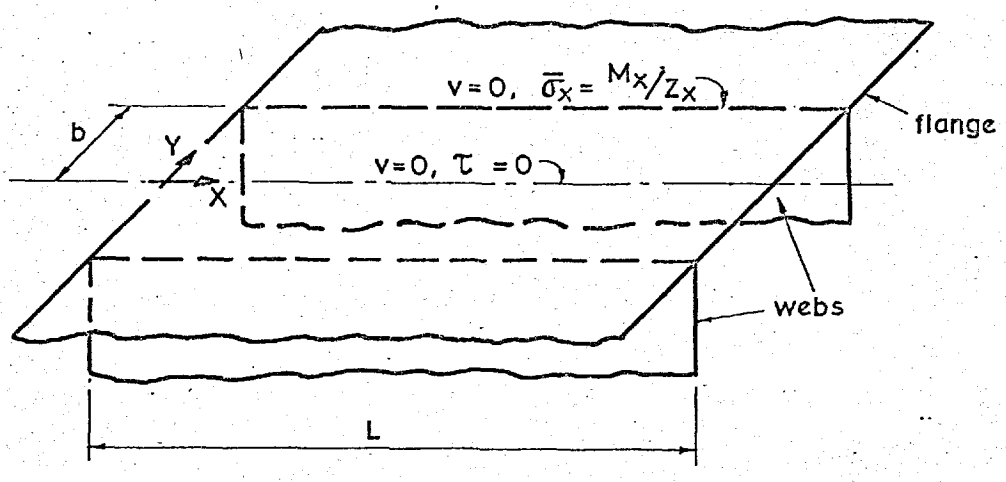

(i) Detail showing boundary conditions

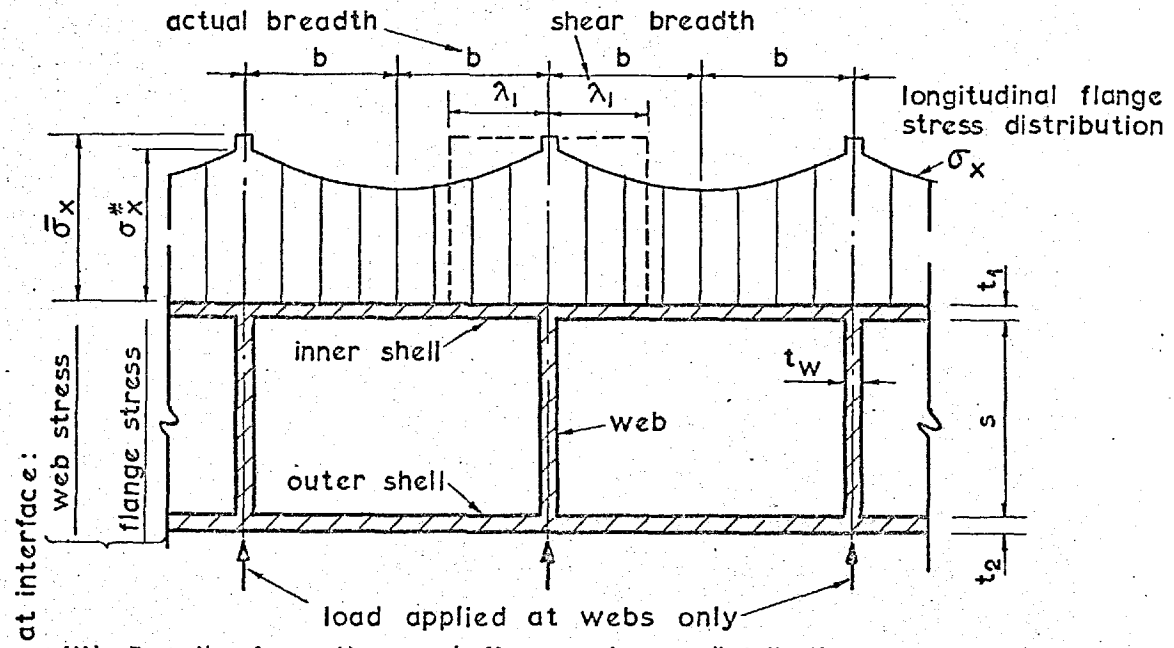

(ii) Detail of section and flange stress distribution.

Fig. 143 : Boundary Conditions and Beam Section and Stress Distribution for Shear Lag Solution.

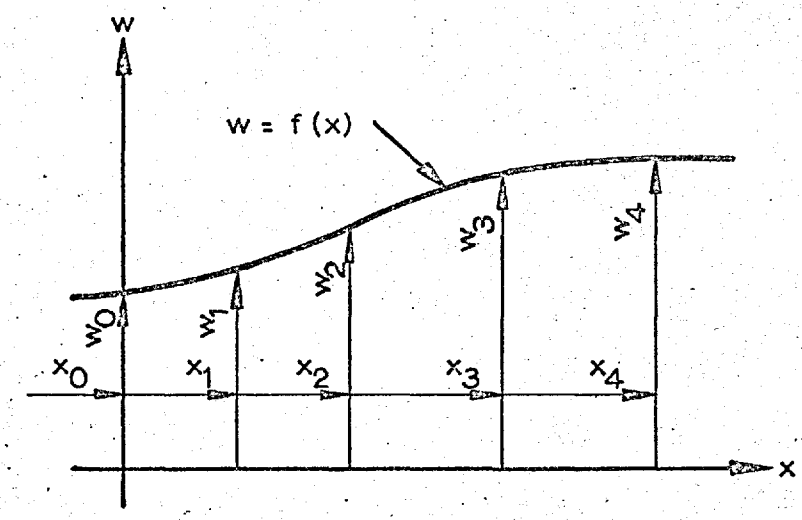

Fig. 144 : Continuous Curve Defined by 5 Points

$$\left[\frac{x_1 - x_0}{y_1 - y_0} = \frac{x_2 - x_1}{y_2 - y_1} = \frac{x_3 - x_2}{y_3 - y_2} = \frac{x_4 - x_3}{y_4 - y_3}\right]$$

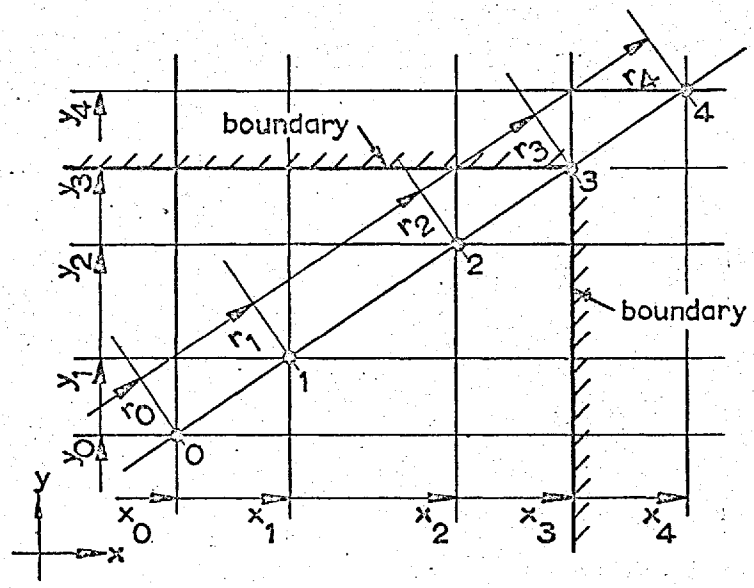

Fig. 145 : Diagonal Extrapolation for Corner Fictitious Point (4)

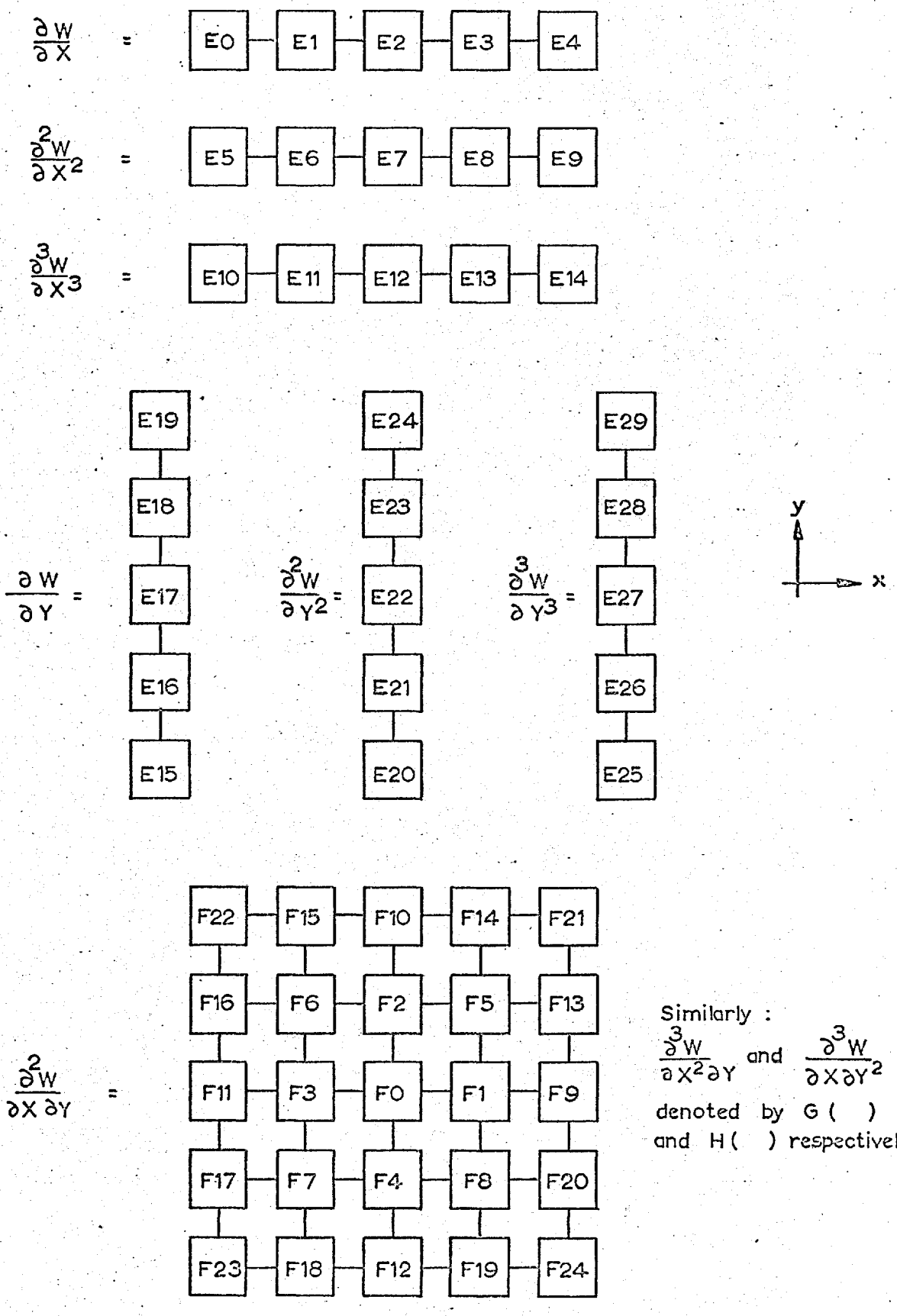

Similarly : $\frac{\partial^3 W}{\partial X^2 \partial Y}$ and $\frac{\partial^3 W}{\partial X \partial Y^2}$ denoted by G( ) and H( ) respectively

Fig. 146 : Mixed Variable Solution – Finite Difference Nets For Derivatives

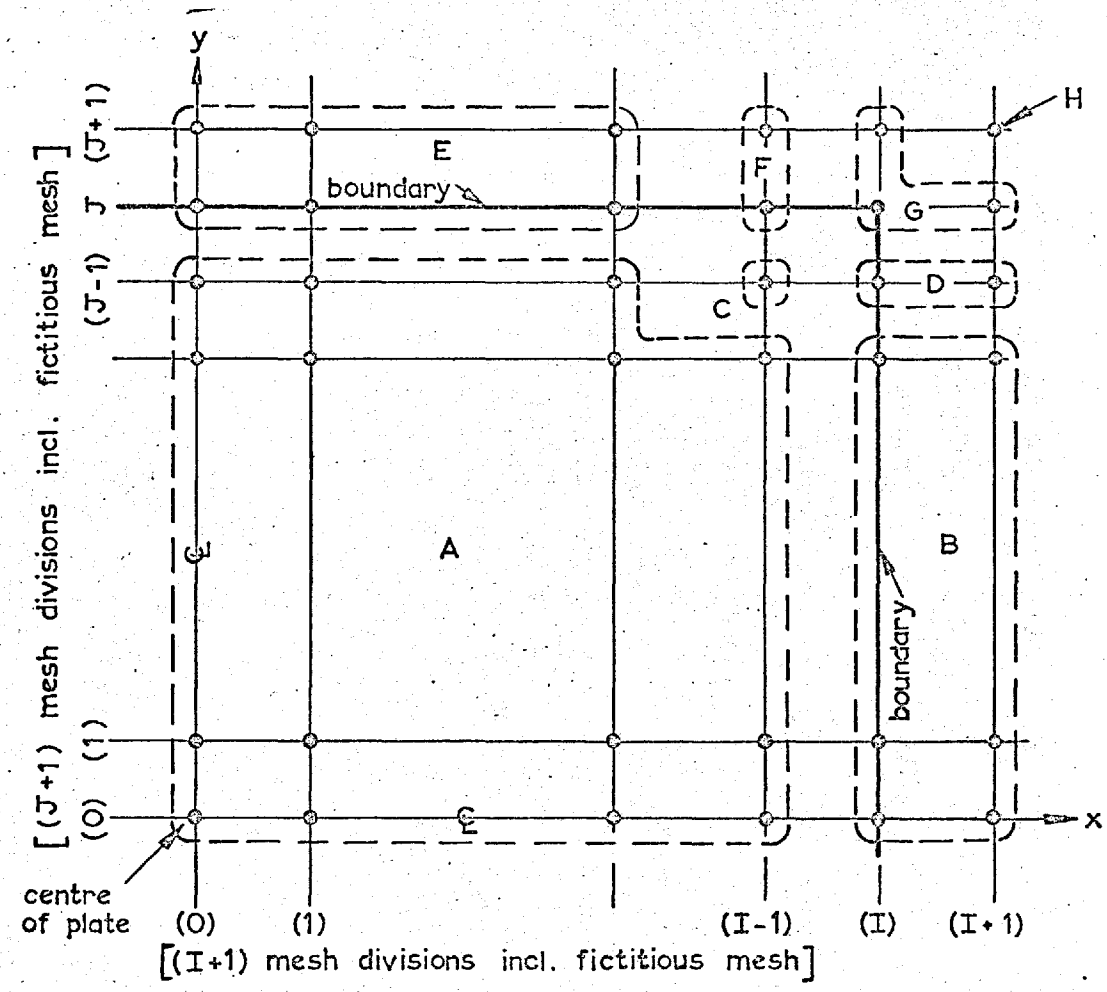

Location	Solution	Uniaxial Derivatives x	Uniaxial Derivatives y	Mixed Derivatives x	Mixed Derivatives y
A	1	central	central	central	central
	2	as for A(1)			
B	1	backward (1)	central	backward (1)	central
	2	as for B(1)			
C	1	central	central	backward (1)	backward (1)
	2	as for A(1)			
D	1	backward (1)	central	backward (1)	backward (1)
	2	as for B(1)			
E	1	central	backward (1)	central	backward (1)
	2	as for E(1)			
F	1	central	backward (1)	backward (1)	backward (1)
	2	as for E(1)			
G	1	backward (1)	backward (1)	backward (2)	backward (2)
	2	backward 1	backward 1	backward (1)	backward (1)

NOTE : (i) Solution 1 - H eliminated by choice of derivatives
2 - H defined by diagonal extrapolation
(ii) Backward (1) and (2) refer to derivatives with respect to nodes once and twice removed from the central node respectively

Fig. 147 : Mixed Variable Solution - Location of Finite Difference Nets

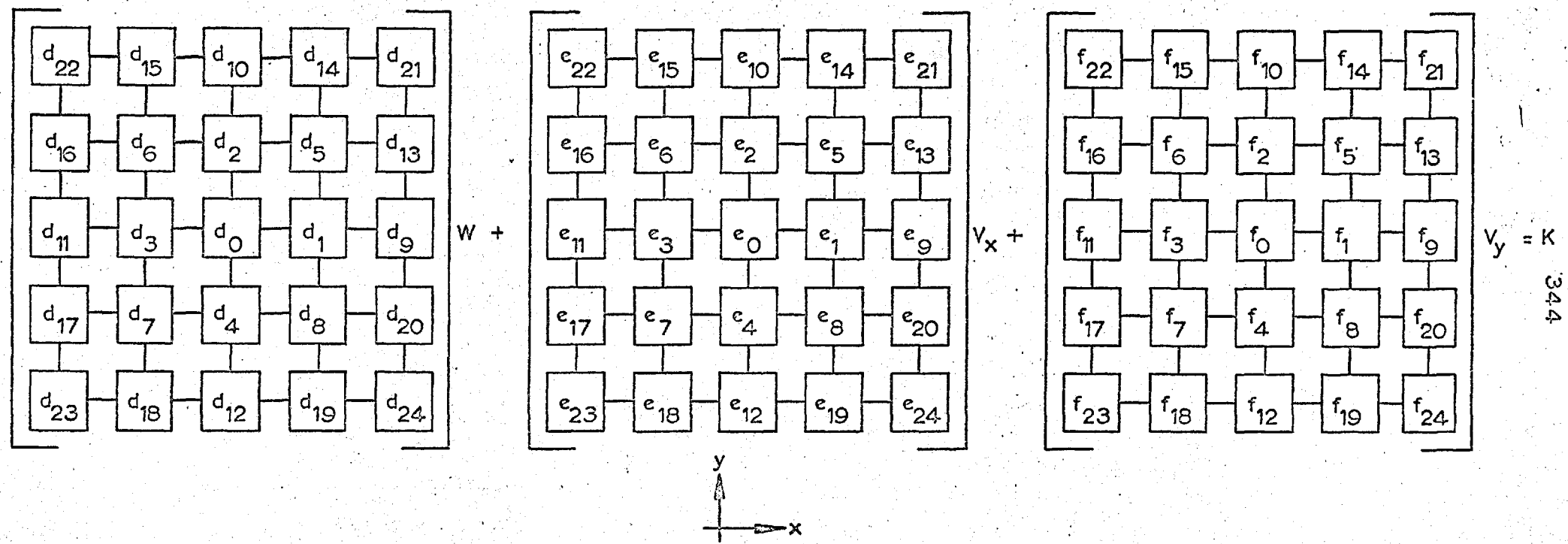

Fig. 148 : Mixed Variable Solution - Finite Difference Nets For Governing and Boundary Equations

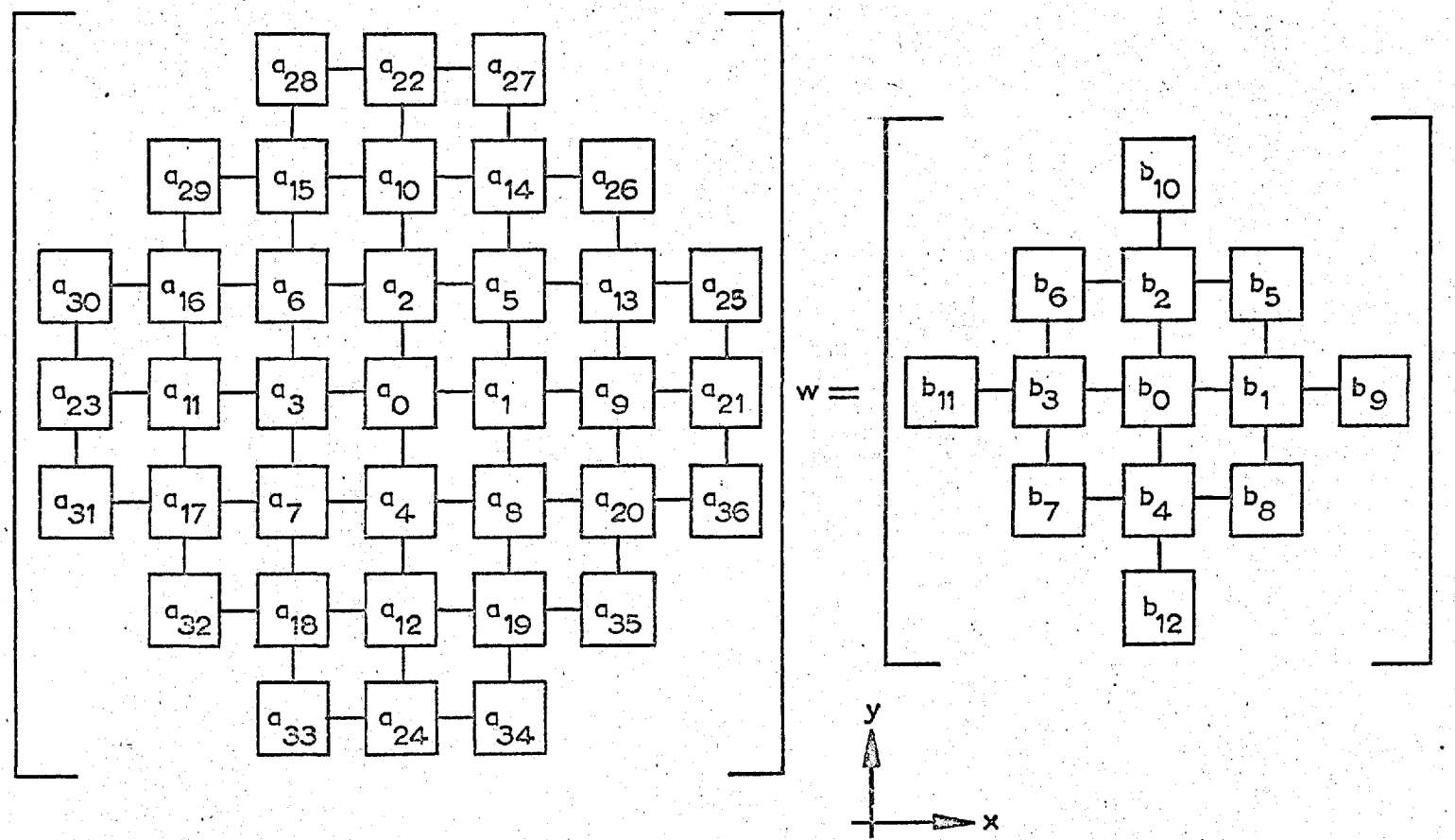

(48)

Fig. 149 : Single Variable Solution for w - Finite Difference Nets for Governing Equation

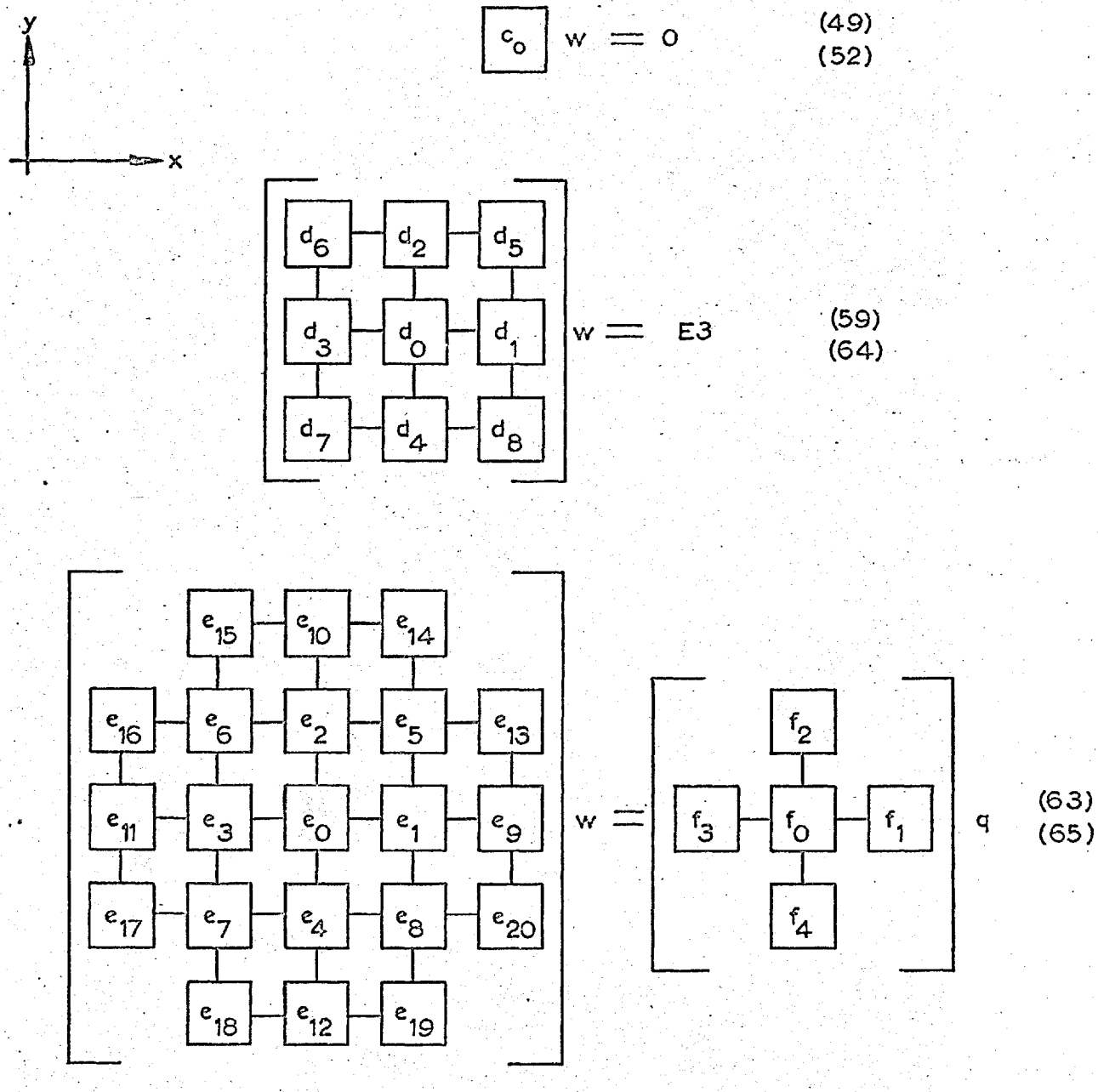

NOTE : (49), (59) and (63) on x = ± a / 2
(52), (64) and (65) on y = ± b / 2

Fig. 150 : Single Variable Solution for w – Finite Differences Nets for Boundary Equations

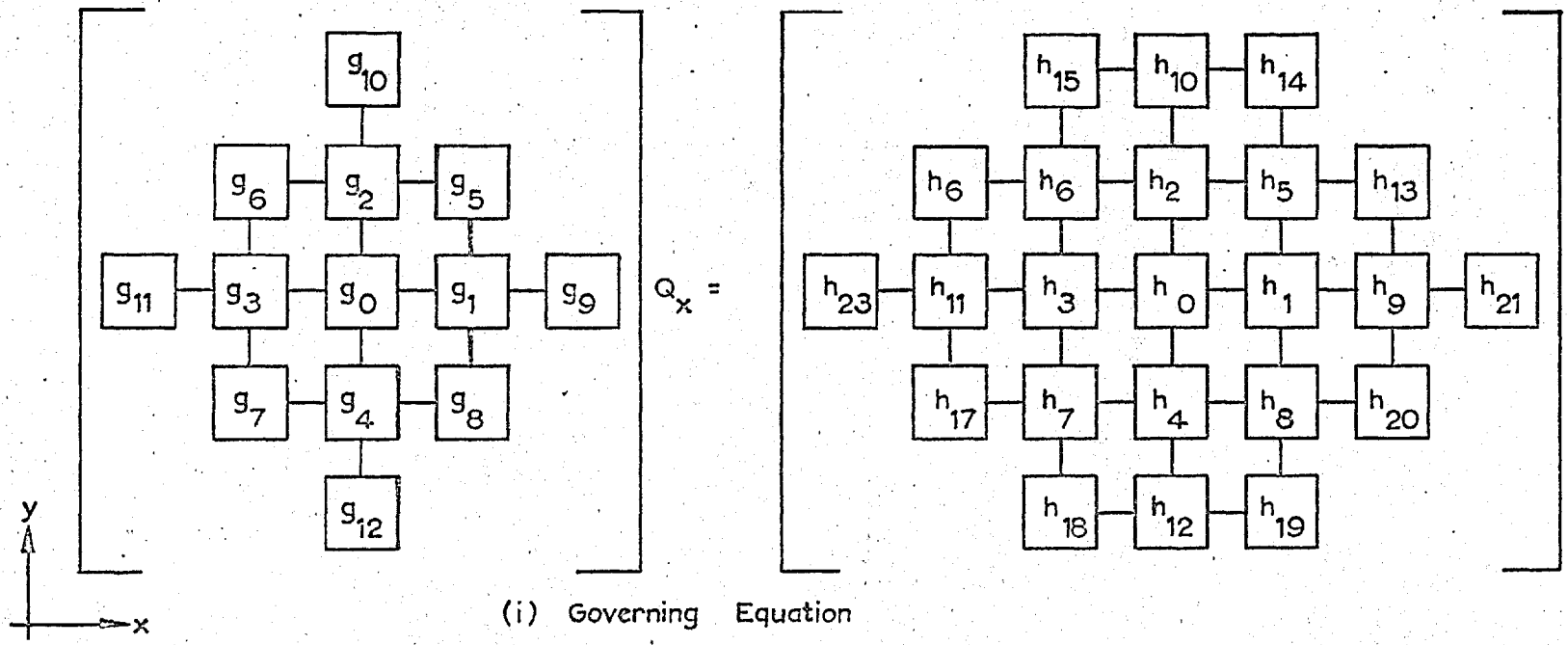

(i) Governing Equation (66)

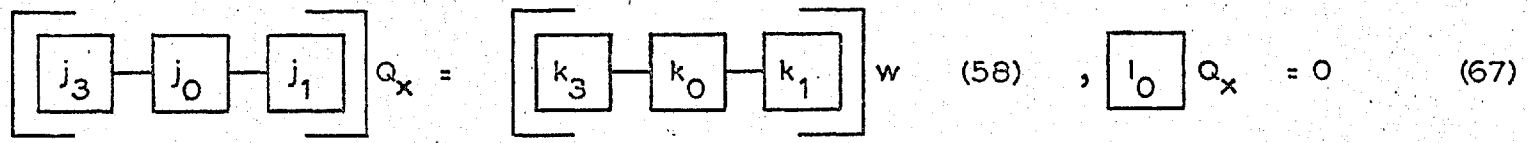

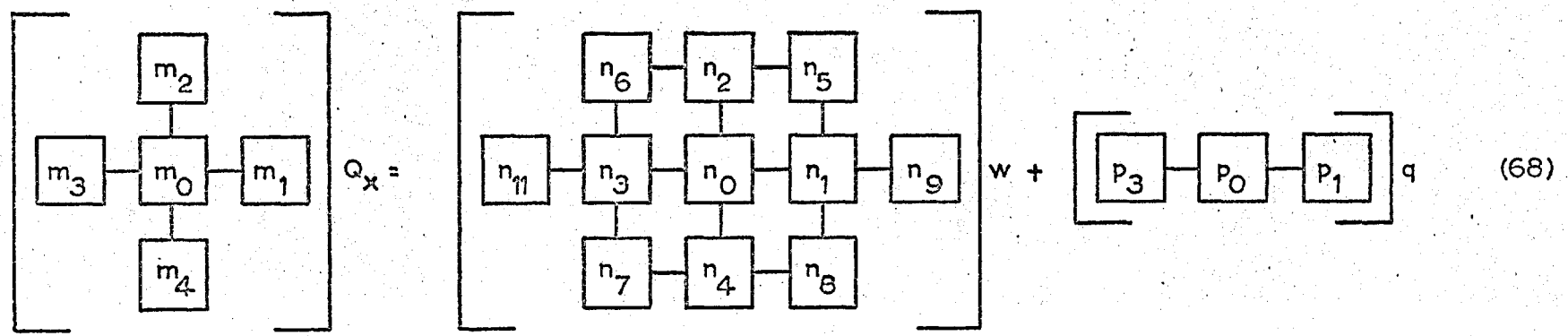

(68)

(ii) Boundary Equations

Fig. 151 : Single Variable Solution for Q_x - Finite Difference Nets